MPHIL

Innovative Cutting Tool Design for Machining Advanced Engineering Materials

Asghari, Saeed

Award date:
2019

Awarding institution:
University of Bath

Innovative Cutting Tool Design for Machining Advanced Engineering Materials

Saeed Asghari

A thesis submitted for the degree of Master of Philosophy

University of Bath

Department of Mechanical Engineering

January 2019

Summary

Machining difficult-to-cut materials such as titanium Ti-6Al-4V, hypoeutectic and eutectic aluminium alloys, Inconel 718 and austenite-ferrite super duplex 2507 are usually accompanied with low productivity, poor surface quality and often short tool life. Despite their increased usage in the aerospace, automotive and nuclear industries, manufacturing facilities are constantly faced with slow production and high manufacturing costs due to the incorrect selection of cutting tools for these materials. However, manufacturing facilities are not to blame for some of the causes of slow productivity.

There are numerous designs of cutting tools currently available in the metal cutting market but are either generic or not specific to the operation, expensive, or only cover a range of materials such as stainless steels. Extensive research has mainly been conducted on machining parameters, coated tungsten carbide inserts, coating technologies and insert tool geometry optimisation, mainly for turning. The continuous development and advancements in tool materials and coating technologies have provided improvements in tool life and productivity for machining difficult-to-cut materials. However, critical factors, including tool geometry are usually missed. Tool design and tool geometry are one of the few critical factors considered when machining difficult-to-cut materials. Cutting tool geometry in end-milling and drilling is a topic which needs further understanding, to evaluate the effect of geometrical parameters in machining of difficult-to-cut materials. This research explores the effect of various cutting tool geometries on tool life and surface roughness in end-milling and drilling of difficult-to-cut materials.

Solid tungsten carbide with cobalt binder cutting tools are commonly used in metal cutting due to their capabilities of enduring high stresses and withstanding heat at the tool-chip interface. Understanding tool geometry and its effect on difficult-to-cut materials can provide a solution to improving tool life, productivity and reducing costs in manufacturing environments. The aim of this research is to investigate the effect of tool geometry on four selected difficult-to-cut materials in end-milling and drilling operations to enhance their performance. A detailed research study, exploring the effect of tool geometry in end-milling and drilling of difficult-to-cut materials was carried out. A methodology was developed for designing and optimising solid tungsten carbide (WC) end-mills and drills. A total of 10 cutting tools, 5 end-mills and 5 drills, were designed and tested to determine a relationship between tool geometry and tool life. Results indicated that using a correct tool geometry can improve tool life and surface finish.

Acknowledgments

There are several people without whom, this work would not have been possible and to whom I am deeply indebted.

First and foremost, I would like to express my sincerest gratitude to Dr. Alborz Shokrani and Prof Stephen T. Newman for their supervision, patience, friendship and for giving me the opportunity to undertake this enormous project. I would like to extend my sincere appreciation for Dr. Alborz Shokrani for guiding me through the project and for trusting me every step of the way. I would not be where I am without his support and guidance.

I would also wish to extend my sincere appreciation to Nick Reade, Chris Wands and the staff at Scorpion Tooling UK Ltd. for trusting me and looking after me for the duration of the project. I would like to especially thank Nick Reade and Chris Wands for their teachings and patience.

Last but not least, I owe my deepest gratitude to my family for their support throughout my studies. A special thanks to my mum who always encouraged me to strive for greatness and my sister for always believing in me.

Table of Contents

List of Acronyms

3FL	Three Flute
ADoC	Axial Depth of Cut
Al	Aluminium
AlCrN	Aluminium Chromium Nitride
ANOVA	Analysis of Variance
BS	British Standardisation
BUE	Built-up-edge
CAD	Computer Aided Design
CAM	Computer Aided Manufacturing
CBN	Cubic Boron Nitride
CE	Cutting Edge
CNC	Computer Numerical Control
Co	Cobalt
CrAlSiN	Chromium Aluminium Silicon Nitride
CVD	Chemical Vapour Deposition
DF	Degrees of Freedom
DoC	Depth of Cut
DoE	Design of Experiments
EFM	Environmentally Friendly Machining
FEA	Finite Element Analysis
HB	Brinell Hardness
HPM	High Precision Machining
HSM	High Speed Machining
HSS	High Speed Steel
ISO	International Organisation for Standardisation
LPM	Low Pollution Machining
Mo	Molybdenum
MQL	Minimum Quantity Lubrication
MS	Adjusted Mean Squares
NbC	Niobium Carbide
Ni	Nickel
PCD	Polycrystalline Diamond
PH	Precipitation Hardening
RDoC	Radial Depth of Cut
SAF	Sandvik Austenite Ferrite
SFL	Striaght Flute
SS	Adjusted Sum of Squares
TaC	Tantalum Carbide
Ti	Titanium

TiAl	Titanium Aluminide
TiAlN	Titanium Aluminium Nitride
TiAlSiN	Titianium Aluminium Silicon Nitride
HSM	High Speed Machining
HSS	High Speed Steel
TiC	Titanium Carbide
TiN	Titanium Nitride
TiSiN	Titanium Silicon Nitride
TiVN	Titanium Vanadium Nitride
V	Vanadium
VB	Flank Wear Land Width
WC	Tungsten Carbide

List of Figures

List of Tables

1. Introduction

Cutting tools have undergone drastic changes with the introduction of CNC machinery [1] and the growing trends towards high speed machining (HSM), low pollution machining (LPM) and sustainability in engineering design [2]. As a result, various designs (Appendices A-C) [3], tool materials (Appendix D) [4–7] and coating technologies (Appendix J) [8–11] have been introduced in the cutting tool market to address the trends in metal cutting production facilities and manufacturing environments [1]. The introduction of difficult-to-cut materials in various engineering sectors and the need for more complex components has caused a surge in research and development of high-performance cutting tools. A high-performance cutting tool should exhibit good tool life and provide substantial resistance to wear when machining difficult-to-cut materials. This will have a ripple effect on efficiency throughout high and low volume CNC machining environments [4], potentially increasing productivity including cost savings of up to 20%. This saving can be a result of reduction in cutting tool consumption and the amount of downtime in tool change and machining set up [12,13].

Difficult-to-cut materials possess astounding mechanical and physical properties as they can endure high pressures and temperatures. The machinability of difficult-to-cut materials is still not entirely understood; there are numerous variables involved when machining these materials. Fig. 1 shows the specific strength (MPa) of difficult-to-cut alloys versus temperature (K, Kelvin) for comparison.

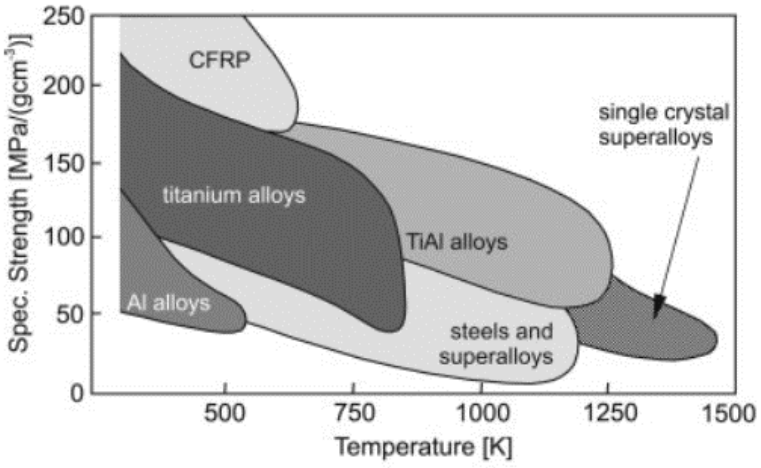

Fig. 1: Specific strength vs. use temperature of selected structural materials compared with titanium alloys and aluminides [5]

The term “difficult-to-cut”, in milling or drilling, relates to materials exhibiting poor machinability [4] due to their abnormal characteristics such as poor thermal conductivity, strain hardening, resistance to wear and chemical reactions. An investigation of environmentally conscious machining of difficult-to-cut materials, with regard to cutting fluids, by Shokrani et al. [14], states that “difficult-to-cut alloys” usually come with a variety of disadvantages such as “low

productivity, poor surface quality and short tool life". The difficulties of machining difficult-to-cut materials is usually visible in examples such as hypoeutectic aluminium alloys, titanium alloys, nickel-based alloys, and austenitic-ferritic alloys.

One example of a difficult-to-cut alloy is hypoeutectic aluminium alloy 6082-T6 which represents the largest consumption of aluminium alloy across many engineering sectors. Practically used in numerous industries for its properties and its commercial availability. The addition of silicon, Si, allows higher temperature strength and better wear resistance, all thanks to the crystallisation and microstructural strength that Si particles add to alter the characteristics of the material [15–17]. Hypoeutectic alloys contain less than 12-13% silicon. Other aluminium alloys such as eutectic and hypereutectic aluminium alloys have a much higher percentage of silicon (>12% and above) and can withstand tougher environments. However, the introduction of silicon, and its increase as an alloying content, brings a set of difficulties in CNC machining. This results in reduction of tool life and restricts the performance of the cutting tool. These types of alloys are notorious for built-up-edge (BUE) [18,19]; can cause disruptions in machining and obstruct the flow of cut chips away from the cutting tool [20]. Chip evacuation is a major challenge when machining aluminium alloys in drilling and milling [21,22]. Tools with sharp cutting edges are produced by manufacturers to counteract these issues. The automotive and aerospace industries generally machine hypoeutectic, eutectic, and hypereutectic aluminium alloys with high contents of Si. The lightweight, corrosive resistant and high temperature tolerance are some of the reasons why they are used as pistons in the automotive industry [23].

Tool geometry has been recognised as a critical factor in designing cutting tools for difficult-to-cut materials which needs to be broken down and investigated in detail. Other factors such as the selection of tool material, coating and machining techniques also effect the tool life but investigating the tool geometry is the primary factor determining the performance and the cutting tool behaviour of a high-performance tool. This research reported in this thesis investigates the effect of cutting tool geometry on the performance of solid carbide end-mills and drills specifically designed for difficult-to-cut materials. A robust methodology was developed for this study and was followed to study the effect of various cutting geometries on tool life and surface roughness. This report outlines the research conducted into machining four difficult-to-cut alloys and the approach taken to achieve a better tool life.

1.1 Report Structure

The first chapter of this report introduces the challenges of machining difficult-to-cut materials and the need for high-performance cutting tools, followed by the overall aim and objectives in Chapter 2. A detailed literature review of cutting tool technology with focus on solid carbide end-mills and drills is presented in Chapter 3, as well as the author's review of past studies – including limitations of previous research. Chapter 4 highlights the methodology employed to

carry out the experiments based on tool geometry. In Chapter 5, the experimental results are presented and manipulated along with the analysis based on the results obtained. Chapter 6 provides discussion based on results and analysis as well as performance enhancement on further optimisation, using coating and tooling technologies. The study is then concluded in Chapter 7 where the learning outcome of this research is presented, with Chapter 8 providing suggestions for future work as the final part of this research. Additional supporting information relevant to the research has been provided in the appendices.

2. Scope of Research

This chapter represents the aim, objectives, and the research scope as well as research boundaries of this study. The research aim will define the purpose behind why this study is being tackled. Following the aim, the research objectives are presented with a break down structure of the goals needed to accomplish the overall aim. Finally, a description is presented on research areas to be investigated to achieve the proposed aim and objectives.

2.1 Research Context

Productivity, power consumption and cost-effectiveness are some of the challenges to overcome in engineering industries according to Ezugwu [4], Hong et al. [24], and Pervaiz et al. [25]. Shokrani et al. [14] mentions that to accomplish these goals extensive research and resources are used to provide novel solutions for machining difficult-to-cut materials effectively both in tool design and machining techniques. The introduction of difficult-to-cut materials has brought many challenges for manufacturing environments. For example, the growth in using titanium alloys in the aerospace industry is shown by the increased use of Ti-6Al-4V and the introduction of newer alloys such as Ti-55531 [6] alloy in the Airbus A380 and Boeing 787 aircraft [26]. Cui et al. [26] describes that the total amount of titanium required to produce a single Boeing 787 is approximately 91 tonnes. The rest of the aircraft is mostly made of aluminium, steel, and advanced composites. Investigating the material response during machining processes is a general strategy to understand the machinability of any material.

Tool wear is one of the biggest challenges to overcome in machining difficult-to-cut alloys as it can occur rapidly on the cutting tool and shorten tool life. This process can be costly, time consuming and unproductive for manufacturing centres. There are many challenges to overcome in the machinability of difficult-to-cut engineering materials but overcoming these requires innovative thinking and experimentation to, obtain tool geometry and design for a high-performance cutting tool. However, machining difficult-to-cut alloys remains one of the major bottlenecks in many engineering industries. This is mainly due to the specific challenges that these difficult-to-cut alloys exhibit during machining [14]. One alternative resolving some of the challenges faced during machining of difficult-to-cut alloys is to design cutting tools with tailored tool geometries.

2.2 Research Aim

The aim of this research is to develop a range of cutting tools for optimising the performance of solid tungsten carbide end-mills and drills for difficult-to-cut alloys such as aluminium alloy 6082-T6, titanium Ti-6Al-4V, Nickel alloy Inconel 718 and austenitic-ferritic (super duplex) stainless-steel 2507. For the purpose of this research, tool performance is measured by tool life and surface roughness.

2.3 Research Objectives

With reference to the aim, the following objectives were identified:

i. To complete a comprehensive literature review on cutting tool technology; identifying the importance of tool design for end-mills and drills focusing on the importance of tool geometry, tool wear, chip formation and coating technology.
ii. To design and realise a methodology for optimising cutting tools for advanced engineering materials
iii. To conduct milling and drilling experiments in difficult-to-cut materials such as 6082-T6, Ti-6Al-4V, Inconel 718 and super duplex alloy 2507 detailing the steps taken to achieve the optimised tool geometry.
iv. To evaluate the experimental results and identify the significance of the geometrical factors based on tool life and surface roughness.

2.4 Research Scope

Much of this thesis focuses on generating a range of cutting tools, mainly solid WC-Co end-mills and drills, for difficult-to-cut alloys. A major element of the research will be defining the new enhanced tool geometry through experimentation for various difficult-to-cut materials.

2.5 Research Boundaries

This report mainly outlines the techniques and steps required to realise an optimised cutting tool for a specific advanced engineering material namely 6082-T6, Ti-6Al-4V, Inconel 718 and super duplex stainless-steel 2507. The cutting tools have been developed after a range of different materials have been evaluated in the 2nd and 3rd years of this research and will form the major contribution of the research aim.

The major machining operations which have been considered have been defined as roughing and finishing with solid carbide end-mills and drilling with solid tungsten carbide cutting tools.

This research is limited to the optimisation of the cutting tool geometry to maximise tool life, improve surface roughness (Ra) and analyse chip morphology. Specifically, the mechanism of material cutting, material microstructure changes, machining strategies, cutting parameters, energy consumption and cooling/lubricating techniques are outside the boundaries of this research. Moreover, this research does not cover the cost analysis for machining of difficult-to-machine materials.

3. A Review of Cutting Tool Technology

In this chapter, a review of relevant existing literature related to the advancement of cutting tool technology for solid tungsten carbide (WC-Co) end-mills and drills is presented. Firstly, this will explore the science of cutting tools for WC-Co end-mills and drills, providing detailed information on their designs, tool materials and existing coating technologies. Key tool geometrical factors that influence the performance of the end-mills and drills when machining difficult-to-cut materials are described in more detail with the use of nomenclature. Then, the chip formation and tool wear mechanisms, as well as tool wear types will be discussed. Therefore, providing further information on the failure of cutting tools in machining of difficult-to-cut materials; such as aluminium alloys, titanium alloys, nickel-based alloys, and austenitic-ferritic alloys. Finally, a literature critique outlines the gaps of existing literature and reasons behind carrying out this valuable study to fill in the gaps in knowledge.

3.1 Cutting Tool Technology

The term “cutting tools” in the context of machining and CNC machining refers to single-point tools such as inserts, for the use in turning, or multi-point cutting tools for milling, drilling or thread-milling operations. Solid WC-Co or insert tools tend to be the most popular choice for material removal (by shearing) in the form of chips for difficult-to-cut alloys [4,7]. Cutting tools can vary in design and shape, as shown in Fig. 2, and their selection is purely dependant on the specific machining operation(s) involved. Designs of cutting tools can vary depending on the need of the machine operator. In the case of inserts, the WC-Co tips can come in various shapes as shown in Fig. 3 and may vary in tool geometry, tool material and coating technology.

Fig. 2: Current cutting tool designs and cutting tool technology [27,28]

The same principles are applied to solid WC-Co cutting tools such as end-mills and drills where the number of cutting edges, shape and end profile design varies depending on the machining operations and the workpiece material. The design and the tool geometry of these cutting tools (Fig. 4 & Fig. 5), to some extent, determines the material removal behaviour and the capability of the cutting tool as well as its performance [7].

Fig. 3: Various WC-Co insert tip designs [2]

Fig. 4: Various designs of end-mills with multiple cutting edges [3]

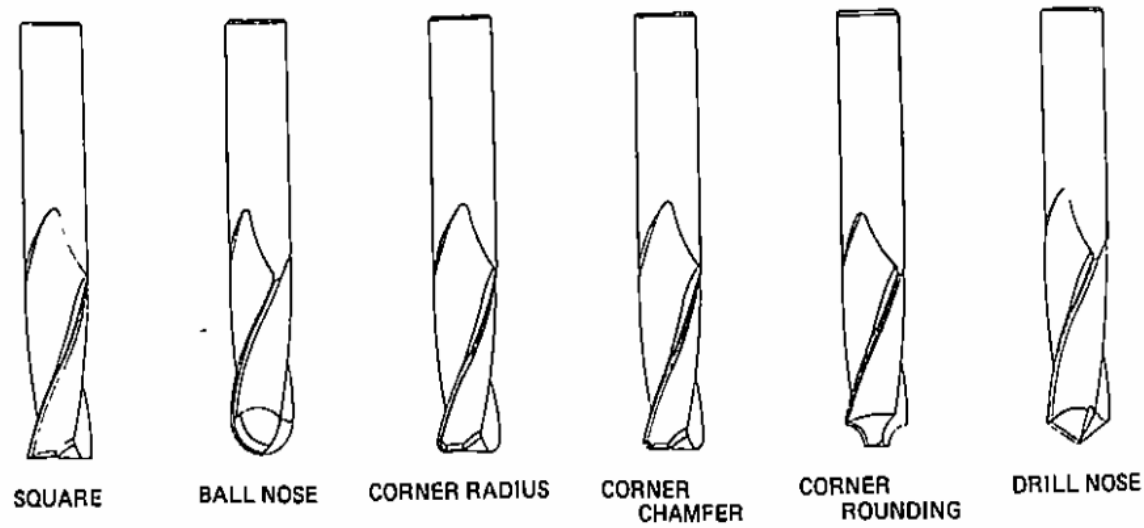

Fig. 5: Different end profile designs; each specific for a certain machining operation such as chamfering and drilling [29]

Cutting tools can be found in various engineering production facilities such as aerospace, automotive and oil & gas industries where complex components are produced using sophisticated CNC machinery. As sustainability in engineering design evolves, the need for more complex parts becomes more evident, which prompts engineers to look for alternative materials. However, new alternative materials introduce new challenges and material removal becomes a problem. As a result of these challenges, cutting tools, coating technologies and tool materials are in a constant race to catch up with the advancements in material science to

meet the new manufacturing industry requirements and the trends in machining technology. Three main areas are currently being focused upon in manufacturing environments [7]:

1. High speed machining (HSM)
2. High precision machining (HPM)
3. Low pollution machining (LPM)

The need for HSM is a critical factor for manufacturing economics. Machining complex components in difficult-to-cut materials is costly and time consuming. High speed machining comes with its own set of challenges and several factors should be considered. Increasing machining speed increases machining efficiency and in turn reduces production costs, as long as other conditions are the same [30]. However, the consequences of increased machining speed are reduction in tool life and increase in tool wear because of higher cutting temperatures at the tool-chip interface. Therefore, the correct selection of tool material, tool geometry and coating becomes critical in higher machining speeds [2,7,31]. High precision machining (HPM) determines the product quality as well as its reliability. The geometrical error of cutting tools and poor design has enormous effects on surface roughness which is significant in determining the quality of the machined surface [7,31]. Therefore, to get high standards in quality and reliability, high rigidity in machine tools and precise cutting tools are needed; which in turn reduces the chance of material scrappage [7]. The final trend in machining technology is the environmentally friendly machining (EFM) or LPM and the use of novel techniques such as minimum quantity lubrication (MQL) and hybrid machining [7,13,14,32]. Shokrani et al. [13] for example, analysed the effect of cryogenic cooling when milling titanium alloy Ti-6Al-4V and compared it against other cooling techniques to understand whether using this technique improve tool life and surface integrity. It was concluded that cryogenic cooling improves surface roughness by as much as 31% when compared to conventional emulsion cooling technique. Hong et al. [33] also investigated cryogenic machining Ti-6Al-4V in the turning of alloy Ti-6Al-4V and found that this method can be a vital operation in extending tool life. Conventional cooling techniques such as flood coolant can cost approximately 15 percent of the life-cycle operational cost of a machining process [34]. It is important to note that there are other hidden factors in conventional cooling techniques. These include the costs associated with procurement, filtration, separation, disposal, delivery and documentation for environmental protection [7].

To overcome the challenges set by the trends in machining technology, high-performance, high-precision cutting tools with low chemical affinity and high rigidity are required. Difficult-to-cut materials tend to possess high material strength and toughness, poor thermal conductivity, and high temperature hardness, depending on their properties. As a result of these material properties, machining difficult-to-cut components becomes challenging and makes tool life unpredictable. One way to overcome the challenges of machining difficult-to-cut materials and

controlling the unpredictability of tool life is to design cutting tools with specific tool geometries. Further enhancement to tool performance can be accomplished in tool design when the tool geometry is combined with the correct tool material and coating, as shown in Fig. 6.

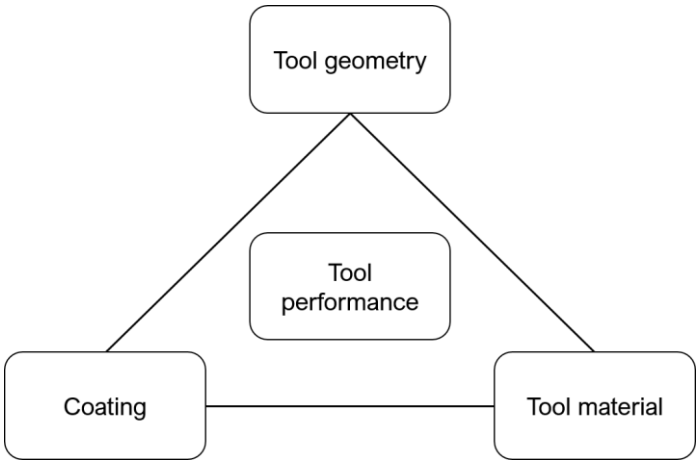

Fig. 6: Three fundamental factors contributing to cutting tool performance

3.1.1 Tool Geometry

One critical factor which can affect tool life in machining of difficult-to-cut materials is the tool geometry [2,6,7,35]. Other factors such as the grade of tool material [36], coolant, coating [37] and machining techniques [38] can also play a vital role when machining a difficult-to-cut material. Additional factors that play an important role in machining are coolant delivery method, workpiece material, machining techniques or strategies and unstable conditions in CNC machining. In most cases, it is the lack of knowledge and inadequate experience in tooling and tool material [38] which generates problems in various areas such as machining environment, tooling, lack of information on the workpiece material being machined [35], coatings and coolant. Therefore, the reason why the productivity of these materials is extremely low, becomes clear.

Previously, the importance of cutting tools in manufacturing environments were usually ignored due to little financial support or technical expertise in the area [2]. However, tool design is now considered to be one of the most important aspects of the machining process design [2]. In tool design, it is important to thoroughly consider tool geometry, tool material, surface treatment, coating technology and their combination to improve the total machining performance. Tool geometry is of utmost importance due to the direct effect it has on [31]:

- Tool life
- Surface finish and quality
- Chip flow

Consider a two-dimensional orthogonal cutting with a single-point cutting tool (Fig. 7).The rake angle (γ) is the angle of the rake surface where the chip is being formed as the tool cuts the material [39]. The flank angle (θ) denoted as (α) shown in Fig. 7, is the clearance angle

between the cutting tool and the freshly cut surface to prevent friction between flank face and workpiece. The cutting edge can be described as a theoretical point at which the rake and flank surfaces meet. Astakhov and Davim [31] define the cutting edge at the first point of contact as the tool moves towards the workpiece. Cheng [7] mentions that the rake angle, flank angle and the cutting edge are three major geometrical parameters with rake angle being the most critical. It should be noted that three-dimensional tools where helix angle is present, such as end-mills and drills, the rake angle becomes harder to define and model. An example of this can be found in drills where there is no nominal rake angle. The effective rake angle is dependent on the helix angle at the cutting point [7,31].

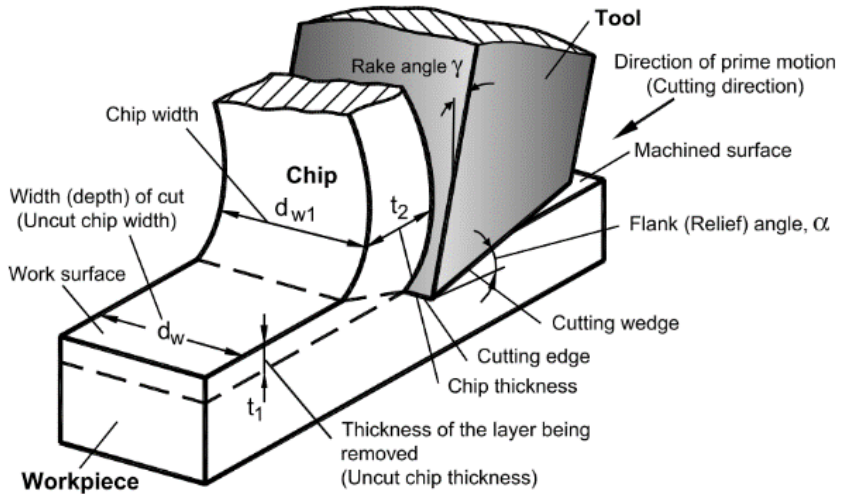

Fig. 7: Visualisation of basic terms in orthogonal cutting [31]

The magnitude of cutting tool wear is dependent on the tool material, tool geometry and workpiece material according to Davim [6] and Astakhov [31]. Understanding tool geometry is essential as different materials react differently during cutting operations. Discovering the geometry fit for the workpiece material requires a series of experiments, analysis and understanding. Astakhov [31] describes that tool geometry influence factors such as:

i. Uncut chip thickness – which in turn will maximise the productivity of machining (also known as maximum chip load) and prevent burnishing or galling.
ii. Chip flow direction – the geometry defines the direction of the chip flow and evacuation.
iii. Cutting forces – An essential and important aspect of understanding tool geometry. If the forces are irregular and the performance of the tool is poor, then the tool geometry for that material is not suitable. This downside can also increase the power consumption of the machines used for similar operations.
iv. The quality and surface finish – the geometry and the cutting tool together define the surface quality. Tool geometry defines surface topography or in other words the quality

of the surface finish. There is a relationship between cutting tool geometry and surface finish.

v. Tool life – tool geometry affects the tool life of the cutting tool directly and it is a simple way of understanding the effect of geometry on the material.

3.1.2 Drills

One major operation in CNC machining of difficult-to-cut materials is the hole making operation, also known as drilling. Drilling covers up to 40-60% of the total material removal in structural frames of an aircraft [40,41]. Typically, there are two types of drilling: short hole drilling and deep hole drilling. Short hole drilling tends to cover holes with a small depth to diameter ratio having diameter up to 30 mm and a depth of no more than 7 times the diameter [40,42–45]. Meanwhile deep hole drilling covers holes requiring more than 30 mm of diameter and drill deeper depths [40,45]. Drilling penetration and the speed at which a hole can be drilled is crucial to CNC machining centres because of operating costs involved. Increasing the drill penetration rate by 50% could amount to yearly savings per machine [31]. That is if one is factoring a 75% efficiency for loading/unloading, tool setup and tool change. In the case of this study, short hole drilling has been adopted for investigation and ease of manufacturing. The geometrical parameters of a helical twist drill are presented in Fig. 8. The major geometrical parameters of a drill are the rake angle, point angle, clearance angle and chisel edge angle. It should be noted that the rake angle is usually specified as the helix angle at the periphery.

In drilling, the cutting tool usually consists of either two or three cutting edges and rotates about its axis in order to remove material via the flute. During machining, the cutting edges are continuously removing material from the workpiece; this is in contrast to turning in which there is one continuously engaged cutting edge. In a twist drill, material removal occurs by extrusion near the chisel edge (the cutting speed is negligible at this particular point on the drill). On the cutting edges however, material is removed by shearing the workpiece. Chips are then evacuated up along the drill flute, which is oriented at an angle to the drill axis, the helix angle.

There are numerous variables which affect the performance of the drill in CNC machine operations. Productivity and tool life are usually the main objectives in drilling but if hole quality is introduced then the approach to the drilling method might have to be revised. The workpiece material, machine type and hole concentricity are some of the other factors that can determine the tool life and the productivity of the drill [31]. Therefore, different designs are required to fulfil the operational needs of CNC machining centres and manufacturing cells. There are many designs of drills, as shown in Fig. 9, yet not all designs are optimised for their specific use on difficult-to-cut materials.

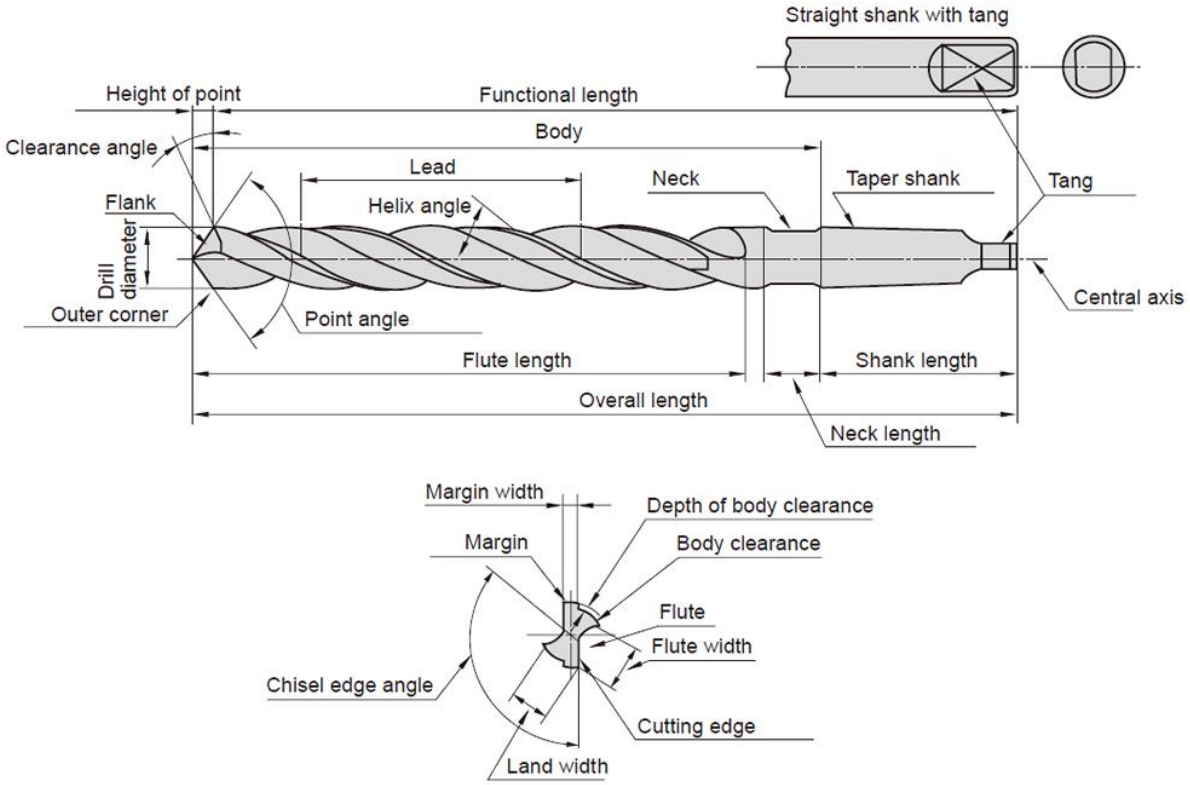

Fig. 8: Nomenclature of a helical twist drill geometry [27]

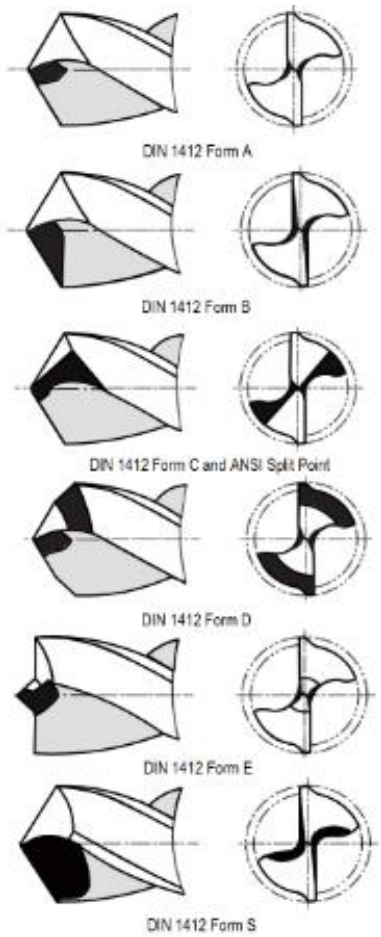

Fig. 9: DIN. 1412 drill point designs [31]

Numerous recent studies have been conducted on drilling of Inconel 718, a difficult-to-cut alloy [42,43,46,47]. These studies have evaluated tool performance and tool life based on design, machining parameters, cooling techniques and wear mechanisms. In addition, most studies carried out on tool geometry have concentrated their efforts and resources on carbide inserts [48–50]. Prolonging tool life provides positive effects on productivity, costs, and efficiency. A study by Ulutan et al. [51] on high performance cutting tools in end-milling of nickel-based alloys showed that tool life can be extended by 27% if the right selection of tool material and coating is used. However, the geometry of the high-performance tool was not studied. The selection of the right tool material and design of cutting tools in combination with new advancements in coatings and cooling technologies could, drastically increase tool life in difficult-to-cut materials. This was illustrated by Li et al. [44] when comparing a high-performance drill against standard drills. It was noted that there is a significant research gap on optimising the cutting tool geometry for solid tungsten carbide (WC-Co) drills.

It is extremely important to understand the causes of tool wear, but this can be minimised if tool geometry is involved. Batzer et al. [20] conducted a similar experiment to [46] where drilling of high-strength cast aluminium alloy 308 and 390 was carried out. Different drill designs such as three-flute and zero helix angle drills as well as two types of tool materials were investigated during the study. Cutting tools made of WC-Co showed a better performance when compared to high speed steel (HSS) tools. Li et al. [44] carried out a study based on three types of drills when drilling titanium alloy Ti-6Al-4V evaluating the effect of tool life, thrust force, energy and burr formation. The study concluded that the tool life of a drill can be increased by as much as 10 times when spindle through coolant and a specific design of drill are used. Li et al. [44] demonstrated that, using stable drilling parameters, spiral point drill geometry and fine-grained WC-Co tool material, high drilling penetration rate of Ti-6Al-4V is achievable. Zeilmann and Weingaertner [52] carried out a study by assessing the temperature of the drill in machining Ti-6Al-4V and applying MQL through the coolant holes and externally, on the outside of the drill. Typically, conventional flood coolant is used for through coolant technology and the high pressure is used to clear chips at the bottom of the drilled hole. Zeilmann and Weingaertner [52] discovered that their internal MQL technique reduced temperature at the tool-chip interface by 50%.

In drilling of stainless-steel materials, the duplex alloys are more difficult to machine than the austenitic grades, though these have better mechanical properties. The common basis for its poor machining behaviour stems primarily not from the resulting high strength of the alloy but being exacerbated by lack of non-metallic inclusions and the low carbon content [53].

There are some studies which have focused on the machinability of duplex and super-duplex alloys. Nomani et al. [53] compared and investigated the machinability of duplex SAF 2205, super-duplex SAF 2507 and 316L austenitic stainless steel in terms of cutting forces and

surface roughness with advancement of tool wear (qualitative and quantitative) during drilling process. They demonstrated that drilling of super duplex 2507 is challenging for the drill bits. Extreme chisel edge and flute damage on the margin and the body clearance of the drill when drilling duplex and super duplex grades, was observed, and documented. Rake face wear was also analysed but severe damage was not observed. Having said this, study on drilling of second-generation duplex alloy (SAF 2507) is extremely limited so far in the literature.

3.1.3 End-mills

Solid carbide WC-Co end-mills are an essential part of most metal cutting processes when machining difficult-to-cut materials. End-milling involves a linear, or multiple-axis feeding motion of a spinning multi-edged cutting tool. Milling operations tend to be an efficient way of removing excess material from a previously fabricated part, or by machining from wrought material [2]. Major geometrical parameters such as helix angle, radial rake angle and radial clearance angles (in this case, radial primary clearance and radial secondary clearance angles) are critical factors when investigating the tool geometry of end-mills. The combination of these factors determines the cutting edge's wedge angle; this greatly influences the strength of the cutting tool [2]. A nomenclature of the geometrical factors on an end-mill is shown in more detail in Fig. 10.

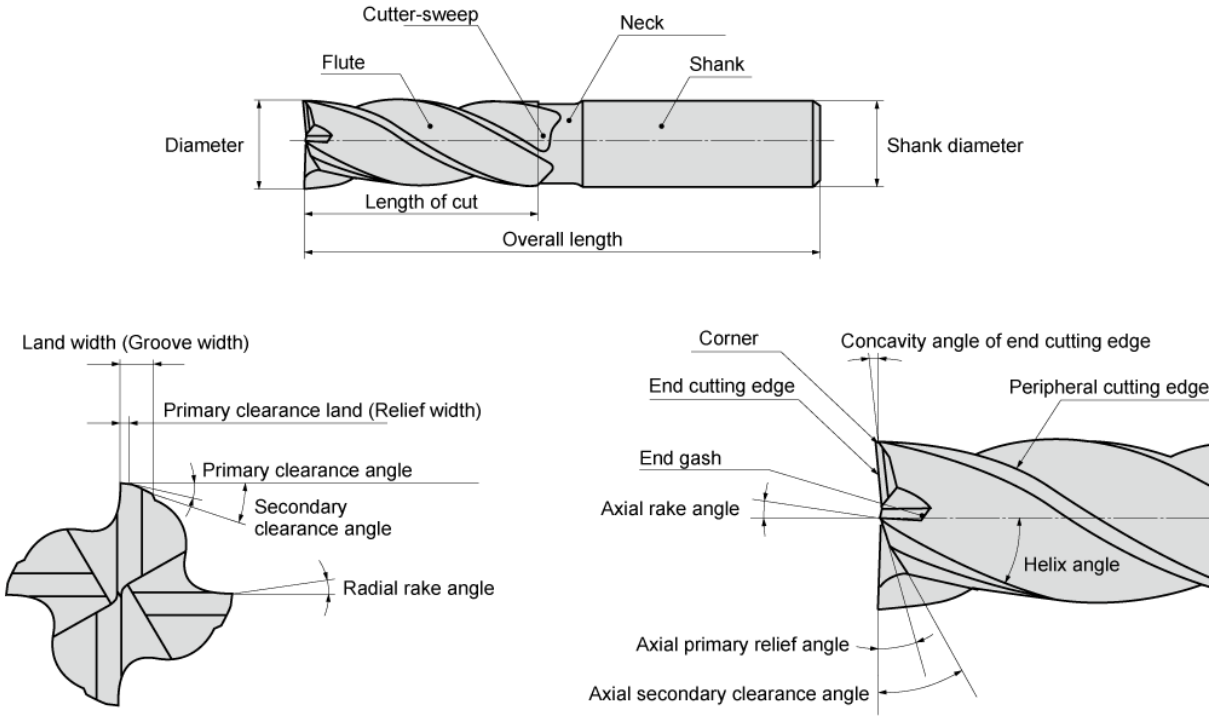

Fig. 10: Nomenclature of end-mill geometry [54]

The design of end-mills is a complicated process. As shown in Fig. 4 and Fig. 5 there are various designs of end-mills with different end profiles. The reason behind the various types of end-mills is mainly due to the operational need in the machining process, roughing or finishing. The milling operations is used to form slots, keyways, pockets, provide better finish and so on

[31]. Fig. 11 provides an overview of the availability of numerous end-mill designs for various machining operations. Several factors such as amount of material removed in a cut, quality of cut, surface finish and wear on the tool should be considered during tool design [31]. Due to multi-tooth interrupted chipping, non-uniform chip loading and the variation of the cutting force direction, the behaviour of the milling process is extraordinarily complex, thus difficult to model.

The workpiece material should also be considered when designing end-mills. For example, in the case of aluminium alloy 6082-T6, end-mills are designed with sharp rake angles and usually do not exceed more than three flutes. This design, for this material, gives better chip evacuation in machining of aluminium alloys due to the size of the chips removed [20]. Increasing the number of flutes in end-mills makes the cutting tool rigid and in return reduces vibrations; it also reduces the available flute space for the evacuation of chips [29,54]. In the case of more difficult-to-cut materials, such as Nickel based alloy Inconel 718 where it is more challenging to remove material, rigidity is of priority over chip evacuation (Fig. 12)

Fig. 11: Different solid WC-Co end-mill designs (courtesy of Scorpion Tooling UK ltd.)

In drilling, the primary function of the helix angle is the evacuation of chips and common perception is that the same principle applies to end-mills. However, this is not the case as the drill is removing material axially. In end-mills, depending on the depth-of-cut (DoC), the helix angle is usually engaged with the workpiece material and removing material axially and radially. According to Astakhov [31] the helix angle of end-mills intended to machine medium carbon steels is 35° while it is higher for machining difficult-to-cut materials.

A helix angle of 30° is considered to be a general-purpose geometry for many applications and standard end-mills because of its acceptable combination of strength, chip removal capacity, balanced cutting forces and versatility. However, an increase in spindle rigidities and rotational

capacity as well as torque has caused a trend to higher helix angles. High helix angles tend to provide a smoother and more efficient entrance to the cut, while lowering the radial forces and tool deflection by transferring stresses vertically. High helix angles, however, also introduce a rapid rise in loading at the tool-workpiece interface; they require shallower cutting depths and they possess less tooth edge integrity [55]. Hricova et al. [21] investigated the influence of tool geometry, mainly focusing on helix angle, and machine parameters in high speed milling of aluminium alloy 6060 in dry and flood conditions. Hricova et al. [21] demonstrated that the effect of helix angle in high speed milling is critical and affects the surface roughness of the finished part. The study also discovered that higher cutting speed reduced the surface roughness in machining alloy 6060. The same principle applies in tool geometry optimisation for end-mills designed for difficult-to-cut materials. The influence of rake angle and the relief angle on the tool life is also another critical factor in end-mill geometry [56].

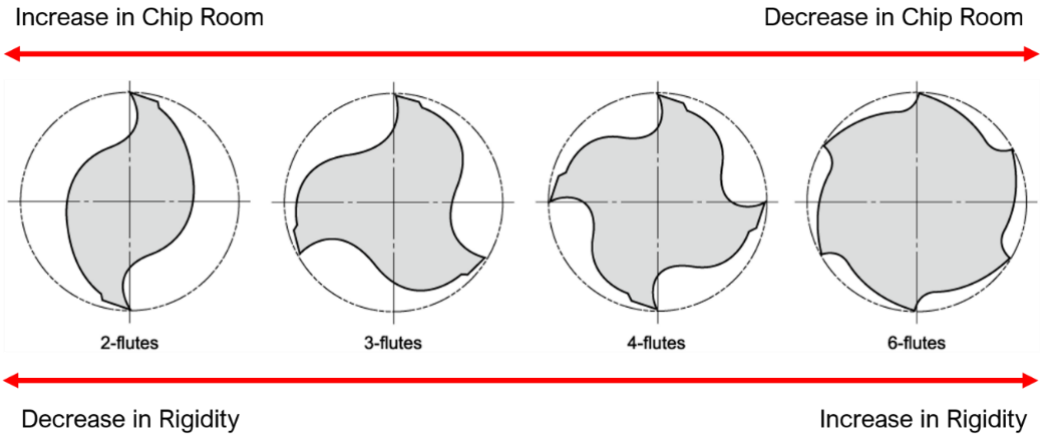

Fig. 12: Representation of different end-mill designs with increasing cutting edges [29,54]

It was found that optimising the tool geometry can lead to improved tool life [57]. Li et al. [57] conducted finite element analysis (FEA) and produced various three-dimensional (3D) solid carbide end-mills with different tool geometries simulating milling of Ti-6Al-4V. The optimum design was later applied to their hypothesis to see whether the optimum tool geometry leads to improved cutting tool performance. A high-speed milling experiment using an ultra-fine substrate of WC-Co for machining titanium alloy Ti-6Al-4V was carried out [58]. The optimised cutting tool from the simulation exhibited longer tool life and produced more refined chips [58]. In a different milling study, Huang et al. [59] analysed the effect of variable pitch and unequal helix in end-milling of Ti-6Al-4V to assess and verify the vibration reduction in machining. Huang et al. [59] designed three end-mills with variable pitch, combination of variable pitch and unequal helix and end-mill with neither methods. They concluded that the energy distribution of variable pitch is more intense, and the amplitude of the cutting force is smaller to standard end-mill design and therefore reduces machining vibration. Chattering and vibration directly affects productivity and surface finish but can be improved with the use of variable pitch and unequal helix on end-mills [60–62]. The design of the end-mill along with the

correct tool material and tool geometry could, theoretically, increase the tool life and the productivity of the cutting tool.

Pleta et al. [51,63] investigated trochoidal milling and conventional end-milling in Inconel 738 using insert tooling to further enhance the tool life by analysing the resultant force, tool wear and surface roughness as output parameters. It was concluded that the efficiency of trochoidal milling was slightly less than conventional end-milling but the productivity in trochoidal milling was far superior. By factoring tool change and cycle time, the overall efficiency of trochoidal milling surpassed standard end-milling technique. In another study by Liao et al. [30] the slot milling and side milling of Inconel 718 was carried out using uncoated cemented tungsten carbide end-mills. Limited information regarding tool geometry was provided by the author, mentioning helix angle of 45° on the end-mills. It was also mentioned that flank wear was the most dominant form of tool wear across the experiments. The authors did not provide further discussion on cutting tool geometry. There are insufficient studies in the end-milling of Inconel 718 using WC-Co end-mills. Furthermore, investigations into tool geometry is very limited due to cost factors and time. The same can be applied for super-duplex 2507 in end-milling [64].

3.1.4 Tool Life and Prediction

Tool life is a critical factor in machining. It determines cost and productivity of operations for engineering applications and cannot be ignored. Yen et al. [65] states that tool wear has a great influence on the economics of machine operations. The cost of cutting tools varies from industry to industry and depends on the complexity of the product or components. Davim [66] describes that the tool cost in an advanced powertrain plant is around 12-15% due to the complexity and the high cost of manufacturing. Whereas for a simpler automotive plant, dealing with mainly turning and milling the cost of tooling is around 5-7%. In the aerospace sector the cost of tooling is significantly higher. However, modelling tool life is very challenging, and for years, researchers have been developing new mathematical models to help manufacturers predict the life of cutting tools more accurately [67–69]. Predicting the life of a cutting tool precisely can help manufacturers estimate their costs more confidently, allowing engineers to focus on other inefficiencies. On average 10% of the finished product cost is attributed to cutting tools. The use of incorrect cutting tools in machining of difficult-to-cut materials introduces unpredictable tool life and performance. This, in combination with high stresses and cutting forces, accelerates tool wear and drastically increases the costs. Though not related to tool wear, machining with the incorrect cutting tool results in higher machine power consumption and can lead to major consequences on the quality of the machined part. If the quality of the machined parts reduces, more work is needed to rectify the problem or in some cases the part is scrapped altogether.

In the early 1900s F.W. Taylor [70] proposed an equation (Eqn. 1, Table 1) to predict the tool life. Taylor [70] gathered data on different tool materials such as carbon tool steels and early

high speed steels developed by Robert Forester Mushet owner of Mushet steels in 1868. Taylor conducted an extensive investigation which lasted 26 years trying to determine the suitable cutting speed, feed rate, for machining a certain material. His pioneering work led to the start of many investigations in materials engineering, tribology, etc. Kattan and Currie [71] contributed by adding that the research in cutting tools and metal cutting has expanded in scope and complexity since the introduction of Taylor's first equation. Since then, notable contributions by Merchant [72], Zorev [73] and Colding [69] in the art of metal cutting have been recorded. Merchant [72] carried out research analysing the metal cutting process in terms of geometry and strain-stress conditions. Merchant is known for providing the oversimplified orthogonal force model known as Merchant's force circle diagram, or defined by Davim [66] as a condensed force diagram. Zorev [73] provided a detailed analysis of the chip formation by the peripheral edge. According to Davim [66], Zorev [73] studied the velocity hodograph, associated plastic deformation and flows in the region (cutting zone) to provide a visualisation of the chip formation. Colding [69] discovered a relationship between specific energy and tool life and surface finish based on a novel shear angle relationship as a function of tool life. Colding's [74] tool life model also provides good validity in machining applications such as turning and drilling based on the study carried out by Hägglund [75]. Other studies related to tool life by Johansson et al. [76] show that with the right conditions, the cutting speed (v_c), can be predicted to less than 1% error for a given tool life when using Colding's equation. Johansson et al. [67] go further and apply Colding's equation for varying tool coatings.

Astakhov [31] mentions that this formula, although widely used is the main focus of major studies in metal cutting, does not suggest that tool geometry affects tool life. According to Marksberry and Jawahir [77] the constants n and C_1 apply to a particular cutting tool and workpiece combination. Marksberry and Jawahir [77] explain that the constants are determined by performing experiments. Therefore, it is not feasible to use Taylor's equation for tool life prediction.

Predicting tool life accurately is challenging because of the different variables in every operation. Hägglund [75] verified Colding's formula and illustrated its applicability in a wide range of different conditions. Johansson et al. [67] mention similar findings. Different engineering materials have different characteristics and behave differently when machined. General tools are not enough, especially when difficult-to-cut materials are involved. Predicting the tool life without sufficient knowledge leads to poor estimations and increased machining costs. Tool geometry is an important aspect of tool life and needs to be studied in more detail and broken down to be included in a new model for tool life prediction.

Table 1: Summary of tool wear and tool life models in machining

No.	Tool Life Equation	Details
1.	$VL^n = C_1$	In the early 1900s F.W. Taylor [70] proposed an equation (Eqn. 1) to predict the tool life of cutting tools Taylor [70] gathered data on different tool materials such as carbon tool steels and early high speed steels developed by Robert Forester Mushet owner of Mushet steels in 1868. Taylor conducted an extensive investigation which lasted 26 years trying to determine the suitable cutting speed, feed rate, for machining a certain material. Where L is the tool life in minutes, cutting speed, V (m/min), or in other cases (v_c) and constants n and C_1 [70,77,78].
2.	$L = \frac{C_2}{(V^P f^q d^r)}$	Researchers such as Hoffman [79], Lau et al. [80], Venkatesh [81] and Wang and Wysk [82] have developed Taylor's tool life equation further by adding factors that provide a more accurate prediction. Hoffman [79] extended Taylor's equation by adding two important factors. The first is the depth of cut (d) and the second, feed rate (f). Equation 2 shows Taylor's extended equation with the added factors. All constants ($C_2, P, q\ and\ r$) are determined experimentally. However, more tool life testing is needed.
3.	$TL^n = C_3$	Another model representing the tool life based on the temperature was later proposed by Oxley [83] and Quinto [84]. They describe the equation as temperature (T) based and dependant. Marksberry and Jawahir [77] mention the equation is set only on an empirical basis. The equation does not seem convenient enough to be used on a shop floor environment where operations are dependent on cutting speed, depth of cut and feed rate. Trying to measure the temperature

		of the cut is complicated in a manufacturing environment where emulsion is used to cool the tool and workpiece. It is also mentioned that constant (n) is between the values 0.01 and 0.1 with (C_3) being determined through experiments.
4.	$C_1 \propto \left[(\cot\beta - \tan\alpha)\theta(\alpha,\beta)^{\frac{1}{\varepsilon}}\right]^{-1}$	Lau et al. [80] investigated the relationship between tool geometry and Taylor's constant (C_1). The study provided relationship between tool life, rake and clearance angles but seems too complicated. Lau et al. [80] attempted to relate the cutting tool geometry to Taylor's constant analytically. Equation 4 shows the mathematical formula proposed by Lau at al. [80]. Marksberry and Jawahir [77] mention that the influence of rake angle (α) and clearance angle (β) can be theoretically determined, influenced by Taylor's constant. Lau et al. [80] explains that the θ (α,β) is a suitable function of α and β. Lau et al. [80] explains that (ε) is the index of cutting speed (V) at the mean temperature.
5.	$V = \frac{C_4}{L^m f^q d^q (BHN/_{200})^r}$	Wang and Wysk [82] and Hoffman [79] provide an alternative to Taylor's extended equation by including and accounting for the workpiece hardness. The equation is an extension of equation 2 with the added tool geometry factors. Constants (m,p,q,r,C_4) in equation 5 are all determined through experiments. Yen et al. [65] analysing tool wear through finite element analysis (FEA) indicates the workpiece hardness in Taylor's extended equation as BHN (Brinell scale).
6.	$k + y + bx + cx^2 + dz + hxz = 0$ $k + y + bx + dz = 0$	Although Taylor's equation gave an indication of how to obtain tool life, it is not that accurate. Colding [68,74] noticed that Taylor's equation (Eqn. 1) is used for a wide range of machining data. Therefore, the accuracy of the tool life estimate is

		poor. Colding [74] proposed polynomial relationship containing nine constants to increase the accuracy of tool life prediction. Colding [85] presented a new formula with 5 constants in 1981. Johansson et al. [67] tested Colding's equation for its accuracy in turning of stainless steel 304 concluding that the tool life equation is a well-functioning model. However, it was also mentioned that a disadvantage of Colding's tool life model is that it requires five separate trials, Colding [85,86] represents x as the theoretical chip thickness, y as the cutting speed, and z as the tool life. They are all presented in a logarithm format or a log-log scale. Constants are represented in the form of b, c, d, h, k in the model. Where $x = \ln h_e$, $x = \ln v_c$, and $x = \ln L$
7.	$v_c = e^{\left[K\frac{(\ln(h_e)-H)^2}{4.M}-(N_0-L.\ln(h_e).\ln(T_L))\right]}$	Colding's equation can be represented in a parabolic form, Equation 7. According to Johansson et al. [67] for a specific cutting tool and workpiece the equation describes the relationship between tool life (T_L) of the cutting tool, cutting speed (v_c) and the equivalent chip thickness and constants K, M, N_0 and L. Colding [86] mentions that the equation is based on curve fitting and adjusting on measurement points [67].

3.1.5 Surface Roughness and Quality

Surface roughness is one of the major parameters in determining the quality of a machined surface in machining. Surface roughness is a result of a machined surface based on the movement provided by the machine tool [7]. One factor which contributes to surface roughness is the occurrence of BUE, which over time, increases the roughness of the surface produced. Some geometric factors which affect achieved surface finish in milling and drilling operations include, nose radius, rake angle, relief angle, cutting edge angle, and cutting-edge sharpness and concentricity of the tool [7]. Designing and fabricating high-quality and wear-resistance with low chemical affinity, cutting tools is the first step for high quality machining.

The quality of a machined surface on a difficult-to-cut material is determined by the quality of the cutting tool but also the machine parameters [7,31]. Vibrations in workpiece, cutting tools and machine set-up are other factors contributing to poor surface finish of the workpiece. Sun and Guo [87] investigated the surface integrity by end-milling Ti-6Al-4V using a 12.7 mm, 4-flute solid carbide end-mill with TiAlN coating. They evaluated different cutting parameters and concluded that the increase in feed and radial depth of cut (a_e) causes an increase in surface roughness. Ramesh et al. [88], in a different study, analysing the surface roughness of titanium alloy Ti-6Al-4V also established cutting parameters to be the significant cause of rougher surface finish.

3.2 Chip Formation of Difficult-to-cut Materials

It is crucial to understand the physical mechanisms governing chip formation in difficult-to-cut materials, due to the impact that cut chips can have on stability and the quality of the workpiece [31,89]. The chip formation, as well as relying on machining parameters, also depends on material properties such as metallurgical and thermophysical properties [48,90,91]. In milling and drilling operations of difficult-to-cut materials the shape and size of chips are enormously variable and dependent upon factors such as workpiece material, cutting speeds, tool geometry and cutting temperatures.

Severe plastic deformation occurs during machining with WC-Co cutting tools when the cutting edge is engaged with the workpiece causing discontinuous (segmented) chips to form on the rake face as explained by Odelros [92]. There are two main reasons for chip formation:

1. When the cutting edge is engaged with the workpiece, it causes cracks to grow from the outer surface of the chip. Therefore, producing discontinuous chips as the tool travel through the material [6,93,94].
2. Komanduri et al. and [90] Barry et al. [95] describe that adiabatic shear formation, which is the result of localised shear deformation caused mainly by the thermal softening over strain hardening is the cause of chip formation. A brief step-by-step chip formation as explained by [91,96] has been provided in Fig. 13.

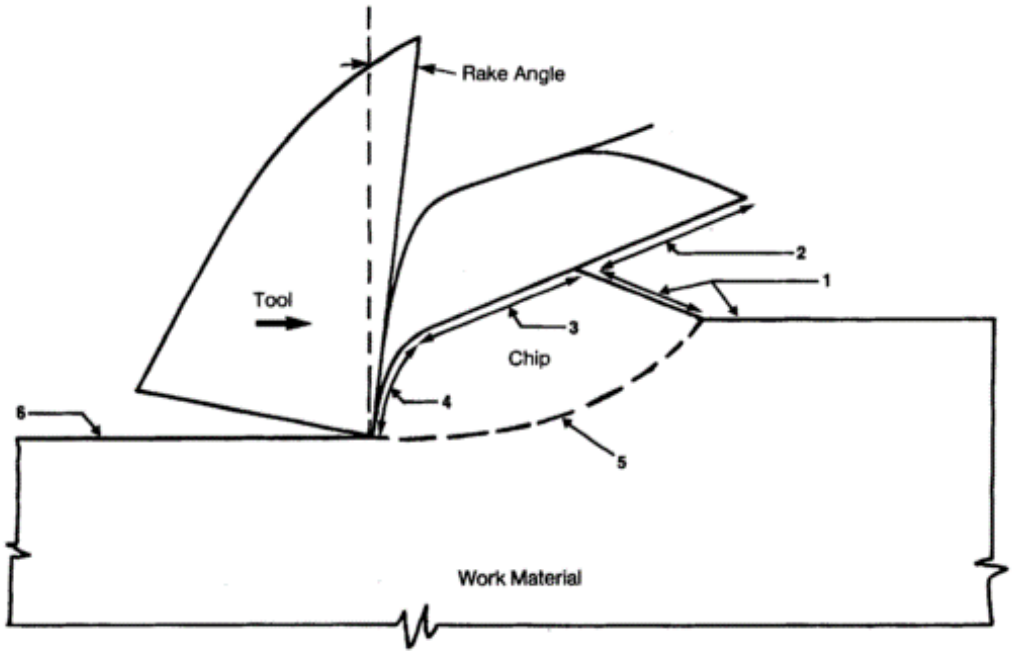

1. Undeformed surfaces
2. Part of the catastrophically shear failed surface separated from the following segment due tointense shear
3. Intense shear band formed due to catastrophic shear during upsetting stage of the segment being formed
4. Intensely sheared surface of a segment in contact with the tool and subsequent sliding on the tool face
5. Intense localized deformation in the primary shear zone
6. Machined surface

Fig. 13: Schematic leading to shear-localised chip formation, with sequence of events [91,96]

In CNC machining, the size, shape, and thickness of chips formed reflects the difficulty in material removal. Davim [6] and Shivpuri et al. [97] state that chips are strongly influenced by the microstructural state of the alloy. Two key chip types are the continuous and discontinuous chips [98,99]. This, again, is dependent upon factors such as workpiece material, cutting speeds, tool geometry, ductility of workpiece material and cutting temperatures. In drilling operations there are two main chip shapes formed; segmented spiral cone and serrated ribbon chips. Sandvik Coromant, a leading manufacturer of cutting tools, describes the ideal chip to be helical, segmented and discontinuous (Fig. 14). Long continuous chips can become tangled around the tool and its holder causing damage to the tool. Drilling operations will be smooth and without problems if chips are well broken [99]. The same can be applied to milling tools.

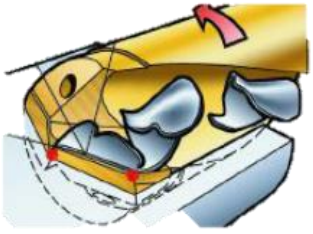

Fig. 14: Ideal chip formation in drilling operations [100]

Consider chip formation in drills. As the drill penetrates the workpiece material, the initial chips formed are always serrated and ribbon like (Fig. 15). As the depth of drilling increases the ribbon chips are transformed into segmented and broken chips. Segmented chips continue to form until the depth of drilling is reached (Fig. 16). The flute of the drill assists with the extraction of the segmented chips during drilling and the use of spindle through coolant (at high pressures) ejects the formed chips in the opposite direction of travel by the drill and out of the drill. This transition from ribbon to segmented chips is swift and occurs at the beginning of the drilling operation. As the drilling depth increases, it becomes very challenging to maintain chip control and the possibility of tool failure becomes more likely [99]. As mentioned before, in this study the author has focused all efforts onto short hole drilling as there were limitations in conducting deep hole drilling studies.

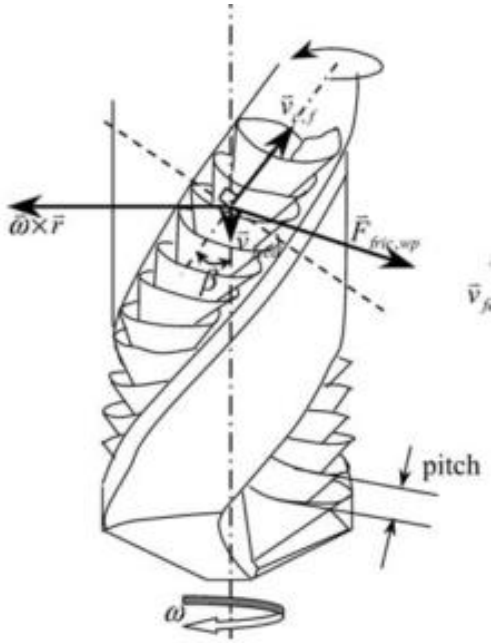

Fig. 15: Serrated ribbon chip formation in drilling [99]

An investigation by Akhavan Farid et al. [101] in the drilling of Al-Si alloys found that the formation of BUE tends to deform cut chips due to unpredictable and uneven chip flow. Therefore, deformed chips tend to adhere to flutes as a result of high tool-chip interface and increase in friction. Similar conclusions have been reported in studies by Kelly and Cotterell [18] as well as Braga et al. [19] who observed BUE formation and tool failure through chip clogging. Furthermore, if the incorrect conditions in drilling of difficult-to-cut materials are used then compressed string like deformed chips are obtained and can cause damage to the cutting tool as well as the workpiece material. An example of this can be observed in Fig. 17 where Álvarez et al. [102] was investigating the build-up of titanium-oxide (TiO) growth, onto the rake face of the drills when drilling Ti-6Al-4V. They reported that the cause of this was due to the workpiece material adhering onto the rake face and obstructing the smooth flow of cut chips. The cause of the rough surface brought problems such as string like compressed chips to wrap

around the cutting tool. This could lead to catastrophic failure of the drill and damage to the workpiece material.

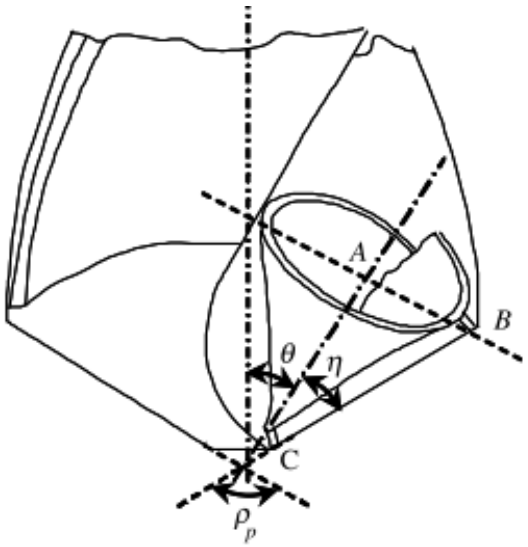

Fig. 16: Segmented chip formation in drilling [99]

An immense amount of strain occurs at the tool-chip interface in a short time and as such, materials cannot withstand this strain without fracture, causing segmented chips. Aluminium and its alloys are well known to produce continuous chips during metal removal [103]. Contrary to this, the investigation completed by Brown et al. [104] found that serrated segmented chips are produced in the machining of age hardened aluminium alloys. Muller et al. [103] confirmed this in 2001 when they produced saw-tooth and fully segmented chips in the machining of age hardened aluminium 7075 alloy. A range of typical chip shapes, including continuous, discontinuous and segmented are shown for ductile metals and alloys (Fig. 18).

Fig. 17: An example of compressed string like chips obstructing drill flutes in machining titanium alloy caused by the accumulation of Ti-6Al-4V in the flutes [102]

Fig. 18: Variation in chip shape for ductile metals and alloys [105]

Segmented and continuous chips are also experienced in milling operations of difficult-to-cut materials and are mainly influenced by tool geometry and machine parameters. For example, in milling of titanium, chips tend to be segmented and thin [2]. Two major chip formations are encountered when machining difficult-to-cut alloys. The first form being segmented chips and the second continuous chips. Continuous chips in machining of titanium alloy occur at lower speeds whereas segmented or shear-localised chips are formed at machining speeds, 50-80 m/min [106–109]. However, serrated chips on these two types of chip formation can be observed when machining titanium alloys for example. According to Shokrani et al. [14] serrated or saw-toothed are produced in the machining of titanium alloys due to the localised adiabatic shear bending at the primary shear zone where the workpiece material experiences an intense shear rate. This is mainly caused by the shear strength of titanium alloys and the temperature between the tool and chip at the tool-chip interface. The formation of serrated chips in machining of difficult-to-cut materials could result in machining instability, fluctuations in force and chattering which can cause chipping on the cutting edge when in contact with the workpiece material [48,106,110–112]. Chip formation was studied by Liao et al. [30] in end milling of Inconel 718 using cemented WC-Co under various cutting speeds and machining strategies such as slot and side milling. According to [30] Inconel 718 chips, at a lower speed of 22.6 m/min, were segmented but became continuous chips when cutting speed was increased to 90.5 m/min as shown in Fig. 19. Liao et al. [30] concluded by explaining that the increase in cutting speed is related closely to cutting force and tool wear/failure in slot milling of Inconel 718. It was also concluded that the feed was insignificant in their study. The same

effects in drilling such as accumulation of workpiece material on the rake face, BUE, chipping and variation in chip formation can occur in milling of difficult-to-cut alloys but they are dependent on several factors that the author discussed earlier when explaining chip formation.

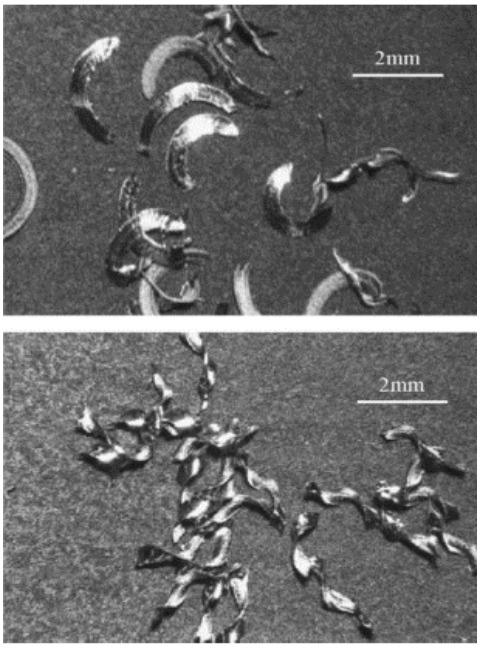

Fig. 19: Segmented and continuous chips obtained in slot milling of Inconel 718 [30]

3.3 Tool Materials

According to Davim [66] wear resistance is the least understood characteristic of a cutting tool which is defined as the *"attainment of acceptable tool life before tools require replacement"*. Since difficult-to-cut materials exhibit poor machinability in milling and drilling processes, the tool materials required to withstand the extreme machining conditions, should have the following characteristics [14,110,113]:

- High hot hardness
- High Strength and toughness
- High Chemical and thermal stability
- High Thermal shock resistance
- High thermal conductivity
- Low chemical affinity

The ability to maintain hardness at elevated temperatures or hot hardness, is a critical factor in machining difficult-to-cut materials, because of the occurrence of very high temperatures at the cutting zone [6,66]. Greater fracture toughness is required in a tool material to withstand shock load, chipping, vibration, runouts etc. Chemical reactivity between the cutting tool and the workpiece material should be kept to a minimum to minimise welding or fusing of workpiece material to the tool material surface at high temperatures in the cutting zone [14,113]. The right balance of hardness and toughness in tool material is dependent upon the workpiece material and should be considered in production planning. The ability to maintain hardness at elevated temperatures is called hot hardness [6,66]. The tool material should be able to maintain its integrity at high temperatures and not soften, since difficult-to-cut materials have a low thermal conductivity and therefore high thermal conductivity of a tool material is also important. Titanium alloy Ti-6Al-4V and nickel-based alloy Inconel 718 for example have low thermal conductivity of 6.6 W/mk and 11.4 W/mk, respectively. This means that the temperature at the cutting zone will be mostly transferred onto the tool material, causing the tool material to soften and rapidly wear [46]. Temperatures as high as 900 °C have been recorded in Inconel 718 at cutting speed of 30 m/min; even higher temperatures in the region of 1300 °C when machining at 300 m/min [114]. A review on the machining of nickel-based alloys shows that cemented tungsten carbide tends to soften at around 1100 °C, [4,115] leading to mechanical and thermal fatigue within the tool material. High strength and hardness, in combination with wear mechanisms such as diffusion, attrition and abrasion, increases the tool wear rate and can even cause premature failure [48].

In depth review of cutting tool materials has led the author to cemented tungsten carbide tools, as their properties and price meet the criteria for machining difficult-to-cut alloys. Cemented tungsten carbide (WC-Co) also known as solid carbide is one of the tool materials commonly

selected when machining difficult-to-cut materials [4,6,106,110]. The right balance of hardness and toughness as well as the grain size and structure of the WC-Co are three factors in increasing tool life of the cutting tool. In most machining operations tungsten carbide is the desired tool material [6]. Carbide tools comprise a high modulus of elasticity, high thermal conductivity, and high hardness over a range of temperatures. They are extremely effective at removing material and are desirable to carry out metal removal in various different machining operations. The use of carbide tools allows for higher cutting speeds, three to five times higher than that of HSS (Fig. 20) [116]. Fig. 20 illustrates the effect of temperature on hardness of various tool materials. High speed steel (HSS), carbon tool steels, carbides, ceramics and polycrystalline diamond (PCD) tools, are amongst some of the tool materials available.

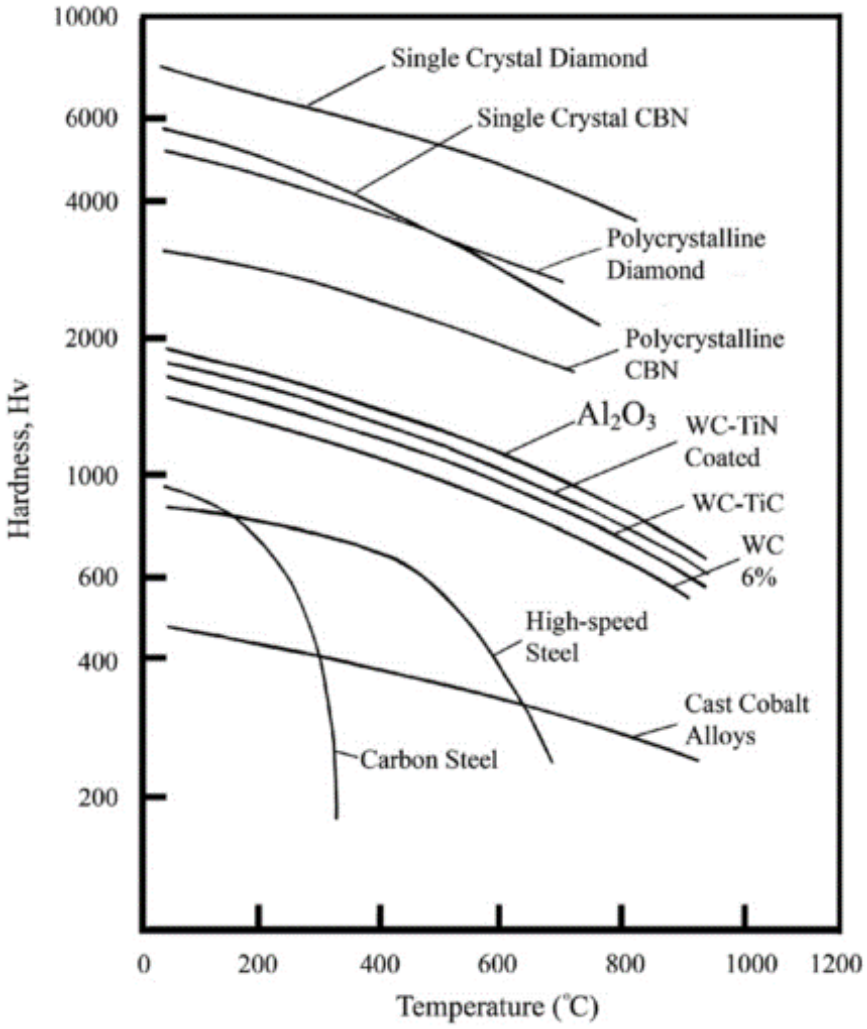

Fig. 20: Hardness of tool materials vs. temperature [117]

Ezugwu [4], Ezugwu and Wang [106] state that cemented solid tungsten carbide tools maintain their superiority in all machining processes involving difficult-to-cut materials. Table 2 shows the softening point temperature of commercially available tool materials used for machining difficult-to-cut materials while Fig. 21, illustrates the effective range of hardness and toughness of various current tool materials. WC-Co can withstand higher temperatures and are still able

to retain good toughness. Note that WC-Co, when coated, covers a wider range of hardness and toughness when compared to high speed steel (HSS) and ceramics.

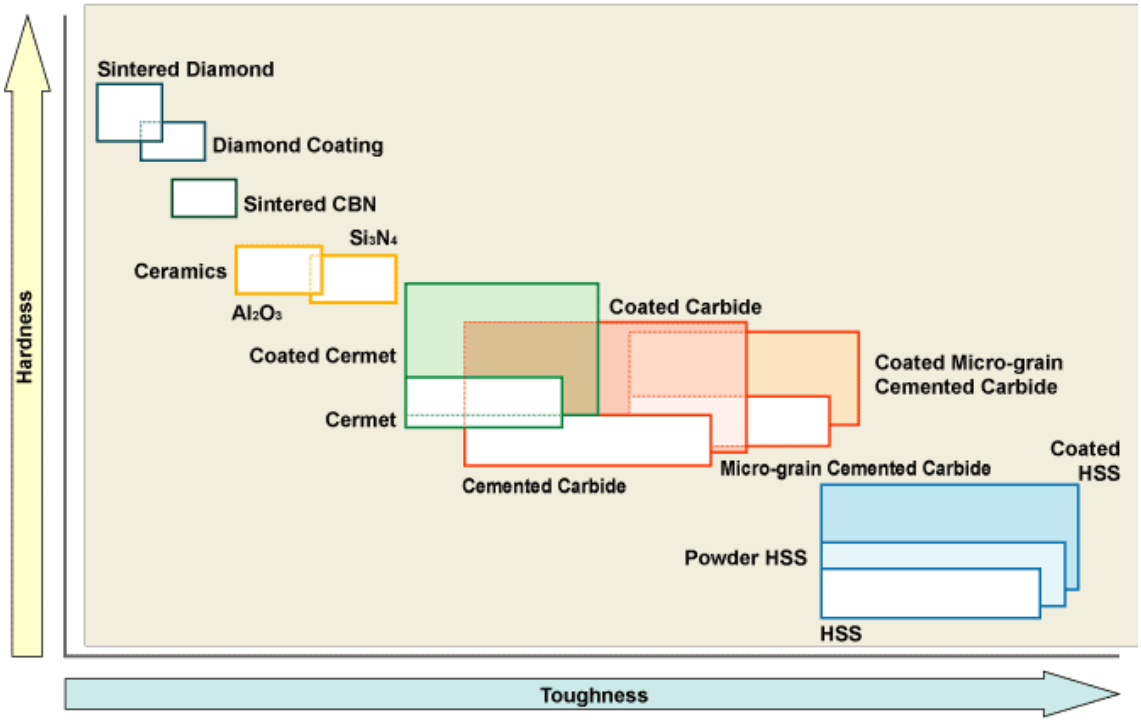

Fig. 21: Hardness versus toughness for some conventional cutting tool materials. [2]

Table 2: Softening points of tool materials [4,115]

Tool Materials	Softening Temperature (°C)
High speed steel (HSS)	600
Cemented carbide (WC)	1100
Aluminium oxide (Al_2O_2)	1400
Cubic boron nitride (CBN)	1500
Diamond	1500

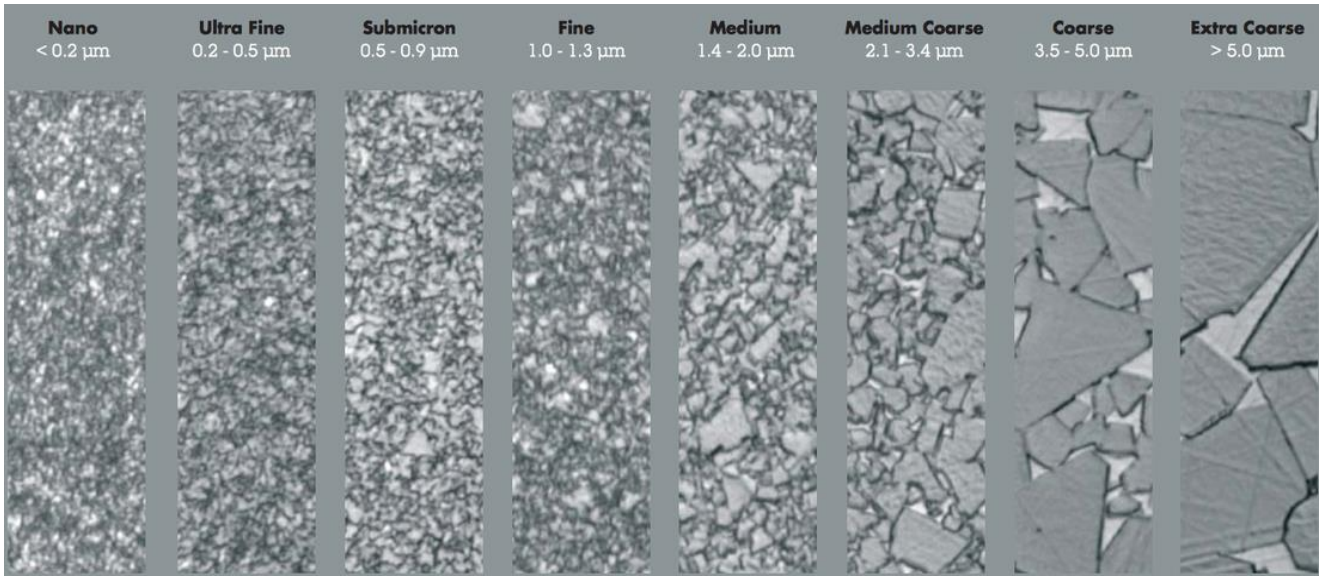

Fig. 22: Variation in grain size in WC-Co [118]

The material composition of WC-Co consists of a binder element, cobalt (Co), and tungsten carbide (WC) along with additives such as titanium carbide (TiC), tantalum carbide (TaC) and niobium carbide (NbC), etc. The additives assist with the modification to the properties of the WC-Co. The grain structure and the amount of Co (wt.%) also contribute to the changes in material properties. If the amount of Co is increased, then the toughness of the cutting tool increases. However, Odelros [92] points out that reduced amount of Co causes an increase in hardness and a decrease in toughness and strength. The composition and grain structure of solid WC-Co can be altered by changing the grain size and the amount of metal binding material (Cobalt, Co). Their grain size structure ranges from 0.2 μm (Nano grain size) up to 5 μm (Extra-Coarse) Fig. 22. However, in cutting tools the range is mainly from 0.2 μm-~1.4 μm.

3.4 Coating Technology

Further enhancement to cutting tools can be attained by high performance coating technology in milling and drilling. Around 85% of all cemented carbide tools are now coated [119]. The purpose of coatings and the development of coatings has been targeted on wear protection, against abrasion and adhesion. However, Bobzin [119] states that the most important requirement for cutting tool coatings, is to provide protection against oxidation and to minimise diffusion between the workpiece and tool material. Various coatings such as TiN, TiAlN, TiC, and TiSiN with high hardness and low friction are used to reduce the high temperatures at the cutting zone and provide adequate protection from diffusion between the cutting tool and difficult-to-cut material. Coating technology has been developing since the introduction of first chemical vapour deposition (CVD), TiC coating in 1969, with later development in the 1980s and use of physical vapour deposition (PVD) to produce newer coatings such TiAlN in the 1980s and AlCrN in 2003 [119]. With the introduction of nanostructured PVD coatings in 2005, newer coatings such as TiSiN, TiAlSiN and CrAlSiN have now been introduced to the cutting tool market.

Revankar et al. [120] indicates that reducing the coefficient of friction enhances the tribological effect and therefore reduces adhesion wear. Coatings are mainly used as a mean of increasing the tool life, by increasing the cutting tools' hardness, reducing adhesion and delaying heat build-up between the tool and the workpiece [119,121]. Ginting and Nouari [122] also examined cutting parameters using chemical vapour deposition (CVD) on coated carbide tools and concluded that cutting conditions as well as flank wear on the cutting tool affect the surface integrity of the titanium alloy workpiece. Jawaid et al. [123] compared the effects of inserts coated with CVD against PVD coated tools and found that CVD coating TiCN+Al_2O_3 coating improved the surface roughness more than PVD-TiN coating. Another study by Uddin et al. [124] showed that PVD-TiAlN produces a better surface finish, 31% lower, when compared to an uncoated tool. Jawaid et al. [123] evaluated the effect of coating in the milling of Ti-6Al-4V comparing TiN coating against TiCN+Al_2O_3 coating and concluded that TiCN+Al_2O_3 coating on the cutting tool can extend the tool life to a certain extent. Uddin et al. [124] investigated the effect of coated and uncoated cutting tools in milling of Ti-6Al-4V. The results showed that coating can improve tool life and surface roughness when compared to an uncoated end-mill. The experiments showed that the end-mill with TiAlN coating exhibited improved tool life with approximately 44% lower flank wear when compared to the uncoated tool. In addition, 31% lower surface finish was achieved using coated tools. Polini and Turchetta [10] investigated the performance of TiAl and TiAlN coating in milling of Ti-6Al-4V at 38 m/min, 63 m/min and 88 m/min at various cutting depths of 5 mm, 10 mm, 15 mm and 20 mm. The study later concluded that the TiAlN coating exhibited better tool life at lower and higher cutting speeds

when compared to TiAl coating for example. Flank wear was also measured at intervals with TiAlN showing less wear.

New advancements in PVD coating and innovative methods in applying these coatings at nanometric level has provided a new set of coatings, attracting great interest in industrial applications [11]. Applying coatings such as TiAlN, TiSiN and TiVN provides superior high hardness, wear resistance and tribological performance to various applications, WC-Co cutting tools included. These new coatings have been under development to reduce the built-up material on the cutting edges and to reduce the formation of crater wear. Chang *et al.* [11] investigated the microstructure characterisation of TiVN, TiSiN multi-layered TiVN/TiSiN coatings and whether their applications could improve wear resistance further. The study concluded that multi-layered coatings such as TiVN/TiSiN can increase wear resistance in machining of 7000 series aluminium alloys.

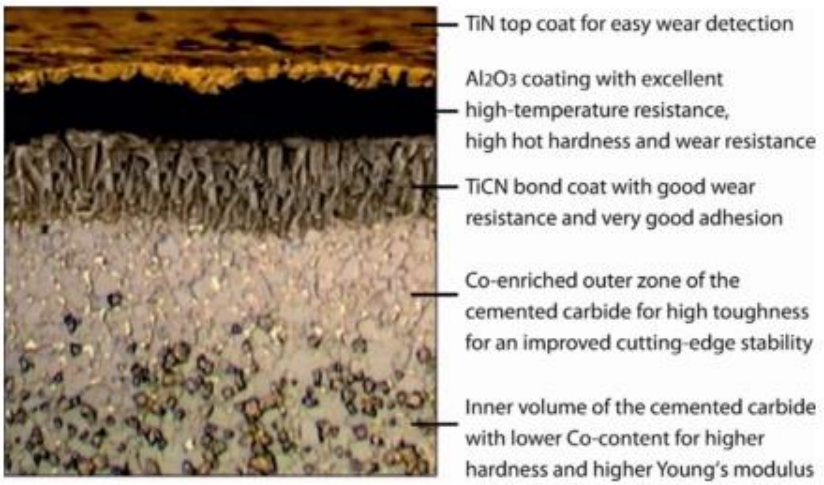

Fig. 23: Multilayer composite of an Al2O3-coated indexable insert made of graded cemented carbide, Sandvik Coromant [119]

3.5 Difficult-to-Cut Materials (Benefits and Disadvantages)

Titanium alloys are also classified as difficult-to-cut and are the preferred choice of material in the aerospace, chemical, medical and sports industries due to their mechanical and excellent corrosion resistance properties. Titanium's high specific strength-to-weight ratio is extremely valuable across many engineering applications [5,6,92,125]. The density of titanium is only about 60% of that of steel or nickel-based super alloys. Yet, the cost of titanium is four times higher than stainless steel and not very cost effective in some cases [125]. Its benefits however do not prevent its regular use in numerous industries from aerospace to consumer goods. Ribeiro et al. [126] identified that 75% of the global consumption of titanium alloys is within the aerospace industry. Titanium alloys, such as Ti-6Al-4V, are able to endure high temperatures in extreme conditions and not deform under high pressures. Inagaki et al. [127] gives an example in their assessment of application and features of titanium for the aerospace industry and states that Ti-6Al-4V is used as fan blades, fan case and the intake section of jet engines where temperatures of around 300-400 °C can be reached. Peters [5], Donachie [125] and Ezugwu [106] describe that nearly all commercially used titanium alloys operate around or below 538 °C. In the medical sector, titanium alloys are one of the prime choices for prosthetic devices and other biological materials due to their mechanical properties, resistance to corrosion as well as biocompatibility [26]. According to Cui et al. [26] the low modulus of elasticity of titanium alloys is a biomechanical advantage. It can result in smaller stress shielding in artificial hip joints for example.

The problems associated with machining titanium alloys include poor thermal conductivity, high machining costs and tendency to maintain its hardness and material strength at high and low temperatures; these are some of the contributors to cutting tool failures and poor surface finish. An example of such material can be found in alpha-beta titanium alloy Ti-6Al-4V. Low thermal conductivity of titanium is a major issue in machining of the alloy [6]. This phenomenon gives rise to high pressures at the tool-chip interface and increases plastic instability resulting in localised adiabatic shear bands, [90] and tool wear by thermal fatigue and diffusion [128]. Narutaki et al. [129] investigated the effect of localised heat generation in machining titanium alloys and mentioned that heat generated from strong adhesion between cutting tool and workpiece is dissipated through the WC-Co. The heat generated at the cutting zone in machining of Ti-6Al-4V, for example, cannot be dissipated through the titanium workpiece or cut chips effectively due to the alloy's low thermal conductivity of 6.6 W/mk. The generated heat at the cutting zone is transferred onto the cutting tool instead, causing it to and soften which will lead to premature tool failure and vulnerable to chipping [6,31]. It is discussed that 80% of the heat generated when machining Ti-6Al-4V is absorbed by the cutting tool with the remaining heat generation retained in the chips [106].

Low modulus of elasticity, work hardening, and chemical reactivity also contribute to the wear on cutting tools when machining Ti-6Al-4V. There are different types of wear mechanism that contribute to various problems when machining difficult-to-cut materials. Abrasion, adhesion, diffusion, and chemical wear are some of these mechanisms causing wear on cutting tools. Wear mechanisms lead to different types of wear that usually occur on the cutting tools. One or several types of wear could occur at the same time during an operation.

Inconel 718 is a nickel-based superalloy that is extensively used in the aerospace sector for high temperature components of gas turbine engines [46]. According to Schafrik et al. [130] this alloy with its combination of strength and ductility to about 650 °C, weldability and precipitate stability, is the material of choice in aircraft engines. It is also found in applications where resistance to corrosion and high-temperatures are critical factors in component specifications [48]. The difficulty of dislocation through the microstructure is the result of Inconel 718's high tensile and yield strength and therefore dubbing this material as difficult-to-cut. This dynamic material has high material strength and hardness which are also responsible for the poor machinability of the alloy. The low thermal conductivity of this alloy (11.4 W/mk) leads to high temperatures at the tool-workpiece interface causing the tool material to soften and rapidly wear [46]. A review on the machining of nickel-based alloys shows that cemented carbide tends to soften at around 1100 °C [4,5,115] which leads to mechanical and thermal fatigue of the tool material. High strength and hardness in combination with wear mechanisms such as diffusion, attrition and abrasion, increases the tool wear rate and can even cause premature failure [48]. Nickel-based alloys are also extremely sensitive to strain hardening and work harden, which leads to chipping and notch wear of the cutting edges.

The consumption of stainless steels has gradually increased by around 5% yearly on a global scale over the past 20 years, which is more than other metals in manufacturing [131,132]. Stainless steel is usually classified under 5 types. These are ferritic, austenitic, martensitic, duplex and precipitation hardening (PH) alloys. Duplex alloys are classified as difficult-to-cut due to their high tendency to work harden; toughness and relatively low thermal conductivity [53,133–135]. Additional problems arise from their high fracture toughness, which increases temperatures at the tool-chip interface leading to poor surface finish and tool failure. Built-up-edge (BUE) formation has also been observed when machining at elevated cutting speeds. One of the most difficult-to-cut stainless steel categories are the duplex alloys. Duplex alloys are desirable engineering materials that come with several benefits such as, corrosion resistance, high tensile strengths and relative low cost due to lower contents of nickel (Ni) and molybdenum (Mo) [131,136]. Duplex alloys are quite popular in the marine, industrial and construction applications as well as chemical processing industries. The low cost of duplex steels is mainly due to its manufacturing technique and the control of nitrogen in the process [132]. The lower cost feature of duplex makes it a desirable material in applications of highly

corrosive environments where other materials providing similar performance are significantly more expensive.

The austenite-ferrite microstructure of duplex alloys is the reason behind the superior mechanical properties of this class of stainless steel. It consists of approximately 50% austenitic and 50% ferritic. The austenite phase is responsible for the relative ductility and resistance to uniform corrosion; while ferrite phase is responsible for the superior strength as well as corrosion resistance [53,137]. Furthermore, due to the high strength compared to the 300 series such as 304 and 316L stainless steels, duplex stainless steels are increasingly used as an alternative material to austenitic stainless steels.

3.6 Critique of the Literature

Based on the literature in the previous review sections the following research gaps have been identified. Table 3 summarises these findings from the literature:

1. Extensive research has been conducted on difficult-to-cut materials and their machinability in various operations such as turning, milling and drilling [10,13,33,42,46,123,126]. However, research in the context of tool geometry is limited (Table 3). Knowledge and understanding on this subject can lead to better productivity and longer tool life for cutting tools when machining difficult-to-cut materials. For example, in the case of Inconel , referring to a family of austenitic nickel-chromium-based high-performance alloys, further research and development is required to understand and acknowledge the behaviour and machinability of this family of nickel-based advanced material [30,42,43,46,114]. This is also true for other difficult-to-cut alloys such as Ti-6Al-4V and super duplex stainless steel (grade 2507) [53,64]. Investigating these materials at a microscopic level to evaluate their structure, is a key area that will further enable high performance cutting tools and therefore prolong their tool life. The knowledge obtained through material analysis could be used in future simulation studies [32,138].
2. Most research studies evaluating tool geometry solely focus on the optimisation of WC-Co inserts, either in the form of turning or the use of indexable inserts in milling [24,25,33,49,126]. Studies on solid carbide end-mills, along with their performance analysis are inadequate [10,13,21,58]. Research studies focusing on drilling operations use solid WC-Co but do not investigate the WC-Co in difficult-to-cut materials [42,43,46,47]. Numerous research studies have been conducted on solid carbide drills and some have provided optimised geometry and machining techniques [45,114], but more in-depth knowledge is needed to understand the performance of these tools on other advanced engineering materials. It is important to note that there are other major machining operations with different cutting mechanisms, such as thread-milling and reaming, which need further and in-depth research to determine the optimum geometry. This can potentially promote better and more efficient processes in industrial environments.
3. Geometrical factors that affect the performance of tool life need to be analysed for specific materials and tested thoroughly. Developing cutting tools with an optimised geometry will need extensive development, testing and analysis. Further evaluation of cutting tool geometry in solid WC-Co for difficult-to-cut materials is needed, to better understand the cause and effect and to identify solutions.
4. Moreover, to meet the trends in manufacturing such as HSM and LPM, the use of new coating, machining strategies, cooling and tool material technologies should be

considered and studied in more detail. By combining these technologies with high-performance cutting tools potential increase in productivity in machining and emissions could be attained. The development of such technologies alongside the cutting tool design should not be forgotten in manufacturing environments.

5. The author understands the importance and the impact which coating technology has on tool life and cutting performance but has decided that in order to accelerate tool wear on cutting tools all experimental tools will be tested without the use of coating technologies. The author's main objective is to investigate and assess the effect of tool geometry in difficult-to-cut materials but recommends that all cutting tools should be coated to enhance the performance of end-mills and drills.

Table 3: Literature summary and the gaps in research

Ref.	Author(s)	Machining Operation	Material	Limitations
[10]	Polini and Turchetta	End-milling	Ti-6Al-4V	✓ Good investigation into tool life, surface integrity and cutting force × No investigation in tool geometry investigation in milling Ti-6Al-4V ✓ Two types of coatings analysed × New coatings were not assessed × Chip morphology
[13]	Shokrani et al.	End-milling	Ti-6Al-4V	✓ Machine parameters investigated × Investigation into tool geometry
[18]	Kelly and Cotterell	Drilling	ACP 5080	× No investigation into design and geometry ✓ Good investigation into cooling technologies × Tool material investigation
[19]	Braga et al.	Drilling	SAE 323	✓ Diamond coating investigated ✓ MQL assessed × Tool geometry and tool material investigation
[20]	Batzer et al.	Drilling	SAE 308 and 390	× Detailed investigation of tool geometry ✓ Compared High Speed Steel tool material against WC-Co × No tool geometry investigation
[21]	Hricova et al.	End-milling	6060-T6	✓ One geometrical parameter investigated (helix angle) ✓ Three flute designs investigated × No tool material investigation × No investigation into tool geometry
[22]	Hricova	End-milling	6082-T6	× No satisfactory results were obtained ✓ Chip morphology ✓ Machine parameters for HSM
[24]	Hong et al.	Turning	Ti-6Al-4V	× Uncoated insert investigated ✓ Investigated cryogenic cooling × No tool geometry investigation
[25]	Pervaiz et al.	Turning	Ti-6Al-4V	× Investigated turning operation using inserts ✓ Investigated power consumption in machining titanium alloys

				× Investigated at various cutting speeds but not in milling or drilling ✓ Investigated coated inserts against uncoated inserts
[30]	Liao et al.	End-milling	Inconel 718	✓ Limited tool geometry investigation × Tool life was not investigated × Uncoated WC-Co used
[33]	Hong et al.	Turning	Ti-6Al-4V	× Inserts used in experiments × No geometry investigation ✓ Cryogenic cooling investigated × Tool life investigated
[42]	Vimalesh et al.	Drilling	Inconel 718	× No detailed information on tool material or geometry ✓ Machinability of Inconel 718
[43]	Chen and Liao	Drilling	Inconel 718	× No investigation in design or geometry × Spindle through coolant not used ✓ Machinability of Inconel 718 covered ✓ Coated drills were investigated against uncoated drills × Chip morphology was discussed
[44]	Li et al.	Drilling	Ti-6Al-4V	✓ Investigation covered tool material, design, and cooling techniques ✓ Tool geometry investigation was not detailed
[45]	Rahim and Sasahara	Drilling	Ti-6Al-4V	× Solid WC-Co was not used. Exchangeable-tips were used × Limited discussion in tool geometry × Minimum quantity lubrication used in experiments
[46]	Sharman et al.	Drilling	Inconel 718	✓ Limited investigation in tool geometry ✓ Various drill designs investigated × Limited tool material assessment ✓ Limited in coating technology with one tool without coating
[47]	Kivak et al.	Drilling	Inconel 718	✓ Two coatings tested against uncoated drills × Basic information regarding drill design and tool material × Tool geometry investigation
[49]	Devillez et al.	Turning	Inconel 718	✓ Analysis of cutting forces × Inserts investigated × No geometry analysis

[51]	Ulutan et al.	End-milling	Nickel-based alloy	✓ Compared ceramic tool against carbide tools ✓ Coatings were investigated × Tool geometry was no investigated
[52]	Zeilmann and Weingaertner	Drilling	Ti-6Al-4V	× Tool life and tool geometry was not investigated in detail ✓ Temperature analysis in drilling of Ti-6Al-4V
[53]	Nomani et al.	Drilling	2205 and 2507	× No investigation in tool material, geometry, or coating technology ✓ Assessment of the machinability of 2205 and 2507 × Problems associated with machining duplex alloys discussed
[56]	Razak et al.	End-milling	Inconel 718 Plus	× Insert WC-Co were used during the investigation × Tool geometry was not investigated
[57]	Li et al.	End-milling	Ti-6Al-4V	✓ Tool geometry was investigated via simulation ✓ Different designs were modelled in simulation ✓ Detailed analysis of cutting tool
[58]	Li et al.	End-milling	Ti-6Al-4V	✓ Tool geometry was selected from previous study and applied to experiment ✓ Optimum geometry from simulation was tested ✓ Two types of coatings were tested ✓ Fine grade and ultra-fine grade were tested
[59]	Huang et al.	End-milling	Ti-6Al-4V	✓ Vibration study was carried out × Tool design was covered but geometry was not
[63]	Pleta et al.	End-milling	Inconel 738	× Coated indexable inserts were used in milling tests ✓ Tool geometry was not studied
[64]	Airao et al.	End-milling	2507	× Indexable inserts were used in milling tests × Tool geometry was not studied ✓ Machine parameters were investigated in 2507
[87]	Sun and Guo	End-milling	Ti-6Al-4V	✓ Surface integrity was investigated × Tool life was not the focus of the study × Cutting tool geometry was not discussed in detail
[102]	Álvarez et al.	Drilling	Ti-6Al-4V	✓ Chip morphology and chemical reaction in dry machining was investigated ✓ Interaction between material and coating investigated ✓ Titanium Oxide behaviour examined

				× Tool geometry was not investigated
[114]	Kitagawa et al.	End-milling and turning	Inconel 718 Ti-6Al-6V-2Sn	✓ Machining parameters and temperature at the cutting zone was investigated ✓ Ceramic tools and WC-Co was investigated ✓ End-milling and turning investigated × Tool geometry was not studied
[123]	Jawaid et al.	End-milling	Ti-6Al-4V	× Inserts were used for the study ✓ Geometrical details for inserts were provided
[124]	Uddin et al.	End-milling	Ti-6Al-4V	× Details of geometrical parameters were provided but not investigated in detail ✓ Coated and uncoated tools were tested
[126]	Ribeiro et al.	Turning	Ti-6Al-4V	× Inserts used instead of solid WC-Co × No geometry investigation ✓ Detailed assessment of Ti-6Al-4V × WC-Co not explored
[138]	Shokrani et al.	End-milling	Inconel 718	✓ Cooling technologies were investigated × Tool geometry was not investigated but was mentioned in detail
[139]	Dornfeld et al.	Drilling	Ti-6Al-4V	✓ Burr formation was investigated × Geometry was not investigated
[140]	Shokrani et al.	Drilling	Grade 5 titanium ELI	✓ Cooling technologies were investigated ✓ Tool geometry was not investigated but was mentioned in detail
[141]	Zhu et al.	Drilling	Aluminium 2024-T351/Ti-6Al-4V	✓ Different designs were investigated ✓ Chip morphology was conducted on all designs ✓ Burr formation analysis was conducted ✓ Tool wear analysis was conducted as well × Tool geometry was not carried out for different designs

× Areas not covered by author(s)

✓ Areas covered by author(s)

4. Methodology

An effective approach to obtain the experimental results for the proposed theory is to create a methodology and establish the effect of cutting tool geometry on tool life. The methodology, generated by the author, will provide guidance for future work and the approach on optimising cutting tool geometry for a specific alloy. The author's optimisation methodology ensures that the future experiments follow clear step-by-step instructions to reach the objective.

Li et al. [57] assessed tool geometry in end-mills designed for Ti-6Al-4V using finite element analysis (FEA). However, determining the optimum cutting tool using FEA is computationally expensive, time consuming and complex. Moreover, the computational models are based on a series of assumptions, which are not necessarily correct in a Multiphysics environment such as machining. Experimentations are costly; however, their benefits can assist with understanding the interaction between the cutting tools and difficult-to-cut materials in more detail; providing live feedback on stresses, chip size, thermochemical reaction between cutting tool and workpiece, etc. Using statistical analysis, a relationship between the material and the cutting tool may become apparent. In order to design a successful experiment, to determine the optimum cutting tool geometry for end-mills, specifically designed for milling and drilling of difficult-to-cut materials, a systematic process is required to illustrate the steps needed to reach the objectives.

An overview of the experimental work procedure has been displayed through the use of process flowcharts which function as a modelling approach. The simplified experimental process for this study illustrating the steps needed in establishing the optimum geometry for cutting tools is shown in Fig. 25. The process is initiated with the specification of the cutting tools and machining operations set for the difficult-to-cut material under evaluation. For this research, two operations namely, end-milling and drilling were chosen for machining four workpiece materials, e.g. 6082-T6, Ti-6Al-4V, Inconel 718 and super duplex stainless steel 2507 as defined in section 4.2. This section covers much of the process which involved the design, manufacture of prototypes and final designs, testing and collection of data from the experiments. The use of 3D, CAD modelling, allowed for changes in design before manufacturing the experimental tools, or in this case prototypes, for testing and evaluation. Prototypes were used to confirm the flute depth, design type (such as variable helix and variable pitch) and number of flutes for specific operations. The final tool design was determined based on the prototypes. Data collected after testing and evaluation phase determined the significance of geometrical parameters and their interactions. If results were inconclusive or undetermined, new geometrical values were carried out and steps were repeated to re-evaluate the design and the geometrical parameters, until satisfactory results

of the performance of the cutting tools were obtained. No further experiments were necessary after this process.

The resources required for the experimental study on the effect of tool geometry on difficult-to-cut materials are illustrated in Fig. 24. The diagram provides an outlook on the research study and the three major areas where resources were identified. The resources have been separated into three areas. They include, (1) background and preparation, (2) machine requirements and (3) experimental requirements. Resources such as literature, DoE, standards and knowledge on problem description or alloy, are required to implement a successful experiment. The CNC machinery, software and equipment needed to carry out the experiments in the present study are listed under machine requirements. The final resource tool is the experimental requirements for analysing the results. Experimental tools such as statistical software and the use of microscopes, are an essential part in understanding the cause of tool wear and the performance of the cutting tool. The outcome of the methodology provides an in-depth understanding on optimum geometry, tool design, tool wear, chip morphology and surface roughness.

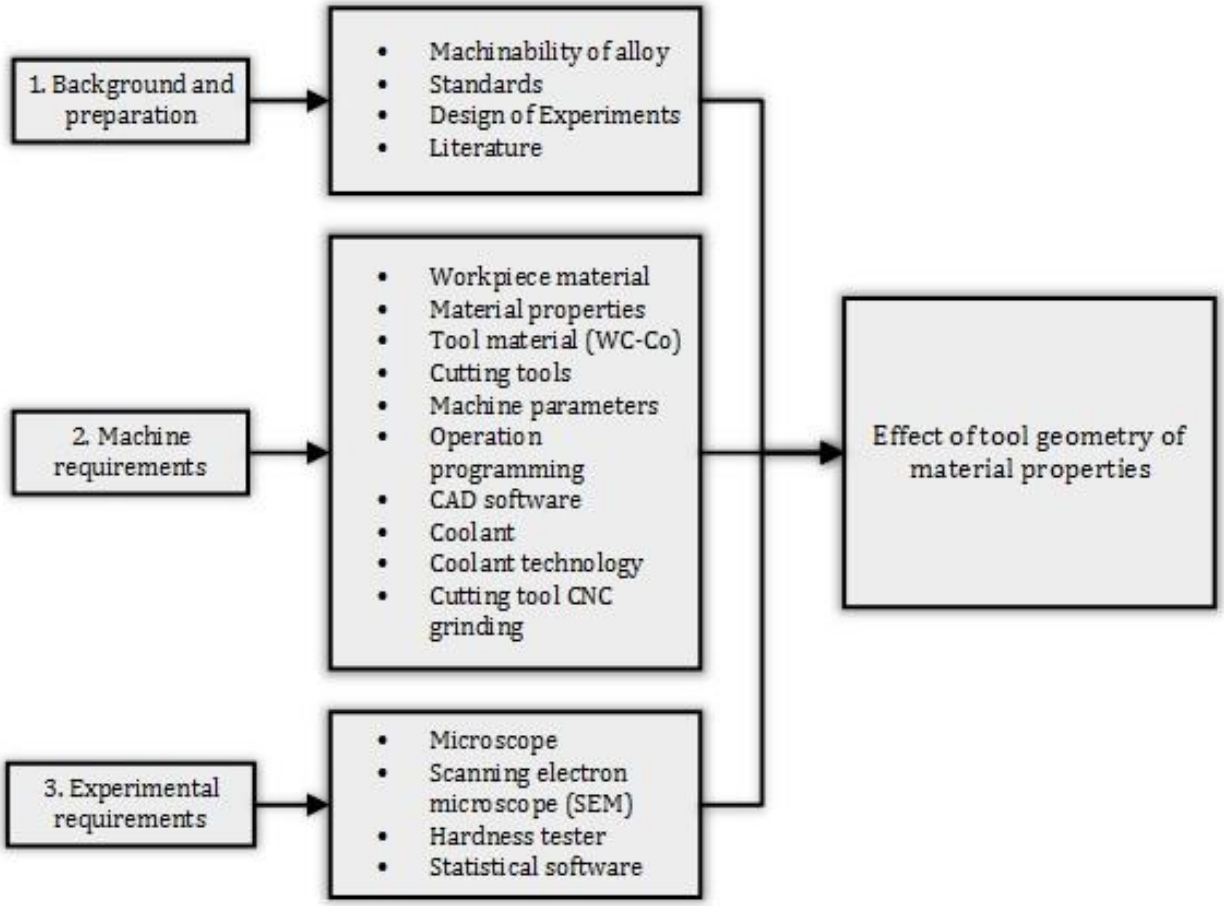

Fig. 24: Representation of the research resources diagram

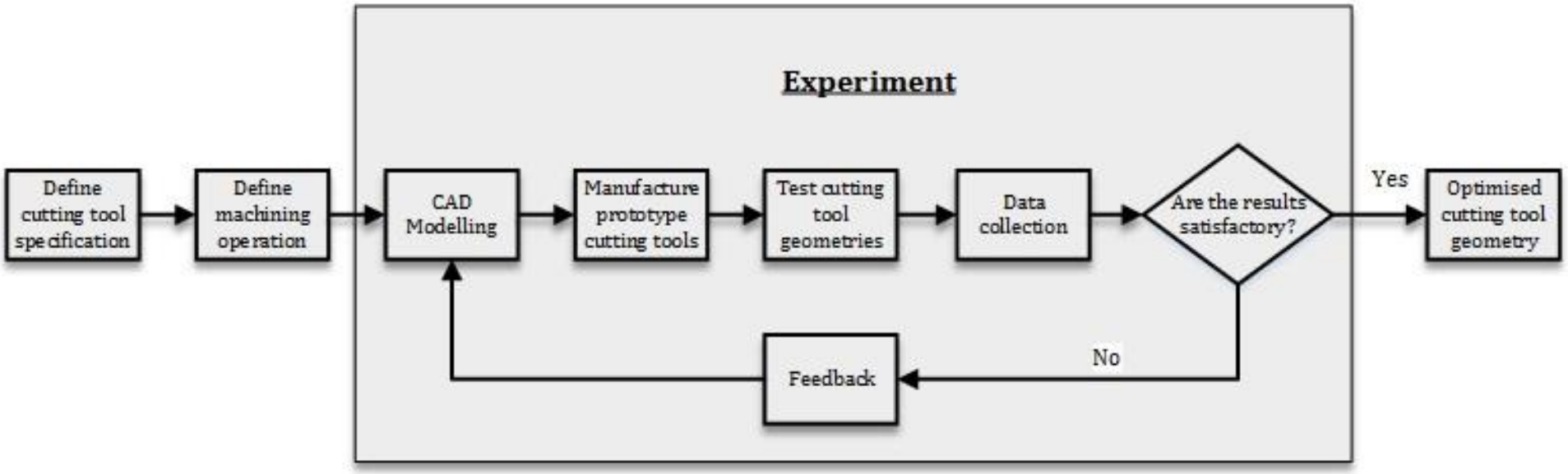

Fig. 25: An illustration of the overall process in designing end-mills with optimum geometry

4.1 Procedure

A flowchart presented in Fig. 26 illustrates the experimental procedure planned for the study, along with the inputs and outputs throughout the experiments. The combination of preliminary knowledge in literature and machining technology, as well as problems associated with machining difficult-to-cut materials acquired is utilised to plan the DoE. The knowledge provides a framework in which it can be used to plan for the number of experiments needed and the approach to take during the analysis stage. After completing the experiments, several outputs such as machined parts, cut chips and worn tools are obtained. The data collected was then analysed with the use of microscopes and later statistical/mathematical software to establish the cause of tool wear, tool life and to determine the significance of geometrical factors. The author would like to clarify that the same procedure as Fig. 26 was applied for end-mills and drills with minor changes to the ISO standards.

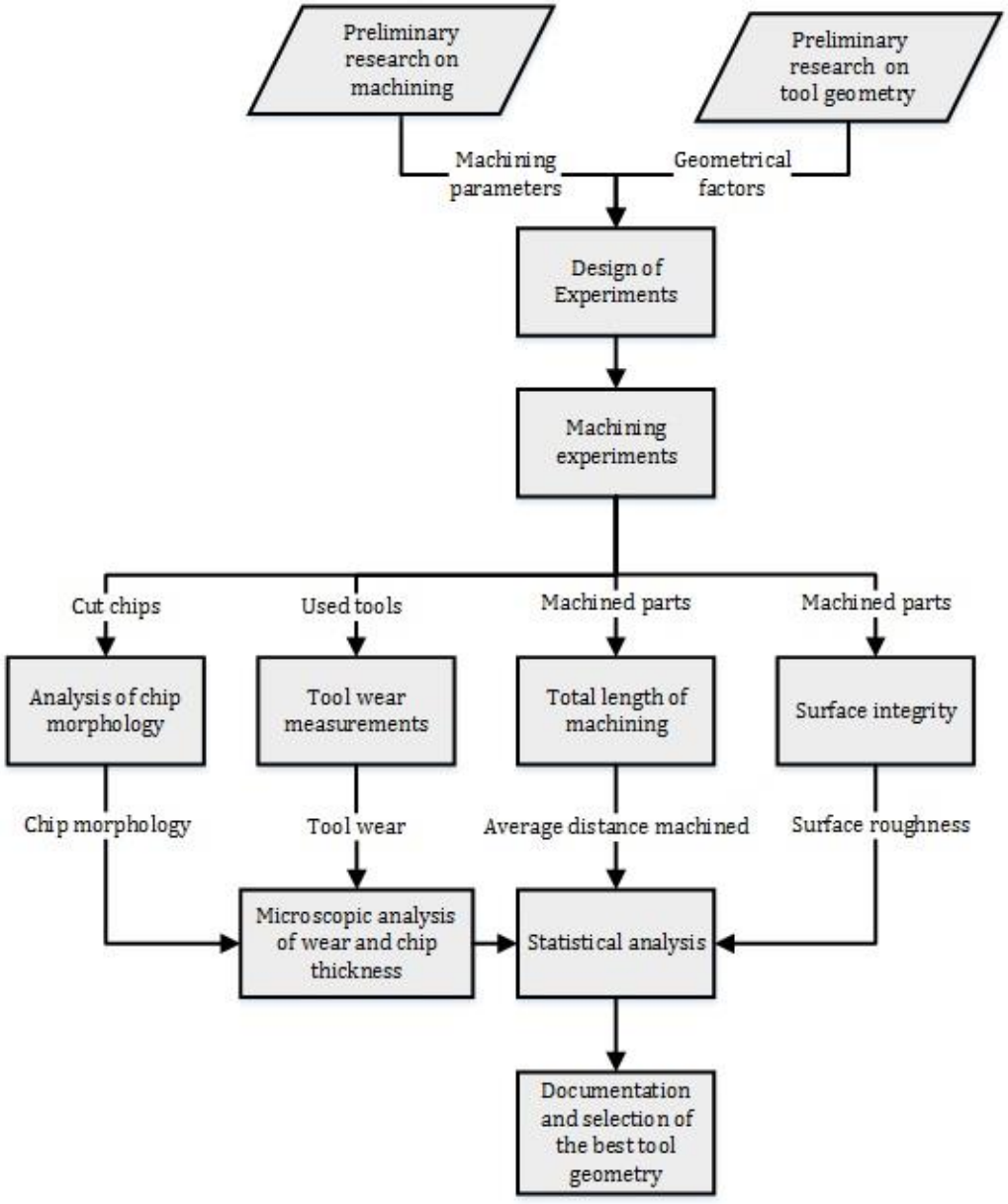

Fig. 26: Illustration of the analytical process to determine the optimum tool geometry

The author would like to clarify that due to time and budget limitations, replicates for some experiments were not carried out. These included the experiments on aluminium 6082-T6 and super duplex 2507 as well as drilling experiments on Inconel 718. The author realises the importance of experimental repetitions for increasing statistical repeatability, but it should be noted that experiments are costly and time consuming. As a result of this, replicates were not produced for experiments on 6082-T6, Inconel 718 and super duplex 2507. Experiments where repeats were required as a result of human error were carried out where deemed necessary. This was applied to all end-milling and drilling experiments.

4.1.1 Design of Experiments

Design of Experiments (DoE), refers to the collection process of data acquisition through experimentation and analysing the results using statistical techniques to obtain meaningful results to reach a conclusion. British standards, BS ISO 3534-3 [142] provides detailed instructions on how the experiment should be conducted, so that feasible results are obtained. However, the selection of experimental parameters or factors for an investigation is itself a very crucial stage. It should also be noted that optimising geometrical parameters individually, while keeping remaining geometrical parameters constant is not conclusive and will not provide useful information. A full factorial design of experiment consists of all possible combinations of the parameters at different levels.[142]. This method allows for the study of the effect of each factor on the response variable, as well as the effects of interactions between factors on the response variable. It is crucial to understand the effect of all factors at the same time and then establish their significance through statistical analysis.

For the purpose of this research study, the author adopted full factorial design technique for all experiments on end-mills and drills to establish whether tool geometry can increase tool life and improve performance. Using DoE techniques such as full factorial, the number of experiments, dependant variables, independent variables and machine parameters can be established. Furthermore, the importance of each of these variable parameters on the desired outcome, e.g. tool life can be identified.

A total of 10 experimental series were proposed and later generated with the use of DoE. Geometrical parameters investigated on end-mills included factors such as helix, radial rake, radial primary clearance and radial secondary clearance angles (Table 4). Four different set of geometrical factors were investigated in drills. Factors under investigation in drilling included helix angle, drill point angle, cutting angle and relief angle (Table 5). On several occasions hybrid full factorial designs were created to ensure that the all geometrical levels are included in the investigation. Randomisation used in the experiments created a homogenous series of experiments to eliminate biases or judgments. Validation experiments on Ti-6Al-4V and Inconel 718 in end-milling and drilling experiments were conducted, to confirm the analytical results.

4.1.2 Experimental Constants

Throughout this study of tool geometries on end-mills and drills, it was essential for all other key machining parameters to remain constant. The following parameter selections were based on industry recommendations and existing literature as well as the outcomes from preliminary tests. Full details of machining parameters have been provided in 4.1.3.

i. The cutting speed and feed rate for each experimental series, associated with the material under evaluation, varied due the mechanical properties and machinability of the difficult-to-cut alloy. However, once the appropriate machine parameters were selected for the operation under evaluation, the author made sure that the parameters stayed constant throughout the experiments. Further details are provided in Table 6 and Table 7.
ii. In end-milling experiments the axial depth of cut (ADoC) and radial depth of cut (RDoC) varied, depending on the difficult-to-cut alloy and operation. This enabled tool wear to be observed over a sufficient length of cutting edge; the profilometer stylus to fit on the workpiece shoulder to measure surface roughness and to efficiently utilise the workpiece material for all experiments. Once the appropriate depth of cut was selected, it was then kept the same throughout the experiments.
iii. Climb milling was utilised instead of conventional milling to reduce tool wear and the higher cutting temperatures at the cutting zone (Fig. 27).
iv. Continuous drilling was adopted for all drilling experiments. No peck drilling was carried out in any experiment.
v. In drilling operations, where necessary, spindle through coolant was used to regulate the machining temperature and provide better lubrication at the cutting zone. This provided a constant evolution of tool wear which was then used for analysis.
vi. All drilling experiments were specified to produce blind holes and not drill through the workpiece material. Exit burr or burr formation was not investigated.
vii. Machining was performed with flood coolant. The coolant concentration, when mixed with water was kept within 10%-15% in all experiments.
viii. All tools were uncoated, in an effort to accelerate the tool wear when machining the limited workpiece material. This would examine the suitability of the tool geometries without introducing additional wear resistance to the tool.
ix. Cutting tool diameters where kept to 10 mm and 8.5 mm for end-mill and drills, respectively.
x. The tool holder secured each tool 30 mm from the end to maintain a consistent tool deflection and vibration during machining. In drilling, this length was kept to 65 mm for all experiments.

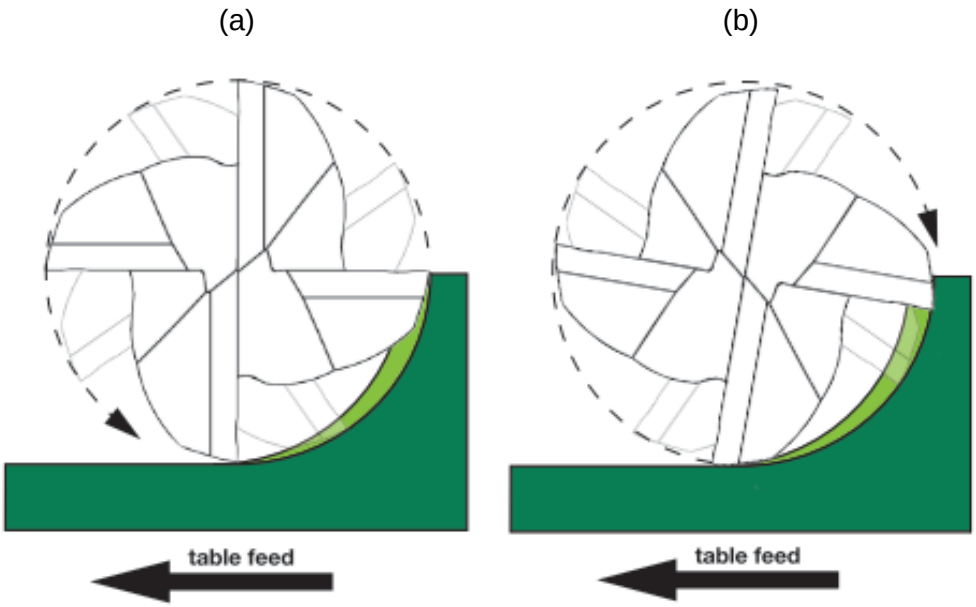

Fig. 27: Illustration of (a) conventional milling and (b) climb milling [3]

Each tool was assigned a unique coding or experiment I.D. for reference and clear identification during the analysis stage. The example below represents corresponding letters in an experimental I.D.

A	B	C	D	E
Ti	**1**	**R**	**24**	**1**

Where,

A – Workpiece material, in the case of the example used, titanium (Ti) alloy Ti-6Al-4V. Inconel 718 (INCO), 6082-T6 (AL) and super duplex 2507 (SDX)

B – Experimental series number indicating the order of iterations in an operation

C – Signifies the machining operation where (R) corresponds with roughing, (F) corresponds with finishing and (D) for drilling

D – Total number of experiments in an allocated series

E – Experiment number

Table 4: DoE levels chosen for each geometrical factor for end-mills

	6082-T6		**Ti-6Al-4V**			**Ti-6Al-4V**		**Inconel 718**			**2507**			
	Level		**Level**			**Level**		**Level**			**Level**			
Geometrical Parameters	*Low*	*High*	*Low*	*Medium*	*High*	*Low*	*High*	*Low*	*Medium*	*High*	*Low*	*Medium*	*High*	*Very High*
Helix angle	45°	55°	A	-	B	40°	45°	34°	36°	38°	C	-	-	B
Radial rake angle	16°	16°	12°	14°	16°	8°	14°	8°	10°	12°	8°	10°	12°	14°
Radial primary clearance angle	12°	12°	10°	-	12°	10°	14°	10°	12°	14°	10°	-	-	14°
Radial secondary clearance angle	23°	23°	25°	-	30°	23°	23°	23°	23°	23°	23°	23°	23°	23°
End-mill designs								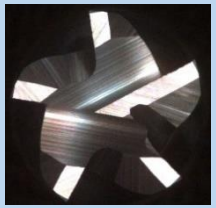			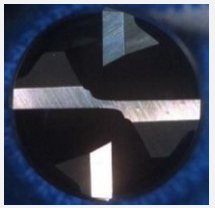			

Table 5: DoE levels chosen for each geometrical factor for drills

	6082-T6		6082-T6			Ti-6Al-4V		Inconel 718		2507	
	Level		Level			Level		Level		Level	
Geometrical Parameters	*Low*	*High*	*Low*	*Medium*	*High*	*Low*	*High*	*Low*	*High*	*Low*	*High*
Helix angle	30°	35°	0°	-	0°	30°	30°	30°	34°	30°	30°
Cutting angle	15°	15°	0°	-	0°	3°	5°	0°	5°	0°	-5°
Drill point angle	130°	135°	120°	-	130°	130°	140°	130°	140°	130°	140°
Relief angle	10°	10°	12°	16°	20°	10°	16°	6°	10°	10°	12°
Drill designs			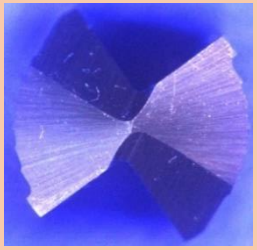			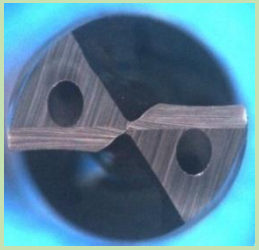		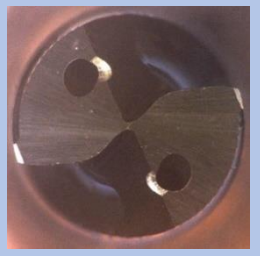		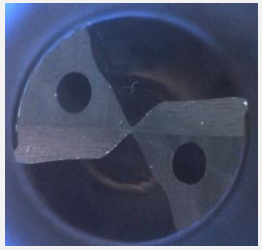	

4.1.3 Machine Parameters

A total of 10 cutting tools, 5 end-mills and 5 drills, were proposed for the experiments. Two end-mill designs were allocated for Ti-6Al-4V and two drills for 6082-T6. In the case of end-mills designed for titanium, the author wanted to investigate and evaluate two different machining operations, roughing and finishing in end-milling of Ti-6Al-4V. The two drill designs for 6082-T6 were recommended from the industrial partner. All other materials were allocated a single cutting tool design due to limited funding and materials. Preliminary experiments were carried out to establish suitable machining parameters to be able to gather data for analysis. The machine parameters for end-mills and drills allocated for each design is presented in Table 6 and Table 7.

With the use of CAM software, the author made sure that incremental cuts where taken at certain RDoC and ADoC, to track the progression of tool wear. An example is provided in Fig. 28-Fig. 30. The same procedure was followed in all other milling experiments. High speed machining (HSM) is a crucial factor in increasing productivity and therefore the machine parameters chosen for these experiments were recommendations, based on current machining methods and other cutting tool manufacturers. The machining parameters selected for the experiments had to satisfy the HSM requirements and produce tangible results for tool life and tool wear analysis. The author's review of literature from past research studies did not provide optimum machining parameters and as a result, preliminary tests were conducted to make sure that chattering and vibrations caused by unsuitable machine parameters, were eliminated from the end-milling experiment. Preliminary tests were also carried out for drilling experiments.

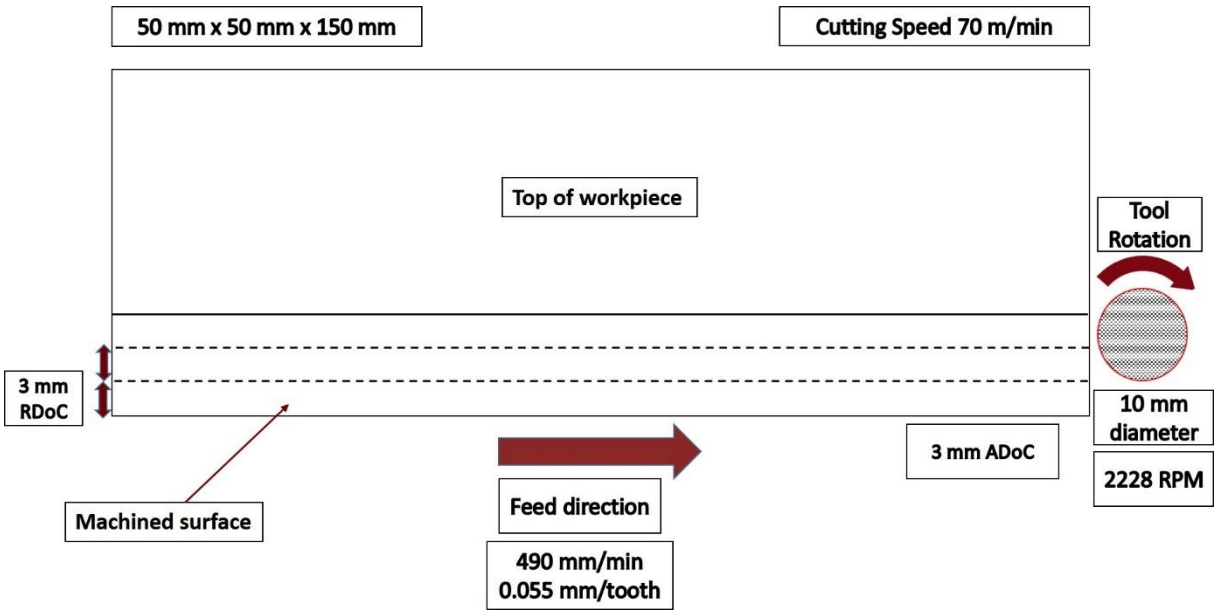

Fig. 28: An illustration of the machining method used on Ti-6Al-4V using 4-flute end-mill

Table 6: Machine parameters set for *end-milling* experiments

Machine Parameter	Unit	6082-T6	Ti-6Al-4V	Ti-6Al-4V	Inconel 718	2507
Number of teeth, z	-	2	4	6	5	4
Cutting speed, V_c	m/min	200	70	70	30	40
Feedrate, f_z	mm/z	0.180	0.055	0.050	0.030	0.070
Spindle speed, n	rpm	6366	2228	2228	955	1273
Feed, V_f	mm/min	2292	490	668	143	357
ADoC, a_p	mm	3	3	20	3	5
RDoC, a_e	mm	6	3	1	2.5	4

Table 7: Machine parameters set for *drilling* experiments

Machine Parameter	Unit	6082-T6	6082-T6	Ti-6Al-4V	Inconel 718	2507
Number of teeth, z	-	2	3	2	2	2
Cutting speed, V_c	m/min	150	180	30	30	40
Feedrate, f_z	mm/rev	0.100	0.200	0.120	0.102	0.090
Spindle speed, n	rpm	5617	6741	1123	1123	1498
Feed, V_f	mm/min	562	1348	135	115	135
ADoC, a_p	mm	40	40	31.5	21.5	24

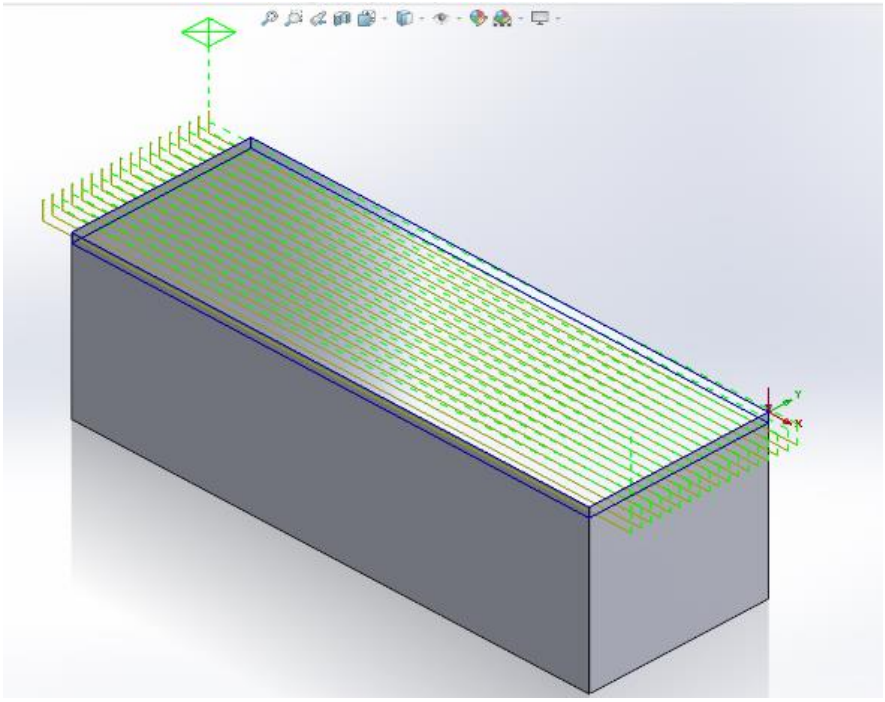

Fig. 29: CAM software design for end-milling Ti-6Al-4V

Fig. 30: Machining process in Ti-6Al-4V

The depth of drilling varied for all different materials, due to the limitations in through coolant pressure and the availability of workpiece material. An example of the design of drilling procedure in Inconel 718 has been provided in Fig. 31-Fig. 33. Drilling method had to be utilised to be able to increase the number of drilled holes (Fig. 33).

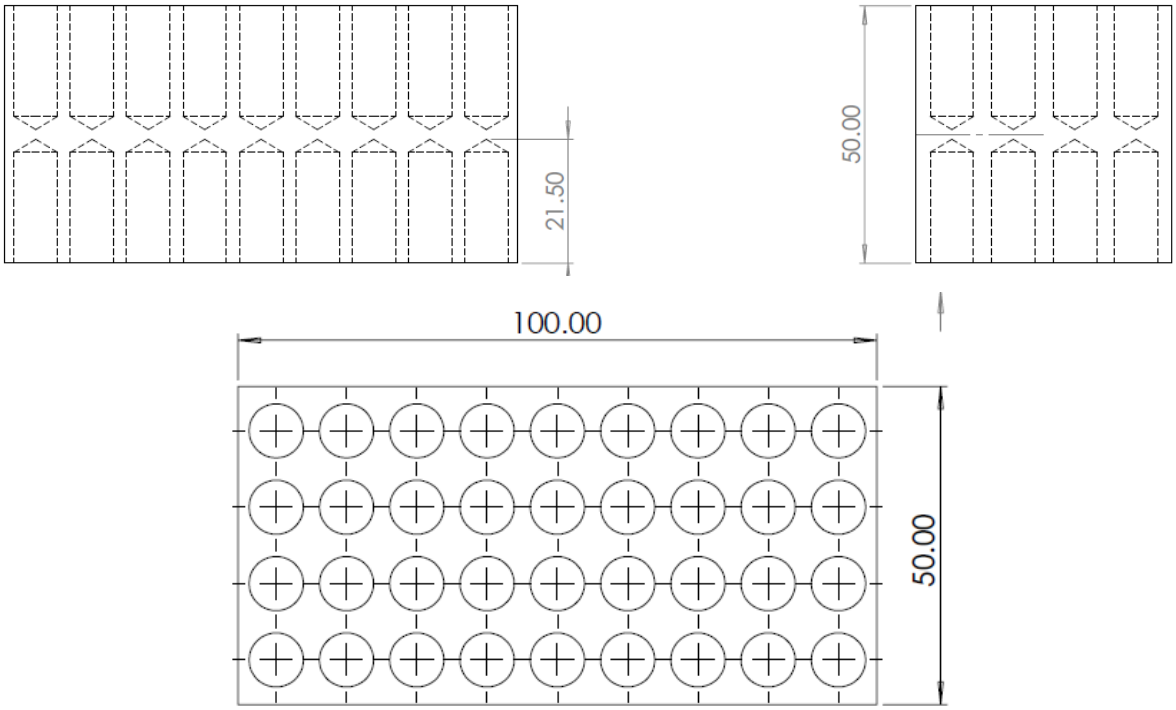

Fig. 31: An example of drilling operation plan on CAM software in machining Inconel 718

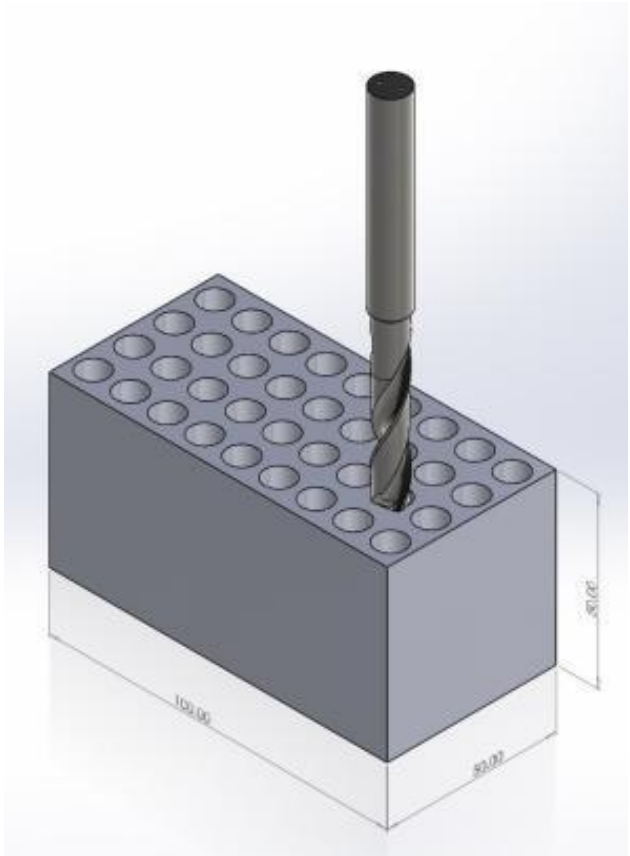

Fig. 32: CAM software design for drilling Inconel 718

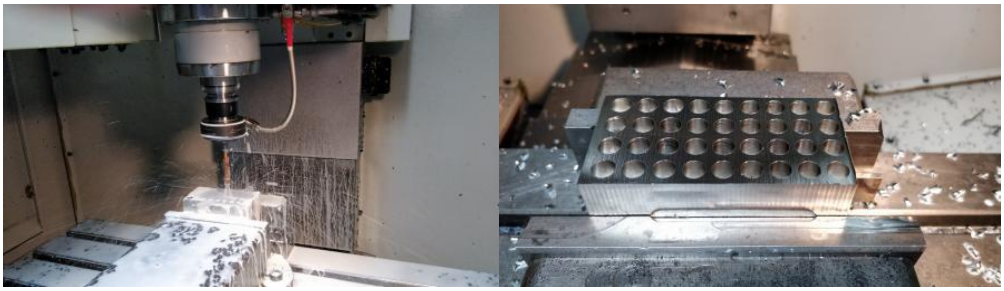

Fig. 33: Applied CAM design to experiment in drilling of Inconel 718

Three axis Eumach, Axe and Status V16 vertical CNC machine, with a 3.7 kW motor and Fanuc 0-MD series employing a continuously variable spindle speed up to a maximum of 10,000 rpm, was used to perform experimental runs. The machine tool was cleaned prior to experimentation and new coolant was prepared. Water soluble coolant BF222 was selected, due to its high performance for general heavy-duty machining on titanium alloys. A vice was used for holding workpiece material in place, as shown in Fig. 34, to ensure the workpiece is placed above the top of the vice and sits straight when machining. A BR30-ER32-070 collet chuck was used to hold the cutting tools. Tool concentricity was measured using a clock and recorded before every experiment.

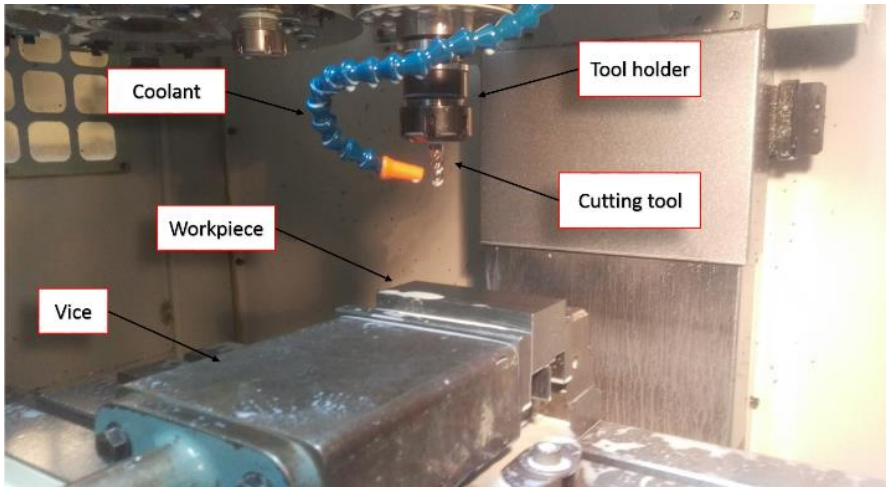

Fig. 34: Experimental environment and workpiece holding technique

4.1.4 Drill Designs

Findings from literature and expertise from industry, directed the author towards several designs for drills for the selected workpiece materials. The designs of drills were based on factors such machinability of the material, previous designs and recommendations from literature [44,46,53,143]. Geometrical parameters such as helix, angle, cutting angle, drill point angle and relief angle were chosen for the study (Fig. 35).

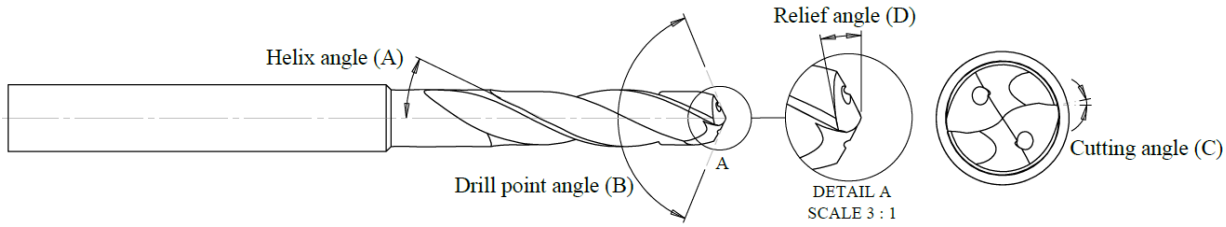

Fig. 35: Geometrical parameters investigated in drilling

The same procedure as end-mills were followed for drills. But British Standardisation BS ISO 7079:2016 [144] was used for dimensional clarification. Drill diameter of 8.5 mm, with an overall length of 110 mm, shank diameter of 10 mm and a flute length 5 times the diameter (5xD) was proposed and adopted for all drilling experiments. All tools were used by the author and manufactured at Scorpion Tooling UK Ltd. The peripheral cutting edges of the drills were prepped by the author, before experiments as recommended by Denkena and Biermann [145]. No coatings were used during any drilling experiments, to encourage wear and to assist with the examination of wear. Further information has been provided in Table 8 and Appendix C.

Table 8: Summary of drill designs for each difficult-to-cut material

Drill Designs for Difficult-to-Cut Materials (Appendix C)				
Materials selected	6082-T6	Ti-6Al-4V	Inconel 718	SDX 2507
No. of flutes (z)	2 and 3	2	2	2
Corner geometry (μm)	N/A	N/A	250	N/A
WC-Co grade	YL10.2	CTS20D	CTS20D	CTS20D

4.1.5 End-mill Designs

Major parameters such as helix angle, radial rake angle (cutting angle), and clearance angles, in this case radial primary clearance and radial secondary clearance angles, were chosen for evaluation in this study because of the effect that they bring to the performance of the cutting tool (Fig. 10). All end-mills were initially designed on CAD software, SolidWorks, to get a better understanding of the tool and for record keeping of the designs for future reference and use. The British Standardisation BS-ISO 1641-1:2016 [146] for cutting tools was adopted and all dimensions were met during the design and manufacturing stage. A cutting tool with a diameter of 10 mm, overall length of 72 mm and a length of cut of 22 mm was proposed for all milling experiments (Fig. 36). All tools were manufactured at Scorpion Tooling UK Ltd. The peripheral cutting edge of all the flutes were prepped before the experiments as recommended by Denkena and Biermann [145]. It was allocated that cutting tools will be tested without coating to encourage wear and to assist with the examination of wear on the peripheral cutting edge.

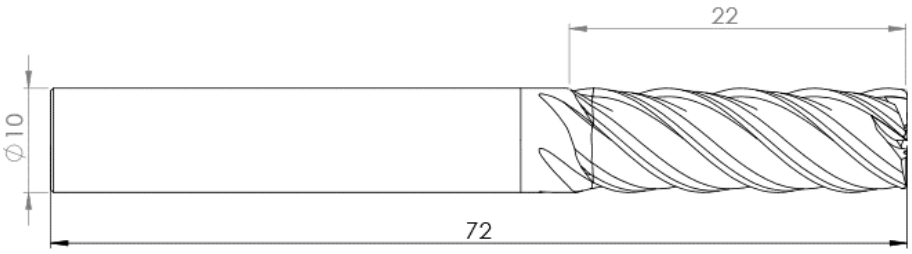

Fig. 36: Design of end-mills on SolidWorks with dimensions based on BS-ISO 1641-1:2016

To minimise the amplification of harmonic vibrations in 4-flute end-mills, variable helix was used to counter the chattering effects caused by harmonic vibrations. Sun et al. [147] investigating the characteristics of the cutting forces and chip formation in machining titanium alloys, states that the vibration frequency increases when machining. Budak [61] and Budak and Kops [60] proved that the productivity and the surface finish can be improved significantly by using variable pitch angle on cutting tools. Huang et al. [59] investigated unequal pitch and concluded that it does reduce the vibration frequency. Variable pitch was adopted for 5-flute and 6-flute end-mills designed Ti-6Al-4V and Inconel 718 Experiments, to reduce chattering and allow the cutting tool to perform at its optimum. Further information such as the WC-Co used and the corner geometry on end-mills for each difficult-to-cut material is presented in Table 9. All end-mill designs are presented in Appendix C for further review.

Table 9: Summary of end-mill designs for each difficult-to-cut material

End-mill Designs for Difficult-to-Cut Materials (Appendix B)				
Materials selected	6082-T6	Ti-6Al-4V	Inconel 718	SDX 2507
No. of flutes (z)	2	4 and 6	5	4
Corner geometry (μm)	None	500 and 200	250	500
WC-Co Selected	YL10.2	EMT100	EMT100	YL10.2

4.1.6 Tool Material Selection

According to Shokrani et al. [14], Cheng [7], Davim [6,66], Denkena and Biermann [145] and Childs et al. [148] the ideal cutting tool should have superior performance in 5 distinct areas.

1. Hot hardness: the ability to maintain hardness at elevated temperatures
2. Low chemical affinity: not to react with the material under high pressures and temperatures
3. Toughness: to resist external loads either static or dynamic and mechanical stresses.
4. Resistance to thermal shock: to withstand sudden temperature fluctuations causing stress on the tool material.

5. Resistance to oxidisation: ability not chemically reacting with Oxygen in machine operations.
6. High thermal conductivity: tolerate elevated temperatures

Based on the literature review and WC-Co manufacturer recommendations the author decided to select three solid WC-Co for end-mill and drilling experiments. Information regarding the WC-Co grades such as chemical composition and physical data have been provided in Table 10. Images of grain structure have been provided in Appendix B.

Table 10: Properties of WC-Co selected for this study

Chemical Composition	**EMT100**	**YL10.2**	**CTS20D**
Cobalt, Co (%)	6.0	10	10
Tungsten carbide, WC (%)	93.0	89	89
Other (%)	1.0	1.0	1.15
Physical Data	**EMT100**	**YL10.2**	**CTS20D**
Density (g/cm^3)	14.80	14.45	14.38
Hardness HV30	1740 - 1860	1600	1600
Coercive force (kA/m)	22.2 - 25.8	20.5	20.69
Transverse rupture strength (N/mm^2)	3900	4000	4000
Grain size (µm)	0.8	0.8	0.7

Cemented Tungsten Carbide (WC-Co) EMT100 with submicron grain structure of 0.8 µm was chosen as the preferred material to produce the cutting tools for the experiments on roughing and finishing operations in Ti-6Al-4V and roughing experiments in Inconel 718. A lower percentage of cobalt (Co), 6%, and 93% WC-Co was chosen. Lowering the Co% content in the WC decreases the toughness of the solid carbide but in return it increases the hardness and strength, [31,92].

According to researchers such as Davim [66], Ezugwu and Wang [106], Hartung et al. [107] and Che-Haron [149], one of the most preferred grades of carbide for machining titanium and titanium alloys is the straight grade cemented carbide (WC-Co) comprising of 6 wt.% Cobalt and 94 wt.% tungsten carbide with grain size structure ranging 0.8 µm-1.4 µm. Hartung et al. [107] reported that that low amounts of cobalt presence (lower than 6%), in the WC increases crater wear when machining titanium. Che-Haron [149] analysing tool life and surface integrity in turning titanium alloys Ti-6Al-2Sn-4Zr-6Mo mentioned that the straight grade cemented carbide, gave optimum performance and therefore was chosen for the present study. Choosing the correct carbide for the experiments is a crucial factor. Shokrani et al. [138,140]

evaluated cryogenic and hybrid cooling technology in Ti-6Al-4V and Inconel 718 chose carbide YL10.2 with 10% Co as binder for both studies. As a result of, the WC-Co grade was selected for studies on drilling and milling of aluminium 6082-T6 and milling of super duplex 2507. With a binder percentage of 10% Co this solid tungsten carbide was used for its higher toughness based on the information provided by Scorpion Tooling UK ltd. when compared to EMT100. The final grade of WC-Co, CTS20D, was mainly chosen, based on carbide manufacturers and the their recommendations for drilling difficult-to-cut materials [150]. This grade was used in drilling of Ti-6Al-4V, Inconel 718 and super duplex 2507 because of its improved toughness, increased transverse rupture strength and optimised hardness.

4.1.7 Manufacture of Cutting Tools

All cutting tools were manufactured on site at Scorpion Tooling UK. Schneeberger Norma with GE Fanuc Series 160i-MB software and Schneeberger Gemini with GE Fanuc Series 160i-MB were used to produce end-mills and drills, respectively. The same machines, cutting tool holders and same grade of grinding wheel, where used on all cutting tools during manufacture. Cutting tools were gauged at zero for concentricity before being grounded and a Schunk high precision sleeved tool holder (Fig. 37), was used to make sure that the WC-Co blanks stayed concentric throughout the grinding process. An example of 6-flute end-mill for Ti-6Al-4V and drill for Inconel 718 after manufacture is presented in Fig. 38 and Fig. 39.

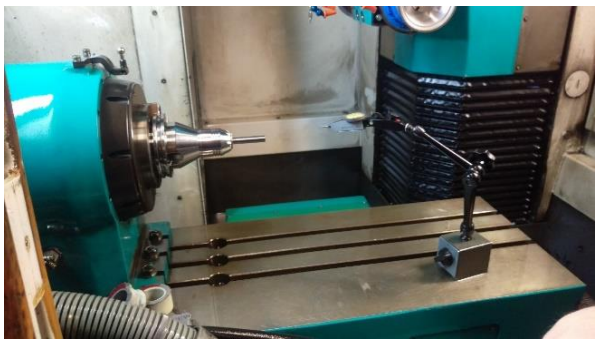

Fig. 37: Preparations and production set up on Norma Schneeberger

(a) (b)

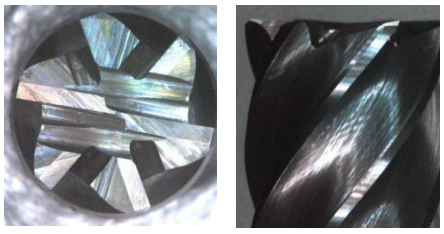

Fig. 38: Example of end-mill designed and produced for Ti-6Al-4V (a) face view (b) side view

(a) (b)

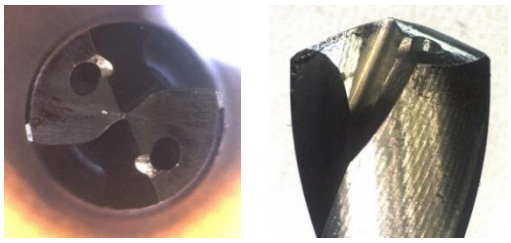

Fig. 39: Example of drill designed and produced for Inconel 718 (a) face view (b) side view

4.2 Workpiece Material

Four difficult-to-cut workpiece materials were chosen for this study. They are as follows:

1. Aluminium 6082-T6
2. Titanium alloy Ti-6Al-4V
3. Nickel-based alloys Inconel 718
4. Austenitic-ferritic super duplex stainless steel 2507

The selected workpiece materials were mainly chosen for the present study, because of their popularity and wide use in aerospace, power generation, defence, and medical industries according to industrial partner (Scorpion Tooling UK Ltd.). The poor machinability of these materials was also considered due to the challenges faced in machining. The chemical composition of all four materials are presented in Table 11-Table 14. A summary of the mechanical properties of the workpiece materials selected for this study have been presented in Table 15. The author made sure that all workpiece materials, when acquired, were from the same batch of ingots. The workpiece materials varied from 100-150 mm in length, but the width and depth of the materials were kept to 50 mm.

Table 11: Chemical composition (%) of Ti-6Al-4V

Ti-6Al-4V	**Al**	**V**	**Fe**	**C**	**O**	**N**	**H**	**Ti**
Alloying (%)	6.23	4.02	0.15	0.16	0.14	0.01	0.002	Remainder

Table 12: Chemical composition (%) of 6082-T6

6082-T6	**Si**	**Fe**	**Cu**	**Mn**	**Mg**	**Cr**	**Zn**	**Ti**	**Al**
Alloying (%)	0.96	0.26	0.04	0.56	0.82	0.01	0.02	0.015	Remainder

Table 13: Chemical composition (%) of super duplex 2507

2507	**Cr**	**Ni**	**Mo**	**Mn**	**Cu**	**Si**	**N**	**P**	**C**	**S**	**Fe**
Alloying (%)	26	8.0	5.0	2.0	1.0	1.0	0.35	0.35	0.03	0.015	Remainder

Table 14: Chemical composition (%) of Inconel 718

Inconel 718	**Ni**	**Cr**	**Nb**	**Mo**	**Ti**	**Al**	**Co**	**Si**	**Cu**	**Mn**	**C**	**Fe**
Alloying (%)	52.57	19.16	5.26	2.89	1.14	0.58	0.18	0.1	0.05	0.07	0.002	Remainder

Table 15: Mechanical properties of the workpiece materials selected for this study

Workpiece material	**Young's Modulus (GPa)**	**Thermal Conductivity (W/mk)**	**Hardness (HB)**
6082-T6	71	180	91
Ti-6Al-4V	114	7	315
Super Duplex 2507	200	15	266
Inconel 718	200	11	392

4.3 Data Collection

The subsequent activity involves the collection of raw data throughout each trial. Machined material, tools and workpiece chips are all analysed within this section. In chronological order, the first stage involved measuring the total milling distance for end-milling and number of holes in drilling experiments. Secondly, concurrently with machining trials, cut chips from the initial machined surface and drilled hole were collected and compared to swarf at the end of the experiment for each tool. Thirdly, tool wear measurements were taken using optical microscopy once the cutting tool had reached the tool wear criteria. Please see 4.3.1 below, for more information on tool wear criteria for all experiments. Finally, the surface profilometry was used to establish a relationship between tool wear and workpiece surface roughness.

4.3.1 Tool Wear Measurements

Quantifying wear can either be achieved directly, through wear land measurements under an optical toolmaker's microscope, or indirectly by recording cutting forces or power, which can be related back to actual tool wear. ISO 8688-2, the standard for tool life testing in end milling, recommends that the width of flank wear land, VB (Fig. 40) is measured directly for use as a tool life criterion, although each form of deterioration should be recorded once it becomes visible [151]. Flank wear is widely used in metal cutting because it has a direct influence on workpiece accuracy and surface roughness, and the flank wear land is close to parallel to the direction of cutting. Flank wear was selected as the governing type of tool wear for tool life, for end-milling and drilling operations. The author has provided further details of flank wear on end-mills and drills in Fig. 40 and Fig. 41. The radial flank wear on drills was not measured but has been discussed in the Chapter 0.

ISO 8688-2:1989 [151] was used as reference to carry out tool wear measurements in end-milling and drilling experiments (Table 16). For metal cutting, a flank wear tool life criterion is set as $VB = 0.3\ mm\ (300\ \mu m)$ for uniform wear and $VB = 0.5\ mm\ (500\ \mu m)$ for irregular wear. A similar threshold has not been defined for drilling operations in standards. However, based on drilling experiments carried out [152,153] and preliminary experiments carried out by the author, a $VB = 0.1\ mm\ (100\ \mu m)$ is set for uniform wear and $VB = 0.3\ mm\ (300\ \mu m)$ for irregular wear or localised wear on the cutting edge. In the case of occurrence of chipping on the cutting edges, the tool wear type was treated as localised wear meaning it would equal to $500 \mu m$ for end-mills and $300 \mu m$ for drills as a tool life end point [151]. According to [151] catastrophic failure (cutting tool breakage) should not be used a primary criterion for tool life end point. Experiments were repeated when faced with tool breakage.

Table 16: Minimum and maximum tool wear criteria set for end-milling and drilling experiments

Operation	Uniform Wear (VB_{min}) (averaged over all cutting edges)	Localised Wear (VB_{max}) (maximum on any individual tooth)
End-milling	300 µm	500 µm
Drilling	100 µm	300 µm

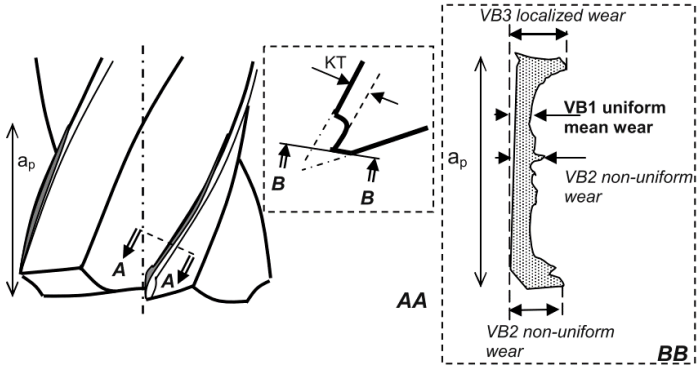

Fig. 40: Wear of end-milling tools, BS ISO 8688 [154]

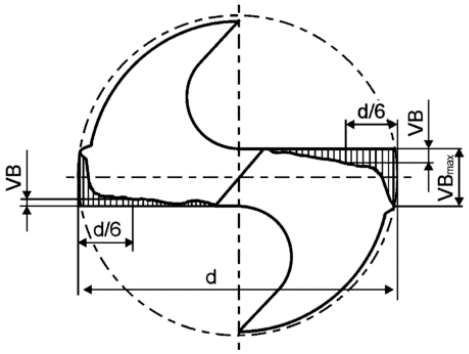

Fig. 41: Flank wear on drills to determine tool life [152]

Flank wear measurements were taken across the allocated length of cut for end-mills for each experimental series on selected difficult-to-cut materials. The ADoC varied for each material but measurements were taken across the worn peripheral cutting edge using the method provided by ISO 8688-2:1989. For example, in the case of end-mills, Due to the high zoom of the microscope, three separate images were taken to capture the cutting edge of each drill as shown in Fig. 42.

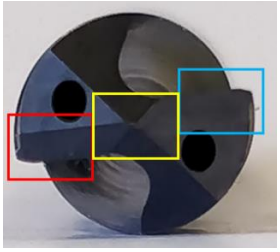

Fig. 42: Tool regions analysed during tool wear measurements

After machining experiments, the cutting tools were cleaned with the use of pressurised air and were cleared of any oil and debris for examination. Optical microscopy for tool wear was used to measure the wear on the cutting tools. A Nikon tool makers' microscope was used to measure the tool wear on the cutting tools. The extent of the wear land progression along the tool edge was examined under a Nikon toolmaker's microscope, retrofitted with a Moticam digital camera for image acquisition. Fig. 43. Images were taken using the software acquired from the manufacturer. Before use, the microscope and the digital camera were calibrated, and the same method was followed throughout.

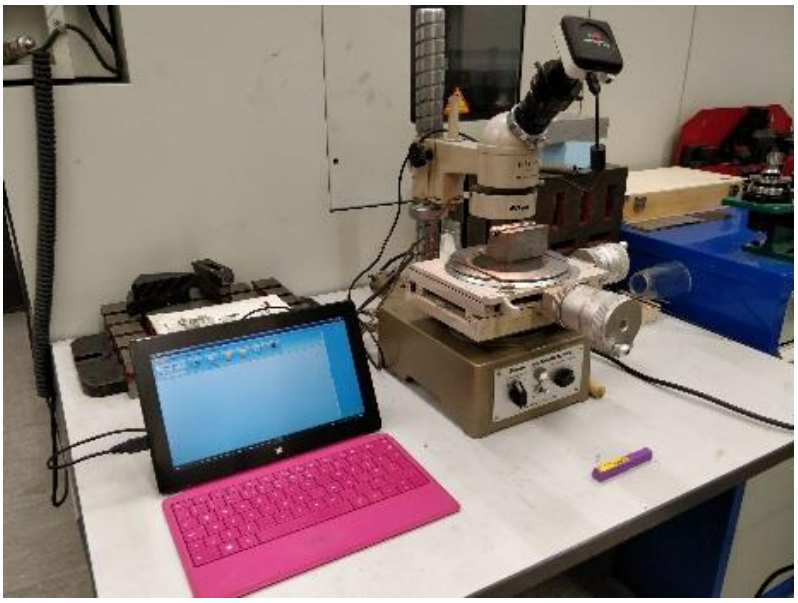

Fig. 43: Nikon tool makers' microscope and set-up for measuring tool wear

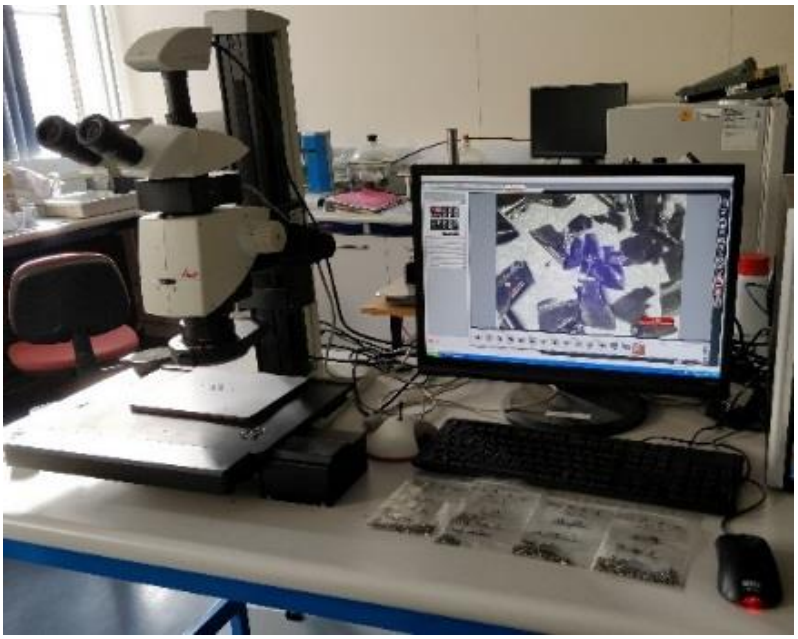

Fig. 44: Leica M205 C microscope and set-up when analysing titanium chips

A second microscope was used for analysing cut chips collected from experiments. The LEICA M205 C, shown in Fig. 44 came with an integrated Leica MC170 HD digital camera fitted inside the microscope which allowed for the analysis of the cut chips. All chips were collected after the first machining pass and the final pass or the first drilled hole and the last. The chips were analysed under this microscope. After the collection of chips from each experiment they were left to dry to let the water from the coolant evaporate. Later chips were cleaned to remove any residues or signs of oil.

4.3.2 Surface Roughness Equipment

The surface roughness of workpiece materials in 6-flute end-mill experiments and all drills analysed after completing the experiments. The average wall surface finish of the titanium workpiece materials was measured in the finishing experiments on Ti-6Al-4V. A Mitutoyo SJ-201P portable surface roughness tester, as shown in Fig. 45, was used to measure the surface finish of the titanium blocks from the finishing experiments. The surface roughness was calibrated to 3 µm (calibration stated by the manufacturers). Before taking measurements of the titanium alloys, the workpiece was cleaned, and pressured air was used to dry the samples and remove any other residues. Surface roughness measurements were taken at the beginning, middle and end of the machined faces. Fig. 46 shows the designated areas A, B and C where the surface roughness measurements were recorded. Three measurements were taken at each designated area. In drilling experiments, it was decided, by the author, that the surface roughness of the first and last hole of every row of drilled holes was to be measured.

Fig. 45: Mitutoyo SJ-201P portable surface roughness tester calibration

Each measurement was taken three times at each point to increase statistical reliability. In drilling operations, the first and last hole of every row of holes was measured. The same procedure as end-mills was followed where measurements were taken three times at each point to increase statistical reliability.

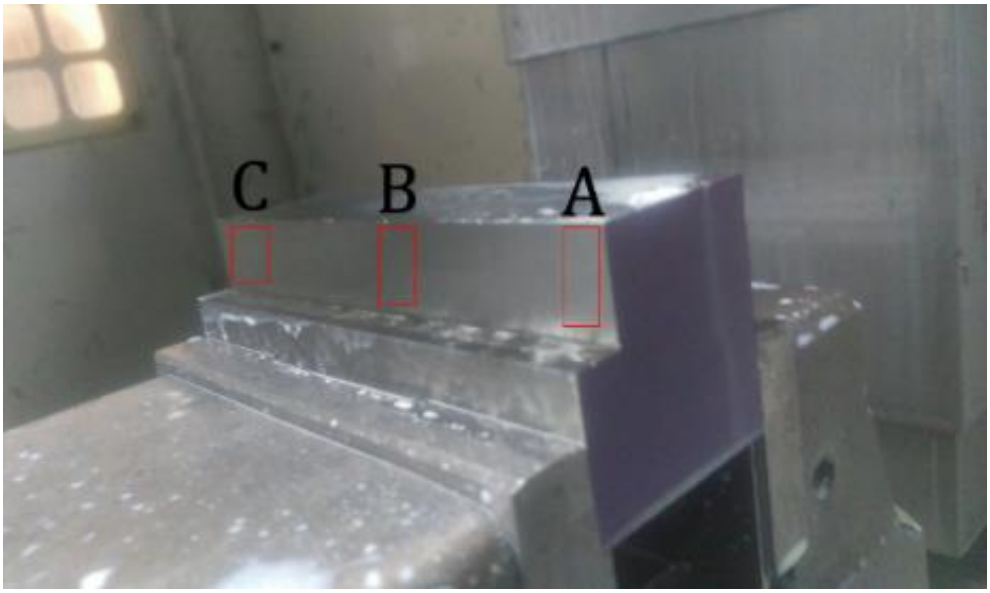

Fig. 46: Designated areas where surface finish values were recorded

5. Results and Analysis

The following section presents the experimental results and the subsequent analysis performed in order to achieve meaningful conclusions relative to the project aims and objectives outlined in Chapter 2. Sections 5.2 and 5.3 will cover the author's analysis based on the response factors such as tool life. Firstly, results based on tool life, obtained from end-milling and drilling experiments for each difficult-to-cut workpiece material is presented and discussed. The author expands further by evaluating the geometrical factors in each experimental series and their effect on tool life performance using analysis of variance (ANOVA) and visual statistical representations such as a Pareto ANOVA chart. The author then focuses on the types of wear encountered during tool wear assessment and the likely or potential causes in end-milling or drilling. Finally, chip morphology and observations in experiments are presented towards the end of each subsection. All images related to experiments are presented in Appendix E. Further information regarding tool life and surface roughness from all experiments is presented in Appendices F and G.

5.1 Experimental Results

Following the experiments on 6082-T6, Ti-6Al-4V, Inconel 718 and 2507, the subsequent data was collected from the end-milling and drilling operations

1. Images of worn cutting tools were obtained from experiments and were used for tool wear analysis (Appendix E).
2. Cut chips were collected throughout experiments for analysis.
3. Data obtained from experiments based on tool life (average distance machined, or average number of holes drilled), were used in statistical analysis to identify and evaluate the importance of geometrical factors.
4. Additional data, such as surface roughness, have been presented in appendices G-J for reference.

Tool wear analysis process, based on the ISO 8688-2:1989 [151] and ISO 3685:1993 [155] was followed thoroughly during the end-milling and drilling experiments, respectively. Images of flank wear on worn cutting tools were captured and used to conclude the end of experiments. Tool wear images of cutting edges (CE) for end-mills and drills were captured and later measured using the tool maker's optical microscope (section 4.3.1) during analysis. Tool wear across each flute was monitored and measured once the tool wear criteria was reached. Worn cutting tool images were tabulated and were assigned by their experimental I.D. for reference, with each flute allocated as cutting edge 1 (CE1), cutting edge 2 (CE2) etc. for comparison (Appendix E). The same procedure was followed for all drilling experiments

with the additional images of the drill point for chisel wear analysis. Further details regarding tool wear criteria for end-mills and drills is detailed in section 4.3.1. It should be noted that the author was unable to reach the tool wear criteria set for end-mills and drills when evaluating the machinability of 6082-T6. This was caused by two factors; the first being the limitations of the CNC machine and its capabilities to reach higher RPMs to accelerate tool wear further, and the second, the limitations in the amount of workpiece material required to encourage tool wear with the second factor was mainly due to budget allocated for workpiece materials as it could not be exceeded. In several experiments cutting tools designed for the difficult-to-cut materials could not reach the tool wear criteria as chipping had occurred on the cutting edges. This was a criterion which was set by the author in the methodology where severe chipping was considered as the end of the experiment. Where it was believed that the external factors were the cause of early tool failure, the author repeated the experiments to eliminate the assumption.

Statistical analysis was used to transform the raw data from the experiments into useful information for analysis. Analysis of variance (ANOVA) was adopted and applied to determine the significance of geometrical parameters based on the results obtained on tool life (total distance milled, or the number of holes drilled). The results from ANOVA provided information on the degrees of freedom (DF), adjusted sum of squares (SS), adjusted mean squares (MS), F-value and P-value. ANOVA results provide information on:

1. Degrees of freedom (DF): the total number of independent pieces of information contributing to the component of variation, minus the number of pieces required to measure it [156]. The value is determined by the number of experiments conducted for each series.
2. Adjusted sum of squares (SS): when conducting ANOVA, the total sum of squares expresses the total variation that can be allocated from various geometrical factors. The adjusted SS are measures of variation for different components of the model in the experiments.
3. Adjusted mean squares (MS): in ANOVA, mean squares are used to determine whether the geometrical parameters in the experiments were conducted are significant.
4. F-value: used in analysis of variance, calculated by dividing two mean squares. The ratio of explained variance to unexplained variance is determined through this calculation. Use of the value helps determine whether the results obtained from the roughing and finishing experiments are statistically significant [157]. In other words, higher F-value determines whether a factor is significant.

5. P-value: strength of evidence for an effect [156], or in this case, the geometrical parameters. A significant effect has a low P-value (P<0.05). By default, this value is set at α = 0.05. The significance value is determined by ANOVA results obtained from both experiments.

All data obtained from the experiments were collected and processed through a normality test (Anderson-Darling) using a statistical analysis software to determine whether the sample data obtained is normally distributed. This is particularly important to ensure that the assumption for ANOVA are not violated. Doncaster and Davey [156] describe ANOVA as an analysis of the relative contributions of explained and unexplained sources of variance in a continuous response, or in other words, variable balanced designs with categorical factors. ANOVA was conducted on the different geometrical parameters at different levels to determine the effect of parameters and their interactions. Several informative visual representations obtained through ANOVA were produced in the form of main effect plots, Pareto charts and probability charts. ANOVA results and their details are tabulated to back the visual representations produced. Please see Appendices F-H for more details.

All results were standardised for evaluation during analysis and were used to produce a visual representation of the factors and their interactions. In the majority of cases a Box-Cox transformation was carried out for the response data (tool life or surface roughness) if the residuals are not normally distributed or do not have constant variance. A better visual representation of ANOVA is the use of Pareto charts to determine the magnitude and the importance of the effects. On the Pareto chart, bars that cross the dotted reference line are statistically significant. The use of John Tukey's box plot was also adopted as another form of graphical tool for better visualisation of the data obtained from end-milling and drilling experiments. The box plot is considered a useful and powerful tool for displaying data obtained from tool for graphical representation of information because it is simple to construct yet easy to understand as it yields a lot of information. The use of box plots allows for the summarisation of the most important statistical characteristics of a frequency distribution for easy understating and comparison [158,159].

The author collected chip samples at the first pass and the final pass in end-milling experiments and repeated the procedure for the drilled, where samples of the first and last hole drilled were collected and recorded. Images of cut chips were taken using the LEICA M205 C stated in section 4.3.1. The shape of the chips collected at the beginning and the end of experiments were compared to each other to (i) compare the shape of the chips when the cutting edges are in perfect condition versus when the cutting edges are worn and (ii) to evaluate the effect of tool geometry on chip formation.

5.2 End-mills

5.2.1 Aluminium 6082-T6

End-mills with 2-flutes and sharp cutting edges were designed and manufactured for machining hypoeutectic aluminium alloy 6082-T6 for swift chip evacuation. Out of the four selected materials chosen for this study, the author considers aluminium 6082-T6 as the least difficult-to-cut as no catastrophic failure was observed. A total of 8 cutting tools, with different geometries, were produced for end-milling study on 6082-T6. Prior to the milling experiments, three workpiece blocks were allocated for each experiment for the machinability studies and to accelerate and encourage tool wear on the cutting edges when machining. Each tool machined a total of 99.45 m (33.15 m per block) before experiments were halted and cutting tools analysed. Since tool life could not be used as a response factor to compare the performance of the cutting tools for this experimental series, the average tool wear, was instead adopted to compare the results against geometrical parameters. Please see Appendix E1 for images of all worn cutting tools from the experiments. Uniform flank wear was observed in the majority of experiments, on the cutting edges of the cutting tools, such as the example shown in Fig. 47.

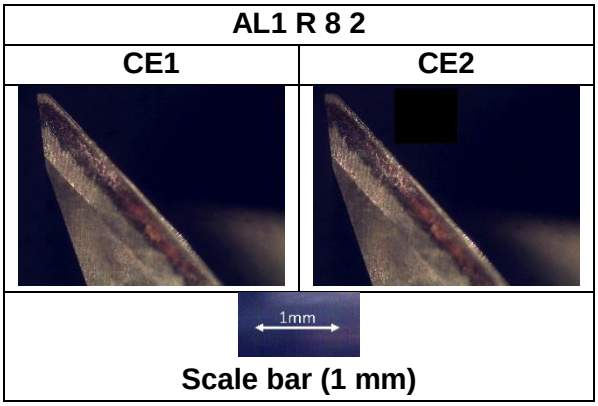

Fig. 47: Typical tool wear on cutting edges in machining of 6082-T6

Chipping was observed on three cutting tools during tool wear analysis. Fig. 48 provides examples where chipping was observed in end-milling of 6082-T6. Experiments AL1 R 8 7 and AL1 R 8 8 were designed with radial rake angles of 20° which provided a very sharp cutting edge, at the cost of a weaker cutting edge, making the cutting edges more likely to chip at the tip of the cutting tools. No signs of BUE or other major types of wear were found on the cutting edges of the 2-flute end-mills for aluminium 6082-T6. Cutting tool wear measurements from this experimental series and has been presented in Fig. 49. Analysis into the surface roughness showed that cutting tools with a lower helix angle of 45° provided better surface finish compared to higher helix angle of 55° Fig. 153. The average surface roughness of experiments 1-4 were around 2 *Ra* (±10%). Whereas experiment 5-8 varied enormously in

average surface finish producing results from 1.042 *Ra* to as high as 9.075 *Ra* (Fig. 153). However, on average, a slightly lower tool wear was observed on cutting tools with helix angle of 55°.

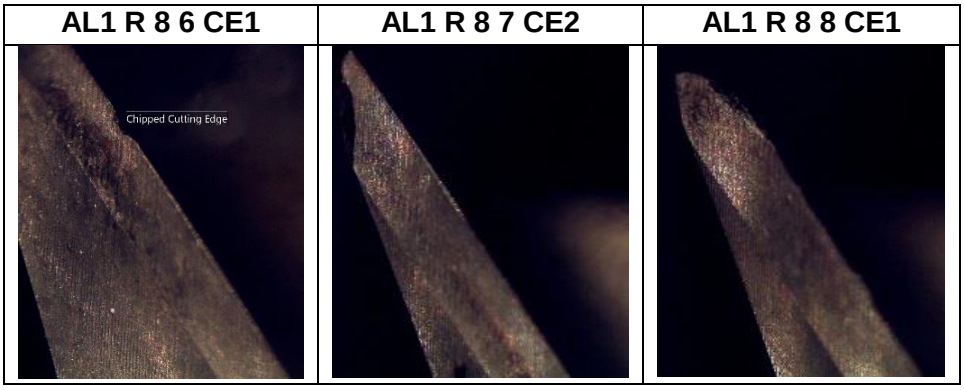

Fig. 48: Examples of chipping on flutes in end-milling experiments of 6082-T6

Results based on tool life could not be obtained in end-milling of 6082-T6 due to the factors which the author explained in 5.1. Instead, the author assigned a set tool life for each experiment and analysed the tool wear based on the geometrical differences in each experiment. Box plots based on the interaction between geometrical factors were produced to summarise the distribution of the data, central tendency and variability. As shown in Fig. 50-Fig. 52 the data is normally distributed because of even distance at the inter-quartile range. However, further experiments and analysis to be able to conclude the best geometry of the 2-flute end-mills for 6082T6.

A visual representation of the effect of geometrical parameters at different levels, based on tool wear has been presented in the form of a main effects plot (Fig. 54). The plot indicates that on average high helix angle in combination with high radial rake angle and radial primary clearance produce lower tool wear (4-11 μm difference). To support the significance of the geometrical parameters in main effects plot, ANOVA was carried out on each factor as well as their interactions. A Pareto ANOVA chart based on the effects of the geometrical parameters with tool wear as the response output was produced. On the Pareto chart, bars that cross the dotted reference line are statistically significant. However, in Fig. 53, the bars that represent geometrical factors, do not cross the reference line that is at 12.71. Based on the results obtained from the end-milling experiments on 6082-T6, no significance between geometrical factors or their interactions were observed during analysis. These factors are statistically insignificant at the 0.05 level with the current model terms. The Pareto chart has been expanded in Table 17 where the P-value (significance) of each geometrical parameter and their interactions are listed to support the Pareto ANOVA.

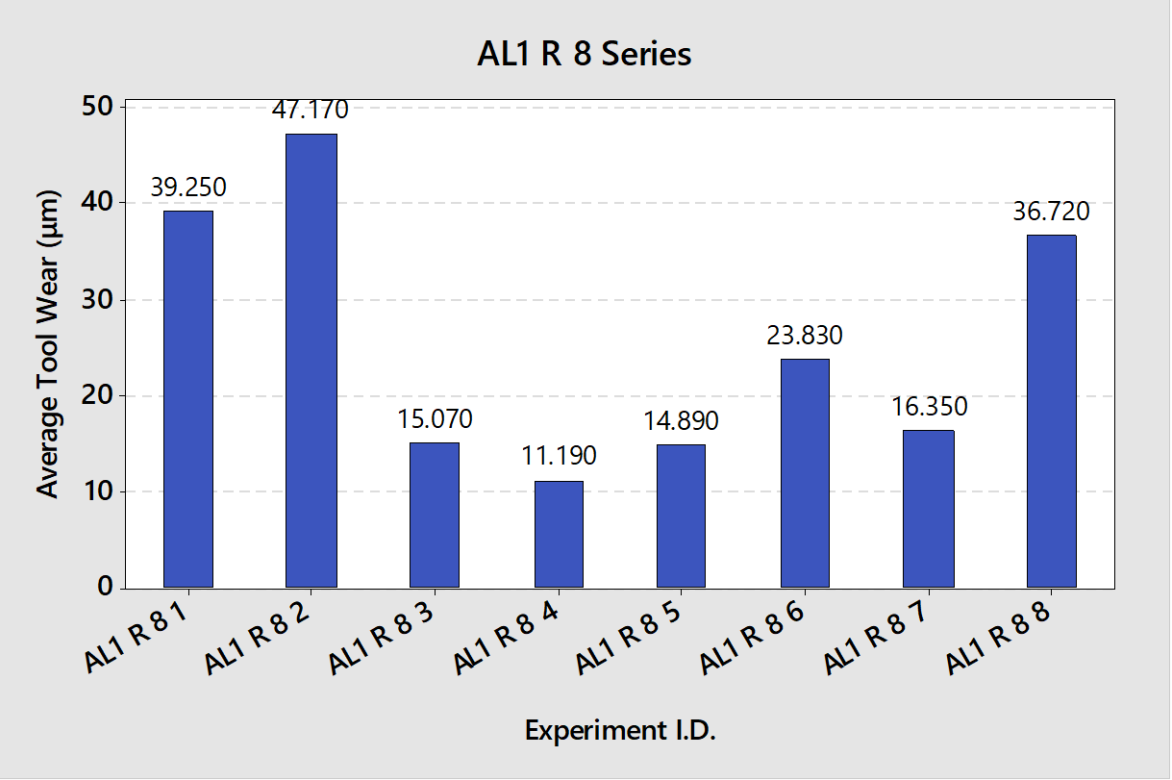

Fig. 49: Cutting tool wear measurements from end-milling experiments on 6082-T6

Table 17: Analysis of variance for trnaformed response (tool life) in end-milling of 6082-T6

Parameters	(DF)	Adj (SS)	Adj (MS)	F-value	P-value
Model	6	11.7844	1.96407	3.45	0.390
Linear	3	4.0727	1.35756	2.39	0.436
Helix angle (A)	1	0.2875	0.28751	0.51	0.607
Radial rake angle (B)	1	2.5799	2.57986	4.54	0.279
Radial primary clearance angle (C)	1	1.2053	1.20530	2.12	0.383
Two-way Interactions	3	7.7117	2.57057	4.52	0.330
A*B	1	6.6043	6.60431	11.61	0.182
A*C	1	1.1047	1.10472	1.94	0.396
B*C	1	0.0027	0.00269	0.00	0.956
Error	1	0.5689	0.56886	-	-
Total	7	12.3532	-	-	-

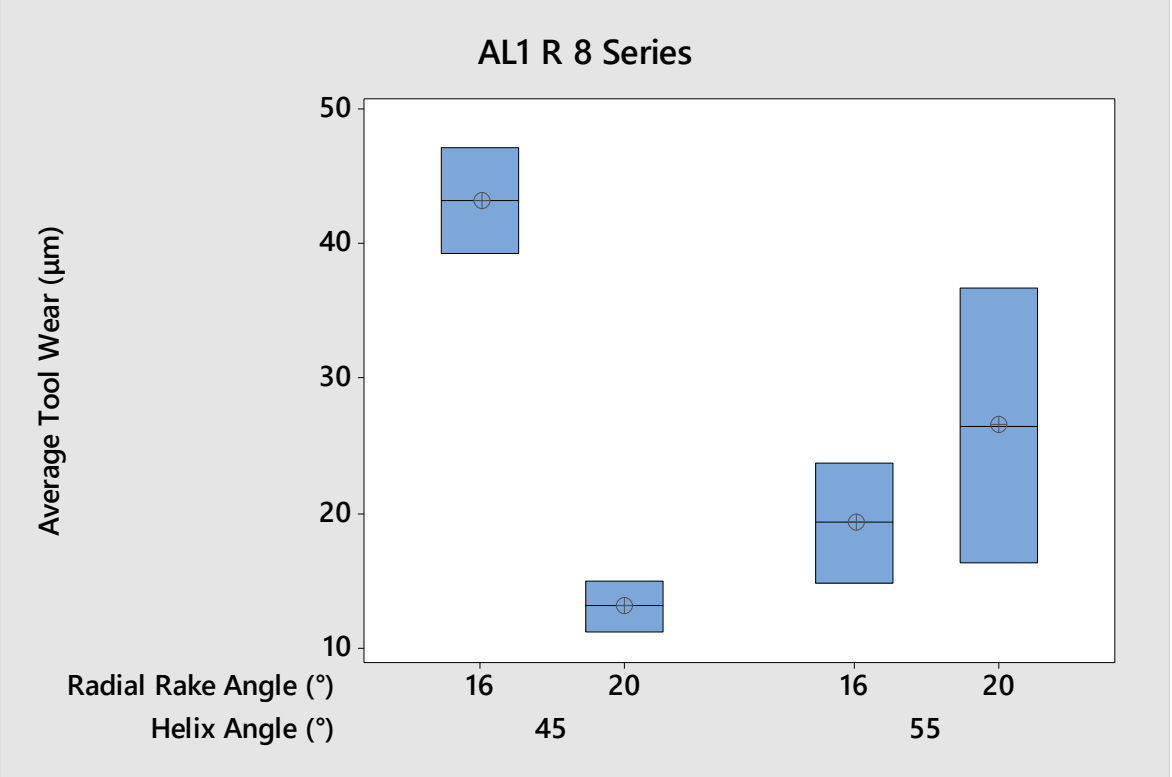

Fig. 50: Box plot of interactions between helix angle and radial rake angle of 2-flute end-mills based on the average tool wear results obtained from experiments on 6082-T6

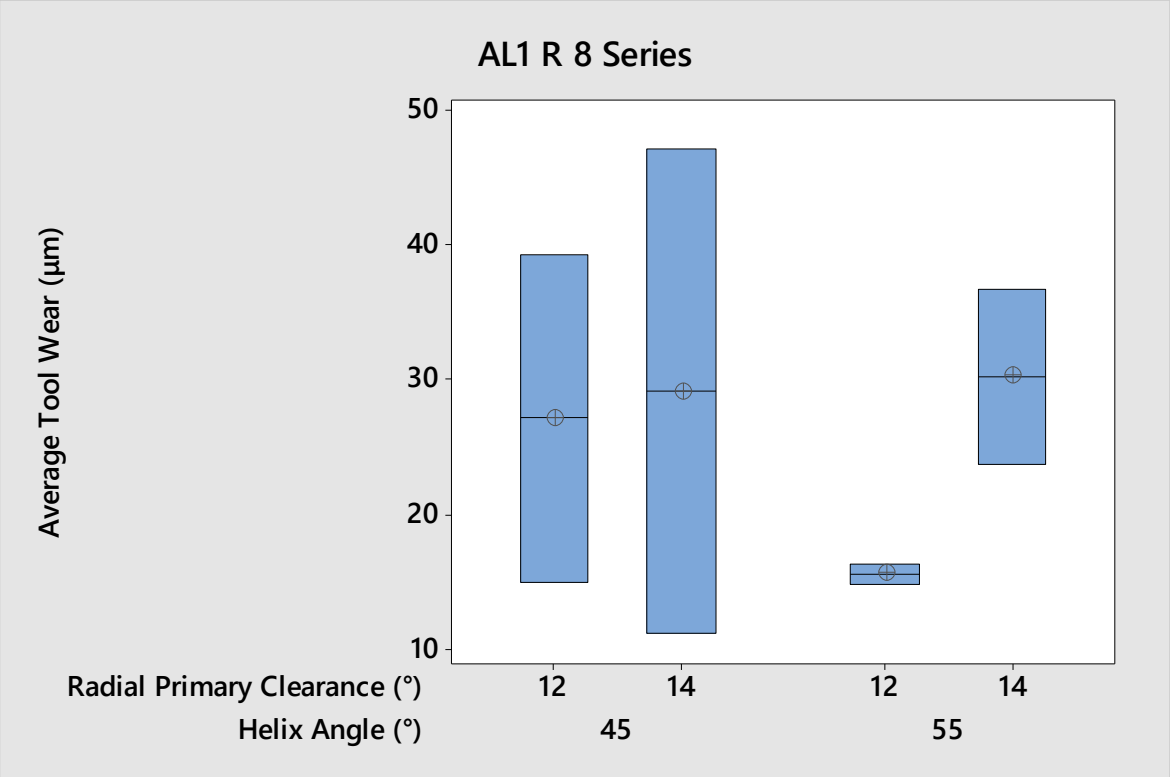

Fig. 51: Box plot of interactions between helix angle and radial primary clearance angle of 2-flute end-mills based on the average tool wear results obtained from experiments on 6082-T6

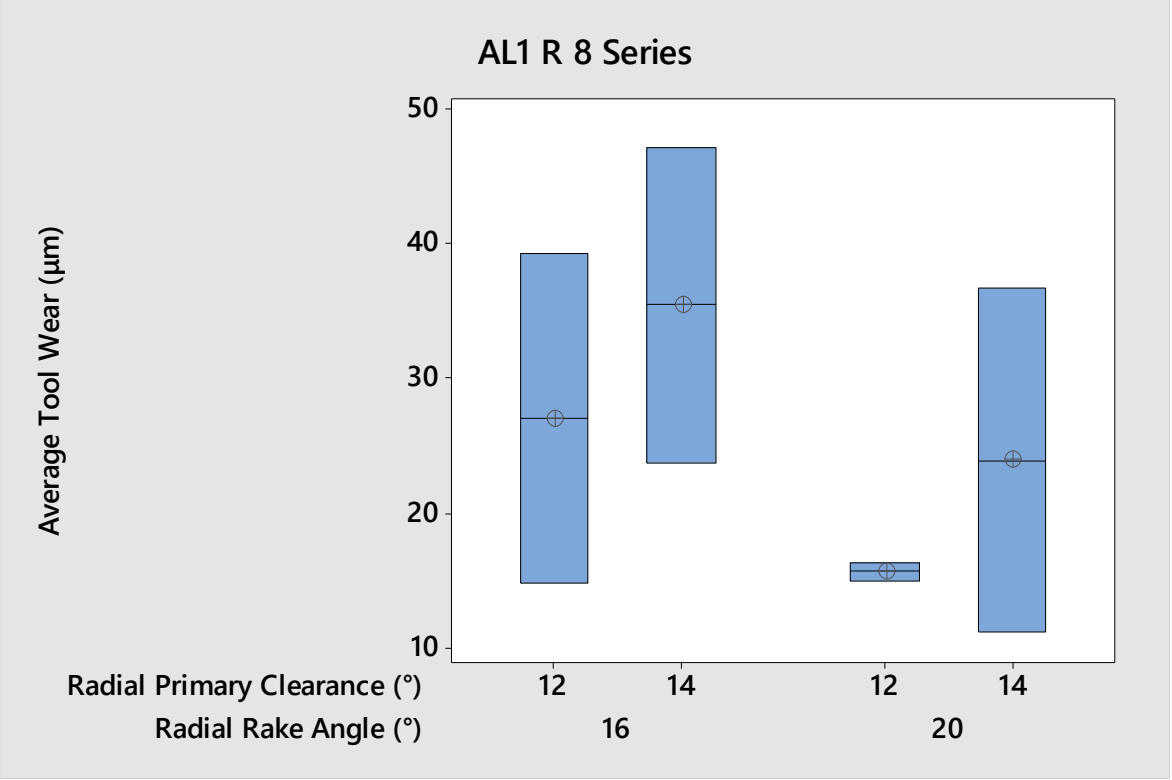

Fig. 52: Box plot of interactions between radial rake angle and radial primary clearance angle of 2-flute end-mills based on the average tool wear results obtained from experiments on 6082-T6

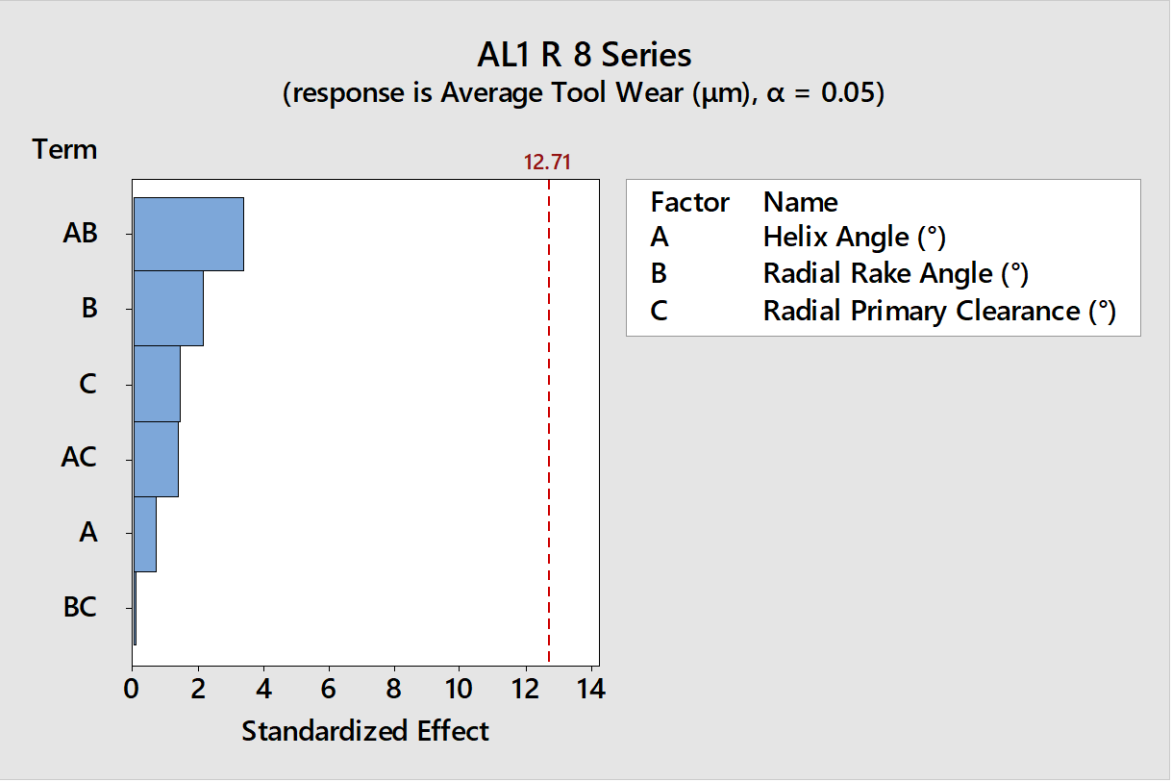

Fig. 53: Pareto ANOVA of geometrical parameters in end-milling of 6082-T6

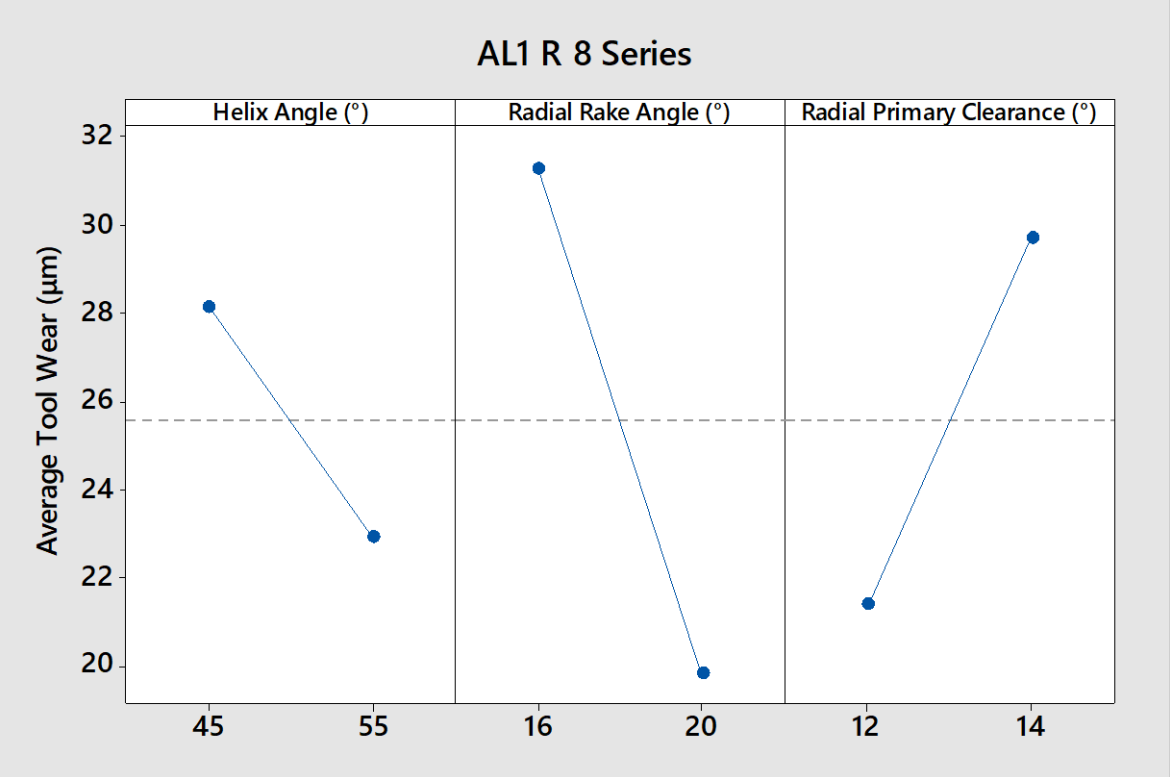

Fig. 54: Main effects plot of average tool wear in end-milling of 6082-T6 using the selected geometrical paramters presented in the plot

Cut chips were collected at the beginning and the end of each experiment for chip morphology. Fig. 55 and Fig. 56 show example of chips collected from two separate experiments, AL1 R 8 2 and AL1 R 8 5. In the case of Fig. 55, the saw-tooth edge is not as pronounced as Fig. 56. These figures also show that when comparing an unworn and worn tool (a) and (b), respectively, there is a negligible difference between the segmentation of a worn and unworn cutting tool.

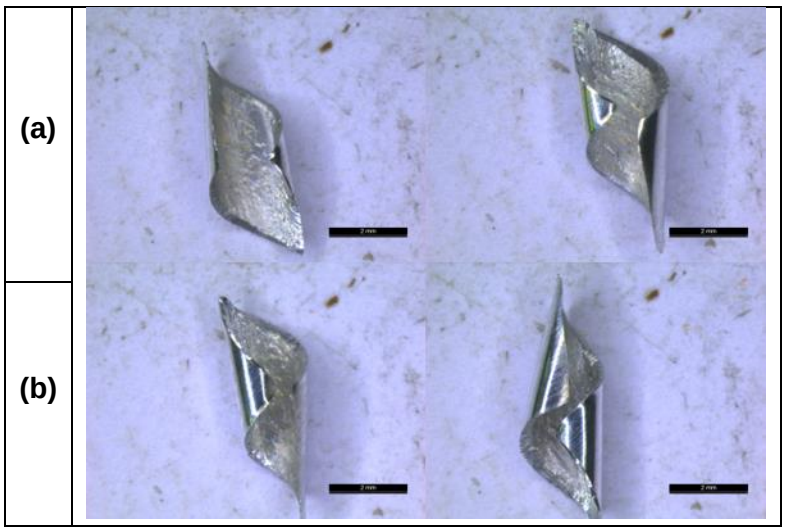

Fig. 55: Chips obtained from AL1 R 8 2 end-milling 6082-T6 - (a) chips collected after the first pass, (b) chips collected after the final pass

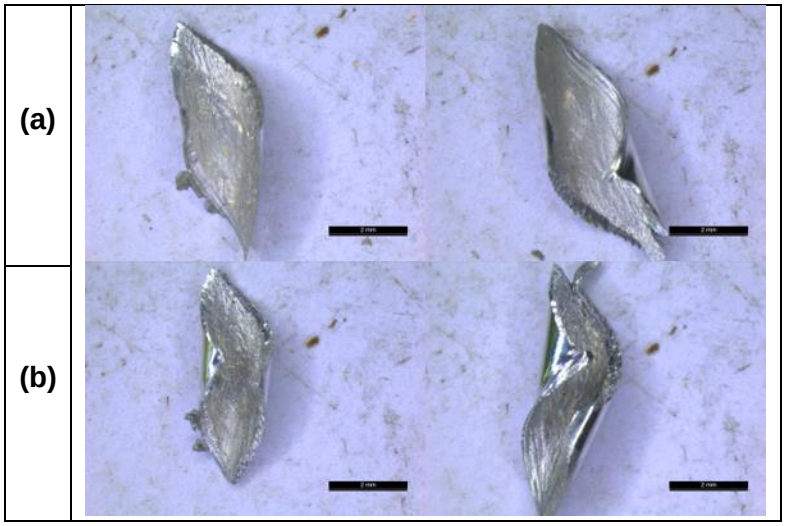

Fig. 56: Chips obtained from AL1 R 8 5 end-milling 6082-T6 - (a) chips collected after the first pass, (b) chips collected after the final pass

5.2.2 Ti-6Al-4V

Two series of experiments were completed on end-milling titanium alloy Ti-6Al-4V evaluating the effect of geometrical parameters such as helix angle, radial rake angle, radial primary and radial secondary clearance angles. The first series of experiments were conducted using 4-flute end-mills to assess their performance based on tool life. The roughing series comprised of 24 experiments along with replicates, denoted as (Rep). The second series of experiments proposed for end-milling Ti-6Al-4V, assessed the performance of 6-flute end-mills in a finishing operation where the RDoC and ADoC varied from the experiments on 4-flute end-mills. A total of 8 tools with replicates were produced and tested to collect data on tool life and wall surface roughness. Tool life, measured in millimetres, were allocated as the output response to assess the effect of factors in this study in both end-milling series. Fig. 146 and Fig. 147 (Appendix F) provide a summary of tool life in end-milling of Ti-6Al-4V with 4-flute and 6-flute end-mills, respectively. Tool wear and surface roughness progression was monitored throughout all end-milling experiments on Ti-6Al-4V. Tool wear measurements were taken across the cutting edge (CE) of every flute in roughing and finishing experiments on Ti-6Al-4V. An additional output parameter, surface roughness, was measured in the finishing experiments since surface roughness is a crucial factor in finishing operations. Experiments were conducted until the set tool wear criteria were reached. It should be noted that the author stopped experiments where chipping had been identified as this was allocated to be a tool wear criterion. However, no chipping was observed in the experiments on 6-flute end-mills for Ti-6Al-4V.

In the experiments carried out on 4-flute end-mills, uniform and non-uniform flank wear was identified as the most dominant type of wear in end-milling of Ti-6Al-4V. This common type of wear was observed across the length of the cutting edges (CE) on all four flutes of the cutting

tools (Fig. 57). The cause of this type of wear is the result of contact between tool material and the workpiece material, due to the tribological effect occurring at the contact point between the two materials. However, other forms of tool wear such as crater wear and notch wear, mainly caused by excessive adhesion, were also discovered throughout the tool wear analysis phase. Examples where crater and notch wear were observed during tool wear analysis have been presented in Fig. 58. The occurrence of crater wear and notch wear at the tip of cutting edges (CE) caused further difficulties in material removal of Ti-6Al-4V and the introduction of BUE on the cutting edges. The result of the combination of abrasive, adhesive and diffusion wear as well as high temperatures at the cutting zone, provided space for the workpiece particles to be deposited and to be welded onto the worn areas on the cutting edges, causing BUE. Examples of BUE are clearly visible in Fig. 57-Fig. 60. Chipping on the cutting edges was also observed in several cases where the cutting edge had deteriorated. An example has been provided in Fig. 59. Tool life results obtained from the experiments were used to produce the main effects plot shown in Fig. 61 based on the 4-flute experiments conducted. Geometrical parameters, helix angle, radial primary and radial secondary clearance angles were investigated at two levels in this series. Whereas, the radial rake angle was investigated at three levels. Radial rake angle of 14° proved to be extremely effective in providing a better performance in end-milling of Ti-6Al-4V. On average, cutting tools with a radial rake angle of 14° managed to reach a tool life in the region or excess of 14 m.

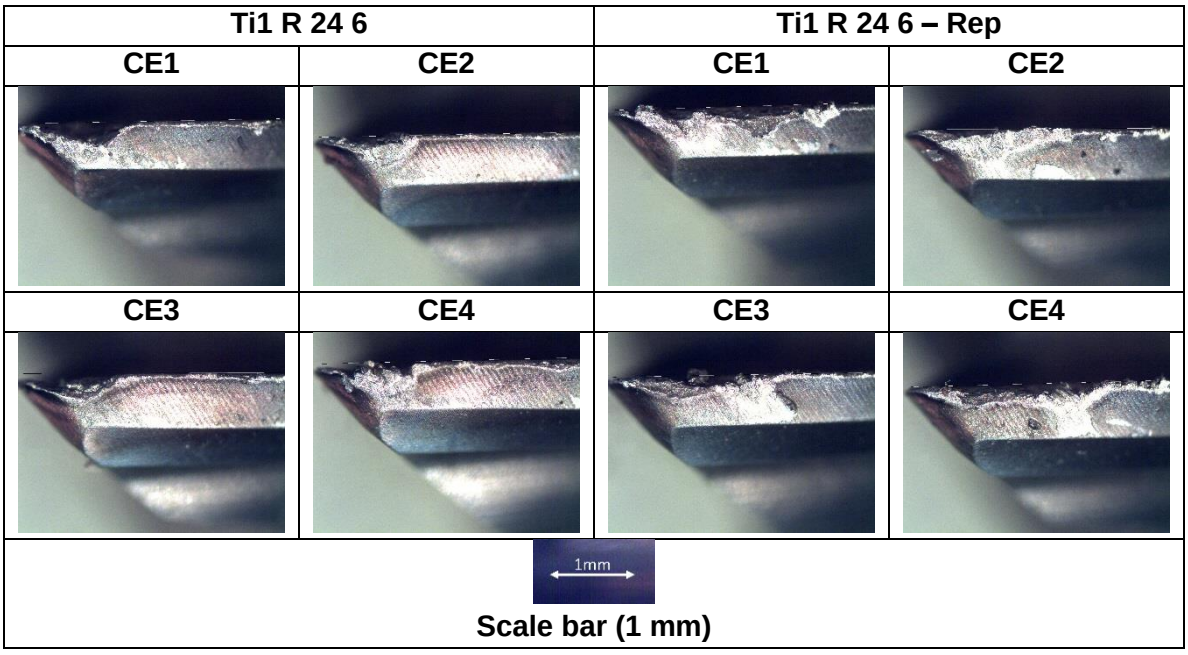

Fig. 57: An example of tool wear in end-milling of Ti-6Al-4V (4-flute end-mills)

Furthermore, the main effects plot is supported by ANOVA results obtained from the experiments. The ANOVA results showed that the radial rake angle was the most significant geometrical factors with a P-value of 0.050, with the remaining geometrical being insignificant

in causing performance enhancement in end-milling of Ti-6Al-4V. No major significance was observed between the interactions of the geometrical factors during analysis and therefore were not presented.

Table 18: Analysis of variance (N-way) obtained from 4-flute end-milling experiments on Ti-6Al-4V

Parameters	(DF)	(SS)	MS	F-value	P-value
Helix angle (A)	1	1019410	1019410	0.06	0.809
Radial rake angle (B)	2	119722000	59860800	3.55	0.050
Radial primary clearance angle (C)	1	5758380	5758380	0.34	0.566
Radial secondary clearance angle (D)	1	9103860	9103860	0.54	0.472
Error	18	303653000	303653000	-	-
Total	23	439256000	-	-	-

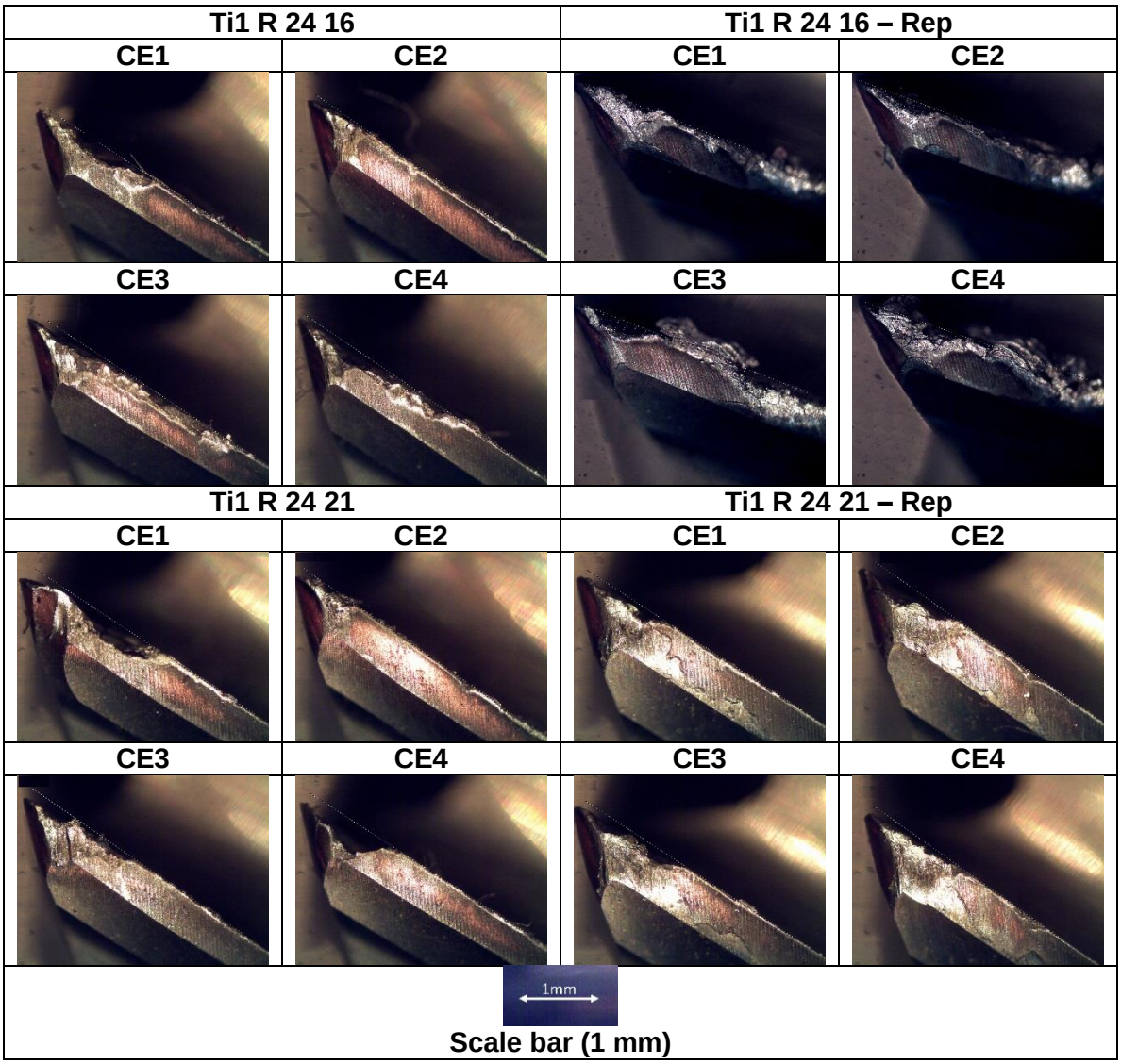

Fig. 58: Examples of extreme crater and notch wear in end-milling of Ti-6Al-4V

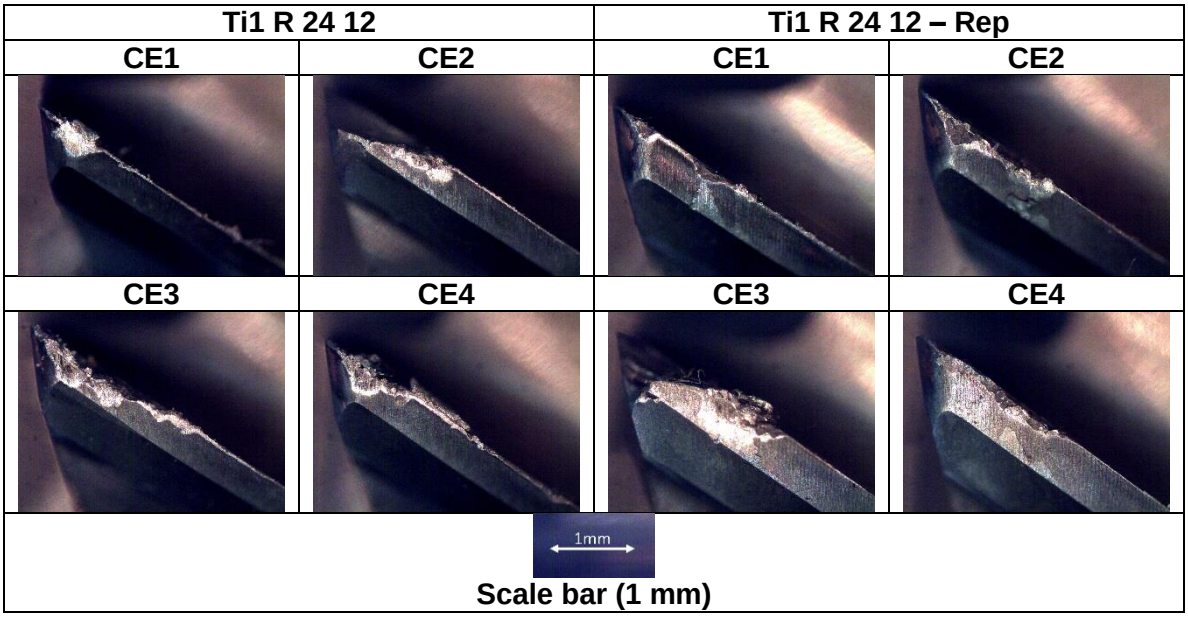

Fig. 59: An example of chipping at the corner in experiment Ti1 R 24 12

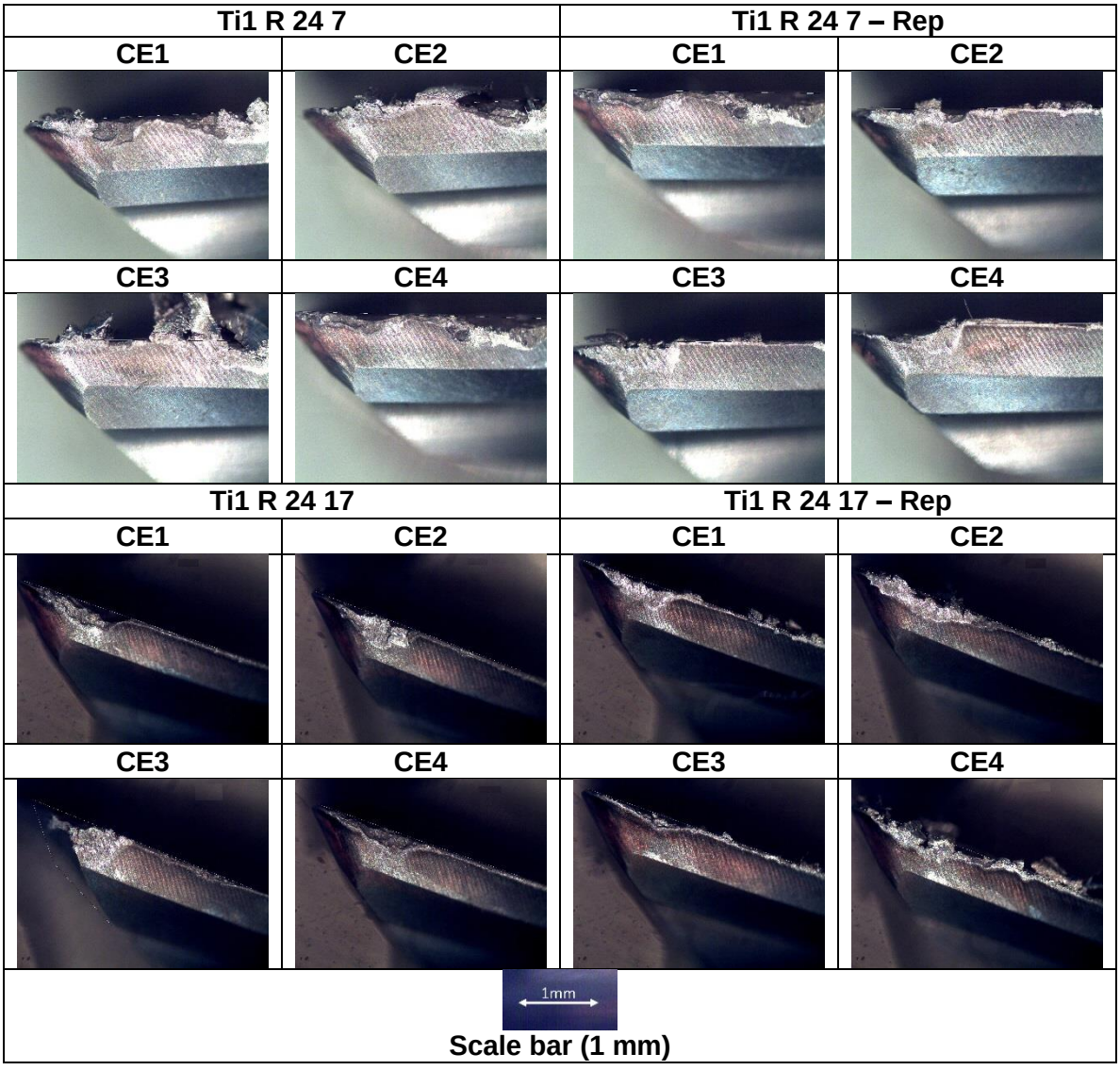

Fig. 60: Examples of occurrence of BUE in milling of Ti-6Al-4V

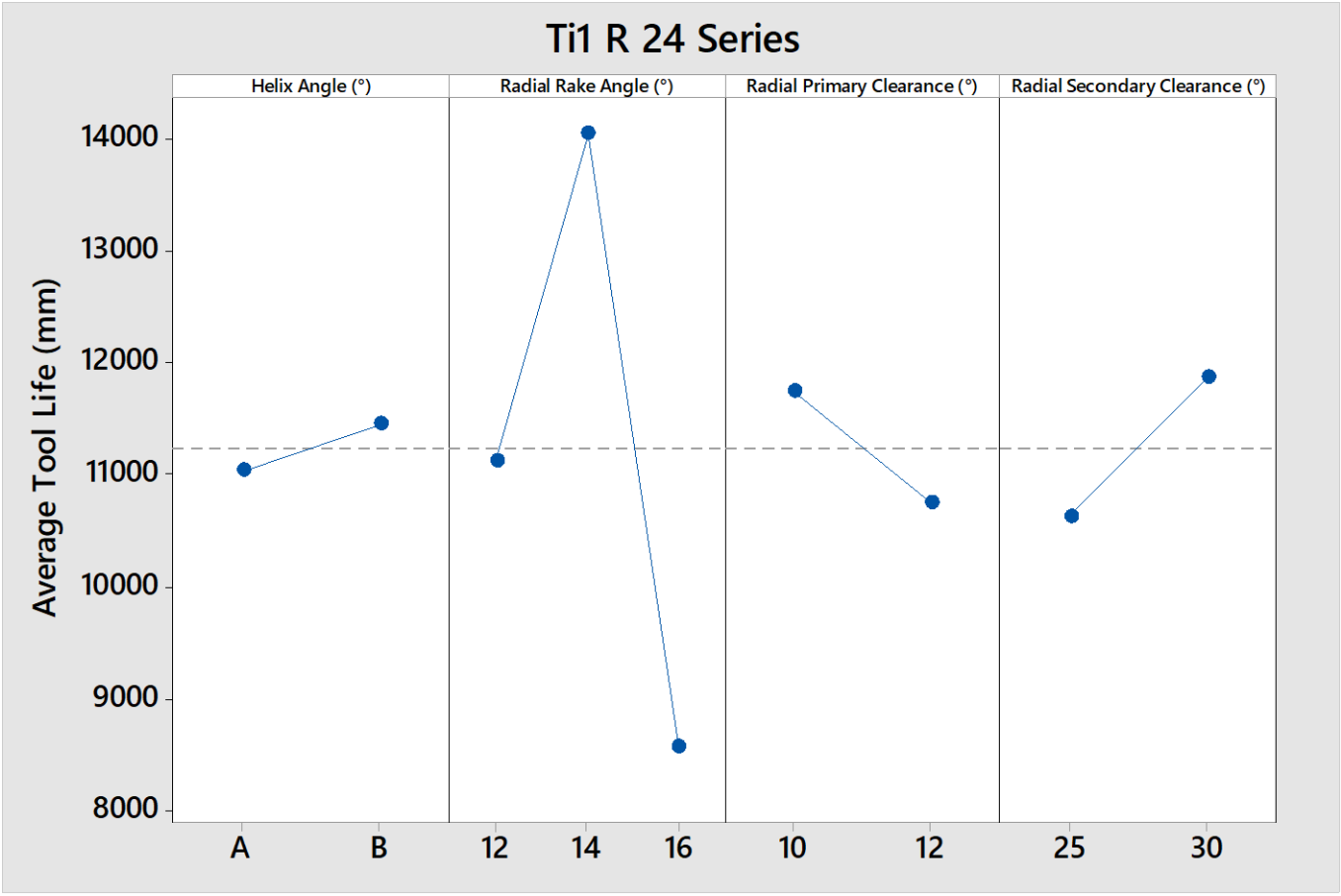

Fig. 61: Main effects plot of average tool life in end-milling of Ti-6Al-4V with 4-flute end-mills

Box plots were used once more to analyse the distribution of tool life against the interaction fo geometrical factors at different levels. No outliers were detcted in the results for this series of experiemnts. Box plots,

Fig. 62 - Fig. 67, support Fig. 61 and Table 18, showing that the radial rake angle is the most important geometrical factor with the remaining factors such as helix angle, radial primary and secondary angles as being not so significant in affecting the performance of the 4-flute end-mills when machining Ti-6Al-4V.

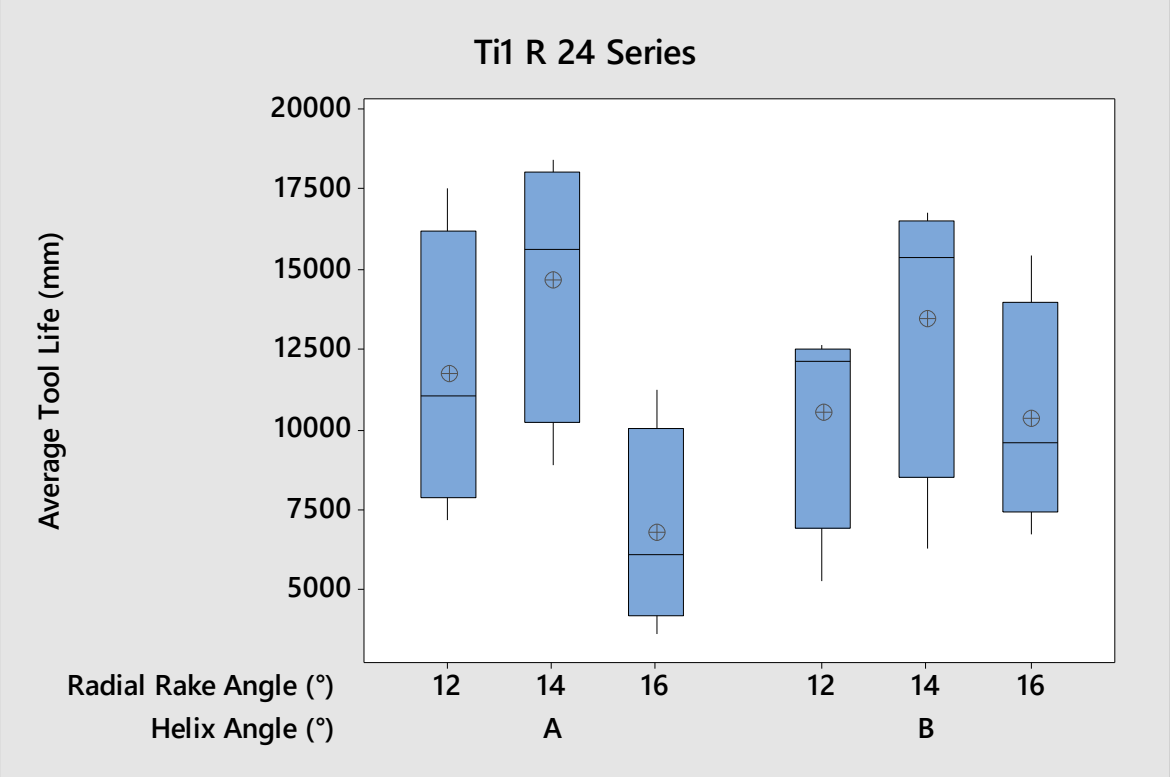

Fig. 62: Box plot of interactions between helix angle and radial rake angle at different levels based on tool life data collected from end-milling of Ti-6Al-4V using 4-flute end-mills

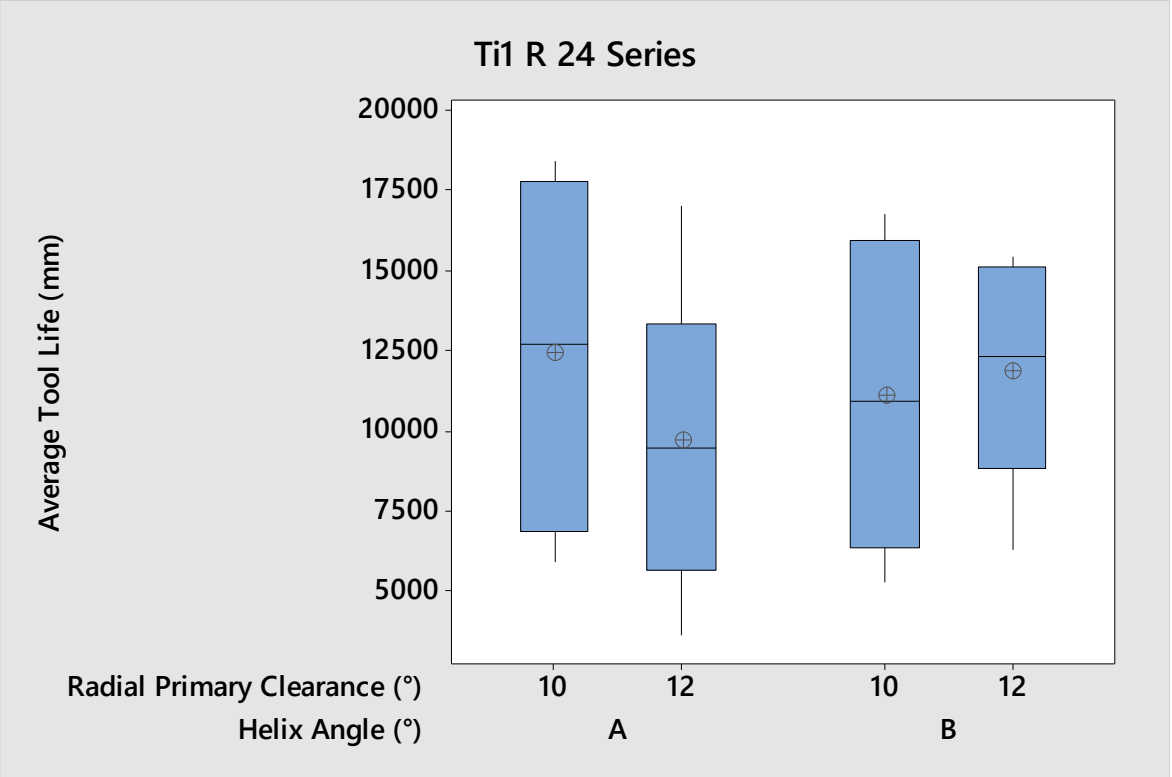

Fig. 63: Box plot of interactions between helix angle and radial primary clearance angle at different levels based on tool life data collected from end-milling of Ti-6Al-4V using 4-flute end-mills

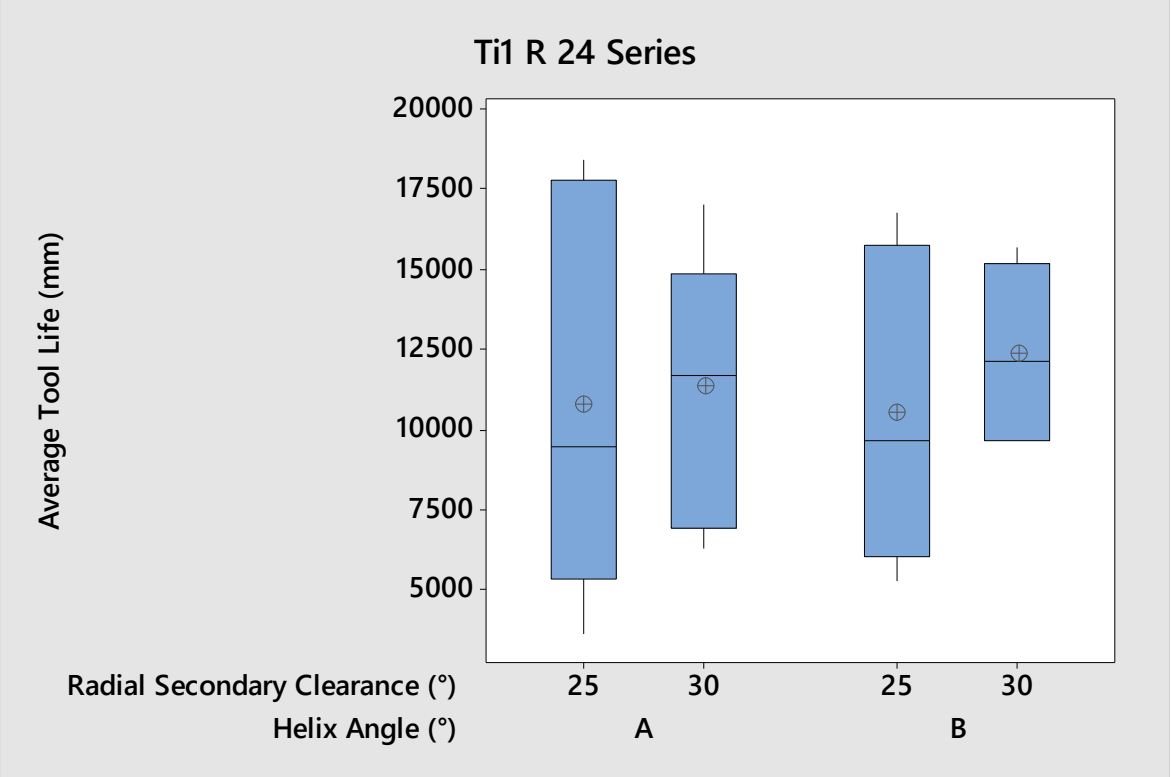

Fig. 64: Box plot of interactions between helix angle and radial secondary clearance angle at different levels based on tool life data collected from end-milling of Ti-6Al-4V using 4-flute end-mills

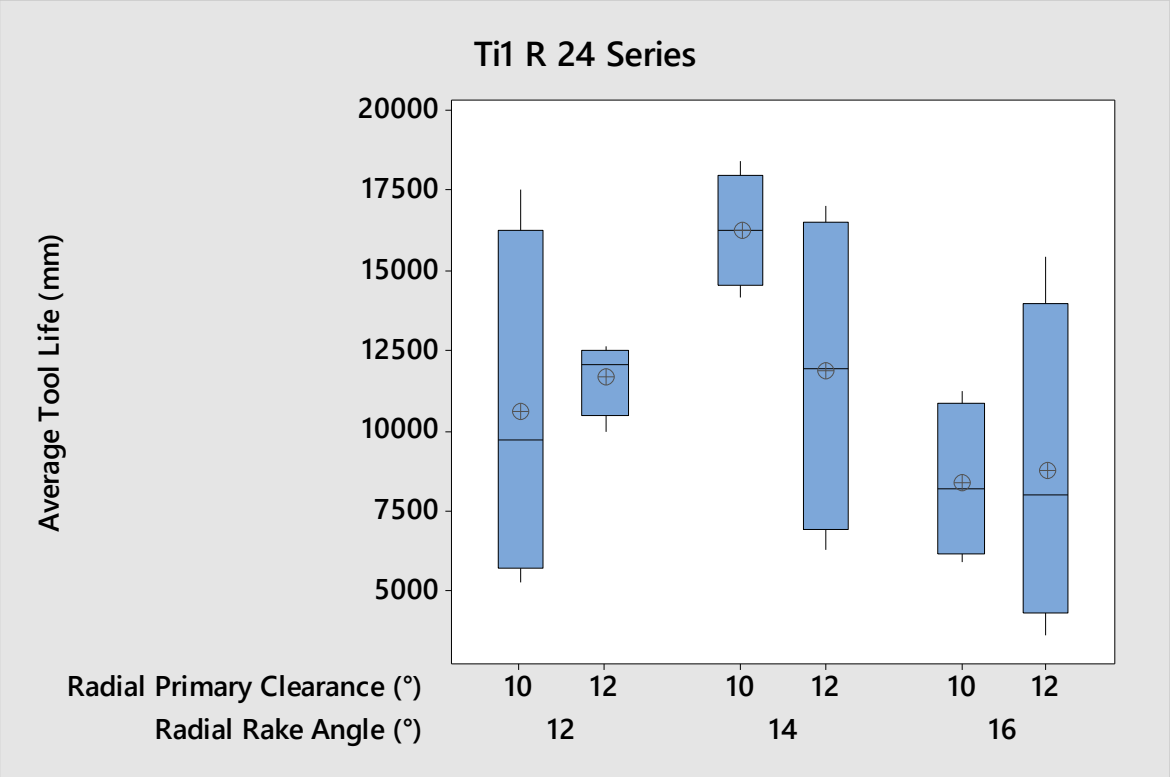

Fig. 65: Box plot of interactions between radial rake angle and radial primary clearance angle at different levels based on tool life data collected from end-milling of Ti-6Al-4V using 4-flute end-mills

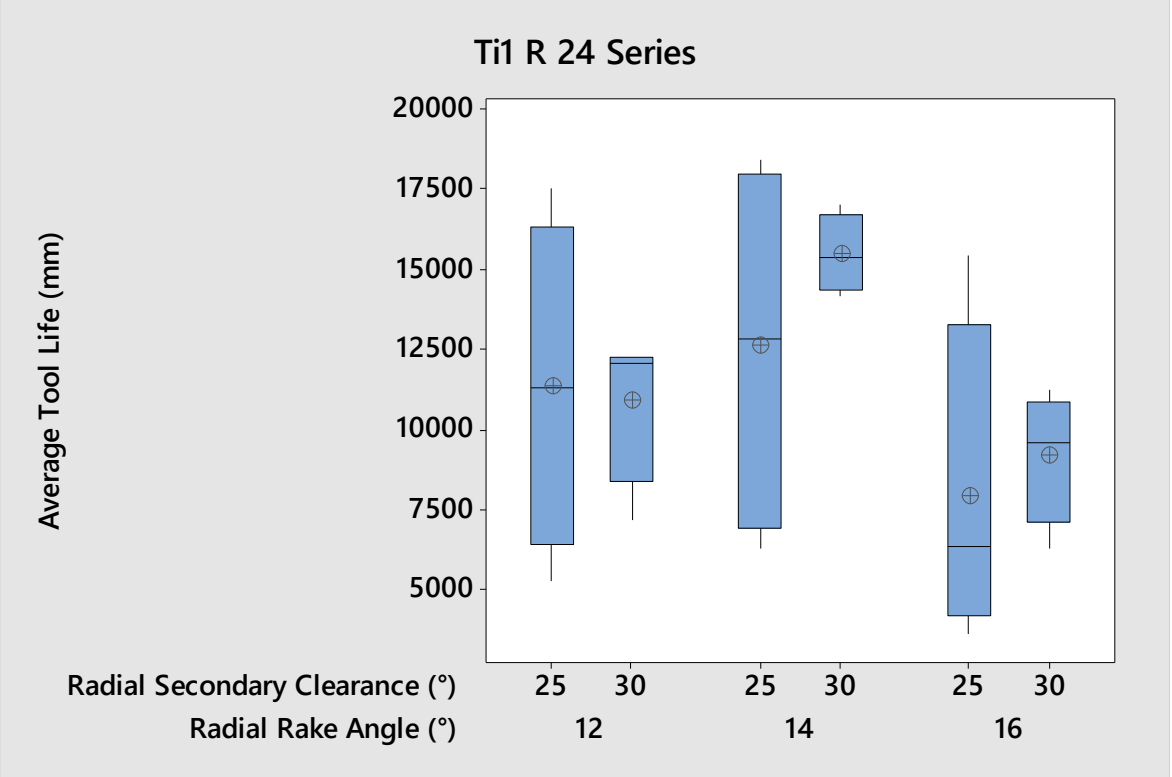

Fig. 66: Box plot of interactions between radial rake angle and radial secondary clearance angle at different levels based on tool life data collected from end-milling of Ti-6Al-4V using 4-flute end-mills

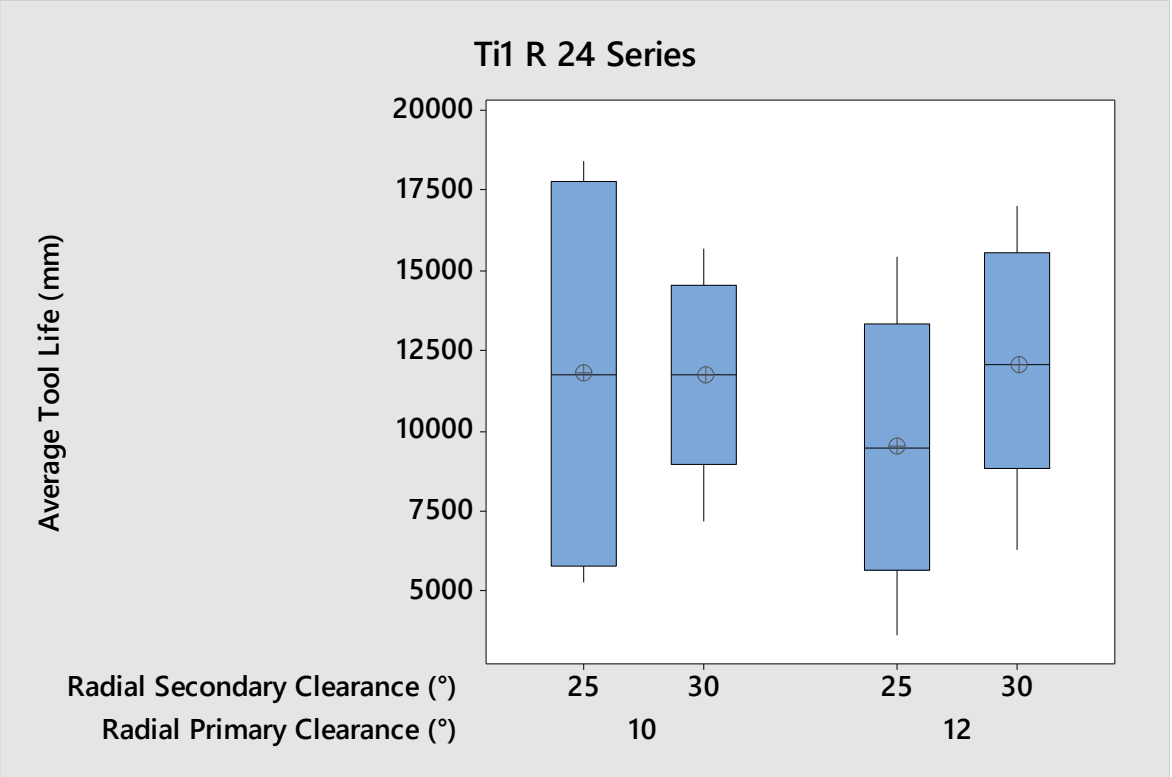

Fig. 67: Box plot of interactions between radial primary clearance angle and radial secondary clearance angle at different levels based on tool life data collected from end-milling of Ti-6Al-4V using 4-flute end-mills

A similar experimental procedure was conducted on the second series of experiments in end-milling of Ti-6Al-4V using 6-flute end-mills. Slight changes were made to the methodology for the evaluation of tool wear in this experiment as discussed earlier in 5.2.2. All experiments, along with their replicates, were conducted and data, based on tool life and wall surface roughness were collected. Results based on tool life and wall surface finish can be found in Appendices F and G. The geometrical factors experimented in this experimental series included the helix angle, radial rake angle and the radial primary clearance angle, which were tested at two levels. Previous results obtained from the 4-flute end-mills showed that a radial rake angle of 14° and a radial primary clearance angle of 10° on average gave a better performance. Therefore, the author decided to adopt the same values when experimenting in 6-flute end-mills and investigate the effects of different levels in in radial rake angle and radial primary clearance angle. Instead the author decided to explore higher helix angles such as 40° and 45°.

Uniform flank wear was identified as the dominant tool wear across all cutting edges and along the 20 mm depth of cut. However, BUE was identified during and after completion of the experiments (Fig. 68 and Fig. 76). Over time as the tool wear progressed, tool material particles detached and separated from the surface of the cutting tool causing further tool deterioration and providing more room for workpiece materials to weld onto the cutting edges. Chipping had also occurred in some experiments but mainly dominating the tip of the cutting edges (Fig. 75). Flank wear is caused by abrasion due to contact between the cutting edge and the workpiece, as tool wear progressed on the cutting edges of the end-mills, the workpiece surface finish became worse; indicating that the cutting tool has lost its integrity at the periphery and is unable to continue machining.

However, additional forms of tool wear such as crater wear and notch wear, mainly caused by excessive abrasion and adhesion, were not discovered throughout the tool wear analysis phase. Abrasive wear remained as the main cause of tool wear throughout the analysis phase on 6-flute end-mills. As a result of abrasive wear, increased BUE was encountered across the cutting edges of the end-mills. In the case of experiment Ti1 F 8 8, different forms of BUE were experienced. The first cutting tool used for experiment Ti1 F 8 8, exhibited small particles of titanium on the cutting edges CE1, CE3, CE4, CE5 and CE6. In the same experiment, the replicated cutting tool displayed long, thin strands of Ti-6Al-4V, welded onto the worn cutting edges. Signs of BUE are clearly visible in Fig. 68.

The ANOVA results in Table 19 support the Pareto ANOVA chart (Fig. 69) providing compelling evidence that factors, helix angle and radial primary clearance angle, are significant enough to affect tool life. With P-values of 0.020 and 0.022, respectively, the helix angle and the radial primary clearance angles support the visual representations of the main

effects plot of tool life (Fig. 70) in this set of experiments. Interactions between geometrical factors did not show a significance effect on the performance of the cutting tools. With regards to the finishing experiment, experiment 7 (Ti F 8 7) produced the best tool life, with an average of 30732.47 mm achieved. On average, cutting tools with a higher helix angle produced better surface finish (Fig. 71) and outperformed tools with lower helix angle of 40°. Using the John Tukey's box plots the distribution of data the interaction between geometrical factors based on tool life (measured in millimetres) were produced, Fig. 72 - Fig. 74. The normally distributed data from Fig. 73 shows that the helix angle and the radial primary clearance angles are significant with 45° helix and 10° radial primary clearances angles giving the best interquartile range. The radial rake angle seemed to be quite negligible in this series of experiments.

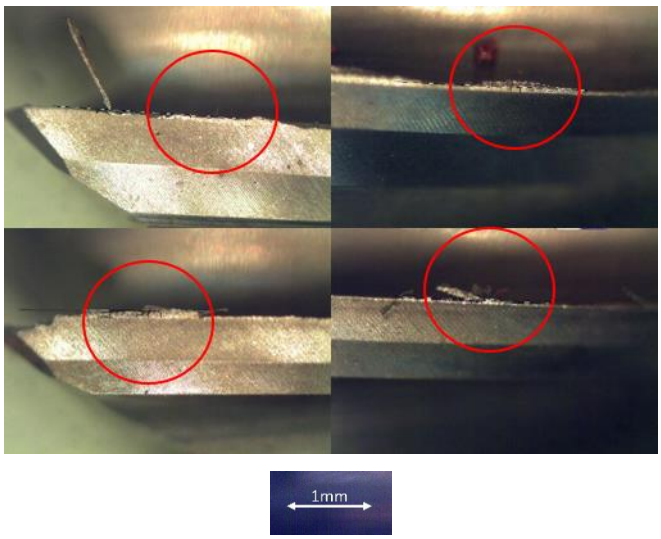

Scale bar (1 mm)

Fig. 68: Examples of BUE in the cutting edges of the end-mills during experiments

Table 19: Analysis of variance for transformed response of tool life in end-milling of Ti-6Al-4V

Parameters	(DF)	Adj (SS)	Adj (MS)	F-value	P-value
Source	6	17353.3	2892.21	330.23	0.042
Linear	3	16534.4	5511.47	629.29	0.029
Helix angle (A)	1	9010.8	9010.75	1028.84	0.020
Radial rake angle (B)	1	15.0	14.99	1.71	0.415
Radial primary clearance angle (C)	1	7508.7	7508.67	857.33	0.022
Two-way interactions	3	818.9	272.96	31.17	0.131
A*B	1	377.3	377.27	43.08	0.096
A*C	1	11.4	11.37	1.30	0.459
B*C	1	430.2	430.24	49.12	0.090
Error	1	8.8	8.76	-	-
Total	7	17362.0	-	-	-

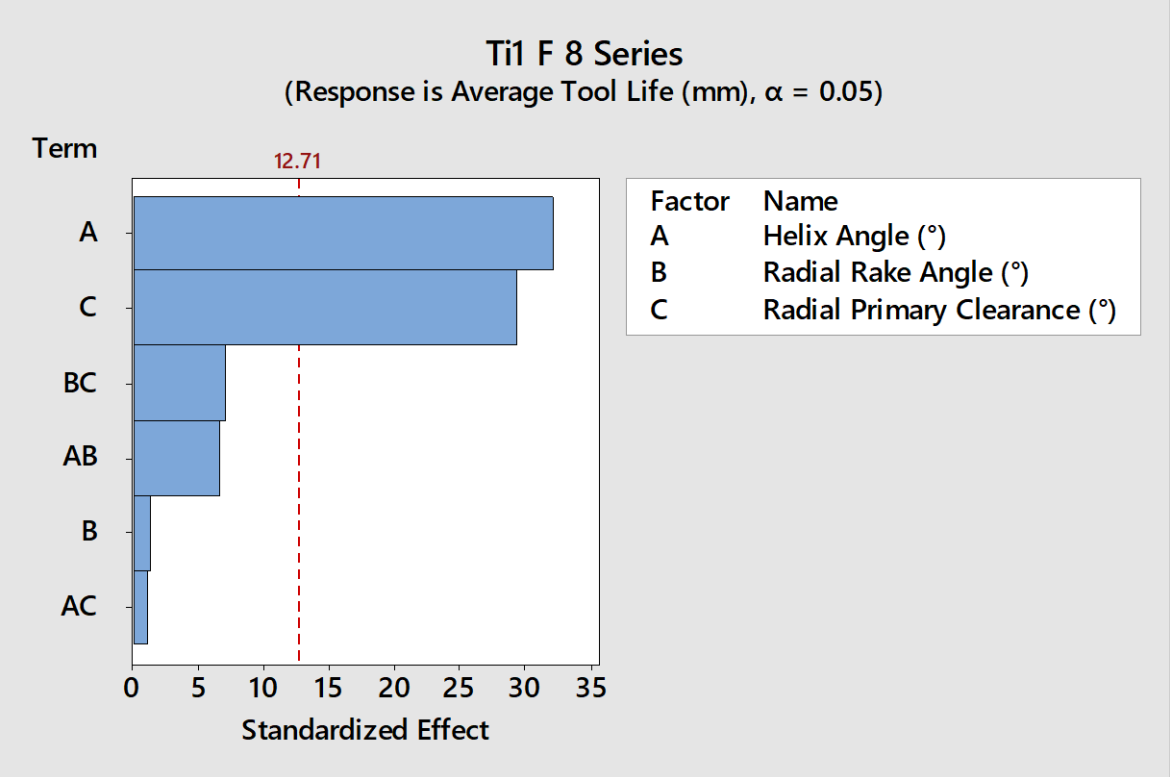

Fig. 69: Pareto chart of the effect of geometrical factors on tool life in end-milling of Ti-6Al-4V

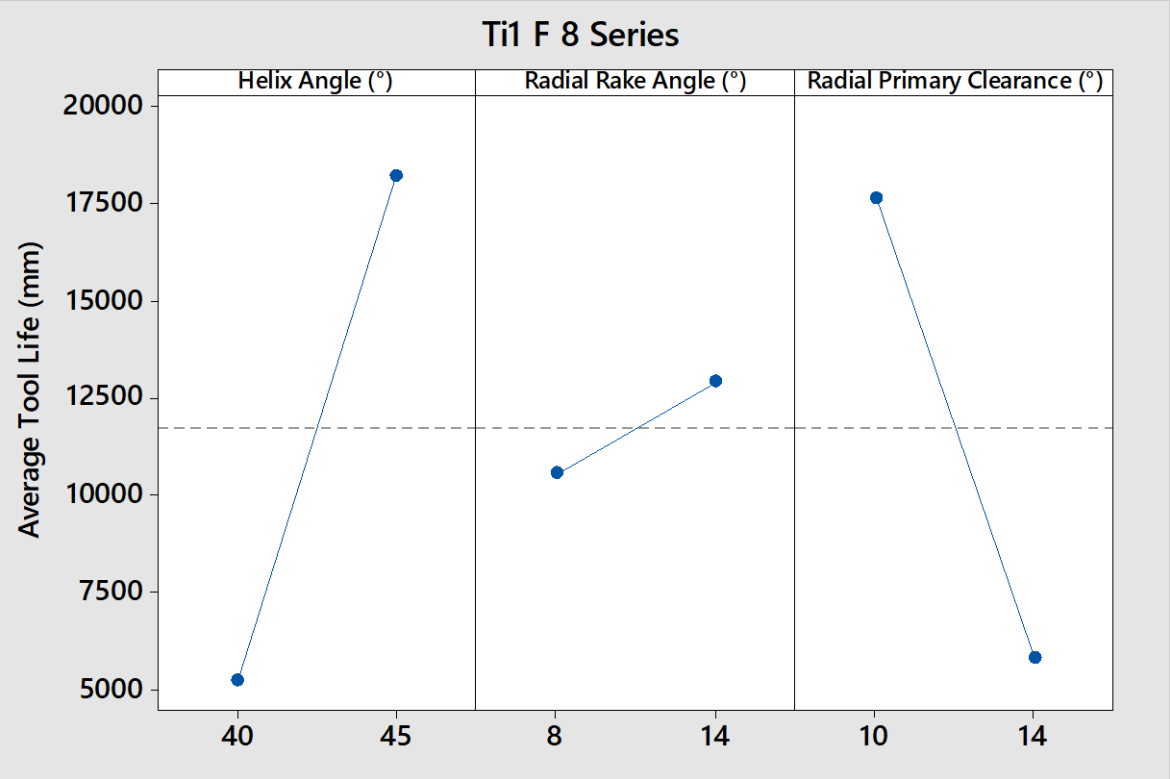

Fig. 70: Main effects plot of average tool life in end-milling of Ti-6Al-4V with 6-flute end-mills

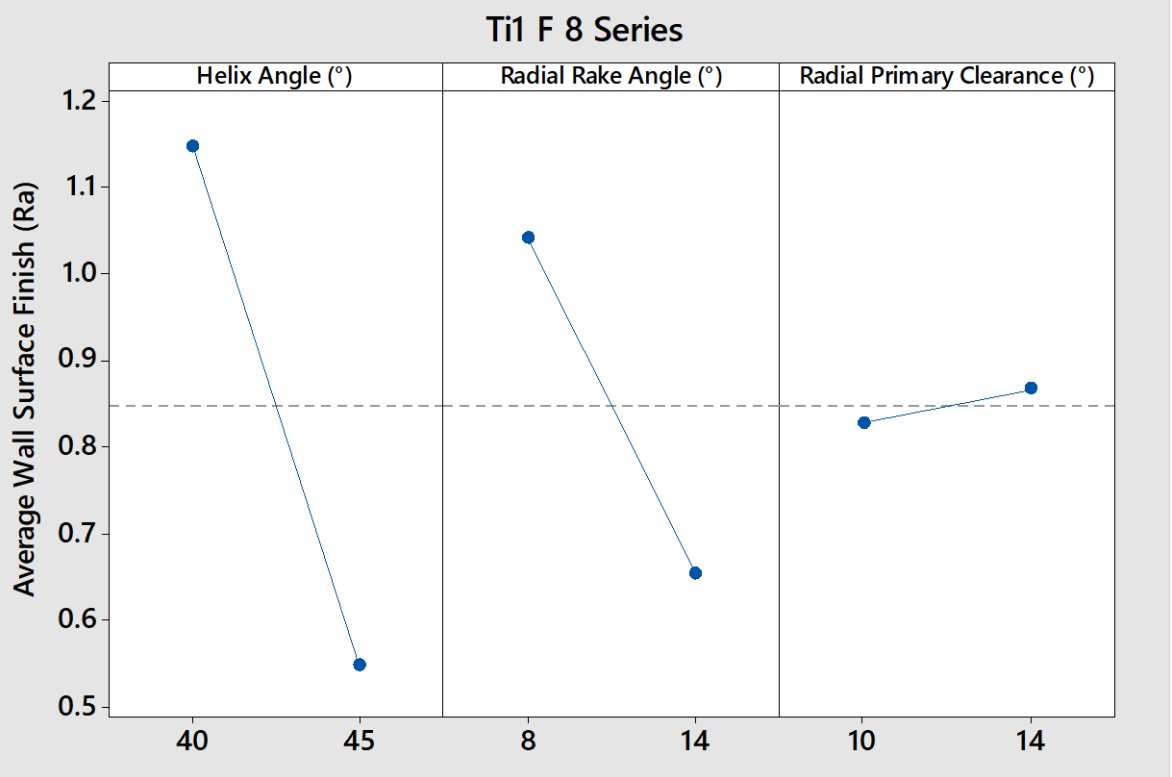

Fig. 71: Main effects plot of average surface finish in end-milling of Ti-6Al-4V with 6-flute end-mills

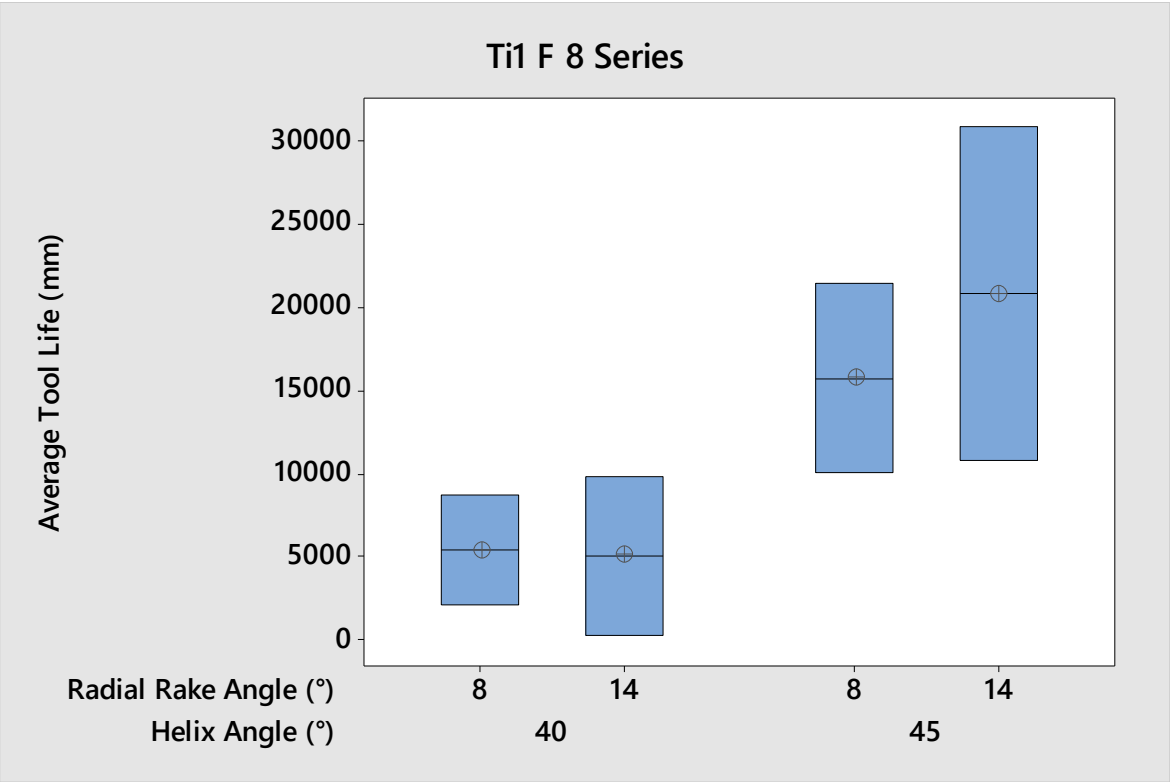

Fig. 72: Box plot of interactions between helix angle and radial rake angle at different levels based on tool life data collected from end-milling of Ti-6Al-4V using 6-flute end-mills

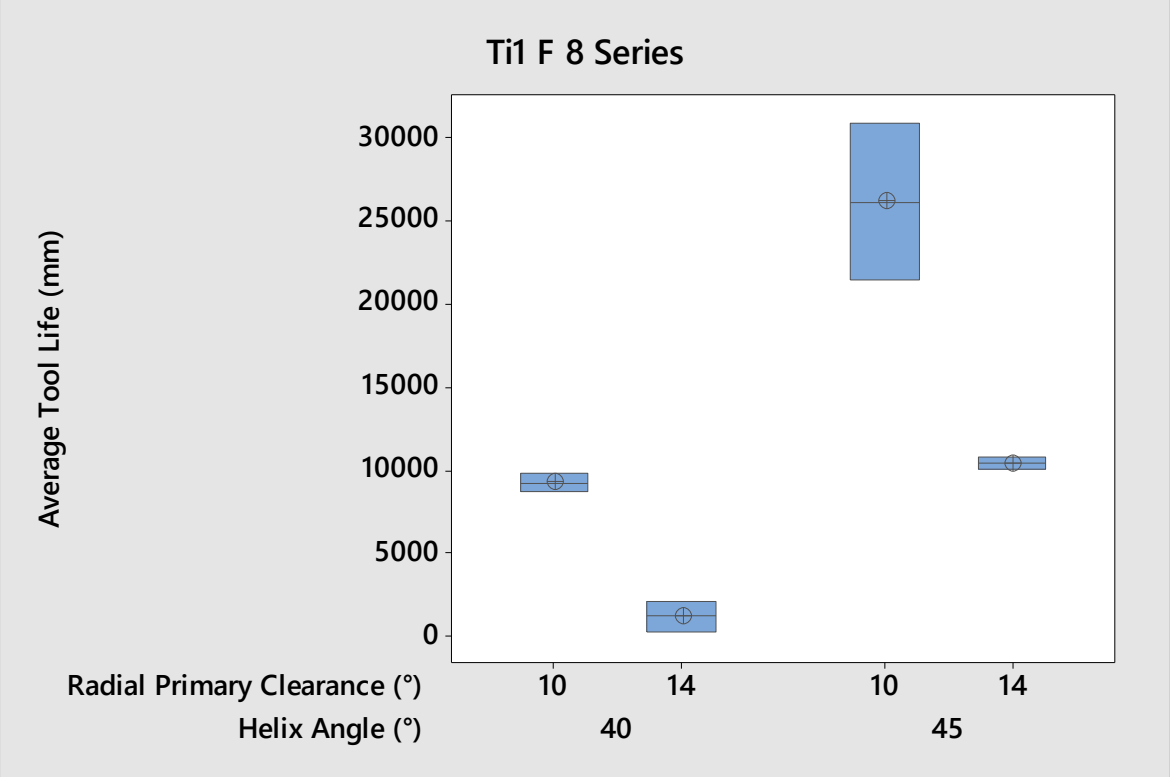

Fig. 73: Box plot of interactions between helix angle and radial primary clearance angle at different levels based on tool life data collected from end-milling of Ti-6Al-4V using 6-flute end-mills

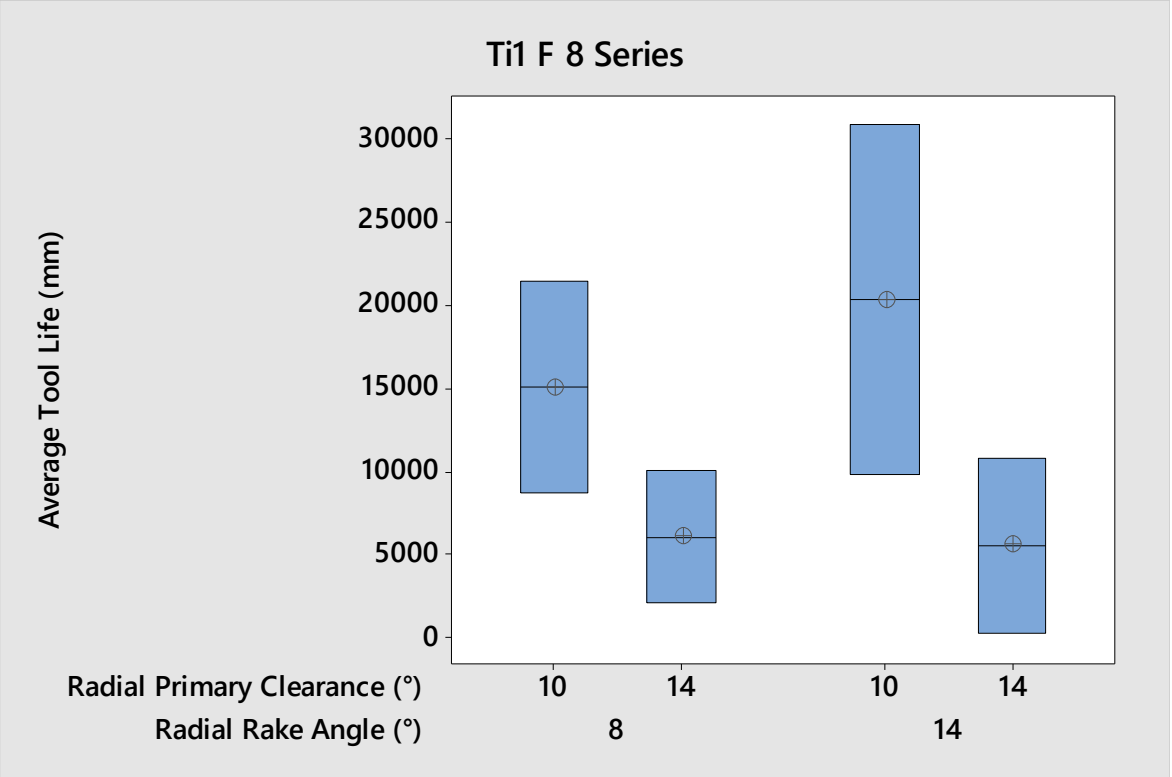

Fig. 74: Box plot of interactions between radial rake angle and radial primary clearance angle at different levels based on tool life data collected from end-milling of Ti-6Al-4V using 6-flute end-mills

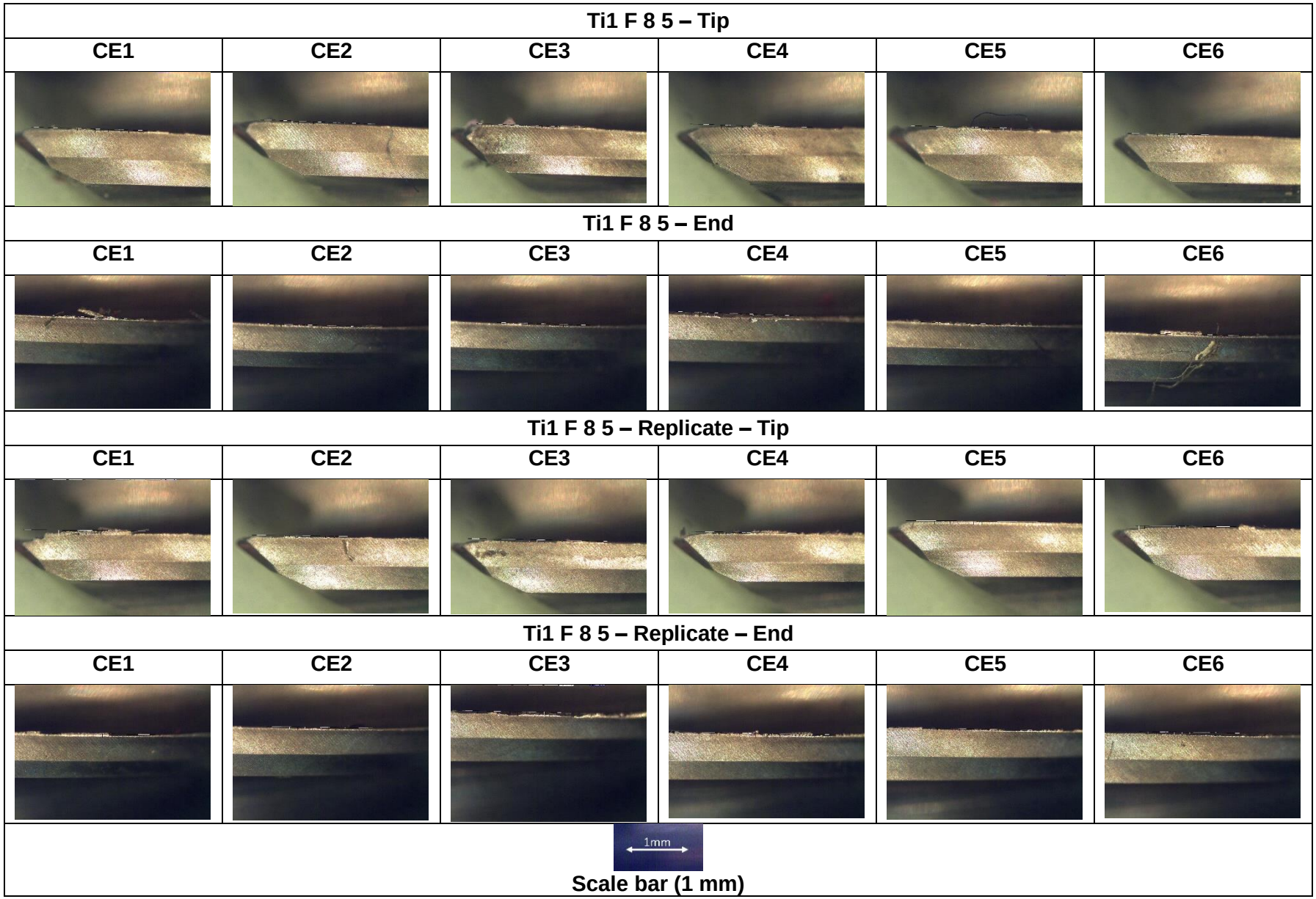

Fig. 75: Example of cutting tool wear in end-milling of Ti-6Al-4V using 6-flute end-mills as well as signs of chipping at the tip of Ti1 F 8 5, CE3 and replicate CE1

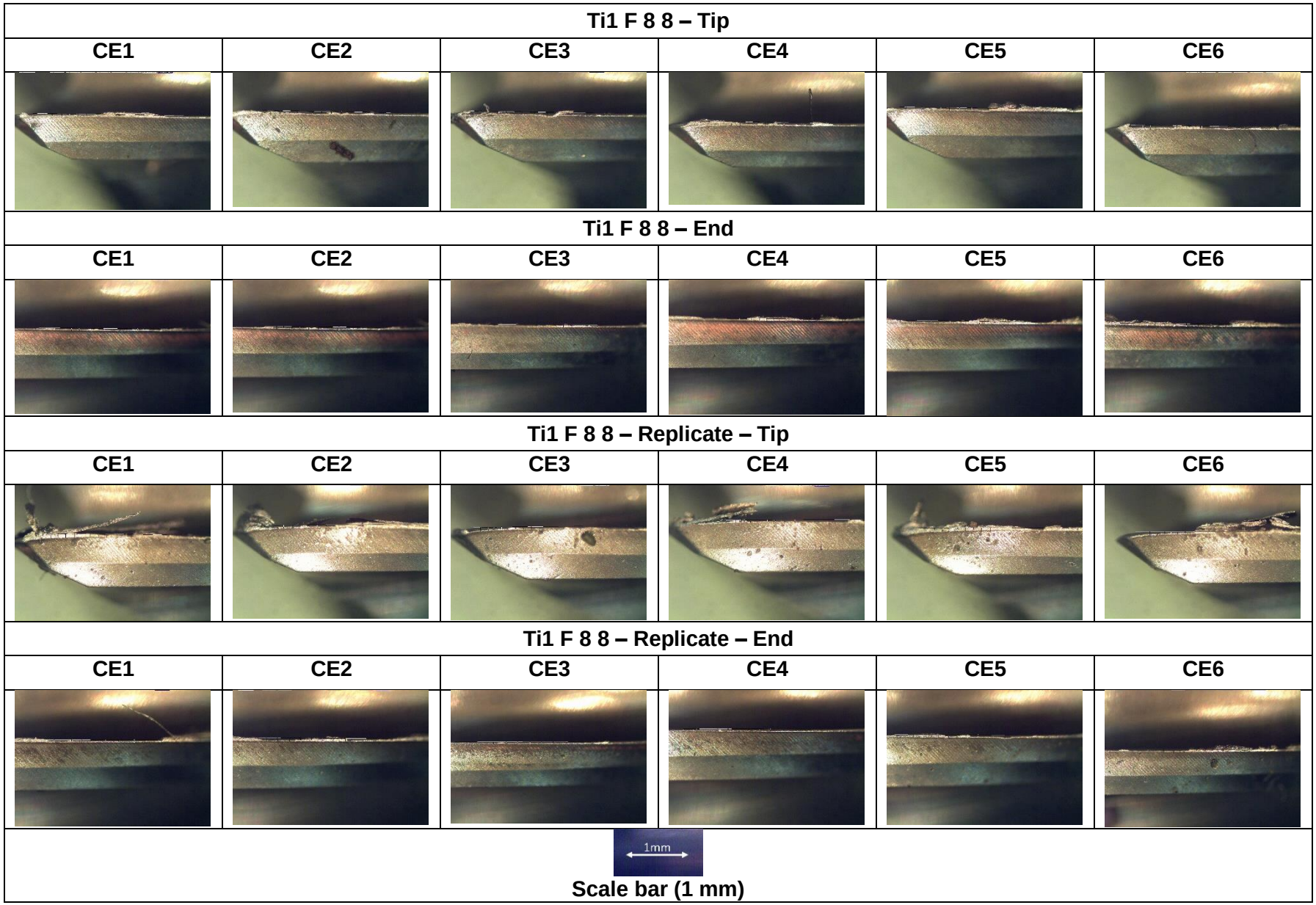

Fig. 76: Example of BUE in end-milling of Ti-6Al-4V using 6-flute end-mill

Examples of chips produced by 4-flute and 6-flute end-mills are provided in Fig. 77 and Fig. 78. Segmented chips were produced in all experiments for 4-flute and 6-flute end-mills. The smaller segmented chips produced by 4-flute roughing end-mills produced curved chips after the first machine pass Fig. 77 (a). Gradual tool wear caused changes in chip formation and as a result, saw-toothed like chips shown in Fig. 77 (b) were produced. A similar analysis was conducted on the chips produced by 6-flute end-mills. The chips produced from finish milling experiments, Fig. 78, are longer due to the deeper axial depth-of-cut. Similar observations to that of 4-flute end-mills were made. Chips collected after the final machine pass in the finish milling experiments also exhibited saw-toothed. Fig. 78 provides a close-up image of the chip formation in 6-flute end-mills. No major differences, other than worn chips being serrated, were observed between the worn and unworn chips collected from the end-milling experiments on Ti-6Al-4V.

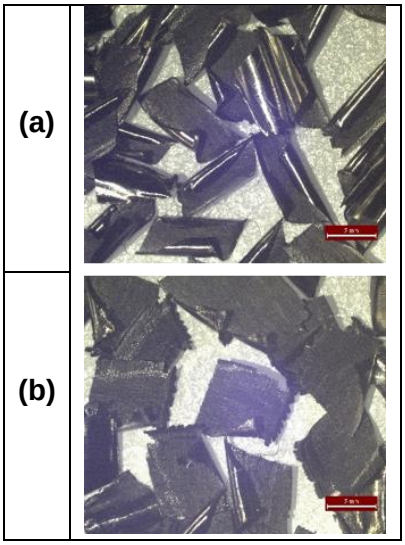

Fig. 77: Chips obtained from Ti1 R 24 5 end-milling Ti-6Al-4V - (a) chips collected after the first pass, (b) chips collected after the final pass

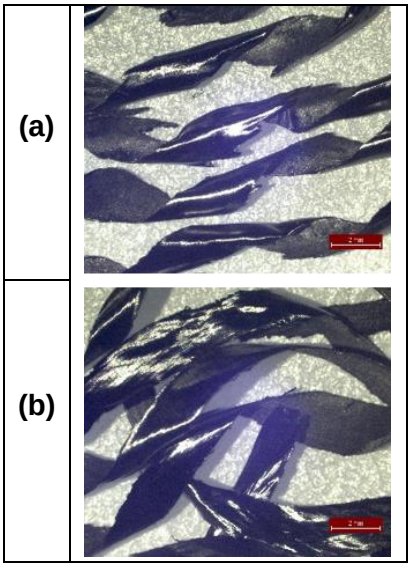

Fig. 78: Chips obtained from Ti1 F 8 7 end-milling Ti-6Al-4V - (a) chips collected after the first pass, (b) chips collected after the final pass

5.2.3 Inconel 718

End-milling experiments on Inconel 718 were conducted on three geometrical factors at three levels (Fig. 79). A total of 16 experiments were performed by following the step-by-step guide provided in the methodology to obtain meaningful results. Geometrical factors, helix angle, radial rake angle and primary clearance angle were once more chosen for evaluation, when designing the 5-flute end-mills with various geometries. Information regarding the performance of each cutting tool and tool wear measurements have been provided in Appendices F and G.

Following the analysis based on tool life, Table 20 and Fig. 80 were produced to identify the importance of the geometrical parameters and support the statistical results obtained. According to Fig. 80 the helix angle and radial primary clearance angle were the only two geometrical parameters to cross the reference line of 2.086. This is backed up and confirmed by the P-values of 0.005 and 0.004 respectively in Table 20. The experiments showed that high helix angle in combination with high radial rake angle and primary clearance angle showed a better performance when contrasted to lower level.

Table 20: Analysis of variance for transformed response of tool life in end-milling of Inconel 718

Parameters	(DF)	Adj (SS)	Adj (MS)	F-value	P-value
Model	6	396.718	66.120	4.52	0.005
Linear	3	325.210	108.403	7.41	0.002
Helix angle (A)	1	144.739	144.739	9.90	0.005
Radial rake angle (B)	1	21.550	21.550	1.47	0.239
Radial primary clearance angle (C)	1	158.922	158.922	10.87	0.004
Two-way Interactions	3	71.508	23.836	1.63	0.214
A*B	1	9.034	9.034	0.62	0.441
A*C	1	41.242	41.242	2.82	0.109
B*C	1	21.232	21.232	1.45	0.242
Error	20	292.397	14.620	-	-
Total	26	689.114	-	-	-

Once more, flank wear seemed to dominate the cutting edges, regardless of tool geometry, on the end-mills with particles on Inconel 718 deposited on the cutting edges (BUE), as shown in Fig. 84. The various geometries and their performance intensified the amount of flank wear measured during the analysis (Fig. 85). The author did not observe any crater wear on the rake face of the cutting edges but instead assessed the notch wear on flutes mainly found at the end of the ADoC of 3 mm (Fig. 86). The burr formation of Inconel 718 after each cut seemed to increase the intensity of the notch wear on the radial primary clearance. High radial primary clearance angles showed better resistance against the hardened burr on the workpiece material. Chipping was also observed in the experiments which mainly occurred at the tip of the flute end-mills (Fig. 84 and Fig. 85). The data distribution of box plots based on the

interaction between helix angle, radial rake angle and radial primary clearance angle supports Fig. 79 and Fig. 80. The skewness of the plots varies between different levels indicating a positive or negative skew in the normal distribution of the data (tool life). The skewness in the box plots could be resolved if more data points or experiments are carried out to bring about a more normal distribution.

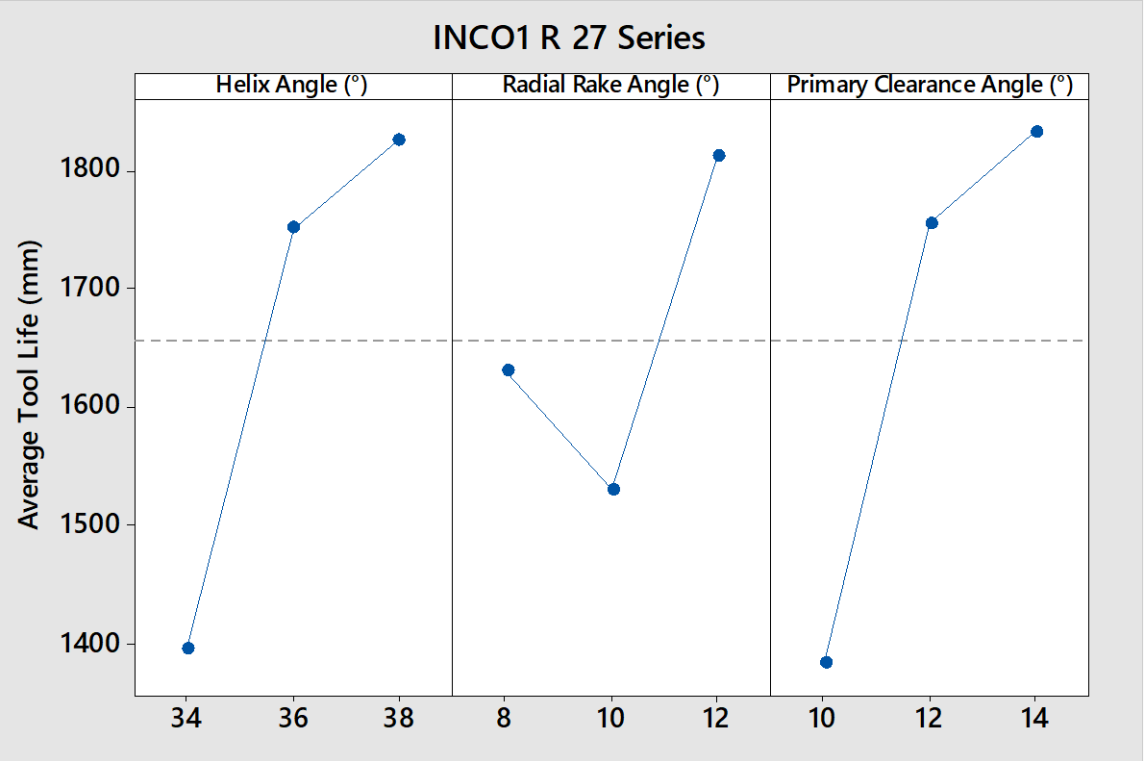

Fig. 79: Main effects plot of average tool life in end-milling of Inconel 718 with 5-flute end-mills

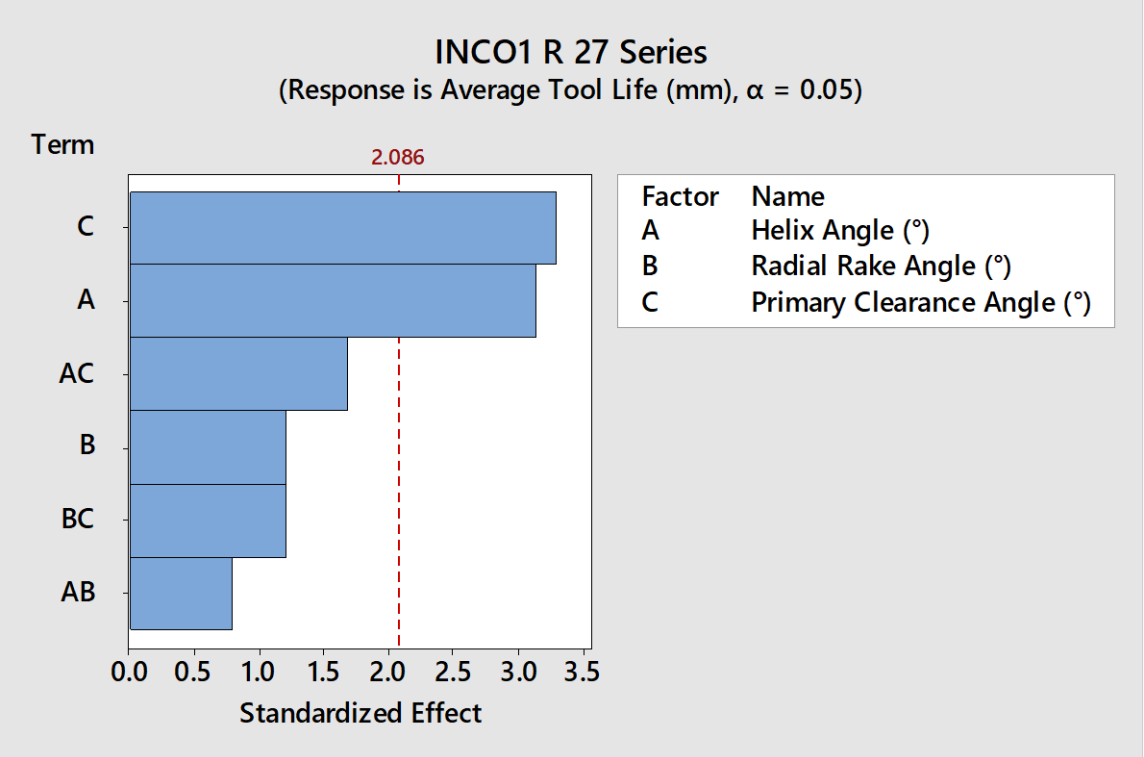

Fig. 80: Pareto ANOVA of geometrical parameters in end-milling of Inconel 718

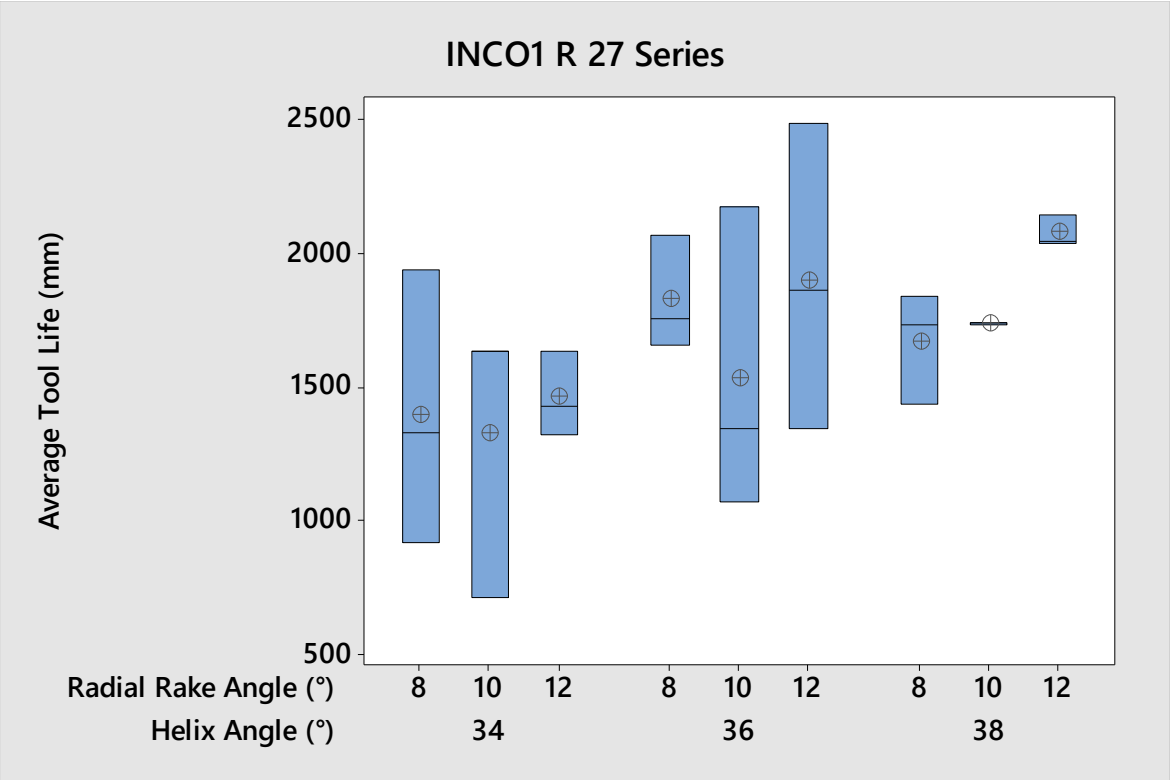

Fig. 81: Box plot of interactions between helix angle and radial rake angle at different levels based on tool life data collected from end-milling of Inconel 718 using 5-flute end-mills

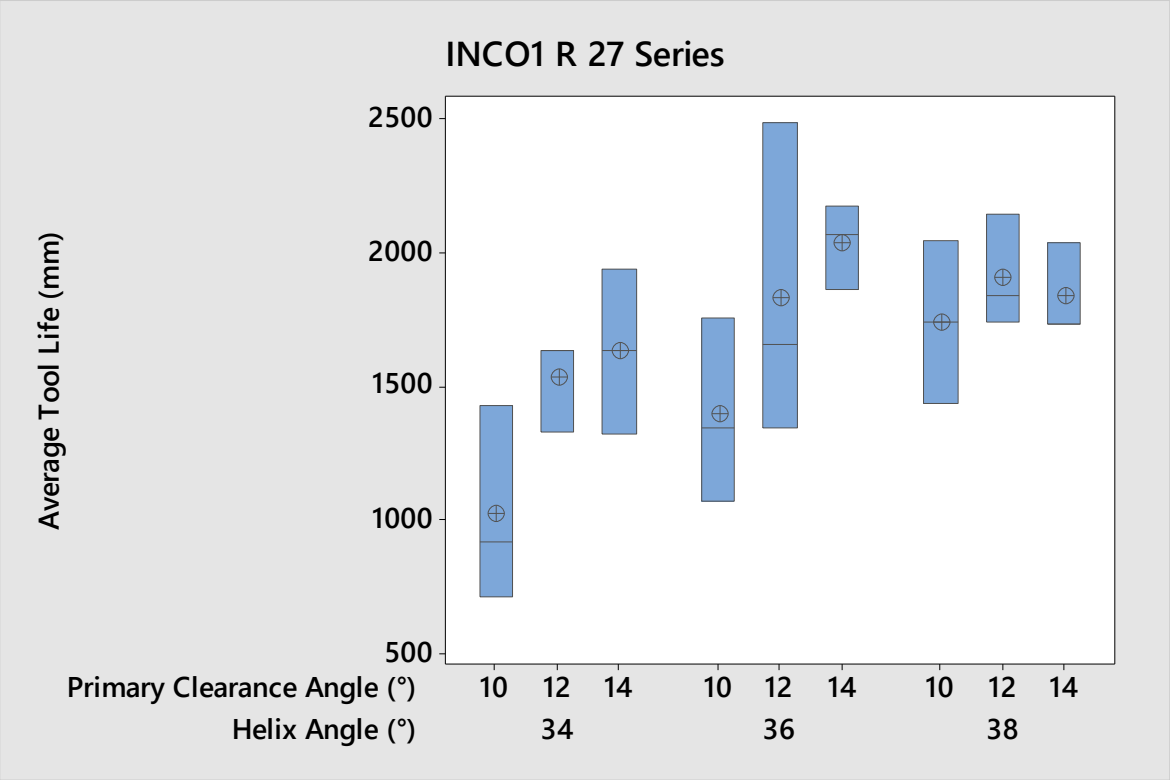

Fig. 82: Box plot of interactions between helix angle and radial primary clearance angle at different levels based on tool life data collected from end-milling of Inconel 718 using 5-flute end-mills

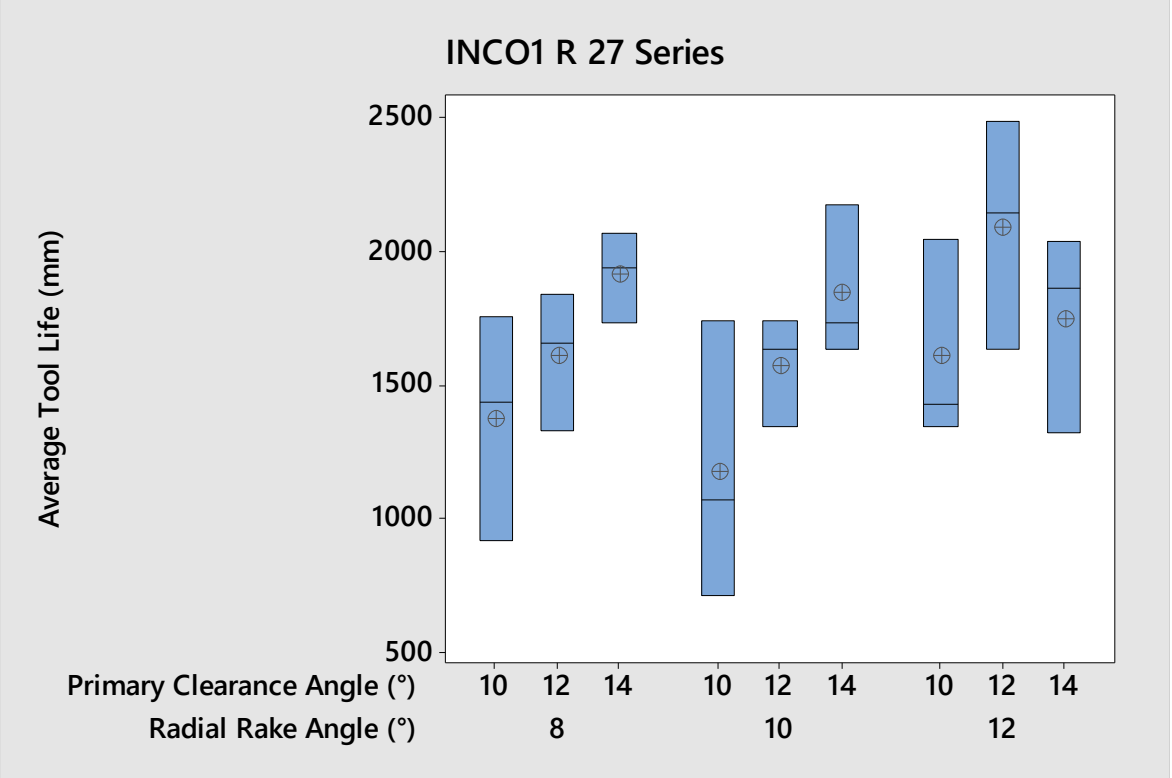

Fig. 83: Box plot of interactions between radial rake angle and radial primary clearance angle at different levels based on tool life data collected from end-milling of Inconel 718 using 5-flute end-mills

Analysis carried out on the chips formed in end-milling experiments on Inconel 718 showed smooth and rough edges on collected samples, Fig. 87 (a). Cut chip samples at the beginning of every experiment seemed inconsistent and irregular in shape. Both smooth and serrated chips were observed after the initial pass in every experiment, regardless of tool geometry. As the tool wear gradually evolved on the cutting edges of the end-mills chips began to become more jagged, uneven and irregular, Fig. 87 (b). Inconel 718 and its mechanical properties such as high Young's Modulus of 200 GPa and a hardness of 392 Brinell (HB), reduce the performance of the cutting tool and cause rapid tool wear on cutting edges and loss integrity in end-milling this nickel-based alloy, producing uneven chips.

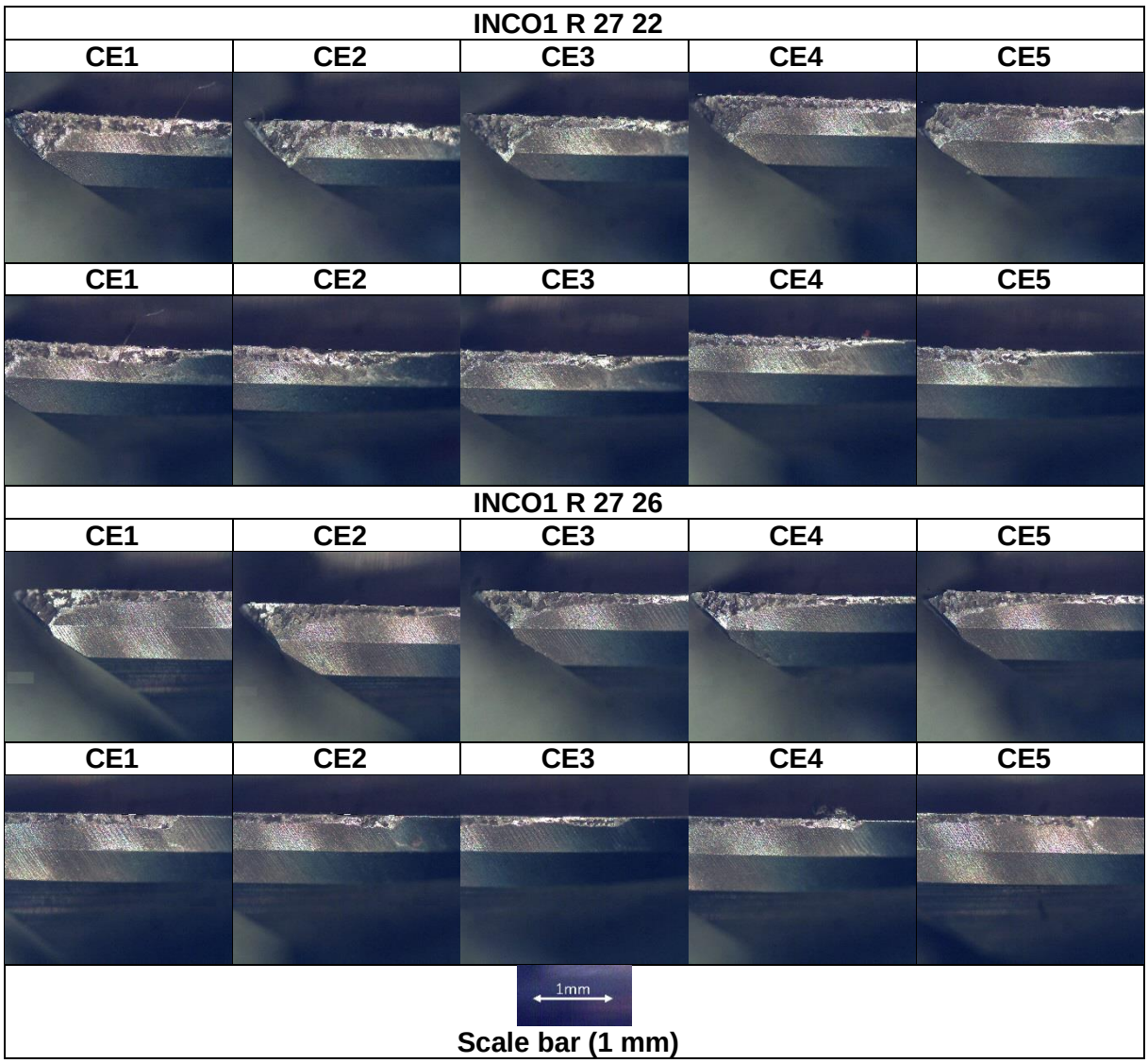

Fig. 84: Examples of flank wear, chipping and BUE on the cutting edges when milling Inconel 718

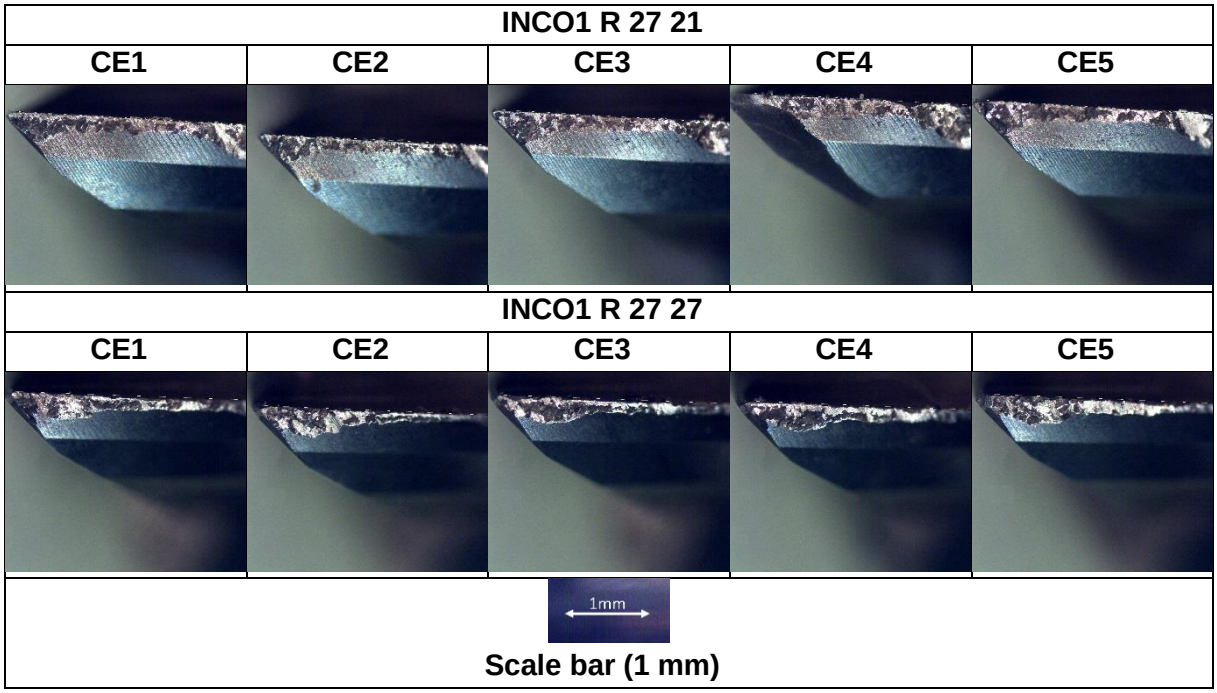

Fig. 85: Excessive cutting tool wear due to abrasive wear in end-milling of Inconel 718

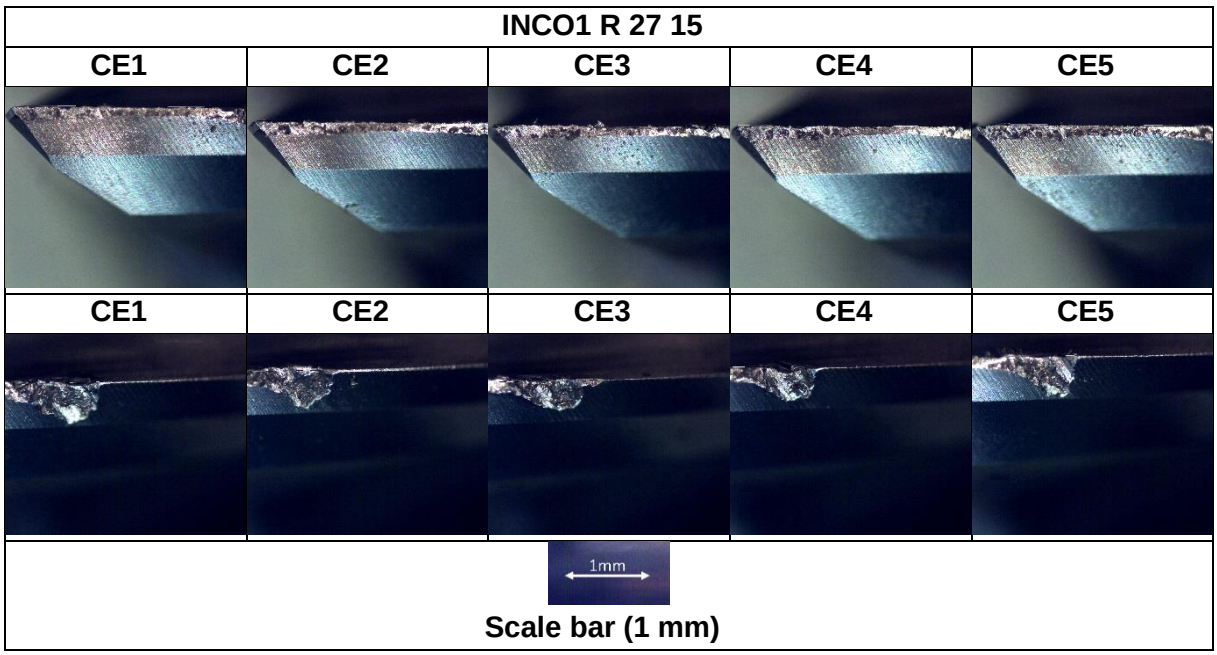

Fig. 86: Examples of the occurrence of notch wear in the end-milling experiments of Inconel 718

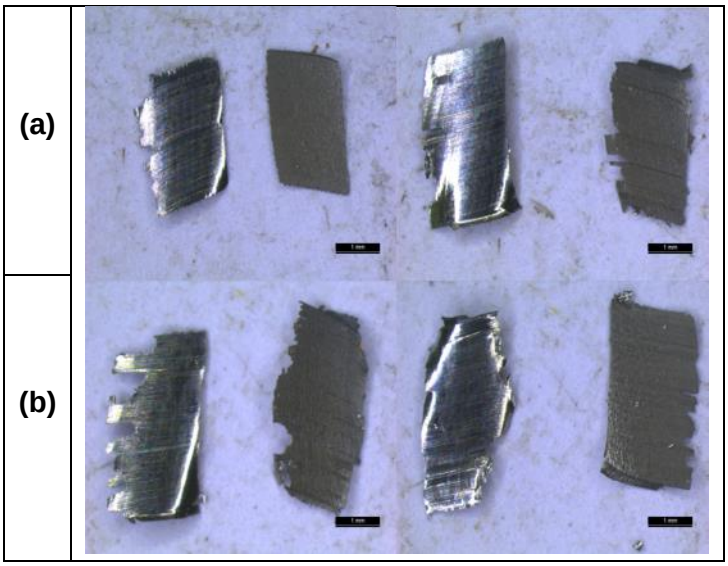

Fig. 87: Chips obtained from INCO1 R 27 18 in end-milling of Inconel 718 - (a) chips collected after the first pass, (b) chips collected after the final pass

5.2.4 Super Duplex 2507

The use of different helix angles, radial rake angles and radial primary clearance angles appears to have had limited impact on the performance of the 4-flute end-mills designed for machining alloy 2057. This suggestion is reinforced by an ANOVA test of between-subject effects which found no statistical significance between any of the three factors used in the evaluation of tool geometry (Table 21). This is shown by the significances in the final (P-value) column for all factors and interactions, where no values were below 0.05, the 95% confidence interval. However, based on Fig. 89, the radial rake angle of 10° seems to improve tool life when compared to other levels chosen for evaluation. Based on the main effects plot, the helix angle and the radial primary clearance angle do not seem to make a difference. Whereas, on the Pareto ANOVA (Fig. 88), it seems that the interaction of helix angle and radial primary clearance angle is closer to the reference line in Fig. 88, followed by the interaction between radial rake angle and radial primary clearance angle. Further investigation at different levels may be required to establish the effect of geometrical parameters on tool life in end-milling alloy 2507. The box plot analysis on 4-flute end-mills designed for super duplex stainless steel 2507, Fig. 90 - Fig. 92, could not support the ANOVA results obtained from Table 21. Further experiments at different levels may be required to identify the effect of each geometrical parameter as well as their interactions in end-milling of super duplex 2507.

Table 21: Analysis of variance for transformed response of tool life in end-milling of super duplex 2507

Parameters	(DF)	Adj (SS)	Adj (MS)	F-value	P-value
Model	6	217.853	36.309	0.73	0.640
Linear	3	0.737	0.246	0.00	0.999
Helix angle (A)	1	0.390	0.390	0.01	0.932
Radial rake angle (B)	1	0.049	0.049	0.00	0.976
Radial primary clearance angle (C)	1	0.298	0.298	0.01	0.940
Two-way Interactions	3	217.116	72.372	1.45	0.292
A*B	1	8.494	8.494	0.17	0.690
A*C	1	139.193	139.193	2.79	0.129
B*C	1	69.430	69.430	1.39	0.269
Error	9	449.536	49.948	-	-
Total	15	667.389	-	-	-

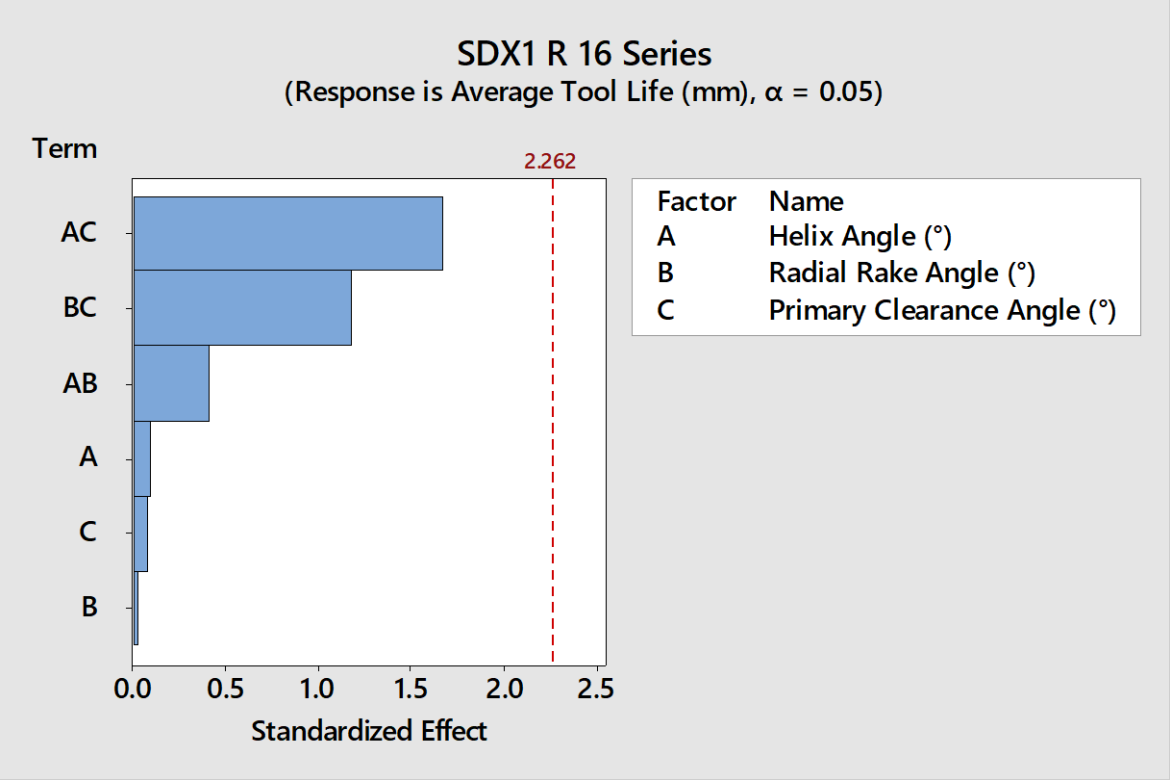

Fig. 88: Pareto ANOVA of geometrical parameters in end-milling of super duplex 2507

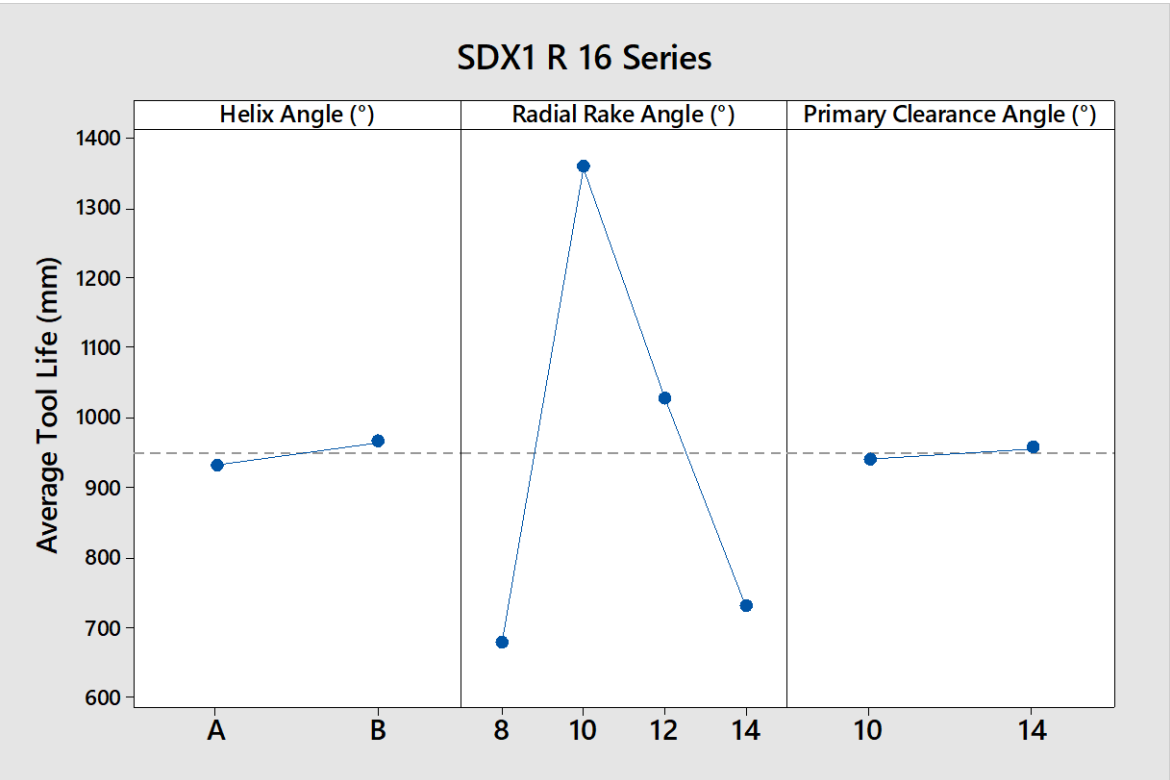

Fig. 89: Main effects plot of average tool life in end-milling of super duplex 2507 with 4-flute end-mills

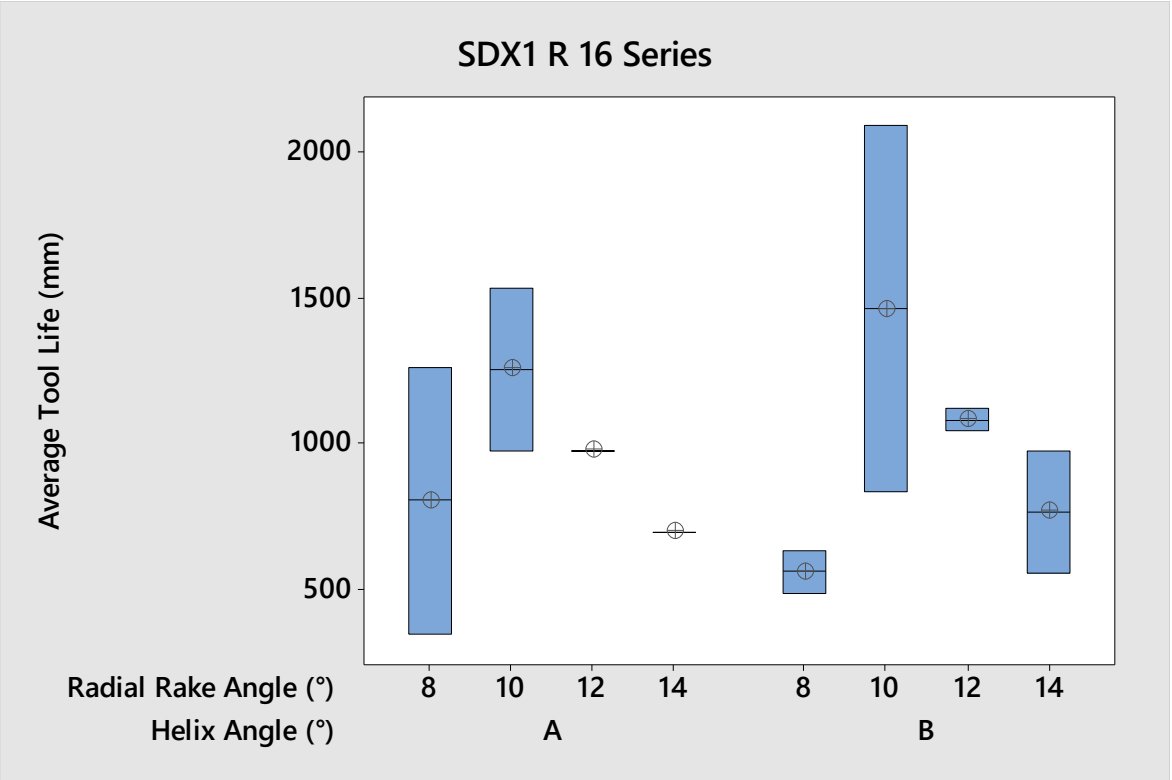

Fig. 90: Box plot of interactions between helix angle and radial rake angle at different levels based on tool life data collected from end-milling of super duplex 2507 using 4-flute end-mills

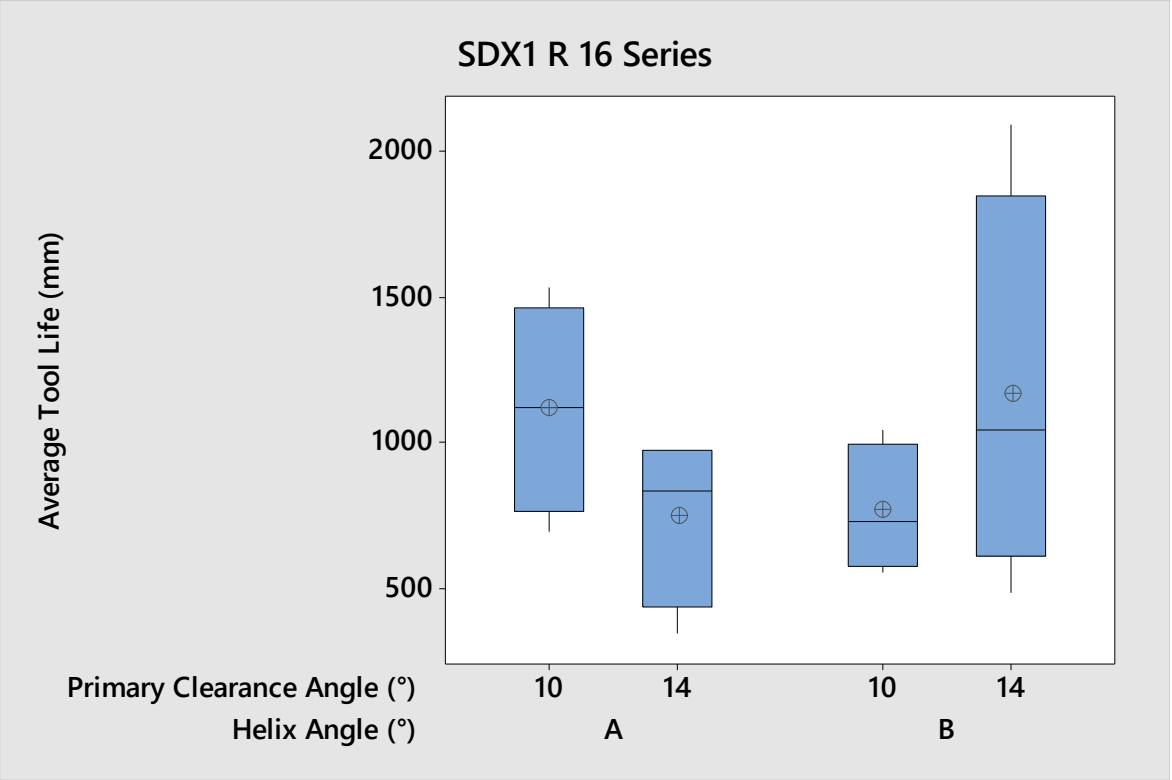

Fig. 91: Box plot of interactions between helix angle and radial primary clearance angle at different levels based on tool life data collected from end-milling of super duplex 2507 using 4-flute end-mills

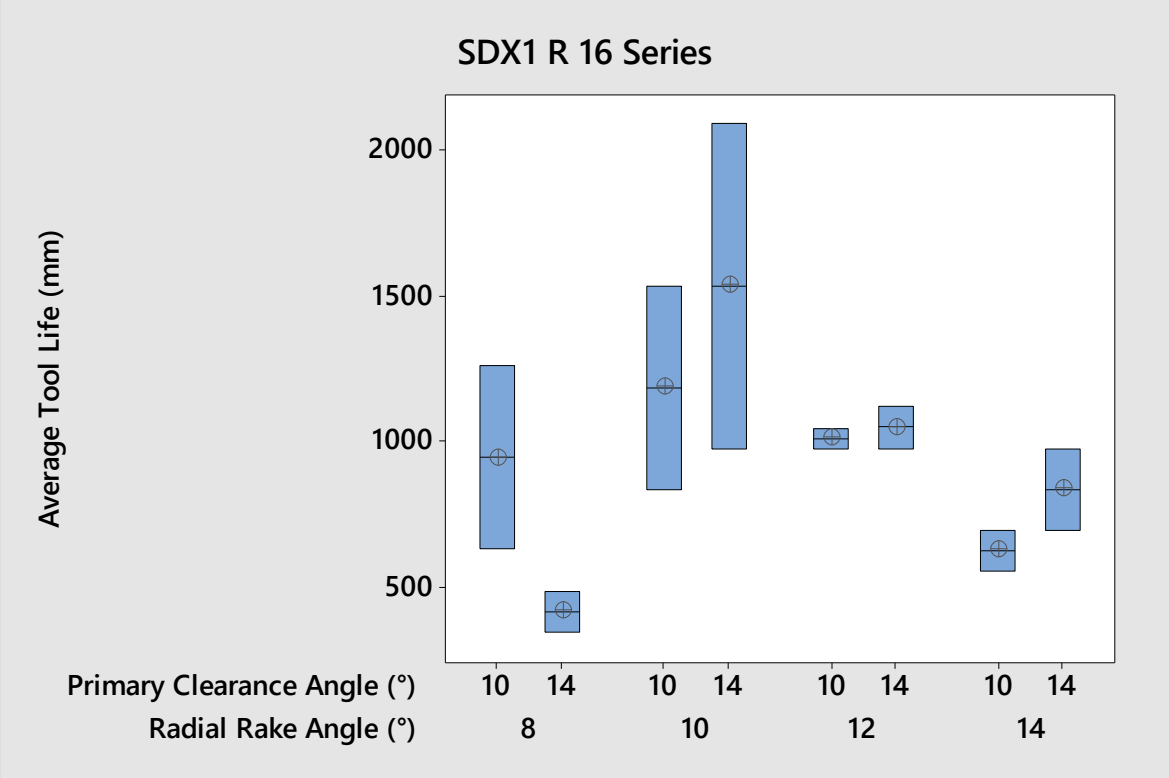

Fig. 92: Box plot of interactions between radial rake angle and primary clearance angle at different levels based on tool life data collected from end-milling of super duplex 2507 using 4-flute end-mills

The flank wear measurements at the tool corner (Fig. 93 and Fig. 94) increased somewhat erratically instead of following the steady wear progression expected with abrasion and microchipping. This may have been a consequence of the use of incorrect tool geometry, machine parameters or tool material since it is often challenging to distinguish the optimum cutting parameters for machining a difficult-to-cut material. Many of the experimental cutting tools exhibited chipping and crater wear as well as BUE on their cutting edges (Fig. 93). Tool life results obtained from the experiments seemed inconsistent for obtaining a conclusion. The cutting tool with the best performance in this series was experiment SDX R 16 12 with a tool life of 2088.15 mm (Appendix F). Further investigation is required to be able to locate the optimum geometry in end-milling of 2507.

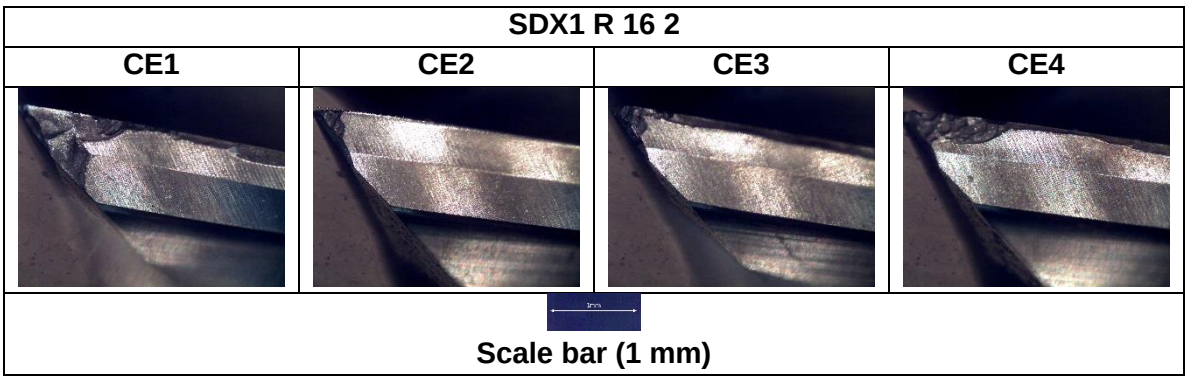

Fig. 93: Examples of BUE and chipping on the cutting edges when milling super duplex 2507

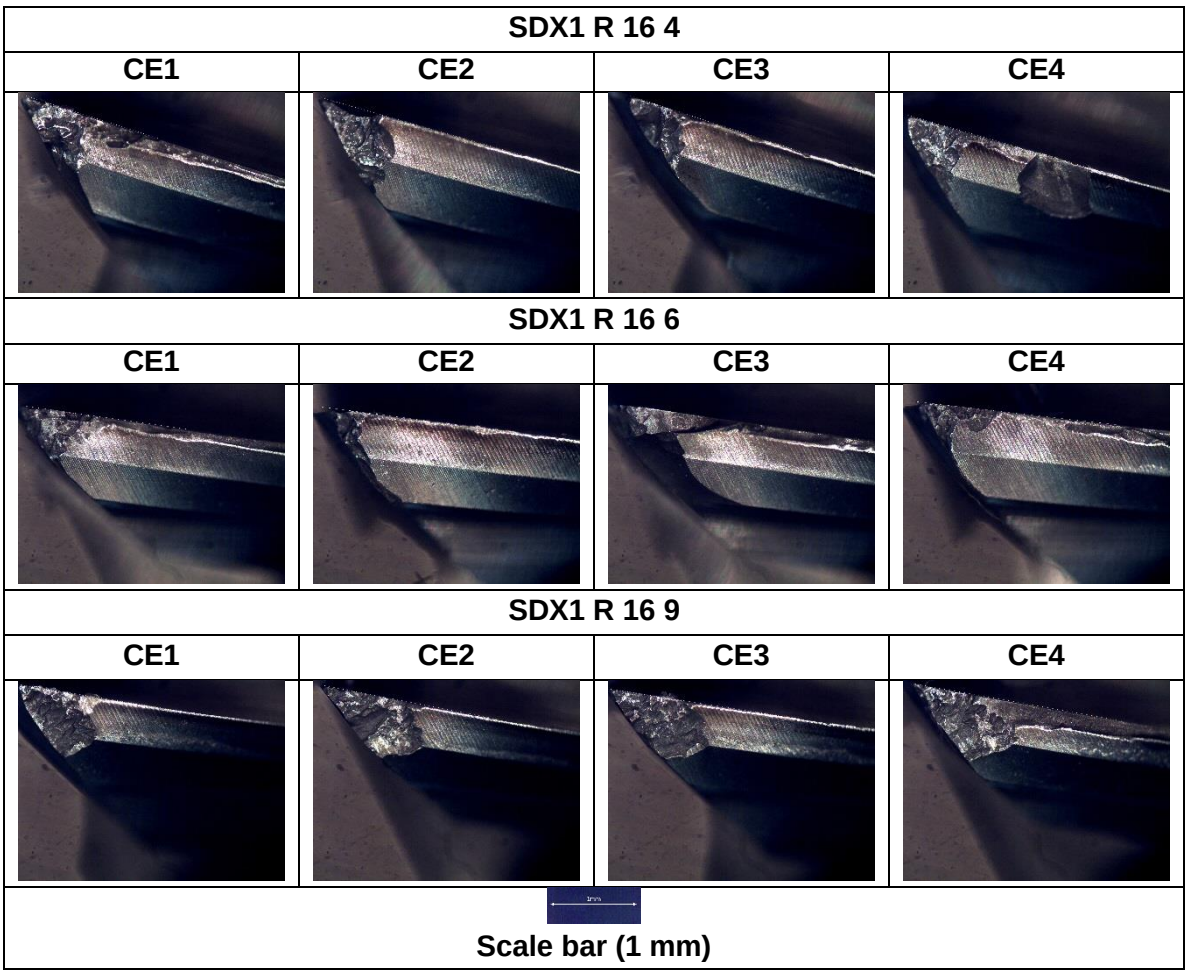

Fig. 94: Example of extreme abrasive wear and notch wear in end-milling of super duplex 2507

An example of chips collected from the end-milling experiments on super duplex 2507 is shown in Fig. 95. All chips collected at the beginning of the experiments were regular in size with smooth edges Fig. 95 (a).

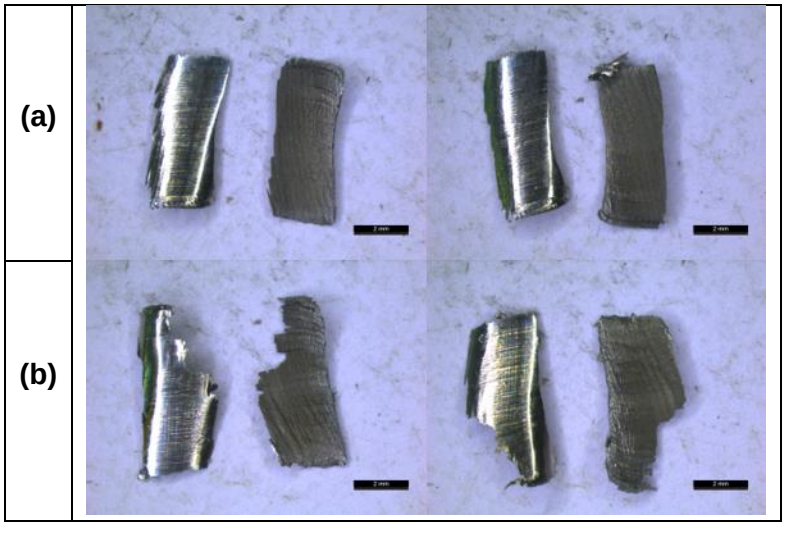

Fig. 95: Chips obtained from SDX1 R 16 12 end-milling 2507 - (a) chips collected after the first pass, (b) chips collected after the final pass

However, they were not as curved as chips compared to aluminium or titanium chips. Worn chip samples collected, did not exhibit extreme or long saw-tooth edges when compared to Inconel 718 chips. Instead, they were regular in shape with rough edges due to tool wear over the course of the experiment.

5.3 Drills

5.3.1 Aluminium 6082-T6

The soft nature of aluminium 6082-T6 (with a hardness of 91 HB) allowed for new drill designs in this study, instead of the conventional 2-flute twist drill design used in drilling operations of difficult-to-cut materials. Based on the literature review conducted on drills 4.1.4 the author decided that it would be best to explore two separate drill designs in machining of 6082-T6. The first design, a 2-flute, with no helical angle labelled as straight flute (SFL) was selected for this study. The second design was a 3-flute (3FL) twist drill selected to combine the design of a spot drill and conventional drill for penetration stability in drilling of aluminium alloys. Spindle through coolant was not utilised in the experiments, firstly due to costs of tool material, limited workpiece material resources and to increase tool wear rate on the cutting edges.

Since tool life could not be used as a response factor in the analysis to compare the performance of the cutting tools for this experimental series, the average tool wear and surface roughness of drilled holes were adopted instead to establish the importance and relationship between geometrical factors. In the case of both drilling experiments (3FL and SFL) each tool was allocated and limited to drill 84 holes in a single block of 6082-T6 at a depth of 40 mm (total of 3.36 metres) at the machine parameters allocated in 4.1.3. In the SFL experiments, drill point angle and relief angle were chosen for investigation, whereas helix angle and drill point angle were selected for the 3FL design. Three levels and two levels were selected for the factors for SFL and 3FL designs, respectively.

Based on the Pareto ANOVA on tool wear, Fig. 157, the geometrical factors, under evaluation, were found to be insignificant (Table 22). Neither geometrical factors evaluated in SFL experiments crossed the reference line to exceed below the 0.05 statistical significance value. Moreover, the number of experiments and their duration were insufficient to arrive at a viable conclusion. Further investigation is required to assess the performance of the geometrical factors based on tool wear. However, as discussed in 4.3.2, the surface roughness of the workpiece material is also a critical response factor if the Pareto ANOVA based on surface roughness (Fig. 158) of drilled holes was taken into account, it becomes clear that the relief angle is significant. The relief angle showed a P-value of 0.046 followed by the drill point angle just shy of the reference line on the Pareto ANOVA on surface roughness (Fig. 158). The results based on surface roughness show that increasing drill point angle and relief angle produce a lower surface roughness (Fig. 159). Tools 3, 6 and 9 (AL1 D SF 9 3, AL1 D SF 9 6 and AL1 D SF 9 9) all had a relief angle of 20° with a drill point of 140°. All three drills produced a better finish and showed less flank wear on the cutting edges (Appendix H, Fig. 156). The cutting tool wear on the drills, were mainly focused on the drill point where extreme flank wear on the chisel edge of the drill was observed as shown in Fig. 97. Other than flank wear, the author did not observe any noticeable wear on the cutting edges of the drills.

Table 22: Analysis of variance for transformed response of tool wear in drilling of 6082-T6

Parameters	(DF)	Adj (SS)	Adj (MS)	F-value	P-value
Model	3	1.3477	0.4492	0.81	0.540
Linear	2	0.8805	0.4403	0.80	0.501
Drill point angle (A)	1	0.4276	0.4276	0.77	0.420
Relief angle (B)	1	0.4530	0.4530	0.82	0.407
Two-way Interactions	1	0.4672	0.4672	0.84	0.400
A*B	1	0.4672	0.4672	0.84	0.400
Error	5	2.7668	0.5534	-	-
Total	8	4.1146	-	-	-

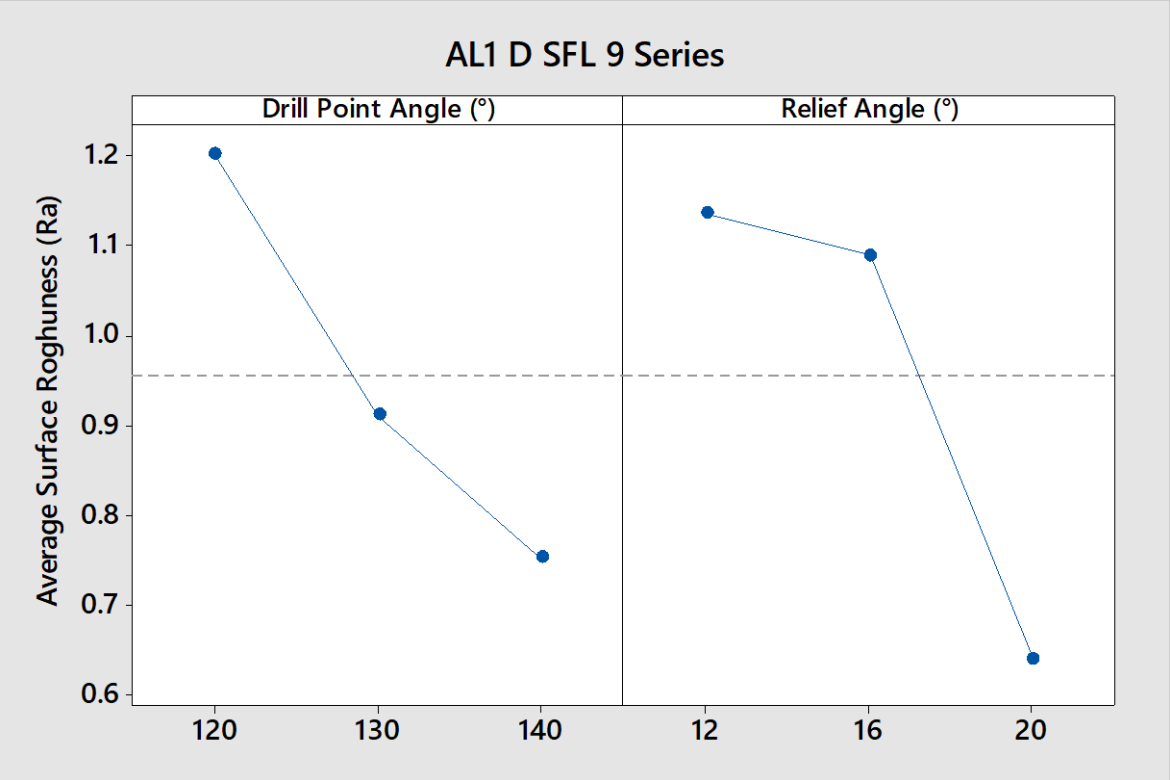

Fig. 96: Main effects plot of geometrical parameters based on tool wear on striaght flute drill design

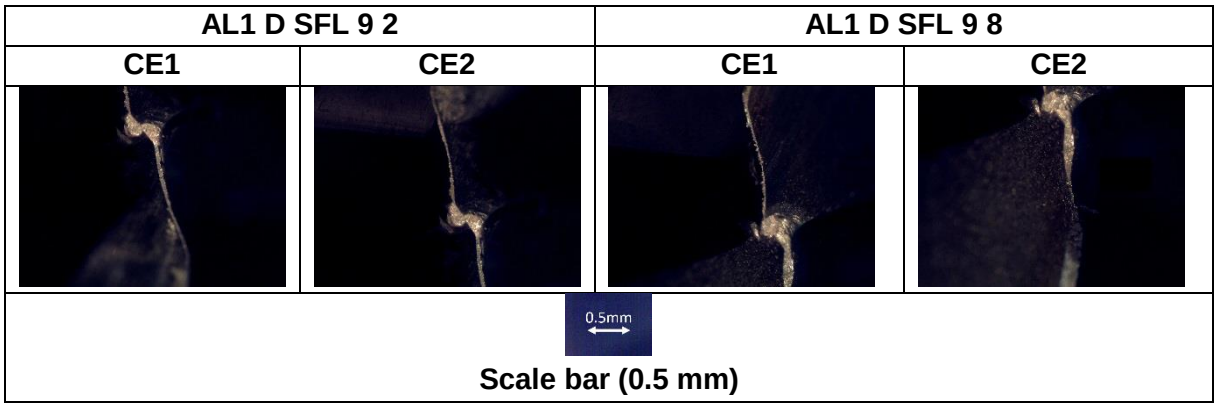

Fig. 97: Flank wear on cutthing edges (AL1 D SFL 9 2) and flank wear on the chisel edge (AL1 D SFL 9 8) straight flute drills for 6082-T6

Chips were collected from the first drilled hole as well as the final hole, Fig. 98. Negligible differences were observed between the initial samples versus the final samples. No major differences could be identified in chip samples from different experiments as cutting tools did not reach the required tool wear criteria. However, based on the analysis carried out in chip formation of drills 0, ideal chip was helical, segmented and discontinuous. Further investigation is required to be able to distinguish the differences in geometry and chip formation in SFL drill designs.

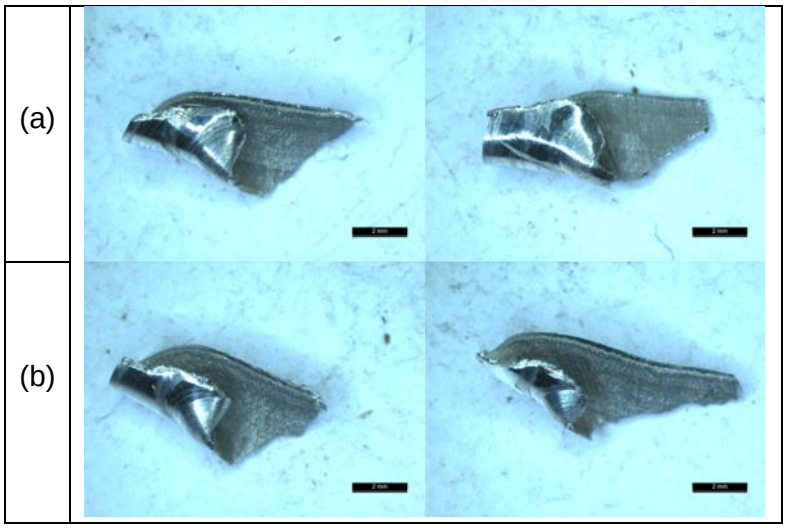

Fig. 98: Chips obtained from drilling experiments on 6082-T6 based on straight flute - (a) chips collected after drilling the first hole, (b) chips collected after drilling the final hole

Results from the drilling experiment on 3FL designs showed that both investigated factors had no major effect on tool wear or surface roughness. The Pareto ANOVA based on tool wear did not show any significance between the factors and their interactions. Insufficient number of experiments meant that a decisive conclusion could not be made by the author. Further experiments are needed to understand the importance of the geometrical factors used in this experimental series.

Uniform flank wear on the relief angle and the cutting edges were experienced throughout tool wear analysis. However, flank wear intensified around the drill point with BUE dominating the small gaps at the tip of the cutting tool Fig. 99. No major failure or tool wears were experienced in drilling of 6082-T6. The author also noticed a particular form of abrasion on the relief angle of the cutting edges which increased in size from the drill point towards the periphery of the cutting tools. An example of this has been provided in Fig. 100. This form of abrasion did not cause any major problems during the experiments but could have been the result of eliminating spindle through coolant and build up oh heat at the cutting zone.

No differences in chip formation were observed in 3FL drilling experiments on 6082-T6. The same experimental procedure as the SFL drills were carried out where samples were collected from the first and last drilled holes in every experiment. Cut samples exhibited a curved and

segmented nature with long tails, due to the high linear selected for the experiments. No serrated edges were observed in the samples collected from the drilling experiments.

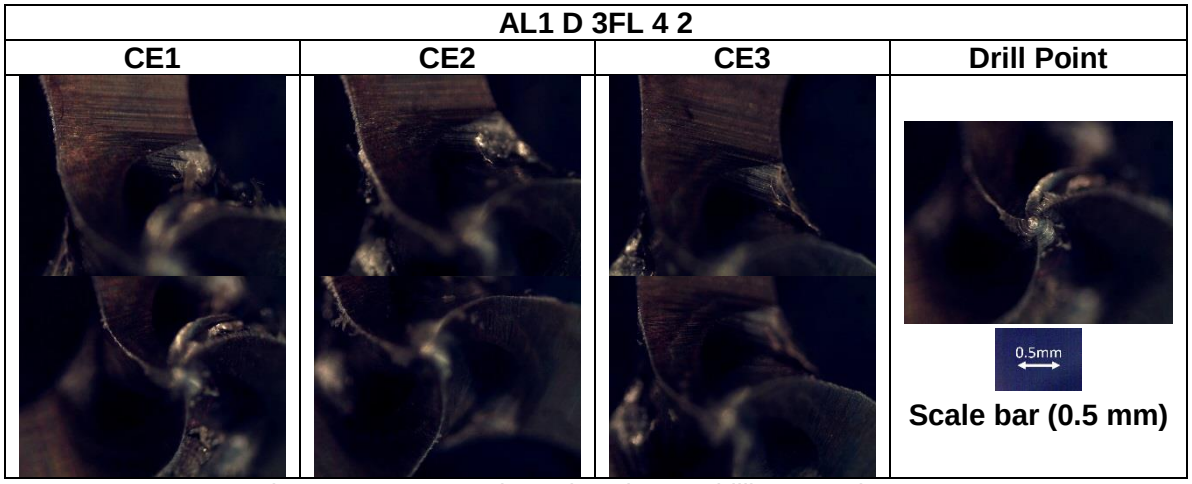

Fig. 99: BUE on Cutting Edges in 3FL drilling experiments

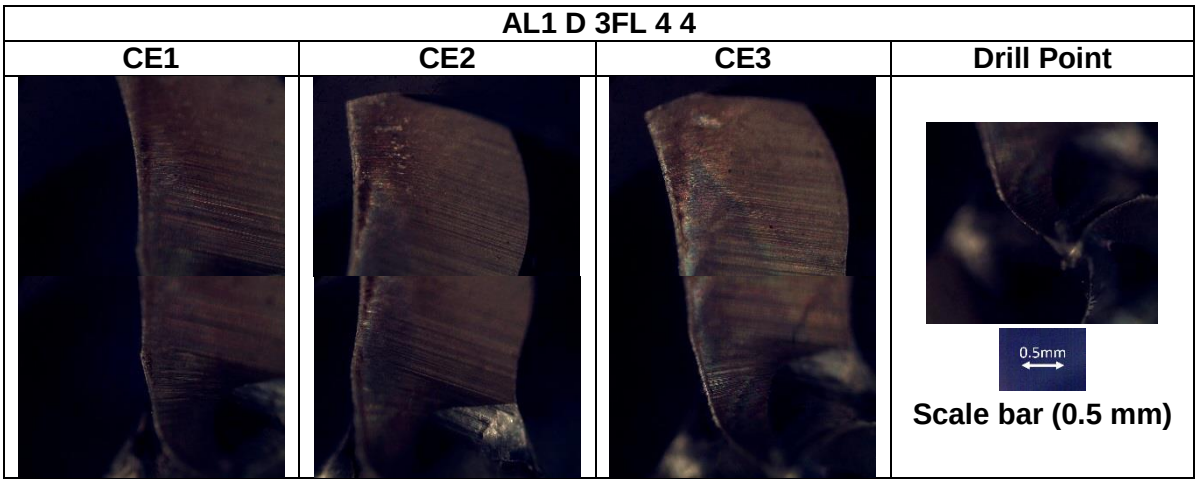

Fig. 100: Signs of smearing on the relief angle of the drill in machining of 6082-T6

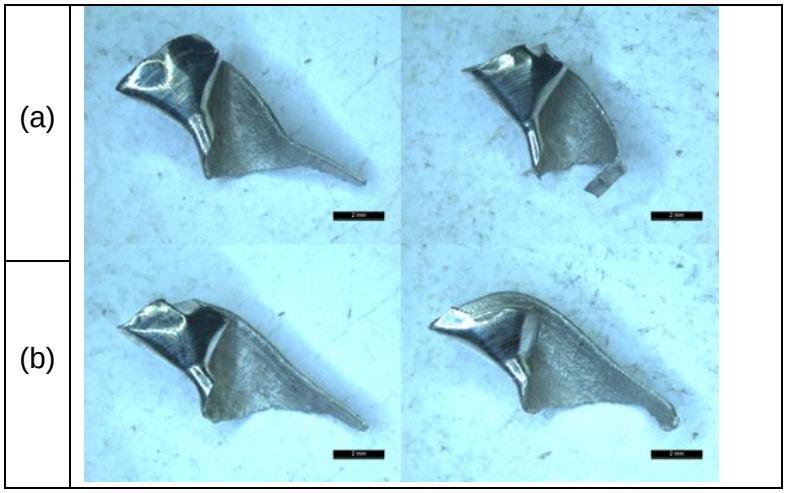

Fig. 101: Chips obtained from drilling experiments on 6082-T6 based on 3-flute - (a) chips collected after drilling the first hole, (b) chips collected after drilling the final hole

5.3.2 Ti-6Al-4V

Drilling experiments on Ti-6Al-4V were performed to better understand the role of geometrical factors and their effect on tool life and tool performance. Eight experiments, with replicates were carried out and tool life, in the form of drilled holes, was measured for each experiment, Appendix F (Fig. 150). Majority of cutting tools, designed for drilling Ti-6Al-4V, irrespective of tool geometry, experienced flank wear on the cutting edges, chisel edge proximity and periphery (Fig. 107, Fig. 108 and Fig. 110). Combination of low thermal conductivity of Ti-6Al-4V and high temperatures at the cutting zone made the cutting tool more vulnerable to tool wear and chipping. Furthermore, this caused cutting chips to weld onto the cutting edges of the drills during machining, in the form of BUE. The drill corners seemed to experience chipping regardless of tool geometry, which was caused by rubbing the outer surface of the drill onto the newly machined surface. The author also observed radial flank wear on the drill margin in all experiments. Though not severe, but presence of flank wear BUE on the margin was quite visible during analysis. Titanium alloy Ti-6Al-4V is known for its strain hardening capabilities. As a result of plastic deformation during cutting, hardness of the machined surface increases. Black burn marks, likely caused by high temperatures and pressures at the drill point, were observed on the flank surface of the tools. Chip evacuation is a critical factor in designing a high-performance drill. Lack of coolant pressure through the spindle through coolant for evacuating chips were also the likely cause of burn marks appearing on the cutting tool flank. The surface roughness of drilled holes in Ti-6Al-4V were measured and averages taken. Averages between 0.38 and 0.54 *Ra* were taken and no outliers were found in the experimental ANOVA was performed on the results and the main effect diagrams were developed as shown in Fig. 102. A Pareto ANOVA diagram based on the sum of squares of the results was developed, Fig. 103, to show the contribution of each parameter and their interactions on tool life. Tough the ANOVA analysis does not provide a clear indication as to which geometrical factor is the main contributor to the performance of the cutting tool, one experiments stands out more than others. However, uniform flank wear was the only form of tool wear which was observed in experiment 7 (Ti1 D 2FL 8 7) after the cutting tool had drilled 178 holes, Fig. 109. This cutting tool with a helix angle of 30°, drill point angle of 140°, cutting angle of 5° and relief angle of 10° managed outperformed all other experiments on Ti-6Al-4V whilst an average tool wear of just under 46 µm was measured across the cutting edges. No chipping on the periphery was observed in both the first tool and its replicate. Further experiments at different levels may be required to confirm the most suitable tool geometry in drilling of Ti-6Al-4V.

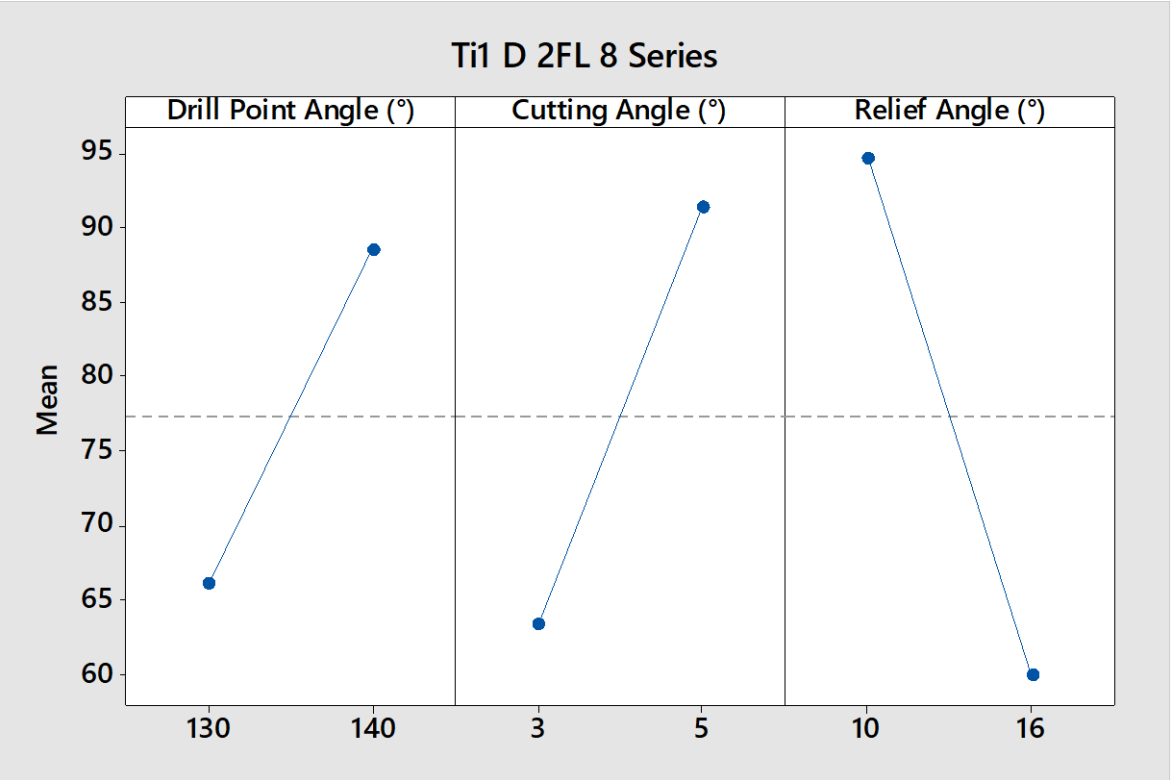

Fig. 102: Main effects plot of drill geometrical parameters investigated in Ti-6Al-4V

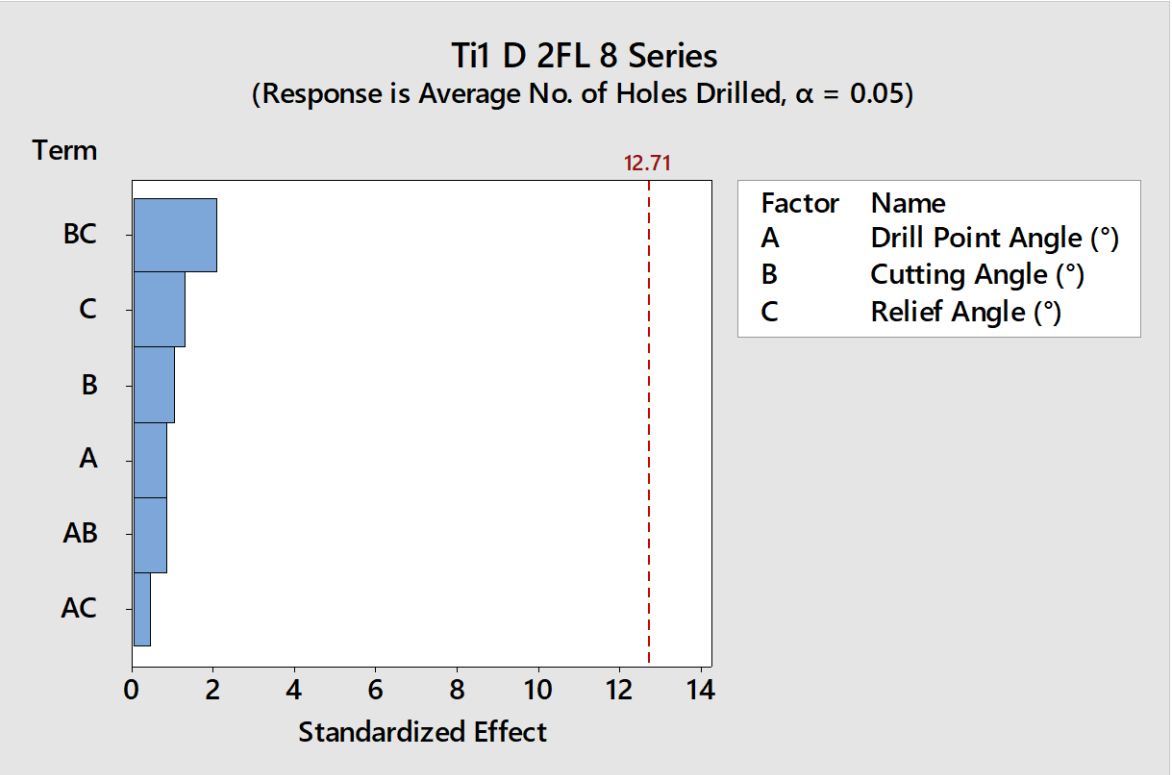

Fig. 103: Pareto ANOVA of geometrical factors in drilling experiments on Ti-6Al-4V

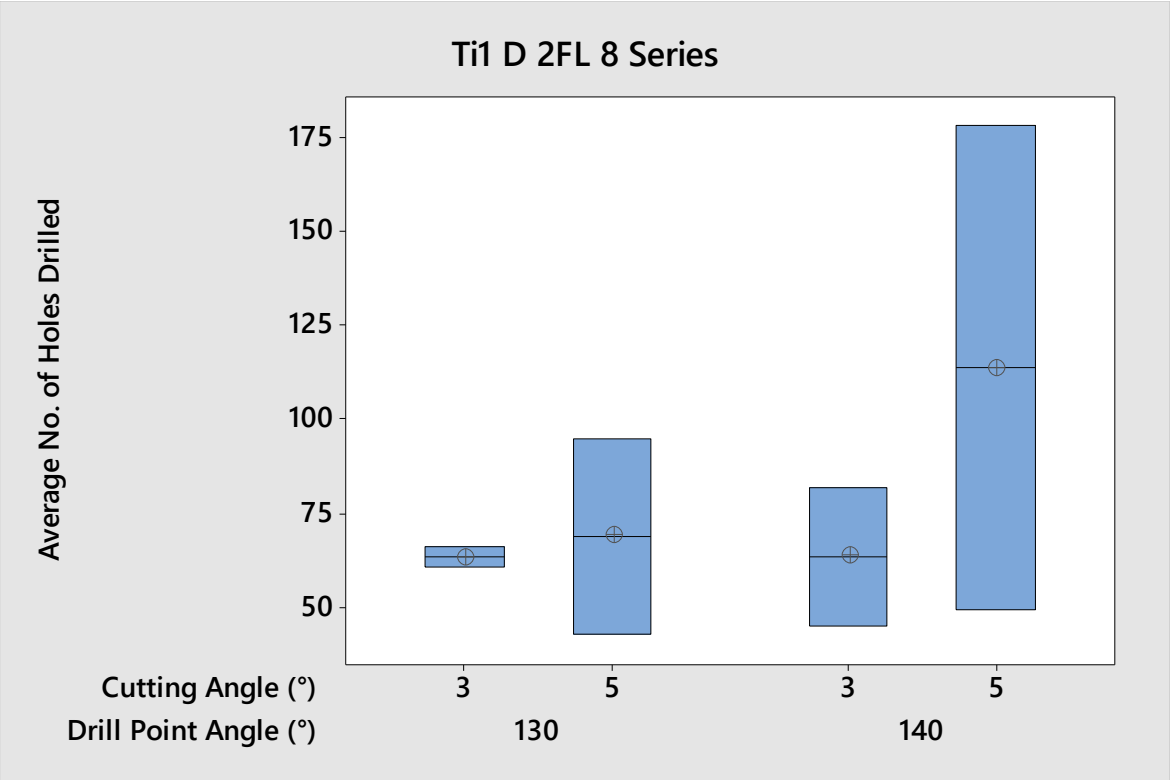

Fig. 104: Box plot of interactions between drill point angle and cutting angle at different levels based on tool life data collected from drilling experiments on Ti-6Al-4V

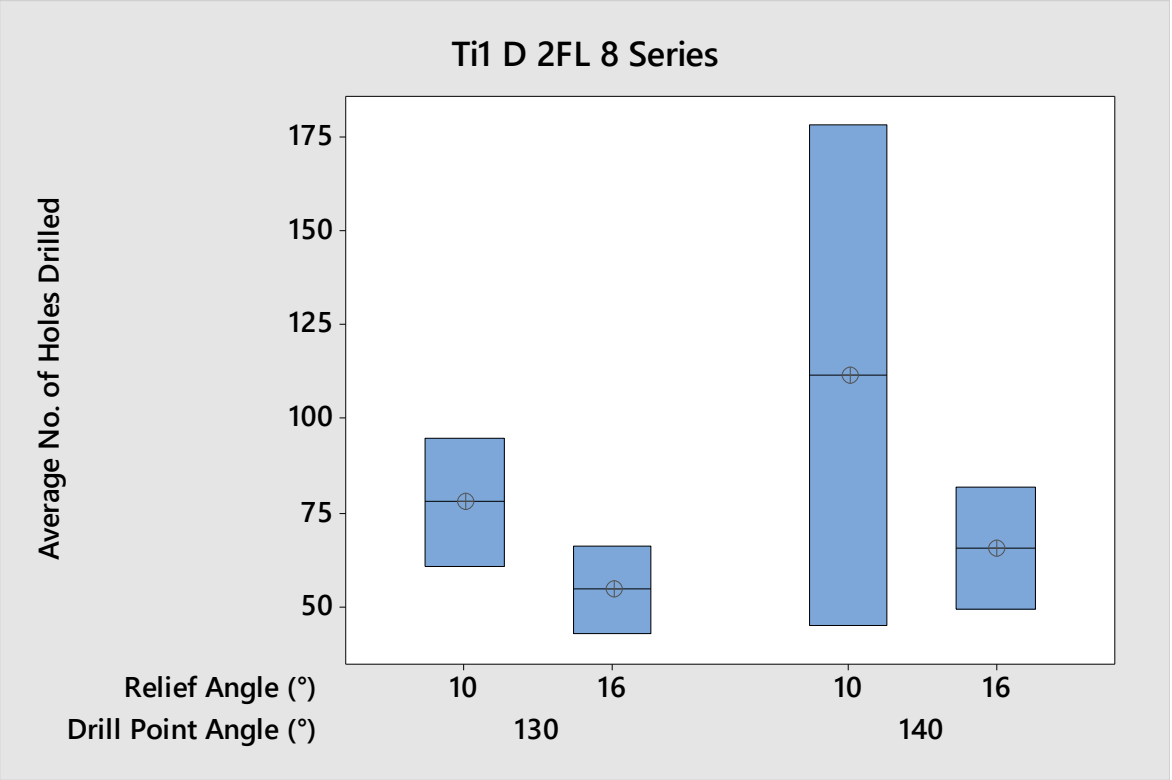

Fig. 105: Box plot of interactions between drill point angle and relief angle at different levels based on tool life data collected from drilling experiments on Ti-6Al-4V

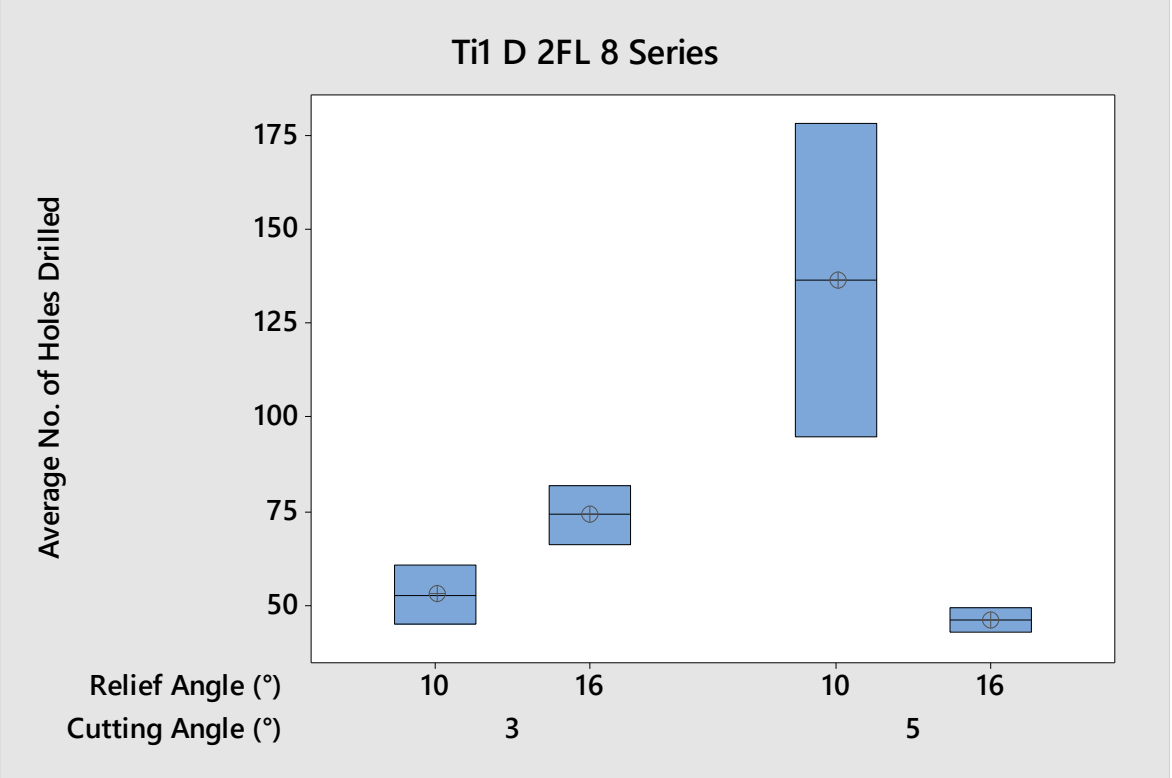

Fig. 106: Box plot of interactions between cutting angle and relief cutting angle at different levels based on tool life data collected from drilling experiments on Ti-6Al-4V

Table 23: Analysis of variance for transformed response of tool life in drilling of Ti-6Al-4V

Parameters	(DF)	Adj (SS)	Adj (MS)	F-value	P-value
Drill point angle (A)	1	990.1	990.12	0.67	0.564
Cutting angle (B)	1	1540.1	1540.13	0.93	0.494
Relief angle (C)	1	2415.1	2415.13	1.63	0.423
A*B	1	990.1	990.13	0.67	0.564
A*C	1	253.1	253.13	0.17	0.751
B*C	1	6216.1	6216.12	4.19	0.289
Error	1	1485.1	1485.13	-	-
Total	7	13889.9	-	-	-

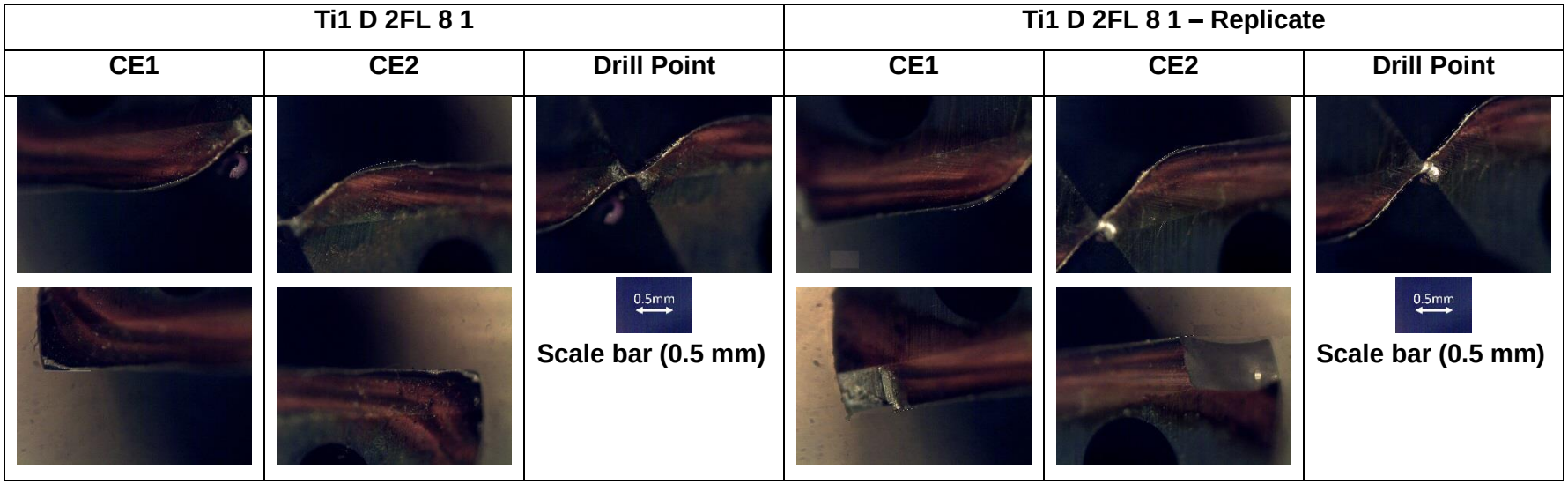

Fig. 107: Chipping at the corners in drilling of Ti-6Al-4V

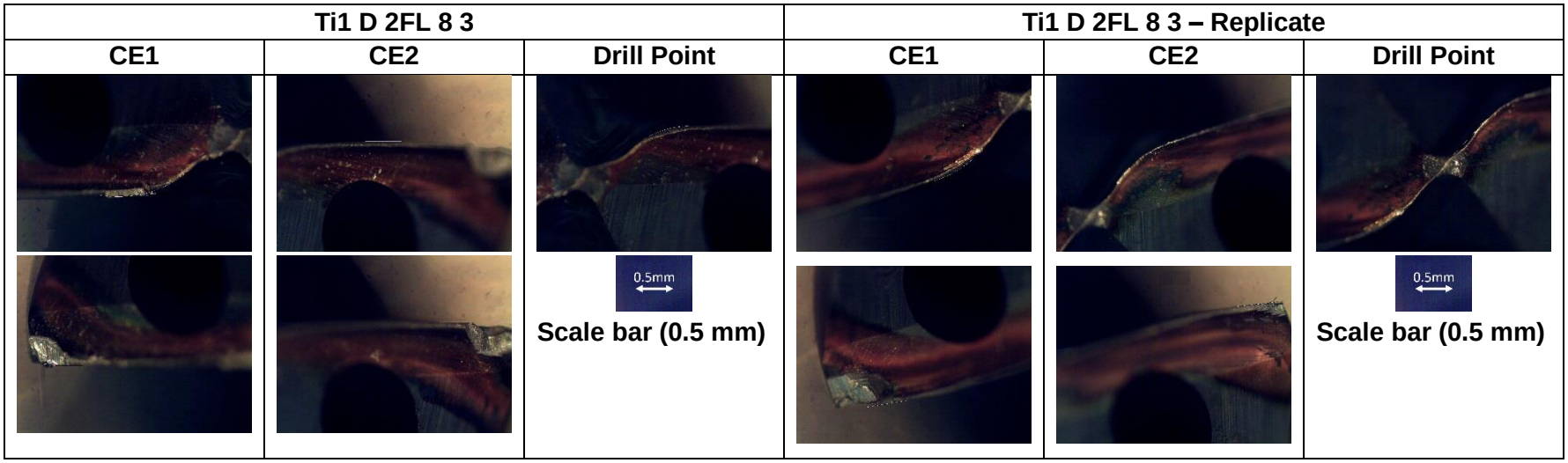

Fig. 108: Examples of BUE on the cutting edges in drilling of Ti-6Al-4V

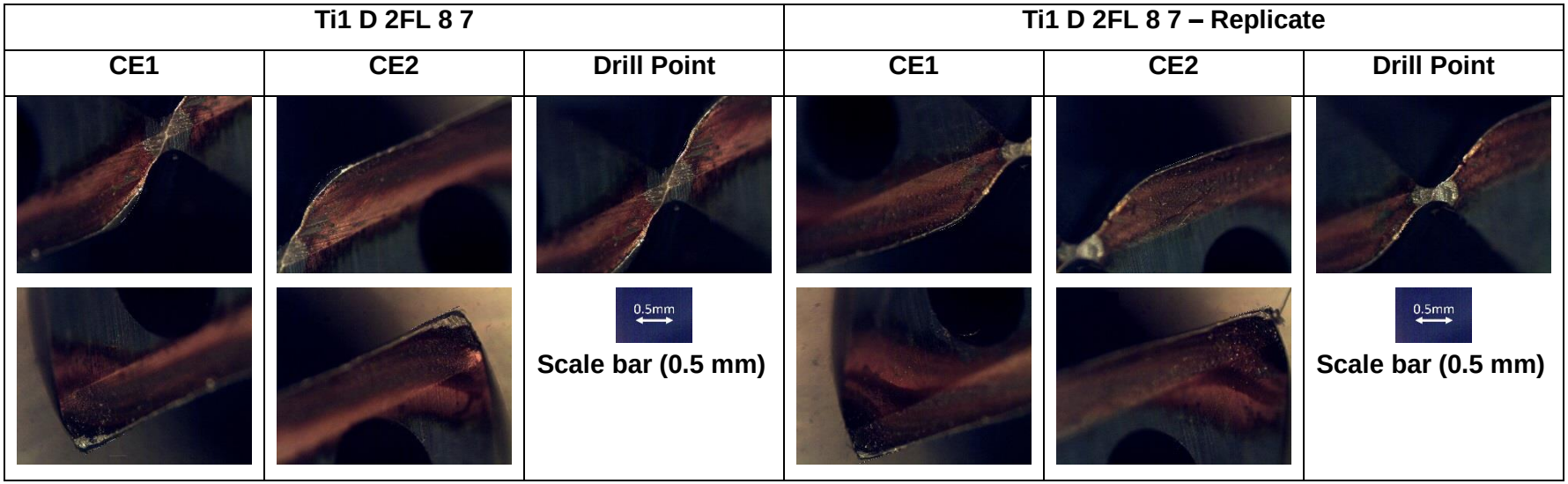

Fig. 109: Cutting tool wear after machining an average of 178 holes

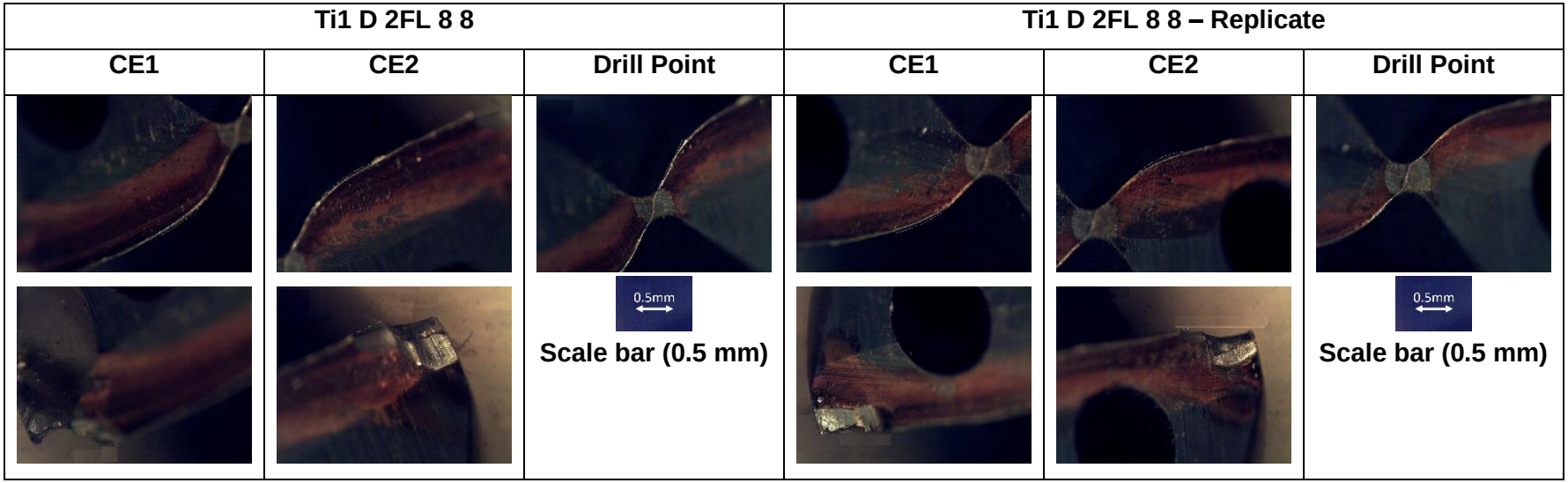

Fig. 110: Extreme cutting tool wear at the corners and chisel edge flank wear at the drill point

On average, worn and unworn cut chip samples acquired from drilling experiments on Ti-6Al-4V varied in shape and size. Excluding the long continuous spiral cone chips produced at the initial cut of every drilling operation, cut chips collected from samples were found to be curved, discontinuous and segmented (Fig. 111 and Fig. 112). However, shapes varied from compressed or folded ribbon like chips to half helical chips (Fig. 111). This was observed in the majority of drilling experiments carried out on difficult-to-cut material, Ti-6Al-4V. Cut chips collected from the first hole and last hole often exhibited smooth edges with short tales. No major differences were observed between unworn and worn chips from the experiments. Due to tool wear and wear at the periphery of the drills the author observed a higher presence of short ribbon like chips towards the end of life of the drills in the majority of experiments. No major or significant changes were observed in the shape and size of unworn and worn titanium chips.

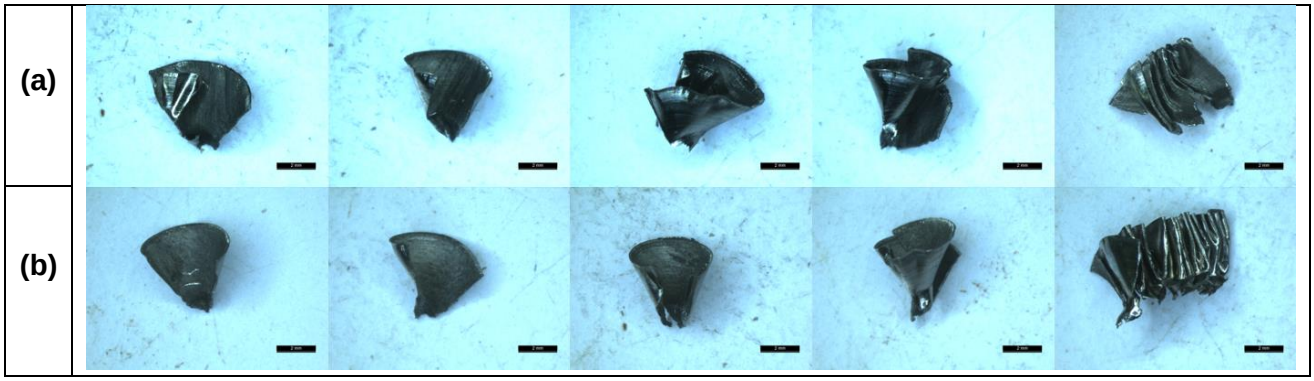

Fig. 111: Examples of various chips obtained from drilling experiments on Ti-6Al-4V based on straight flute - (a) chips collected after drilling the first hole, (b) chips collected after drilling the final hole

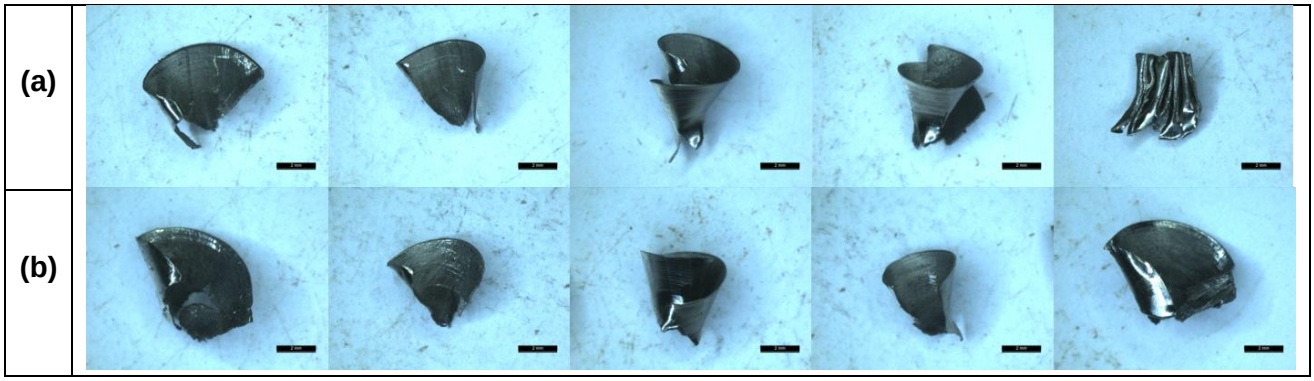

Fig. 112: Examples of various chips obtained from drilling experiments on Ti-6Al-4V based on straight flute - (a) chips collected after drilling the first hole, (b) chips collected after drilling the final hole

5.3.3 Inconel 718

Tool life was measured for each experiment in terms of number of holes as shown in Appendix F (Fig. 151). All cutting tools, irrespective of the geometry, suffered from flank wear in drilling of Inconel 718. Tool wear occurs at a rapid rate at the cutting zone with high temperatures at the tool-chip interface, softening the tool material and making it vulnerable to chipping and abrasive wear. Furthermore, this caused cut chips to weld onto the cutting edge of the tools during machining, blocking the flow of chips on the rake face. The drill cutting speed at the drill point is essentially zero. Though no material is cut at this point, high temperatures due to friction increase the chance of tool failure. Excessive wear was observed on the outer corner of the cutting edges during tool wear analysis of the drills, mostly due to high flank wear and chipping at the corners. This is caused by rubbing the outer surface of the drill onto the newly machined surface (Fig. 122). Inconel 718 is known for its strain hardening capabilities. As a result of plastic deformation during cutting, hardness of the machined surface increases. Together with hard carbide particles present within the material, this results in excessive abrasive wear on the flank face of the tool. Excessive tool wear on the flank face was observed and documented which resulted in chipping on the cutting edges (Fig. 123). High pressures in combination with the high chemical affinity of the workpiece with the cutting tool material are reasons for the built-up of Inconel 718 on the cutting edges (Fig. 121). Black burn marks likely caused by high temperatures and pressures at the drill point were observed on the flank surface of the tools. Chip evacuation is a critical factor in designing a high-performance drill. Lack of coolant pressure and evacuating chips were also the likely cause of burn marks appearing on the cutting tool flank.

Analysis of Variance (ANOVA) was applied to the results obtained from experiments to determine the effect of each geometrical parameter on tool life in drilling Inconel 718. As shown in Table 24, drill point angle, relief angle and their interaction were the most significant parameters affecting tool life. A Pareto ANOVA diagram based on the sum of squares of the results was developed, Fig. 113 to show the contribution of each parameter and their interactions on tool life. As shown in Fig. 113 of the tool life can be effectively controlled by cutting angle, relief angle and the drill point angle and their interactions and supporting the main effects plot of the results Fig. 114.

Table 24: Analysis of variance for transformed response of tool life in drilling of Inconel 718

Parameters	(DF)	Adj (SS)	Adj (MS)	F-value	P-value
Model	10	2510.00	251.00	7.56	0.019
Linear	4	1136.25	284.06	8.56	0.018
Helix angle (A)	1	36.00	36.00	1.08	0.345
Drill point angle (B)	1	144.00	144.00	4.34	0.092
Cutting angle (C)	1	576.00	576.00	17.35	0.009
Relief angle (D)	1	380.25	380.25	11.45	0.020
Two-way Interactions	6	1373.75	228.96	6.90	0.026
A*B	1	100.00	100.00	3.01	0.143
A*C	1	144.00	144.00	4.34	0.092
A*D	1	156.25	156.25	4.71	0.082
B*C	1	169.00	169.00	5.09	0.074
B*D	1	342.25	342.25	10.31	0.024
C*D	1	462.25	462.25	13.92	0.014
Error	5	166.00	33.20	-	-
Total	15	2676.00	-	-	-

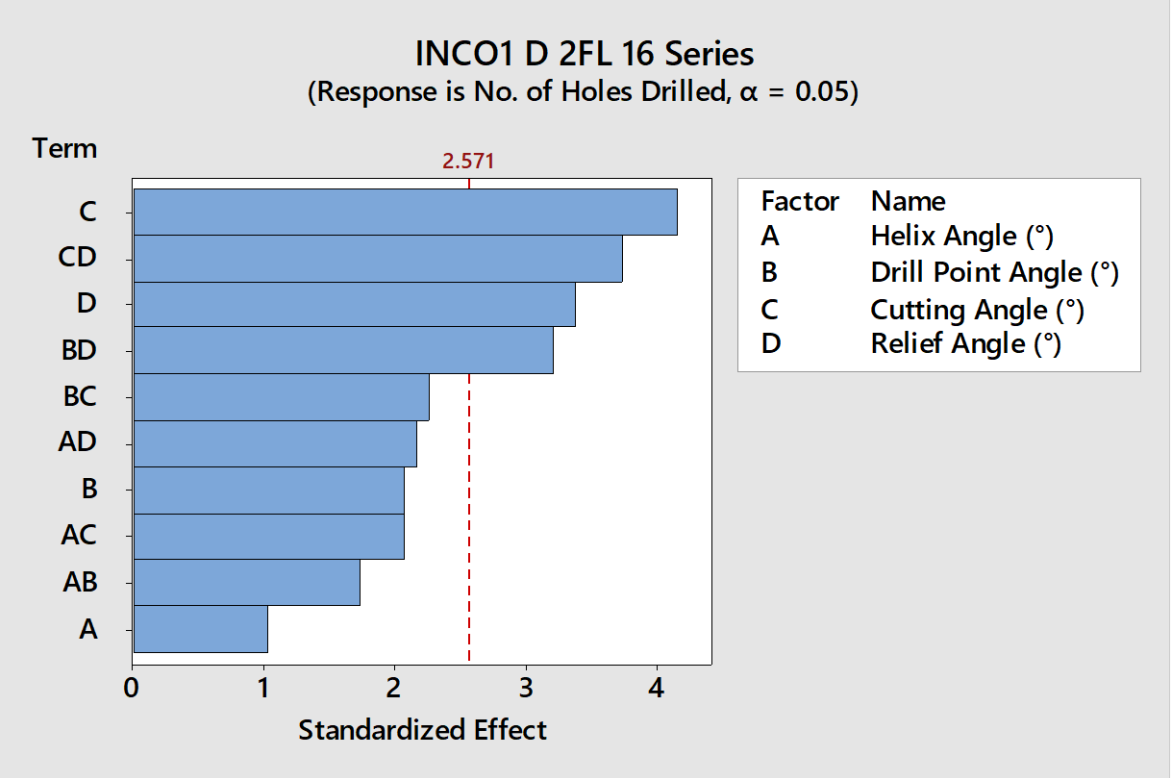

Fig. 113: Pareto ANOVA of geometrical parameters in drilling of Inconel 718

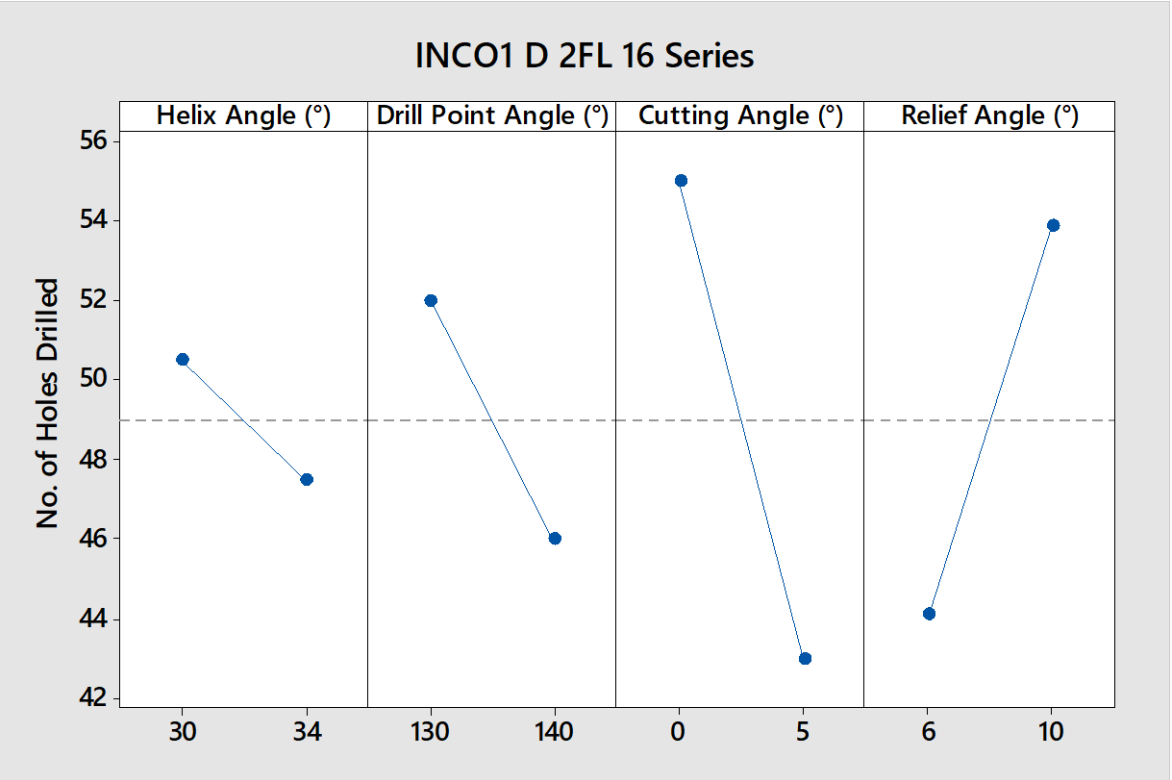

Fig. 114: Main effects plot of drill geometrical parameters investigated in drilling Inconel 718

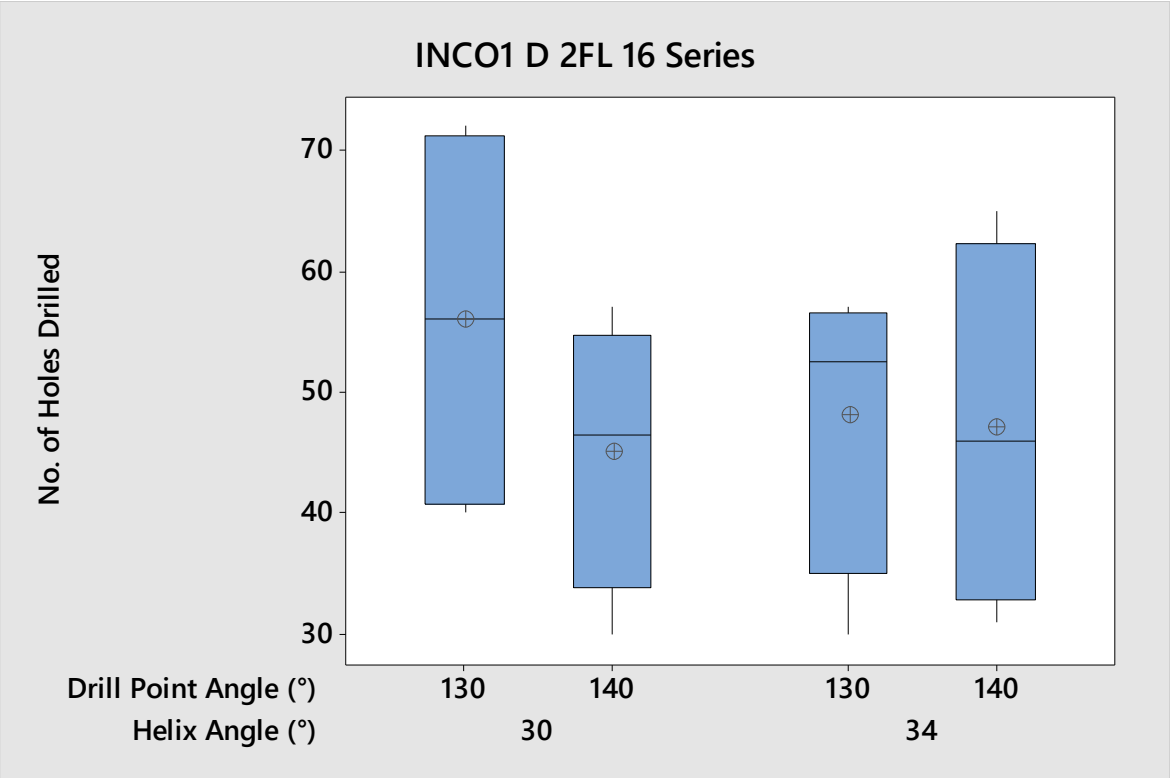

Fig. 115: Box plot of interactions between helix angle and drill point angle at different levels based on tool life data collected from drilling experiments on Inconel 718

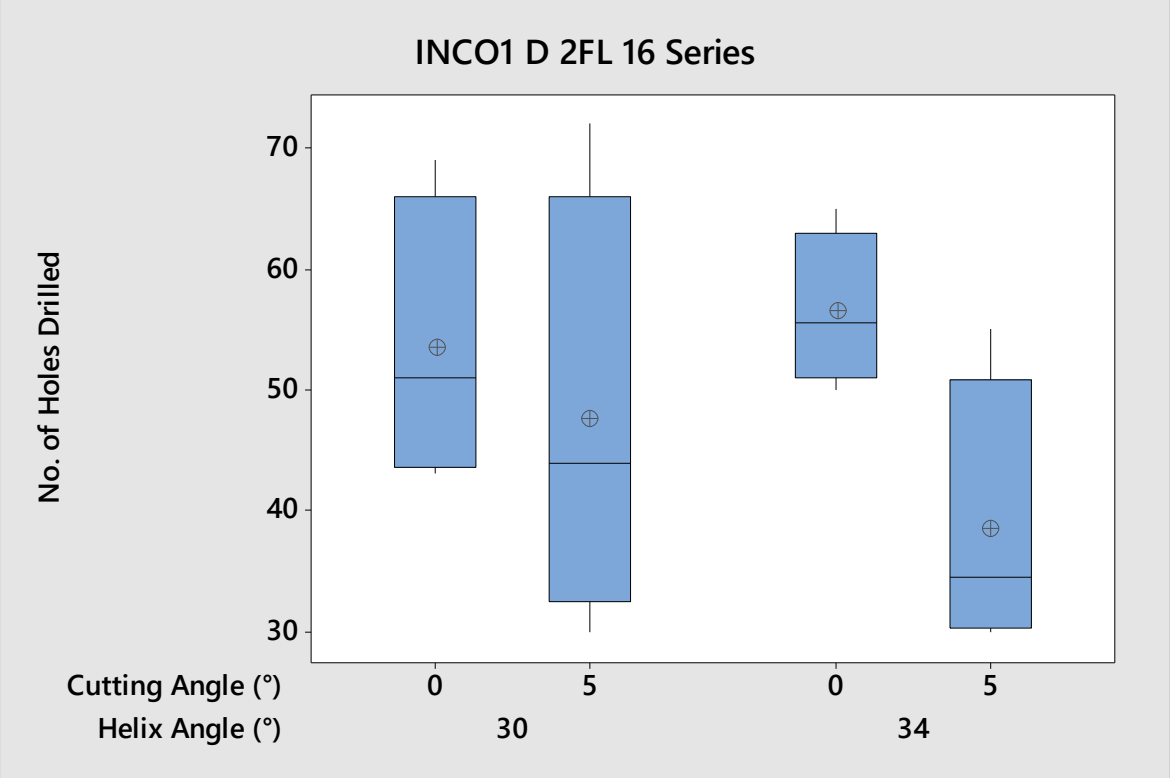

Fig. 116: Box plot of interactions between helix angle and cutting angle at different levels based on tool life data collected from drilling experiments on Inconel 718

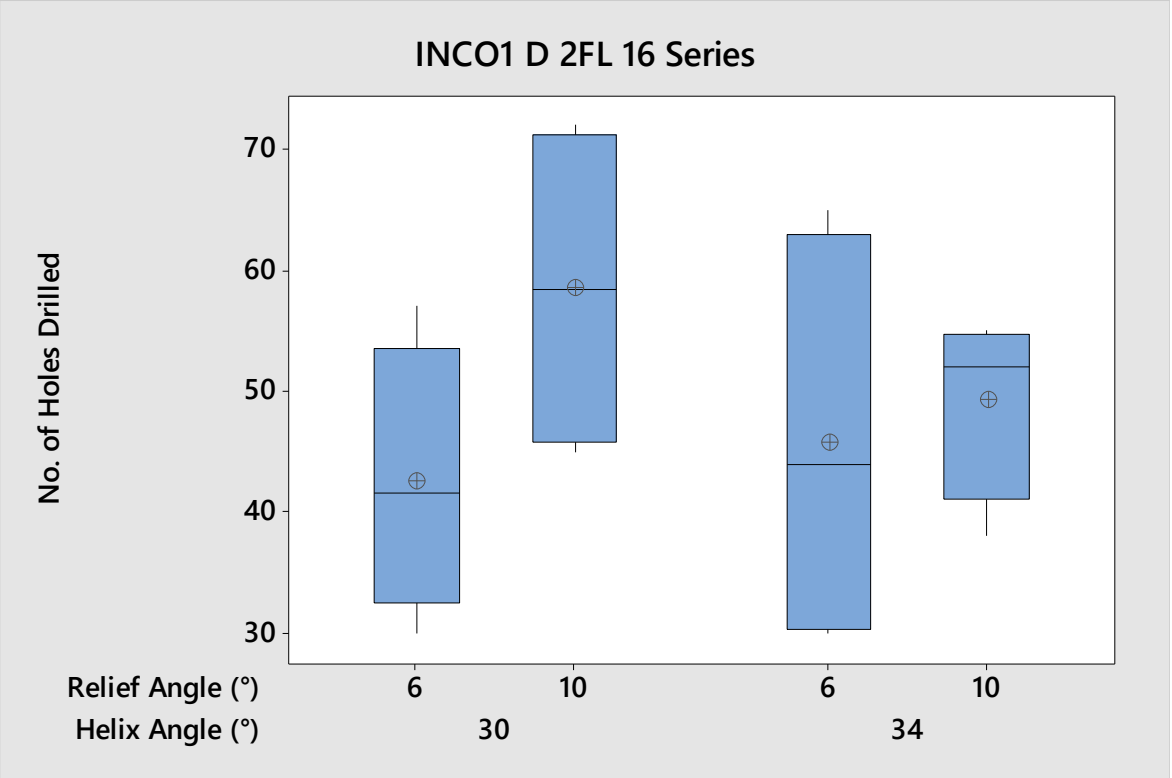

Fig. 117: Box plot of interactions between helix angle and relief angle at different levels based on tool life data collected from drilling experiments on Inconel 718

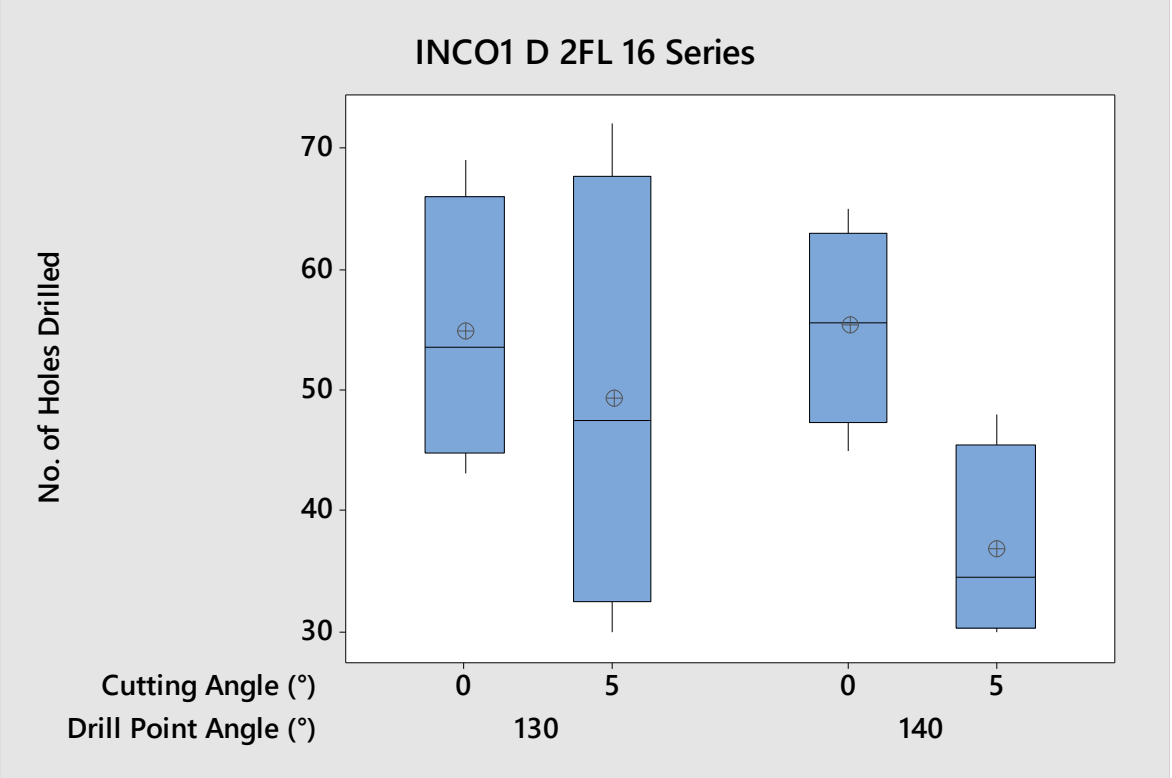

Fig. 118: Box plot of interactions between drill point angle and cutting angle at different levels based on tool life data collected from drilling experiments on Inconel 718

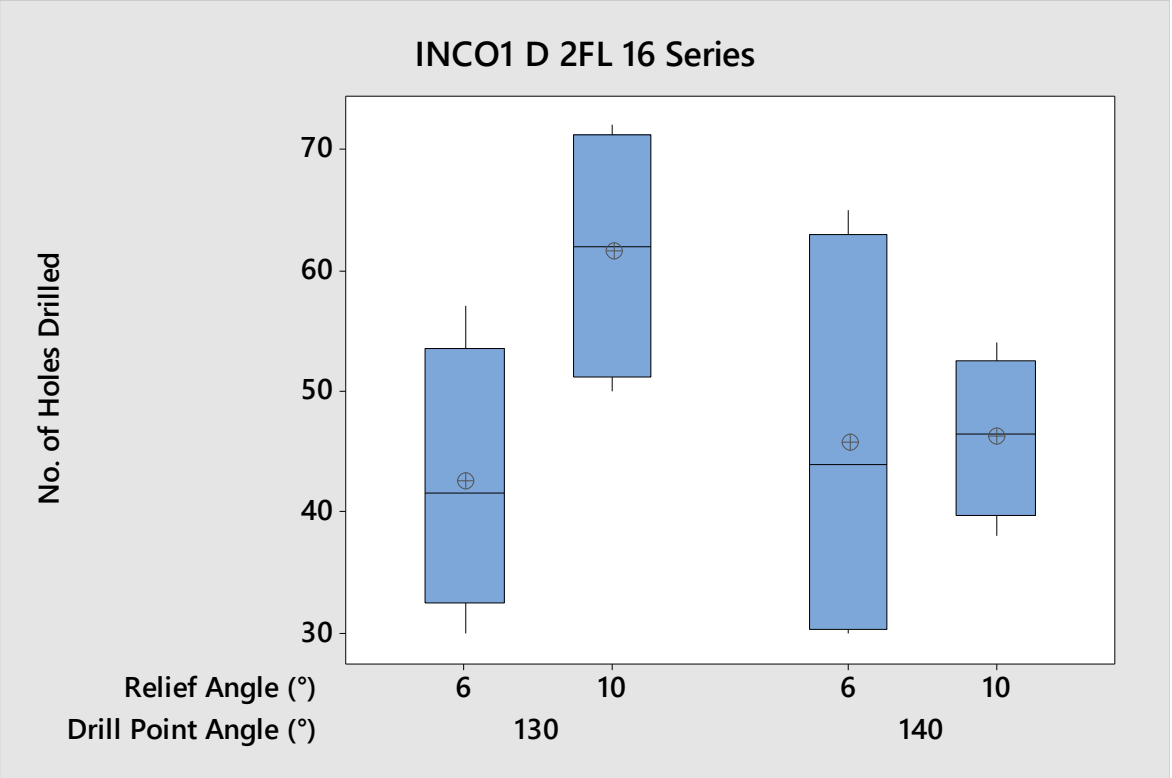

Fig. 119: Box plot of interactions between drill point angle and relief angle at different levels based on tool life data collected from drilling experiments on Inconel 718

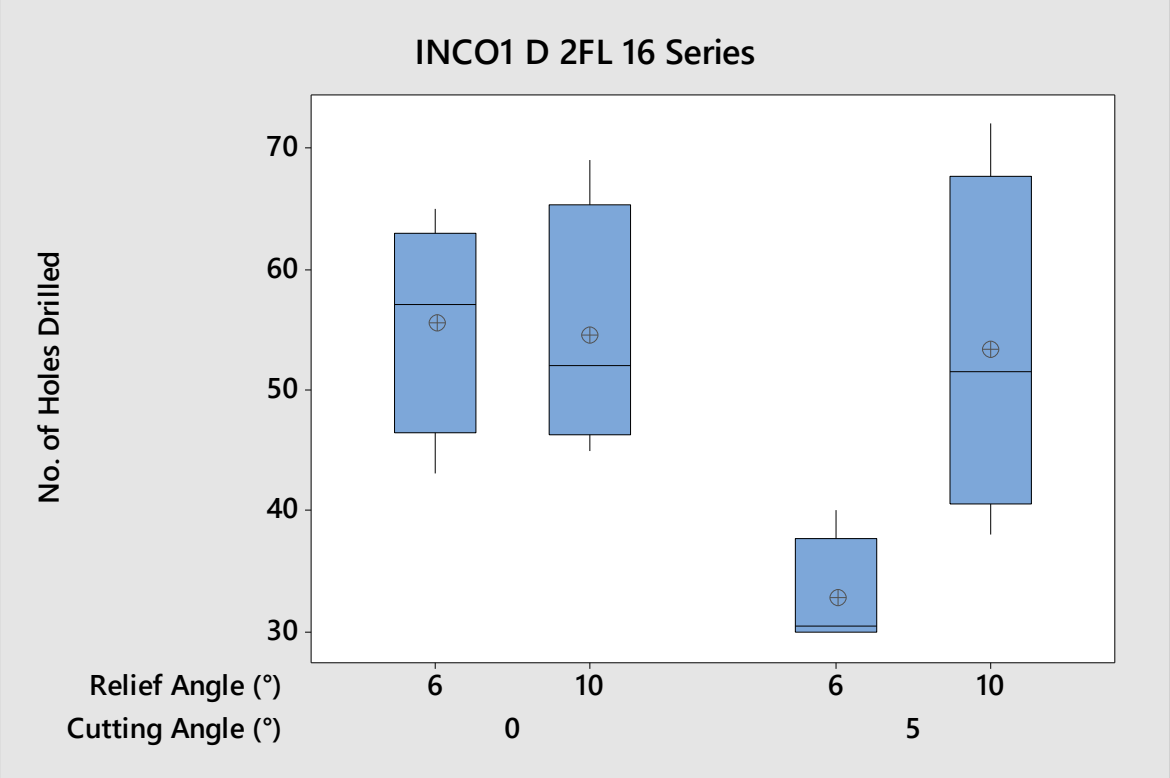

Fig. 120: Box plot of interactions between cutting angle and relief angle at different levels based on tool life data collected from drilling experiments on Inconel 718

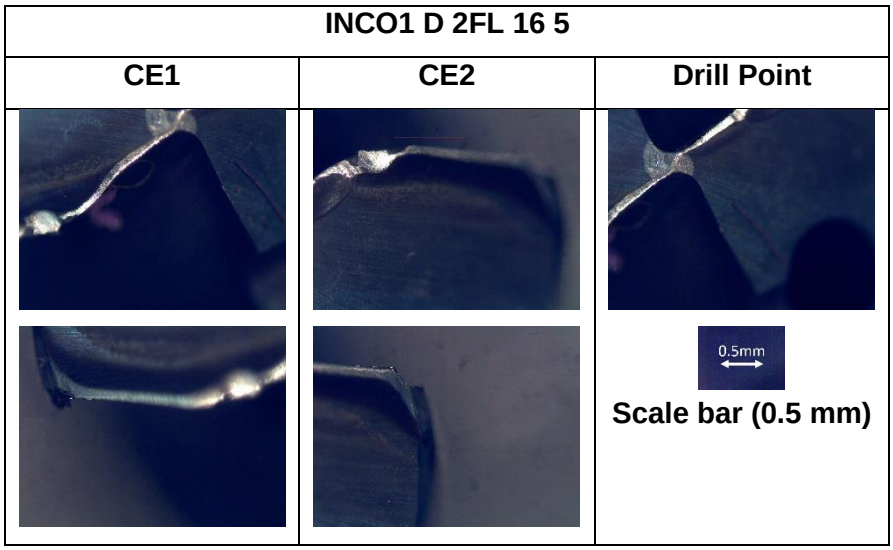

Fig. 121: An example of BUE observed during tool wear analysis in drilling of Inconel 718

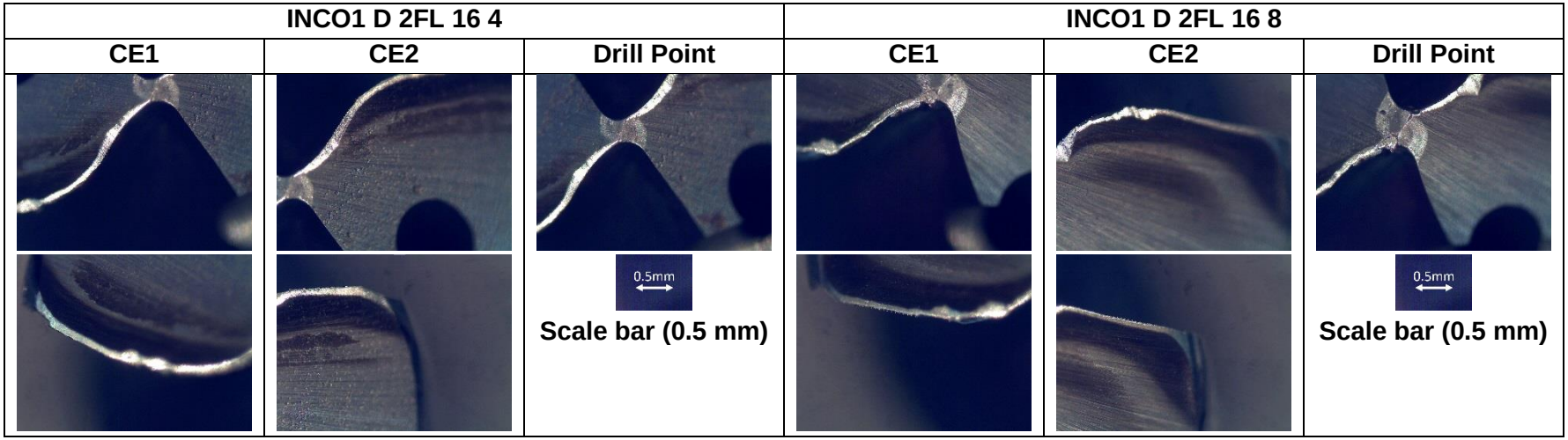

Fig. 122: Examples of flank wear and flank wear on the chisel edge in drilling of Inconel 718

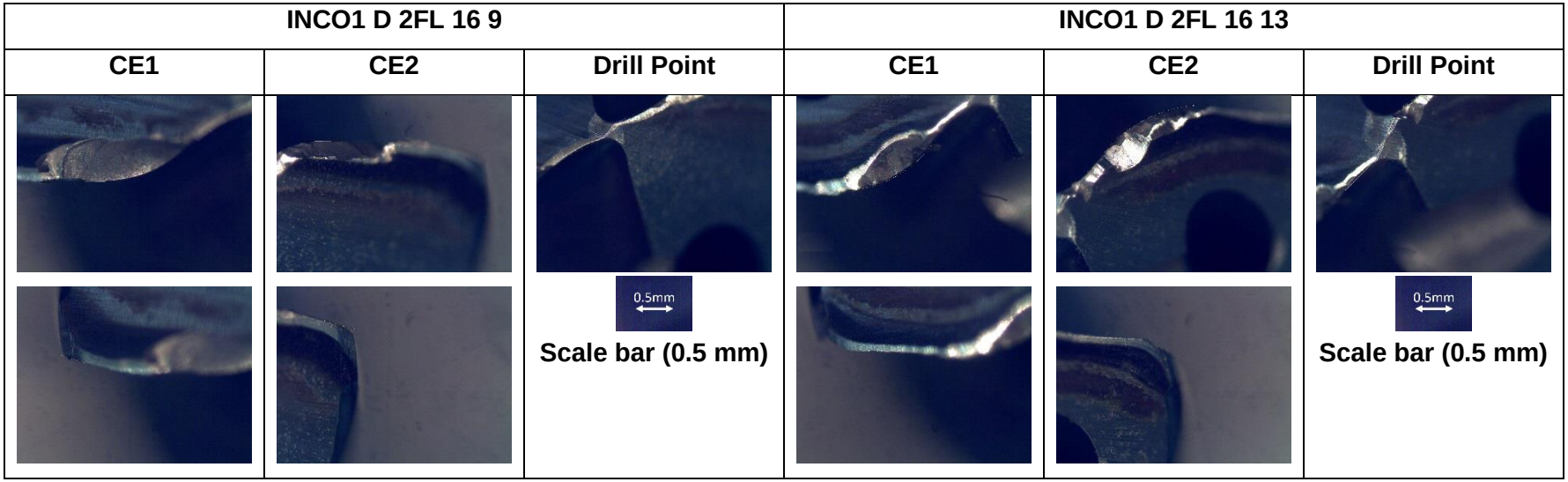

Fig. 123: Examples of chipping in drilling of Inconel 718

An ideal chip should be helical, segmented and discontinuous. Over time, due to tool wear, cut chips begin to change in shape, indicating the end of life of the drill. In drilling experiments conducted on Inconel 718 the chip samples collected matched the ideal chip specifications set by [160]. As shown in Fig. 124 (a) and Fig. 125 (a), two separate experiments, chips collected after drilling one hole in Inconel 718 are fairly regular in shape and size. However, rapid tool wear occurs in machining Inconel 718 and over time irregularity in chips begins to show. For example, in experiments INCO1 D 2FL 16 6, Fig. 124 (a) majority of chips collected after drilling the initial hole in Inconel 718 were similar, and occasionally with long tails. Whereas, samples collected from the same experiment, once the last hole was drilled, were more asymmetrical, Fig. 124 (b), with serrated edges. The experiment with the least amount of irregularities in chip formation was INCO1 D 2FL 16 9, with helical, segmented and discontinuous chips; even after the last hole was drilled. Examples of various chips obtained from the samples collected from the experiment after the first and last drilled hole is shown in Fig. 125 (a) and (b), respectively.

Fig. 124: Various chips obtained from INCO1 D 2FL 16 6 drilling Inconel 718 - (a) chips collected after the first drilled hole, (b) chips collected after the final drilled hole

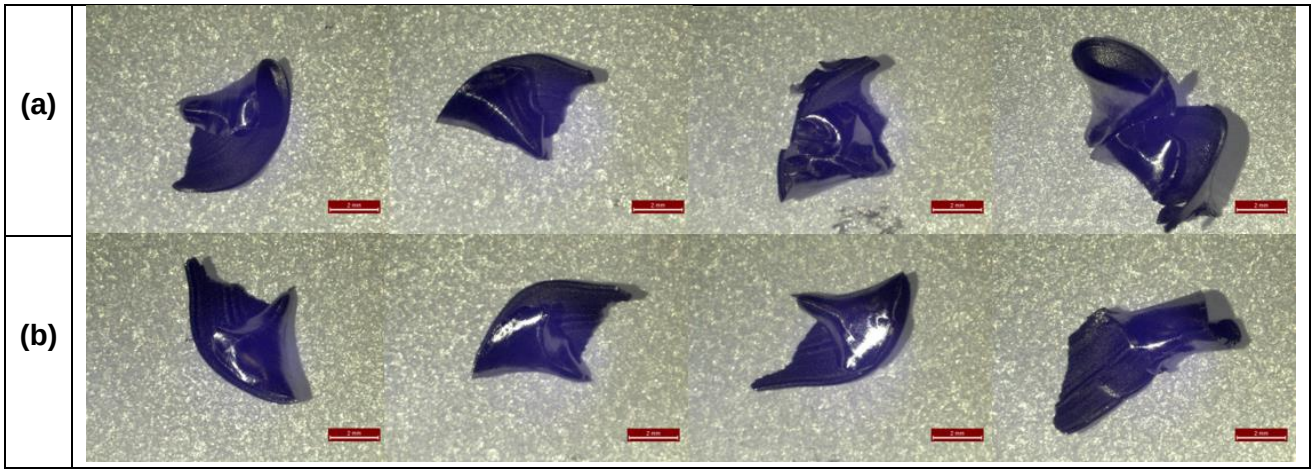

Fig. 125: Various chips obtained from INCO1 D 2FL 16 9 drilling Inconel 718 - (a) chips collected after the first drilled hole, (b) chips collected after the final drilled hole

5.3.4 Super Duplex 2507

The final drilling experiments were conducted on super duplex 2507 where 8, 2-flute, helical drills, with various tool geometries were investigated. No replications for these experiments were carried out in this series due to limited and availability of workpiece material. Three geometrical parameters selected for this series, were the drill point angle, cutting angle and relief angle. The ANOVA results did not show any significance in the three factors under investigation (Fig. 127). This means that further experimentation and testing based on tool geometry is required to be able to determine the most suitable tool geometry in machining of super duplex 2507.

Results of the ANOVA based on tool life, for each factor and their interactions, are presented in Table 25, Irrespective of tool geometry, flank wear was the dominant form of tool wear on the cutting edges in drilling of super duplex alloy 2507 (Fig. 133 and Fig. 134). Abrasion was also observed at the drill point in all experiments due to the contact between the WC-Co grinding against the surface of the workpiece material. The author also observed extreme radial flank wear on the margin of some drills. An example of this form of tool wear has been provided in Fig. 133. It was also noted that drills with a relief angle of 12° exhibited less wear on the drill margin. Chipping near the drill point was observed during the analysis phase which was probably caused by high temperatures at the cutting zone and the lack of coolant pressure going through the spindle through coolant method for delivering lubrication between the cutting edges and the workpiece material (Fig. 126). Consistent surface roughness results, based on drilled holes in 2507, were obtained; varying from 0.7-0.8 *Ra* when measured for each experiment (Fig. 169). The final experiment in this series, SDX1 D 2FL 8 8, or the eighth, experiment stood out from the rest with after it had drilled 166 at a depth of 24 mm and a tool wear of just under 141 μm. Experiment was completed when chipping at the drill point and margin of the drill was observed.

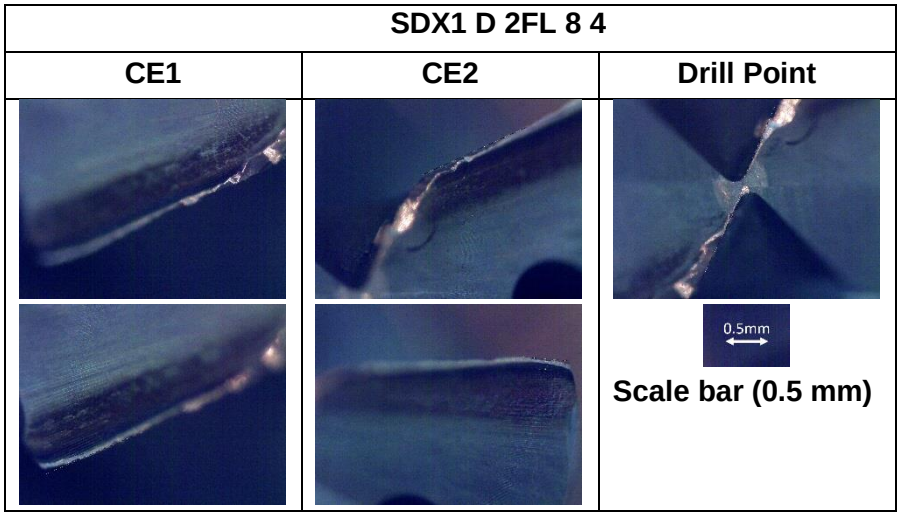

Fig. 126: Chipping near the drill point in drilling of 2507

Table 25: Analysis of variance for transformed response of tool life in drilling of 2507

Parameters	(DF)	Adj (SS)	Adj (MS)	F-value	P-value
Model	6	9845.0	1640.83	0.83	0.686
Linear	3	1230.5	410.17	0.21	0.885
Drill point angle (A)	1	924.5	924.5	0.47	0.619
Cutting angle (B)	1	288.0	288.0	0.15	0.768
Relief angle (C)	1	18.0	18.0	0.01	0.940
Two-way Interactions	3	8614.5	2871.50	1.45	0.533
A*B	1	2450.0	2450.0	1.23	0.467
A*C	1	3200.0	3200.0	1.61	0.425
B*C	1	2964.5	2964.5	1.49	0.437
Error	1	1984.5	1984.5	-	-
Total	7	11829.5	-	-	-

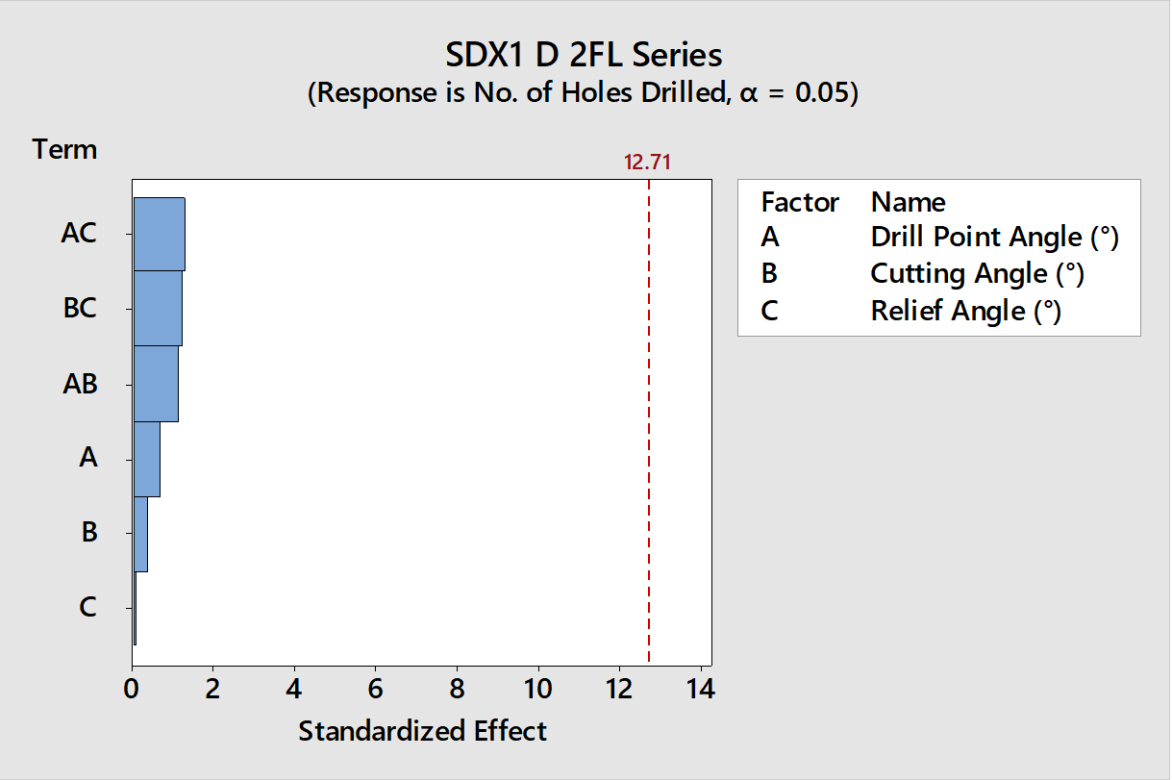

Fig. 127: Pareto ANOVA of geometrical parameters in drilling of 2507

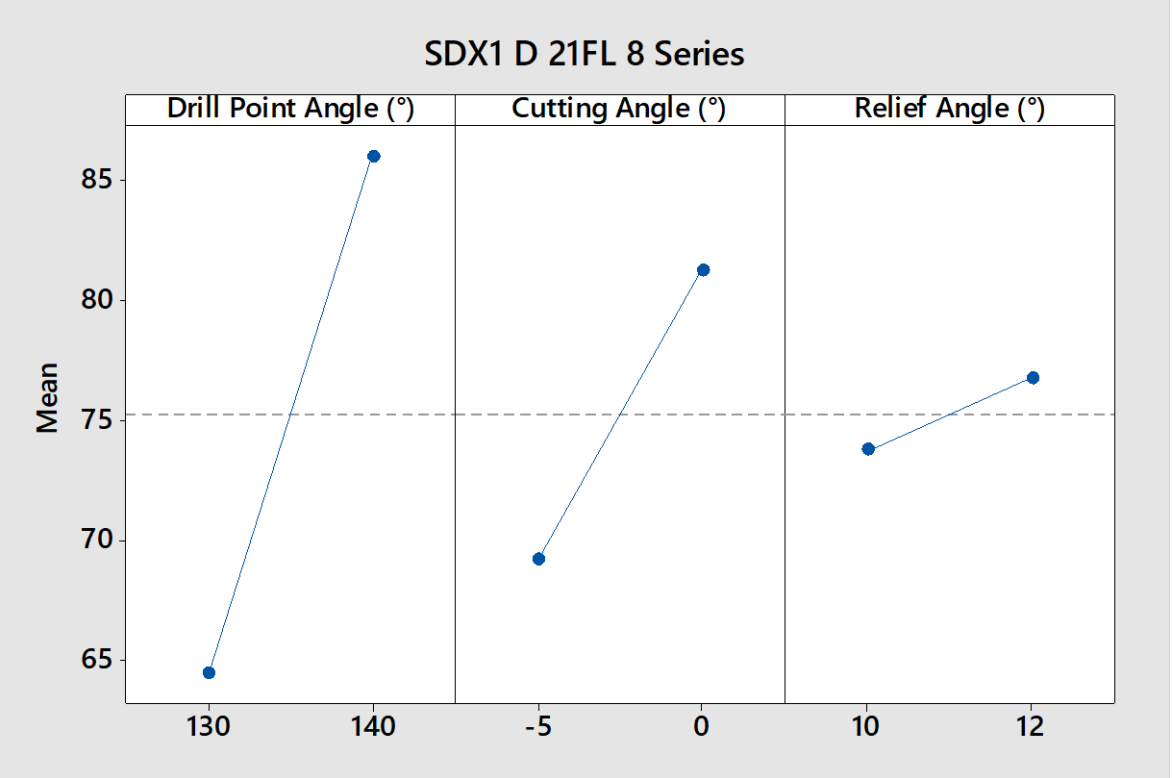

Fig. 128: Main effects plot of geometrical parameters in drilling of 2507

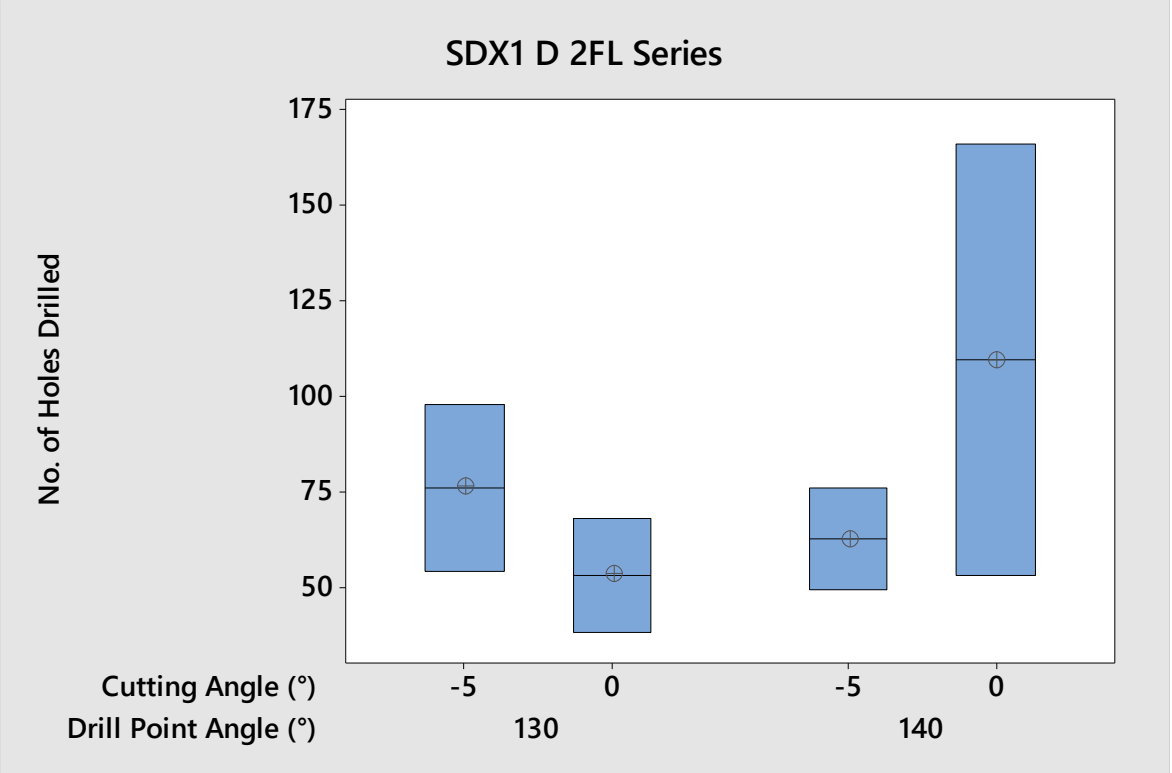

Fig. 129: Box plot of interactions between drill point angle and cutting angle at different levels based on tool life data collected from drilling experiments on Inconel 718

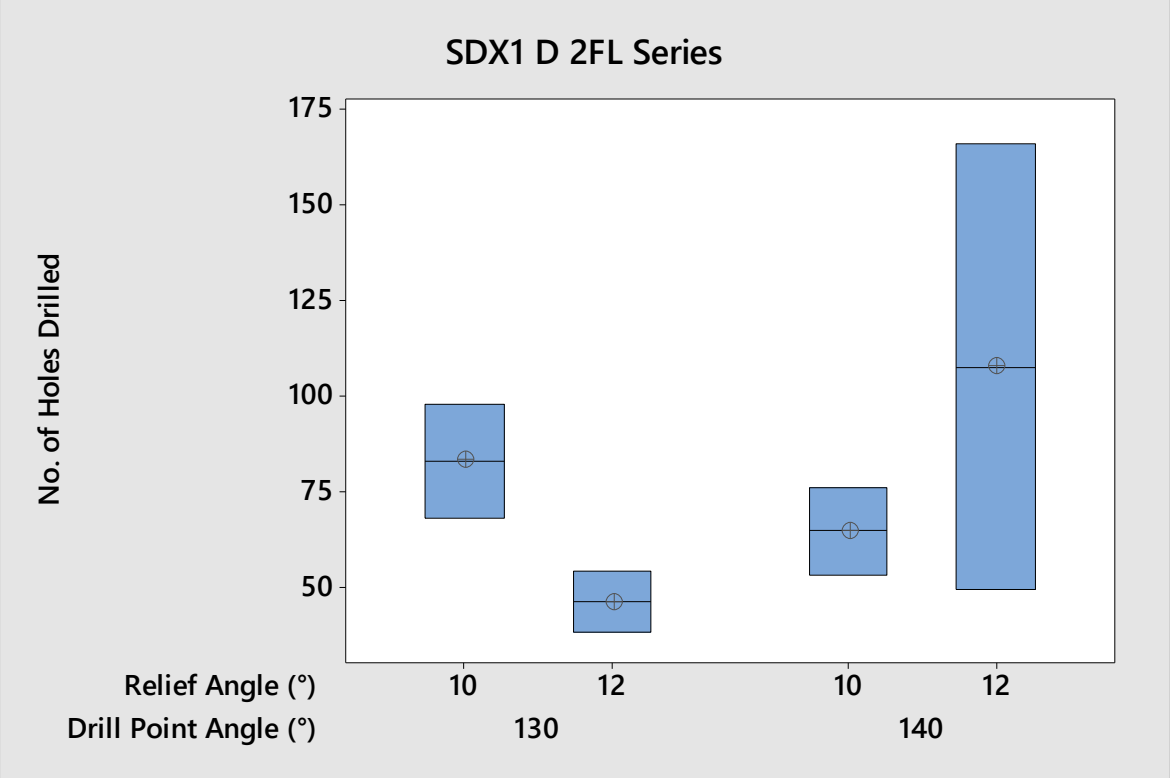

Fig. 130: Box plot of interactions between drill point angle and relief angle at different levels based on tool life data collected from drilling experiments on Inconel 718

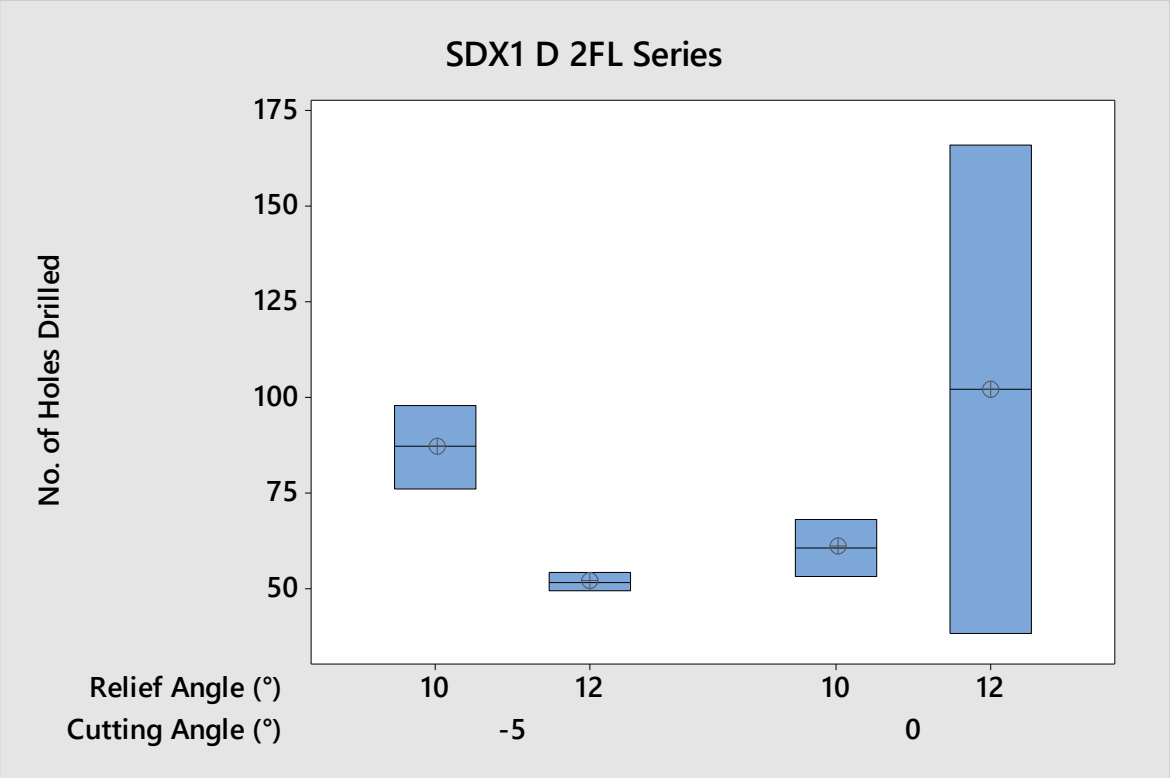

Fig. 131: Box plot of interactions between cutting angle and relief angle at different levels based on tool life data collected from drilling experiments on Inconel 718

When compared to Inconel 718, chips obtained from the drilling experiments on alloy 2507 chips were regular in size and shape with small tails at the cut-off point; where plastic deformation had occurred due to shearing motion of the cutting tool. No significant differences were observed between the initial and final chip samples of all experiments (Fig. 134). Segmented chips with saw-toothed edges were observed and seemed to dominate the samples; however, occasional irregular chips were observed during the analysis phase. Compressed and short-continuous chips were observed at the beginning and the end of experiments, Fig. 132 (first image on the right unworn and worn). These chips occurred randomly during the experiments but did not disturb the experiments. No other important observations were noted in drilling experiments on alloy 2507.

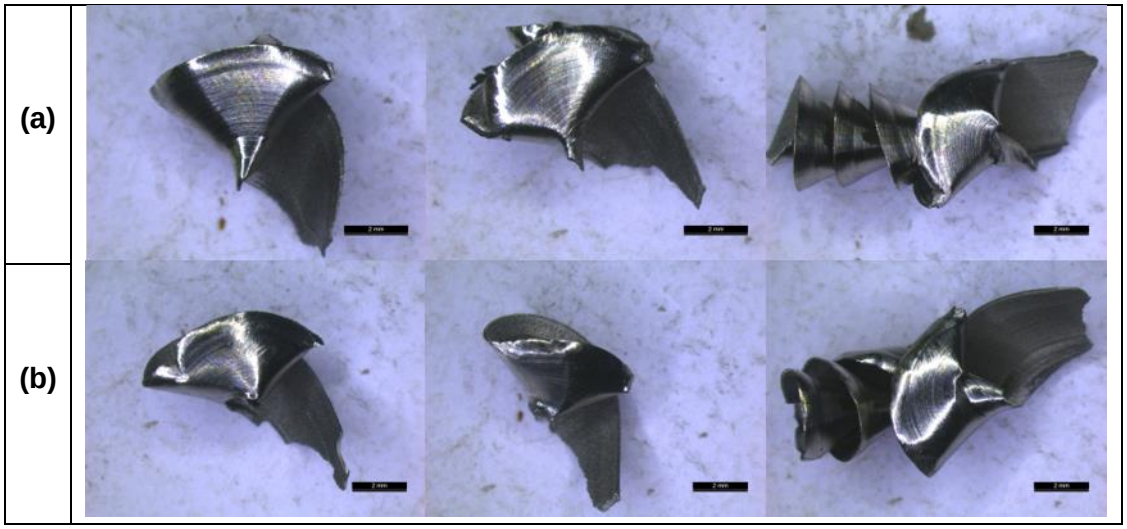

Fig. 132: Various chips obtained from SDX1 D 2FL 8 8 drilling super duplex alloy 2507 - (a) chips collected after the first drilled hole, (b) chips collected after the final drilled hole

SDX1 D 2FL 8 2				
CE1	**CE2**	**Drill Point**	**CE1 - Radial Flank Wear**	**CE2 – Radial Flank Wear**
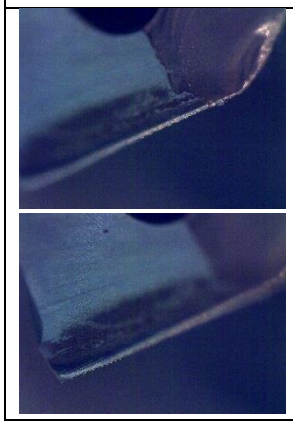	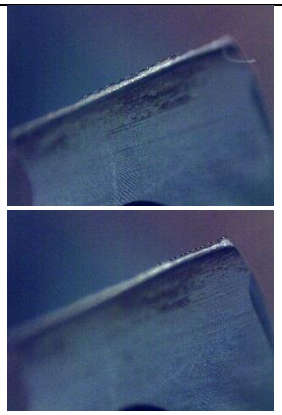	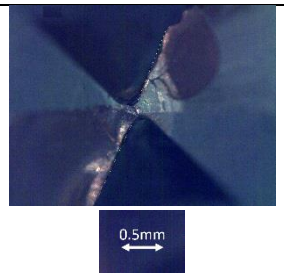 **Scale bar (0.5 mm)**		

Fig. 133: Flank wear on the cutting edges and severe radial flank wear on the margin

SDX1 D 2FL 8 8				
CE1	**CE2**	**Drill Point**	**CE1 - Radial Flank Wear**	**CE2 – Radial Flank Wear**
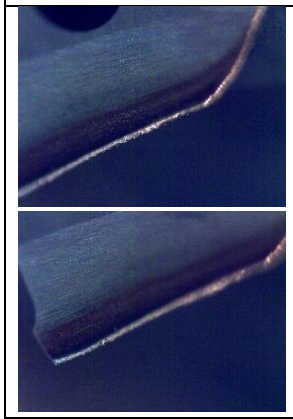	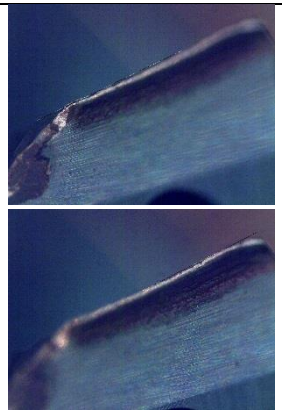	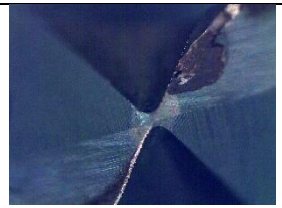 **Scale bar (0.5 mm)**		

Fig. 134: Flank wear and chipping observed after drilling 166 holes

6. Discussion

The aim of this research was to develop a range of cutting tools for optimising the performance of solid tungsten carbide end-mills and drills for difficult-to-cut alloys. Four difficult-to-cut materials, 6082-T6, Ti-6Al-4V, Inconel 718 and 2507, were selected for this research study due to their usage in various engineering sectors and their difficulties associated with machining operations such as milling and drilling. The research study was limited to optimising cutting tool geometry due to constraints in both resources and time. Therefore, other aspects such as microstructure changes in material, energy consumption in machining, cooling and lubricating techniques and other aspects of machining were not included in the investigations. Before delving into the experiments, an in-depth review of cutting tool technology, tool geometry in end-mills and drills, chip formation, tool materials and coating technologies was carried out and provided in Chapter 3 to understand the current limitations in machining difficult-to-cut materials [4,6,14,31,106,110,138].

It was also identified that, though there is currently a substantial amount of information on cutting tool geometry, the subject area has not been studied in detail and has mainly been applied to insert tools. Extensive research has been carried out evaluating tool geometry or drill design, coating and cooling techniques as shown in section 3.6, Table 3. Solid WC-Co end-mills and drills are complex in geometry and design but are part of major machining operations in manufacturing environments. There are limited studies on solid WC-Co cutting tools which could be down to a few factors such as their complexity to production, cost in manufacturing and lack of understanding in tool design and geometry.

A methodology was set in place to carry out the proposed experimental studies on the selected difficult-to-cut materials. Results on tool life, tool wear and surface roughness were obtained from the experiments and analysed. The methodology set in place ensured that the same experimental procedure was followed. However, before following the methodology, preliminary steps were carried out to ensure that the tool material, machine parameters, and tool designs were adequate for the experiments. The methodology would guarantee the repeatability and reproducibility of the experimental results. Throughout this study, small adjustments to the methodology were made to meet the machining criteria for each investigation series. For example, in the investigation of end-milling and drilling of 6082-T6, tool life could not be used as the response factor in the statistical analysis due to the limitations of the spindle motor on the CNC machine. In a different investigation on Ti-6Al-4V, using 6-flute end-mills, the tool wear criteria had to be adjusted as the original values could not be reached.

End-milling experiments, on solid WC-Co tools, varying in design and tool geometry, were conducted to establish the significance of geometrical factors for the selected workpiece materials (section 4.2). The experiments were designed to find a relationship between tool life

and cutting tool geometry when end-milling difficult-to-cut materials. Tool geometry was broken down so that the geometrical factors such as helix, radial rake, radial primary clearance and radial secondary clearance angles can be assessed and understood in more detail. The literature review conducted in Chapter 3, lead the author to select 3 grades of solid tungsten WC-Co 4.1.6. Preliminary experiments were conducted to establish the performance of different grades of WC-Co. A similar process was carried out for the selection of machine parameters. Preliminary tests were carried out to establish the maximum cutting speed in milling and drilling of difficult-to-cut materials, using uncoated carbide 4.1.3. This is mainly due to the fact that different materials are machined at different machine parameters due to their properties. Furthermore, the material properties of difficult-to-cut alloys selected for this study are different to one another and the most suitable cutting parameters are needed to reduce uncertainty and uncontrolled variations in machining and data collection yet still maintain the HSM and HPM machining trends. Prototypes were made and tested in preliminary experiments. Prototype set ground for flute depth, design type (such as variable helix and variable pitch) and number of flutes etc. for end-milling and drilling operations. Completing these stages lead to the design of experiments and manufacturing of cutting tools 4.1.1. Whilst preliminary experiments were carried out, the proposed methodology was adhered to.

A total of 10 experimental series, on the selected difficult-to-cut materials, were conducted in this study. Five experiments were allocated to end-milling and the remaining 5, allocated for drilling. The ANOVA conducted on the results provided visual and detailed summary of the effect each geometrical parameter has on performance. The visual analysis, or in this case the main effects plot and the Pareto ANOVA provided a summary on the significant factors, followed by a table with details of analysis of variance for transformed response performed on the geometrical factors to support the visual representations and to establish the significance of each geometrical parameter and their interactions. Substantial evidence provided by the main effects plot and the ANOVA results showed the significance of these factors.

All experiments conducted, and the results obtained based on statistical significance of geometrical factors have been summarised in Table 26. Radial rake angle, helix angle and radial primary clearance were found to be the significant factors in end-milling of Ti-6Al-4V and Inconel 718, respectively. However, investigation on drilling operation in Inconel 718 resulted in statistical significance (Table 26).

In drilling tests, conclusive results could not be obtained in 6 investigations due to insufficient number of experiments; caused by limitations in budget and time. However, this study provides initial investigation on identifying significant drill bit geometry factors affecting tool life and surface finish in drilling Ti-6Al-4V, 6082-T6, Inconel 718 and Super duplex 2507. Further experimentations are required to ensure the results obtained produce a statistical significance. Investigations on end-milling of aluminium alloy 6082-T6 showed that further experiments are

required to be able to compare tool life and tool wear. Whereas, in end-milling of super duplex alloy 2507, excessive wear was observed in all experiments. Therefore, experiments should be repeated with adjusted cutting parameters. Further investigations are required to distinguish the relationship between geometrical parameters when end-milling super duplex 2507.

Table 26: Summary of experiments and significance of geometrical factors

Operation	Material	No. of Experiments	P-value Obtained	Significant Factor(s)
End-milling	6082-T6	8	No	None
	Ti-6Al-4V	24	Yes	Radial rake angle
	Ti-6Al-4V	8	Yes	Helix angle, radial primary clearance angle
	Inconel 718	27	Yes	Helix angle, radial primary clearance angle
	2507	16	No	None
Drilling	6082-T6	9	No	None
	6082-T6	4	No	None
	Ti-6Al-4V	8	No	None
	Inconel 718	16	Yes	Cutting angle, relief angle
	2507	8	No	None

Four types of tool wear, flank, crater, notch and chipping were encountered during the analysis of the end-mills on difficult-to-cut materials. Flank wear, as well as radial flank wear and chipping dominated the cutting tool edges in experiments involving the drilling operations. A summary of the tool wear experienced in end-milling and drilling difficult-to-cut materials in this research investigation has been provided in Table 27. The author has also matched reported experiments where similar tool wear types were encountered for each material. The majority of cutting tools experienced abrasion and adhesion on the cutting edges as well as the regular occurrence of BUE on the cutting edges as a result of stresses, heat generation and tribological effect, at the tool-chip interface. These effects caused small particles from the carbide tool material would break away and leave a rough rigid surface on the rake face of the cutting tools. The new exposed surface on the tool is then replaced or covered with chip particles, which weld onto the exposed region on the rake face or the peripheral cutting edges and cause wear, failure and poor surface finish on the workpiece material. Additional results on the surface roughness in all experiments obtained, are presented in Appendix G.

Real manufacturing environments can take advantage of the findings and apply it within their processes. Optimised tool geometry can potentially provide fewer down times and tool changes, including savings on cutting tools in milling and drilling operations. Increasing tool life will encourage better productivity and allow manufacturers to keep up with trends such as HSM, HPM and LPM. With the addition of coating and coolant technology further enhancements to cutting tools can be made. The effect of tool geometry on material should be

applied to other tool designs as they are equally as important and should be investigated in the future to determine their optimum tool geometry.

Table 27: Summary of Tool Wear Types and Reported Experiments

Operation	Material	Tool Wear Types During Analysis	Reported Experiments
End-milling	6082-T6	➢ Flank wear ➢ Chipping	[21,22]
	Ti-6Al-4V	➢ Flank wear ➢ Crater wear (only in 4-flute end-mills) ➢ Notch wear (only in 4-flute end-mills) ➢ Chipping	[25,58,123,124,126]
	Inconel 718	➢ Flank wear ➢ Notch wear ➢ Chipping	[30,138]
	2507	➢ Flank wear ➢ Chipping ➢ Notch wear	[161]
Drilling	6082-T6	➢ Flank wear	[19,141]
	Ti-6Al-4V	➢ Flank wear ➢ Flank wear (radial) ➢ Chipping	[44,45,102,140,141]
	Inconel 718	➢ Flank wear ➢ Chipping	[43,46,47]
	2507	➢ Flank wear ➢ Flank wear (radial) ➢ Chipping	[53]

6.1 Coating and Tool Material Selection

The effect of variations in tool geometry on difficult-to-cut materials in end-milling and drilling operations was investigated in this research study, through the use of experimentation. The author decided to further investigate the effect of coating technologies and high-performance solid WC-Co tool materials in end-milling of Ti-6Al-4V. This chapter will provide a brief explanation on the additional experiments which the author completed to evaluate and assess the effect of coating technology and WC-Co on tool geometry in difficult-to-cut materials.

For the end-milling experiments proposed for Ti-6Al-4V, the author decided to adopt the 4-flute end-mill design (Fig. 137), for better tool wear analysis. Helix angle, A (variable helix angle with 34° and 35°), radial rake angle of 14°, primary and secondary of 10° and 25°, respectively. The following tool geometry was chosen based on tool life performance, tool wear and statistical analysis from the previous experiments conducted on Ti-6Al-4V. Three high-performance coatings and WC-Co tool materials were selected and used to determine whether further enhancements are achievable through the best combination of coating and tool material. Three PVD coatings, AlTiN, TiSiN and AlCrN were chosen for end-milling experiments on Ti-6Al-4V. Data based on each coating has been provided in Table 28.

An additional solid WC-Co grade, TSF44, an ultrafine grade (average grain size of 0.4 µm) with 12% Co as binding material, was added to the design of experiments as recommended by the carbide manufacturer. Solid WC-Co YL10.2 and EMT100 were previously selected for end-milling experiments and were included in the performance enhancement experiments on 4-flute end-mills for Ti-6Al-4V. For comparison, end-mills without any coatings were produced again and included in the experiments.

Table 28: Details of coatings used in the experiment

Coating	Thickness	Service Temp.	Hardness (HV 0.05)	Deposition method	Colour
AlTiN [162]	4 µm	1000 °C	3500	PVD	Black
TiSiN [163]	2-4 µm	1100 °C	3500	PVD	Copper
AlCrN [163]	2-4 µm	1050 °C	3000	PVD	Grey

The author made sure that the same machine parameters and conditions were used in the experiments to complete a total of 12 experiments with replicates. Several observations were made during and after the completion of the experiments. They are as follows:

1. A reduction of crater and notch wear was observed in cutting tools with coatings when compared to their uncoated counterparts.
2. Solid WC-Co grade, EMT100 was the worst performing tool material with a tool life of 31332.84 mm when combined with AlTiN

3. Whereas, YL10.2 and TSF44 managed to reach a tool life of 52728.62 mm and 41580.78 mm, respectively, when combined with AlTiN coating (Fig. 135).
4. The correct use of tool material and coating can increase the tool life by as much as 4-8 times, depending on the tool material and coating technology used. In the case of YL10.2 and AlTiN coating, an increase of 8 times was observed when compared to an uncoated YL10.2. In the case of TSF44 with AlTiN coating, an increase of 4 times was observed when compared to its uncoated counterpart.
5. Coating, TiSiN, demonstrated a medium performance when used on all WC-Co grades.
6. Coating, AlCrN, overall, was the worst performing coating in the experiments. However, this does not label the coating as bad coating but rather the wrong coating for the wrong application.
7. Results showed that reduced tool wear and increased tool life can be achieved if the correct combination of tool geometry, coating and tool material are used.

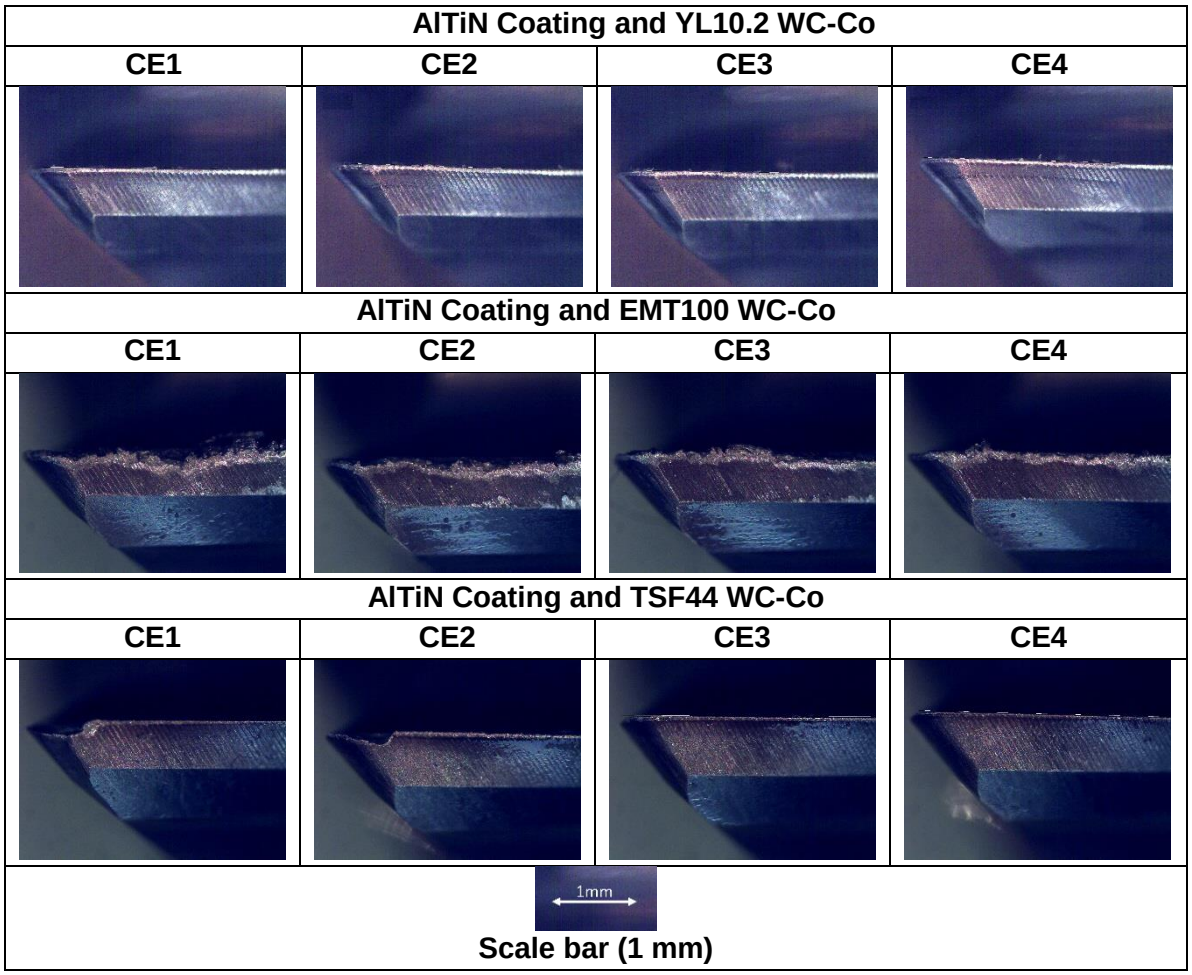

Fig. 135: Tool wear images of three solid WC-Co with AlTiN coating

7. Conclusions

In this research, the effect of tool geometry on difficult-to-cut materials, 6082-T6, Ti-6Al-4V, Inconel 718 and 2507, establishing an improved geometry in milling and drilling operations was investigated. Detailed literature review on cutting tool technology in end-mills and drills in metal removal and difficulties in machinability of difficult-to-cut materials. To clarify whether proposed concept is valid, a series of experiments on end-milling and drilling operations were conducted. A methodology was set in place to be used to carry out the process and the follow a guided procedure in obtaining too life improvement and

Several significant findings were recognised through the end-milling drilling investigations presented in this report. The following conclusions have been drawn:

i. Detailed comprehensive literature review on cutting tool technology and the importance of tool geometry in end-mills and drills was completed. Subjects such as tool geometry, tool life and current tool life prediction models, as well as surface finish, chip formation, tool materials and coating technology were thoroughly reviewed. The author also managed to identify the gaps within the current research and the reason behind this research study.
ii. A methodology was set in place before carrying out the experiments, providing step-by-step instructions on the approach, procedure and data acquisition when optimising tool geometry of cutting tools in machining difficult-to-cut materials.
iii. A total of 10 series of experiments were accomplished, exploring the effect of tool geometry in end-milling and drilling operations, on 4 selected difficult-to-cut materials.
iv. Using statistical analysis (ANOVA) 4 experiments were deemed as successful where significant geometrical factors were obtained. Experiments carried out on Ti-6Al-4V and Inconel 718 showed that improvements in tool life and surface finish are achievable. The hypothesis proposed, confirmed that the changes in geometrical factors can extend tool life, improve the quality of surface finish and the performance of the cutting tool. However, this was not the case in aluminium alloy 6082-T6 and end-milling experiments on super duplex 2507 as further experiments are required to obtain satisfactory results.

8. Future Work

An overview of the future work is discussed in this chapter. A method to design new cutting tools for various difficult-to-cut engineering materials is proposed to further explain the requirements for future work and research in optimising cutting tool geometry. Based on the literature review conducted, research gaps outlined and discussed plans for future work are provided in more detail

The proposed additional research and experiments aim to further develop the understanding of the effect of tool geometry on difficult-to-cut materials and obtaining the optimum tool geometry in end-milling and drilling operations.

In the short term, experiments in aluminium 6082-T6 and super duplex 2507 should be continued to obtain suitable tool geometry with the best tool life performance. As a result, this includes the continuation and repeatability of experiments until significant geometrical parameters are discovered. The same tool optimisation methodology should then be applied to other cutting tool designs such as thread-mills.

In the longer term, in addition to tool geometry, extensive research should be conducted into the comparison of different grades WC-Co and coating technologies for their suitability with the optimum geometries obtained for the 4 selected materials to further enhance the tool life of the cutting tools. Experiments are required to understand the effect of carbide substrates on advanced alloys [118,124,164]. To enhance the cutting tools, further coating technologies should be investigated to test the effects of TiN, TiAlN, TiSiN, AlCrN and new, potential multilayer coating technologies to further improve tool life [11,119,124]. The introduction of alternative and novel machining solutions (such as MQL) has shown great improvements in tool life, productivity and power consumption [13,14,138,140].

The final objective revolves around productivity to be able to meet the demands of HSM, HPM and LPM by applying the optimised cutting tools in various manufacturing environments to collect data based on the performance of the cutting tools. This would provide a clear understanding of the limitations of the cutting tools in real machining environments. With the development in finite element modelling and improved accuracy of the results, there is a potential to incorporate findings from simulation into design of cutting tools with complex geometries in future.

References

[1]. Erdel BP. High-speed machining. Dearborn, Mich.: Dearborn, Mich. : Society of Manufacturing Engineers; 2003.

[2]. Graham T. S. Cutting Tool Technology: Industrial Handbook. Igarss 2014. 2008;(1):1–606.

[3]. Helical Solutions. Machining Guidebook. 2016.

[4]. Ezugwu EO. Key improvements in the Machining of Difficult-to-cut Aerospace Superalloys. International Journal of Machine Tools and Manufacture. 2005;45(12–13):1353–67.

[5]. Peters M. Titanium and Titanium Alloys. Leyens C, Peters M, editors. Vol. 1, Titanium and Titanium Alloys Fundamentals and Applications. Weinheim, FRG: Wiley-VCH Verlag GmbH & Co. KGaA; 2003. 513 p.

[6]. Davim JP. Machining of Titanium Alloys. Springer London; 2014. 150 p.

[7]. Cheng K. Machining Dynamics. Cheng K, editor. London: Springer London; 2009. (Springer Series in Advanced Manufacturing).

[8]. Endrino JL, Fox-Rabinovich GS, Gey C. Hard AlTiN, AlCrN PVD Coatings for Machining of Austenitic Stainless Steel. Surface and Coatings Technology. 2006;200(24):6840–5.

[9]. Nordin M, Sundström R, Selinder TI, Hogmark S. Wear and Failure Mechanisms of Multilayered PVD TiN/TaN Coated Tools When Milling Austenitic Stainless Steel. Surface and Coatings Technology. 2000;133–134(134):240–6.

[10]. Polini W, Turchetta S. Cutting force, Tool Life and Surface Integrity in Milling of Titanium Alloy Ti-6Al-4V with Coated Carbide Tools. Proceedings of the Institution of Mechanical Engineers, Part B: Journal of Engineering Manufacture2. 2016;230(4):694–700.

[11]. Chang YY, Chang H, Jhao LJ, Chuang CC. Tribological and Mechanical Properties of Multilayered TiVN/TiSiN Coatings Synthesized by Cathodic Arc Evaporation. Surface and Coatings Technology. 2018;(November 2017):0–1.

[12]. Shokrani A. High Speed Machining of Cobalt Chromium Alloy for Biomedical Applications. 2013;1(5):678.

[13]. Shokrani A, Dhokia V, Newman ST. Investigation of the Effects of Cryogenic Machining on Surface Integrity in CNC End Milling of Ti-6Al-4V Titanium Alloy. Journal of Manufacturing Processes. 2016;21:172–9.

[14]. Shokrani A, Dhokia V, Newman ST. Environmentally Conscious Machining of Difficult-to-machine Materials with Regard to Cutting Fluids. International Journal of Machine Tools and Manufacture. 2012 Jun;57:83–101.

[15]. Nikanorov SP, Volkov MP, Gurin VN, Burenkov YA, Derkachenko LI, Kardashev BK, et al. Structural and Mechanical Properties of Al–Si Alloys Obtained by Fast Cooling of a Levitated Melt. Materials Science and Engineering A. 2005;390:63–9.

[16]. Warmuzek M. Aluminium-Silicon Casting Alloys: Atlas of Microfractographs. ASM Handbook. 2004 Sep 13;9(190):1–10.

[17]. Verma RK, Agrawal L, Awana DS. Effect of Variation of Silicon and Copper Contents in Aluminium-Silicon-Copper Alloy. 2013;4(1):149–56.

[18]. Kelly JF, Cotterell MG. Minimal Lubrication Machining of Aluminium Alloys. Journal of Materials Processing Technology. 2002 Jan 15;120(1–3):327–34.

[19]. Braga DU, Diniz AE, Miranda GWA, Coppini NL. Using a Minimum Quantity of Lubricant (MQL) and a Diamond Coated Tool in the Drilling of Aluminum-silicon Alloys. Journal of Materials Processing Technology. 2002 Mar 5;122(1):127–38.

[20]. Batzer S., Haan D., Rao P., Olson W., Sutherland J. Chip morphology and Hole Surface Texture in the Drilling of Cast Aluminum Alloys. Journal of Materials Processing Technology. 1998 Jul;79(1–3):72–8.

[21]. Hricova J, Kovac M, Sugar P. Experimental Investigation of High Speed Milling of Aluminium Alloy. 2014;3651:773–7.

[22]. Hricova J. Design of End Mill Geometry for Aluminium Alloy Machining. 2014;2014(2):97–105.

[23]. Kamiya M, Yakou T, Sasaki T, Nagatsuma Y. Effect of Si Content on Turning Machinability of Al-Si Binary Alloy Castings * 1. 2008;

[24]. Hong SY, Ding Y, Jeong W cheol. Friction and Cutting Forces in Cryogenic Machining of Ti-6Al-4V. International Journal of Machine Tools and Manufacture. 2001;41(15):2271–85.

[25]. Pervaiz S, Deiab I, Darras B. Power Consumption and Tool Wear Assessment When Machining Titanium Alloys. International Journal of Precision Engineering and Manufacturing. 2013;14(6):925–36.

[26]. Cui C, Hu B, Zhao L, Liu S. Titanium Alloy Production Technology, Market Prospects and Industry Development. Materials & Design. 2011 Mar 1;32(3):1684–91.

[27]. Anonymous. Drill Terminology and Cutting Characteristics [Internet]. Mitsubichi Materials. 2018 [cited 2018 Aug 6]. Available from: http://www.mitsubishicarbide.com/en/technical_information/tec_rotating_tools/drills/tec_drills_technical_top/tec_drilling_terminology

[28]. Sandvick Coromant. Wear on Cutting Edges [Internet]. 2015 [cited 2017 Mar 6]. Available from: http://www.sandvik.coromant.com/en-gb/knowledge/materials/cutting_tool_materials/wear_on_cutting_edges/pages/default.aspx

[29]. Chia Wee Chong. Research and Development of Multi Purpose Carbide End mill. 2005;

[30]. Liao YS, Lin HM, Wang JH. Behaviors of End milling Inconel 718 Superalloy by Cemented Carbide Tools. Journal of Materials Processing Technology. 2008;201(1–3):460–5.

[31]. Astakhov VP. Geometry of Single-point Turning Tools and Drills: Fundamentals and Practical Applications. Vol. 53, Journal of Chemical Information and Modeling. Springer London; 2010. 584 p.

[32]. Newman ST, Shokrani A, Dhokia V. Evaluation of Crygenic CNC Milling of Ti-6Al-4V Titanium Alloy.

[33]. Hong SY, Markus I, Jeong W cheol. New Cooling Approach and Tool Life Improvement in Cryogenic Machining of Titanium Alloy Ti-6Al-4V. International Journal of Machine Tools and Manufacture. 2001;41(15):2245–60.

[34]. Klocke F. Manufacturing Processes 1. Berlin, Heidelberg: Springer Berlin Heidelberg; 2011. (RWTHedition).

[35]. Agnew PJ. What to Consider When Evaluating Solid Carbide End Mill Machining. MoldMaking Technology. 2003;17–8.

[36]. Ku HS, Chia WC. Design of Multi-purpose Carbide End Mill. Animal Genetics. 2008;39(5):561–3.

[37]. Nouari M, List G, Girot F, Coupard D. Experimental Analysis and Optimisation of Tool Wear in Dry Machining of Aluminium Alloys. Wear. 2003 Aug;255(7–12):1359–68.

[38]. Seco Tools. Exploring Solid Carbide End Mill Systems. 2013;

[39]. Carbide Processing Inc. Saw Tip Angles Explained [Internet]. [cited 2017 Feb 27]. Available from: http://www.carbideprocessors.com/pages/saw-blades/saw-tip-angles.html

[40]. Sharif S, Abd E, Sasahar H. Machinability of Titanium Alloys in Drilling. In: Titanium Alloys - Towards Achieving Enhanced Properties for Diversified Applications. InTech; 2012. p. 117–37.

[41]. Brinksmeier E. Prediction of Tool Fracture in Drilling. CIRP Annals - Manufacturing Technology. 1990;39(1):97–100.

[42]. Vimalesh M, Prabhu S, Vijay Sekar KS. Machinability Studies in Drilling of Inconel 718 Super Alloy. Applied Mechanics and Materials. 2015;787(August):480–4.

[43]. Chen YC, Liao YS. Study on Wear Mechanisms in Drilling of Inconel 718 Superalloy. Journal of Materials Processing Technology. 2003;140(1-3 SPEC.):269–73.

[44]. Li R, Hegde P, Shih AJ. High-throughput Drilling of Titanium Alloys. International Journal of Machine Tools and Manufacture. 2007;47(1):63–74.

[45]. Rahim EA, Sasahara H. A Study of the Effect of Palm Oil as MQL Lubricant on High Speed Drilling of Titanium Alloys. Tribology International. 2011 Mar;44(3):309–17.

[46]. Sharman ARC, Amarasinghe A, Ridgway K. Tool Life and Surface Integrity Aspects When Drilling and hole making in Inconel 718. Journal of Materials Processing Technology. 2008;200(1–3):424–32.

[47]. Kivak T, Habali K, Seker U. The Effect of Cutting Paramaters on the Hole Quality and Tool Wear During the Drilling of Inconel 718. Gazi University Journal of Science. 2012;25(2):533–40.

[48]. Ezugwu EO, Wang ZM, Machado AR. The Machinability of Nickel-based Alloys: A Review. Journal of Materials Processing Technology. 1999;86(1–3):1–16.

[49]. Devillez A, Schneider F, Dominiak S, Dudzinski D, Larrouquere D. Cutting Forces and Wear in Dry Machining of Inconel 718 with Coated Carbide Tools. Wear. 2007;262(7–8):931–42.

[50]. Devillez A, Le Coz G, Dominiak S, Dudzinski D. Dry Machining of Inconel 718, Workpiece Surface Integrity. Journal of Materials Processing Technology. 2011;211(10):1590–8.

[51]. Ulutan D, Pleta A, Henderson A, Mears L. Comparison and Cost Optimization of Solid Tool Life in End Milling Nickel-Based Superalloy. Procedia Manufacturing. 2015;1:522–33.

[52]. Zeilmann RP, Weingaertner WL. Analysis of Temperature During Drilling of Ti6Al4V with Minimal Quantity of Lubricant. Journal of Materials Processing Technology. 2006 Oct;179(1–3):124–7.

[53]. Nomani J, Pramanik A, Hilditch T, Littlefair G. Machinability Study of First Generation Duplex (2205), Second Generation Duplex (2507) and Austenite Stainless Steel During Drilling Process. Wear. 2013;304(1–2):20–8.

[54]. Mitsubishi Carbide. End Mill Features and Specification. 2014.

[55]. English T. How the Tool Helix Affects Manufacturing - Manufacturing Lounge [Internet]. 2017 [cited 2018 Jul 24]. Available from: http://www.manufacturinglounge.com/tool-helix-affects-manufacturing/

[56]. Razak NH, Chen ZW, Pasang T. Progression of Tool Deterioration and Related Cutting Force During Milling of 718Plus Superalloy Using Cemented Tungsten Carbide Tools. International Journal of Advanced Manufacturing Technology. 2016;86(9–12):3203–16.

[57]. Li A, Zhao J, Pei Z, Zhu N. Simulation-based Solid Carbide End Mill Design and Geometry Optimization. International Journal of Advanced Manufacturing Technology. 2014;71(9–12):1889–900.

[58]. Li A, Zhao J, Gao X, Wang F. Performance Evaluation of Ultra-fine Grain Carbide in High-speed Milling of Ti-6Al-4V. International Journal of Precision Engineering and Manufacturing. 2014;15(4):593–600.

[59]. Huang P, Li J, Sun J, Zhou J. Study on Vibration Reduction Mechanism of Variable Pitch End Mill and Cutting Performance in Milling Titanium Alloy. The International Journal of Advanced Manufacturing Technology. 2013 Jul 30;67(5–8):1385–91.

[60]. Budak E, Kops L. Improving Productivity and Part Quality in Milling of Titanium Based Impellers by Chatter Suppression and Force Control. CIRP Annals - Manufacturing Technology. 2000;49(1):31–6.

[61]. Budak E. An Analytical Design Method for Milling Cutters With Nonconstant Pitch to Increase Stability, Part 2: Application. Journal of Manufacturing Science and Engineering. 2003;125(1):35.

[62]. Tunç LT, Budak E. Effect of Cutting Conditions and Tool Geometry on Process Damping in Machining. International Journal of Machine Tools and Manufacture. 2012 Jun;57:10–9.

[63]. Pleta A, Ulutan D, Mears L. Investigation of Trochoidal Milling in Nickel-based Superalloy Inconel 738 and Comparison with End Milling. In: ASME 2014 International Manufacturing Science and Engineering Conference, MSEC 2014 Collocated with the JSME 2014 International Conference on Materials and Processing and the 42nd North American Manufacturing Research Conference. ASME; 2014. p. 1–6.

[64]. Airao J, Chaudhary B, Bajpai V, Khanna N. An Experimental Study of Surface Roughness Variation in End Milling of Super Duplex 2507 Stainless Steel. Vol. 5, Materials Today: Proceedings. 2018.

[65]. Yen YC, Söhner J, Lilly B, Altan T. Estimation of Tool Wear in Orthogonal Cutting Using the Finite Element Analysis. Journal of Materials Processing Technology. 2004;146(1):82–91.

[66]. Davim JP. Machining: Fundamentals and Recent Advacnes. London: Springer London; 2008.

[67]. Johansson D, Leemet T, Allas J, Madissoo M, Adoberg E, Schultheiss F. Tool life in Stainless Steel AISI 304: Applicability of Colding's Tool Life Equation for Varying Tool Coatings. Proceedings of the Estonian Academy of Sciences. 2016;65(2):172.

[68]. Colding BN. Machinability of Metals and Machining Costs. International Journal of Machine Tool Design and Research. 1961;1(3):220–48.

[69]. Colding BN. A Predictive Relationship between Forces, Surface Finish and Tool-life. CIRP Annals - Manufacturing Technology. 2004;53(1):85–90.

[70]. Taylor FW. The Art of Cutting Metals. Scientific American. 1907;63(1618supp):25929–31.

[71]. Kattan IA, Currie KR. Developing New Trends of Cutting Tool Geometry. Journal of Materials Processing Technology. 1996 Aug;61(1–2):231–7.

[72]. Merchant ME. Mechanics of the Metal Cutting Process. I. Orthogonal Cutting and a Type 2 Chip. Journal of Applied Physics. 1945 May;16(5):267–75.

[73]. Zorev NN. Metal Cutting Mechanics. Oxford: Pergamon Press; 1996.

[74]. Colding BN. A Wear Relationship for Turning, Milling and Grinding: Machining Economics. [Stockholm]; 1959.

[75]. Hägglund S. Methods and Models for Cutting Data Optimization. Chalmers University of Technology; 2013.

[76]. Daniel Johansson, Fredrik Schultheiss, Volodymyr Bushlya, Jinming Zhou J-ES. Tool Life and Wear Model in Metal Cutting, Part 1 - Influence of Varying Flank Wear Criterion on Colding'S Tool Life Equation. 2013;(1906).

[77]. Marksberry PW, Jawahir IS. A Comprehensive Tool-wear/Tool-life Performance Model in the Evaluation of NDM (Near Dry Machining) for Sustainable Manufacturing. International Journal of Machine Tools and Manufacture. 2008;48(7–8):878–86.

[78]. Jawahir IS, Ghosh R, Fang XD, Li PX. An Investigation of the Effects of Chip Flow on Tool-wear in Machining with Complex Grooved Tools. Wear. 1995;184(2):145–54.

[79]. Hoffman EG. Fundamentals of Tool Design. 2nd ed. Society of Manufacturing Engineers; 1984.

[80]. Lau WS, Venuvinod PK, Rubenstein C. The Relation between Tool Geometry and the Taylor Tool Life Constant. International Journal of Machine Tool Design and Research. 1980 Jan;20(1):29–44.

[81]. Venkatesh V. Computerised Machinability Data. In: Automach Australia. Sydney; 1986. p. 159.

[82]. Wang HP (ben), Wysk RA. An Expert System for Machining Data Section. Computers and Industrial Engineering. 1986 Jan 1;10(2):99–107.

[83]. Oxley PLB. The Mechanics of Machining: an Analytical Approach to Assessing Machinability. Chichester: Halsted Press; 1989. 185 p.

[84]. Quinto DTDT. Mechanical Property and Structure Relationships in Hard Coatings for Cutting Tools. Journal of Vacuum Science & Technology A: Vacuum, Surfaces, and Films. 1988;6(3):2149.

[85]. Colding BN. The Machining Productivity Mountain and its Wall of Optimum Productivity. Dearborn, Mich.: Society of Manufacturing Engineers; 1980.

[86]. Colding BN. A Tool-Temperature/Tool-Life Relationship Covering a Wide Range of Cutting Data. CIRP Annals - Manufacturing Technology. 1991;40(1):35–40.

[87]. Sun J, Guo YB. A Comprehensive Experimental Study on Surface Integrity by End Milling Ti-6Al-4V. Journal of Materials Processing Technology. 2009;209(8):4036–42.

[88]. Ramesh S, Karunamoorthy L, Palanikumar K. Surface Roughness Analysis in Machining of Titanium Alloy. Materials and Manufacturing Processes. 2008;23(2):175–82.

[89]. Jomaa W, Mechri O, Lévesque J, Songmene V, Bocher P, Gakwaya A. Finite Element Simulation and Analysis of Serrated Chip Formation During High–speed Machining of AA7075–T651 Alloy. Journal of Manufacturing Processes. 2017 Apr;26:446–58.

[90]. Komanduri R, Turkovich BFVON, Von Turkovich BF, Turkovich BFVON. New Observations on the Mechanism When Machining Titanium Alloys of Chip Formation. Wear. 1981;69(2):179–88.

[91]. Komanduri R, Hou Z. On Thermoplastic Shear Instability in the Machining of a Titanium Alloy (Ti-6Al-4V). 2002;33(September).

[92]. Odelros S. Tool Wear in Titanium Machining. 2012;(1):1–63.

[93]. Vyas A, Shaw MC. Mechanics of Aaw-tooth Chip Formation in Metal Cutting. Journal of Manufacturing Science and Engineering, Transactions of the ASME. 1999;121(2).

[94]. Obikawa T, Usui E. Computational Machining of Titanium Alloy - Finite Element Modeling and a Few Results. Journal of Manufacturing Science and Engineering, Transactions of the ASME. 1996;118(2):208.

[95]. Barry J, Byrne G, Lennon D. Observations on Chip Formation and Acoustic Emission in Machining Ti-6Al-4V alloy. International Journal of Machine Tools and Manufacture. 2001;41(7):1055–70.

[96]. Komanduri R. Some Clarifications on the Mechanics when Machining Titanium Alloys of Chip Formation. Wear. 1982;76:15–34.

[97]. Shivpuri R, Hua J, Mittal P, Srivastava AK, Lahoti GD. Microstructure-Mechanics Interactions in Modeling Chip Segmentation during Titanium Machining. CIRP Annals - Manufacturing Technology. 2002;51(1):71–4.

[98]. Barish H. Quality Drills Contribute to Successful Titanium Tooling. Cutting Tool Engineering. 1988;40(1):38–9, 41.

[99]. Ke F, Ni J, Stephenson DA. Continuous Chip Formation in Drilling. International Journal of Machine Tools and Manufacture. 2005 Dec;45(15):1652–8.

[100]. Venuvinod PKZ, Djordjevich A. Chip Control. 1996;45:83–6.

[101]. Akhavan Farid A, Sharif S, Idris MH. Chip Morphology Study in High Speed Drilling of Al-Si Alloy. International Journal of Advanced Manufacturing Technology. 2011;57(5–8):555–64.

[102]. Álvarez M, Salguero J, Sánchez JA, Huerta M, Marcos M. SEM and EDS Characterisation of Layering TiOx Growth onto the Cutting Tool Surface in Hard Drilling Processes of Ti-Al-V Alloys. Advances in Materials Science and Engineering. 2011;2011.

[103]. Müller C, Blümke R. Influence of Heat Treatment and Cutting Speed on Chip Segmentation of Age Hardenable Aluminium Alloy. Materials Science and Technology. 2001;17(6):651–4.

[104]. Brown CA, von Turkovich BF. A Practical Method for Estimating Machining Forces from Tool-Chip Contact Area. CIRP Annals - Manufacturing Technology. 1983;32(1):91–5.

[105]. Trent EM, Wright P. Metal Cutting. Vasa. 2000. 288 p.

[106]. Ezugwu EO, Wang ZM. Titanium Alloys and Their Machinability— A Review. Journal of Materials Processing Technology. 1997 Aug;68(3):262–74.

[107]. Hartung PD, Kramer BM, von Turkovich BF. Tool Wear in Titanium Machining. CIRP Annals - Manufacturing Technology. 1982;31(1):75–80.

[108]. RAHMAN M, WANG Z-G, WONG Y-S. A Review on High-Speed Machining of Titanium Alloys. JSME International Journal Series C. 2006;49(1):11–20.

[109]. Colding BN. Machinability Determinations Based on Chip Deformation and Friction. International Journal of Machine Tool Design and Research. 1962 Jul;2(3):297–316.

[110]. Ezugwu E., Bonney J, Yamane Y. An Overview of the Machinability of Aeroengine Alloys. Journal of Materials Processing Technology. 2003 Mar;134(2):233–53.

[111]. Pittalà GM, Monno M. A New Approach to the Prediction of Temperature of the Workpiece of Face Milling Operations of Ti-6Al-4V. Applied Thermal Engineering. 2011;31(2–3):173–80.

[112]. Paul S, Chattopadhyay AB. Environmentally Conscious Machining and Grinding with Cryogenic Cooling. Machining Science and Technology. 2006;10(1):87–131.

[113]. Rahman M, Seah WKH, Teo TT. The Machinability of Inconel 718. Journal of Materials Processing Technology. 1997;63(1–3):199–204.

[114]. Kitagawa T, Kubo A, Maekawa K. Temperature and Wear of Cutting Tools in High-speed Machining of Inconel 718 and Ti-6Al-6V-2Sn. Wear. 1997;202(2):142–8.

[115]. Kramer BM. On Tool Materials for High-Speed Machining. J Eng Ind. 1986;109(May 1987):87–91.

[116]. Grzesik W. Cutting Tool Materials. Advanced Machining Processes of Metallic Materials. 2017;35–63.

[117]. Sreejith PS, Ngoi BKA. Dry Machining: Machining of the Future. Journal of Materials Processing Technology. 2000 Apr 14;101(1):287–91.

[118]. Destiny Tool - The Mark of Performance. Understanding Carbide Substrates used in End Mills - Destiny Tool [Internet]. [cited 2018 Aug 6]. Available from: https://www.destinytool.com/carbide-substrate.html

[119]. Bobzin K. High-performance Coatings for Cutting Tools. Vol. 18, CIRP Journal of Manufacturing Science and Technology. 2017. p. 1–9.

[120]. Revankar GD, Shetty R, Rao SS, Gaitonde VN. Wear resistance enhancement of titanium alloy (Ti–6Al–4V) by ball burnishing process. Journal of Materials Research and Technology. 2016;6(1):13–32.

[121]. Ionbond. Ionbond - Cutting Tool Coatings [Internet]. 2008 [cited 2016 Oct 11]. Available from: http://www.ionbond.com/en/coating-services/cutting-tools/

[122]. Ginting A, Nouari M. Surface Integrity of Dry Machined Titanium Alloys. International Journal of Machine Tools and Manufacture. 2009;49(3–4):325–32.

[123]. Jawaid A, Sharif S, Koksal S. Evaluation of Wear Mechanisms of Coated Carbide Tools when Face Milling Titanium Alloy. Journal of Materials Processing Technology. 2000;99(1):266–74.

[124]. Uddin MS, Pham B, Sarhan A, Basak A, Pramanik A. Comparative Study Between Wear of Uncoated and TiAlN-coated Carbide Tools in Milling of Ti6Al4V. Advances in Manufacturing. 2017;5(1):83–91.

[125]. Donachie, Jr. MJ. Titanium - A Technical Guide (2nd Edition). ASME International. 2000;2:2–4.

[126]. Ribeiro M V., Moreira MR V, Ferreira JR. Optimization of Titanium Alloy (6Al-4V) Machining. Journal of Materials Processing Technology. 2003;143–144(1):458–63.

[127]. Inagaki I, Tsutomu T, Yoshihisa S, Nozomu A. Application and Features of Titanium for the Aerospace Industry. Nippon Steel & Sumitomo Metal Technical Report. 2014;(106):22–7.

[128]. Calamaz M, Coupard D, Girot F. A New Material Model for 2D Numerical Simulation of Serrated Chip Formation when Machining Titanium Alloy Ti-6Al-4V. International Journal of Machine Tools and Manufacture. 2008;48(3–4):275–88.

[129]. Narutaki N, Murakoshi A, Motonishi S, Takeyama H. Study on Machining of Titanium Alloys. CIRP Annals - Manufacturing Technology. 1983;32(1):65–9.

[130]. Schafrik RE, Ward DD, Groh JR. Application of Alloy 718 in GE Aircraft Engines: Past, Present and Next Five Years. Superalloys 718, 625, 706 and Various Derivatives (2001). 2001;1–11.

[131]. Baddoo NR. Stainless Steel in Construction: A Review of Research, Applications, Challenges and Opportunities. Journal of Constructional Steel Research. 2008;64(11):1199–206.

[132]. BSSA. Topic Category: Technical Library [Internet]. British Stainless Steel Association. [cited 2018 Jul 25]. Available from: https://www.bssa.org.uk/topics.php

[133]. Polishetty A, Alabdullah MFA, Pillay N, Littlefair G. A Preliminary Study on Machinability of Super Austenitic Stainless Steel. In: ASME International Mechanical Engineering Congress and Exposition, Proceedings (IMECE). 2015. p. 1–8.

[134]. Kaewkuekool S, Jirapattarasilp K, Pechkong K. A Study of Influence Factors Affecting to Surface Roughness in Stainless Steel Turning. In: 2009 International Conference on Computer Engineering and Technology. IEEE; 2009. p. 299–302.

[135]. Dolinšek S. Work-hardening in the Drilling of Austenitic Stainless Steels. Journal of Materials Processing Technology. 2003;133(1–2):63–70.

[136]. Toor I ul H, Hyun PJ, Kwon HS. Development of High Mn-N Duplex Stainless Steel for Automobile Structural Components. Corrosion Science. 2008 Feb 1;50(2):404–10.

[137]. Saeid T, Abdollah-zadeh A, Assadi H, Malek Ghaini F. Effect of Friction Stir Welding Speed on the Microstructure and Mechanical Properties of a Duplex Stainless Steel. Materials Science and Engineering A. 2008;496(1–2):262–8.

[138]. Shokrani A, Dhokia V, Newman ST. Hybrid Cooling and Lubricating Technology for CNC Milling of Inconel 718 Nickel Alloy. Procedia Manufacturing. 2017 Jan 1;11:625–32.

[139]. Dornfeld D a., Kim JS, Dechow H, Hewson J, Chen LJ. Drilling Burr Formation in Titanium Alloy, Ti-6AI-4V. CIRP Annals - Manufacturing Technology. 1999;48(1):73–6.

[140]. Shokrani A, Huibin S, Dhokia V, Newman ST. Cryogenic Drilling of Grade 5 ELI Titanium Alloy' Paper. :27.

[141]. Zhu Z, Guo K, Sun J, Li J, Liu Y, Zheng Y, et al. Evaluation of Novel Tool Geometries in Dry Drilling Aluminium 2024-T351/Titanium Ti6Al4V Stack. Journal of Materials Processing Technology. 2018;259:270–81.

[142]. British Standards. BSI Standards Publication Statistics — Vocabulary and Symbols Part 3 : Design of Experiments. 2013;

[143]. Hsieh JF, Lin PD. Mathematical Model of Multiflute Drill Point. International Journal of Machine Tools and Manufacture. 2002 Aug;42(10):1181–93.

[144]. BS ISO 7079 : 2016 BSI Standards Publication Core Drills with Parallel Shanks and with Morse Taper Shanks. 2016;

[145]. Denkena B, Biermann D. Cutting Edge Geometries. CIRP Annals - Manufacturing Technology. 2014;63(2):631–53.

[146]. BS ISO 1641-1: 2016 BSI Standards Publication End Mills and Slot Drills Part 1 : Milling Cutters with Cylindrical Shanks. 2016;

[147]. Sun S, Brandt M, Dargusch MS. Characteristics of Cutting Forces and Chip Formation in Machining of Titanium Alloys. International Journal of Machine Tools and Manufacture. 2009;49(7–8):561–8.

[148]. Childs T, Maekawa K, Obikawa T, Yamane Y. Work and Tool Materials. Materials Engineering.

[149]. Che-Haron CH. Tool Life and Surface Integrity in Turning Titanium Alloy. Journal of Materials Processing Technology. 2001;118(1–3):231–7.

[150]. Certatizit. The New CTS Grade Generation - CTS20D. 2013.

[151]. Standards B. BSI Standards Publication Tool life Testing on Milling PArt 2: End Milling. 1989;

[152]. Dolinšek S, Šuštaršič B, Kopač J. Wear Mechanisms of Cutting Tools in High-speed Cutting Processes. Wear. 2001;250–251(1–12):349–56.

[153]. Alves SM, Schroeter RB, Bossardi JC dos S, Andrade CLF de. Influence of EP Additive on Tool Wear in Drilling of Compacted Graphite Iron. Journal of the Brazilian Society of Mechanical Sciences and Engineering. 2011;33(2):197–202.

[154]. Davim JP. Machining of Hard Materials. Machining of Hard Materials. 2011. 1–211 p.

[155]. ISO3685. Tool-life Testing with Single-point Turning Tools. ISO 3685 Second Edition 1993-11-15. 1993;

[156]. Doncaster C, Davey A. Analysis of Variance and Covariance: How to Choose and Construct Models for the Life Sciences. 2007;

[157]. IBM Knowledge Center. IBM Knowledge Center - Política de control de acceso [Internet]. [cited 2017 Nov 1]. Available from: https://www.ibm.com/support/knowledgecenter/en/SS4QC9/com.ibm.solutions.wa_an_overview.2.0.0.doc/c_wa_an_ovrvw_stat_terms.html

[158]. Tague NR. The Quality Toolbox, Second Edition. 2nd ed. Milwaukee, Wisconsin : ASQ Quality Press; 2005. 584 p.

[159]. Munro RA, Ramu G, Zrymiak DJ. The Certified Six Sigma Green Belt Handbook Second Edition. 2nd Editio. American Society for Quality (ASQ); 2015. 1–3 p.

[160]. Sandvik Coromant. Solid Carbide Bits [Internet]. [cited 2018 Sep 17]. Available from: https://www.sandvik.coromant.com/en-gb/knowledge/drilling/wear-and-troubleshooting/wear_types/pages/solid-carbide-drill-.aspx

[161]. Krolczyk GM, Nieslony P, Legutko S. Determination of Tool Life and Research Wear During Duplex Stainless Steel Turning. Archives of Civil and Mechanical Engineering. 2015;15(2):347–54.

[162]. Balzers O. Balinit Latuma [Internet]. 2018 [cited 2018 Oct 22]. Available from: https://www.oerlikon.com/balzers/uk/en/portfolio/balzers-surface-solutions/pvd-and-pacvd-based-coatings/balinit/tialn-based/balinit-latuma/

[163]. Ionbond. Coating Portfolio | Cutting Tools. 2018;

[164]. Wentzel EJ, Allen C. Erosion-corrosion Resistance of Tungsten Carbide Hard Metals with Different Binder Compositions. Wear. 1995;181–183(PART 1):63–9.

[165]. Hildebrandt D. How to Read and Use Histograms. 2012. p. 1–8.

Appendices

Appendix A: DoE

Table 29: Full factorial design of end-mills for 6082-T6

Experiment ID	Helix Angle	Radial Rake Angle	Radial Primary Clearance Angle	Radial Secondary Clearance Angle
AL1 R 8 1	45°	16°	12°	23°
AL1 R 8 2	45°	16°	14°	23°
AL1 R 8 3	45°	20°	12°	23°
AL1 R 8 4	45°	20°	14°	23°
AL1 R 8 5	55°	16°	12°	23°
AL1 R 8 6	55°	16°	14°	23°
AL1 R 8 7	55°	20°	12°	23°
AL1 R 8 8	55°	20°	14°	23°

Table 30: Hybrid full factorial design of 4-flute end-mills for Ti-6Al-4V

Experiment ID	Helix Angle	Radial Rake Angle	Radial Primary Clearance Angle	Radial Secondary Clearance Angle
Ti1 R 24 1	A	12°	10°	25°
Ti1 R 24 2	A	12°	10°	30°
Ti1 R 24 3	A	12°	12°	25°
Ti1 R 24 4	A	12°	12°	30°
Ti1 R 24 5	A	14°	10°	25°
Ti1 R 24 6	A	14°	10°	30°
Ti1 R 24 7	A	14°	12°	25°
Ti1 R 24 8	A	14°	12°	30°
Ti1 R 24 9	A	16°	10°	25°
Ti1 R 24 10	A	16°	10°	30°
Ti1 R 24 11	A	16°	12°	25°
Ti1 R 24 12	A	16°	12°	30°
Ti1 R 24 13	B	12°	10°	25°
Ti1 R 24 14	B	12°	10°	30°
Ti1 R 24 15	B	12°	12°	25°
Ti1 R 24 16	B	12°	12°	30°
Ti1 R 24 17	B	14°	10°	25°
Ti1 R 24 18	B	14°	10°	30°
Ti1 R 24 19	B	14°	12°	25°
Ti1 R 24 20	B	14°	12°	30°
Ti1 R 24 21	B	16°	10°	25°
Ti1 R 24 22	B	16°	10°	30°
Ti1 R 24 23	B	16°	12°	25°
Ti1 R 24 24	B	16°	12°	30°

Where A = 34°/35° and B = 38°/40°

Table 31: Full factorial design of 6-flute end-mills for Ti-6Al-4V

Experiment ID	Helix Angle	Radial Rake Angle	Radial Primary Clearance Angle	Radial Secondary Clearance Angle
Ti1 F 8 1	40°	8°	10°	23°
Ti1 F 8 2	40°	8°	14°	23°
Ti1 F 8 3	40°	14°	10°	23°
Ti1 F 8 4	40°	14°	14°	23°
Ti1 F 8 5	45°	8°	10°	23°
Ti1 F 8 6	45°	8°	14°	23°
Ti1 F 8 7	45°	14°	10°	23°
Ti1 F 8 8	45°	14°	14°	23°

Table 32: Hybrid full factorial design of 5-flute end-mills for Inconel 718

Experiment ID	Helix Angle	Radial Rake Angle	Radial Primary Clearance Angle	Radial Secondary Clearance Angle
INCO1 R 27 1	34°	8°	10°	23°
INCO1 R 27 2	34°	8°	12°	23°
INCO1 R 27 3	34°	8°	14°	23°
INCO1 R 27 4	34°	10°	10°	23°
INCO1 R 27 5	34°	10°	12°	23°
INCO1 R 27 6	34°	10°	14°	23°
INCO1 R 27 7	34°	12°	10°	23°
INCO1 R 27 8	34°	12°	12°	23°
INCO1 R 27 9	34°	12°	14°	23°
INCO1 R 27 10	36°	8°	10°	23°
INCO1 R 27 11	36°	8°	12°	23°
INCO1 R 27 12	36°	8°	14°	23°
INCO1 R 27 13	36°	10°	10°	23°
INCO1 R 27 14	36°	10°	12°	23°
INCO1 R 27 15	36°	10°	14°	23°
INCO1 R 27 16	36°	12°	10°	23°
INCO1 R 27 17	36°	12°	12°	23°
INCO1 R 27 18	36°	12°	14°	23°
INCO1 R 27 19	38°	8°	10°	23°
INCO1 R 27 20	38°	8°	12°	23°
INCO1 R 27 21	38°	8°	14°	23°
INCO1 R 27 22	38°	10°	10°	23°
INCO1 R 27 23	38°	10°	12°	23°
INCO1 R 27 24	38°	10°	14°	23°
INCO1 R 27 25	38°	12°	10°	23°
INCO1 R 27 26	38°	12°	12°	23°
INCO1 R 27 27	38°	12°	14°	23°

Table 33: Hybrid full factorial design of 4-flute end-mills for super duplex 2507

Experiment ID	Helix Angle	Radial Rake Angle	Radial Primary Clearance Angle	Radial Secondary Clearance Angle
SDX1 R 16 1	C	8°	10°	23°
SDX1 R 16 2	C	8°	14°	23°
SDX1 R 16 3	C	10°	10°	23°
SDX1 R 16 4	C	10°	14°	23°
SDX1 R 16 5	C	12°	10°	23°
SDX1 R 16 6	C	12°	14°	23°
SDX1 R 16 7	C	14°	10°	23°
SDX1 R 16 8	C	14°	14°	23°
SDX1 R 16 9	B	8°	10°	23°
SDX1 R 16 10	B	8°	14°	23°
SDX1 R 16 11	B	10°	10°	23°
SDX1 R 16 12	B	10°	14°	23°
SDX1 R 16 13	B	12°	10°	23°
SDX1 R 16 14	B	12°	14°	23°
SDX1 R 16 15	B	14°	10°	23°
SDX1 R 16 16	B	14°	14°	23°

Where C = 36°/38° and B = 38°/40°

Table 34: Full factorial design of straight flute drills for 6082-T6

Experiment ID	Helix Angle	Cutting Angle	Drill Point Angle	Relief Angle
AL1 D SFL 9 1	0°	0°	120°	12°
AL1 D SFL 9 2	0°	0°	120°	16°
AL1 D SFL 9 3	0°	0°	120°	20°
AL1 D SFL 9 4	0°	0°	130°	12°
AL1 D SFL 9 5	0°	0°	130°	16°
AL1 D SFL 9 6	0°	0°	130°	20°
AL1 D SFL 9 7	0°	0°	140°	12°
AL1 D SFL 9 8	0°	0°	140°	16°
AL1 D SFL 9 9	0°	0°	140°	20°

Table 35: Full factorial design of 3-flute drills for 6082-T6

Experiment ID	Helix Angle	Cutting Angle	Drill Point Angle	Relief Angle
AL1 D 3FL 4 1	30°	15°	130°	10°
AL1 D 3FL 4 2	30°	15°	135°	10°
AL1 D 3FL 4 3	35°	15°	130°	10°
AL1 D 3FL 4 4	35°	15°	135°	10°

Table 36: Full factorial design of 2-flute drills for Ti-6Al-4V

Experiment ID	Helix Angle	Cutting Angle	Drill Point Angle	Relief Angle
Ti1 D 2FL 8 1	30°	3°	130°	10°
Ti1 D 2FL 8 2	30°	3°	130°	16°
Ti1 D 2FL 8 3	30°	5°	130°	10°
Ti1 D 2FL 8 4	30°	5°	130°	16°
Ti1 D 2FL 8 5	30°	3°	140°	10°
Ti1 D 2FL 8 6	30°	3°	140°	16°
Ti1 D 2FL 8 7	30°	5°	140°	10°
Ti1 D 2FL 8 8	30°	5°	140°	16°

Table 37: Full factorial design of 2-flute drills for Inconel 718

Experiment ID	Helix Angle	Cutting Angle	Drill Point Angle	Relief Angle
INCO1 D 2FL 16 1	30°	0°	130°	6°
INCO1 D 2FL 16 2	34°	0°	130°	6°
INCO1 D 2FL 16 3	30°	0°	140°	6°
INCO1 D 2FL 16 4	34°	0°	140°	6°
INCO1 D 2FL 16 5	30°	5°	130°	6°
INCO1 D 2FL 16 6	34°	5°	130°	6°
INCO1 D 2FL 16 7	30°	5°	140°	6°
INCO1 D 2FL 16 8	34°	5°	140°	6°
INCO1 D 2FL 16 9	30°	0°	130°	10°
INCO1 D 2FL 16 10	34°	0°	130°	10°
INCO1 D 2FL 16 11	30°	0°	140°	10°
INCO1 D 2FL 16 12	34°	0°	140°	10°
INCO1 D 2FL 16 13	30°	5°	130°	10°
INCO1 D 2FL 16 14	34°	5°	130°	10°
INCO1 D 2FL 16 15	30°	5°	140°	10°
INCO1 D 2FL 16 16	34°	5°	140°	10°

Table 38: Full factorial design of 2-flute drills for super duplex 2507

Experiment ID	Helix Angle	Cutting Angle	Drill Point Angle	Relief Angle
SDX1 D 2FL 8 1	30°	-5°	130°	10°
SDX1 D 2FL 8 2	30°	-5°	130°	12°
SDX1 D 2FL 8 3	30°	0°	130°	10°
SDX1 D 2FL 8 4	30°	0°	130°	12°
SDX1 D 2FL 8 5	30°	-5°	140°	10°
SDX1 D 2FL 8 6	30°	-5°	140°	12°
SDX1 D 2FL 8 7	30°	0°	140°	10°
SDX1 D 2FL 8 8	30°	0°	140°	12°

Appendix B: End-mill Designs

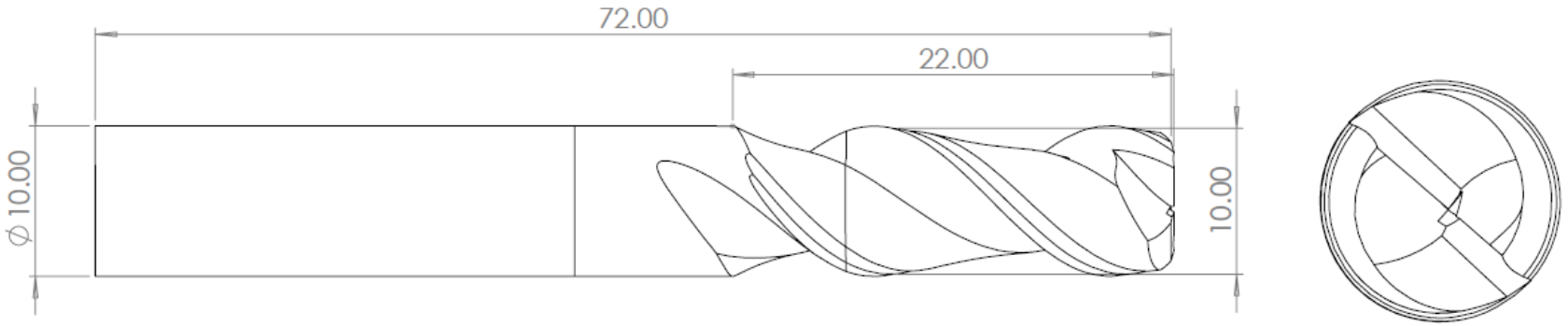

Fig. 136: End-mill design for experiments on 6082-T6, 2-flute

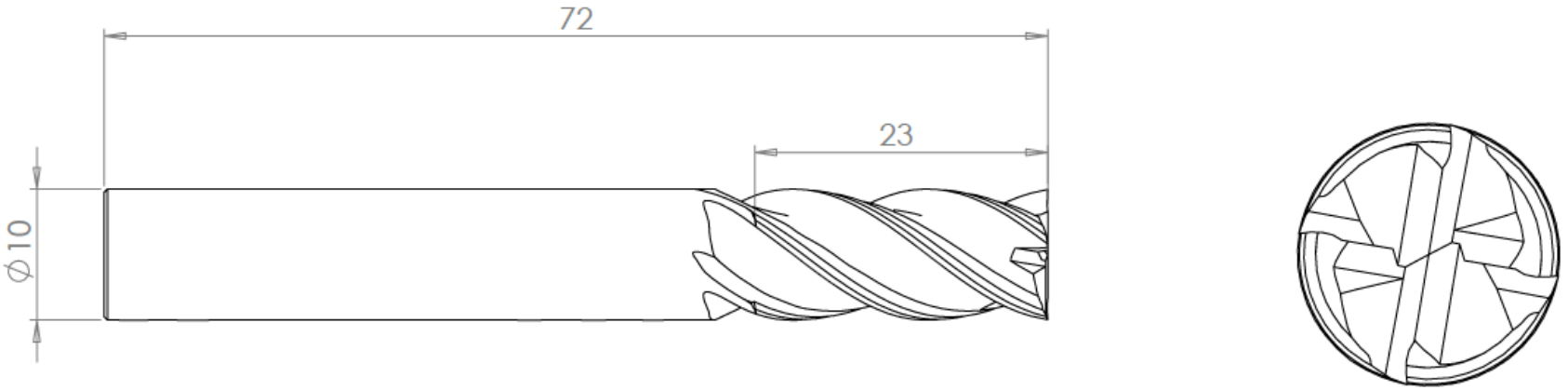

Fig. 137: End-mill design for experiments on Ti-6Al-4V, 4-flute

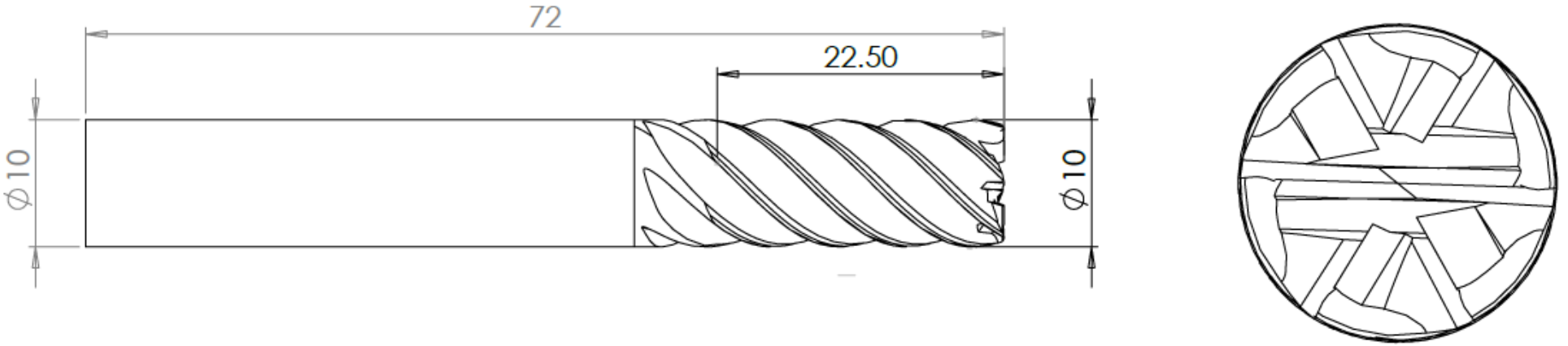

Fig. 138: End-mill design for experiments on Ti-6Al-4V, 6-flute

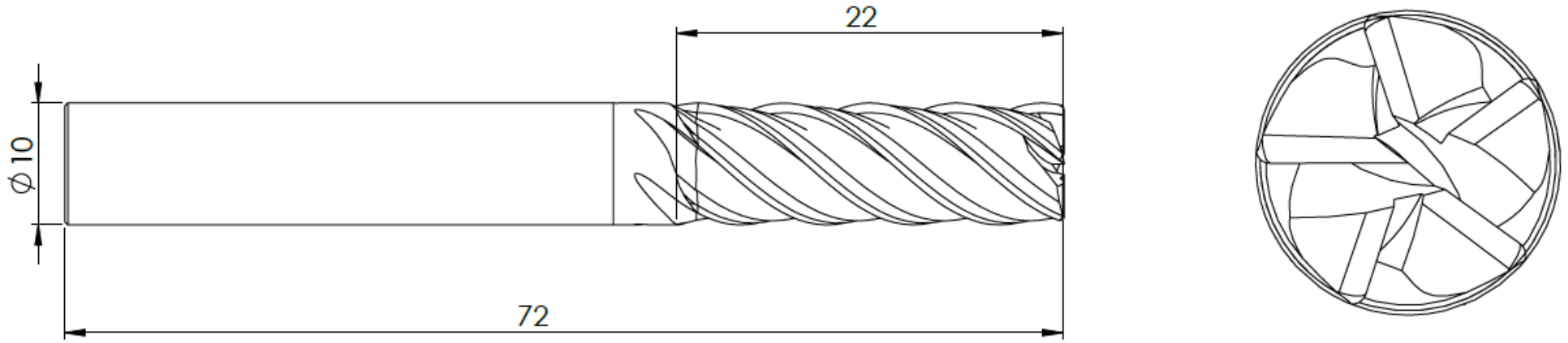

Fig. 139: End-mill design for experiments on Inconel 718, 5-flute

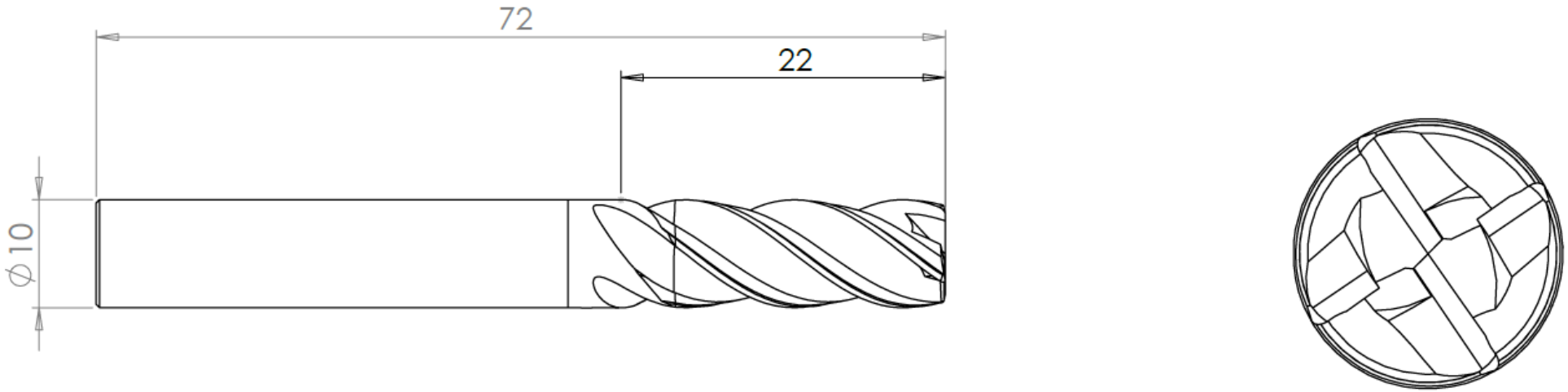

Fig. 140: End-mill design for experiments on super duplex 2507, 4-flute

Appendix C: Drill Designs

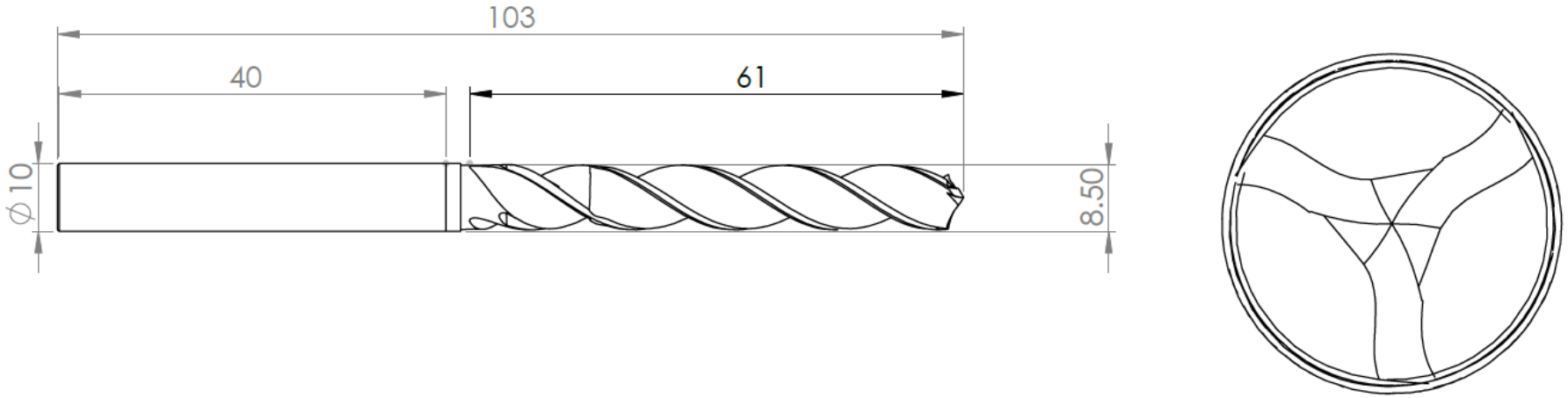

Fig. 141: Drill design for experiments on 6082-T6, 3-flute

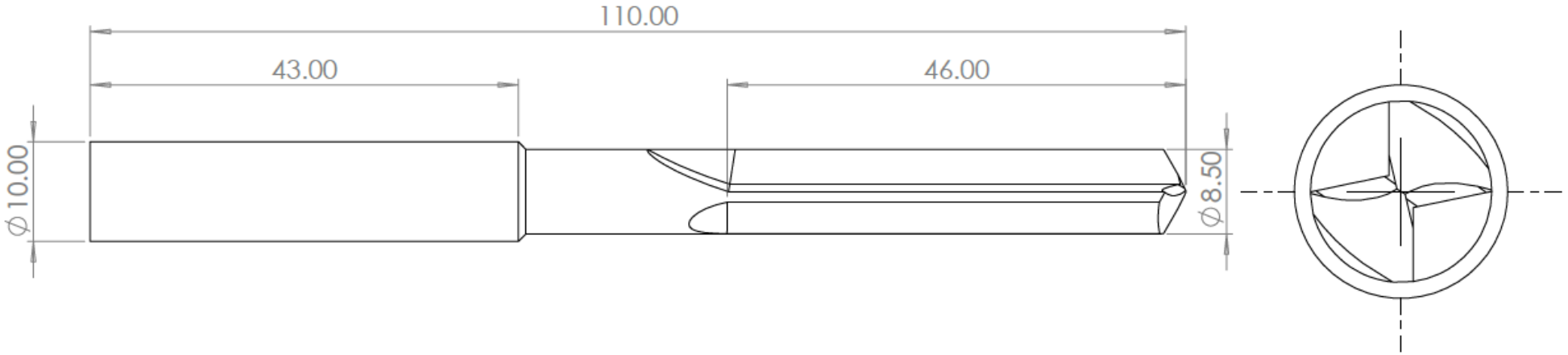

Fig. 142: Striaght flute drill design for experiments on 6082-T6

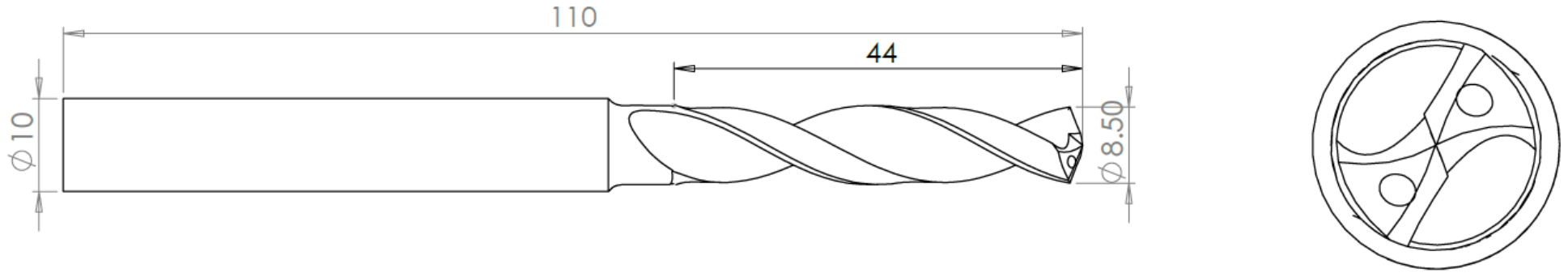

Fig. 143: Drill design for experiments on Ti-6Al-4V

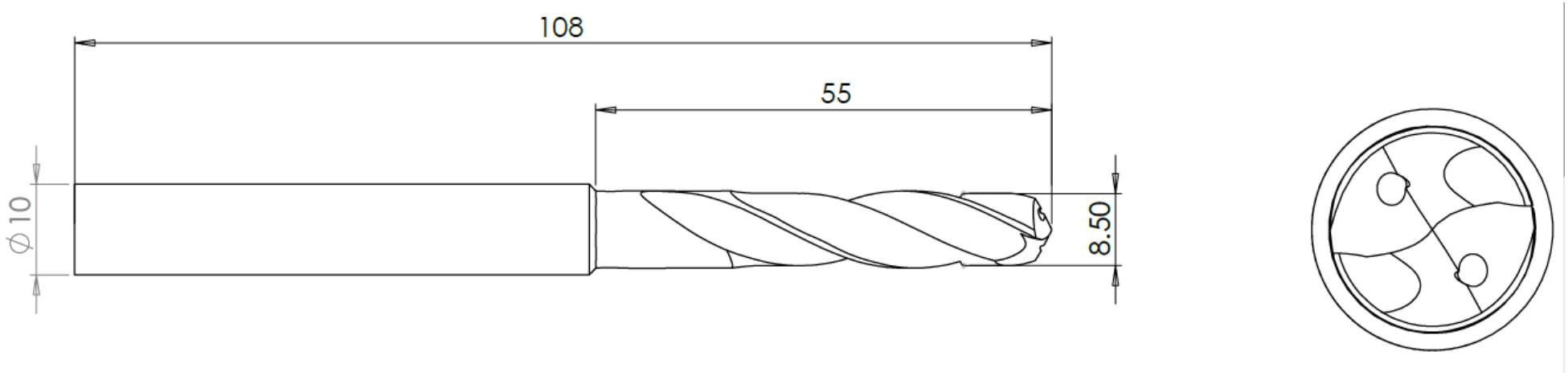

Fig. 144: Drill design for experiments on Inconel 718

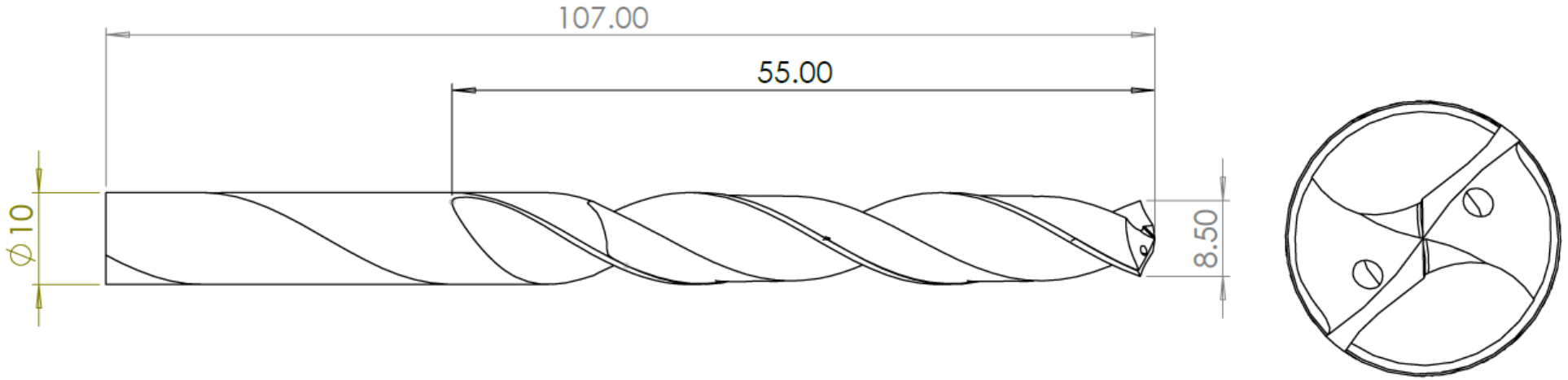

Fig. 145: Drill design for experiments on super duplex 2507

Appendix D: WC-Co Composition

WC-Co	Grain Structure
YL10.2	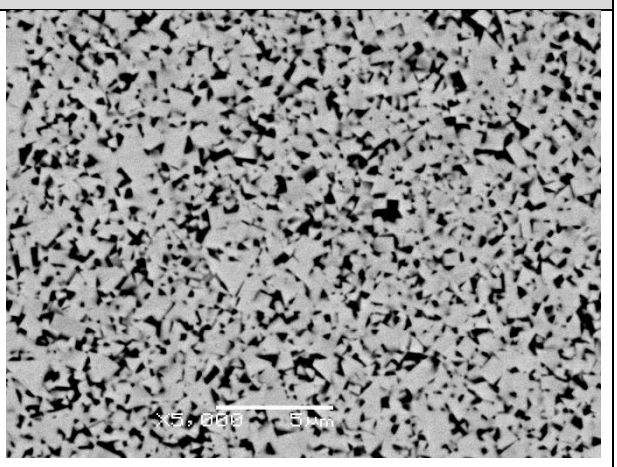
EMT100	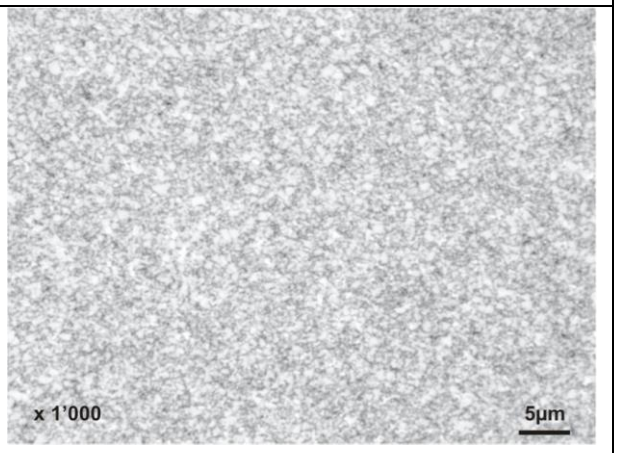
CTS20D	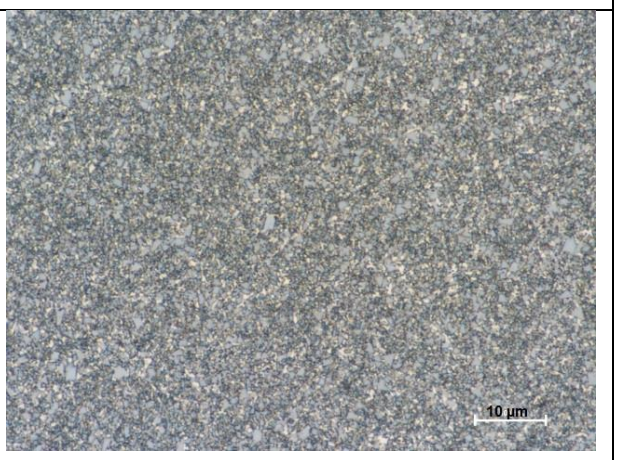

Appendix E: Tool Wear Images

E1.Aluminium 6082-T6

AL1 R 8 1		AL1 R 8 2	
CE1	CE2	CE1	CE2
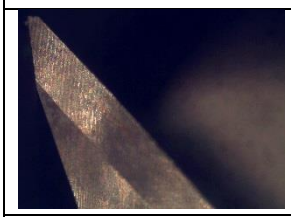	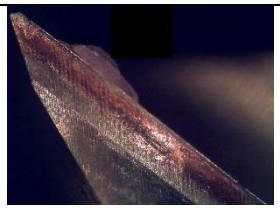		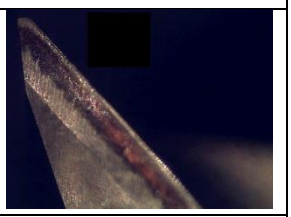
AL1 R 8 3		**AL1 R 8 4**	
CE1	CE2	CE1	CE2
			
AL1 R 8 5		**AL1 R 8 6**	
CE1	CE2	CE1	CE2
			
AL1 R 8 7		**AL1 R 8 8**	
CE1	CE2	CE1	CE2
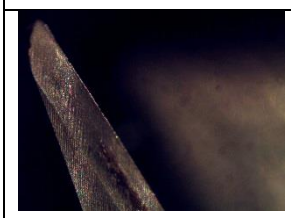			
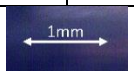 **Scale bar (1 mm)**			

E2.Titanium Ti-6Al-4V

Ti1 R 24 1		Ti1 R 24 1 - Replicate	
CE1	CE2	CE1	CE2
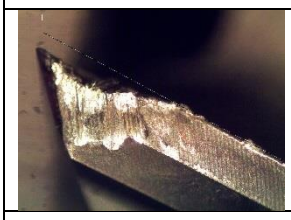		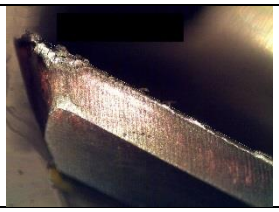	
CE3	CE4	CE3	CE4
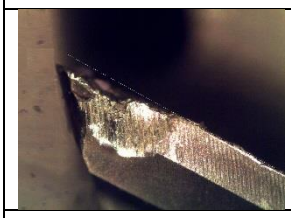			
Ti1 R 24 2		Ti1 R 24 2 – Replicate	
CE1	CE2	CE1	CE2
	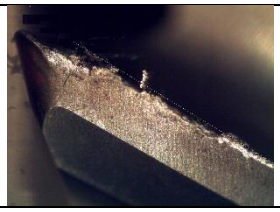		
CE3	CE4	CE3	CE4
			
Ti1 R 24 3		Ti1 R 24 3 – Replicate	
CE1	CE2	CE1	CE2
	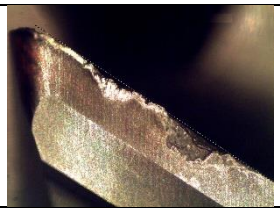		
CE3	CE4	CE3	CE4
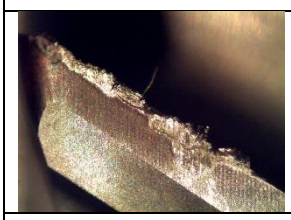			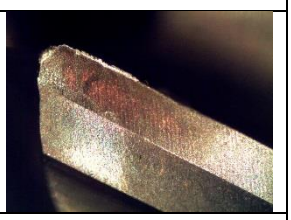
Ti1 R 24 4		Ti1 R 24 4 – Rep	
CE1	CE2	CE1	CE2

	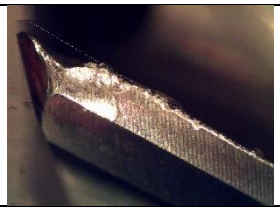		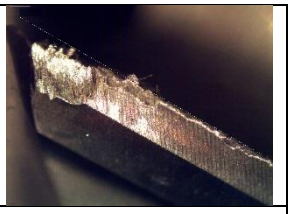
CE3	**CE4**	**CE3**	**CE4**
			
Ti1 R 24 5		**Ti1 R 24 5 – Rep**	
CE1	**CE2**	**CE1**	**CE2**
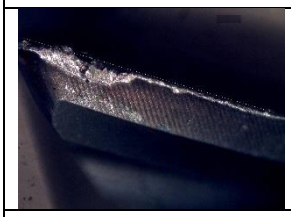			
CE3	**CE4**	**CE3**	**CE4**
	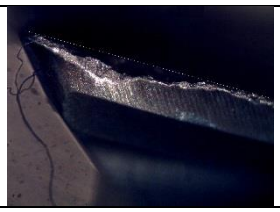	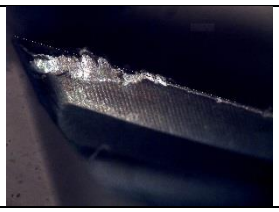	
Ti1 R 24 6		**Ti1 R 24 6 – Rep**	
CE1	**CE2**	**CE1**	**CE2**
	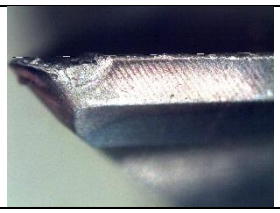	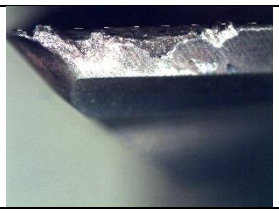	
CE3	**CE4**	**CE3**	**CE4**
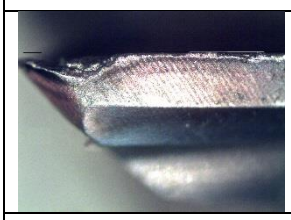	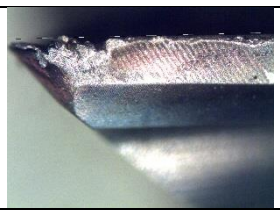	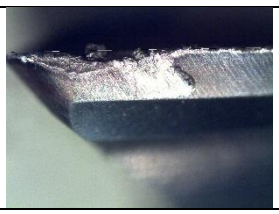	
Ti1 R 24 7		**Ti1 R 24 7 – Rep**	
CE1	**CE2**	**CE1**	**CE2**
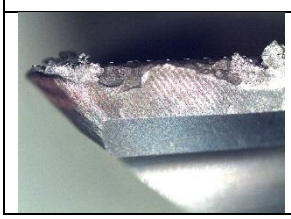	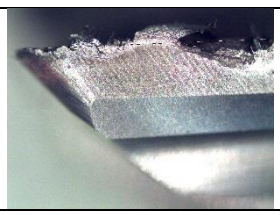	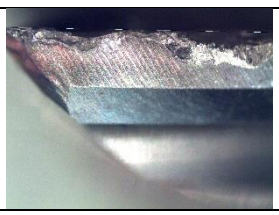	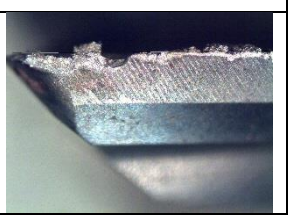

CE3	CE4	CE3	CE4
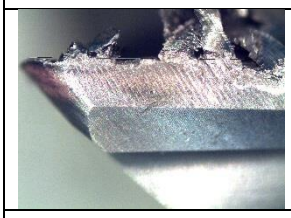	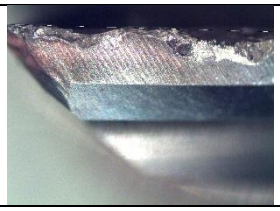	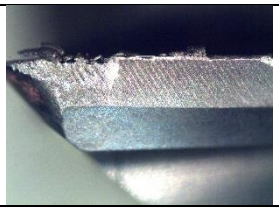	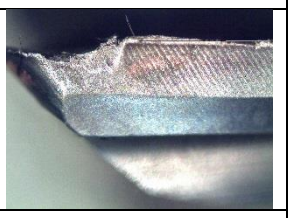
Ti1 R 24 8		Ti1 R 24 8 – Rep	
CE1	CE2	CE1	CE2
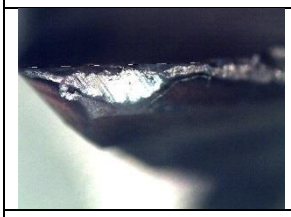	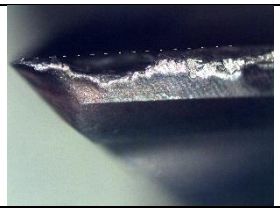	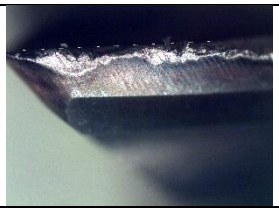	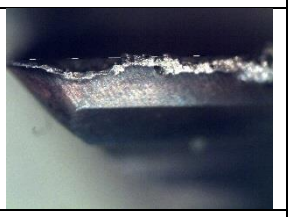
CE3	CE4	CE3	CE4
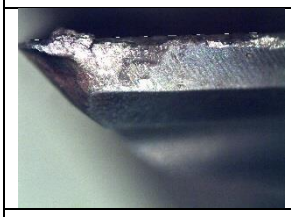		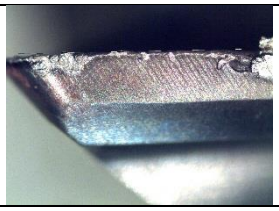	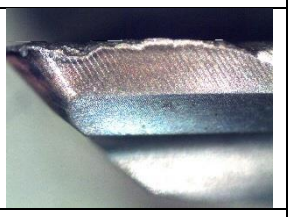
Ti1 R 24 9		Ti1 R 24 9 – Rep	
CE1	CE2	CE1	CE2
	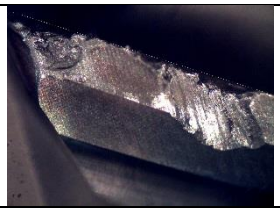	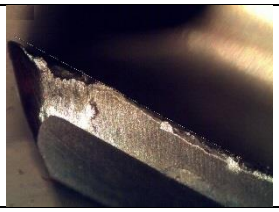	
CE3	CE4	CE3	CE4
			
Ti1 R 24 10		Ti1 R 24 10 – Rep	
CE1	CE2	CE1	CE2
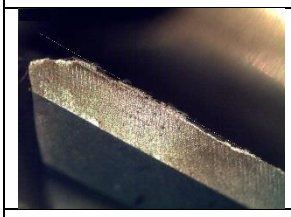	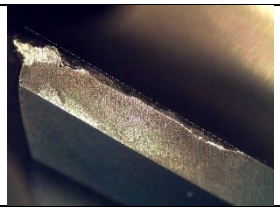	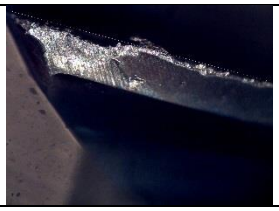	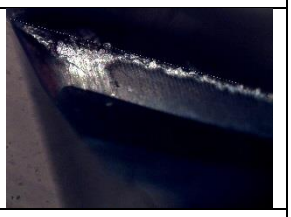
CE3	CE4	CE3	CE4

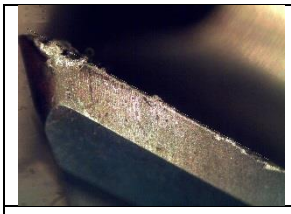	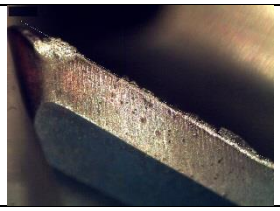		
Ti1 R 24 11		**Ti1 R 24 11 – Rep**	
CE1	**CE2**	**CE1**	**CE2**
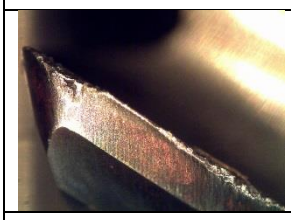			
CE3	**CE4**	**CE3**	**CE4**
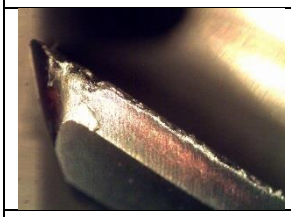	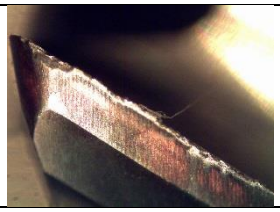		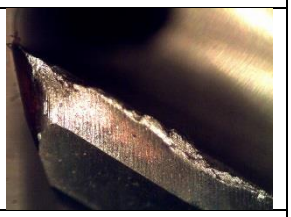
Ti1 R 24 12		**Ti1 R 24 12 – Rep**	
CE1	**CE2**	**CE1**	**CE2**
			
CE3	**CE4**	**CE3**	**CE4**
			
Ti1 R 24 13		**Ti1 R 24 13 – Rep**	
CE1	**CE2**	**CE1**	**CE2**
		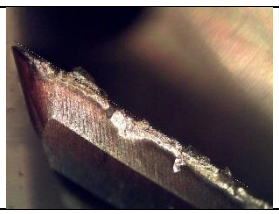	
CE3	**CE4**	**CE3**	**CE4**
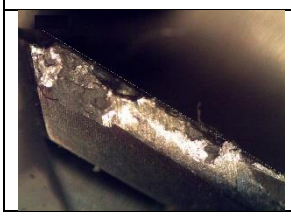		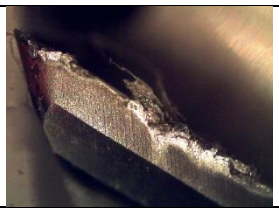	

Ti1 R 24 14		Ti1 R 24 14 – Rep	
CE1	CE2	CE1	CE2
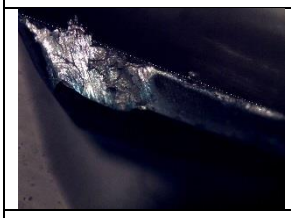		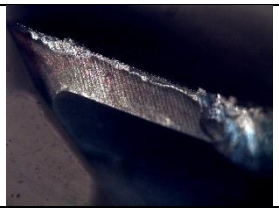	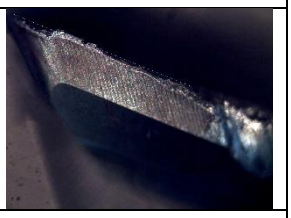
CE3	CE4	CE3	CE4
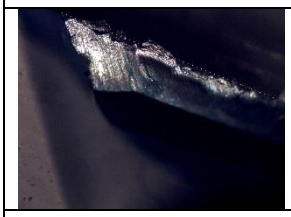			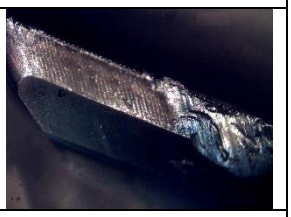
Ti1 R 24 15		Ti1 R 24 15 – Rep	
CE1	CE2	CE1	CE2
			
CE3	CE4	CE3	CE4
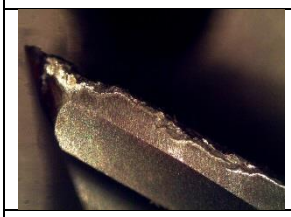			
Ti1 R 24 16		Ti1 R 24 16 – Rep	
CE1	CE2	CE1	CE2
		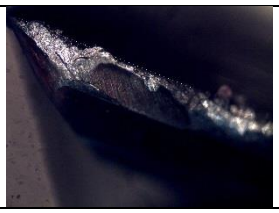	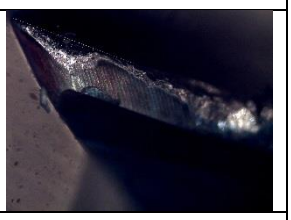
CE3	CE4	CE3	CE4
		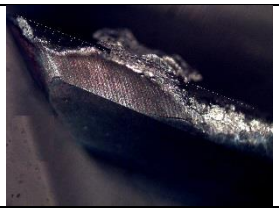	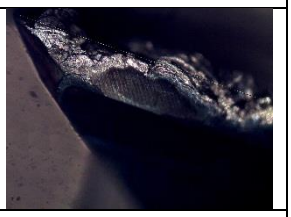
Ti1 R 24 17		Ti1 R 24 17 – Rep	
CE1	CE2	CE1	CE2

		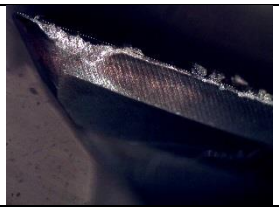	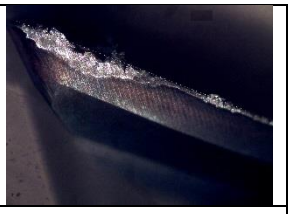
CE3	**CE4**	**CE3**	**CE4**
		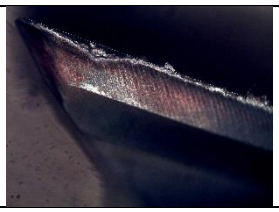	
Ti1 R 24 18		**Ti1 R 24 18 – Rep**	
CE1	**CE2**	**CE1**	**CE2**
	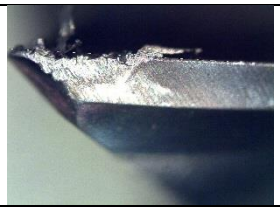		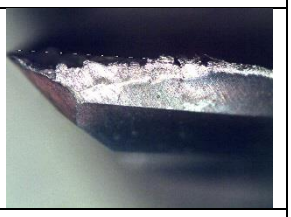
CE3	**CE4**	**CE3**	**CE4**
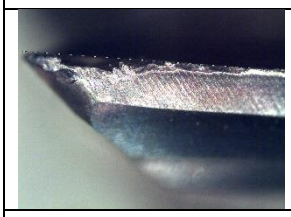	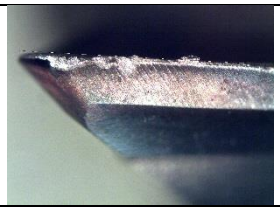	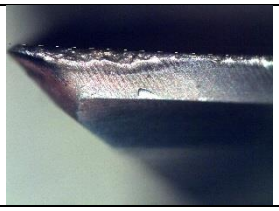	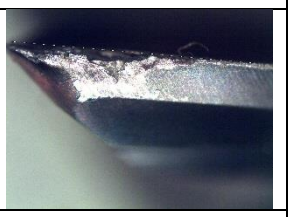
Ti1 R 24 19		**Ti1 R 24 19 – Rep**	
CE1	**CE2**	**CE1**	**CE2**
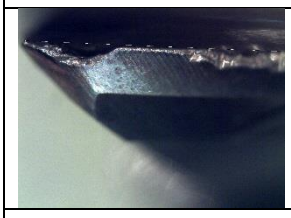	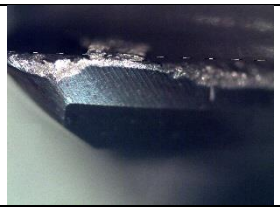	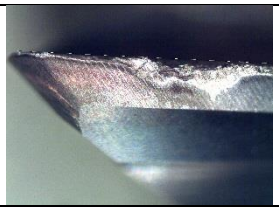	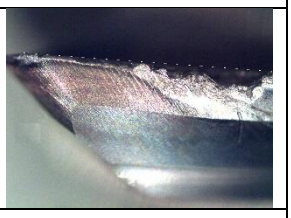
CE3	**CE4**	**CE3**	**CE4**
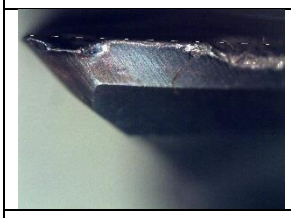	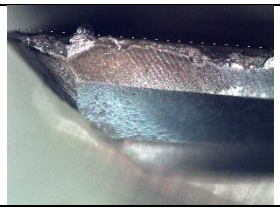	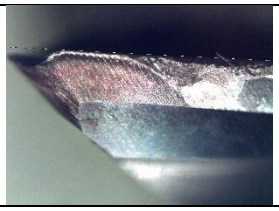	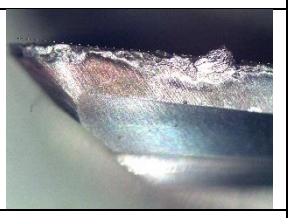
Ti1 R 24 20		**Ti1 R 24 20 – Rep**	
CE1	**CE2**	**CE1**	**CE2**
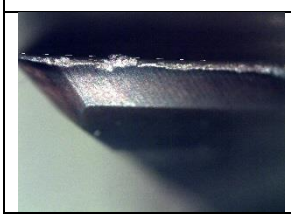	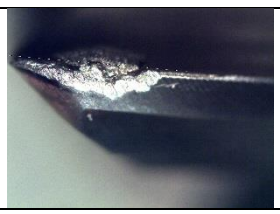	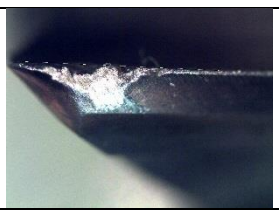	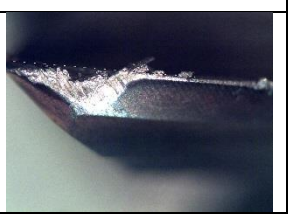

Cutting Edge 3	Cutting Edge 4	Cutting Edge 3	Cutting Edge 4
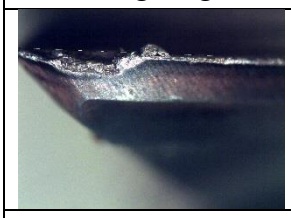	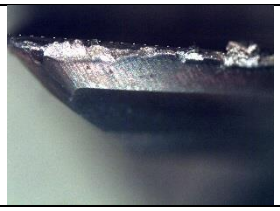		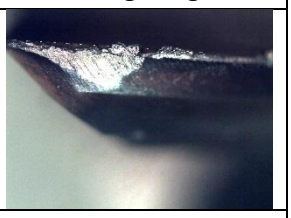
Ti1 R 24 21		**Ti1 R 24 21 – Rep**	
CE1	**CE2**	**CE1**	**CE2**
			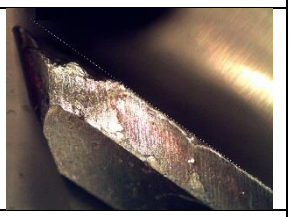
CE3	**CE4**	**CE3**	**CE4**
		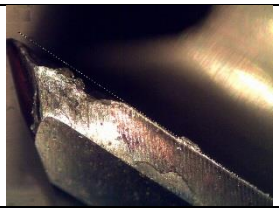	
Ti1 R 24 22		**Ti1 R 24 22 – Rep**	
CE1	**CE2**	**CE1**	**CE2**
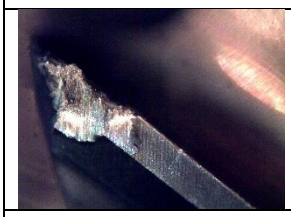			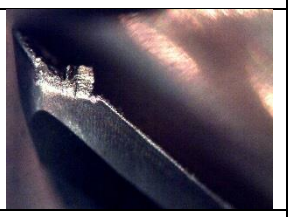
CE3	**CE4**	**CE3**	**CE4**
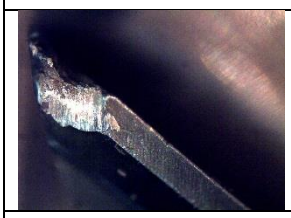			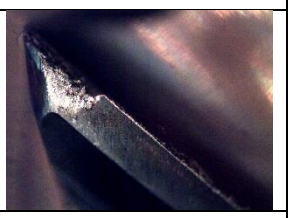
Ti1 R 24 23		**Ti1 R 24 23 – Rep**	
CE1	**CE2**	**CE1**	**CE2**
		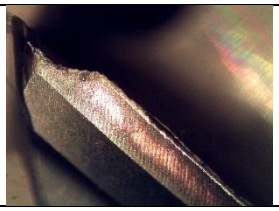	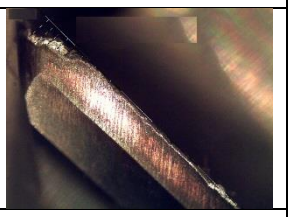
CE3	**CE4**	**CE3**	**CE4**

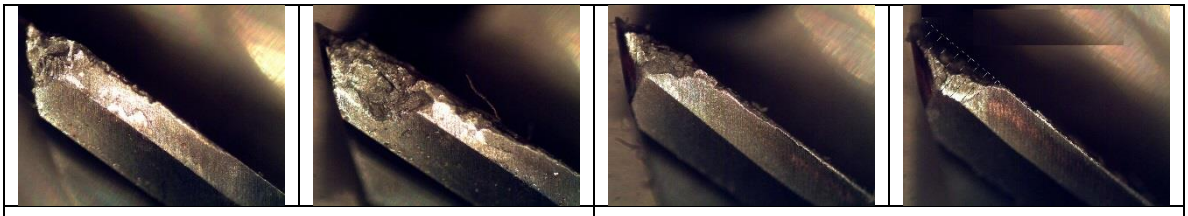			
Ti1 R 24 24		**Ti1 R 24 24 – Rep**	
CE1	**CE2**	**CE1**	**CE2**
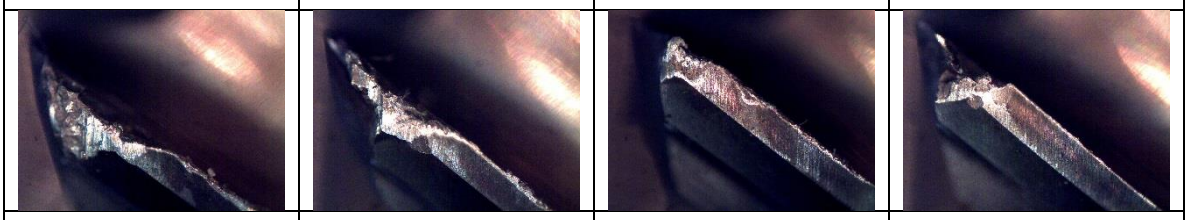			
CE3	**CE4**	**CE3**	**CE4**
			
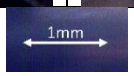 **Scale bar (1 mm)**			

Ti1 F 8 1 – Tip					
CE1	CE2	CE3	CE4	CE5	CE6
	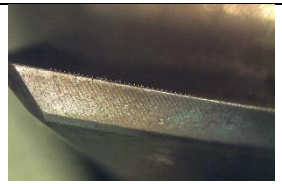		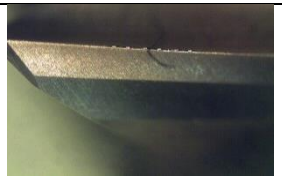	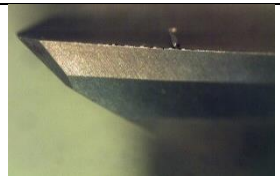	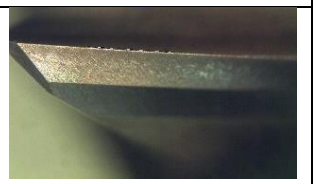
Ti1 F 8 1 – End					
CE1	CE2	CE3	CE4	CE5	CE6
					
Ti1 F 8 1 – Replicate – Tip					
CE1	CE2	CE3	CE4	CE5	CE6
	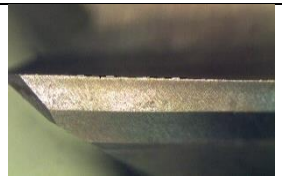	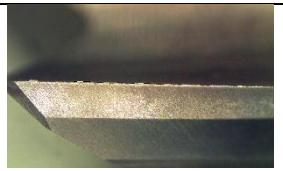	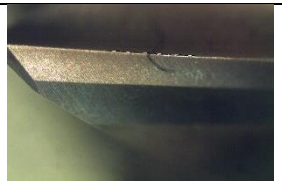	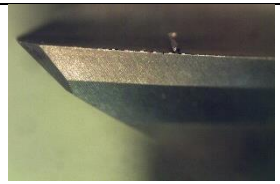	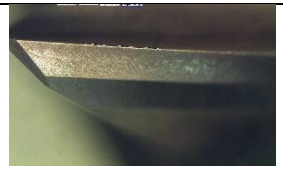
Ti1 F 8 1 – Replicate – End					
CE1	CE2	CE3	CE4	CE5	CE6
					
Ti1 F 8 2 – Tip					

CE1	CE2	CE3	CE4	CE5	CE6
	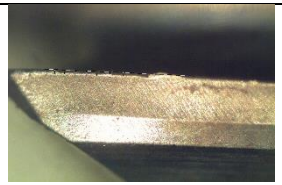		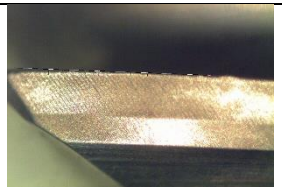		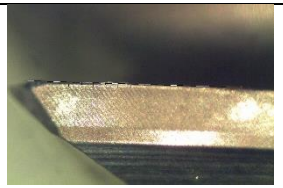
Ti1 F 8 2 – End					
CE1	**CE2**	**CE3**	**CE4**	**CE5**	**CE6**
		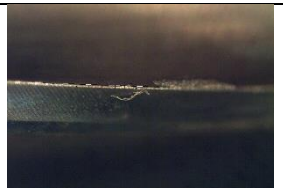	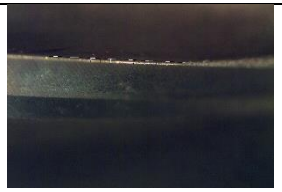	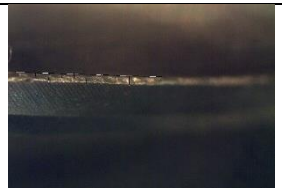	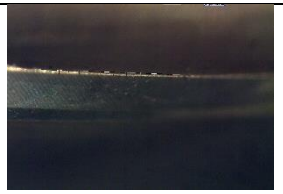
Ti1 F 8 2 – Replicate – Tip					
CE1	**CE2**	**CE3**	**CE4**	**CE5**	**CE6**
	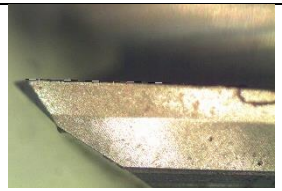	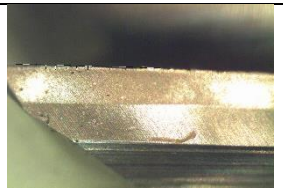			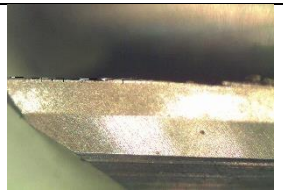
Ti1 F 8 2 – Replicate – End					
CE1	**CE2**	**CE3**	**CE4**	**CE5**	**CE6**
				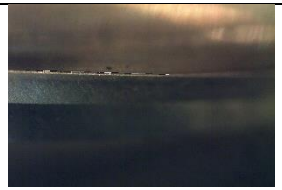	
Ti1 F 8 3 – Tip					
CE1	**CE2**	**CE3**	**CE4**	**CE5**	**CE6**

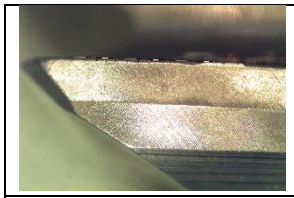	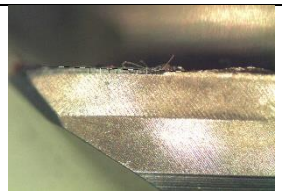	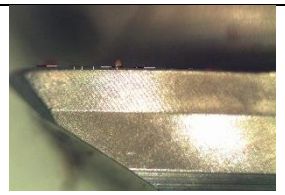	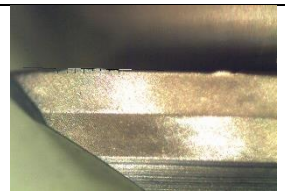	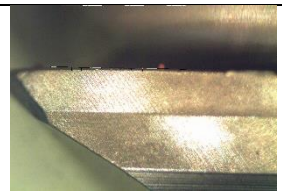	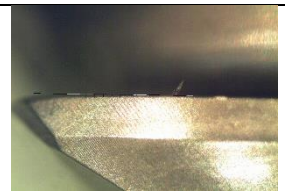
Ti1 F 8 3 – End					
CE1	**CE2**	**CE3**	**CE4**	**CE5**	**CE6**
	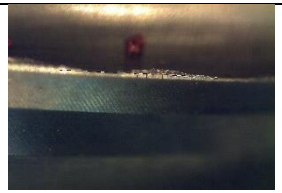			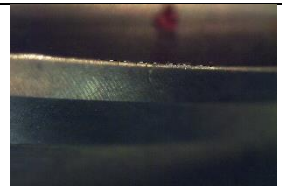	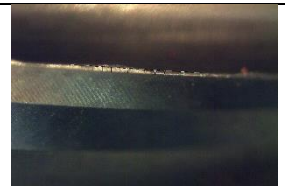
Ti1 F 8 3 – Replicate – Tip					
CE1	**CE2**	**CE3**	**CE4**	**CE5**	**CE6**
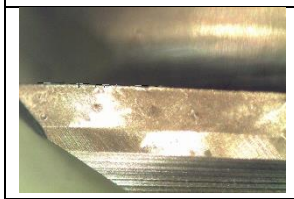	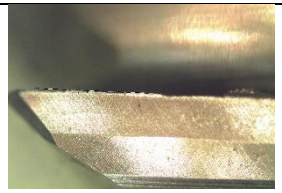	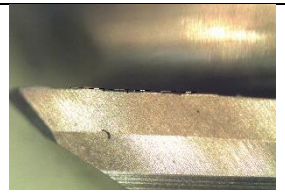	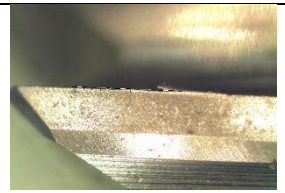		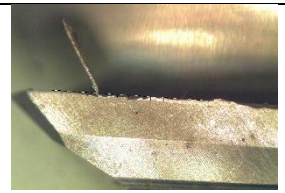
Ti1 F 8 3 – Replicate – End					
CE1	**CE2**	**CE3**	**CE4**	**CE5**	**CE6**
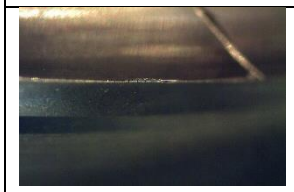	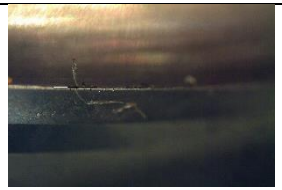			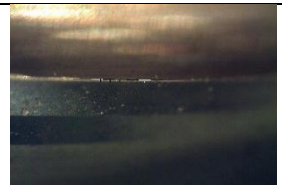	
Ti1 F 8 4 – Tip					
CE1	**CE2**	**CE3**	**CE4**	**CE5**	**CE6**

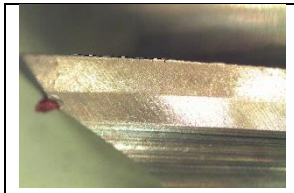	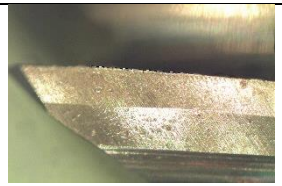	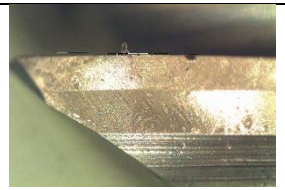	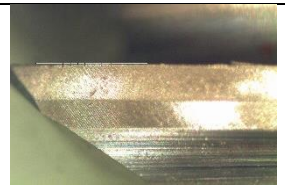	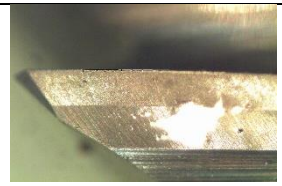	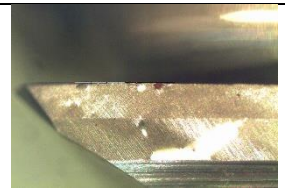
Ti1 F 8 4 – End					
CE1	**CE2**	**CE3**	**CE4**	**CE5**	**CE6**
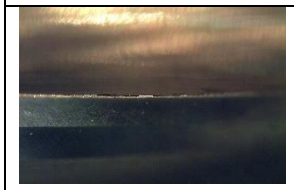	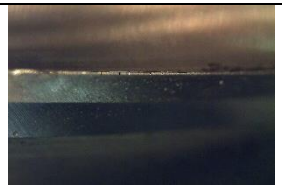	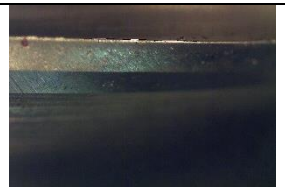	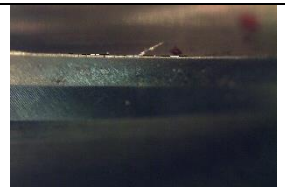		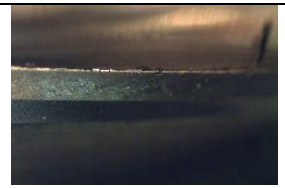
Ti1 F 8 4 – Replicate – Tip					
CE1	**CE2**	**CE3**	**CE4**	**CE5**	**CE6**
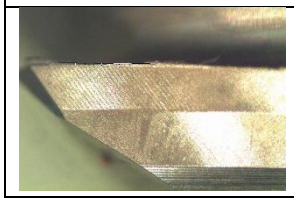	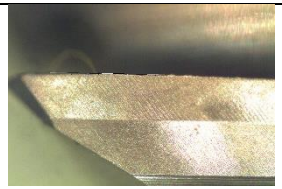	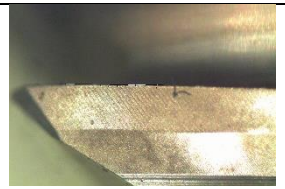	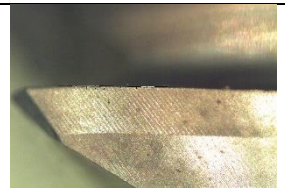	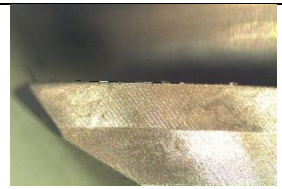	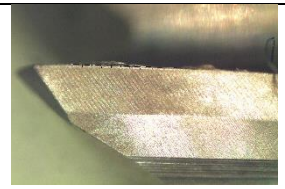
Ti1 F 8 4 – Replicate – End					
CE1	**CE2**	**CE3**	**CE4**	**CE5**	**CE6**
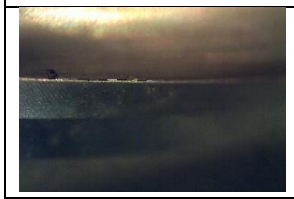	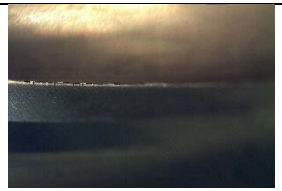	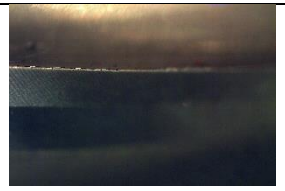		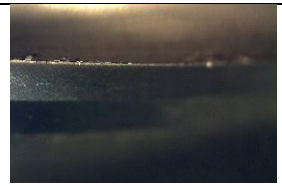	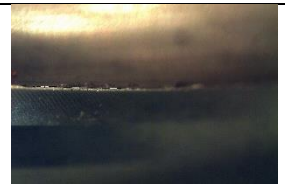
Ti1 F 8 5 – Tip					
CE1	**CE2**	**CE3**	**CE4**	**CE5**	**CE6**

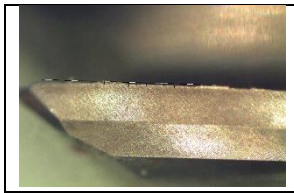	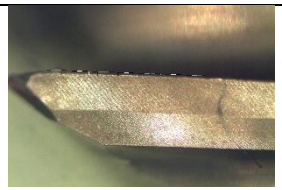	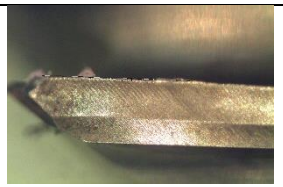		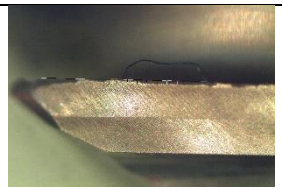	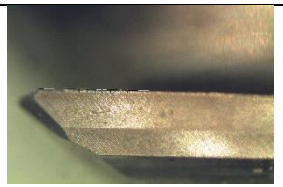
Ti1 F 8 5 – End					
CE1	**CE2**	**CE3**	**CE4**	**CE5**	**CE6**
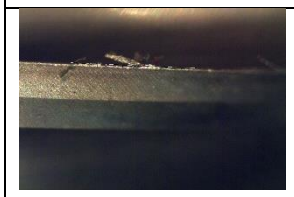	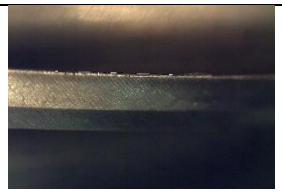				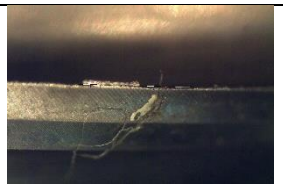
Ti1 F 8 5 – Replicate – Tip					
CE1	**CE2**	**CE3**	**CE4**	**CE5**	**CE6**
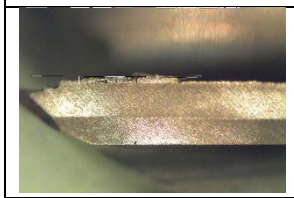	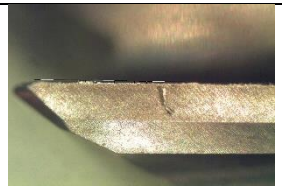		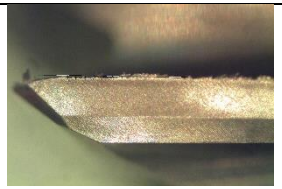	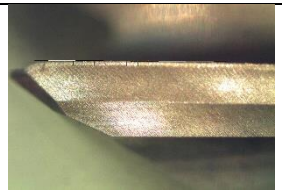	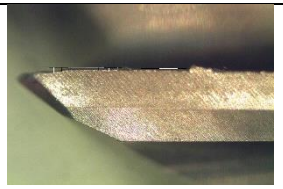
Ti1 F 8 5 – Replicate – End					
CE1	**CE2**	**CE3**	**CE4**	**CE5**	**CE6**
		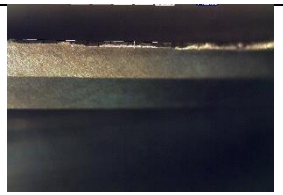		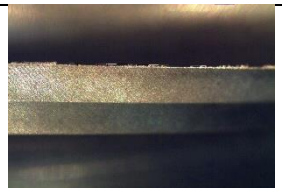	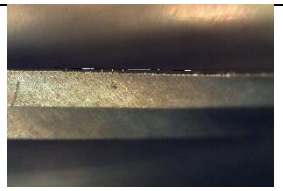
Ti1 F 8 6 – Tip					
CE1	**CE2**	**CE3**	**CE4**	**CE5**	**CE6**

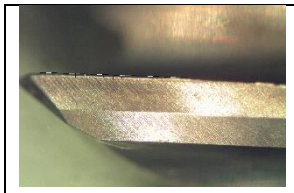	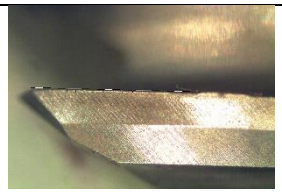		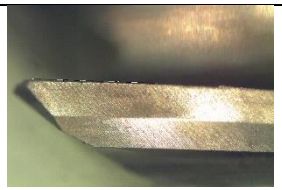	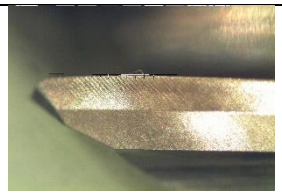	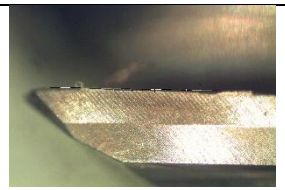
Ti1 F 8 6 – End					
CE1	**CE2**	**CE3**	**CE4**	**CE5**	**CE6**
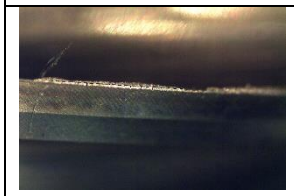	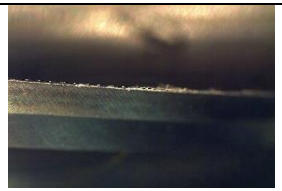	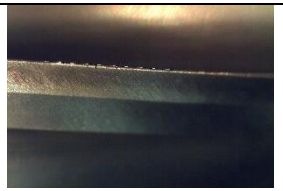		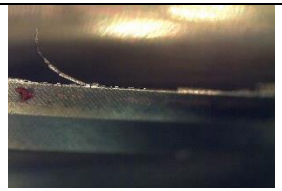	
Ti1 F 8 6 – Replicate – Tip					
CE1	**CE2**	**CE3**	**CE4**	**CE5**	**CE6**
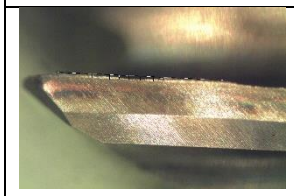	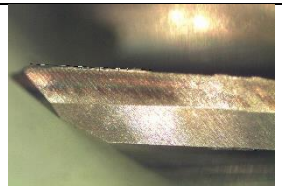	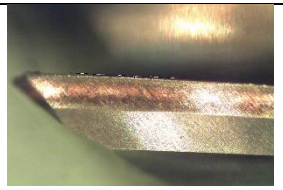			
Ti1 F 8 6 – Replicate – End					
CE1	**CE2**	**CE3**	**CE4**	**CE5**	**CE6**
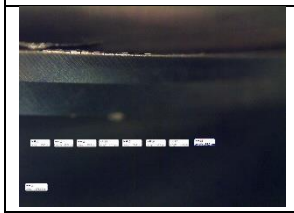	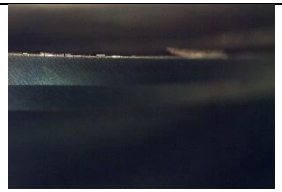		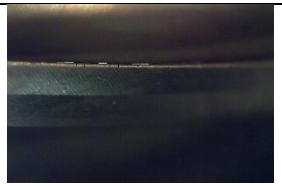		
Ti1 F 8 7 – Tip					
CE1	**CE2**	**CE3**	**CE4**	**CE5**	**CE6**

	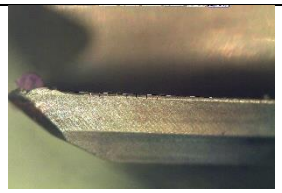	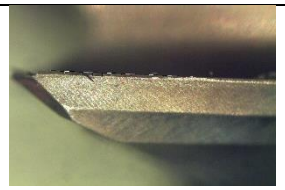	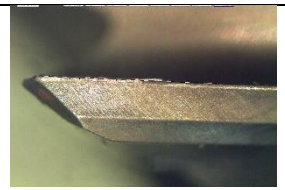	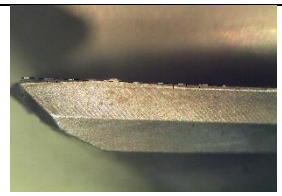	
Ti1 F 8 7 – End					
CE1	**CE2**	**CE3**	**CE4**	**CE5**	**CE6**
	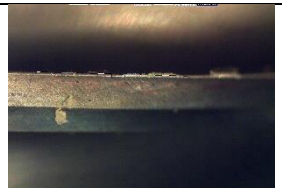	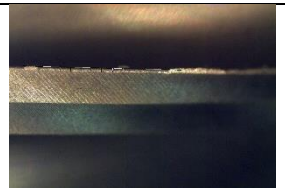	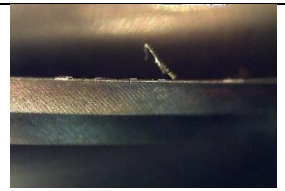	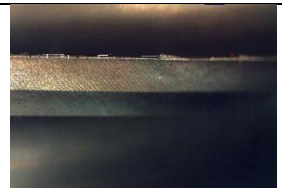	
Ti1 F 8 7 – Replicate – Tip					
CE1	**CE2**	**CE3**	**CE4**	**CE5**	**CE6**
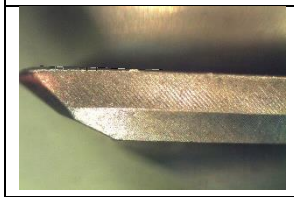	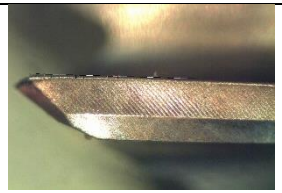	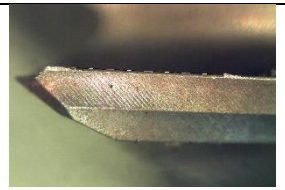	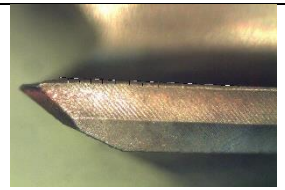	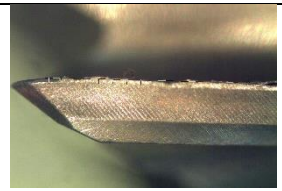	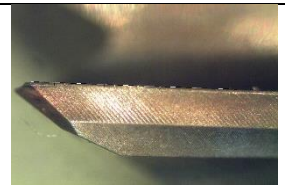
Ti1 F 8 7 – Replicate – End					
CE1	**CE2**	**CE3**	**CE4**	**CE5**	**CE6**
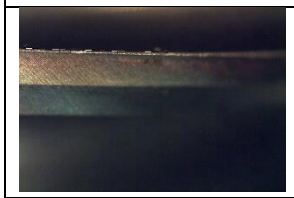	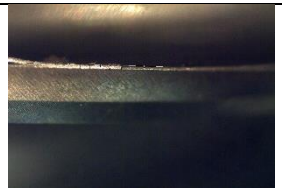	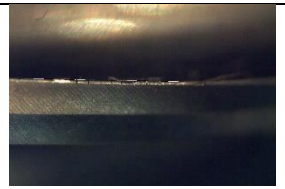	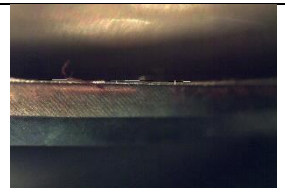	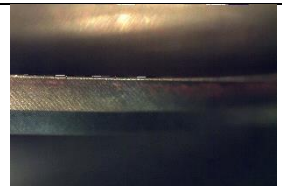	
Ti1 F 8 8 – Tip					
CE1	**CE2**	**CE3**	**CE4**	**CE5**	**CE6**

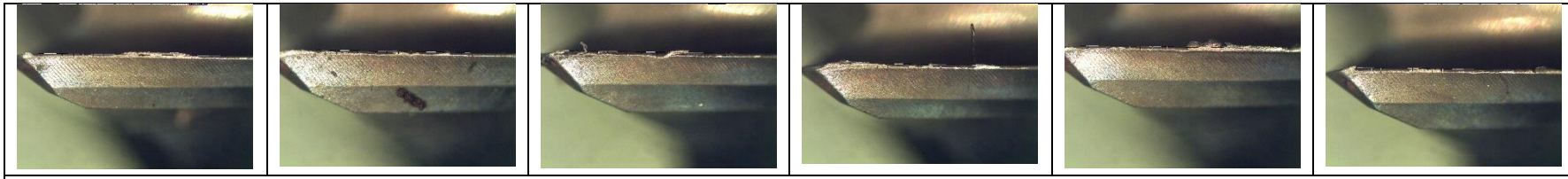

Ti1 F 8 8 – End

CE1	CE2	CE3	CE4	CE5	CE6

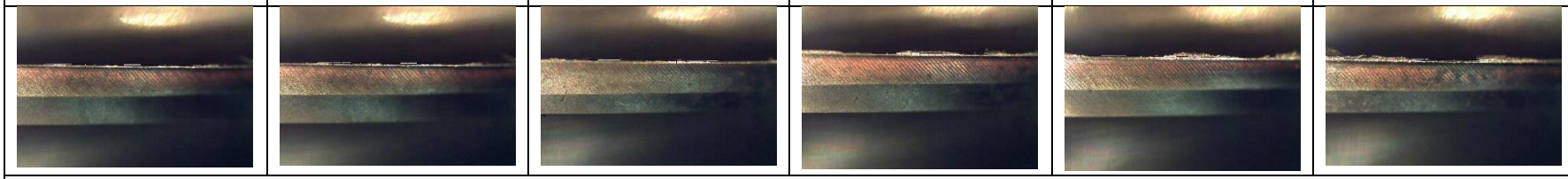

Ti1 F 8 8 – Replicate – Tip

CE1	CE2	CE3	CE4	CE5	CE6

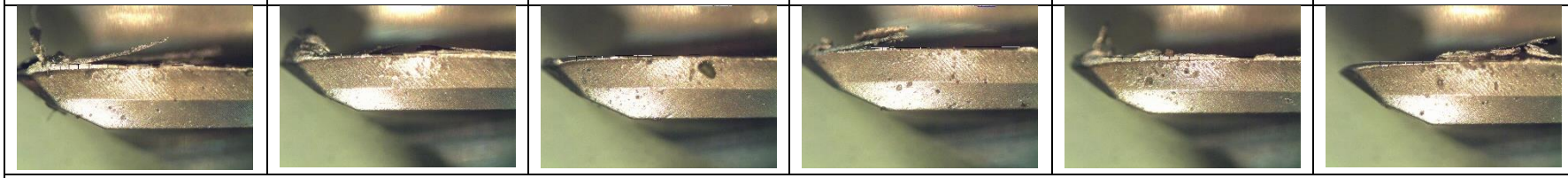

Ti1 F 8 8 – Replicate – End

CE1	CE2	CE3	CE4	CE5	CE6

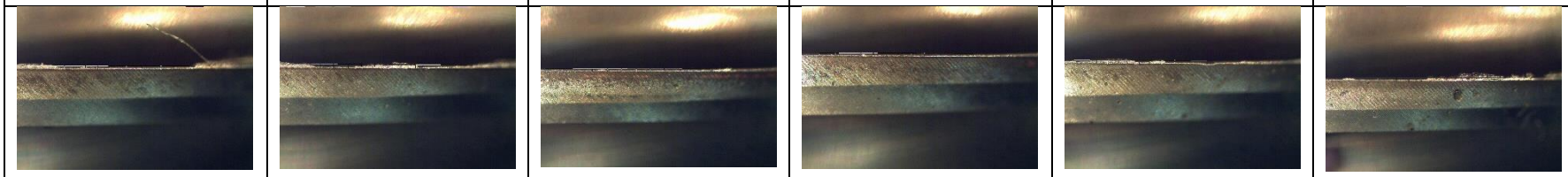

Scale bar (1 mm)

E3.Inconel alloy 718

INCO1 R 27 1				
CE1	CE2	CE3	CE4	CE5
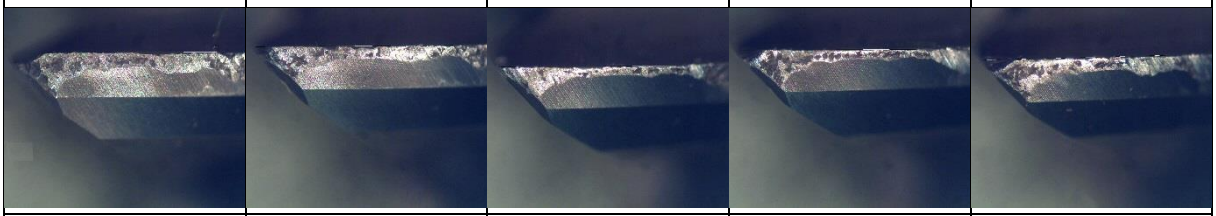				
CE1	CE2	CE3	CE4	CE5
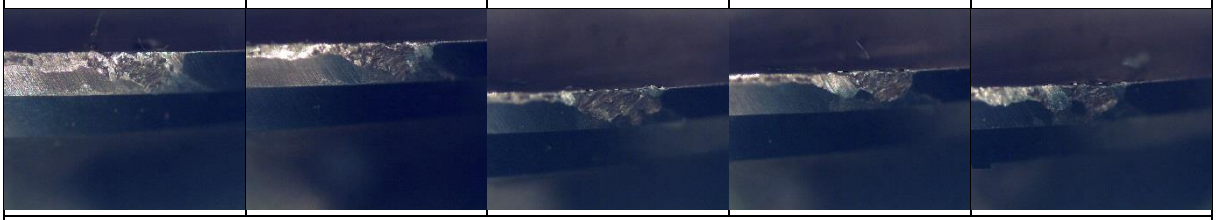				
INCO1 R 27 2				
CE1	CE2	CE3	CE4	CE5
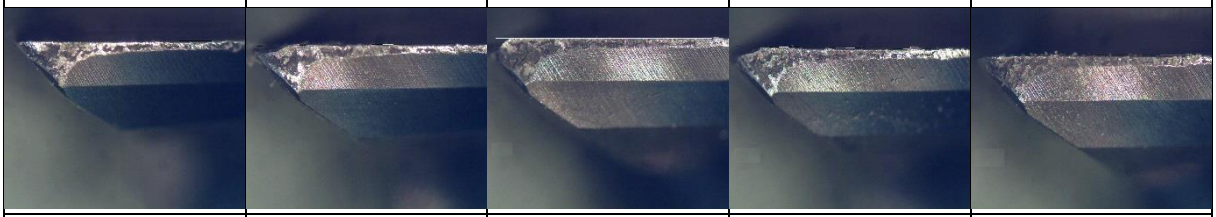				
CE1	CE2	CE3	CE4	CE5
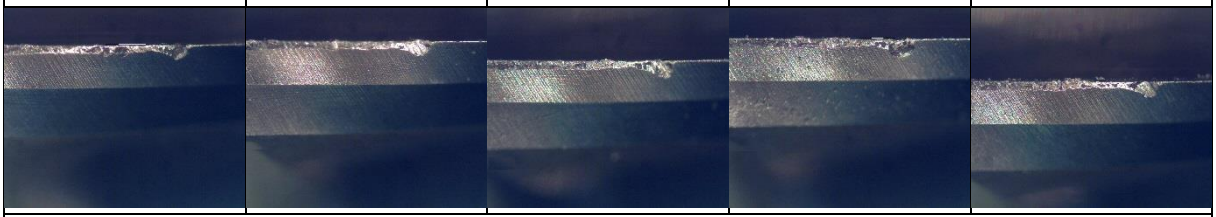				
INCO1 R 27 3				
CE1	CE2	CE3	CE4	CE5
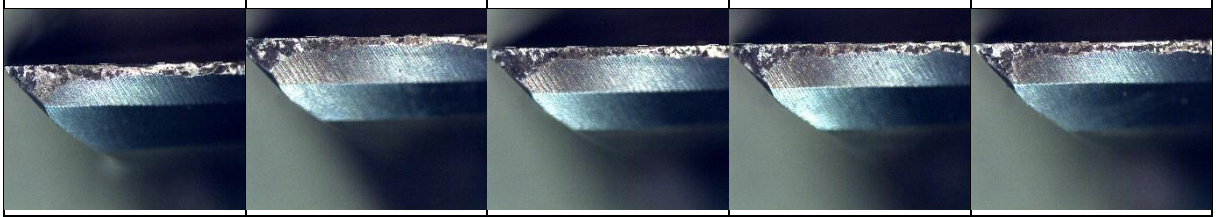				
INCO1 R 27 4				
CE1	CE2	CE3	CE4	CE5
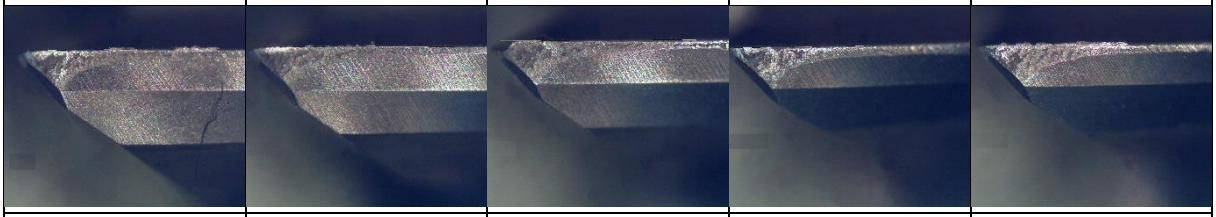				
CE1	CE2	CE3	CE4	CE5

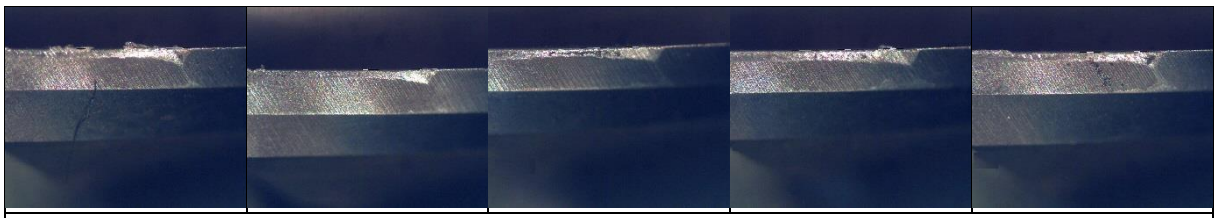				
INCO1 R 27 5				
CE1	**CE2**	**CE3**	**CE4**	**CE5**
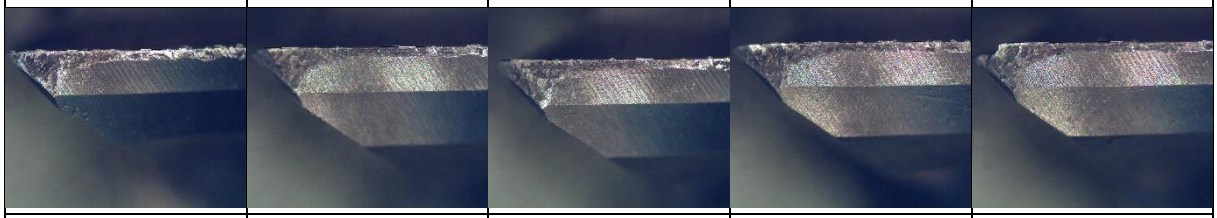				
CE1	**CE2**	**CE3**	**CE4**	**CE5**
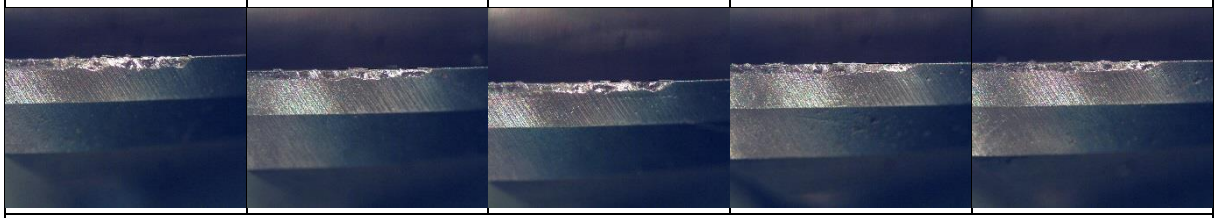				
INCO1 R 27 6				
CE1	**CE2**	**CE3**	**CE4**	**CE5**
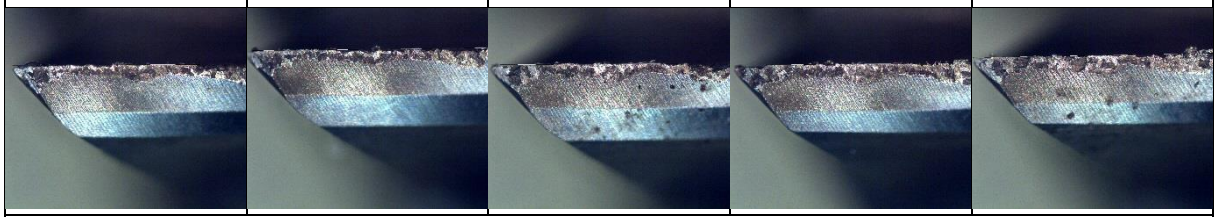				
INCO1 R 27 7				
CE1	**CE2**	**CE3**	**CE4**	**CE5**
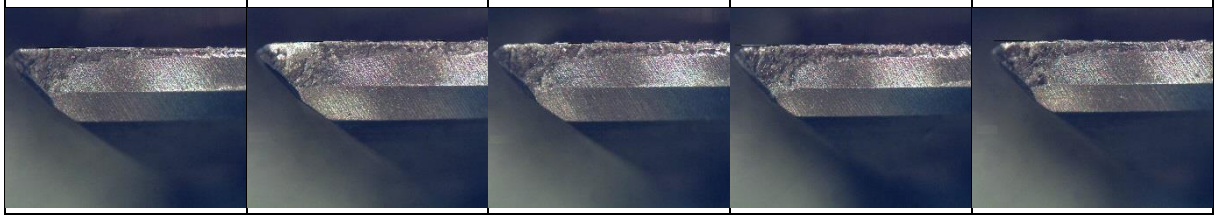				
CE1	**CE2**	**CE3**	**CE4**	**CE5**
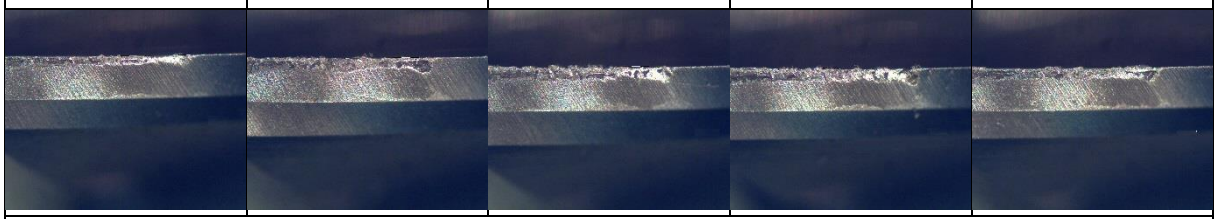				
INCO1 R 27 8				
CE1	**CE2**	**CE3**	**CE4**	**CE5**
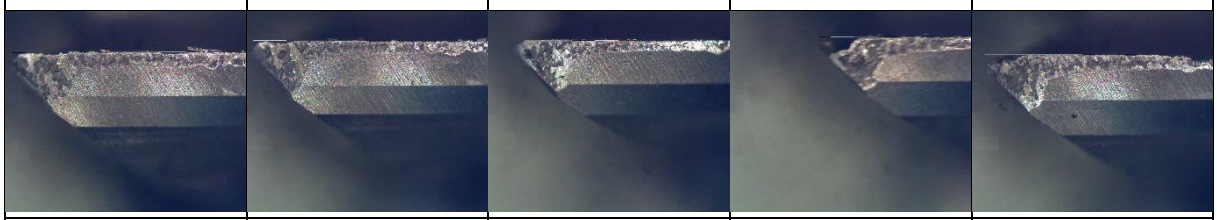				
CE1	**CE2**	**CE3**	**CE4**	**CE5**

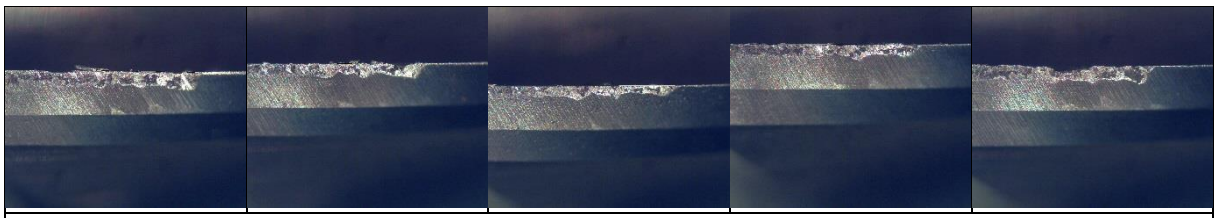				
INCO1 R 27 9				
CE1	**CE2**	**CE3**	**CE4**	**CE5**
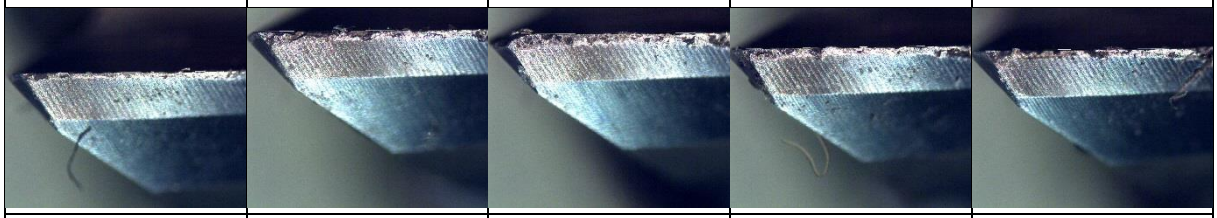				
CE1	**CE2**	**CE3**	**CE4**	**CE5**
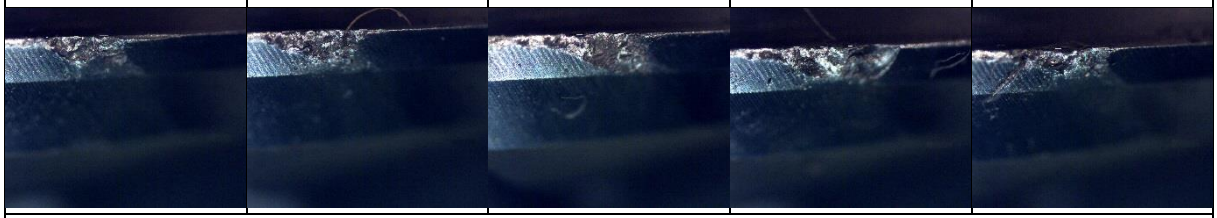				
INCO1 R 27 10				
CE1	**CE2**	**CE3**	**CE4**	**CE5**
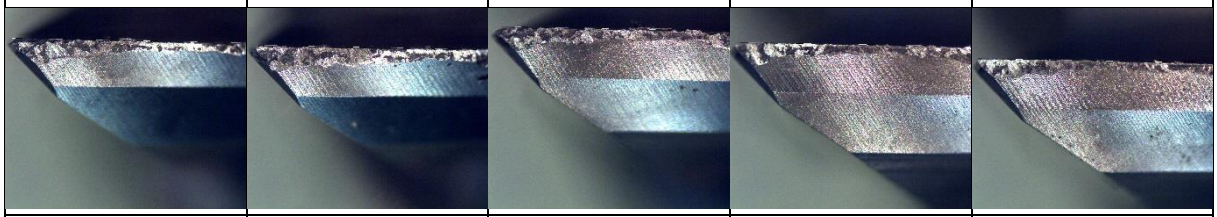				
CE1	**CE2**	**CE3**	**CE4**	**CE5**
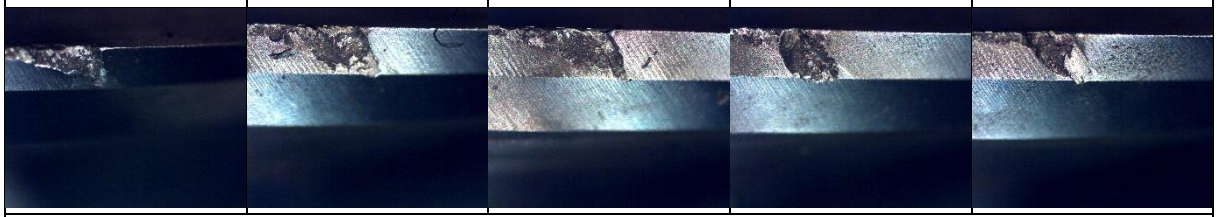				
INCO1 R 27 11				
CE1	**CE2**	**CE3**	**CE4**	**CE5**
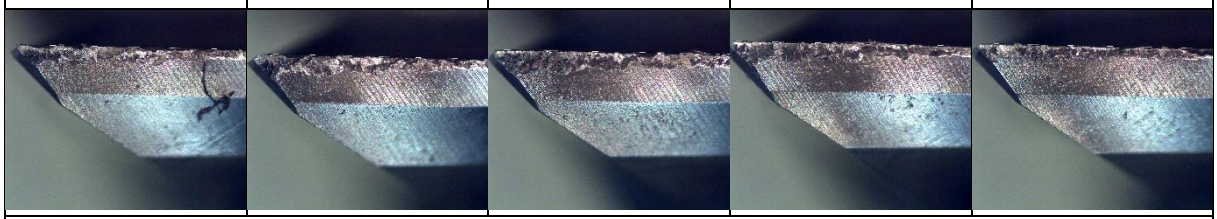				
INCO1 R 27 12				
CE1	**CE2**	**CE3**	**CE4**	**CE5**
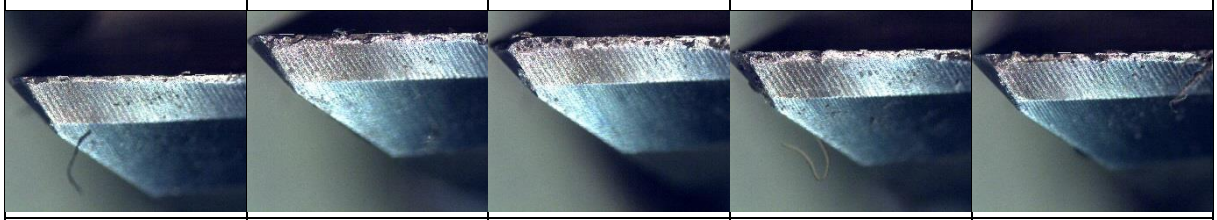				
CE1	**CE2**	**CE3**	**CE4**	**CE5**

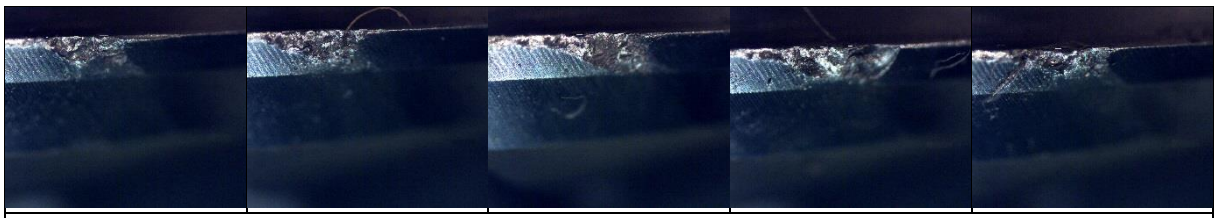				
INCO1 R 27 13				
CE1	**CE2**	**CE3**	**CE4**	**CE5**
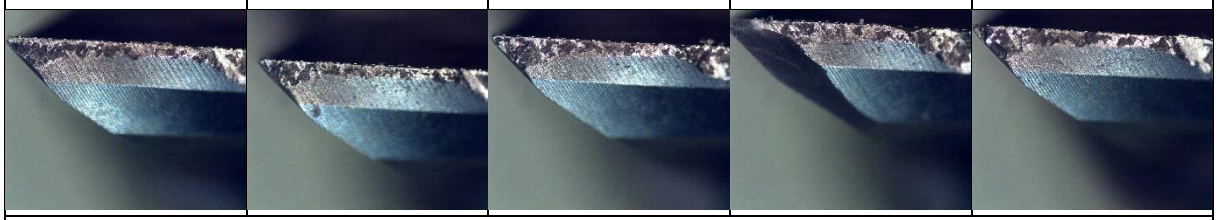				
INCO1 R 27 14				
CE1	**CE2**	**CE3**	**CE4**	**CE5**
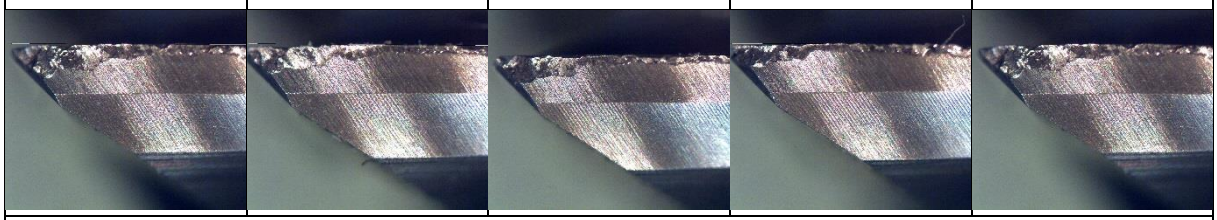				
INCO1 R 27 15				
CE1	**CE2**	**CE3**	**CE4**	**CE5**
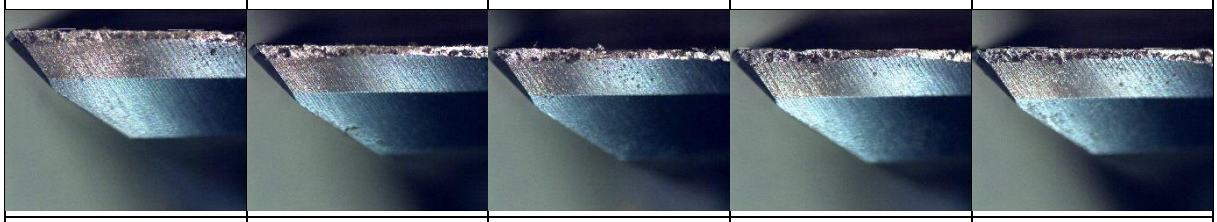				
CE1	**CE2**	**CE3**	**CE4**	**CE5**
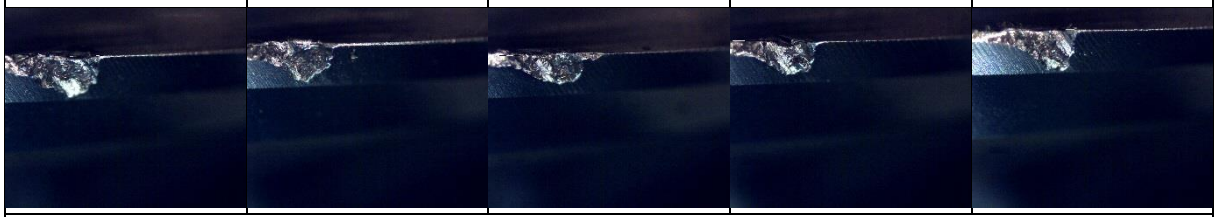				
INCO1 R 27 16				
CE1	**CE2**	**CE3**	**CE4**	**CE5**
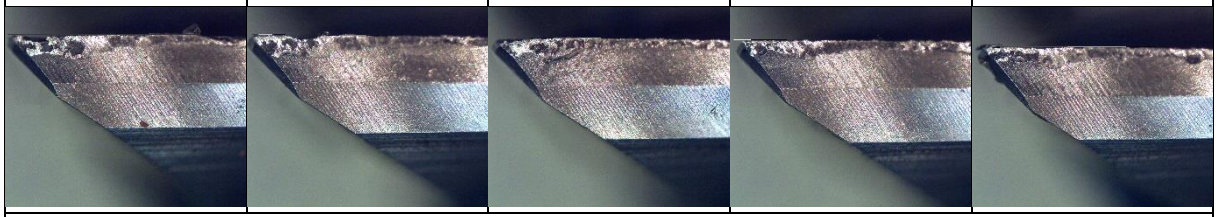				
INCO1 R 27 17				
CE1	**CE2**	**CE3**	**CE4**	**CE5**
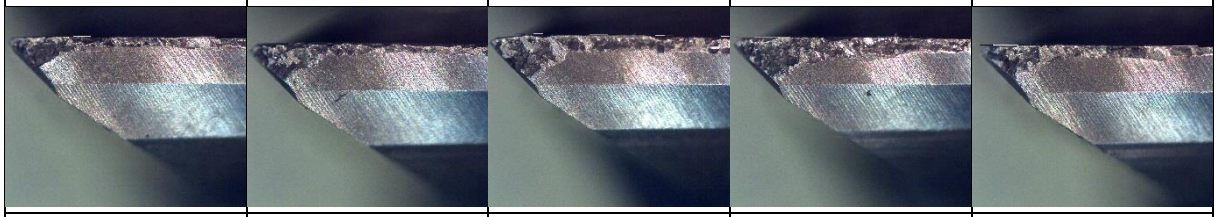				
CE1	**CE2**	**CE3**	**CE4**	**CE5**

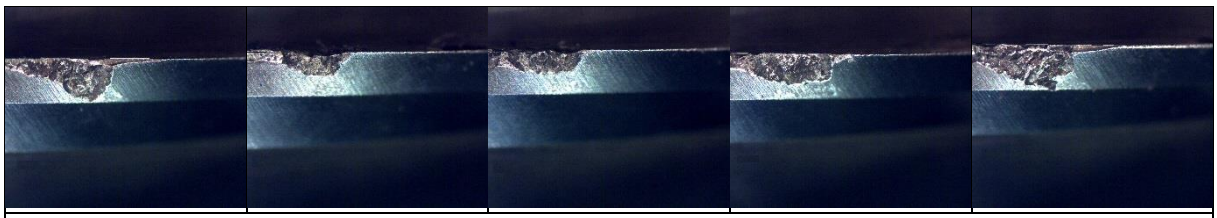				
INCO1 R 27 18				
CE1	**CE2**	**CE3**	**CE4**	**CE5**
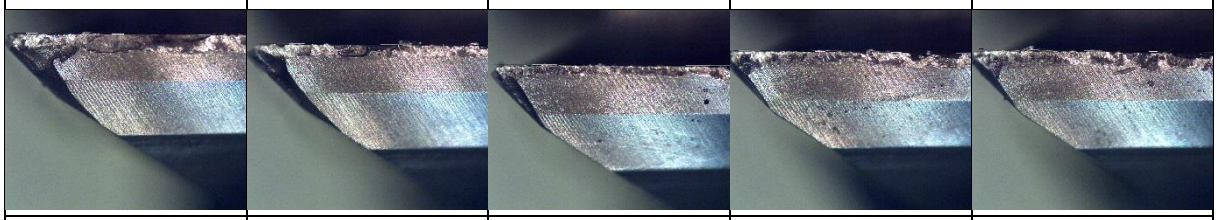				
CE1	**CE2**	**CE3**	**CE4**	**CE5**
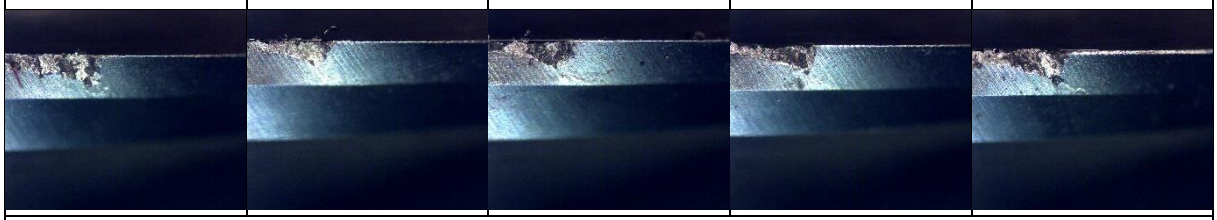				
INCO1 R 27 19				
CE1	**CE2**	**CE3**	**CE4**	**CE5**
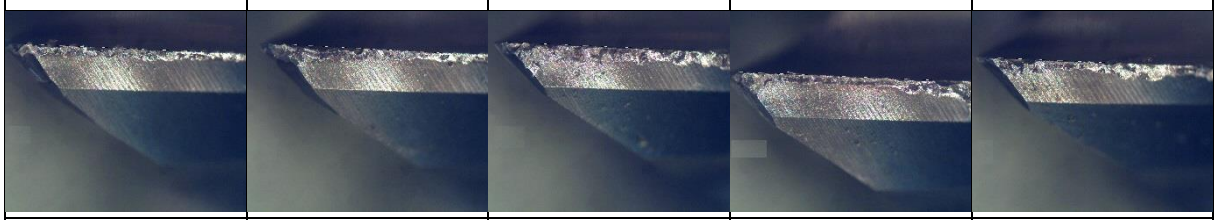				
CE1	**CE2**	**CE3**	**CE4**	**CE5**
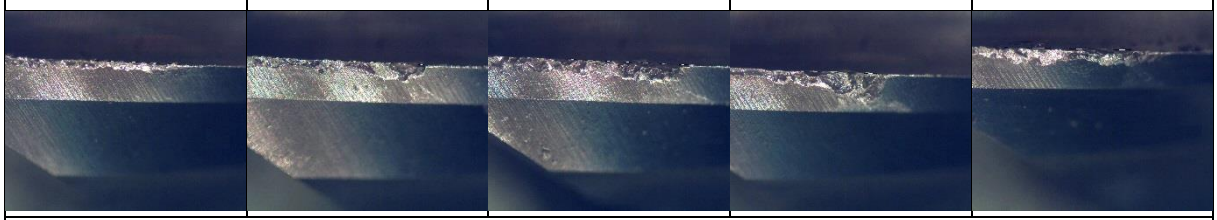				
INCO1 R 27 20				
CE1	**CE2**	**CE3**	**CE4**	**CE5**
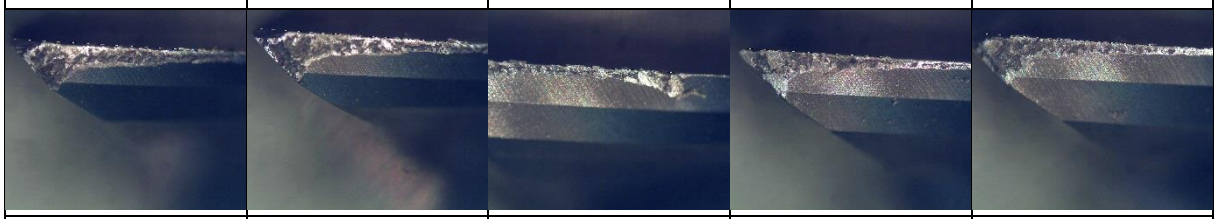				
CE1	**CE2**	**CE3**	**CE4**	**CE5**
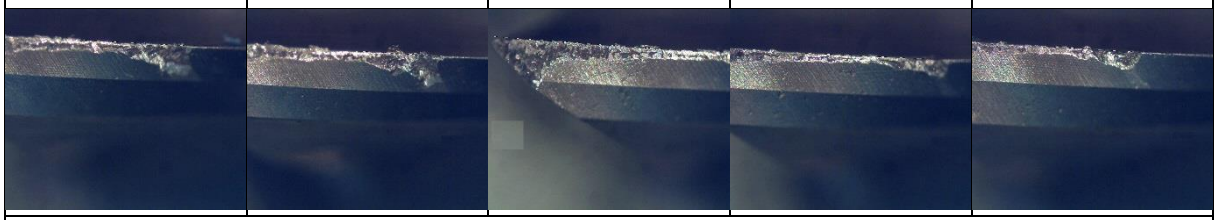				
INCO1 R 27 21				
CE1	**CE2**	**CE3**	**CE4**	**CE5**

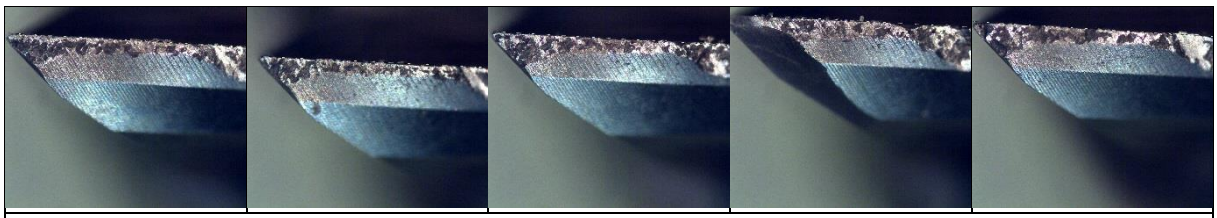				
INCO1 R 27 22				
CE1	**CE2**	**CE3**	**CE4**	**CE5**
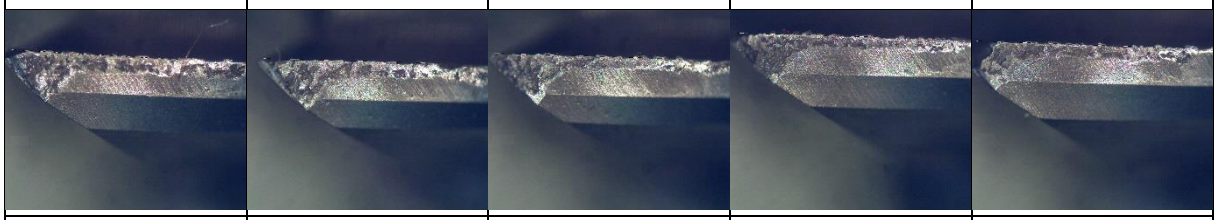				
CE1	**CE2**	**CE3**	**CE4**	**CE5**
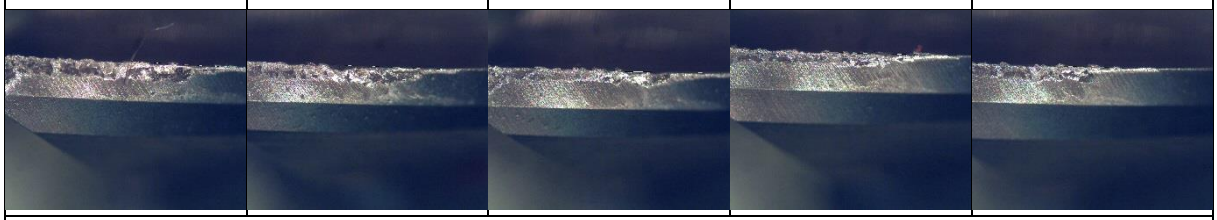				
INCO1 R 27 23				
CE1	**CE2**	**CE3**	**CE4**	**CE5**
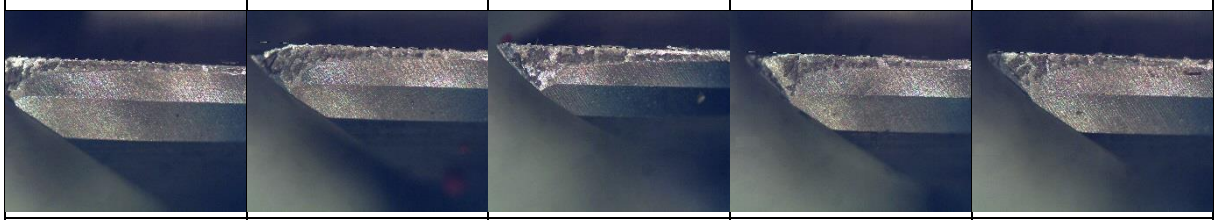				
CE1	**CE2**	**CE3**	**CE4**	**CE5**
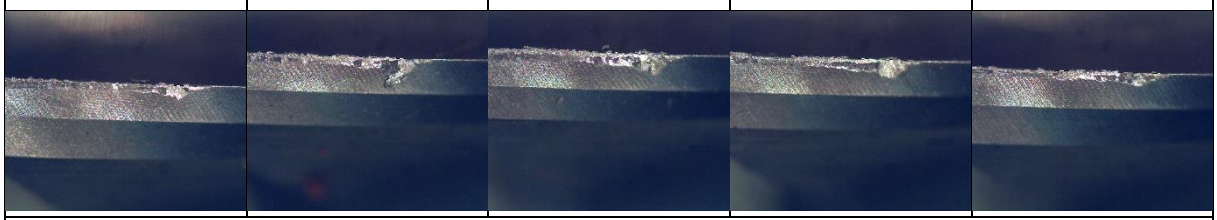				
INCO1 R 27 24				
CE1	**CE2**	**CE3**	**CE4**	**CE5**
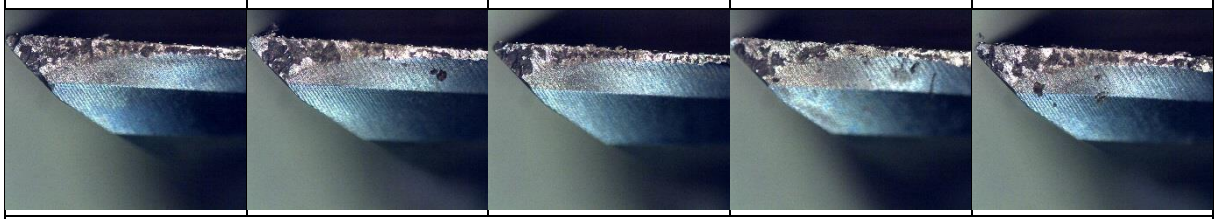				
INCO1 R 27 25				
CE1	**CE2**	**CE3**	**CE4**	**CE5**
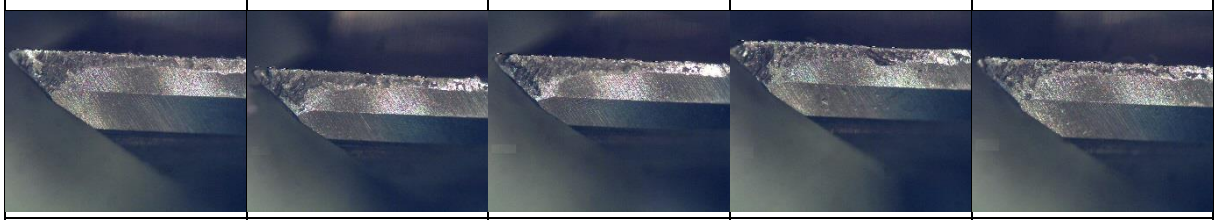				
CE1	**CE2**	**CE3**	**CE4**	**CE5**

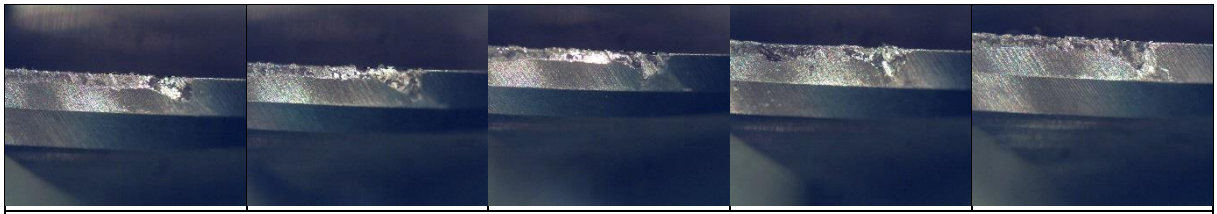

INCO1 R 27 26				
CE1	CE2	CE3	CE4	CE5

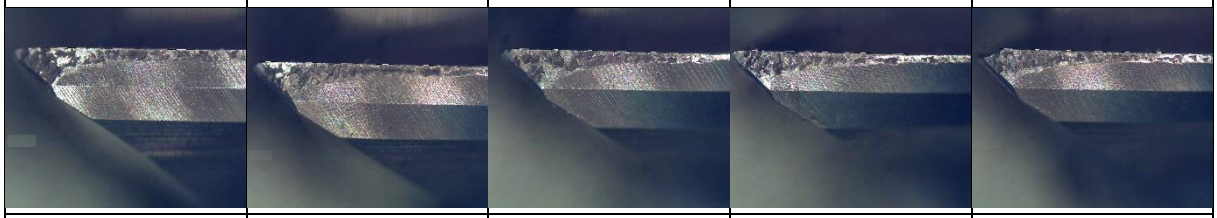

CE1	CE2	CE3	CE4	CE5

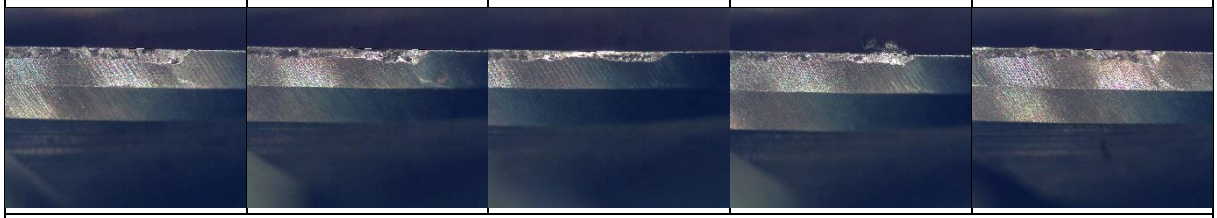

INCO1 R 27 27				
CE1	CE2	CE3	CE4	CE5

Scale bar (1 mm)

E4.Austenitic-ferritic Super Duplex 2507

SDX1 R 16 1			
CE1	CE2	CE3	CE4
			
SDX1 R 16 2			
CE1	CE2	CE3	CE4
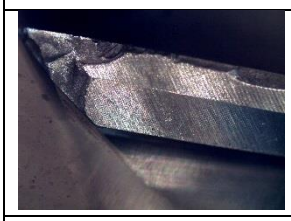	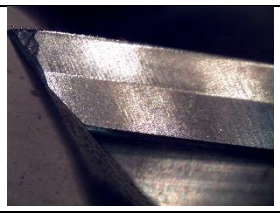	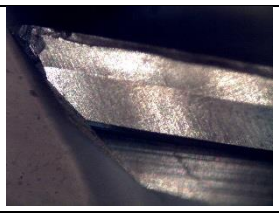	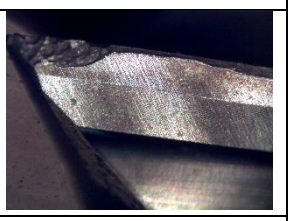
SDX1 R 16 3			
CE1	CE2	CE3	CE4
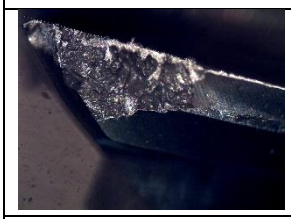		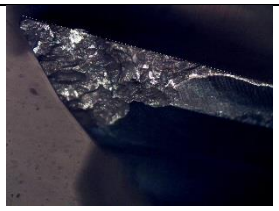	
SDX1 R 16 4			
CE1	CE2	CE3	CE4
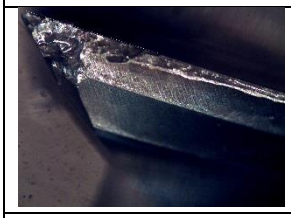		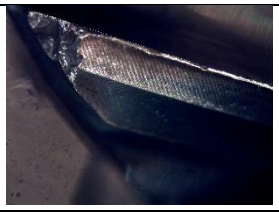	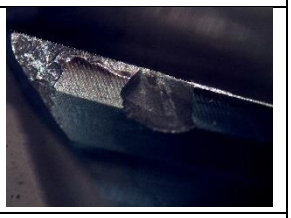
SDX1 R 16 5			
CE1	CE2	CE3	CE4
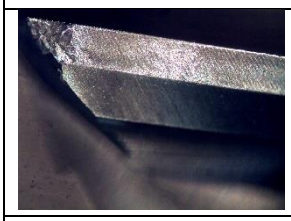			
SDX1 R 16 6			
CE1	CE2	CE3	CE4
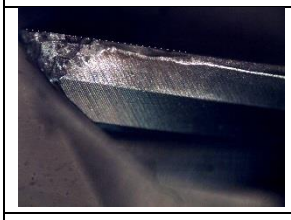	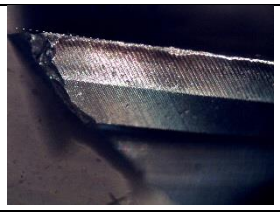		
SDX1 R 16 7			
CE1	CE2	CE3	CE4

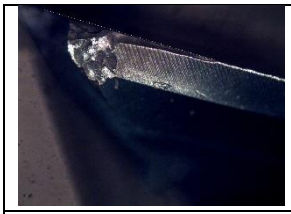	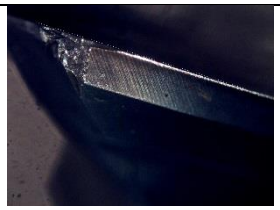		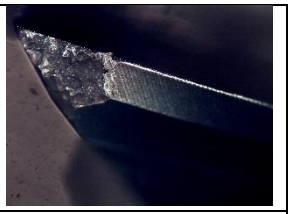
SDX1 R 16 8			
CE1	**CE2**	**CE3**	**CE4**
	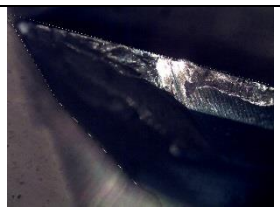	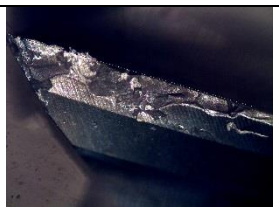	
SDX1 R 16 9			
CE1	**CE2**	**CE3**	**CE4**
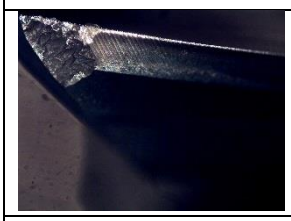		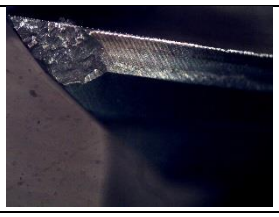	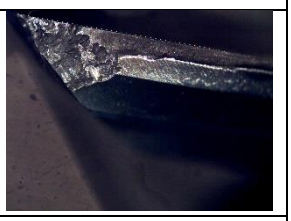
SDX1 R 16 10			
CE1	**CE2**	**CE3**	**CE4**
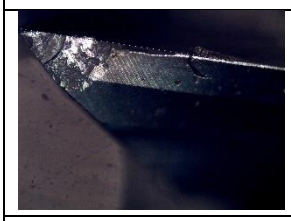	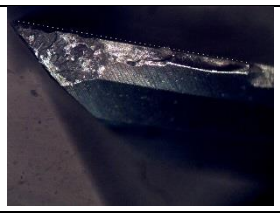	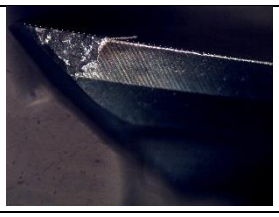	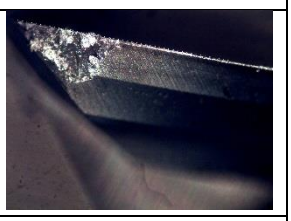
SDX1 R 16 11			
CE1	**CE2**	**CE3**	**CE4**
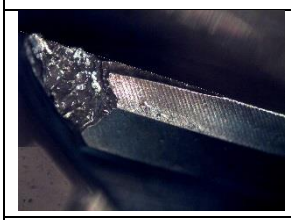		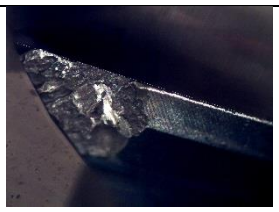	
SDX1 R 16 12			
CE1	**CE2**	**CE3**	**CE4**
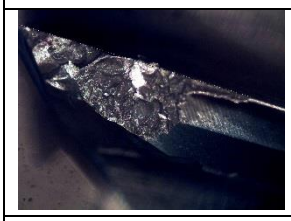		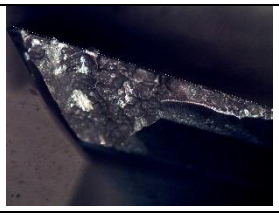	
SDX1 R 16 13			
CE1	**CE2**	**CE3**	**CE4**

		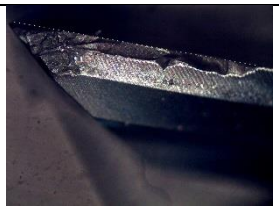	
SDX1 R 16 14			
CE1	**CE2**	**CE3**	**CE4**
	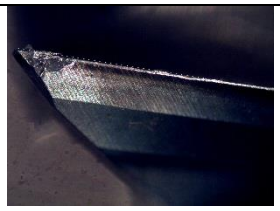	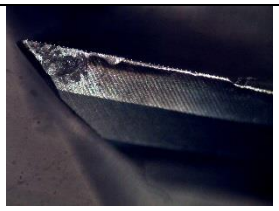	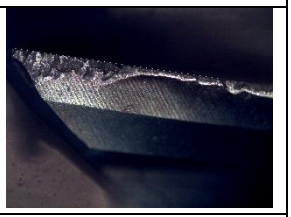
SDX1 R 16 15			
CE1	**CE2**	**CE3**	**CE4**
		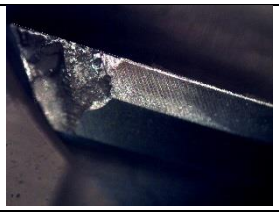	
SDX1 R 16 16			
CE1	**CE2**	**CE3**	**CE4**
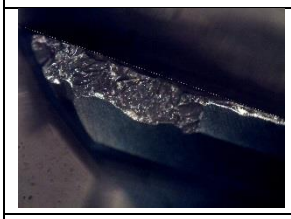			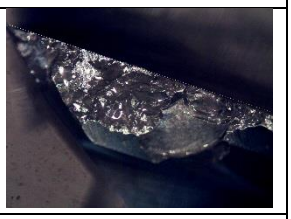
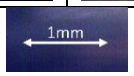			
Scale bar (1 mm)			

E5.Aluminium 6082-T6

AL1 D SFL 9 1	
CE1	CE2
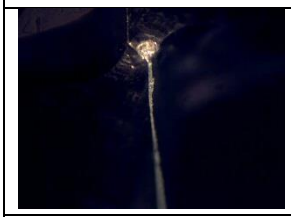	

AL1 D SFL 9 2	
CE1	CE2
	

AL1 D SFL 9 3	
CE1	CE2
	

AL1 D SFL 9 4	
CE1	CE2
	

AL1 D SFL 9 5	
CE1	CE2
	

AL1 D SFL 9 6	
CE1	CE2
	

AL1 D SFL 9 7	
CE1	CE2
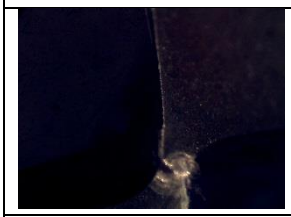	

AL1 D SFL 9 8	
CE1	CE2
	

AL1 D SFL 9 9	
CE1	CE2
	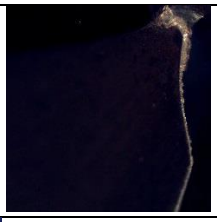
	
Scale bar (0.5 mm)	

AL1 D 3FL 4 1			
CE1	CE2	CE3	Drill Point
			
AL1 D 3FL 4 2			
CE1	CE2	CE3	Drill Point
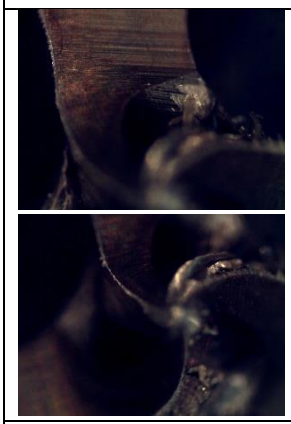			
AL1 D 3FL 4 3			
CE1	CE2	CE3	Drill Point
			
AL1 D 3FL 4 4			
CE1	CE2	CE3	Drill Point

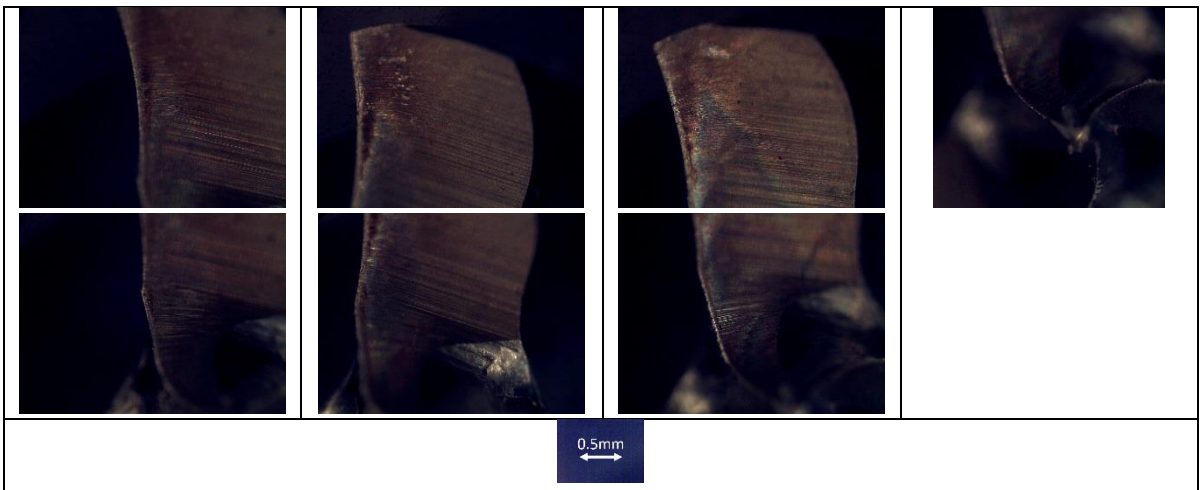

Scale bar (0.5 mm)

E6.Titanium Ti-6Al-4V

Ti1 D 2FL 8 1			Ti1 D 2FL 8 1 – Replicate		
CE1	**CE2**	**Drill Point**	**CE1**	**CE2**	**Drill Point**
					
					
Ti1 D 2FL 8 2			**Ti1 D 2FL 8 2 – Replicate**		
CE1	**CE2**	**Drill Point**	**CE1**	**CE2**	**Drill Point**
					
					
Ti1 D 2FL 8 3			**Ti1 D 2FL 8 3 – Replicate**		

CE1	CE2	Drill Point	CE1	CE2	Drill Point
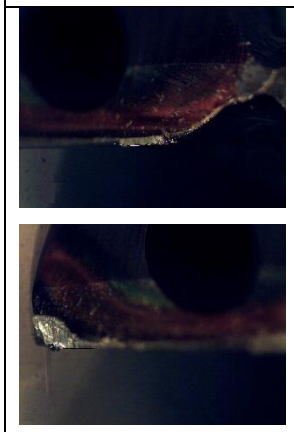					
Ti1 D 2FL 8 4			**Ti1 D 2FL 8 4 – Replicate**		
CE1	**CE2**	**Drill Point**	**CE1**	**CE2**	**Drill Point**
		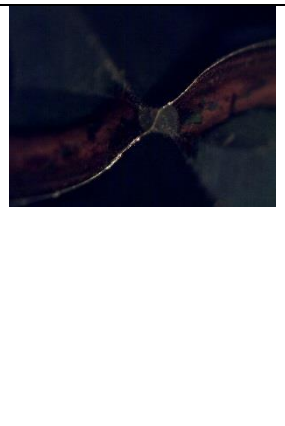			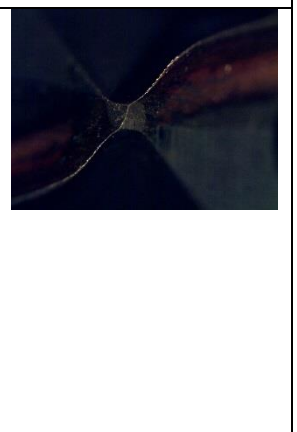
Ti1 D 2FL 8 5			**Ti1 D 2FL 8 5 – Replicate**		
CE1	**CE2**	**Drill Point**	**CE1**	**CE2**	**Drill Point**

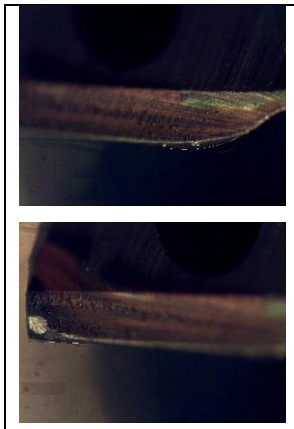		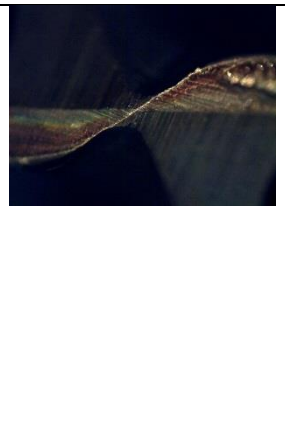	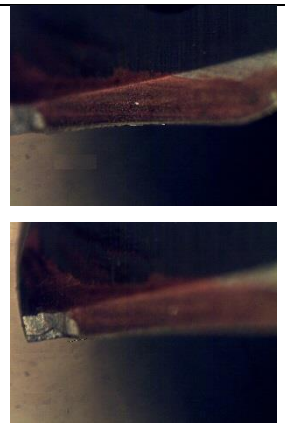	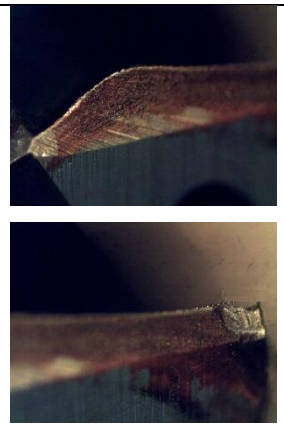	
Ti1 D 2FL 8 6			**Ti1 D 2FL 8 6 – Replicate**		
CE1	**CE2**	**Drill Point**	**CE1**	**CE2**	**Drill Point**
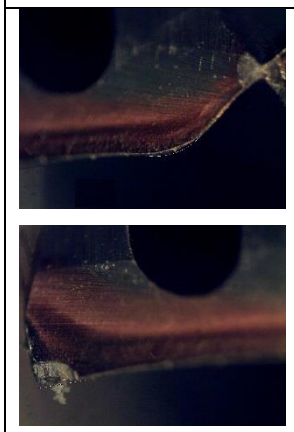	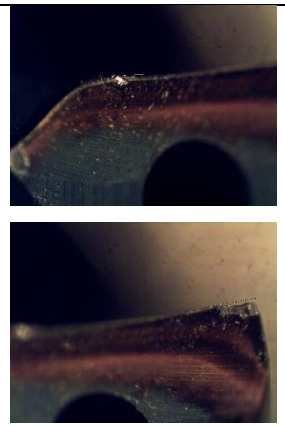				
Ti1 D 2FL 8 7			**Ti1 D 2FL 8 7 – Replicate**		
CE1	**CE2**	**Drill Point**	**CE1**	**CE2**	**Drill Point**

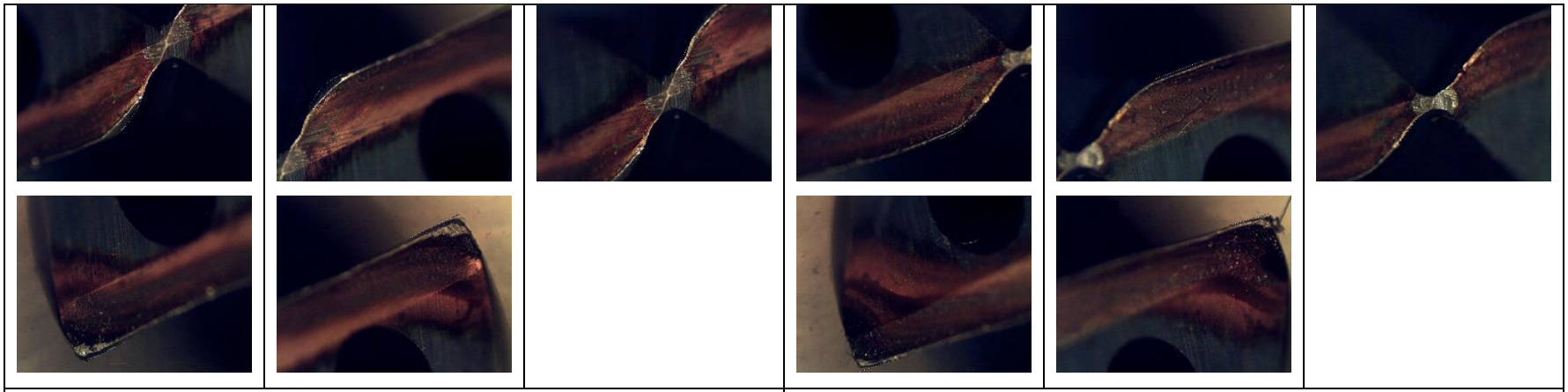

Ti1 D 2FL 8 8			Ti1 D 2FL 8 8 – Replicate		
CE1	**CE2**	**Drill Point**	**CE1**	**CE2**	**Drill Point**

Scale bar (0.5 mm)

E7.Inconel alloy 718

INCO1 D 2FL 16 1			INCO1 D 2FL 16 2		
CE1	**CE2**	**Drill Point**	**CE1**	**CE2**	**Drill Point**
	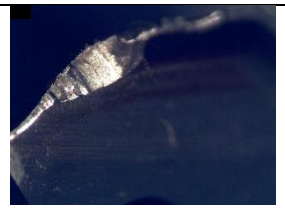	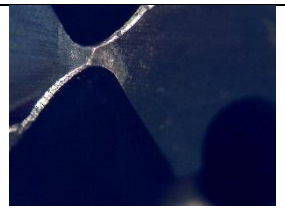		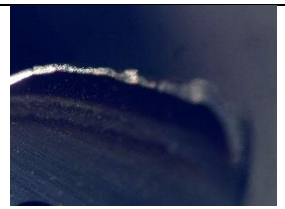	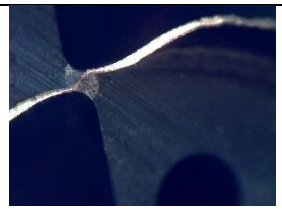
	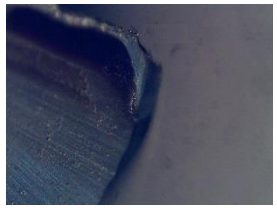		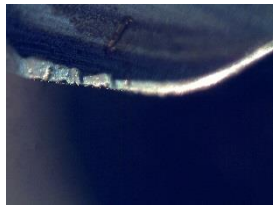		
INCO1 D 2FL 16 3			**INCO1 D 2FL 16 4**		
CE1	**CE2**	**Drill Point**	**CE1**	**CE2**	**Drill Point**
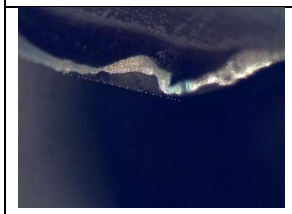	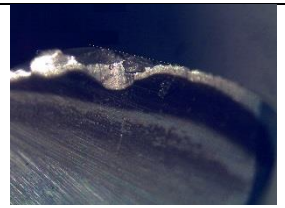	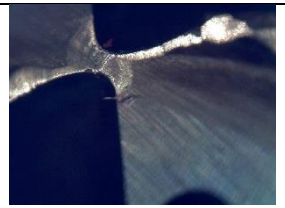	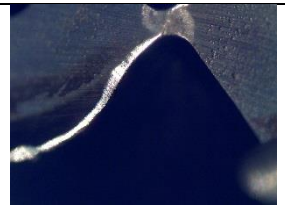	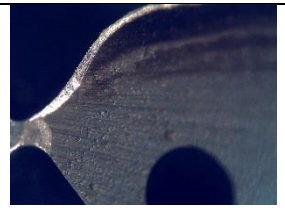	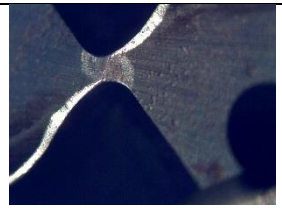
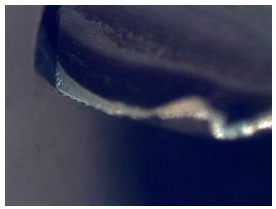	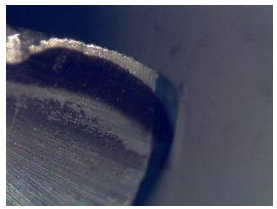		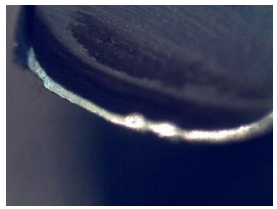	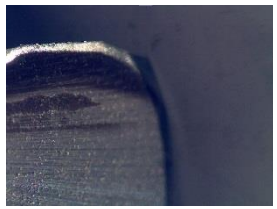	
INCO1 D 2FL 16 5			**INCO1 D 2FL 16 6**		

CE1	CE2	Drill Point	CE1	CE2	Drill Point
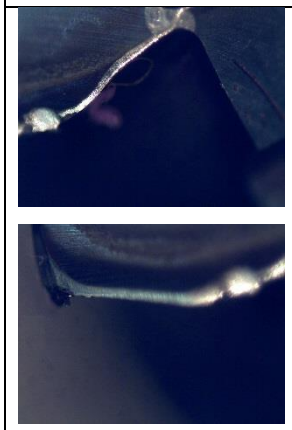	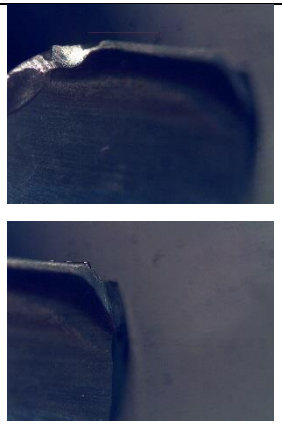		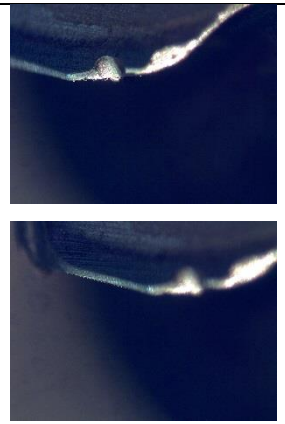	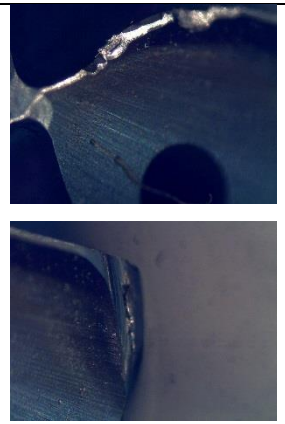	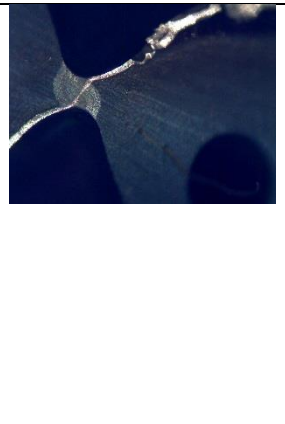
INCO1 D 2FL 16 7			INCO1 D 2FL 16 8		
CE1	CE2	Drill Point	CE1	CE2	Drill Point
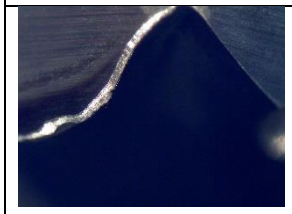	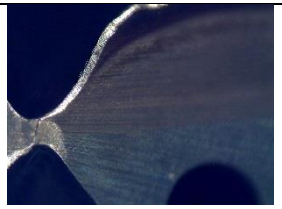	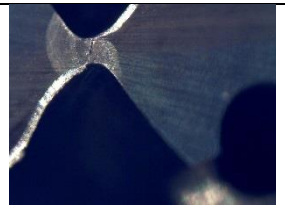		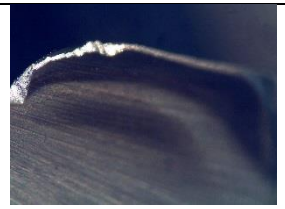	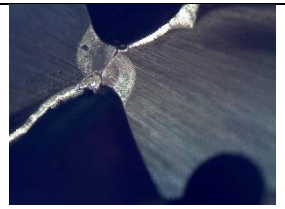
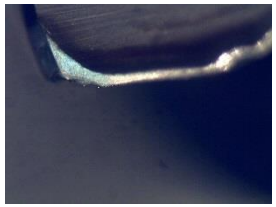	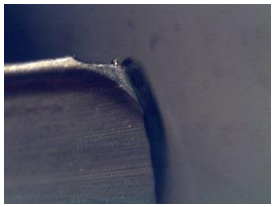		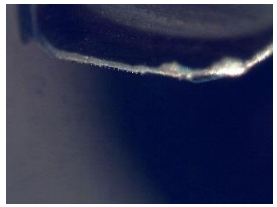		
INCO1 D 2FL 16 9			INCO1 D 2FL 16 10		
CE1	CE2	Drill Point	CE1	CE2	Drill Point

	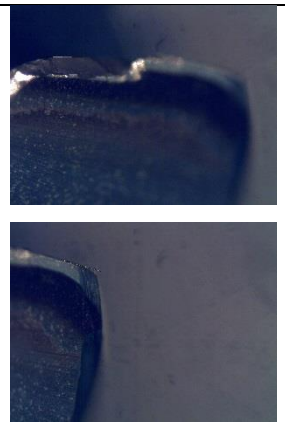		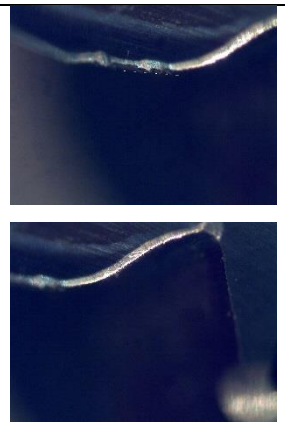		
INCO1 D 2FL 16 11			**INCO1 D 2FL 16 12**		
CE1	**CE2**	**Drill Point**	**CE1**	**CE2**	**Drill Point**
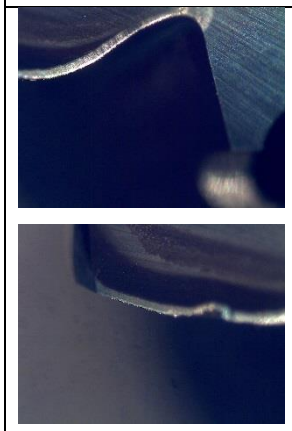	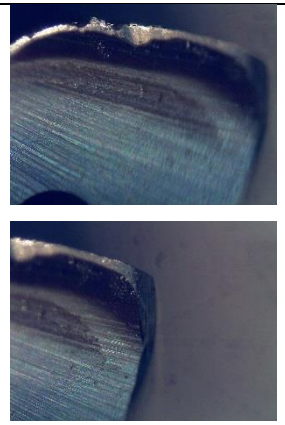		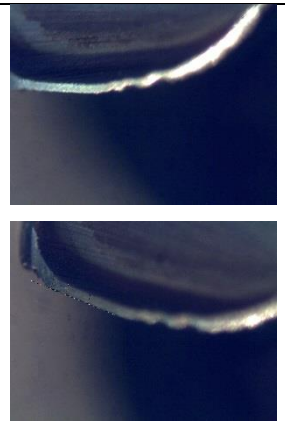	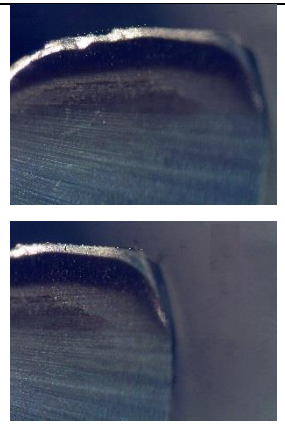	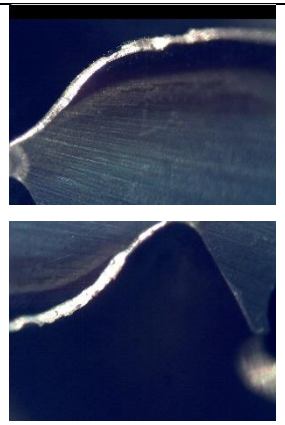
INCO1 D 2FL 16 13			**INCO1 D 2FL 16 14**		
CE1	**CE2**	**Drill Point**	**CE1**	**CE2**	**Drill Point**

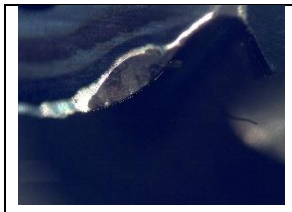
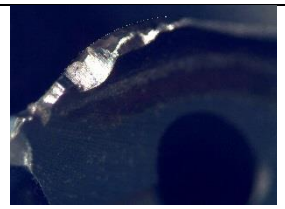
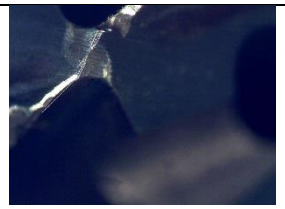
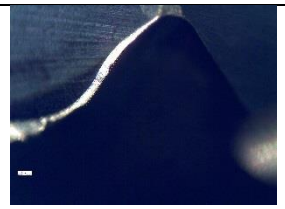
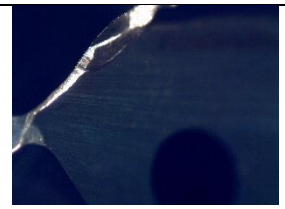

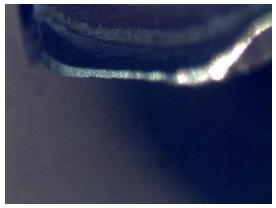

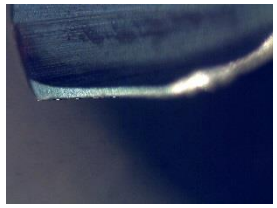
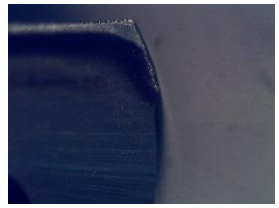

INCO1 D 2FL 16 15			INCO1 D 2FL 16 16		
CE1	CE2	Drill Point	CE1	CE2	Drill Point

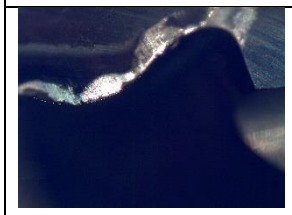
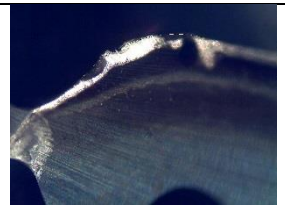
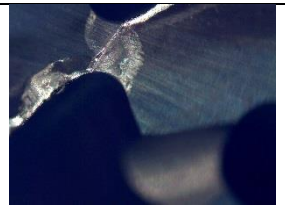

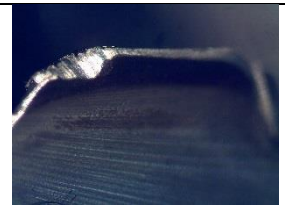
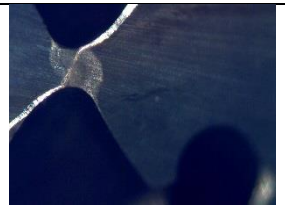
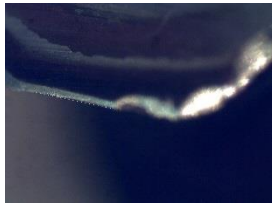
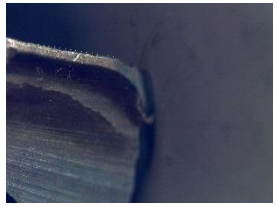
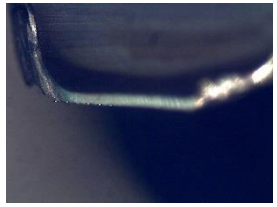
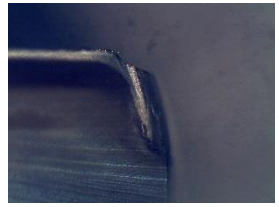

Scale bar (0.5 mm)

E8.Austenitic-ferritic Super Duplex 2507

SDX1 D 2FL 8 1			SDX1 D 2FL 8 2		
CE1	**CE2**	**Drill Point**	**CE1**	**CE2**	**Drill Point**
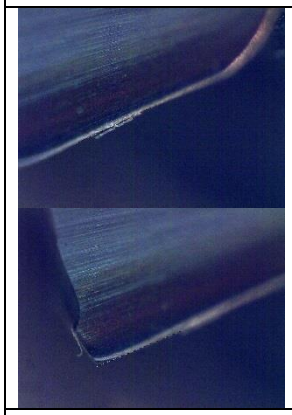	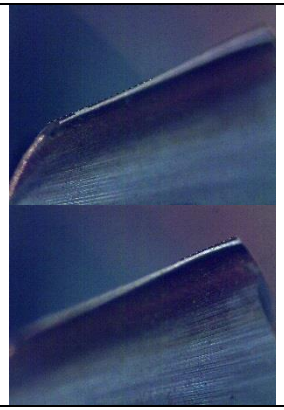	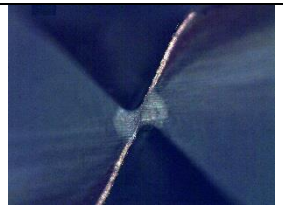	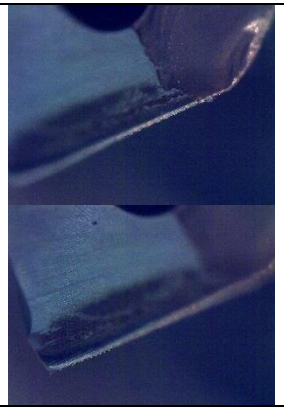	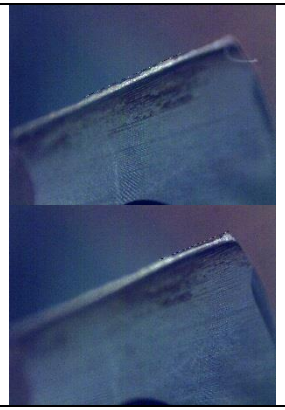	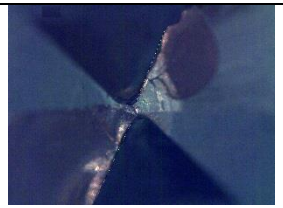
SDX1 D 2FL 8 3			**SDX1 D 2FL 8 4**		
CE1	**CE2**	**Drill Point**	**CE1**	**CE2**	**Drill Point**
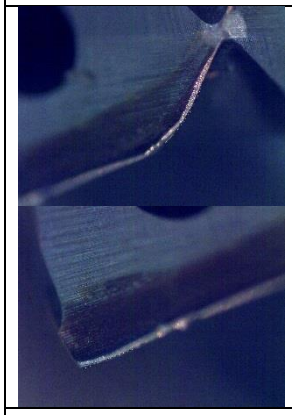	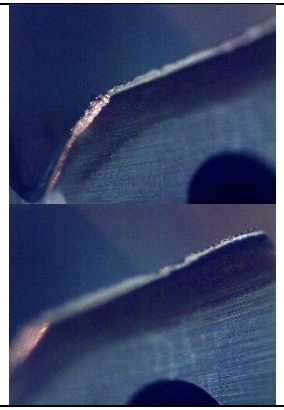	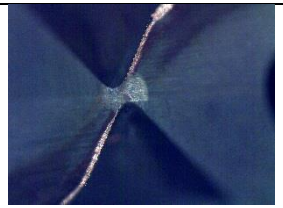	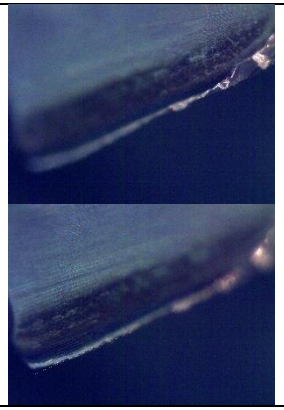	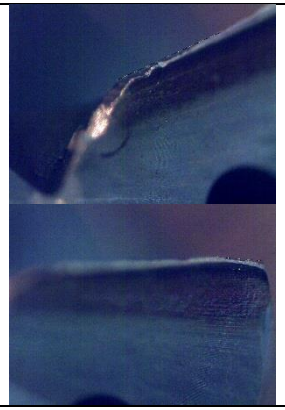	
SDX1 D 2FL 8 5			**SDX1 D 2FL 8 6**		
CE1	**CE2**	**Drill Point**	**CE1**	**CE2**	**Drill Point**

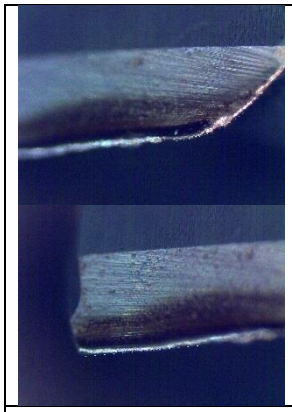
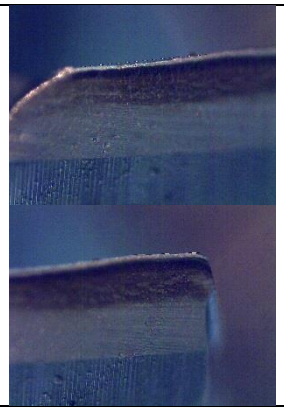
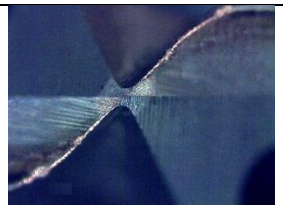
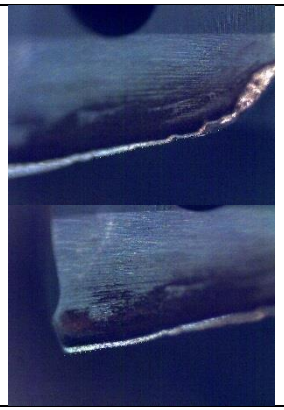
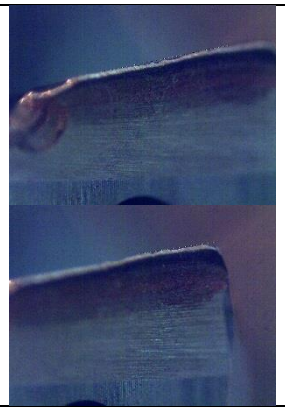
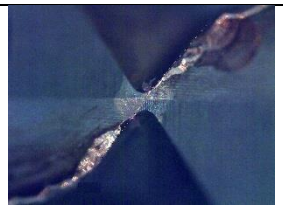

SDX1 D 2FL 8 7			SDX1 D 2FL 8 8		
CE1	CE2	Drill Point	CE1	CE2	Drill Point

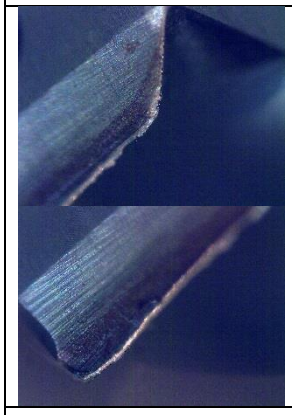
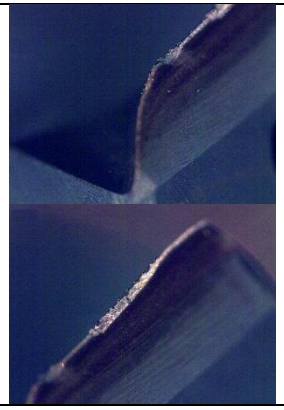

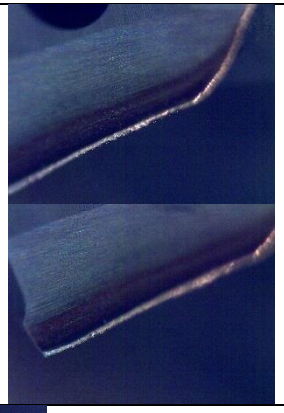
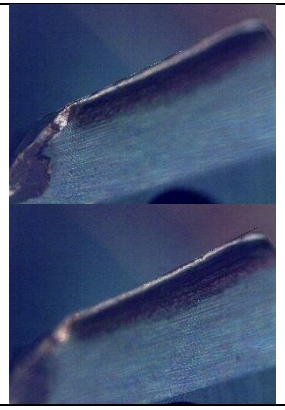
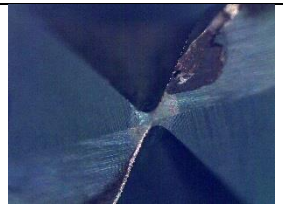

Scale bar (0.5 mm)

Appendix F: Tool Life

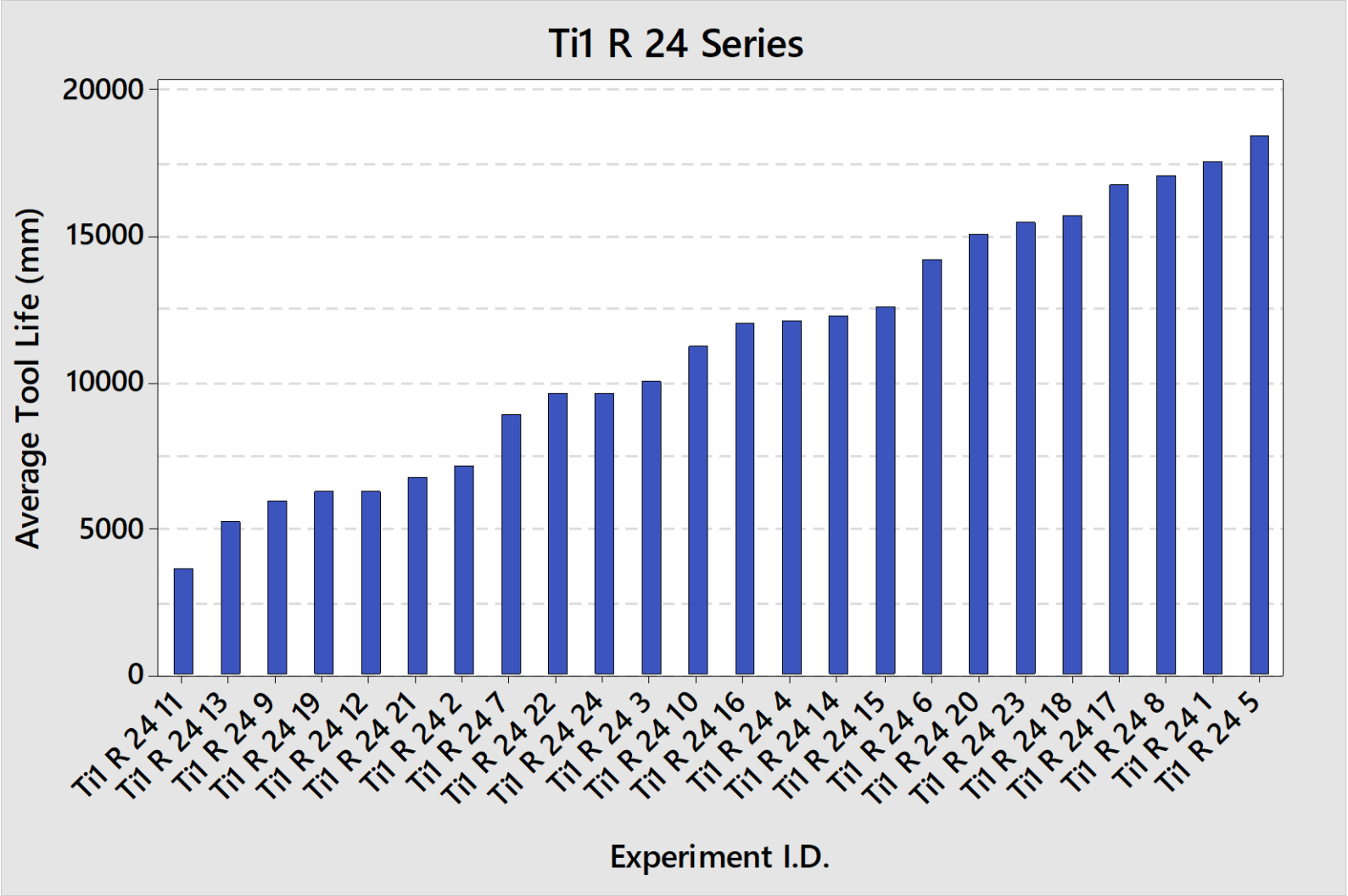

Fig. 146: Tool life results from end-milling experiments using 4-flute end-mills designed for Ti-6Al-4V

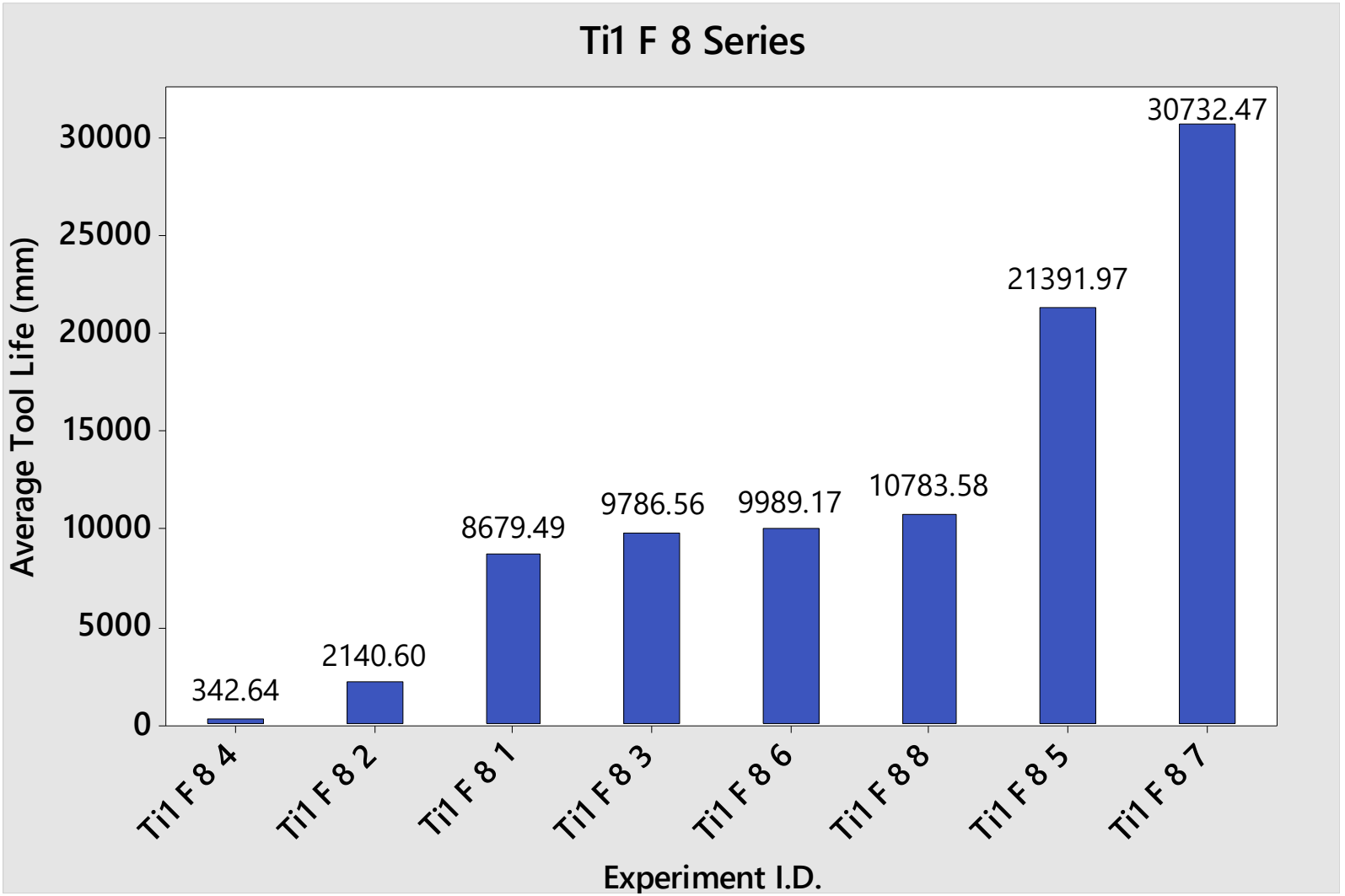

Fig. 147: Tool life results from end-milling experiments using 6-flute end-mills designed for Ti-6Al-4V

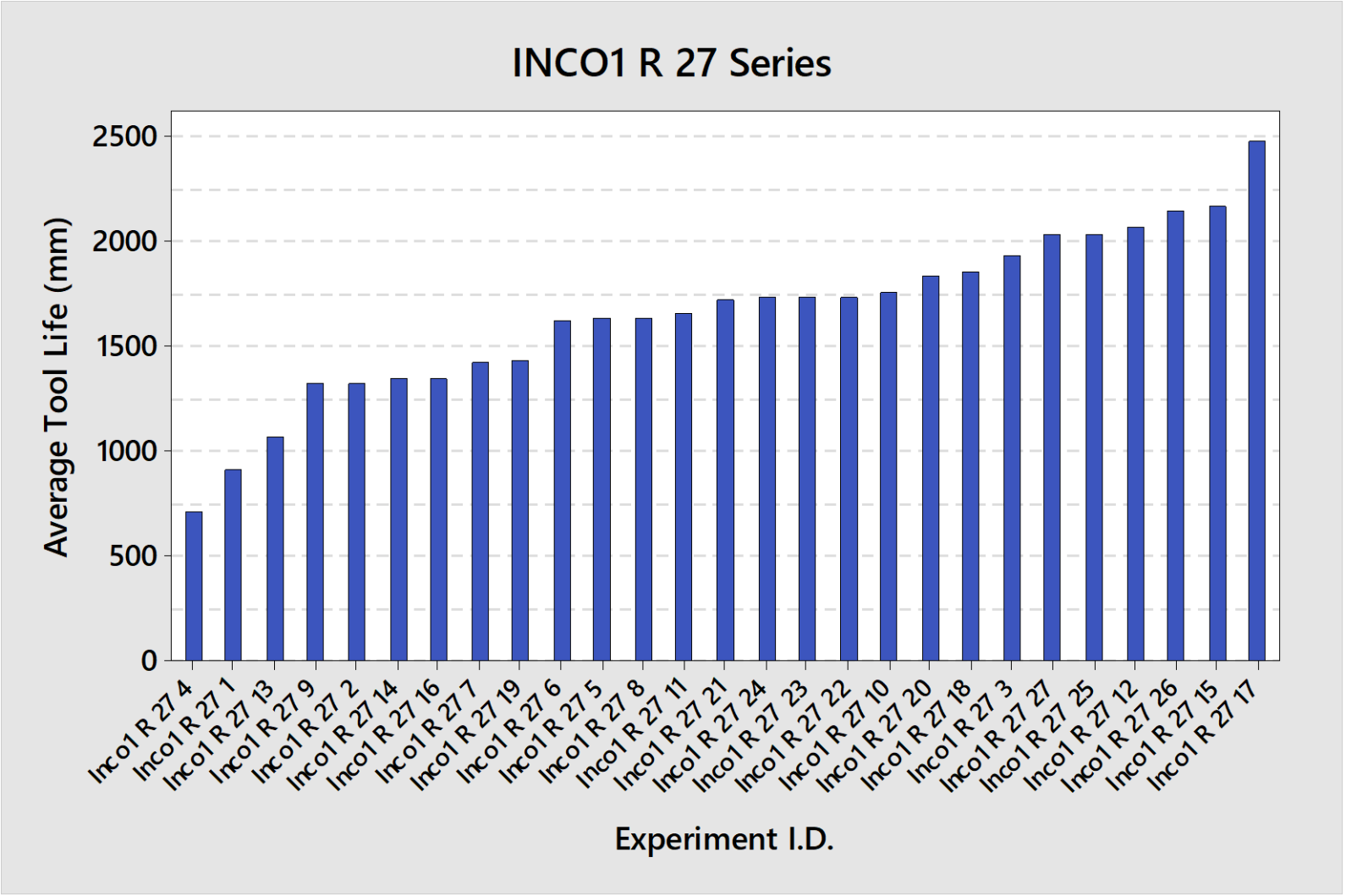

Fig. 148: Tool life results from end-milling experiments using 5-flute end-mills designed for Inconel 718

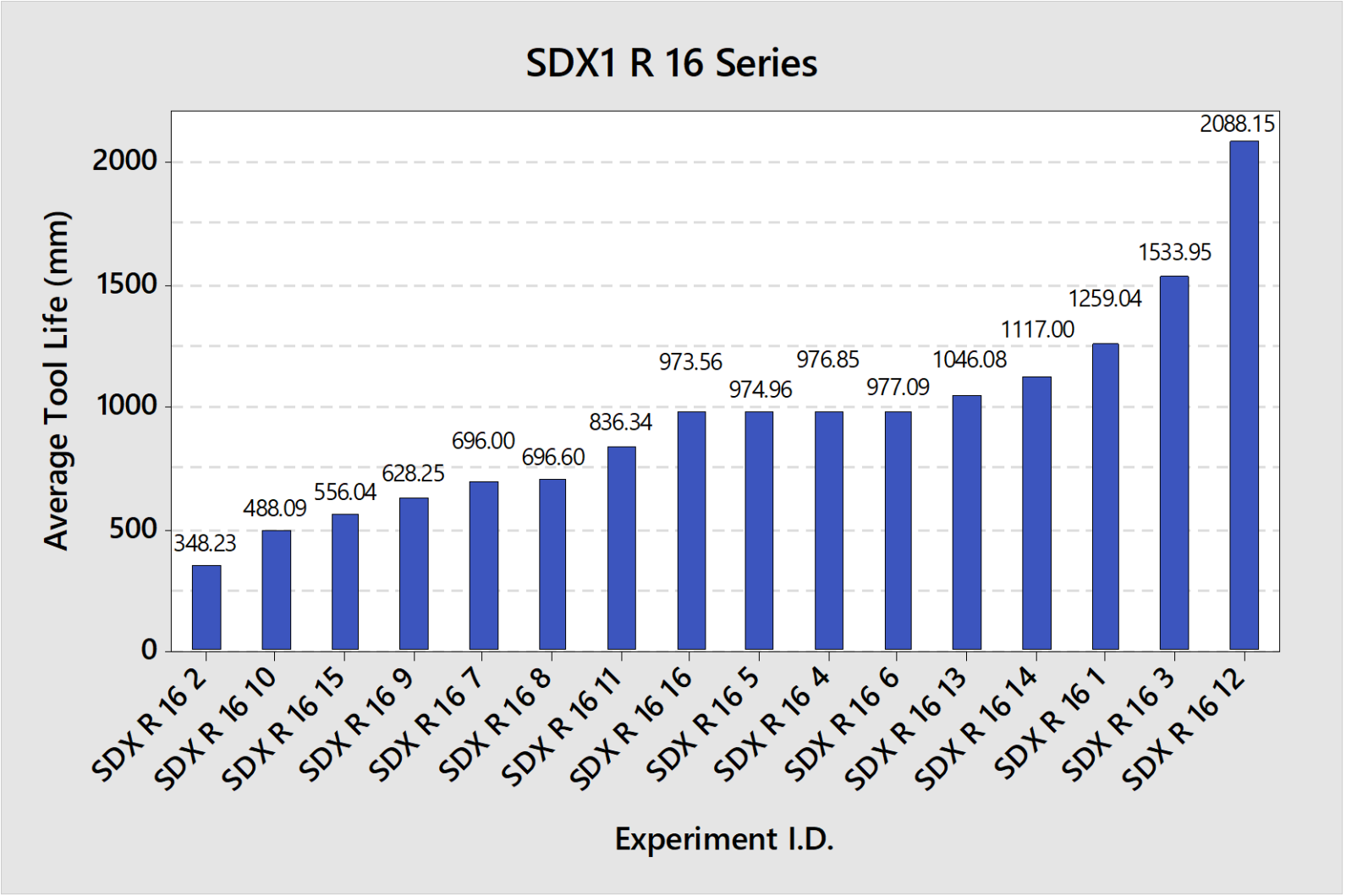

Fig. 149: Tool life results from end-milling experiments using 4-flute end-mills designed for Super Duplex 2507

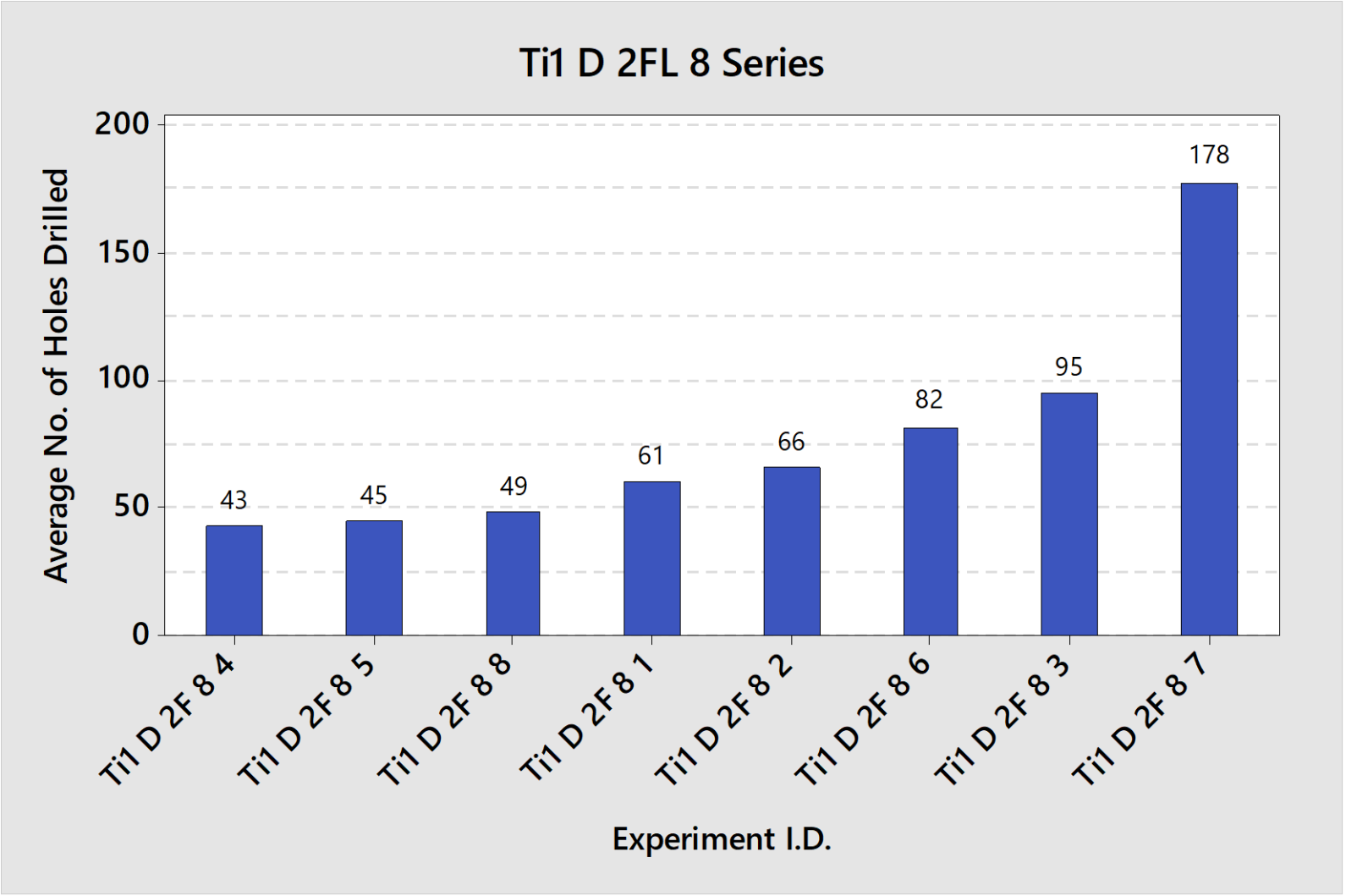

Fig. 150: Number of holes obtained from each experiment in drilling of Ti-6Al-4V

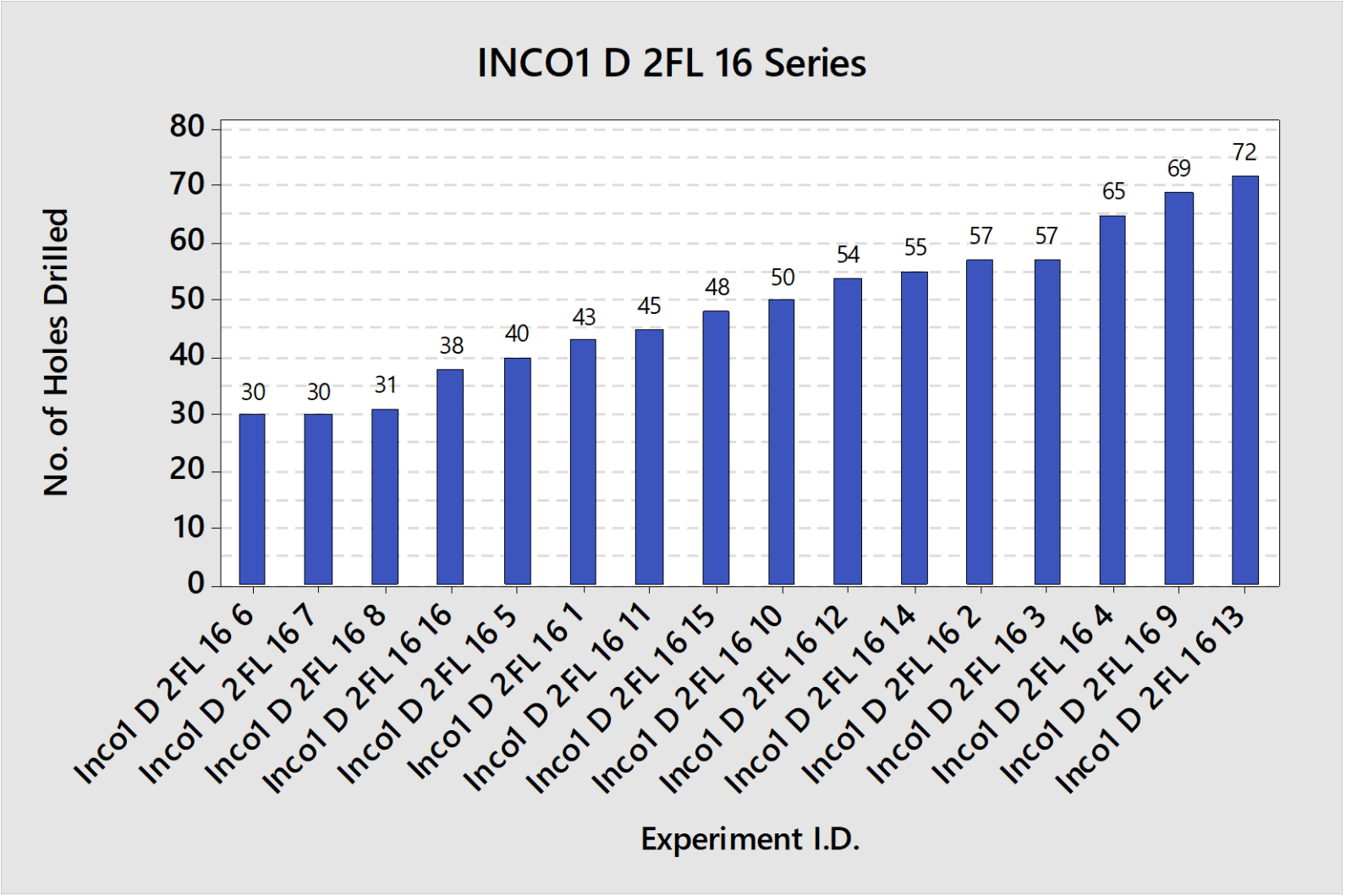

Fig. 151: Number of holes obtained from each experiment in drilling of Inconel 718

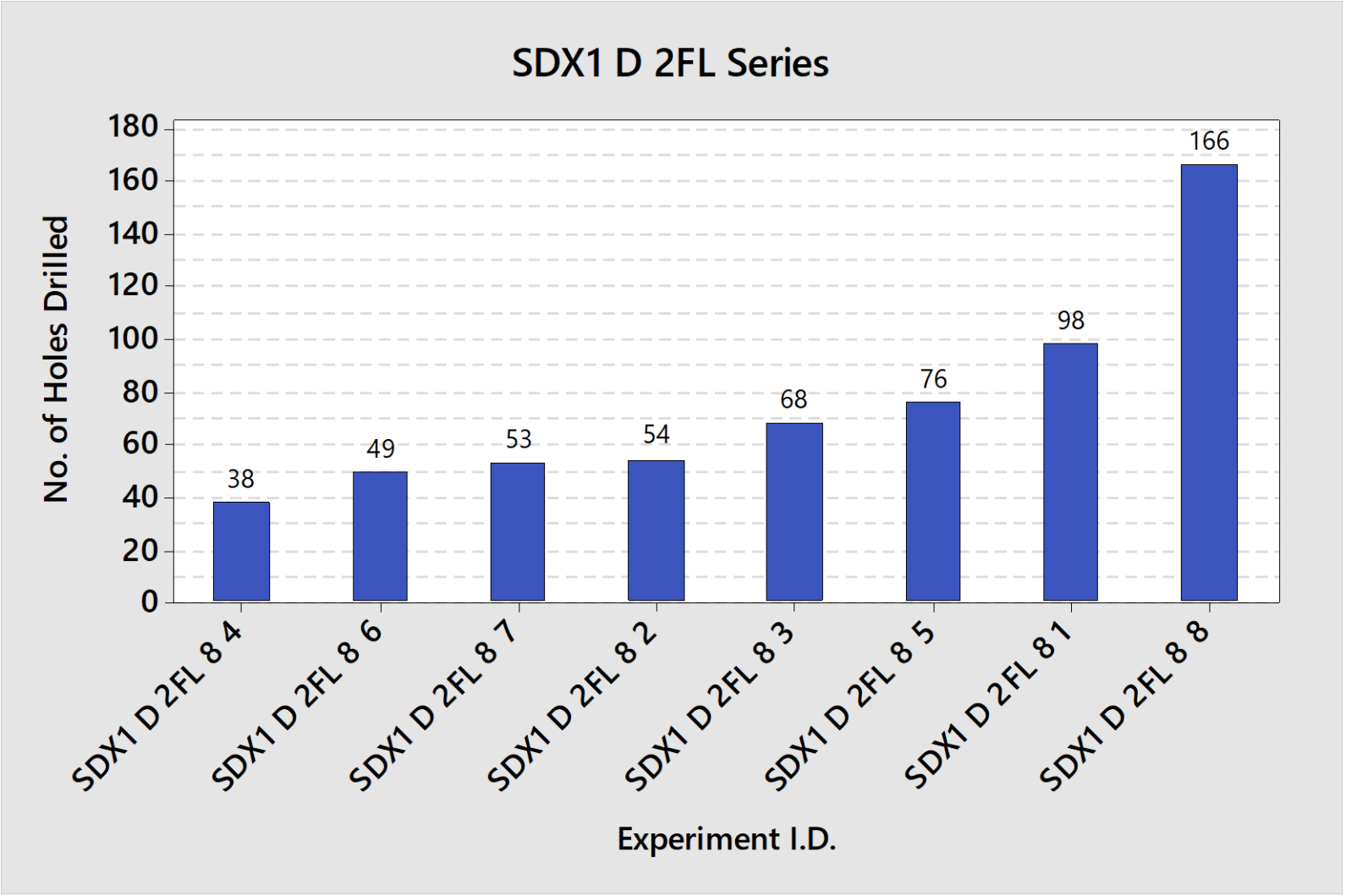

Fig. 152: Number of holes obtained from each experiment in drilling of super duplex 2507

Appendix G: Surface Roughness, Pareto ANOVAs and Main Effect Plots

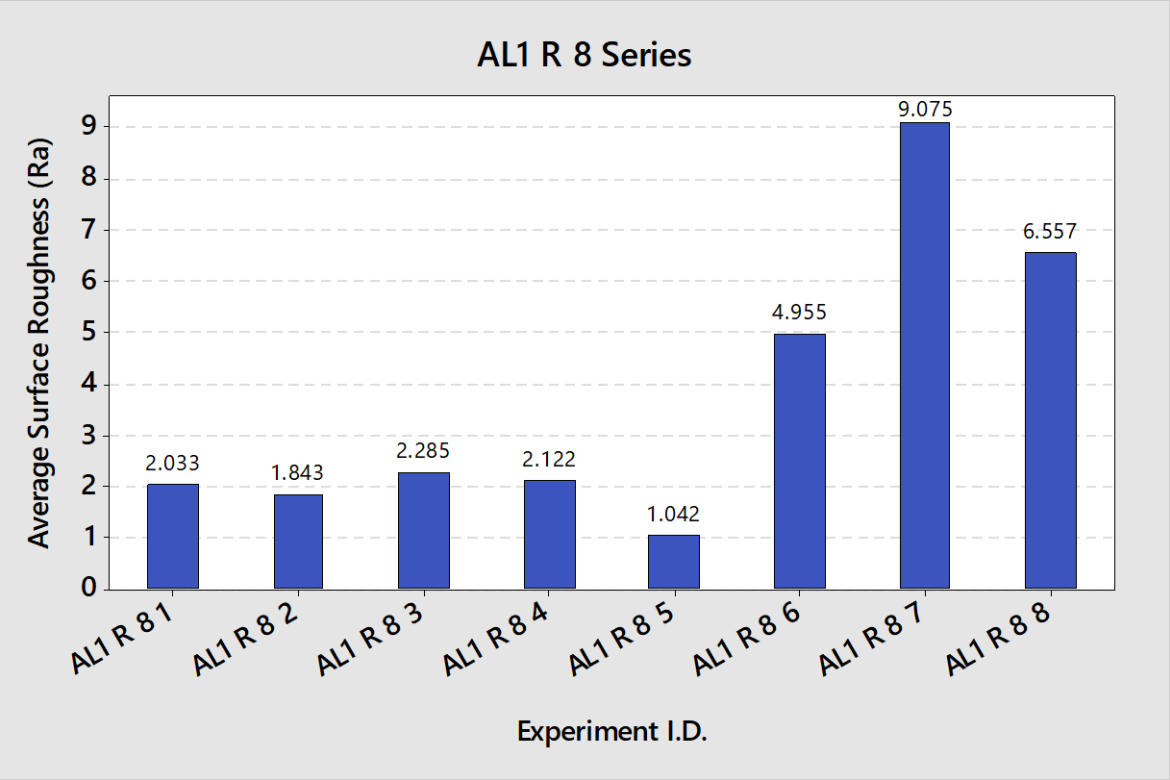

Fig. 153: Surface roughness results obtained from end-milling experiments on 6082-T6

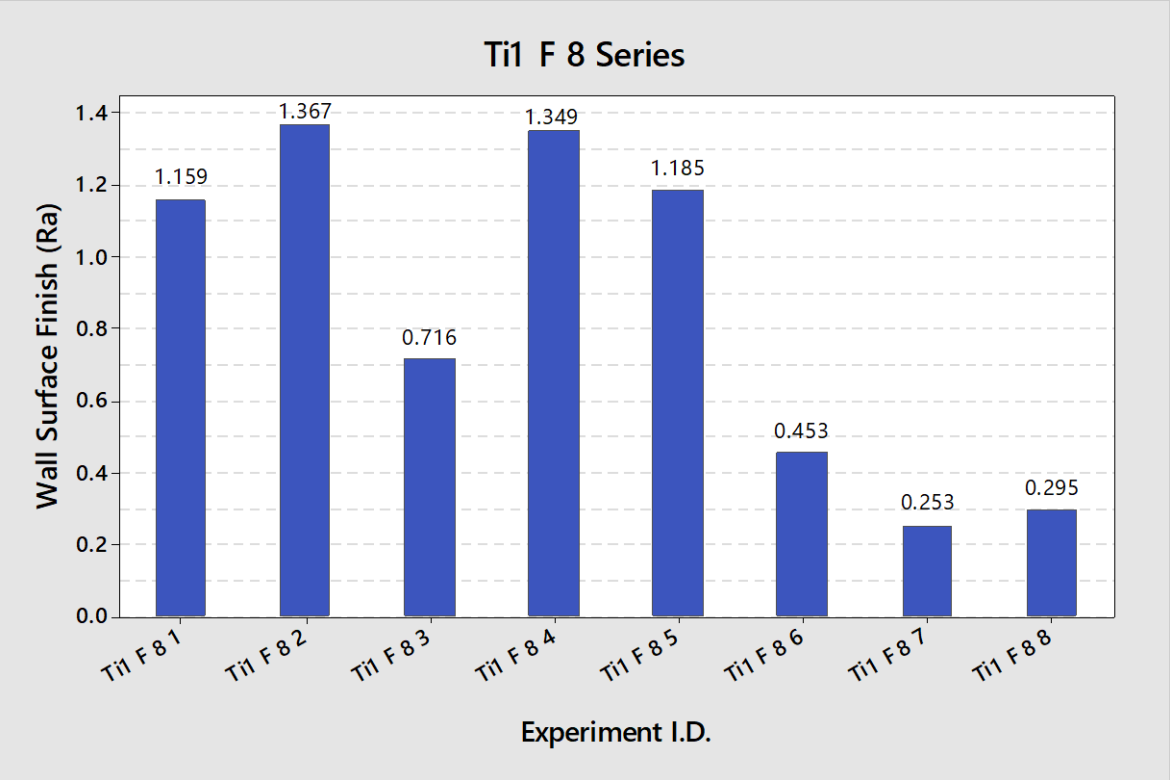

Fig. 154: Wall surface roughness results obtained from end-milling experiments on Ti-6Al-4V using 6-flute end-mills

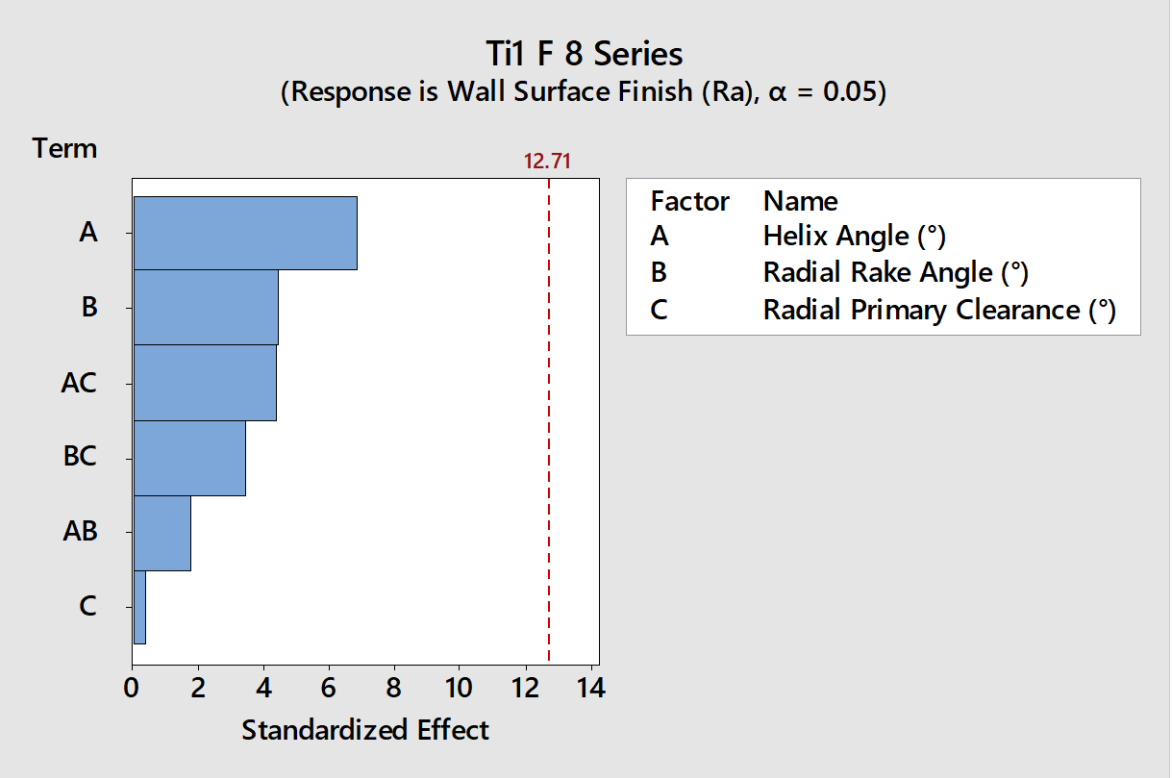

Fig. 155: Pareto ANOVA of geometrical parameters in end-milling Ti-6Al-4V based on wall surface finish

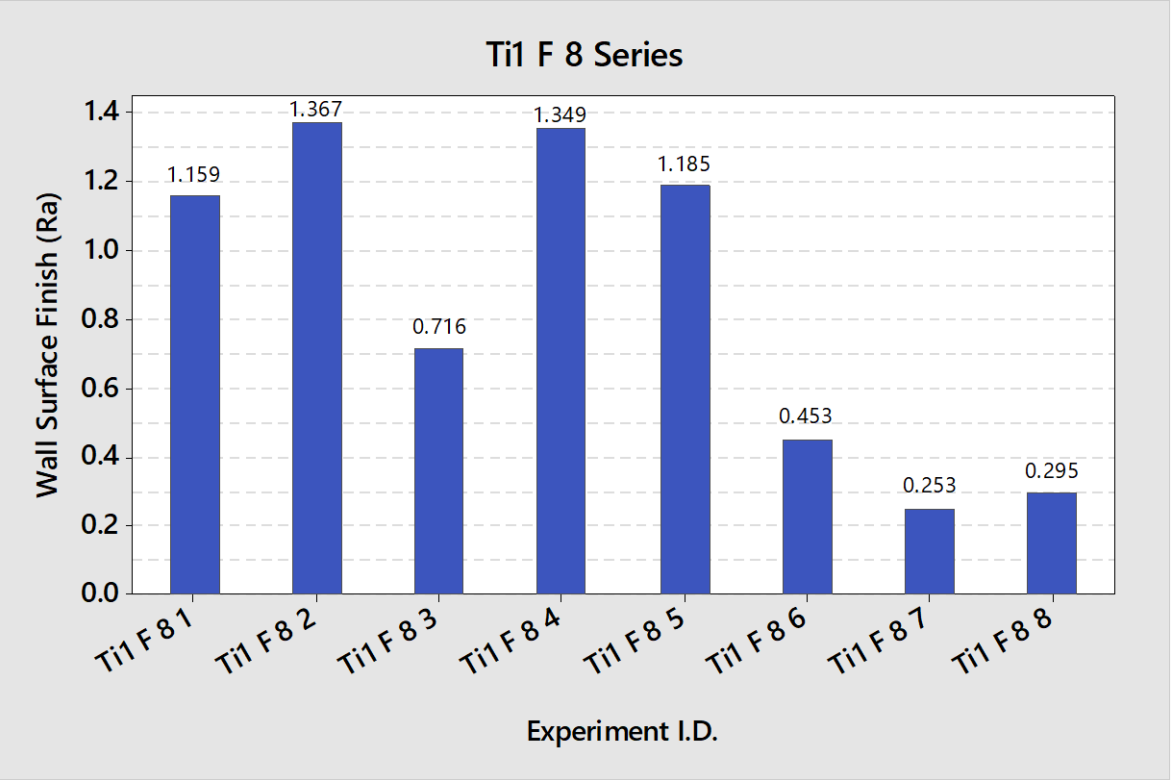

Fig. 156: Surface roughness measurements of drilled holes obtained from experiments on 6082-T6 using straight flute drills

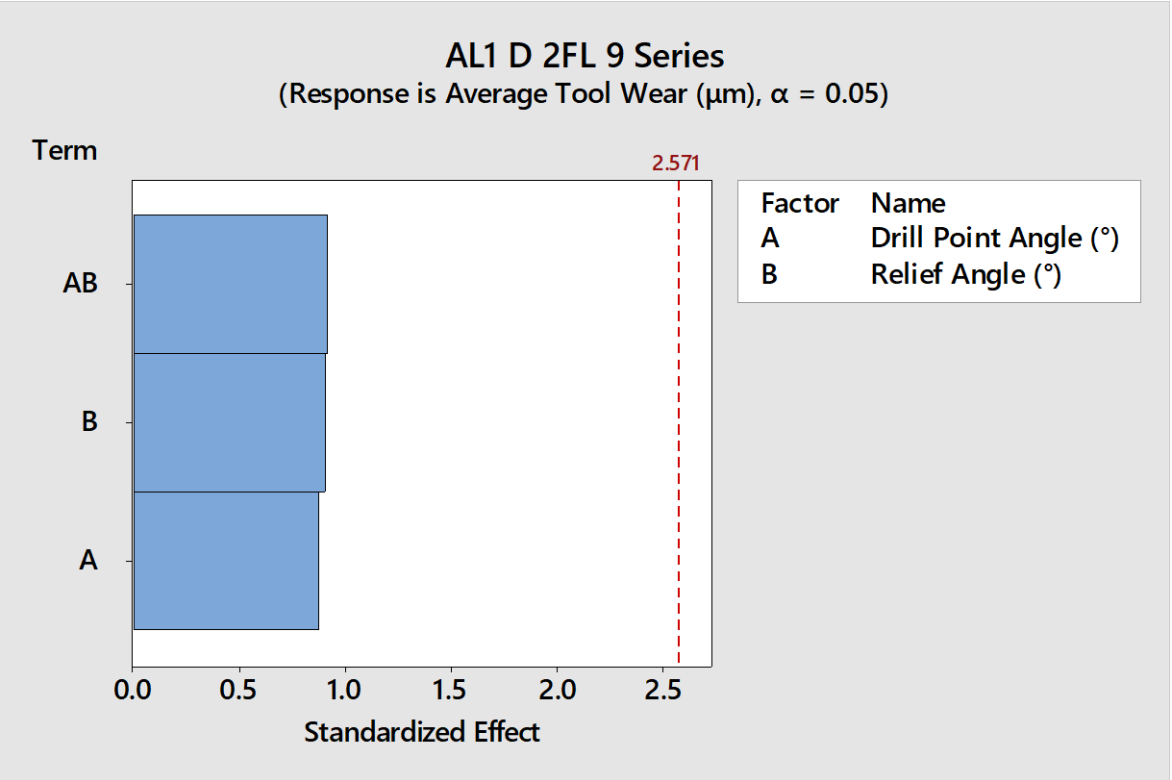

Fig. 157: Pareto ANOVA of tool wear in striaght flute drill deisgns on 6082-T6

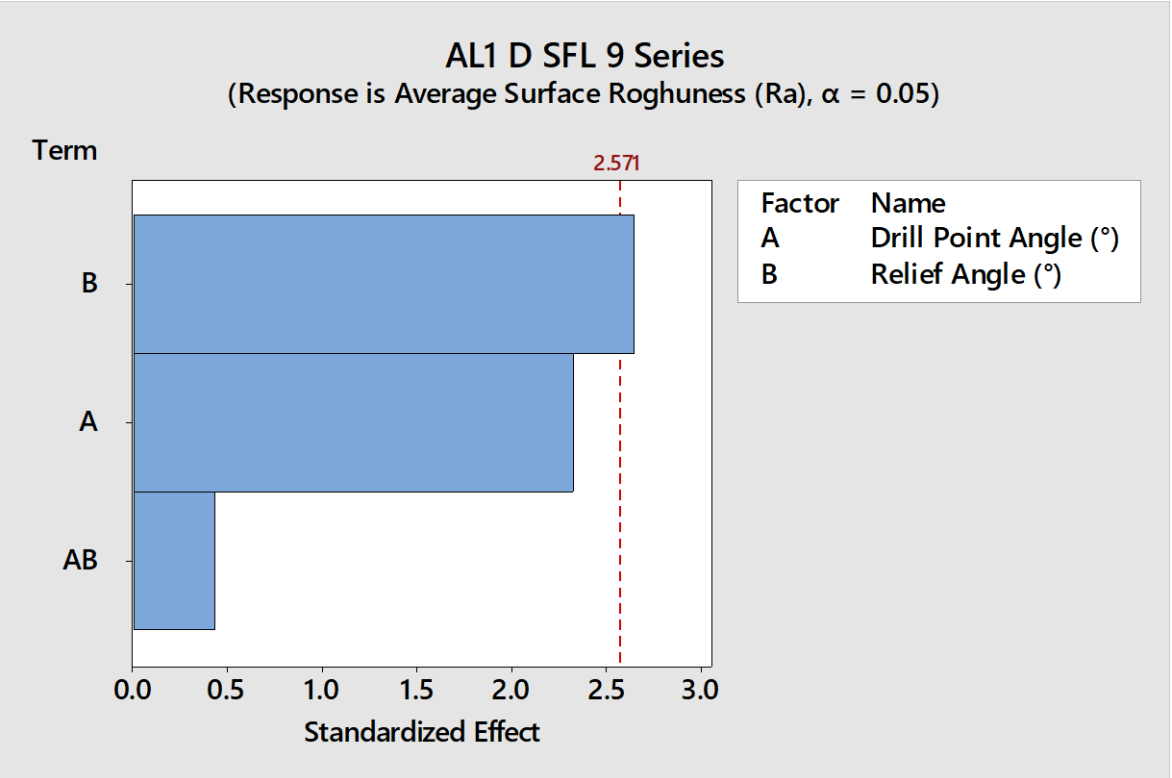

Fig. 158: Pareto ANOVA of geometrical parameters of SFL drills

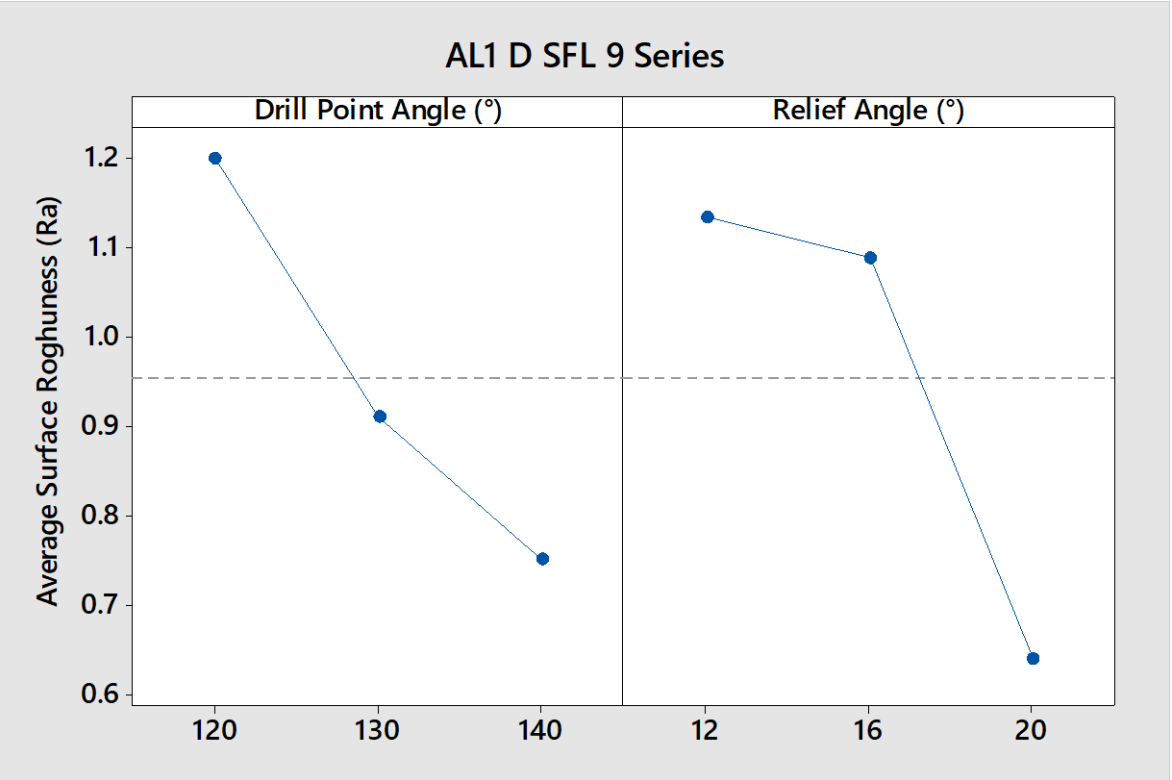

Fig. 159: Main effects plot of geometrical parameters based on surface finish on striaght flute drill design

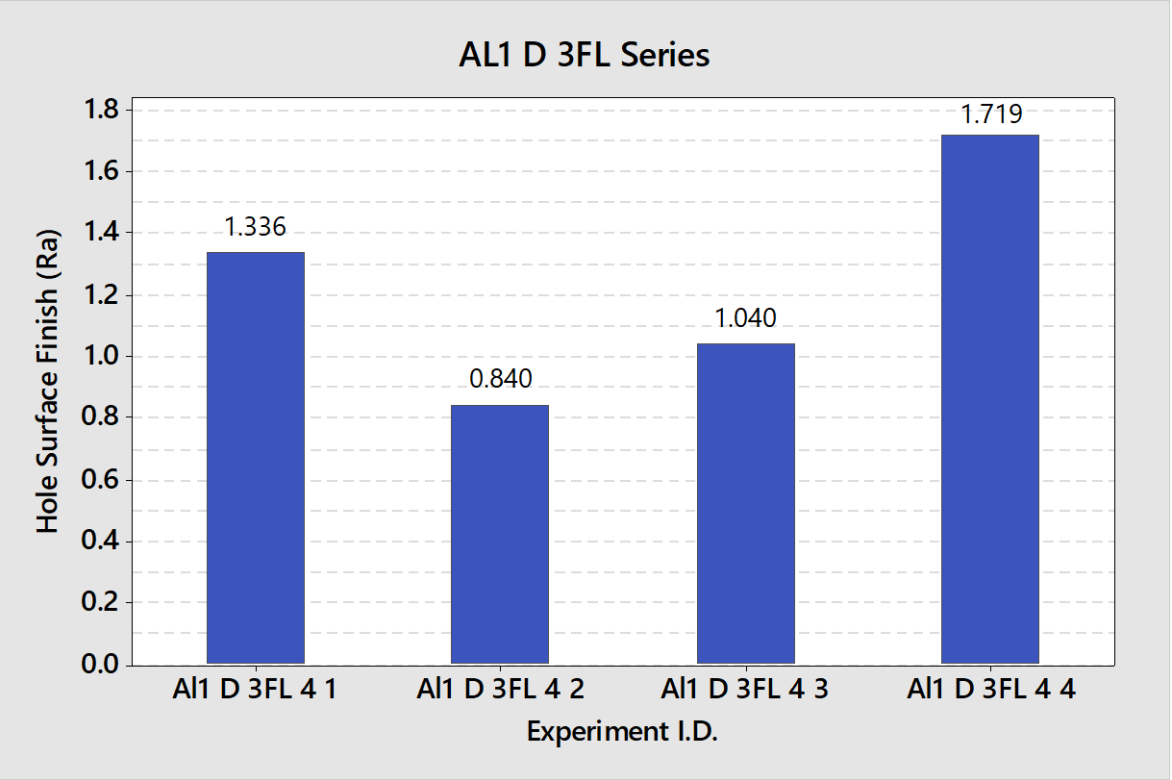

Fig. 160: Surface roughness measurements of drilled holes obtained from experiments on 6082-T6 using 3-flute drills

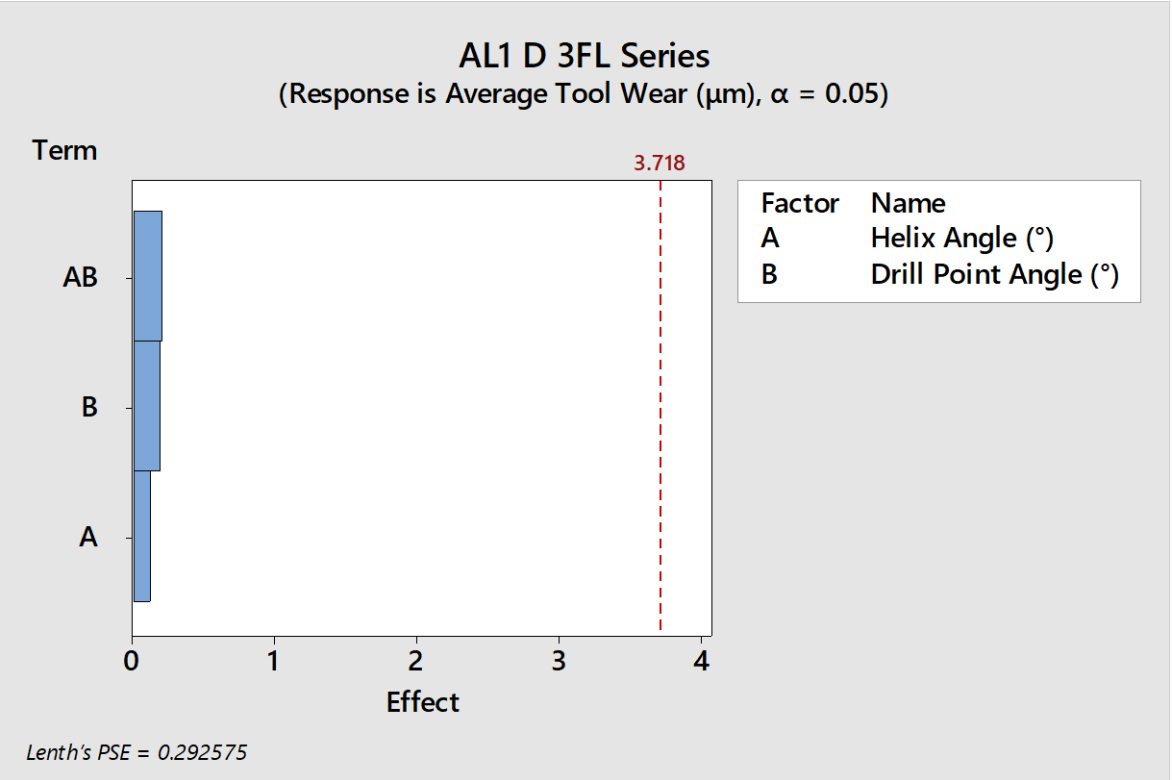

Fig. 161: Pareto ANOVA of tool wear in striaght flute drill deisgns on 6082-T6

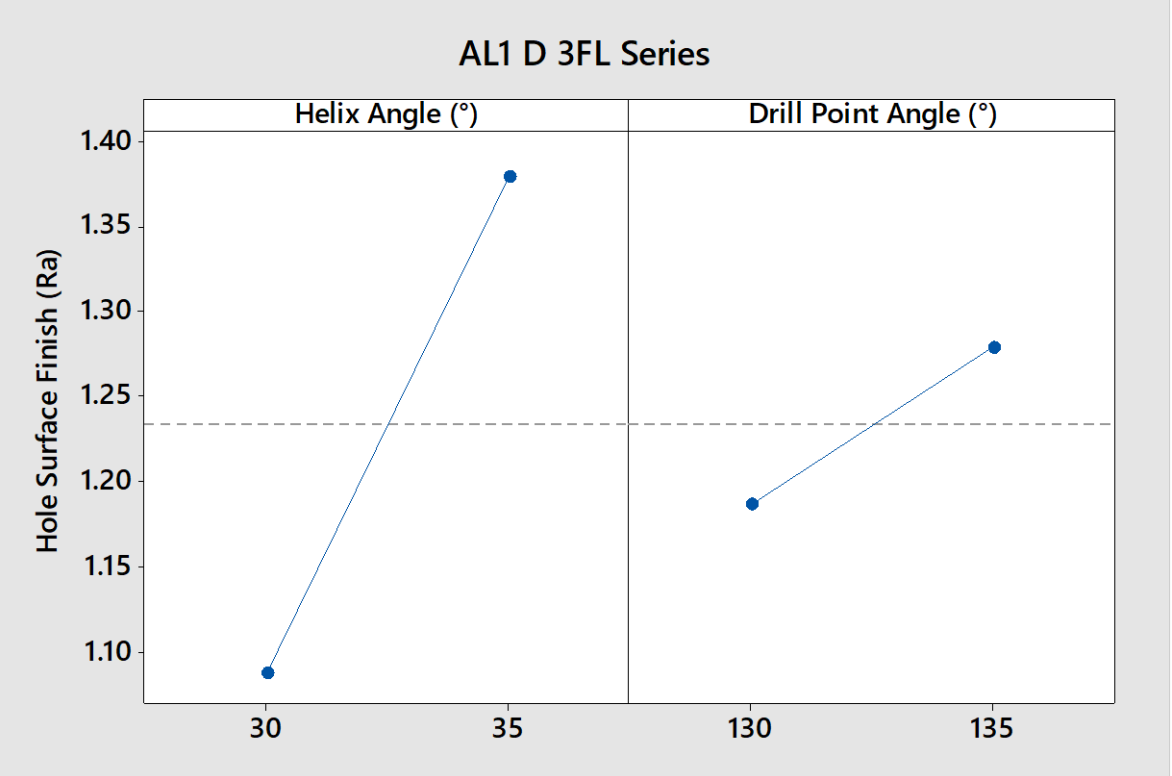

Fig. 162: Main effects plot of geometrical factors based on surface roughness results for 3FL drills

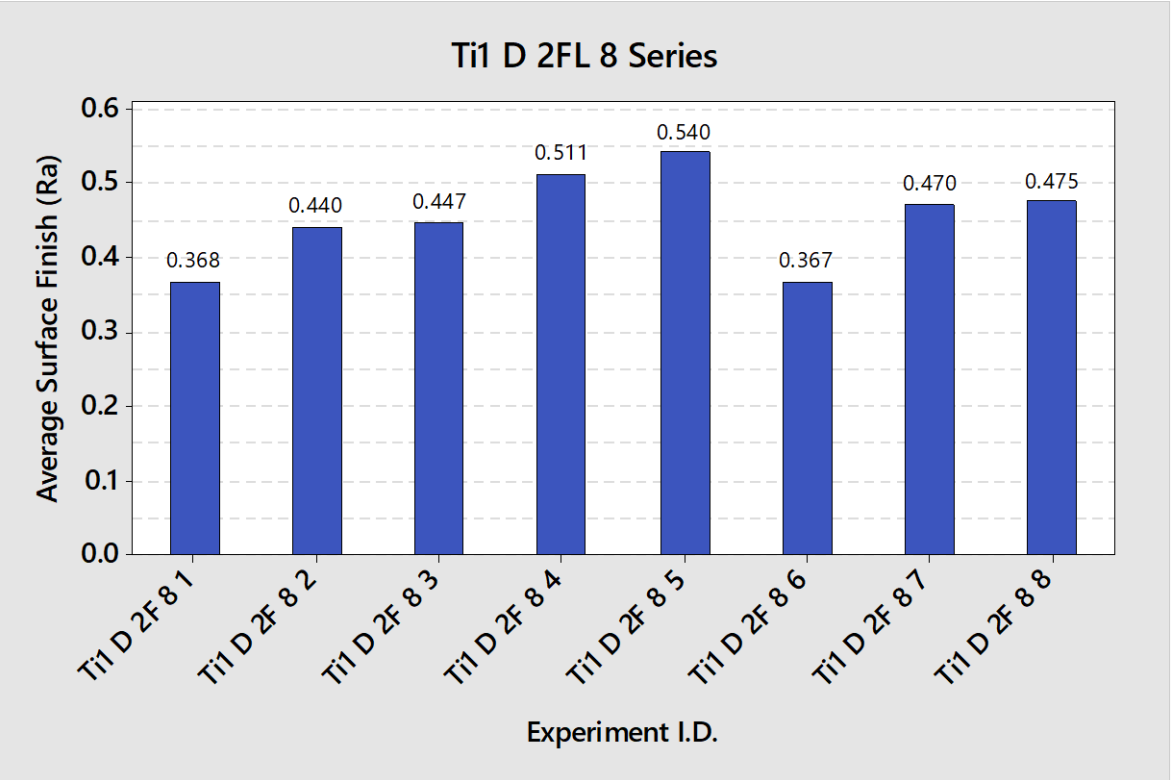

Fig. 163: Surface roughness measurements of drilled holes obtained from experiments on Ti-6Al-4V

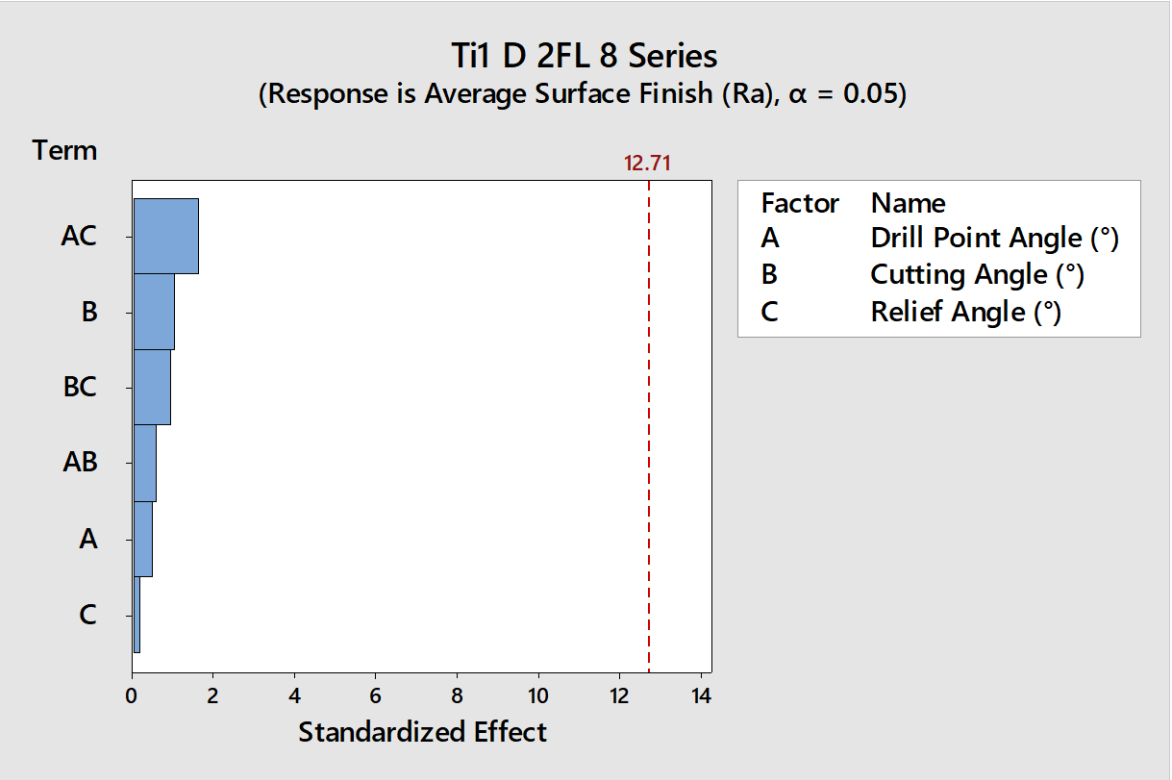

Fig. 164: Pareto ANOVA of geometrical parameters based on surface roghuness drilling Ti-6Al-4V

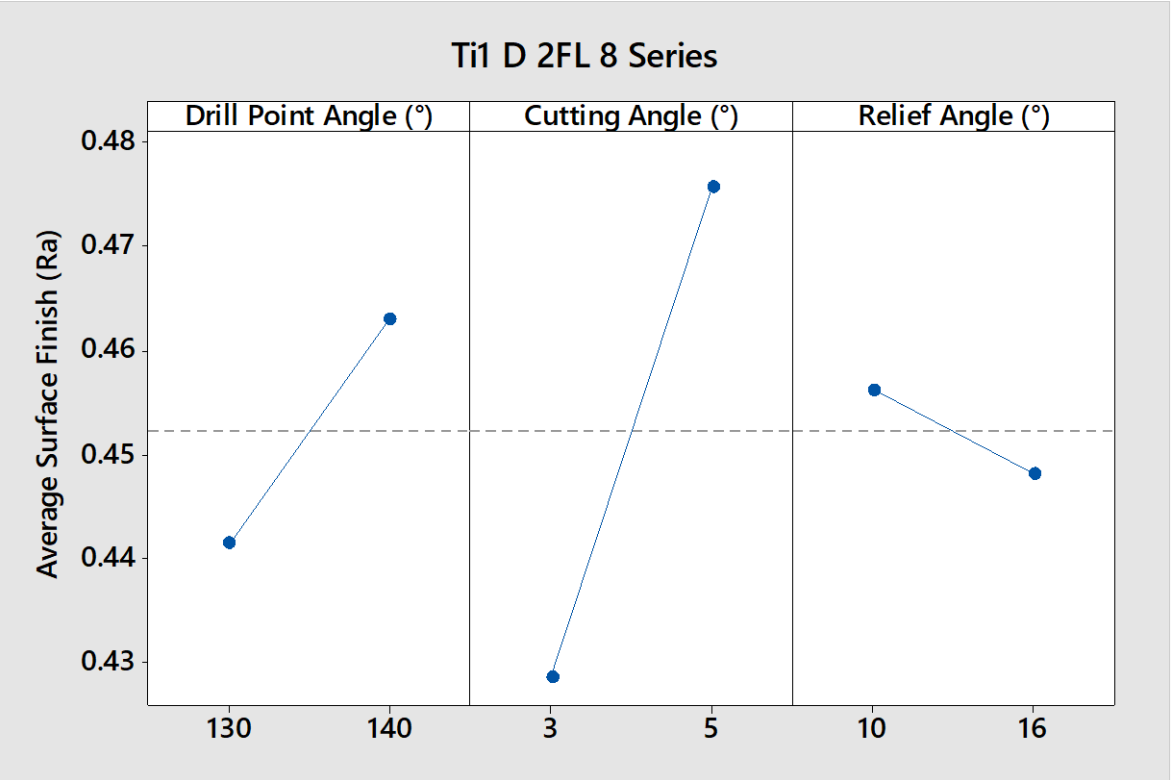

Fig. 165: Main effects plot of geometrical factors based on surface roughness results drills on Ti-6Al-4V

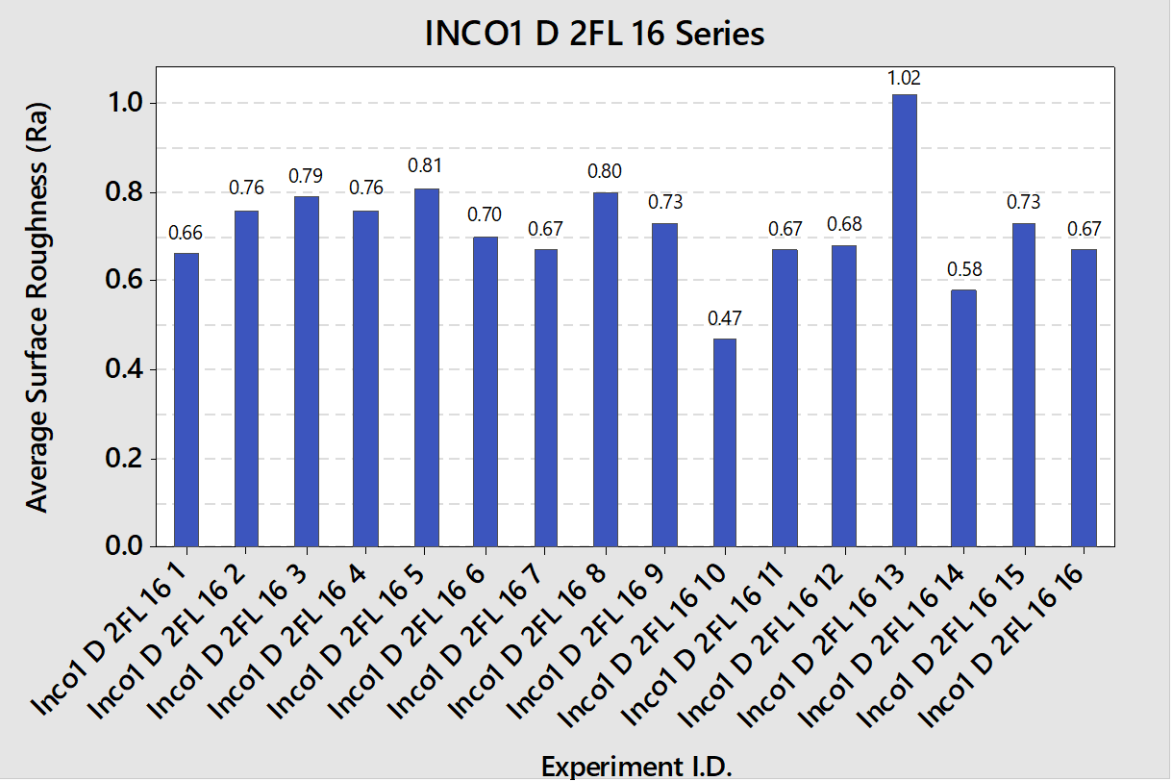

Fig. 166: Surface roughness measurements of drilled holes obtained from experiments on Inconel 718

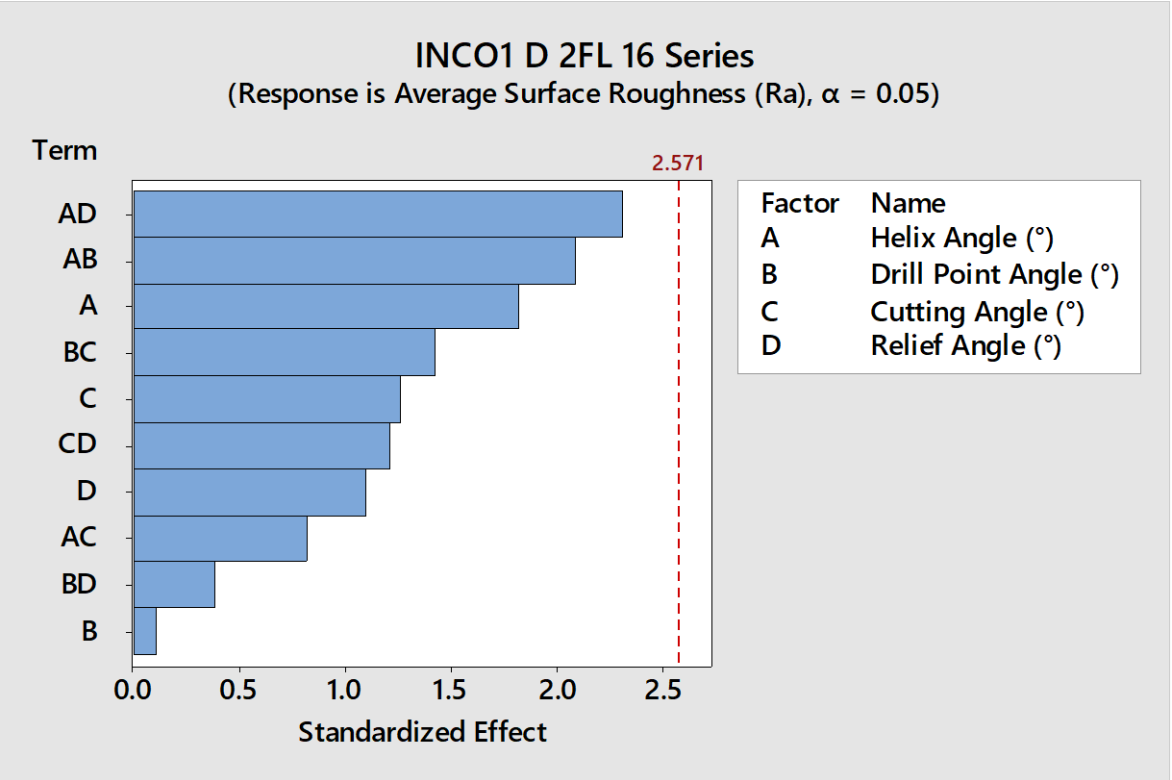

Fig. 167: Pareto ANOVA of geometrical parameters based on surface roghuness in drilling of Inconel 718

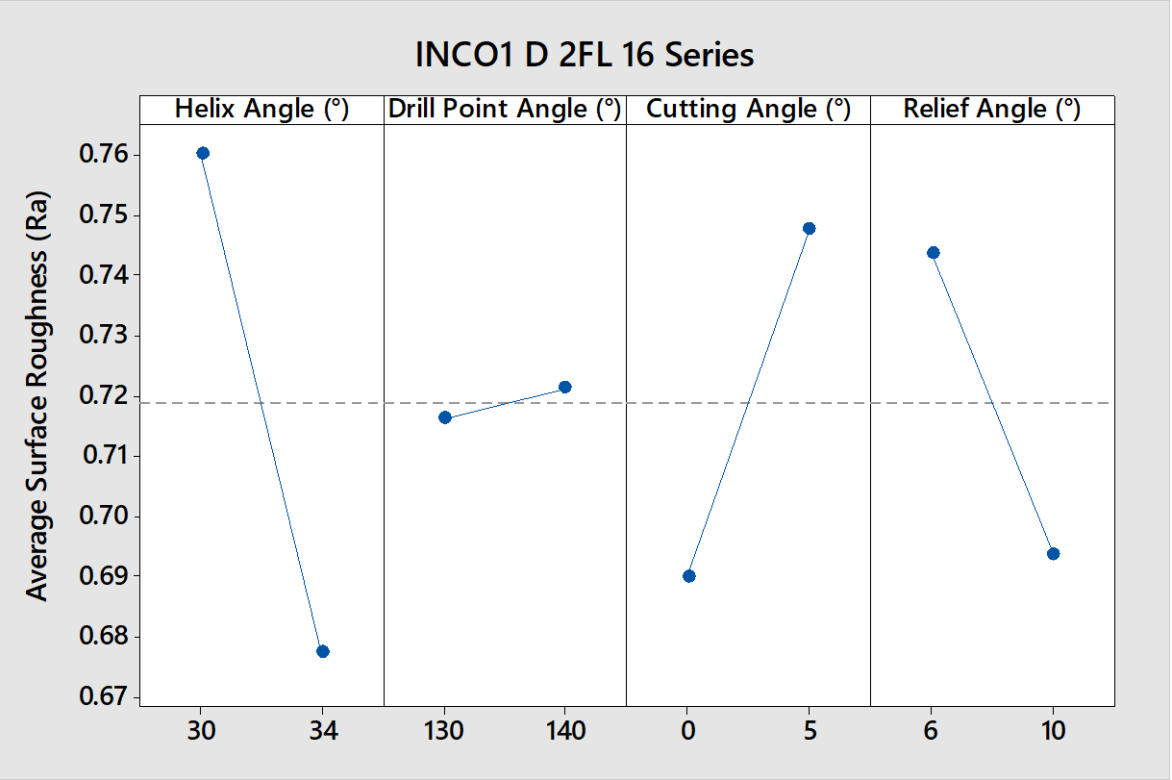

Fig. 168: Main effects plot of geometrical factors based on surface roughness results in drilling of Inconel 718

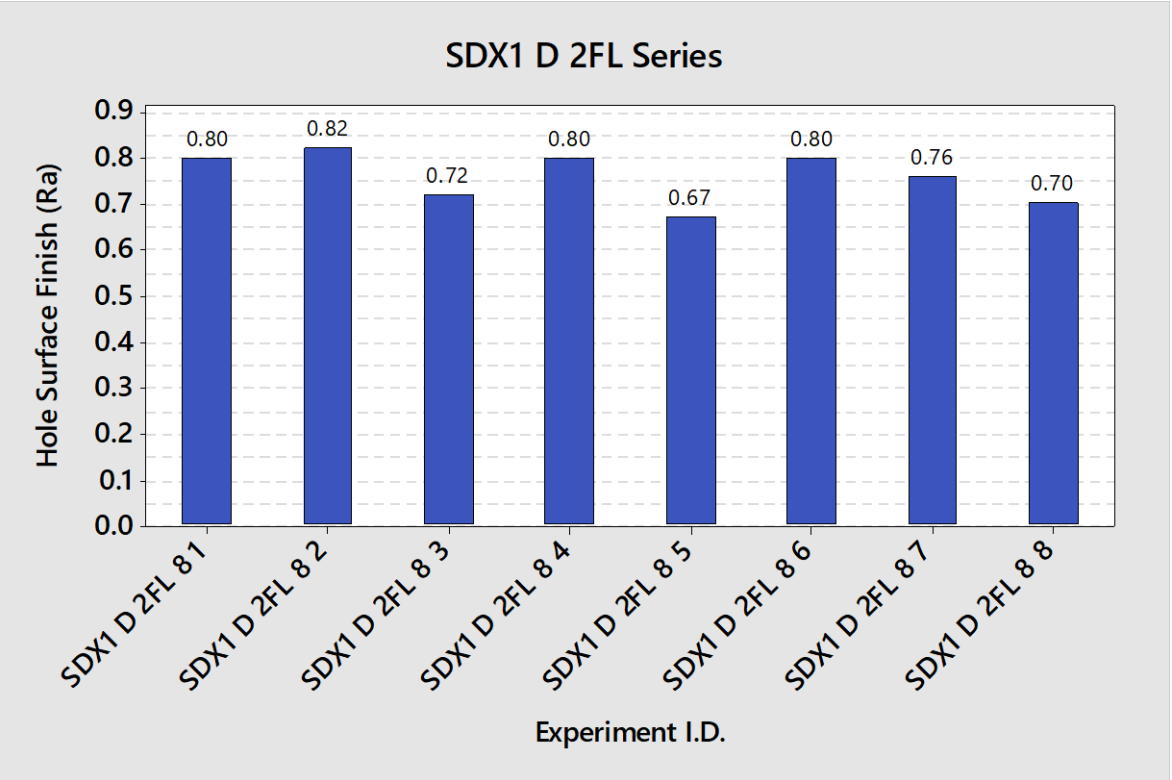

Fig. 169: Surface roughness measurements of drilled holes obtained from experiments on super duplex 2507

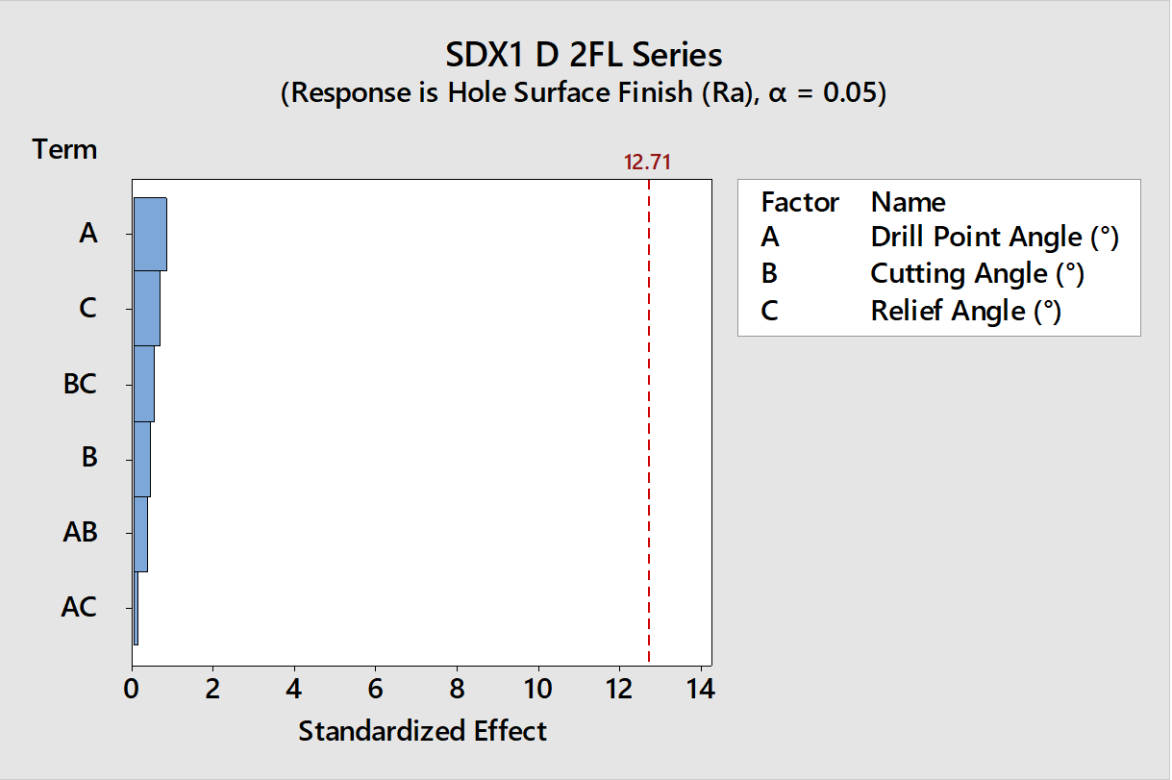

Fig. 170: Pareto ANOVA of geometrical parameters based on surface roghuness in drilling of 2507

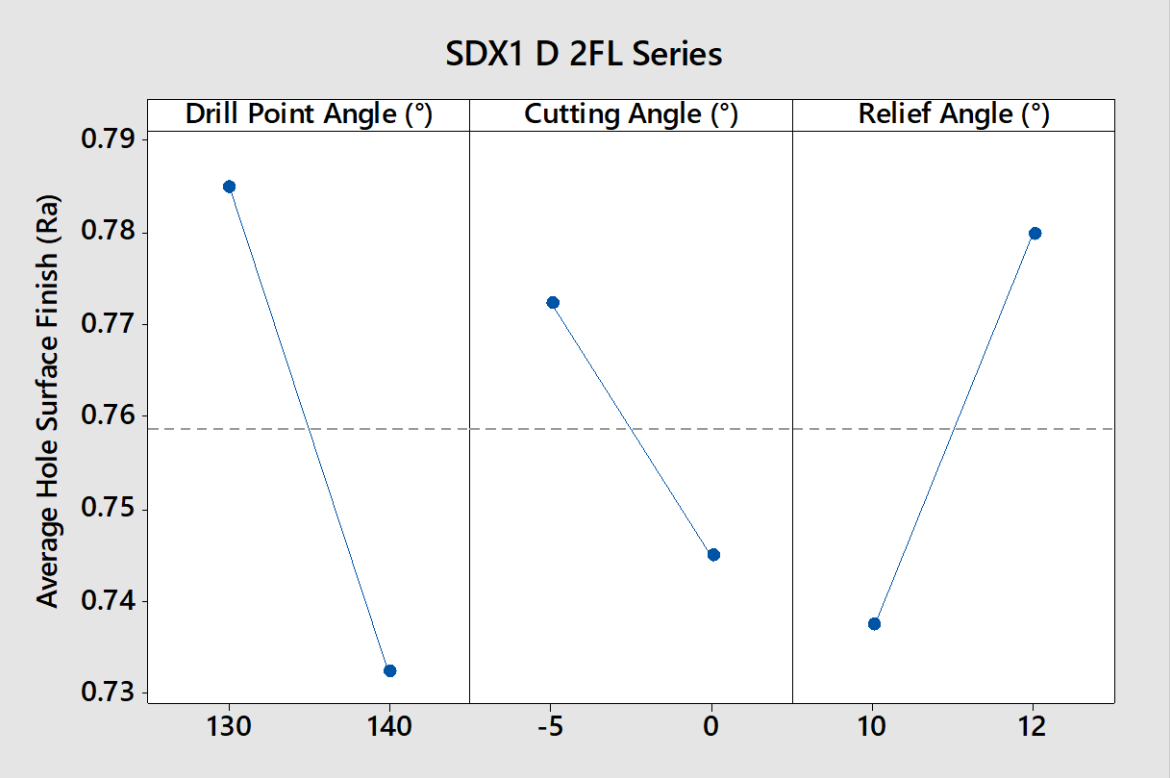

Fig. 171: Main effects plot of geometrical parameters based on results obtained from drilling super duplex alloy 2507

Appendix H: Probability Charts

H1. AL1 R 8 Series

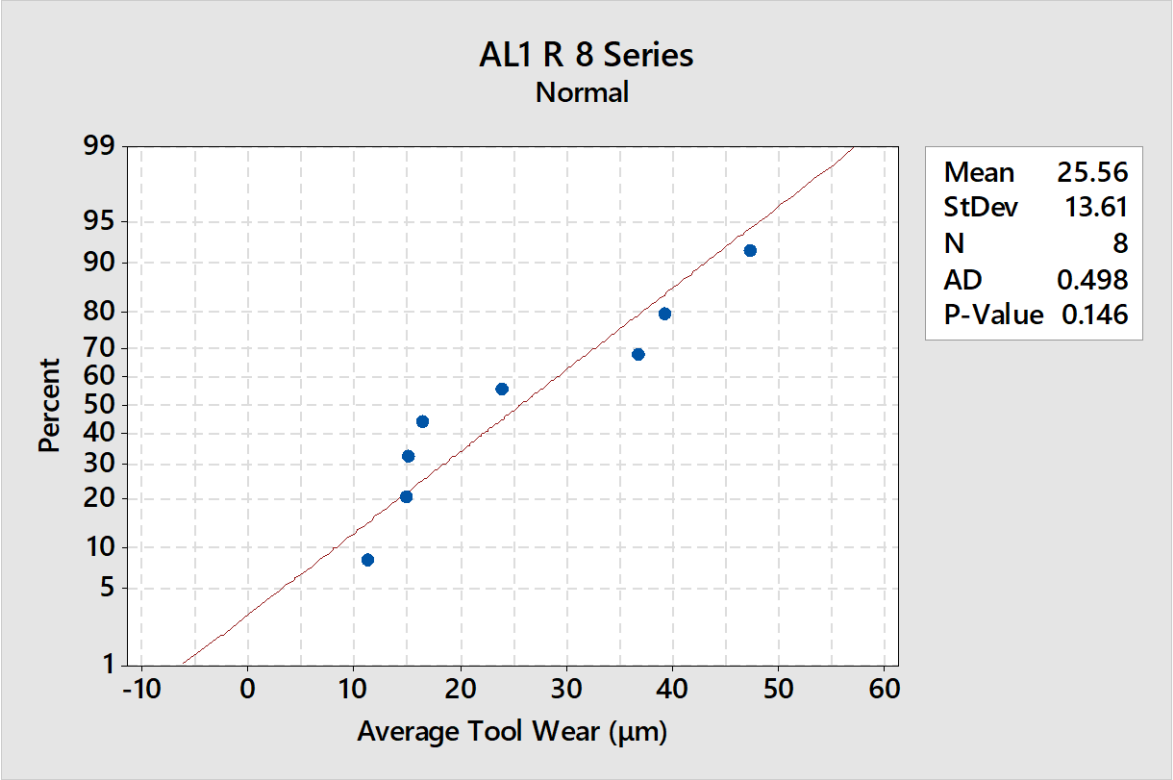

Fig. 172: Probability chart of tool wear results from end-milling experiments on 6082-T6

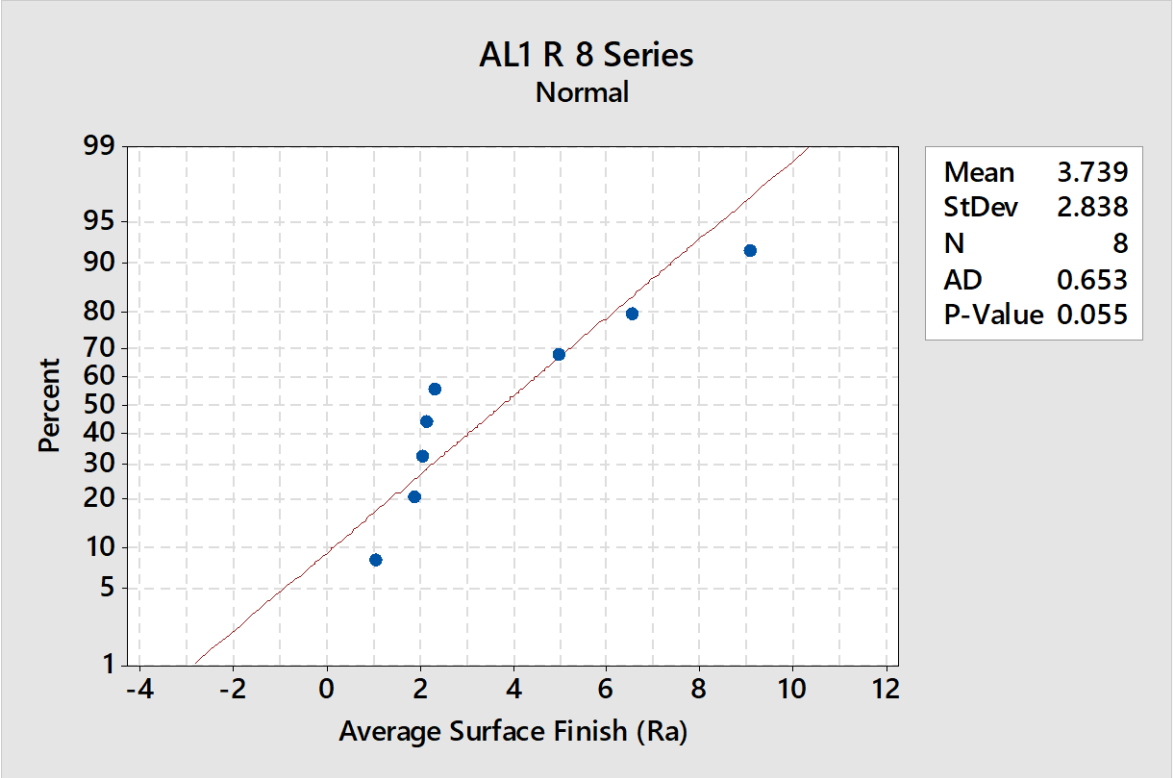

Fig. 173: Probability chart of surface roughness obtained from end-milling experiments on 6082-T6

H2. Ti1 R 24 Series

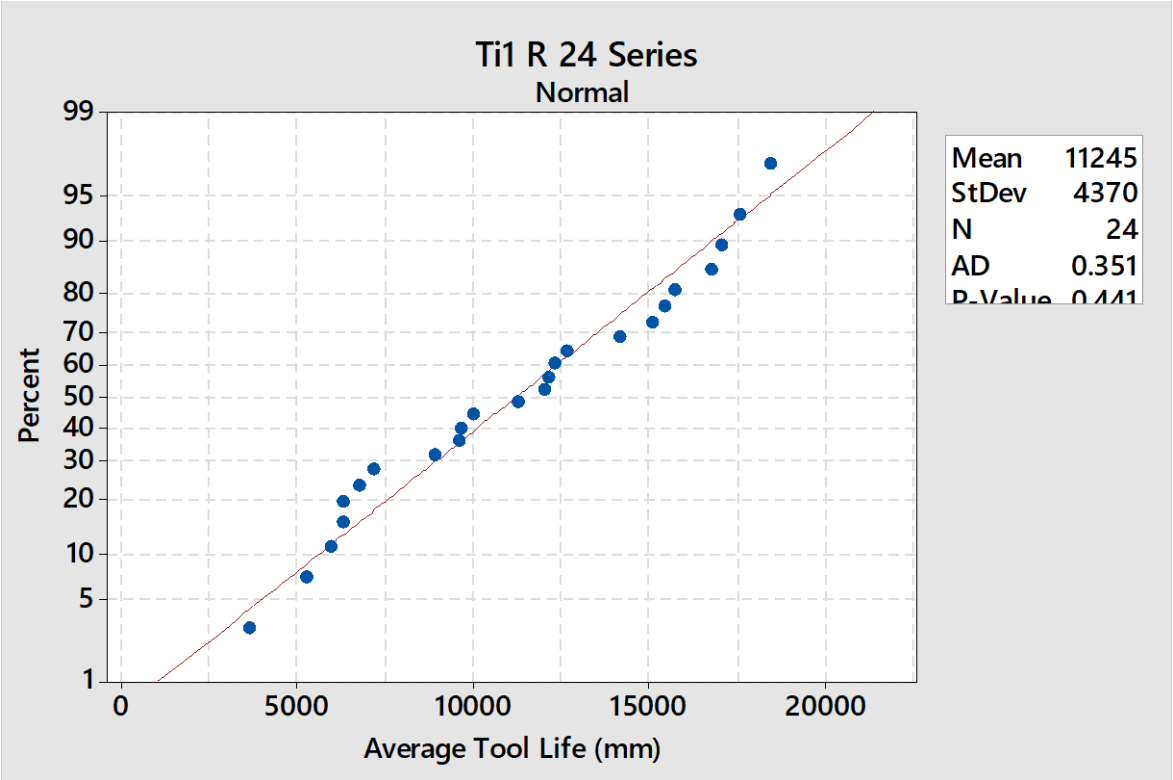

Fig. 174: Probability chart of tool life obtained from end-milling experiments on Ti-6Al-4V

H3. Ti1 F 8 Series

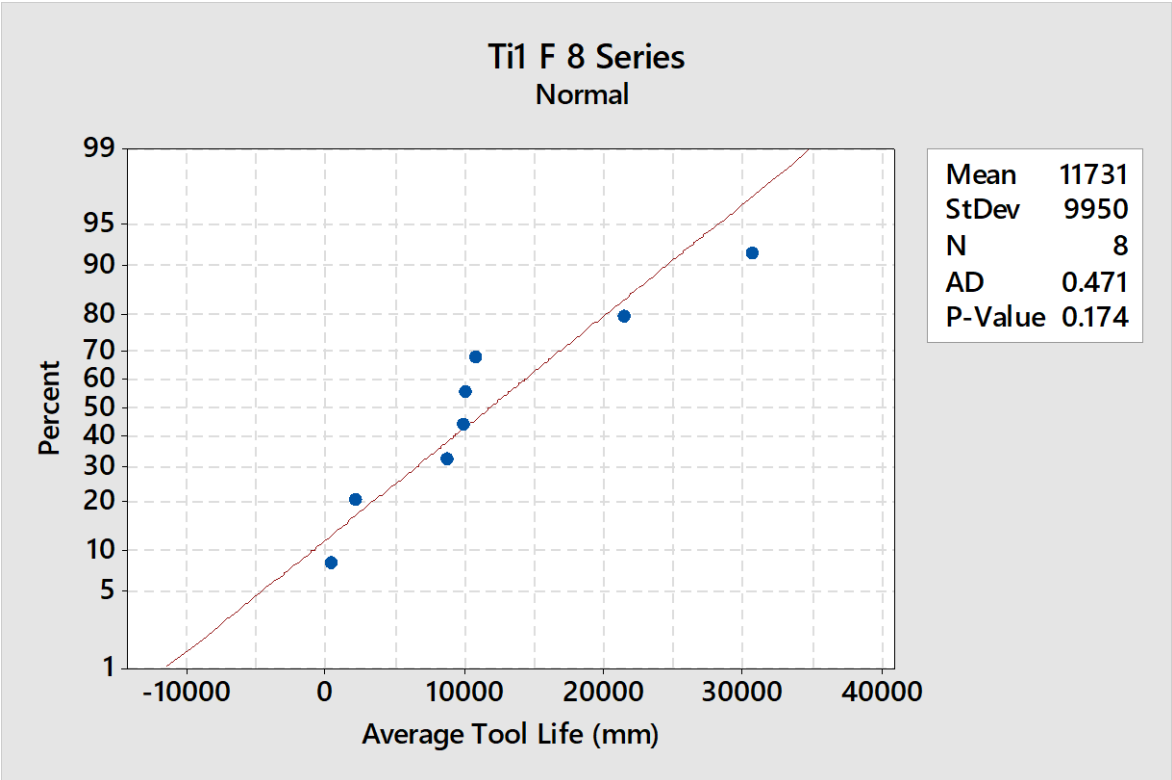

Fig. 175: Probability chart of tool life obtained from end-milling experiments on Ti-6Al-4V

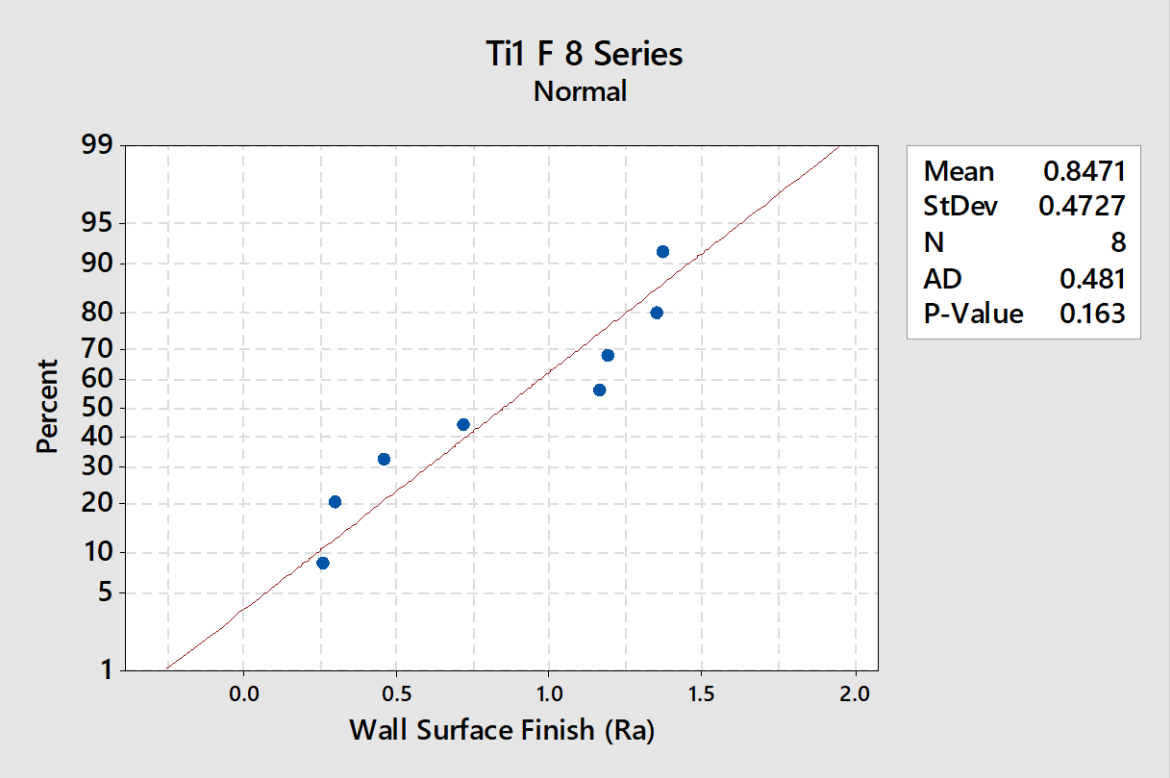

Fig. 176: Probability chart of surface roughness obtained from end-milling experiments on Ti-6Al-4V

H4. INCO1 R 27 Series

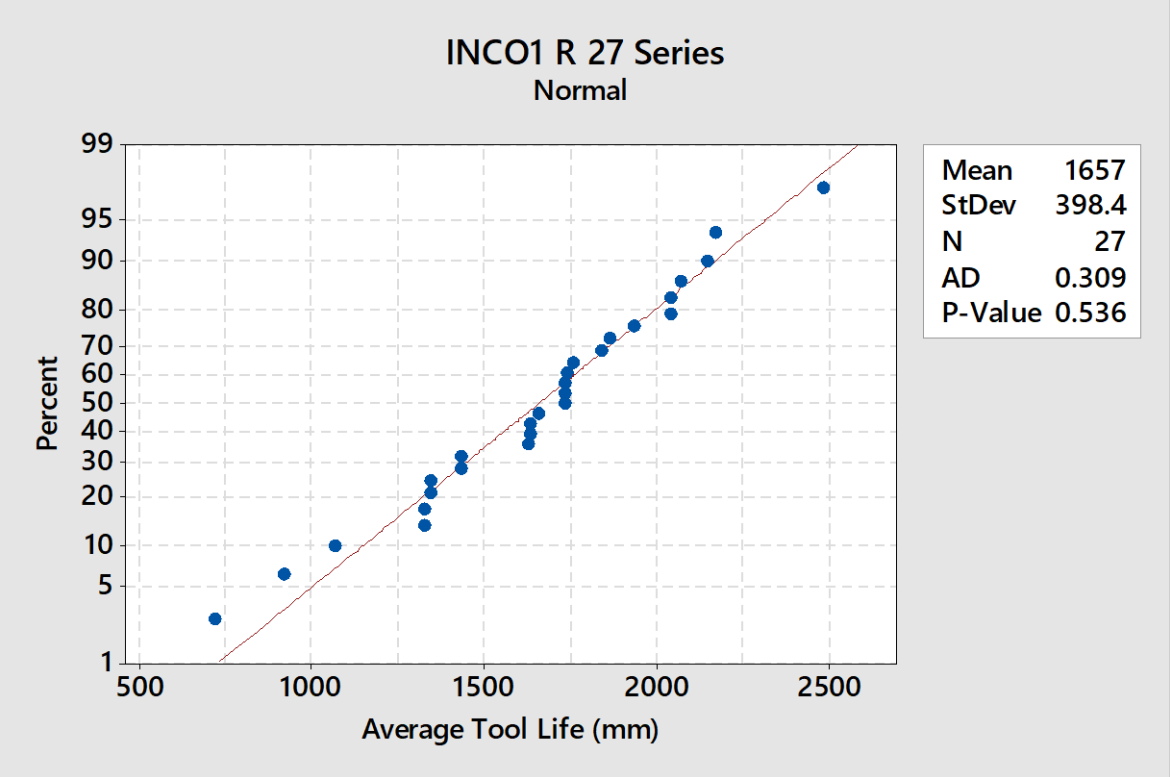

Fig. 177: Probability chart of tool life obtained from end-milling experiments on Inconel 718

H5. SDX1 R 16 Series

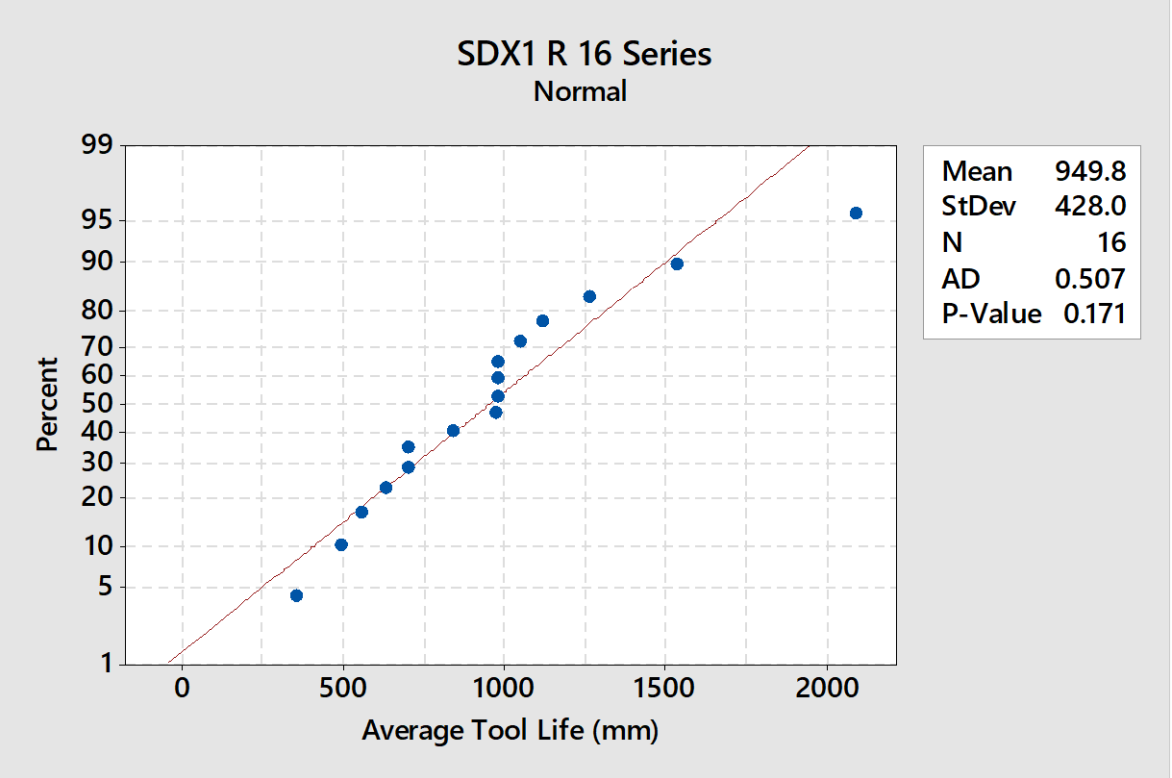

Fig. 178: Probability chart of tool life obtained from end-milling experiments on super duplex 2507

H6. AL1 D SFL 9 Series

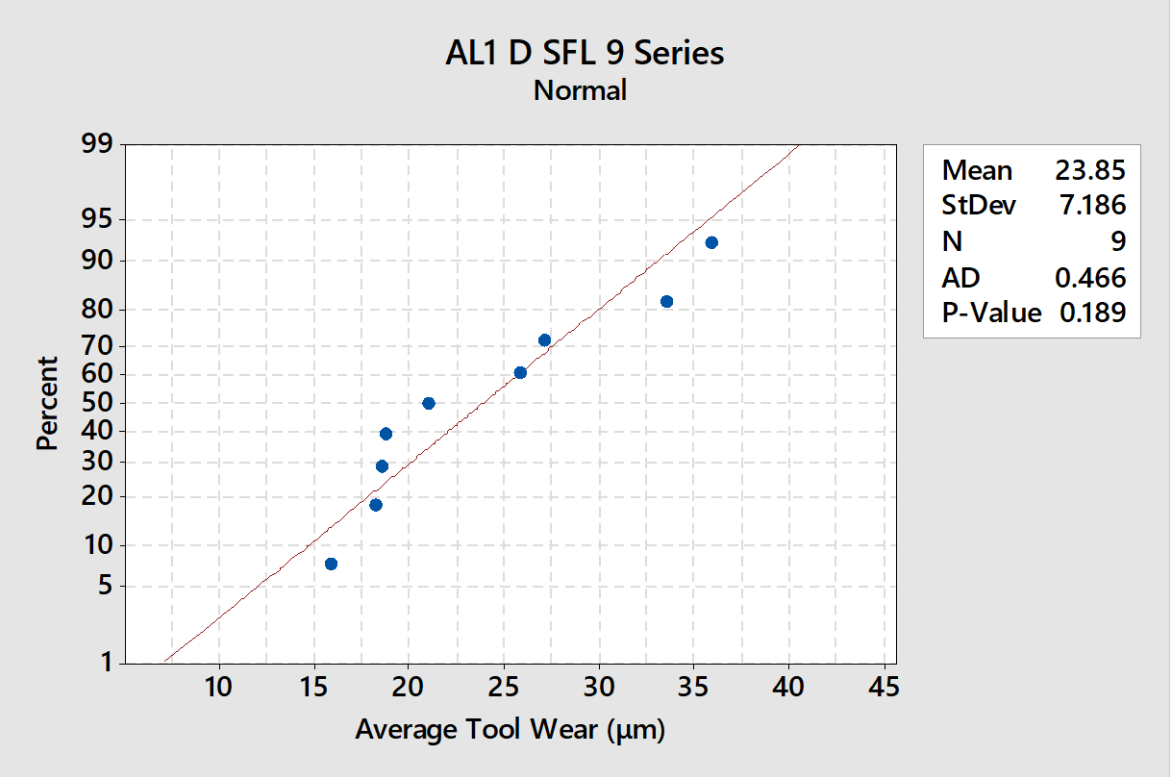

Fig. 179: Probability chart of tool wear obtained from drilling experiments on 6082-T6

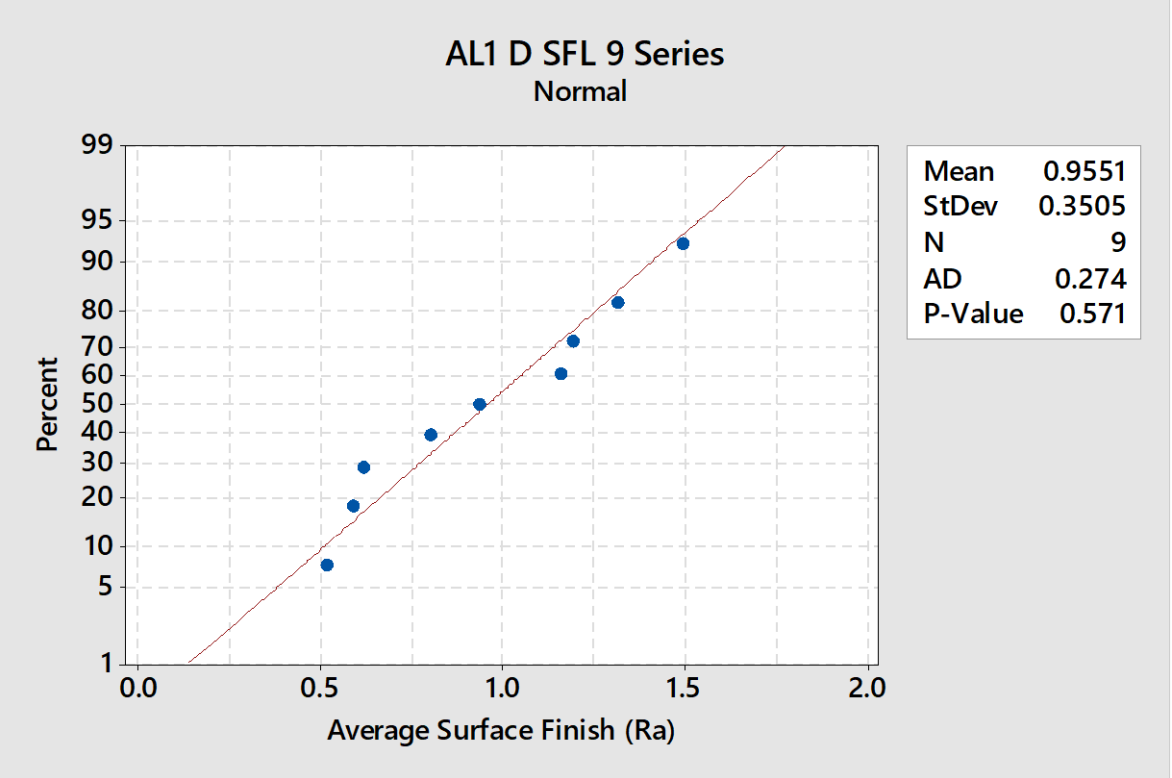

Fig. 180: Probability chart of hole surface roughness obtained from drilling experiments on 6082-T6

H7. AL1 D 3FL 4 Series

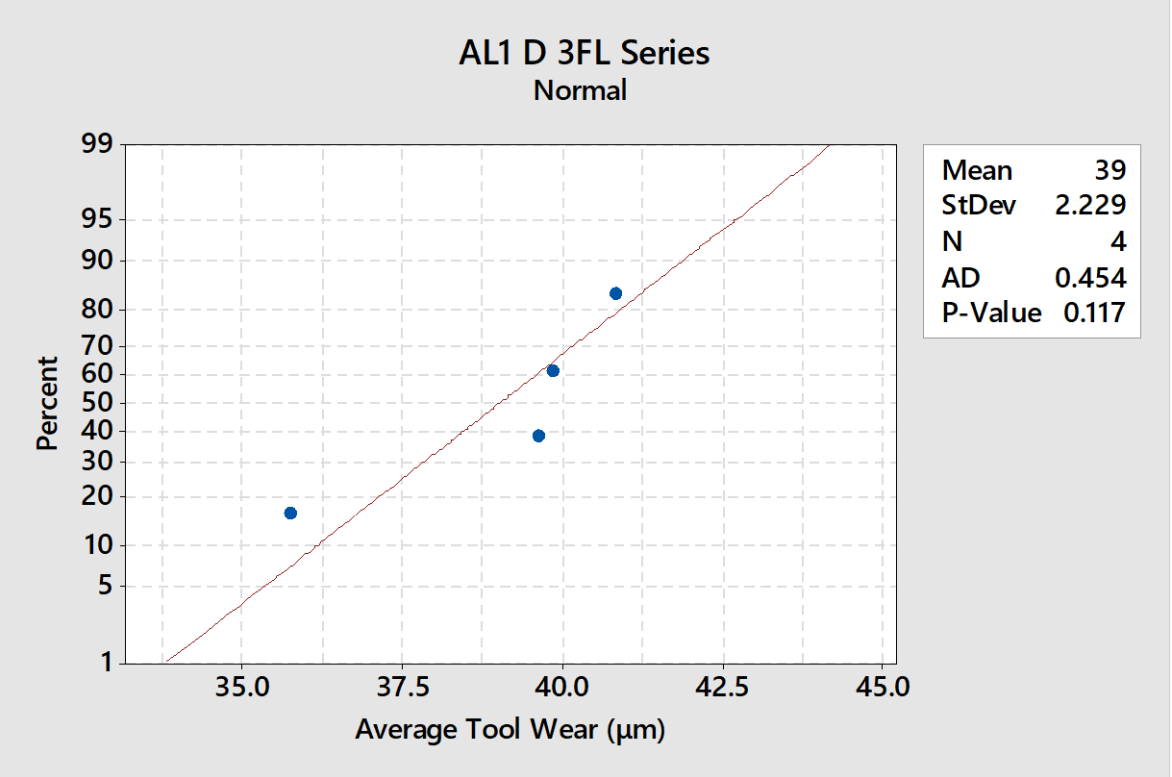

Fig. 181: Probability chart of tool wear obtained from drilling experiments on 6082-T6

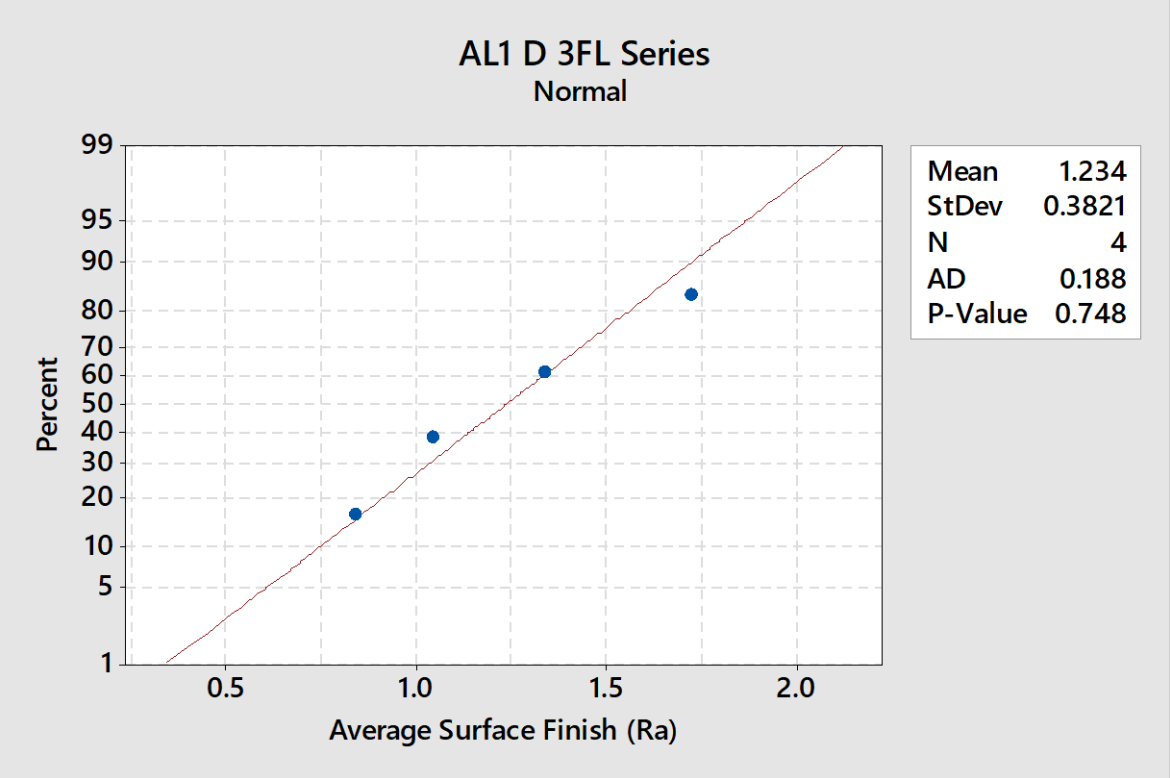

Fig. 182: Probability chart of hole surface finish obtained from drilling experiments on 6082-T6

H8. Ti1 D 2FL 8 Series

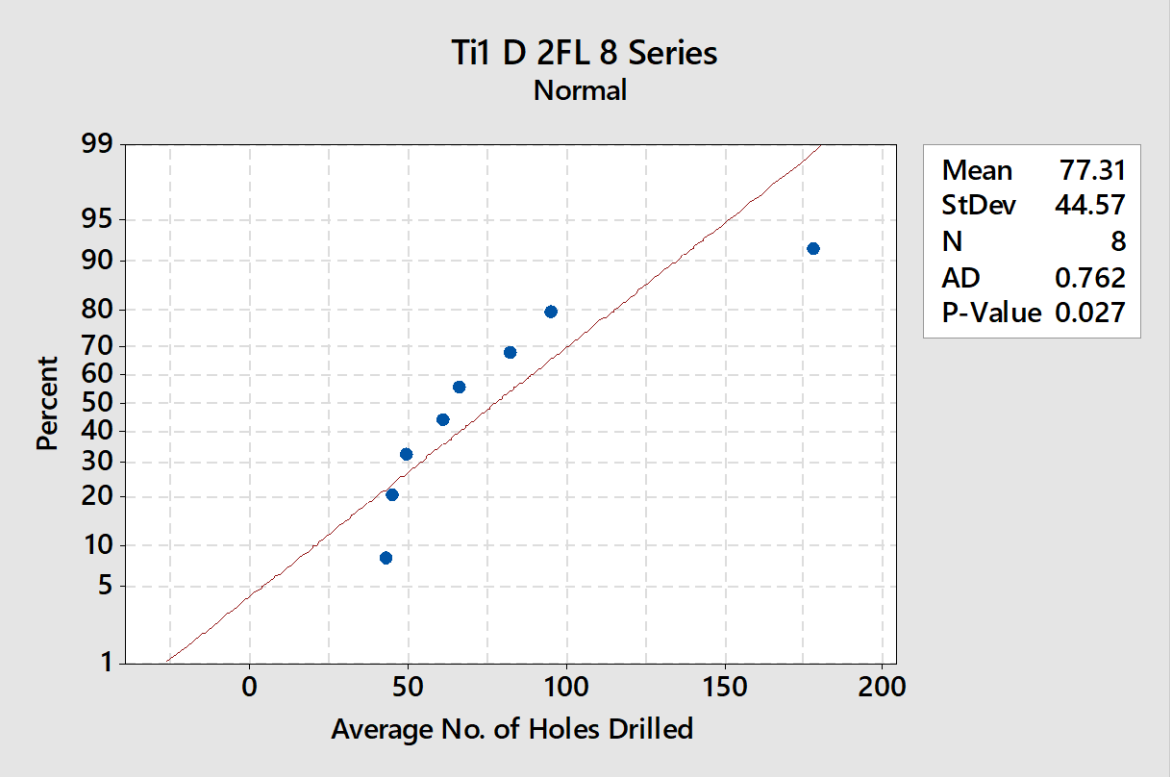

Fig. 183: Probability chart of number of holes drilled obtained from experiments on Ti-6Al-4V

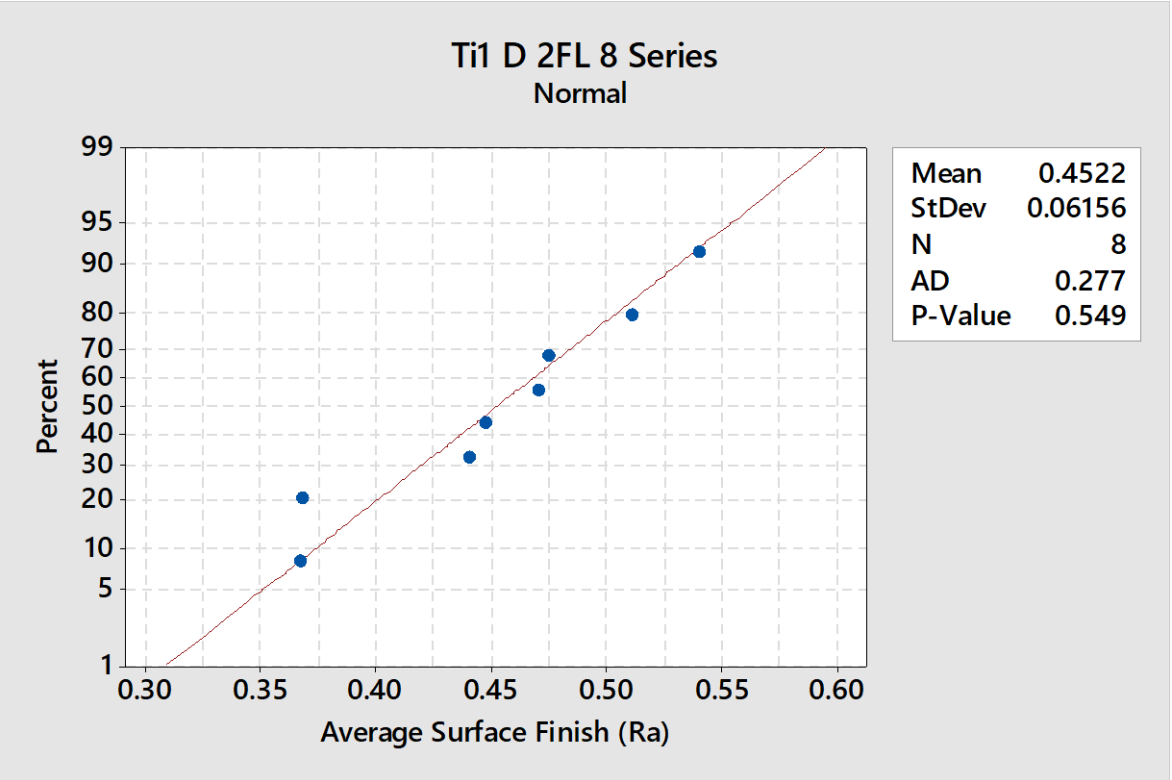

Fig. 184: Probability chart of surface roughness of drilled holes obtained from experiments on Ti-6Al-4V

H9.INCO1 D 2FL 16 Series

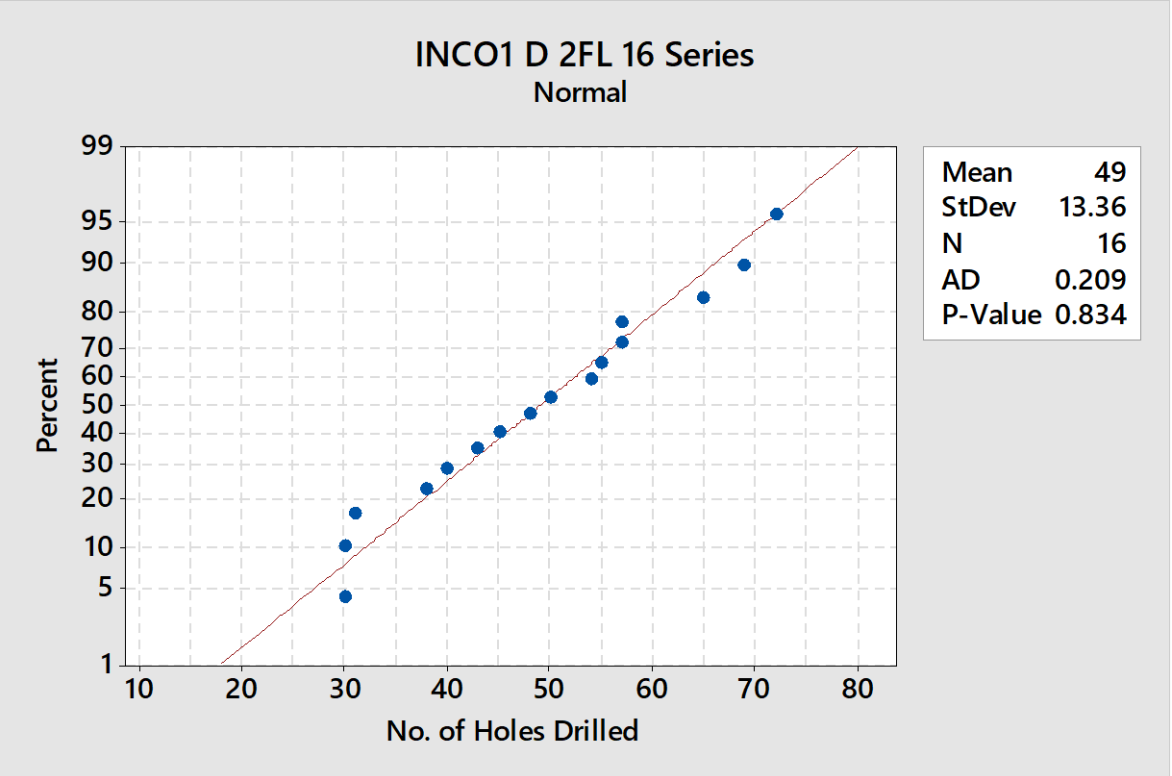

Fig. 185: Probability chart of number of holes drilled obtained from experiments on Inconel 718

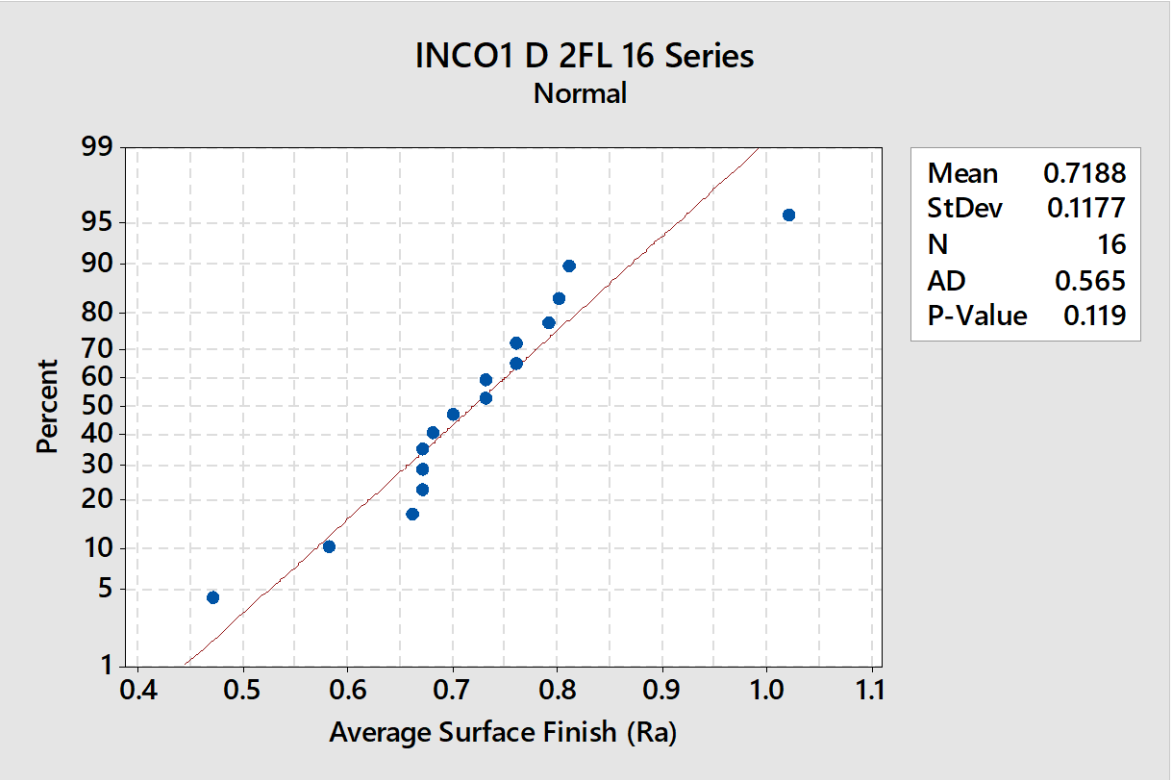

Fig. 186: Probability chart of surface roughness of drilled holes obtained from experiments on Inconel 718

H10. SDX1 D 2FL 8 Series

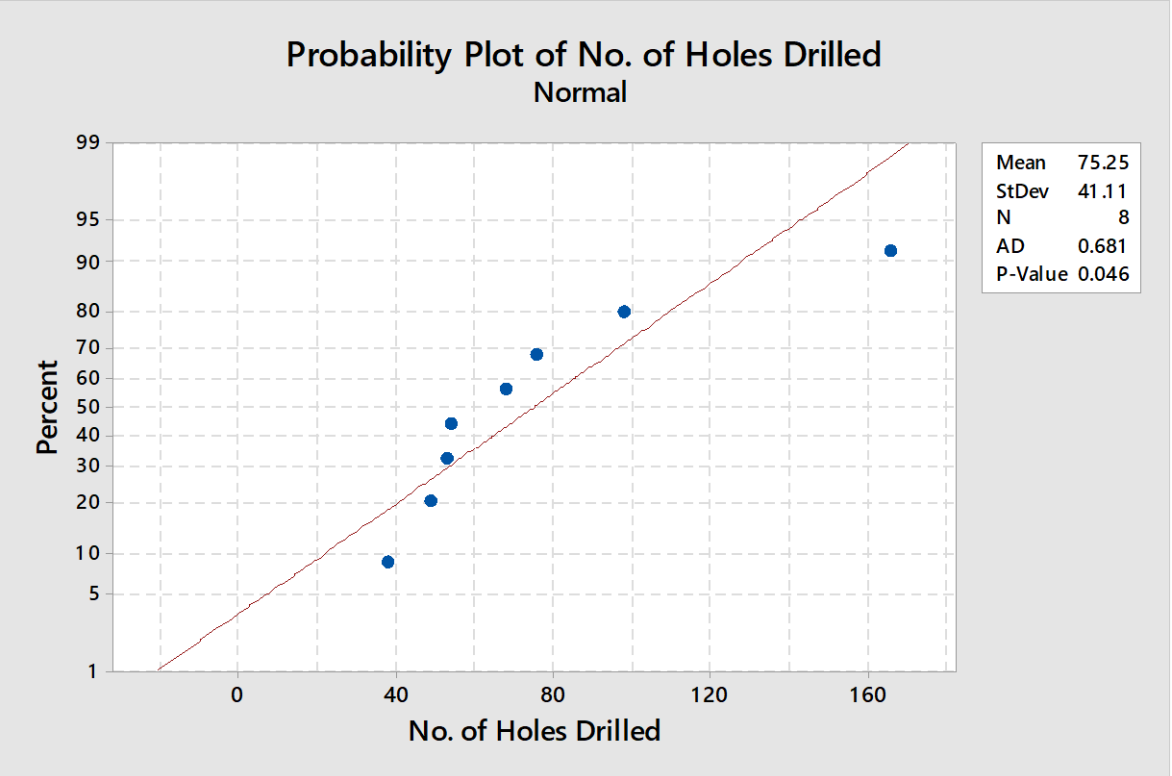

Fig. 187: Probability chart of number of holes drilled obtained from experiments on super duplex 2507

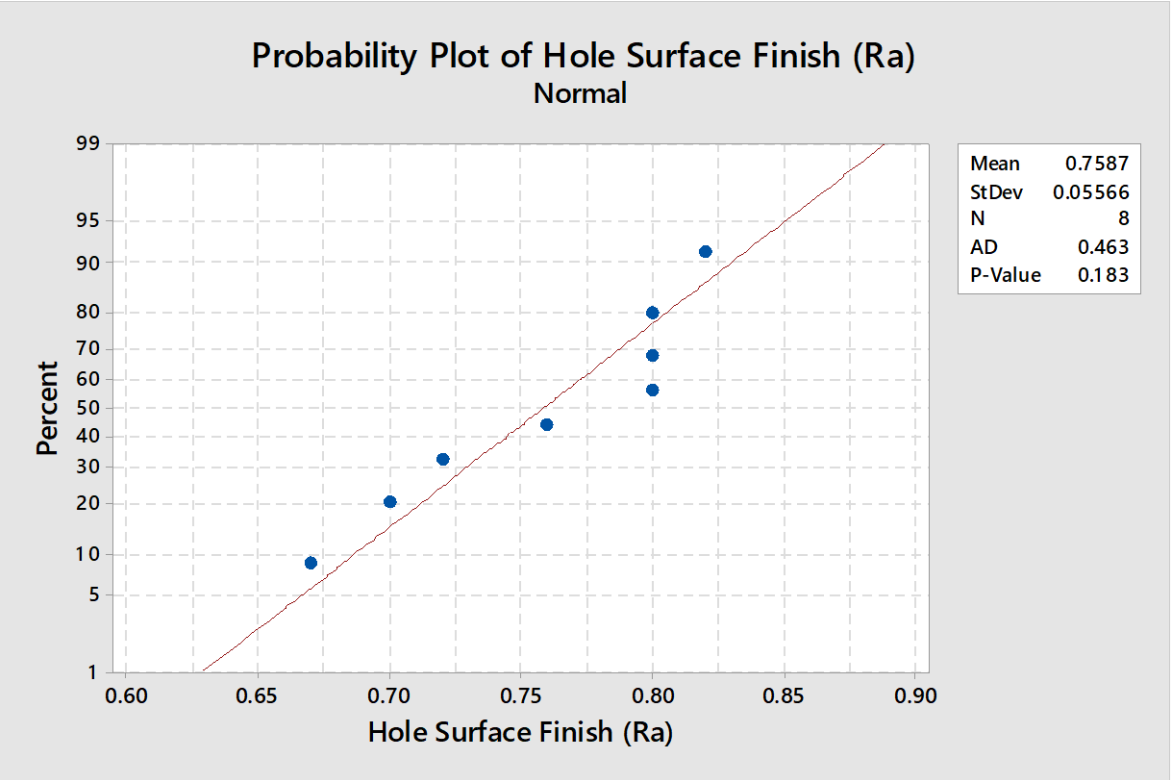

Fig. 188: Probability chart of surface roughness of drilled holes obtained from experiments on super duplex 2507

Appendix I: Box Plots

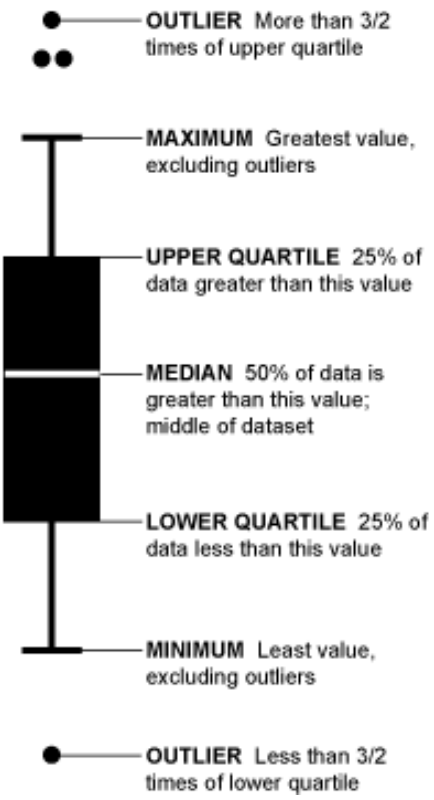

Fig. 189: Detailed representation of a box plot [165]

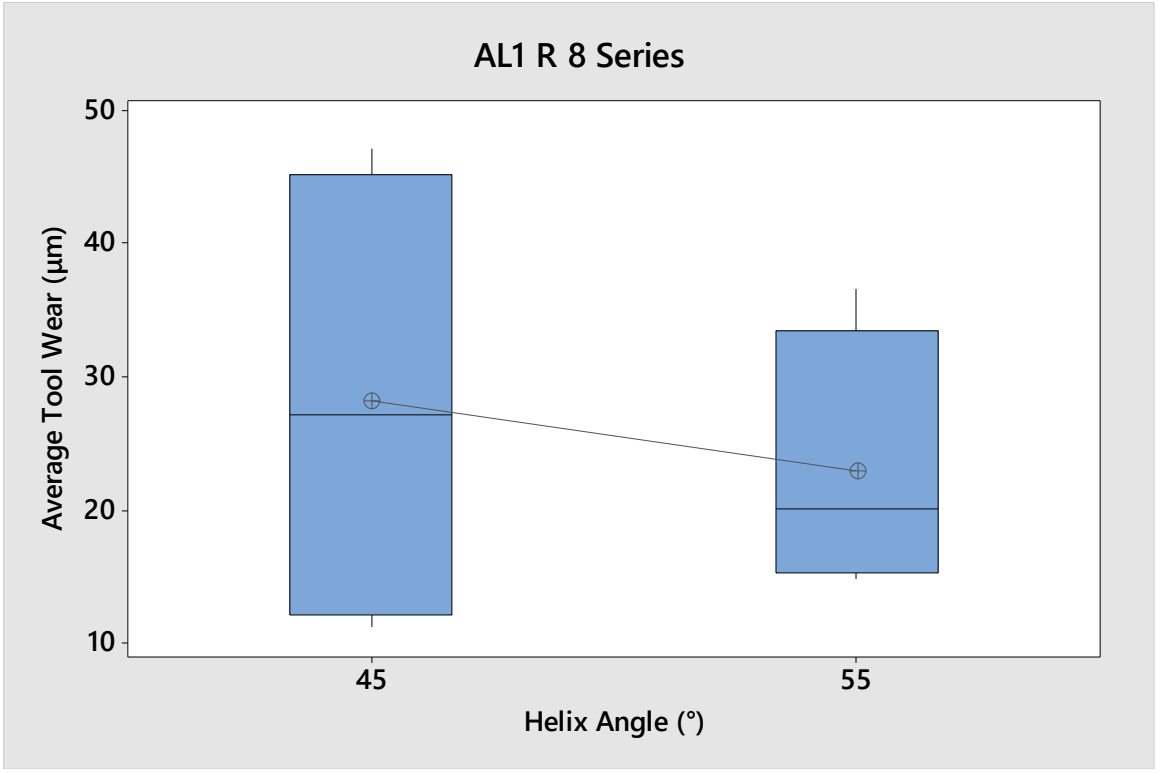

Fig. 190: Box plot of interactions between helix angle at different levels based on average tool wear obtained from end-milling of 6082-T6 using 2-flute end-mills

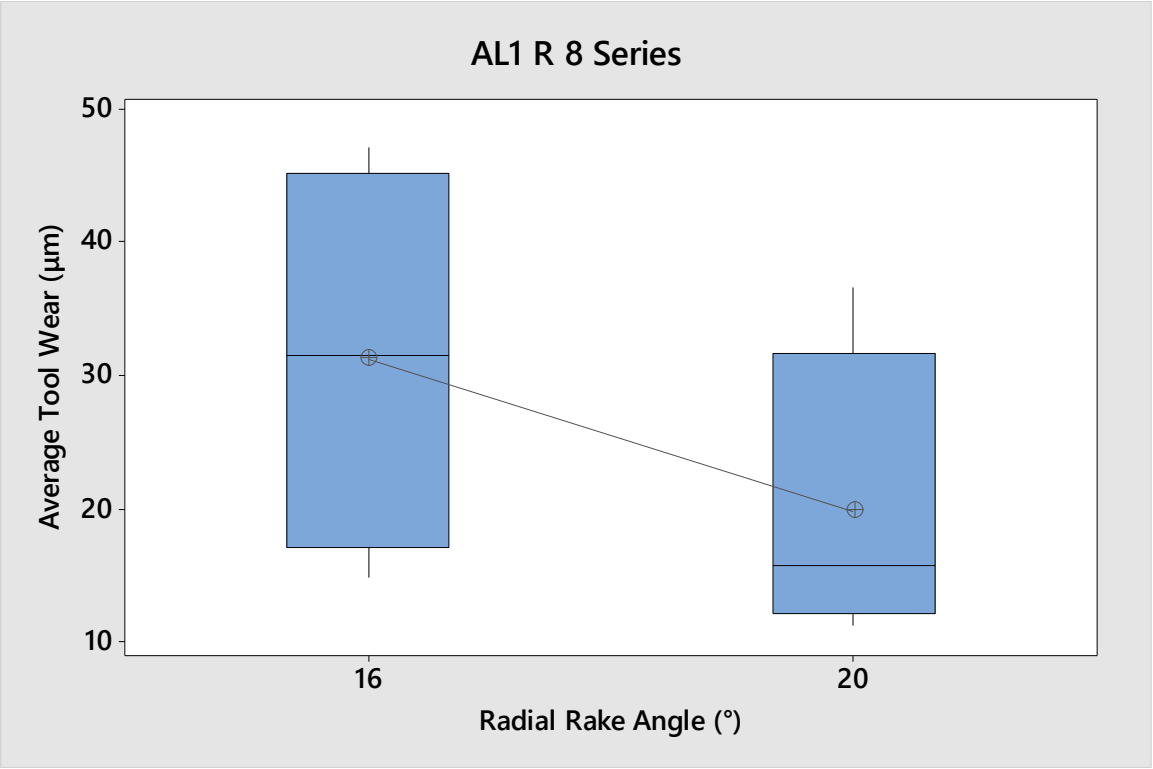

Fig. 191: Box plot of interactions between radial rake angle at different levels based on average tool wear obtained from end-milling of 6082-T6 using 2-flute end-mills

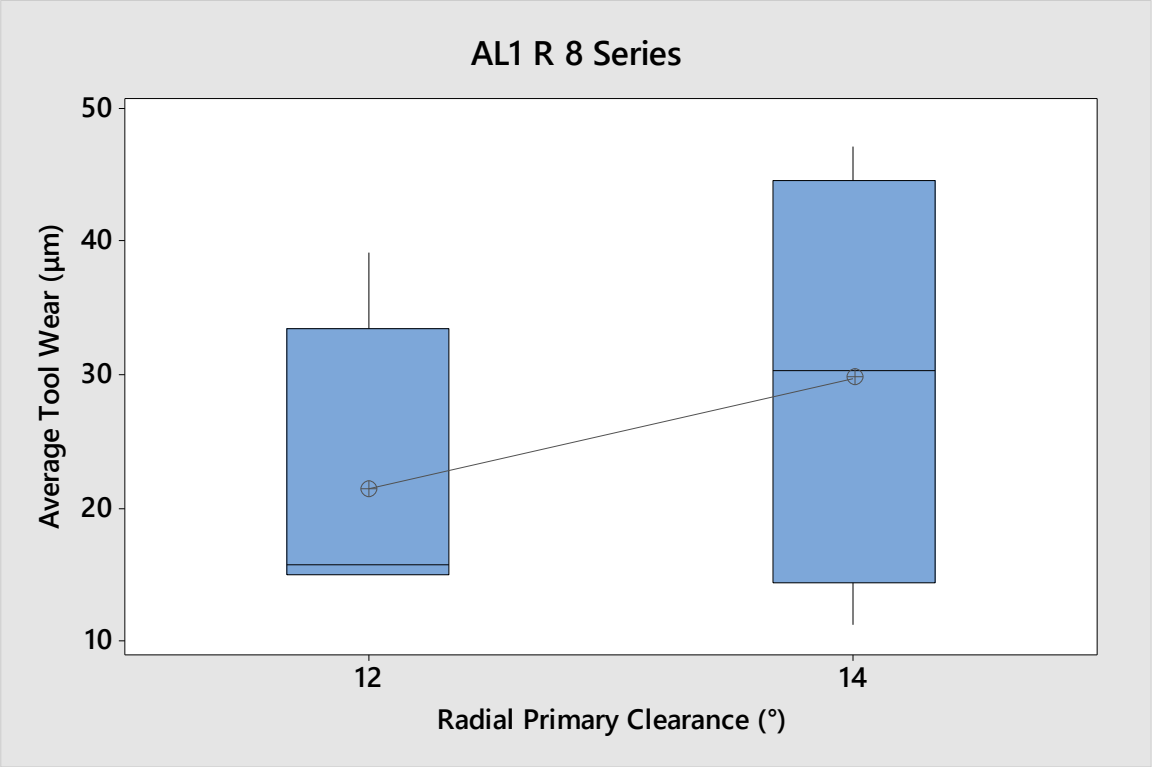

Fig. 192: Box plot of interactions between radial primary clearance angle at different levels based on average tool wear obtained from end-milling of 6082-T6 using 2-flute end-mills

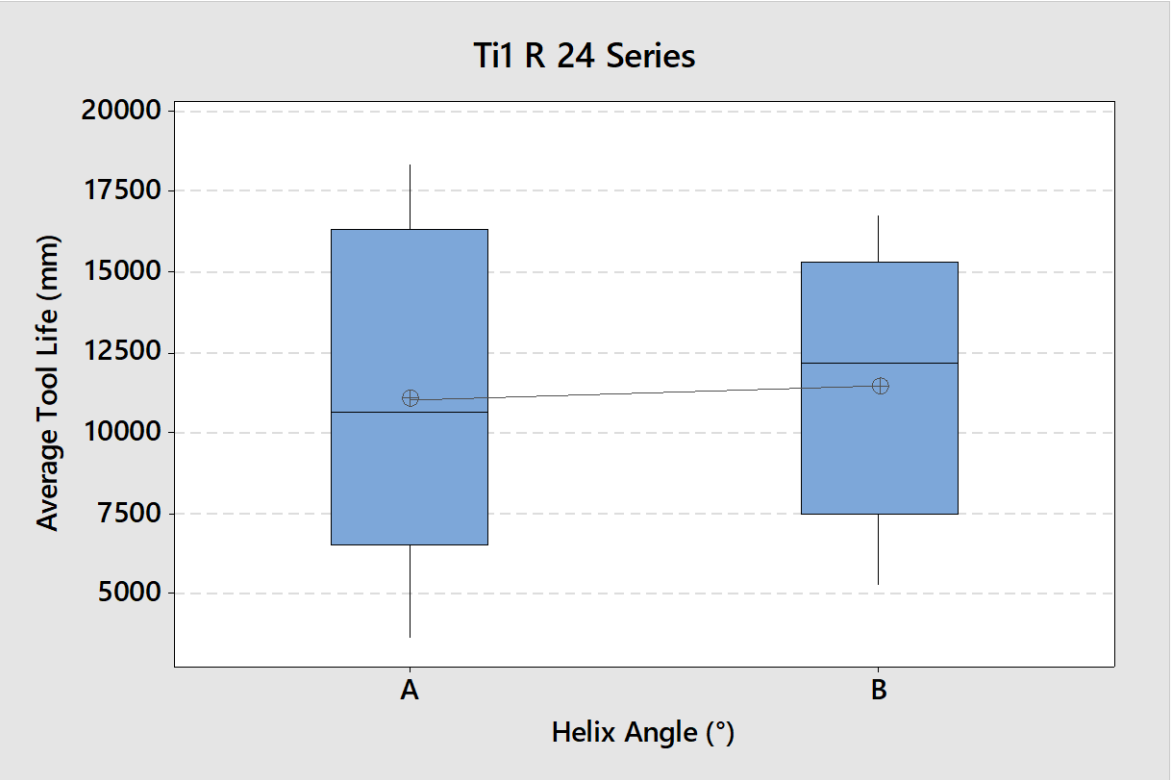

Fig. 193: Box plot of interactions between helix angle at different levels based on average tool life obtained from end-milling of Ti-6Al-4V using 4-flute end-mills

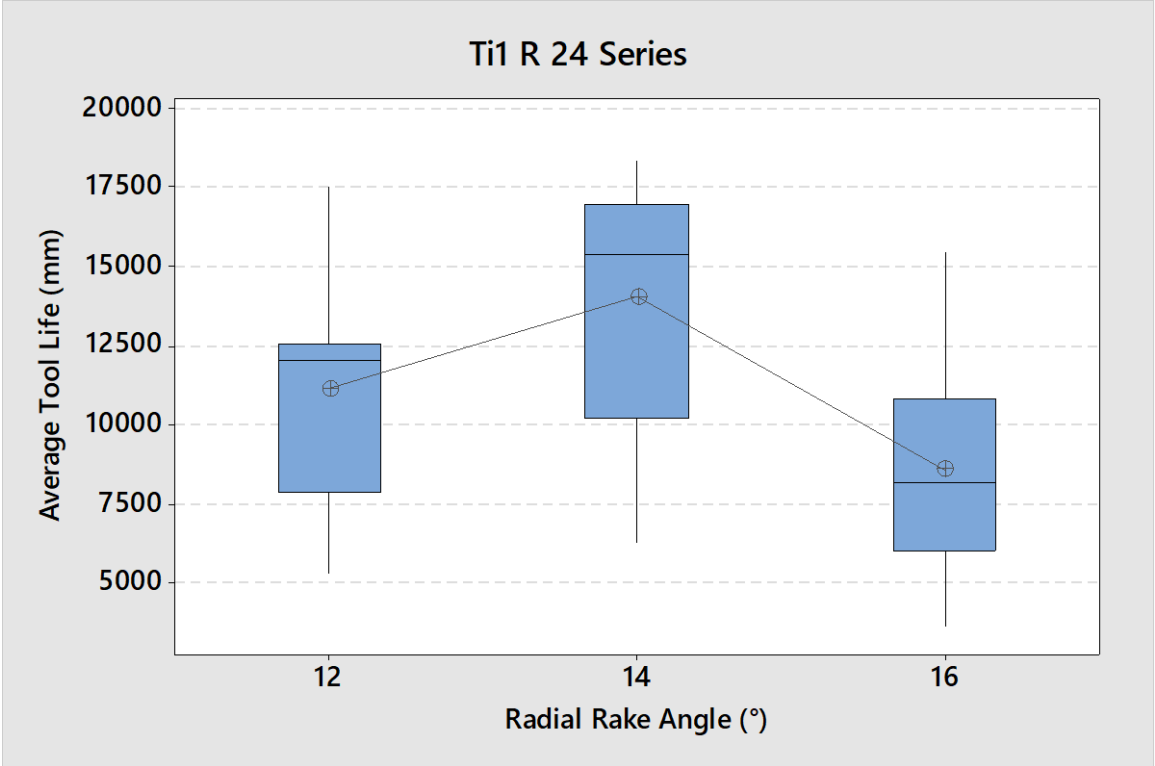

Fig. 194: Box plot of interactions between radial rake angle at different levels based on average tool life obtained from end-milling of Ti-6Al-4V using 4-flute end-mills

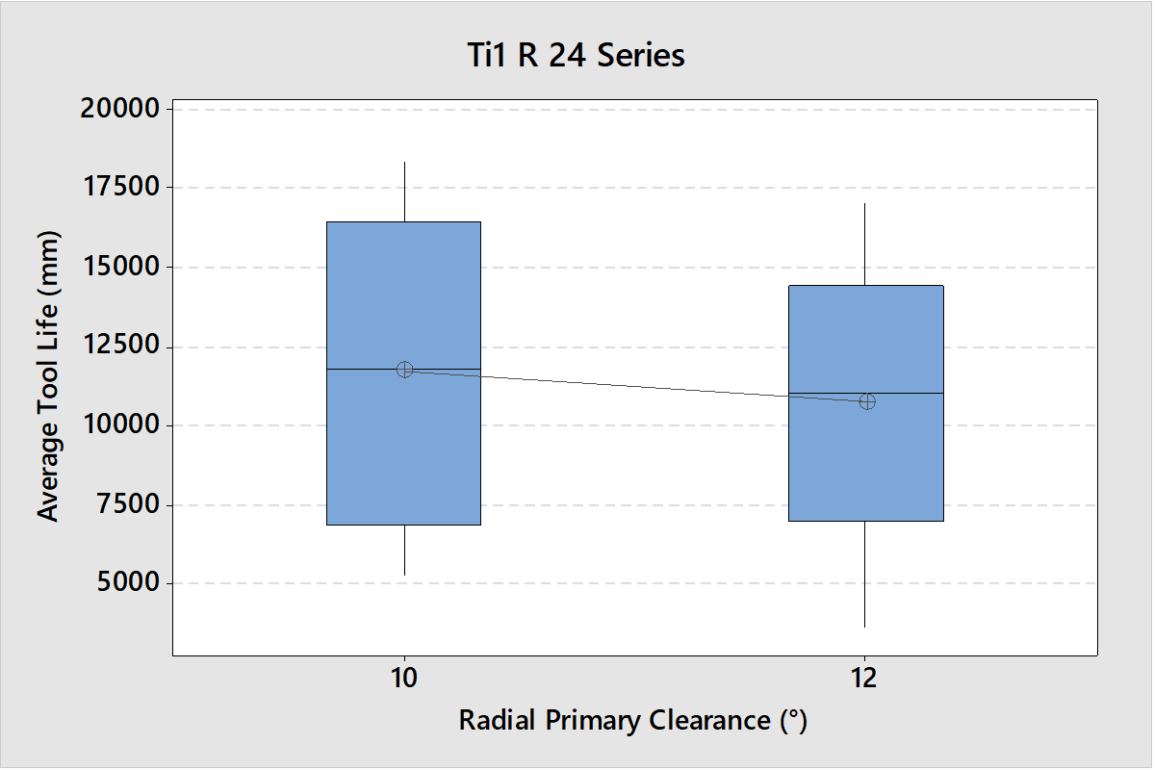

Fig. 195: Box plot of interactions between radial primary clearance angle at different levels based on average tool life obtained from end-milling of Ti-6Al-4V using 4-flute end-mills

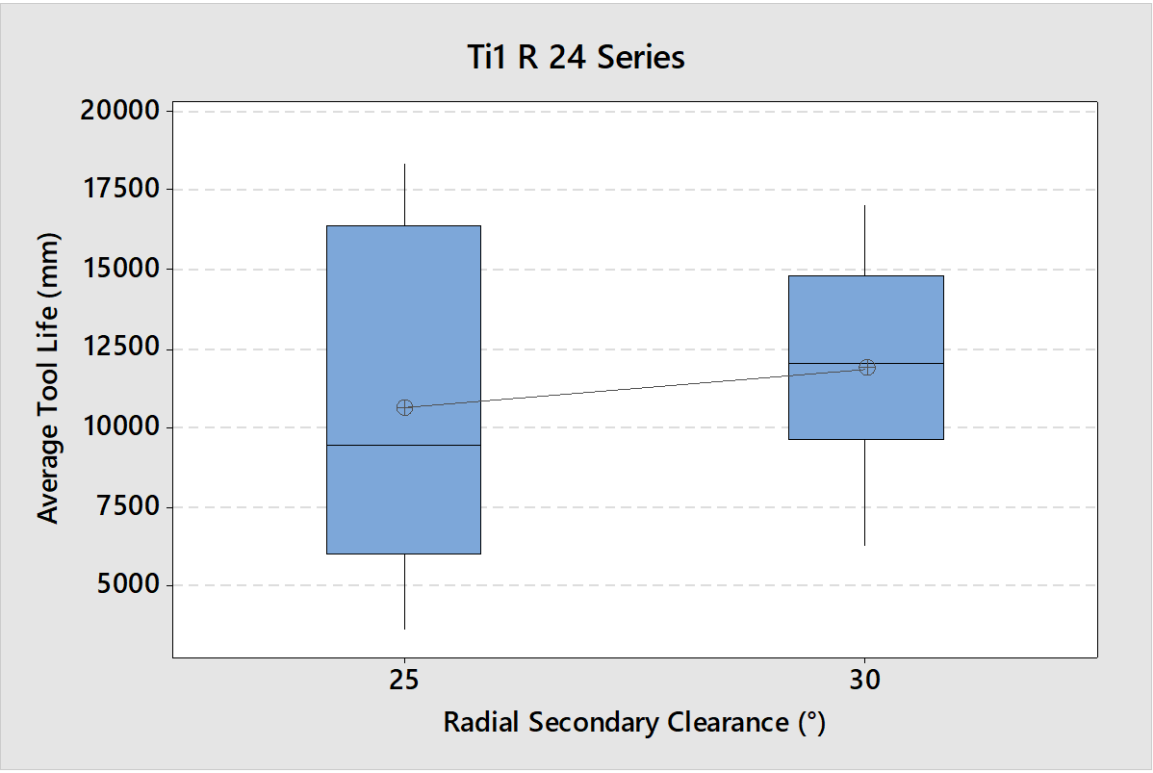

Fig. 196: Box plot of interactions between radial secondary clearance angle at different levels based on average tool life obtained from end-milling of Ti-6Al-4V using 4-flute end-mills

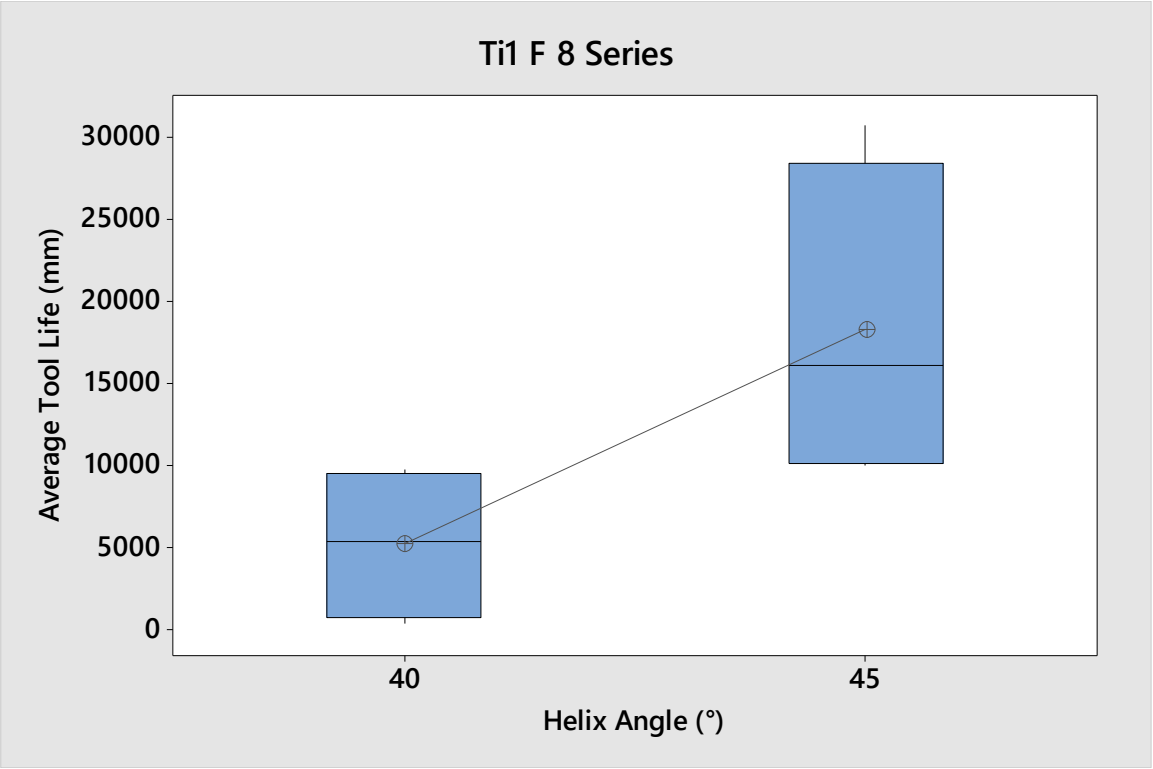

Fig. 197: Box plot of interactions between helix angle at different levels based on average tool life obtained from end-milling of Ti-6Al-4V using 6-flute end-mills

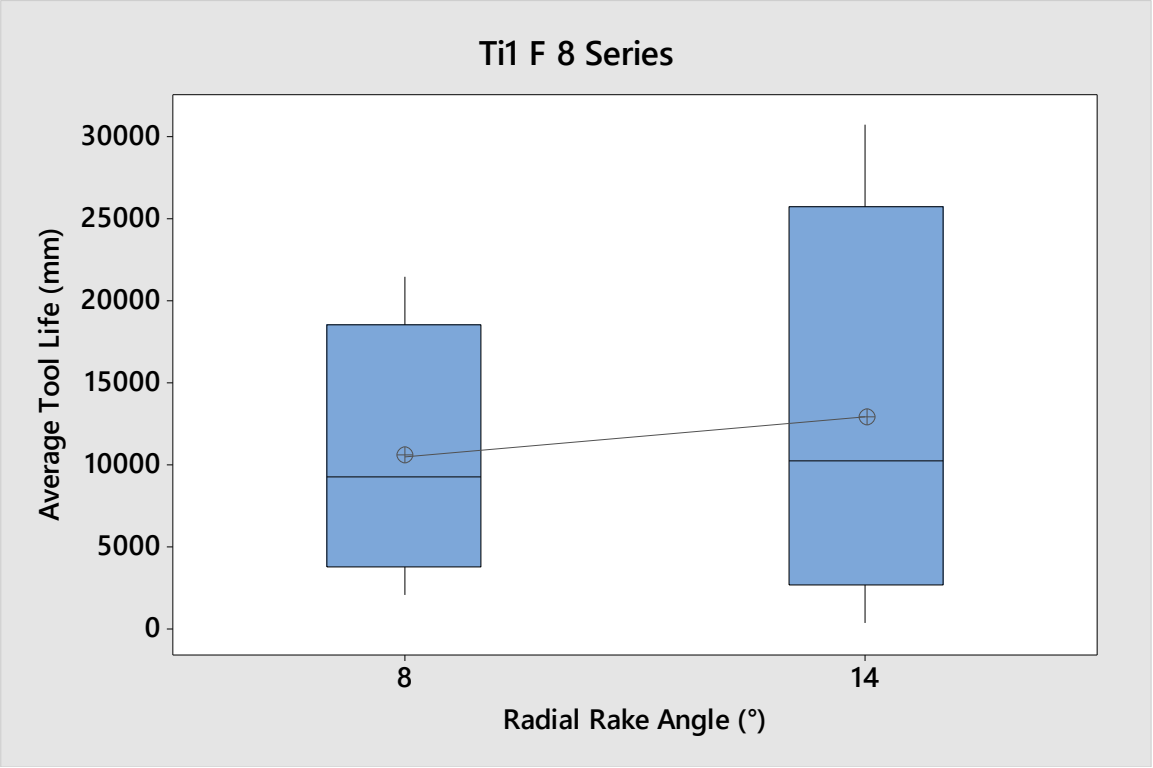

Fig. 198: Box plot of interactions between radial rake angle at different levels based on average tool life obtained from end-milling of Ti-6Al-4V using 6-flute end-mills

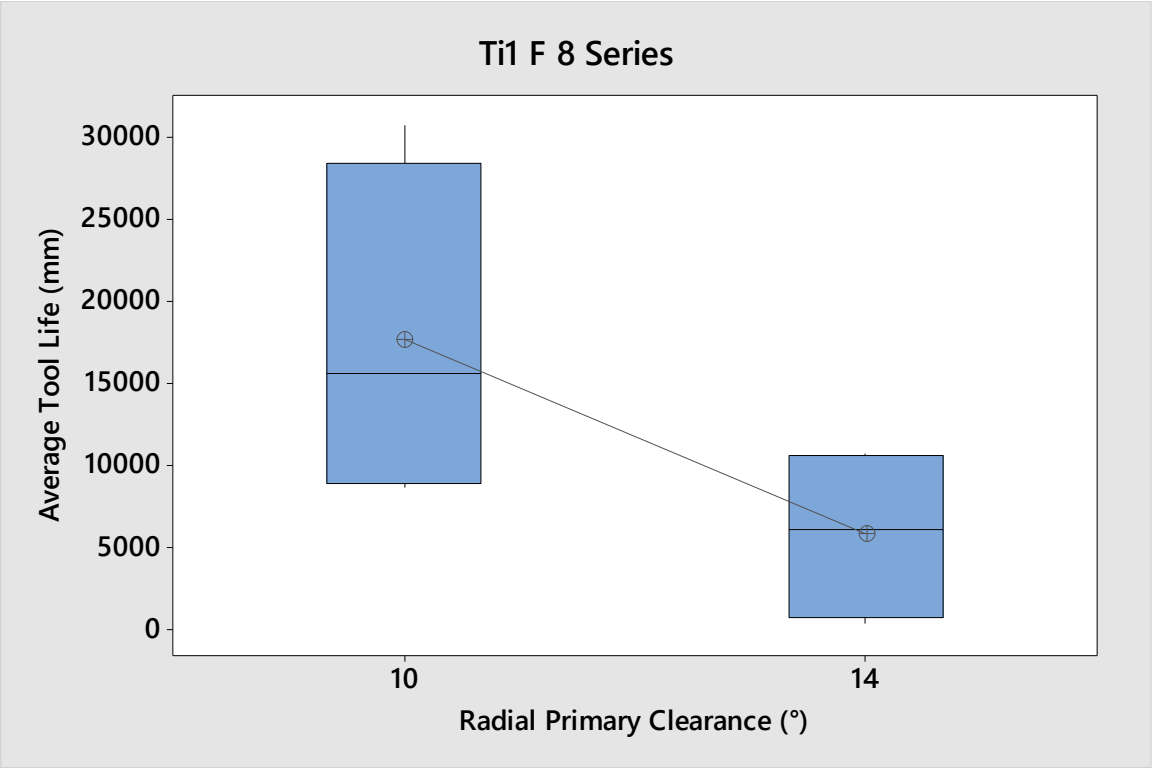

Fig. 199: Box plot of interactions between radial primary clearance angle at different levels based on average tool life obtained from end-milling of Ti-6Al-4V using 6-flute end-mills

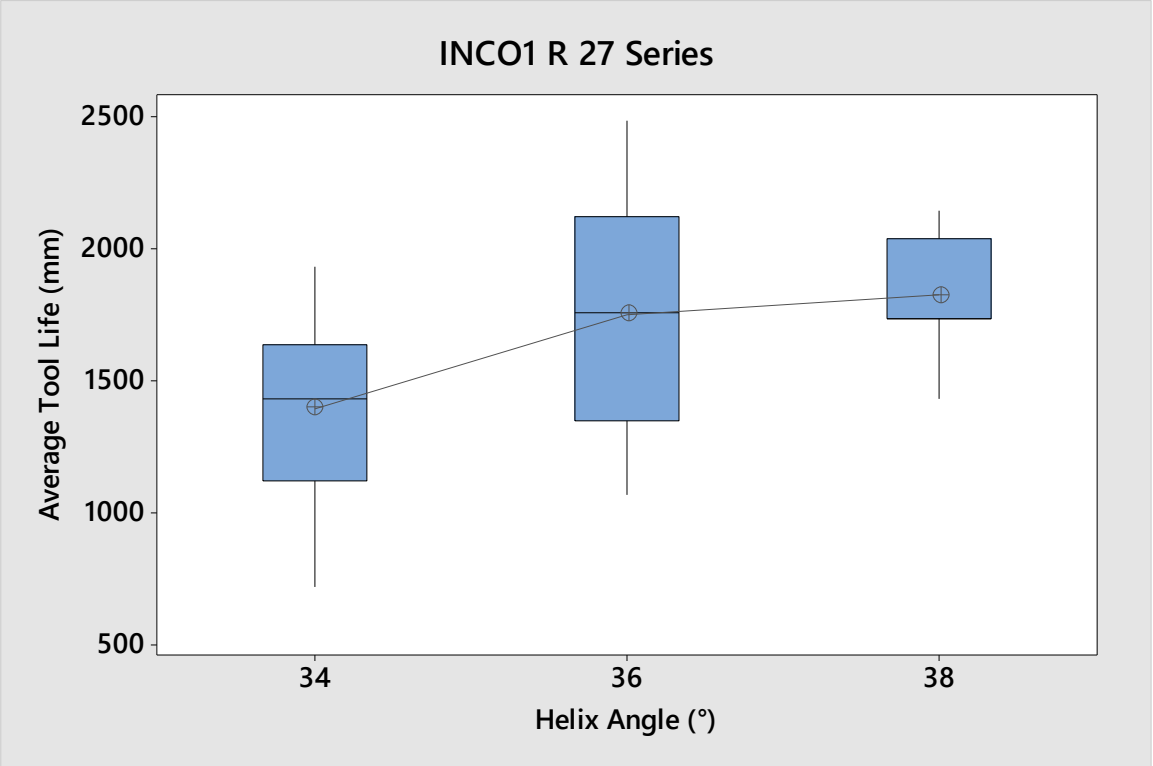

Fig. 200: Box plot of interactions between helix angle at different levels based on average tool life obtained from end-milling of Inconel 718 using 5-flute end-mills

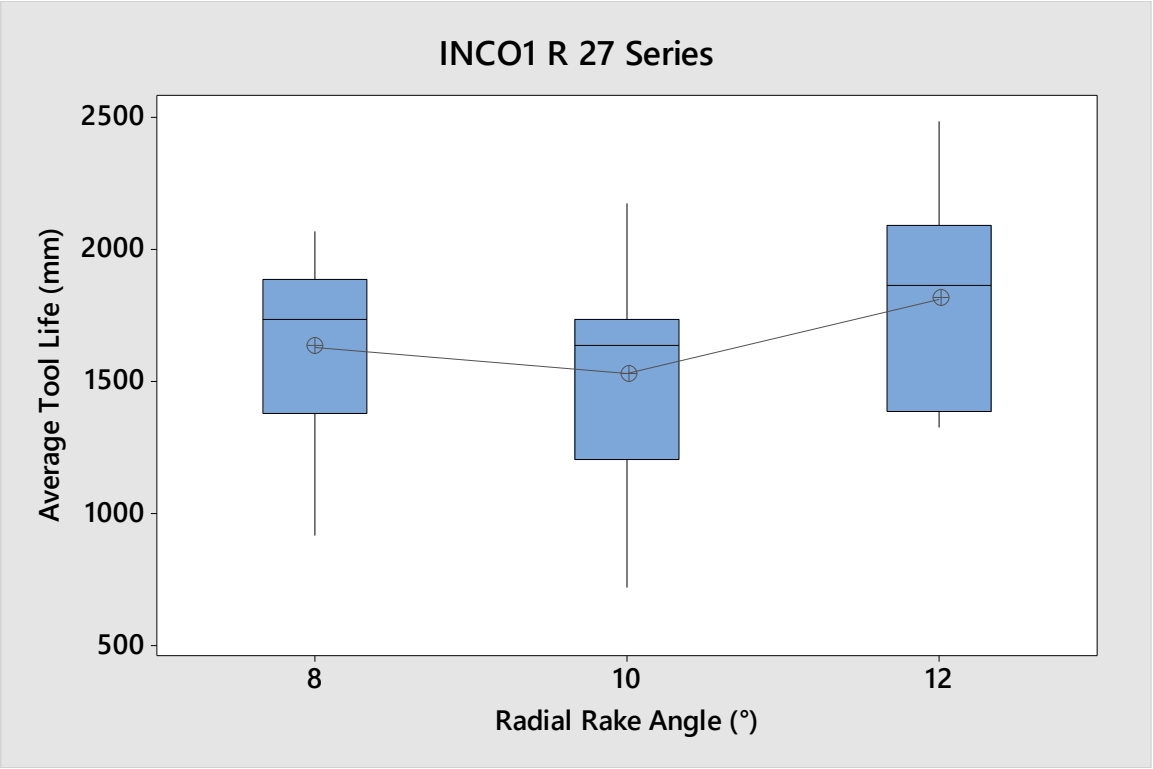

Fig. 201: Box plot of interactions between radial rake angle at different levels based on average tool life obtained from end-milling of Inconel 718 using 5-flute end-mills

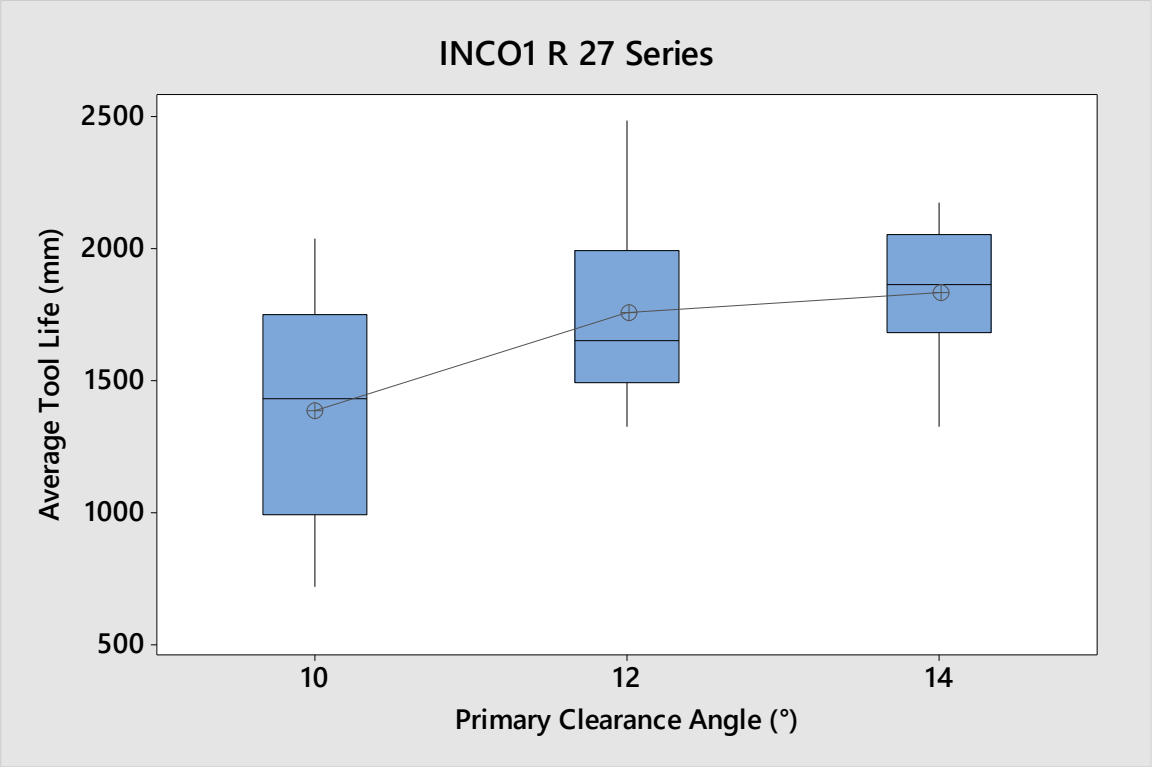

Fig. 202: Box plot of interactions between radial primary clearance angle at different levels based on average tool life obtained from end-milling of Inconel 718 using 5-flute end-mills

Fig. 203: Box plot of interactions between helix angle at different levels based on average tool life obtained from end-milling of super duplex 2507 using 4-flute end-mills

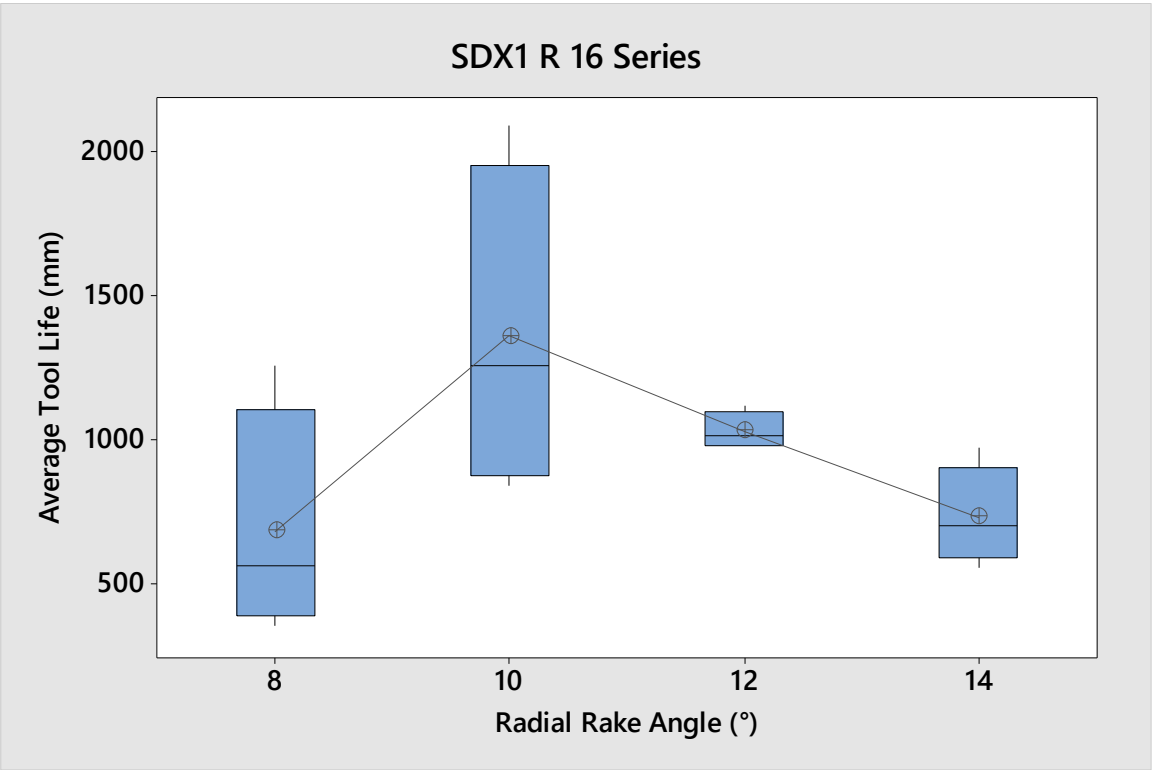

Fig. 204: Box plot of interactions between radial rake angle at different levels based on average tool life obtained from end-milling of super duplex 2507 using 4-flute end-mills

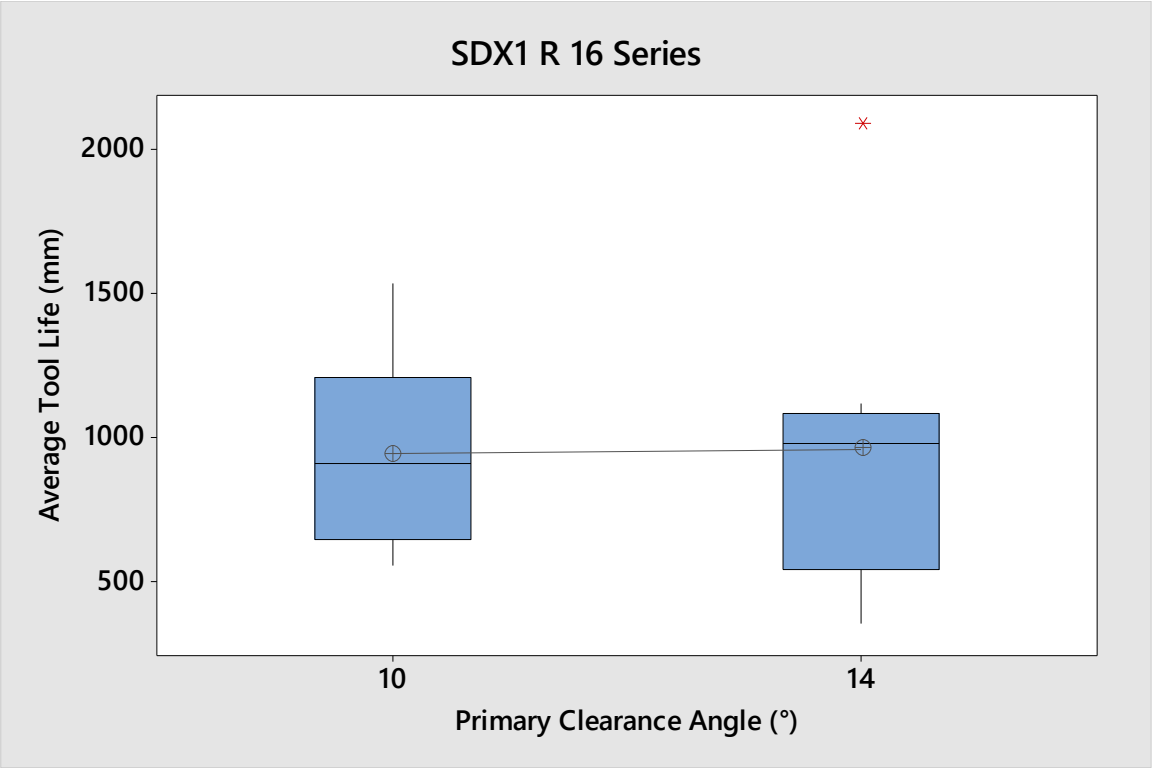

Fig. 205: Box plot of interactions between radial primary clearance angle at different levels based on average tool life obtained from end-milling of super duplex 2507 using 4-flute end-mills

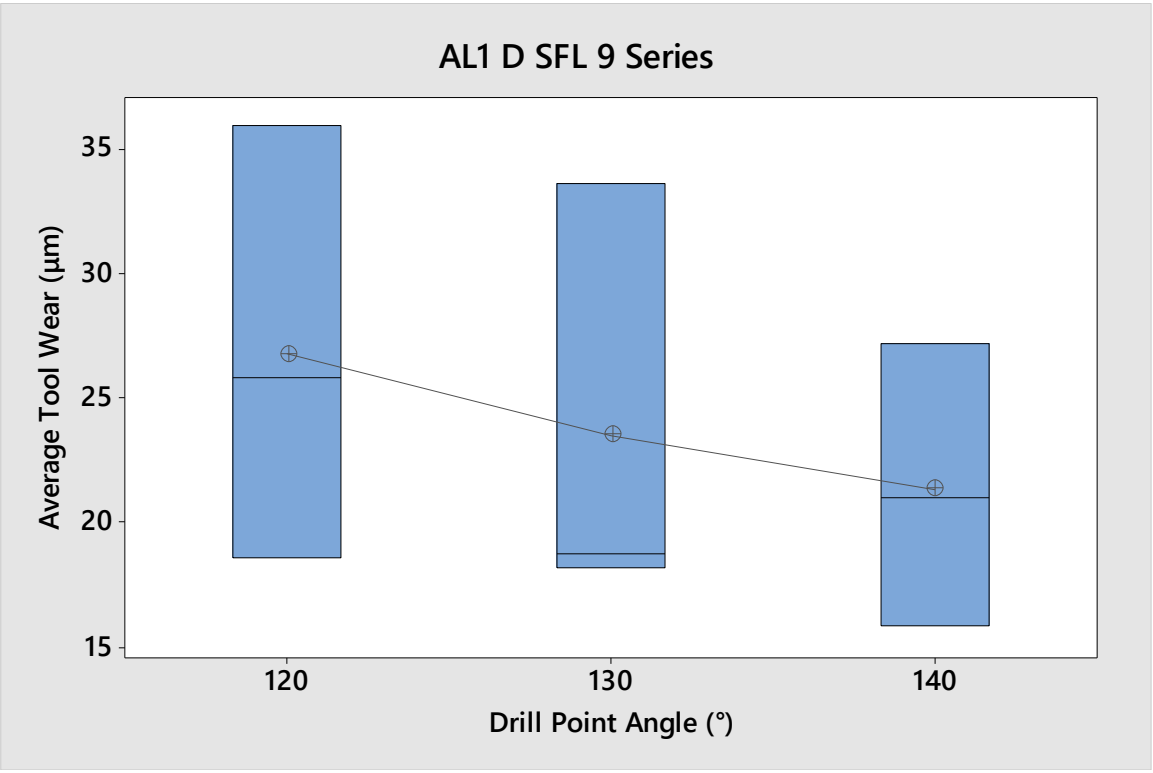

Fig. 206: Box plot of interactions of drill point angle at different levels based on average tool wear obtained from drilling experiments on 6082-T6 using 2-flute drills

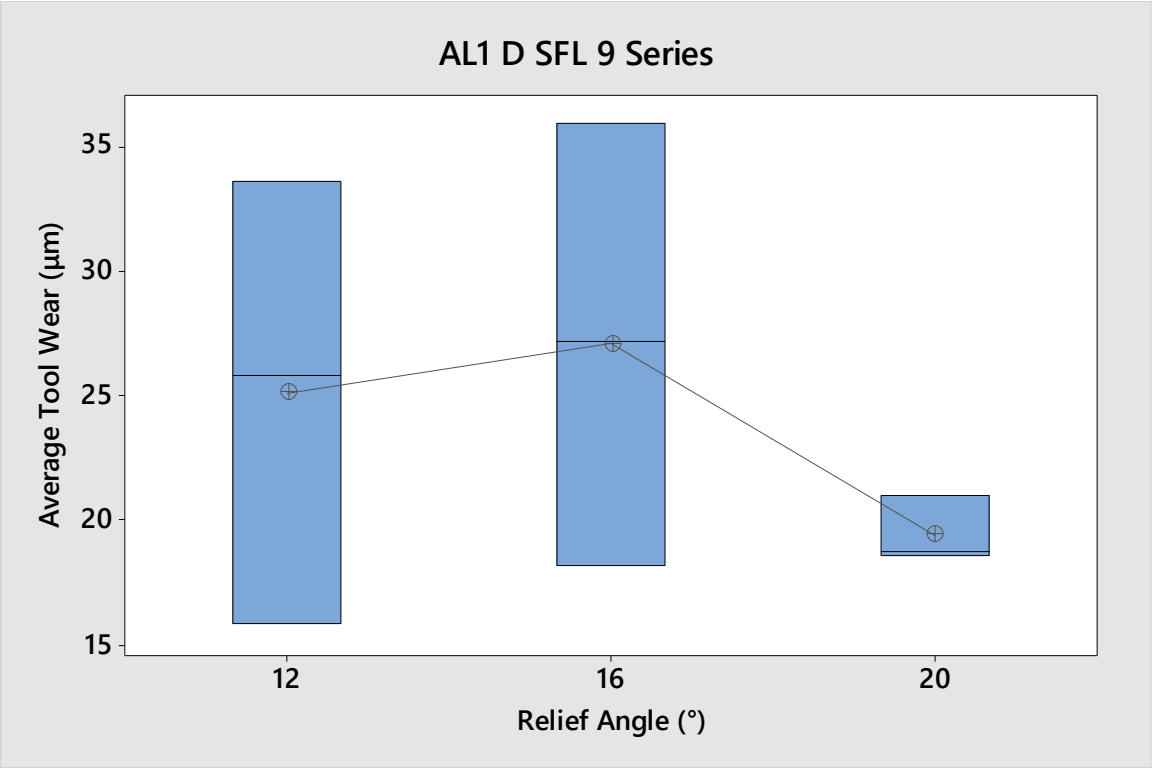

Fig. 207: Box plot of interactions of relief angle at different levels based on average tool wear obtained from drilling experiments on 6082-T6 using 2-flute drills

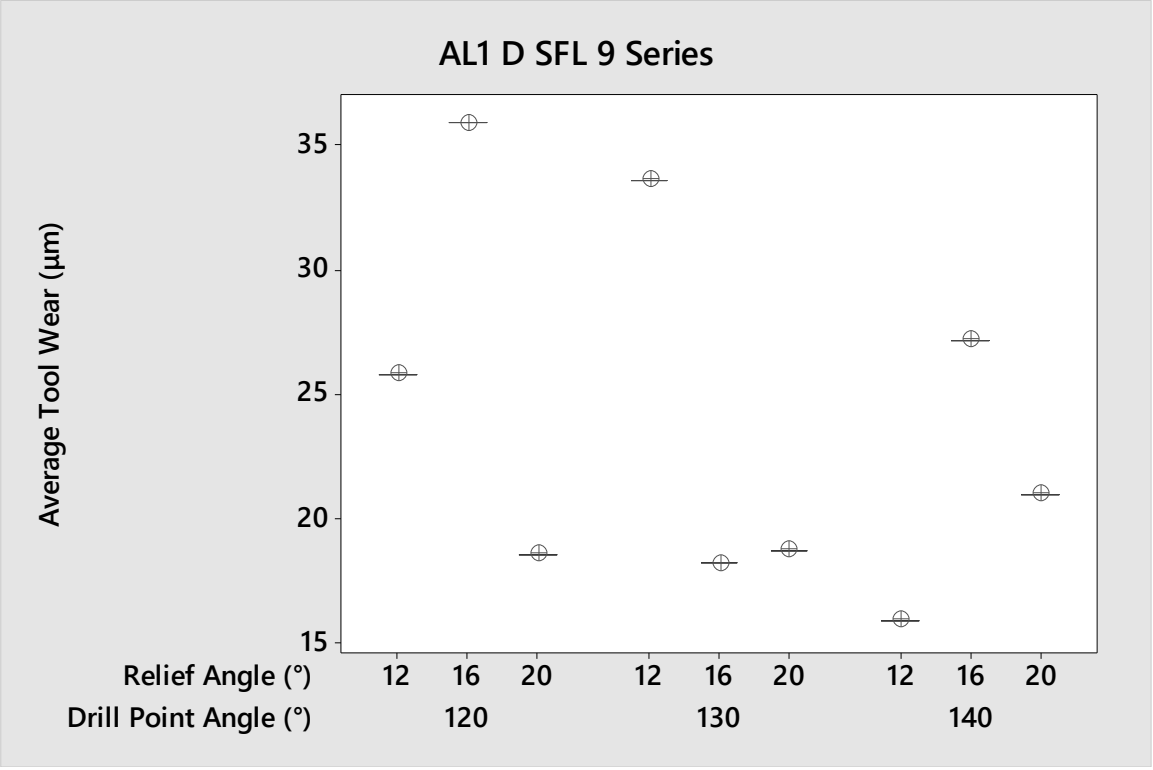

Fig. 208: Box plot of interactions between drill point angle and relief angle at different levels based on average tool wear obtained from drilling experiments on 6082-T6 using 2-flute drills

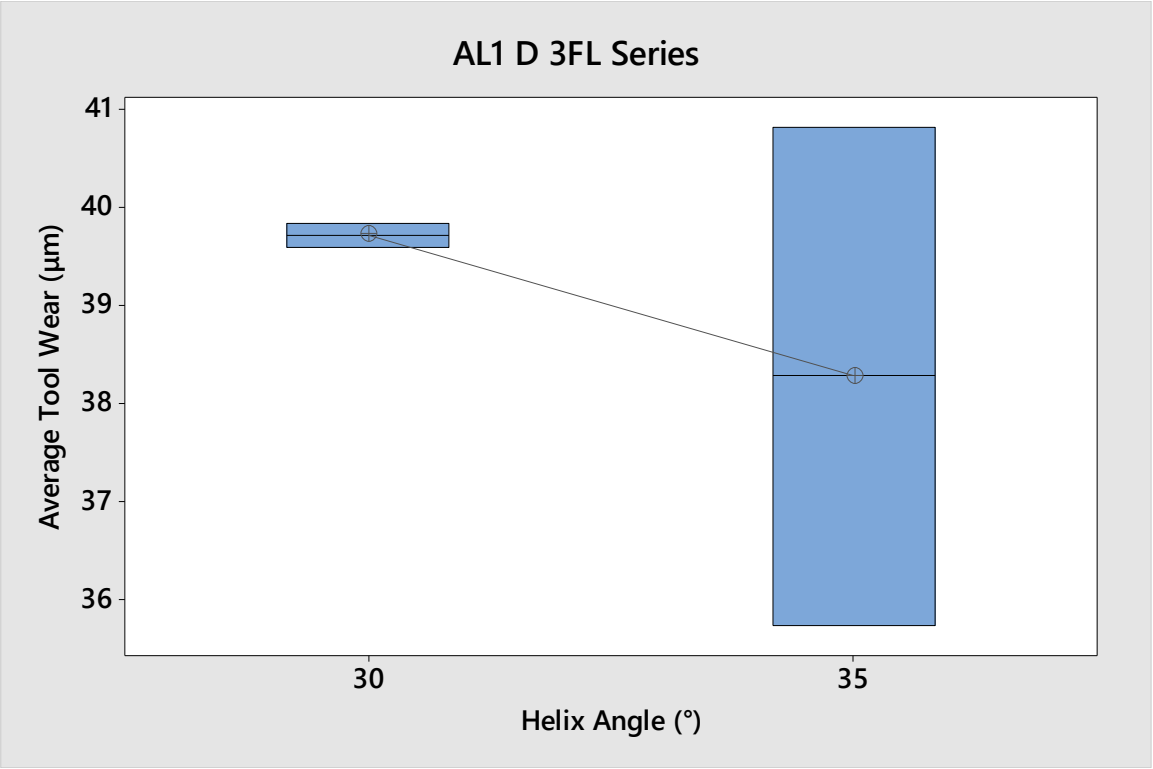

Fig. 209: Box plot of interactions of helix angle at different levels based on average tool wear obtained from drilling experiments on 6082-T6 using 3-flute drills

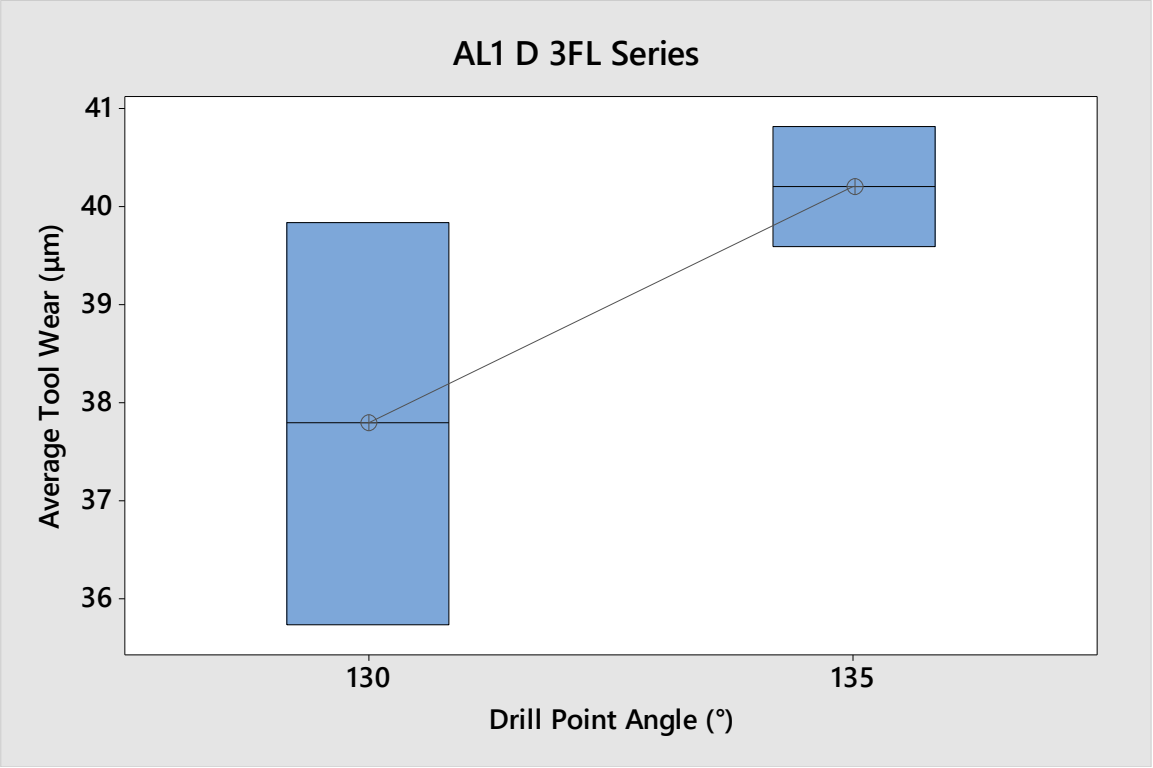

Fig. 210: Box plot of interactions between drill point angle at different levels based on average tool wear obtained from drilling experiments on 6082-T6 using 3-flute drills

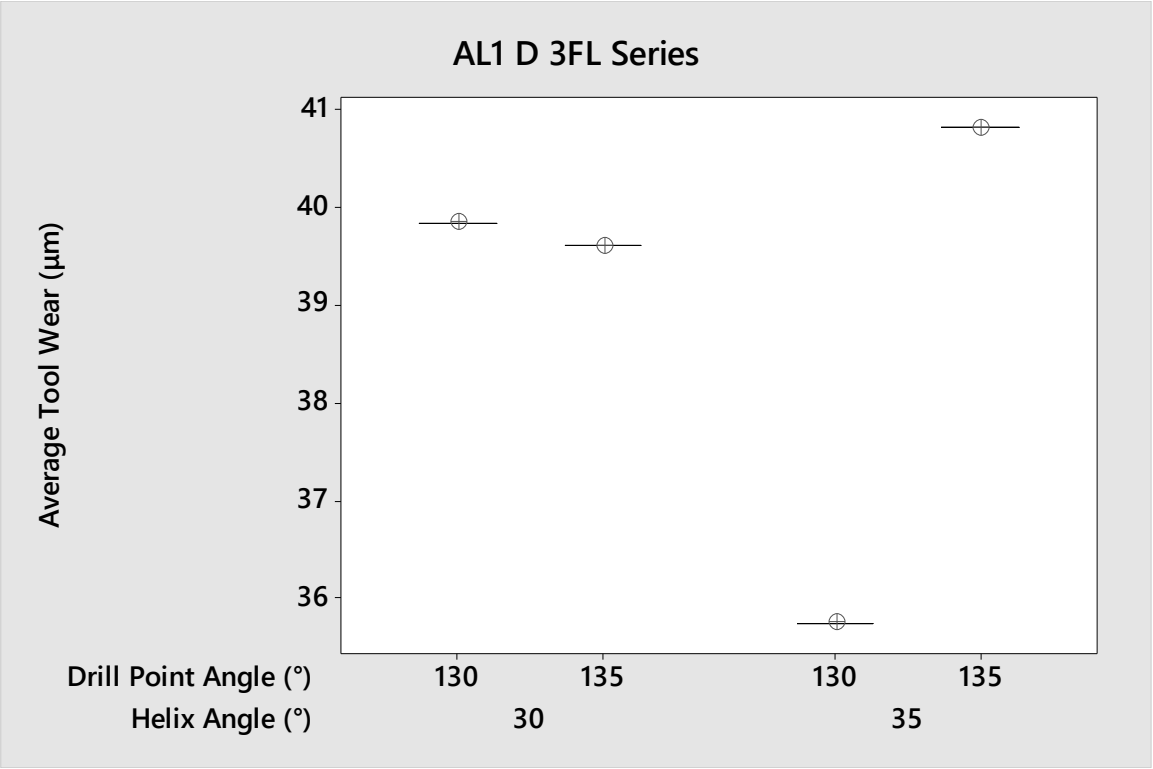

Fig. 211: Box plot of interactions between drill point angle and helix angle at different levels based on average tool wear obtained from drilling experiments on 6082-T6 using 3-flute drills

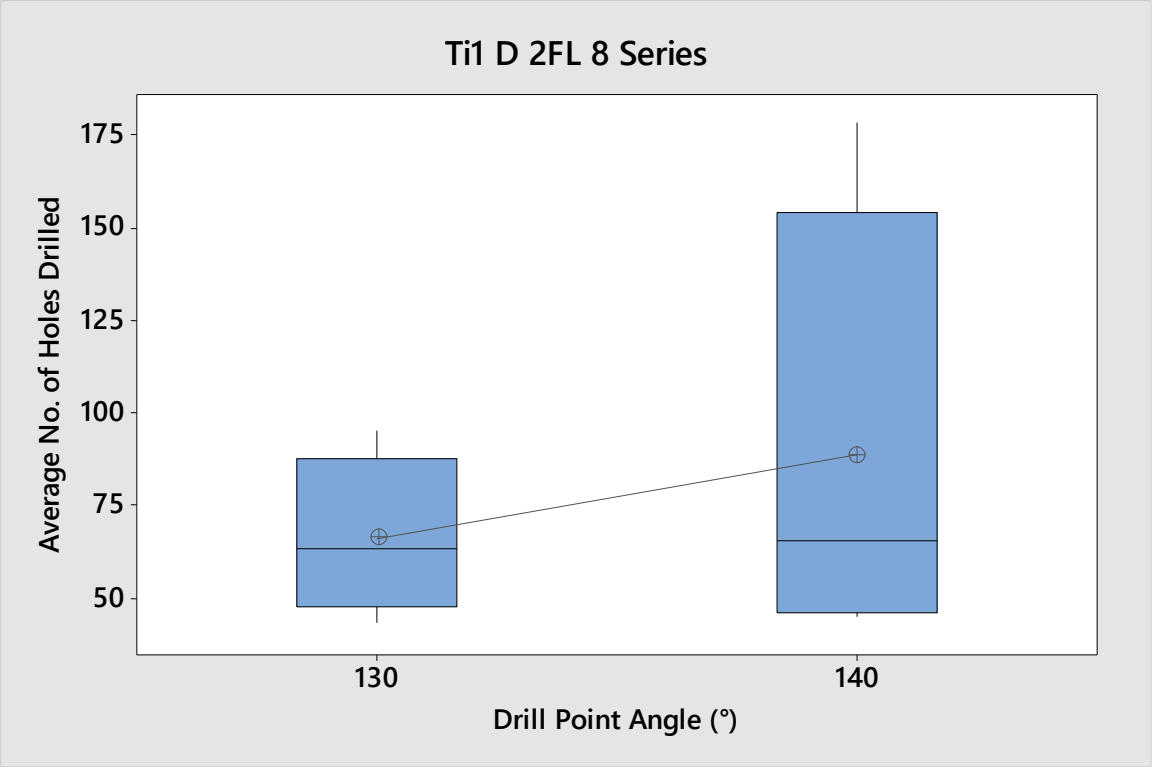

Fig. 212: Box plot of interactions of drill point angle at different levels based on average number of drilled holes obtained from drilling experiments on Ti-6Al-4V

Fig. 213: Box plot of interactions of cutting angle at different levels based on average number of drilled holes obtained from drilling experiments on Ti-6Al-4V

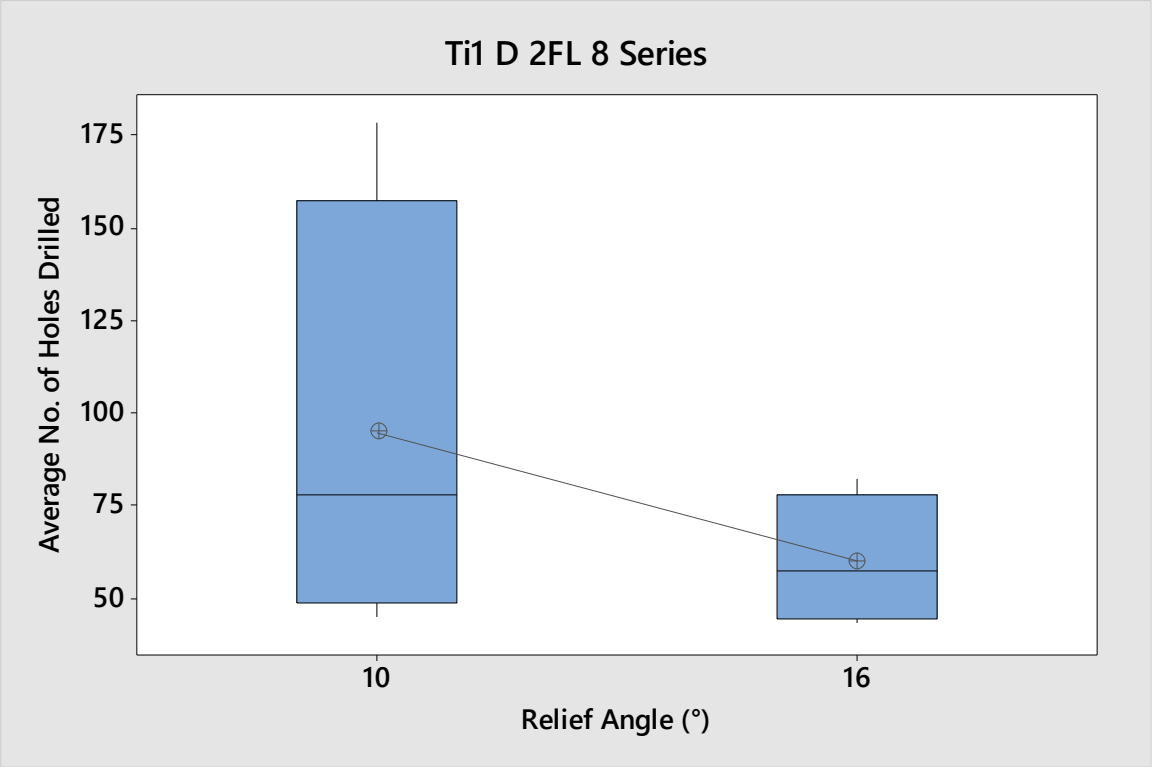

Fig. 214: Box plot of interactions of relief point angle at different levels based on average number of drilled holes obtained from drilling experiments on Ti-6Al-4V

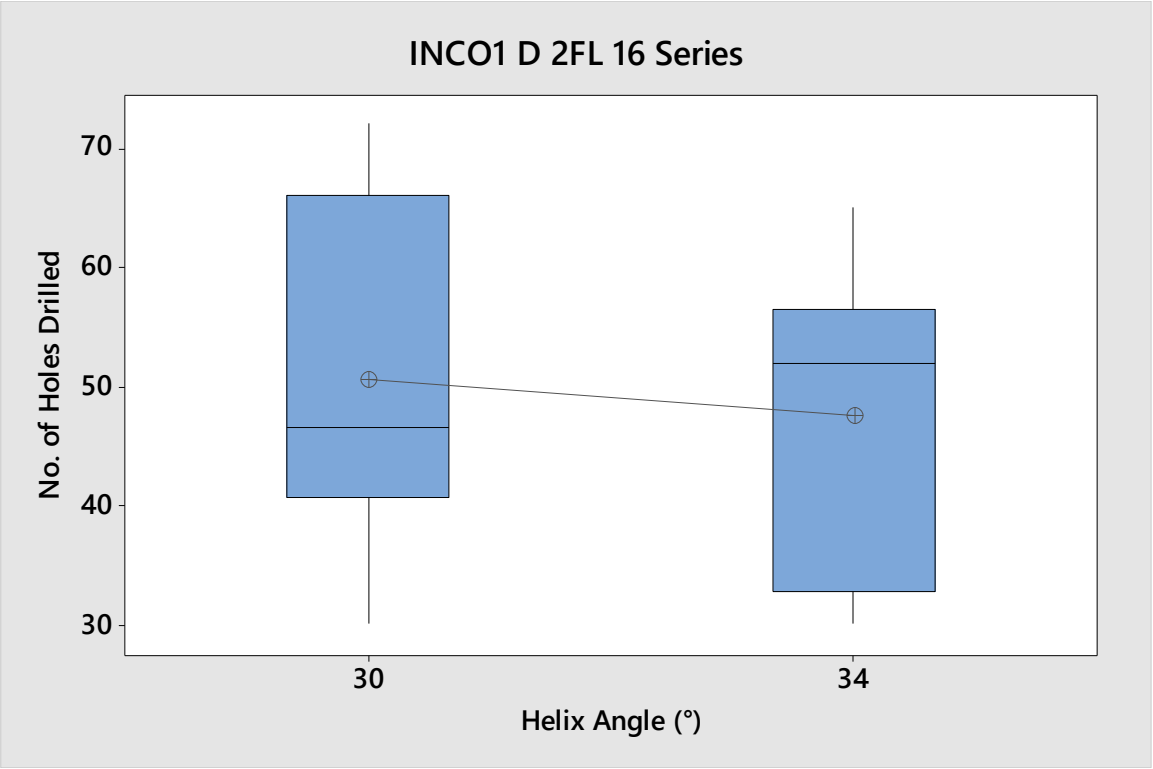

Fig. 215: Box plot of interactions of helix angle at different levels based on average number of drilled holes obtained from drilling experiments on Inconel 718

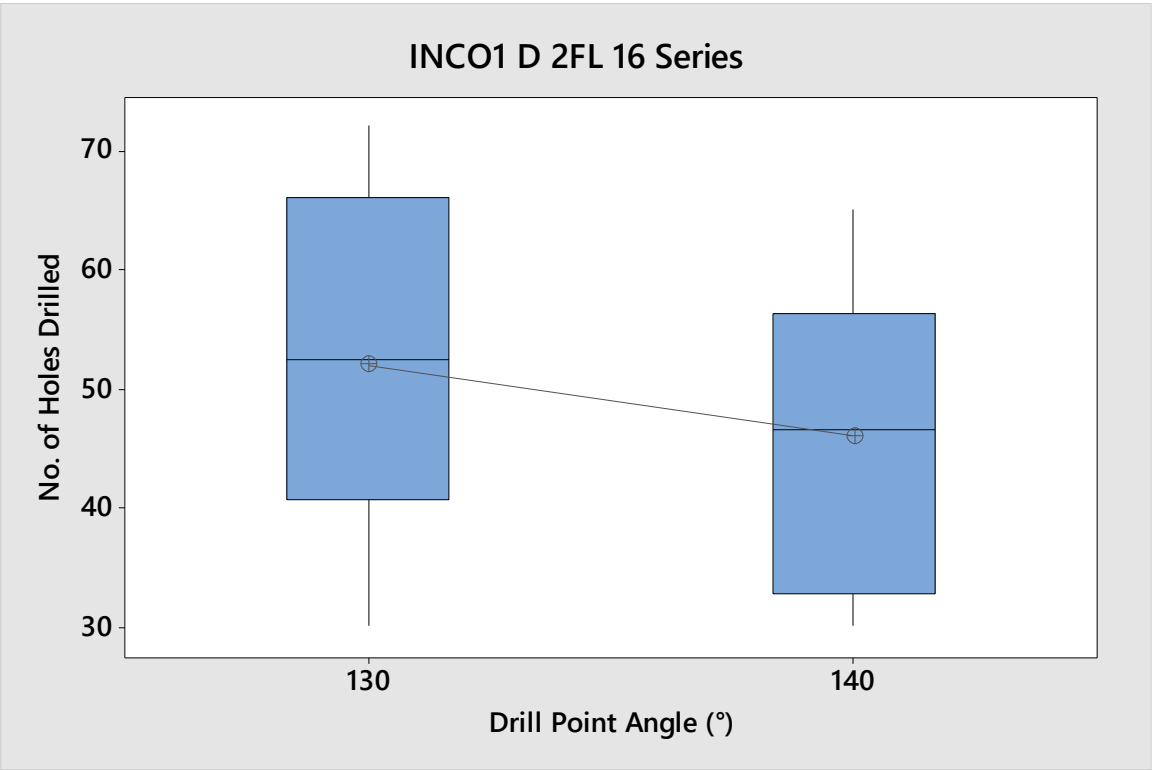

Fig. 216: Box plot of interactions of drill point angle at different levels based on average number of drilled holes obtained from drilling experiments on Ti-6Al-4V

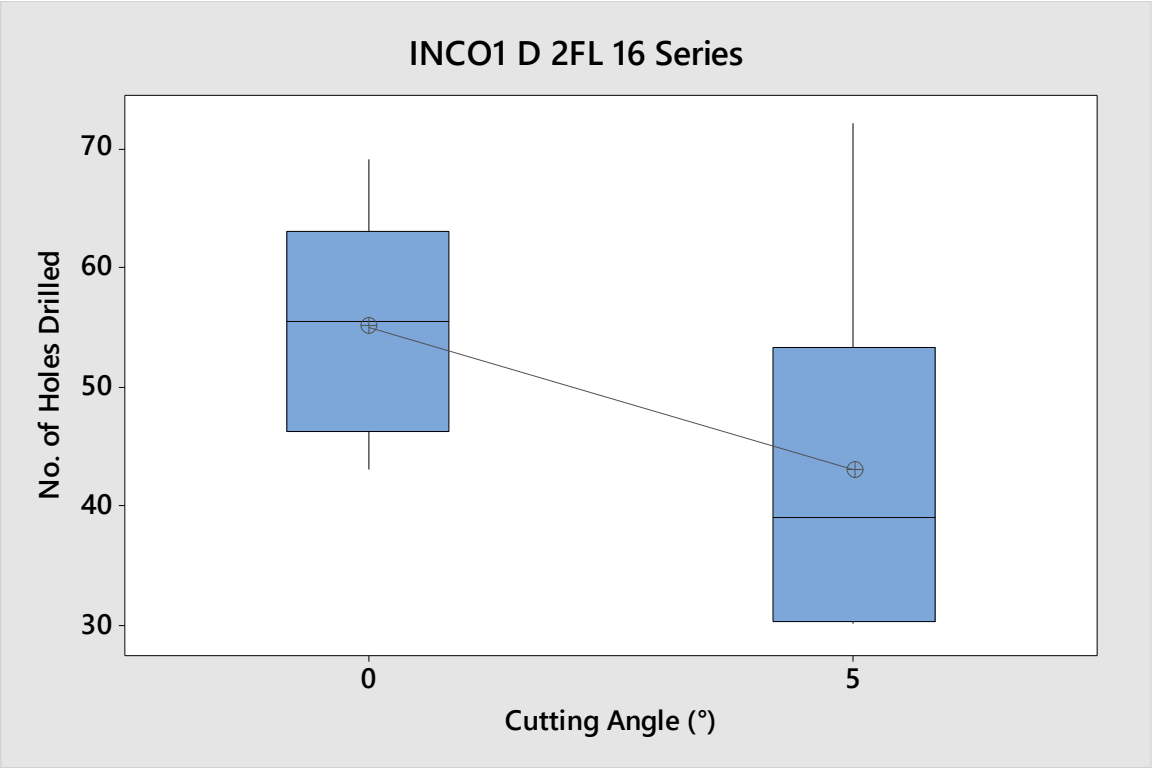

Fig. 217: Box plot of interactions of cutting angle at different levels based on average number of drilled holes obtained from drilling experiments on Inconel 718

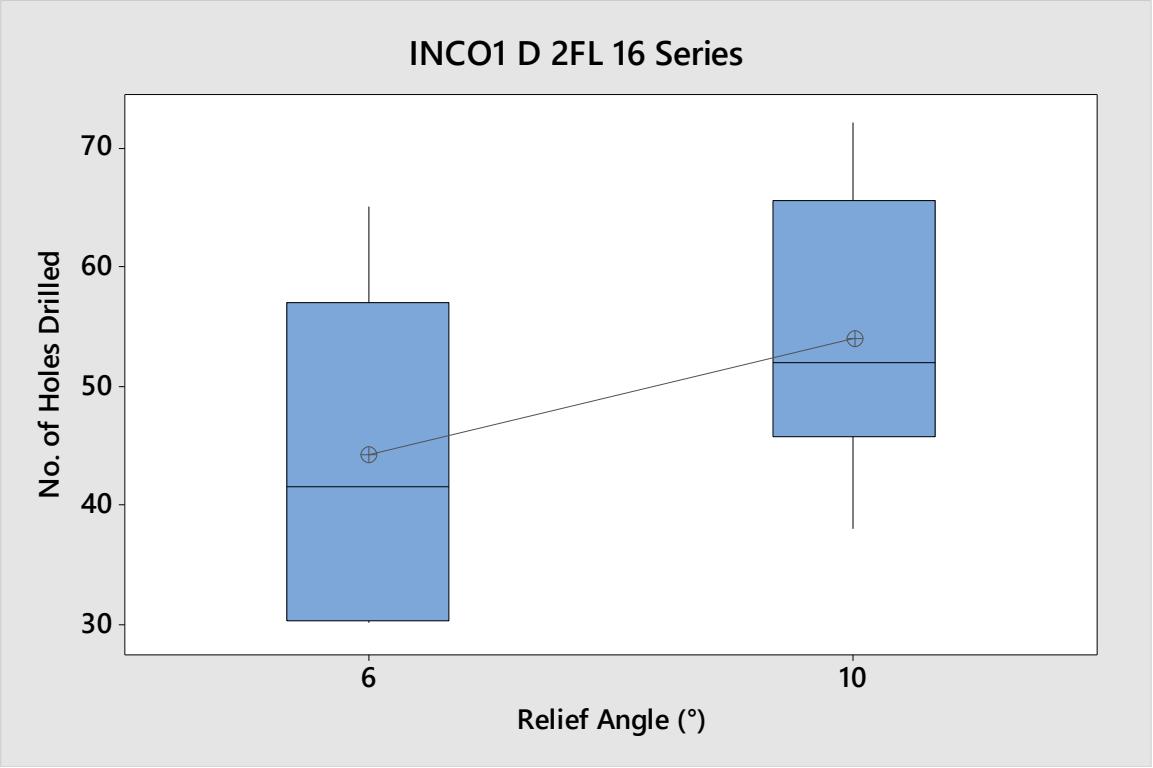

Fig. 218: Box plot of interactions of relief angle at different levels based on average number of drilled holes obtained from drilling experiments on Inconel 718

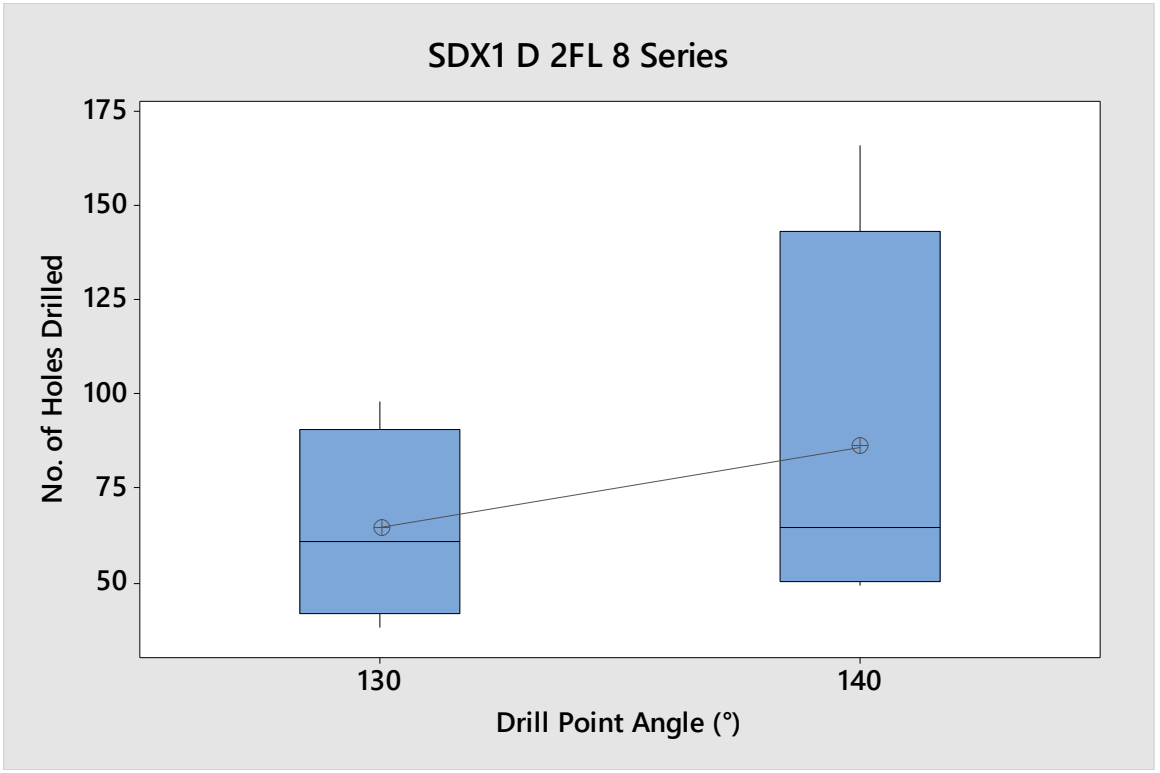

Fig. 219: Box plot of interactions of drill point angle at different levels based on average number of drilled holes obtained from drilling experiments on super duplex 2507

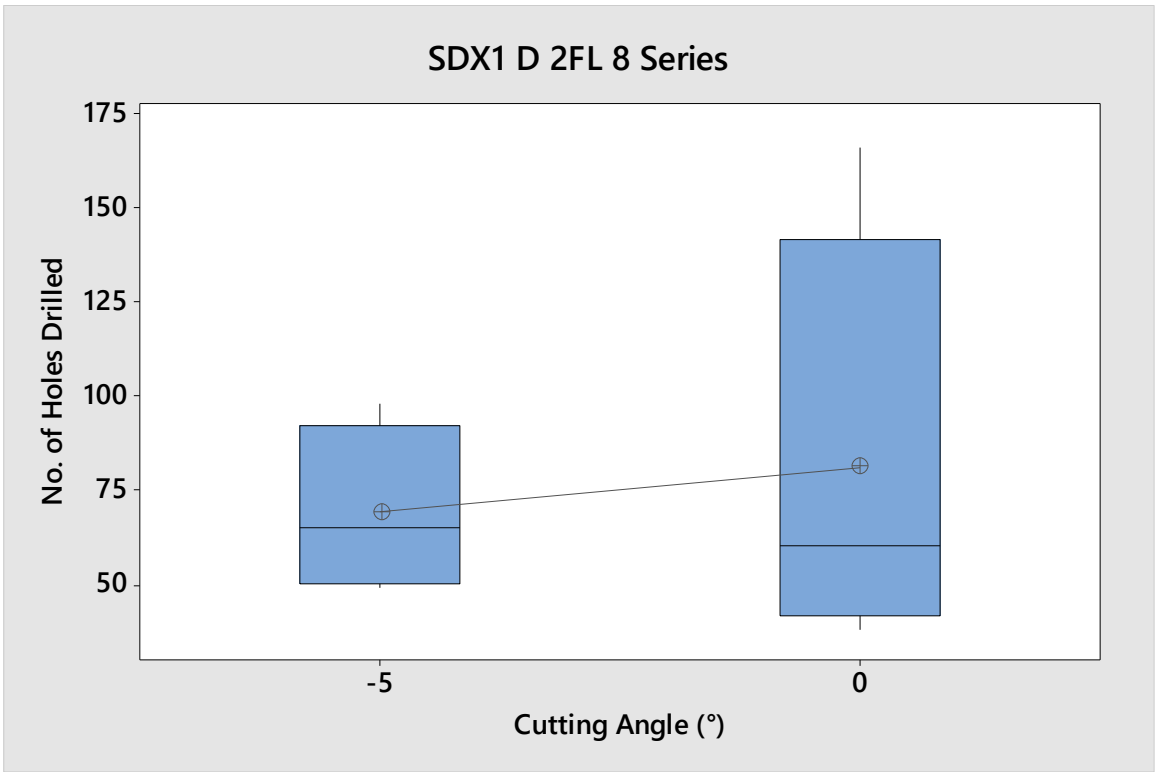

Fig. 220: Box plot of interactions of cutting angle at different levels based on average number of drilled holes obtained from drilling experiments on super duplex 2507

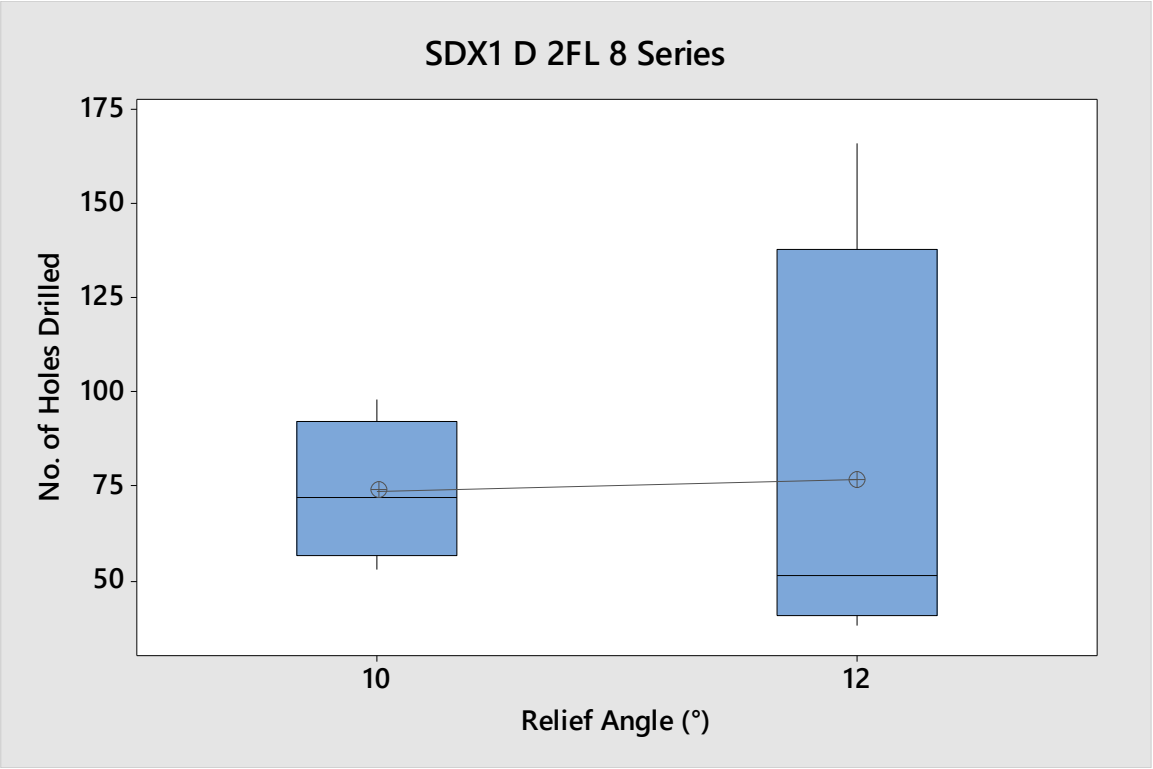

Fig. 221: Box plot of interactions of relief angle at different levels based on average number of drilled holes obtained from drilling experiments on super duplex 2507

Appendix J: Tool Wear – Coated End-mills with Various Grades of WC-Co

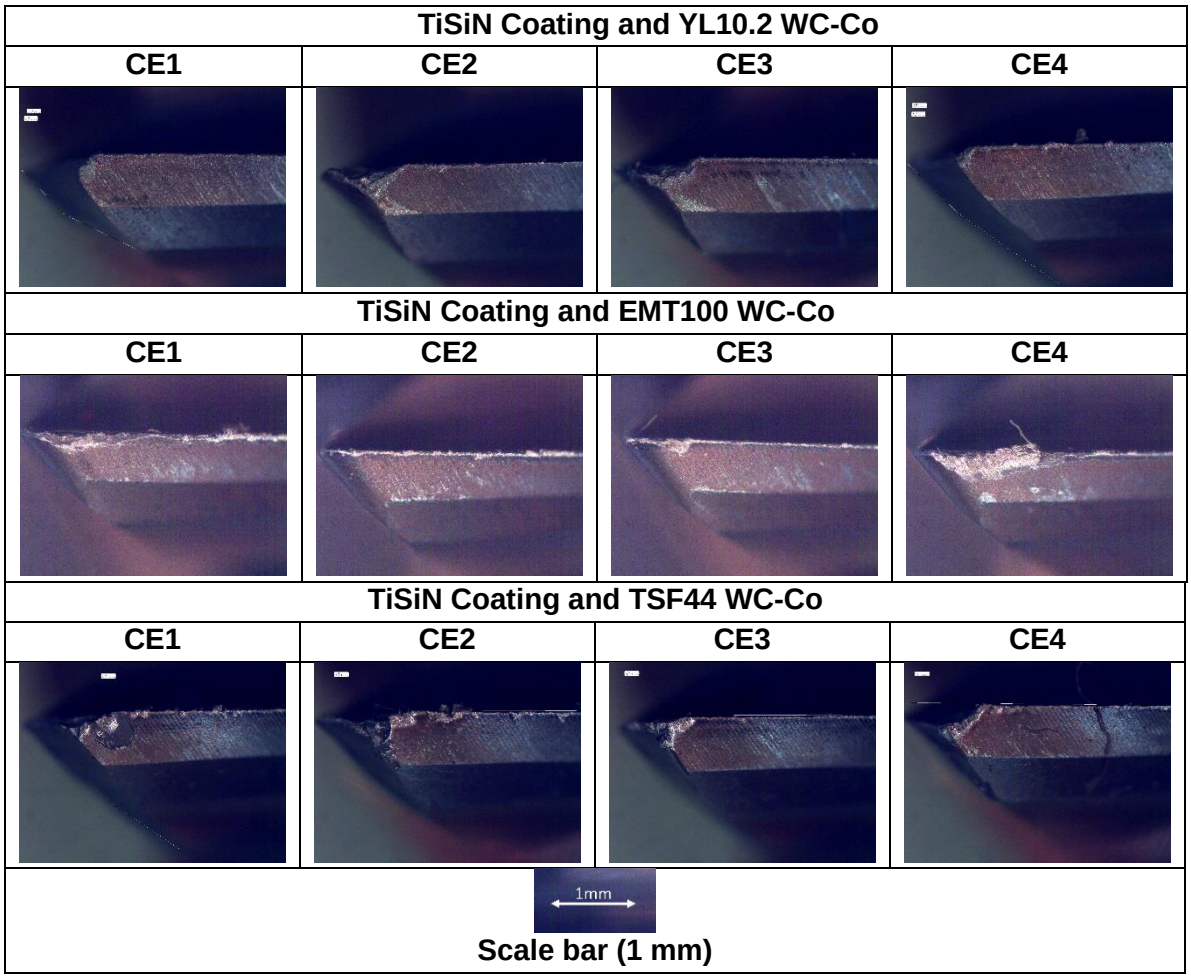

Fig. 222: Tool wear images of various WC-Co with TiSiN coating

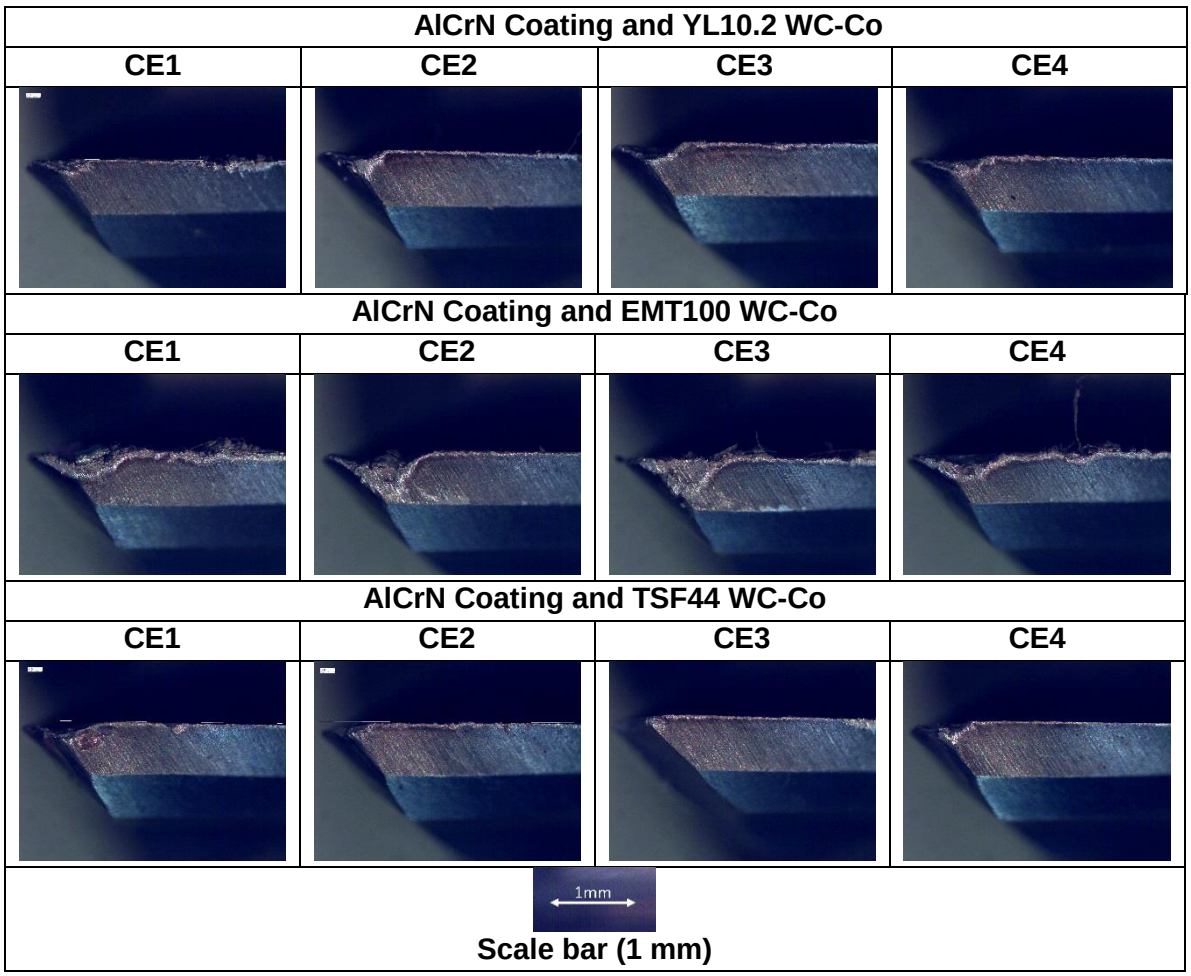

Fig. 223: Tool wear images of three solid WC-Co with AlCrN coating